Le rôle des collisions avec l'hydrogène dans la determination hors-ETL de l'abondance du fer dans les étoiles froides

Rana Ezzeddine

Collège Doctoral du Languedoc-Roussillon

THÈSE

Pour obtenir le grade de

Docteur

Délivré par l'**Université de Montpellier**

Préparée au sein de l'école doctorale **I2S**
Et du **Laboratoire Univers et Particules de Montpellier**

Spécialité: **Physique**

Présentée par **EZZEDDINE Rana**
rana.ezzeddine@umontpellier.fr

Le rôle des collisions inélastique avec l'hydrogène dans la détermination hors-ETL de l'abondance du fer dans les étoiles froides

M. Bertrand Plez	Professeur	Directeur de thèse
M. Marwan Gebran	Maître de conférences	co-directeur de thèse
M. Piercarlo Bonifacio	Directeur de recherche CNRS	Rapporteur
M. Frédéric Thévenin	Directeur de recherche CNRS	Rapporteur
M. Frédéric Paletou	Astronome	Examinateur
M. Matthias Steffen	Professeur	Examinateur

UNIVERSITÉ DE MONTPELLIER

Non-LTE Iron abundance determination in cool stars: The role of Hydrogen collisions

Rana Ezzeddine

December, 2015

Résumé

La détermination d'abondances stellaires très précises est un objectif majeur de la plupart des études spectroscopiques. L'hypothèse de l'équilibre thermodynamique local (ETL), largement utilisée dans les analyses spectroscopiques, est souvent inadéquate pour déterminer les abondances et les paramètres stellaires, particulièrement pour les étoiles géantes ou pauvres en métaux, où les effets hors-ETL dominent. C'est pourquoi, une modélisation hors-ETL des spectres stellaires est cruciale afin de reproduire les observations et ainsi déterminer avec précision les paramètres stellaires. Cette modélisation hors-ETL nécessite l'utilisation d'un grand jeu de données atomiques, qui ne sont pas toujours connues avec certitude. Les taux de collisions avec l'hydrogène sont une des sources d'incertitudes les plus fortes dans le cas des étoiles froides. Ces taux sont souvent approximés en considérant une approche classique (l'approximation de Drawin), et ceci seulement dans le cas de transitions permises liée-liée et d'ionisations. Cette approche classique, tend à surestimer le taux de collision et ne reproduit pas correctement le comportement en fonction de l'énergie de la transition. Je démontre dans cette thèse l'incapacité de l'approximation de Drawin à décrire le taux de collisions avec l'hydrogène. Je présente une nouvelle méthode empirique pour estimer ce taux, par le biais d'ajustement sur des taux quantiques existant pour d'autres éléments. Je montre ensuite que cette méthode d'ajustement quantique (que je nomme QFM) permet de reproduire les résultats des modélisations hors-ETL effectuées avec des taux quantiques existants (cas du Si). J'utilise ensuite cette nouvelle méthode, avec mon propre modèle d'atome de fer, sur des étoiles de référence issues du "*Gaia*-ESO survey", ce qui me permet de déterminer empiriquement les taux de collision avec l'hydrogène. En partant de paramètres photosphériques non-spectroscopiques, je détermine les abondances en fer de ces étoiles de référence dans le cas ETL comme hors-ETL. Les résultats dans le cas hors-ETL montrent un très bon accord entre les abondances de fer neutre et ionisé avec de faibles écarts raie à raie, particulièrement dans le cas des étoiles pauvres en métaux. Finalement cette méthode est validée par une comparaison avec des calculs quantiques très récents et encore non publiés.

Abstract

Determination of high precision abundances has and will always be an important goal of all spectroscopic studies. The use of LTE assumption in spectroscopic analyses has been extensively shown in the literature to badly affect the determined abundances and stellar parameters, especially in metal-poor and giant stars which can be subject to large non-LTE effects. Non-LTE modeling of stellar spectra is therefore essential to accurately reproduce the observations and derive stellar abundances. Non-LTE calculations require the input of a bulk of atomic data, which may be subject to uncertainties. In cool stars, hydrogen collisional rates are a major source of uncertainty, which are often approximated using a classical recipe (the Drawin approximation) for allowed bound-bound, and ionization transitions only. This approximation has been shown to overestimate the collisional rates, and does not reproduce the correct behavior with energies. I demonstrate in this dissertation the inability of the Drawin approximation to describe the hydrogen collisional rates. I introduce a new method to estimate these rates based on fitting the existing quantum rates of several elements. I show that this quantum fitting method (QFM) performs well in non-LTE calculations when detailed quantum rates are not available, and is able to reproduce the results obtained with the quantum rates (the case of Si). I test the newly proposed method, with a complete iron model atom that I developed, on a reference set of stars from the "*Gaia*-ESO survey". Starting from well determined non-spectroscopic atmospheric parameters, I determine 1D, non-LTE, and LTE iron abundances for this set of stars. The non-LTE results show excellent agreement between Fe I and Fe II abundances and small line-by-line dispersions, especially for the metal-poor stars. The method is validated upon comparison with new preliminary Fe I+H quantum calculations, whose fits show an excellent agreement with ours.

“And you run and you run to catch up with the sun but it’s sinking.
Racing around to come up behind you again.
The sun is the same in a relative way, but you’re older.
Shorter of breath and one day closer to death."

— Pink Floyd

Acknowledgements

First and foremost I would like to thank my Ph.D. advisors Bertrand Plez and Marwan Gebran. They helped me realize my dream of becoming a researcher and an Astrophysicist. And for that I am immensely thankful.

Bertrand taught me how to think critically and not to "go with the flow", and not be afraid to take risks and try new ideas. He was supportive and caring. I appreciate all his contributions of time, ideas, and funding and opportunities to make my Ph.D. experience productive. The enthusiasm he has for his research was contagious and motivational for me, even during tough times in the Ph.D. pursuit.

Marwan was the reason I applied for this Ph.D. scholarship and where I stand today. He helped me forever change my life and for that I am greatly indebted. He provided the support and positivity to keep going in the good and tough times all throughout his acquaintance. His immense patience and scientific knowledge and advices were very important to the completion of this work.

One of the most important people contributing to this thesis that I would equally like to thank is Thibault Merle (Brussels). He generously provided me with so much knowledge on non-LTE calculations, the radiative transfer code MULTI, atomic data and models and much much more. Without his help, this thesis would have been much more difficult to accomplish. His respectfulness, kindness and enthusiasm for science made the work all the more interesting. It was a pleasure working and collaborating with you these past three years.

I thank the members of the jury who accepted to asses my work: Frédéric Thévenin, Piercarlo Bonifacio, Frédéric Paletou and Matthias Steffen. Their time and valuable comments are highly appreciated.

In addition to my advisors and collaborators, I am greatly thankful to all the colleagues of LUPM[1] (permanent and non-permanent, administration and technicians). Thank you, first of all, for the directors and co-directors of the lab throughout the past three years: Fabrice Feinstein, Bertrand Plez, Denis Puy, Agnes Lèbre and Georges Vasileiadis for their support and help in solving all encountered administrative problems. A special thank you for the AS[2] team members who have been my surrogate family throughout the last three years when I was away from mine: Fabrice Martins, Ana Palacios, Eric Josselin, Dhabia Tahlbi, Yohann Scribano, Henri Reboul, Nicolas Mauron, Gérard Jasniewicz, Olivier Richard, and Julien Morin (his holy figure for Julianism ☺) for their immense support, kindness, knowledge, guidance and very good sense of humour. I was very happy to be part of your team for the past three years.

A very big thank you goes equally to all the fellow Ph.D. students and postdocs with whome I have spent time at LUPM and outside it throughout these past three years and left a pleasant impact on my life. The great times spent together and your friendship means a lot to me! Thank you for Pierre Ghesquiere, Louis Amard, Anthony Hervé, Lola Faletti, Diane Fernandez, Dimitri Douchin, Morgan Deal, Thibaut Desgardin, Nigel Maxted, Johanna Itam-Pasquet, Marco Padovani, Manal Yassine, Benjamin Tessore (pourquoi t'es malheureux?) and Stephano Magni for all your support.

Thank you for the administration members of the lab and all their help and support: Carole Prevot, Amel Chennouf-Salhi, Sylvianne Colaiocco, Lydie Le-Clainche, Christophe

[1]Laboratoire Univers et Particules de Montpellier
[2]Astrophysique Stellaire

Mercier and all the others. Also I wish to thank the computer technicians for all their help (for the countless number of times my laptop/s decided to stop functioning properly): Nicolas Clementin, Samuel Viscapi, and Claude Zurbach. Thank you for Luisa Arrabito for all her help with the France-Grilles computational grid that allowed me to run the very large number of models.

In addition, I am thankful to all the people/organizations who helped me get financial support that allowed me to continue my Ph.D. and travel to conferences and workshops: François Henn, (vice president délégué aux relation internationales, UM), Ingrid Chanefo (UM), Jean Oppermann (CROUS), Mr. Carlos Gomes (Partenariat Hubert Curien PHC-CEDRE), PNPS (CNRS-France) and Charles Tabet (CNRS-Liban).

I would like to thank Paul Barklem (Uppsala University) for the communication he provided on hydrogen collisions throughout the past three years and for communicating his preliminary data for iron with us, which was indeed vital for this work.

I also thank Roger Hajjar and Bassem Sabra and others who worked so hard to make astronomy and astrophysics in Lebanon a possibility by developing the first astrophysics masters program in the arab region.

Outside the scientific community, many people have played a vital role in providing me with generous support and positivity to keep going. First, I wanna thank my parents, Zainab and Hussein, and my brother Nour for their unconditional love and great sense of humour. Thank you for teaching me to find the full-half part of the cup at all times no matter how hard it gets.

Thank you for my friends: Mona Dib-Awada, Nicolas Milot, Ali Dib-Awada and Marie for the great times spent together and the great support you have provided. I also thank my childhood friend Zahraa, who is the true symbol of strength and kindness. You have managed to lift my spirits and keep me going for countless number of times.

Last but certainly not least, I wanna thank my loving husband Hassan. He provided me with selfless support, endured very difficult three years apart so that I may follow my dreams, yet always managed to stay positive and provide a lot of love, positivity and good sense of humour. I could never have asked for a more special gift than you ♡.

Rana Ezzeddine
16, November 2015

Contents

1 Introduction

The chemistry of the stars holds clues to how the Galaxy was formed and how it evolved through time. The primordial nebulous clouds that formed into the Milky Way consisted merely of the Big Bang elements (Hydrogen, Helium and Lithium), while most other elements were created by the stars (Burbidge et al., 1957). This process involves a chain of fusion of lighter elements, in which several nuclear processes are involved, depending on the mass of the star, which will determine the types of different assortment of elements that will be formed. The answer to when and how these processes take place is largely of the chemical elements that it will contribute to the interstellar medium at the end of its life, which will then create the next generation of stars. By studying the chemical composition of stars in different environments and ages, we can trace this cosmic recycling process.

The total metal content of a star, comprising of all elements except hydrogen and helium, is denoted as its metallicity ([Fe/H]), whose value increase with time. Hence, old stars are more metal poor than younger ones, since the stellar chemical factories from which these stars were born were in their early stages, and there was not enough time to create a great abundance of metals that could be incorporated into the stellar formation from its gaseous nebulae.

The chemical elemental content (abundances) of a star is deciphered from its spectrum, originating from its stellar atmosphere. A significant progress in the field of stellar atmospheres has been achieved in the past few years, making use of rapid advances in multiple areas of astrophysics. Telescopes and detectors became larger, making increasingly precise observations of progressively fainter and more distant objects more feasible, and the analysis of the datasets has surged due to increasing capabilities of computers and networked systems.

With the launch of Gaia spacecraft in December 2013, which will chart our Galaxy and provide a large catalog of the positions and motions of a billion of stars, complementary large-scale studies (*Gaia*-ESO, SDSSIII-APOGEE, RAVE, ...) have started to take place in order to trace the history of stellar populations and the Galaxy. In this context, an important need to characterize in details the chemical composition of these stars, with the highest accuracies possible, has arisen.

Most models of stellar atmospheres adopt the assumption of *Local Thermodynamic Equilibrium* (LTE). Departures from LTE conditions in the atmospheres of cool stars, however, may significantly affect determinations of chemical abundances, in particular the determinations based on spectral lines of minority species. This deviation from LTE grows toward lower metallicities and extended atmospheres, due to decreasing number of electrons donated by metals and decreasing collisional rates. Thus non-LTE modeling of the stellar spectra of these stars becomes important, which in turn requires a good knowledge of a bulk of atomic data for each atom under consideration.

Homogeneous stellar parameters, including effective temperatures, surface gravities and metallicities of the stars are a fundamental cornerstone in any non-LTE study. The iron abundance ([Fe/H]) is a key ingredient, due to its wealth of lines in most stellar spectra, and its common use as a proxy to the total metal content of the star (i.e. its metallicity).

Though stellar parameters determinations are becoming more reliable and less model dependent, lagging far behind in non-LTE modeling of stellar spectra, are the necessary laboratory astrophysics data. A common problem for calculating non-LTE abundances is that they can be subject to errors from uncertainties in the underlying atomic data. Line parameters for the iron atom are a particularly important case. While energy levels, wavelengths, transition probabilities (gf-values) and collisional cross-sections can often be theoretically derived for light, simple atoms, the case is more difficult for atoms as complex as iron.

The influence of inelastic neutral hydrogen collisions on non-LTE spectral line formation remains the most significant source of uncertainty for stellar abundance analysis (Barklem et al., 2011; Osorio et al., 2015). Quantum calculations for hydrogen collisional rates have recently been calculated for a small number of elements including Li (Belyaev and Barklem, 2003), Na (Barklem et al., 2010), Mg (Belyaev et al., 2012), Al (Belyaev, 2013), and Si (Belyaev et al., 2014). For iron and other elements, however, no quantum calculations have been published yet[1]. In the lack of quantum calculations, the tendency is to approximate the hydrogen collisional rates using the classical Drawin (Drawin, 1968, 1969) approximation which is a modified version of Thomson (1912) classical e^- + atom ionization rate equation.

Upon comparison with quantum calculations, the Drawin approximation has been shown to overestimate the collisional rates by several orders of magnitude (Barklem et al., 2011; Lambert, 1993). This is commonly treated by applying a multiplicative scaling fudge factor $\mathbf{S_H}$ to the Drawin rate equation by using different calibration methods on different reference stars. This method however, has been shown to give different scaling factors for different types of stars. This contradicts the fact that collisional cross-sections of an element with an impact species should be model and stellar parameters independent. The failure of the Drawin approximation is clearly seen upon comparison with the quantum calculations for elements like Na, Al, Mg and Si, where the cross-section - transition energy dependence trends are quite different. Thus a multiplicative scaling factor to the Drawin approximation cannot reproduce quantum calculations.

In the light of the inefficiency of the Drawin approximation, a new method to calculate the H-collisional rates is introduced in this dissertation. It is based on fitting the existing quantum data of few elements such as Na, Mg, Al and Si. The aim is to apply this quantum fitting method (QFM) for iron.

[1] See however the very recent, unpublished, results of Paul Barklem (private communication, 2015) presented in Chapter 7

Summary

The following dissertation is organized as follows:

Chapter 2 recaps a brief description of the theory of radiative transfer in stellar atmospheres with a focused concentration on non-Local Thermodynamic Equilibrium.

Chapter 3, reviews a brief history of treatment of inelastic hydrogen collisions with atoms in cool stellar atmospheres, where both the classical and quantum approaches are explained.

Chapter 4 describes a newly developed iron model atom which was used in the calculations.

In Chapter 5, a set of benchmark stars upon which the different methods have been tested are presented with their corresponding atmospheric fundamental parameters which were determined mostly via non-spectroscopic model independent methods.

The Drawin approach to calculating the hydrogen collisional rates, with their results are presented in Chapter 6.

Chapter 7 introduced the quantum fitting method to calculating the hydrogen collisional rates, which was tested on 30 benchmark stars.

2 | Investigating stellar atmospheres

A stellar atmosphere is the transition region from the stellar interior to the interstellar medium. It can be divided into many layers depending on different temperature gradient behaviors (Fig. 2.1). The major part of the visible spectrum originates from the stellar "Photosphere". Higher layers are typically studied at shorter and longer wavelengths.

Everything we know about the stars and systems of stars is derived from the analysis of the radiation emitted by their atmospheres. A great amount of information can be deciphered from the electromagnetic radiation of stars. In order to understand stellar atmospheres, we need to establish the fundamental physics of the energy transport, which is giving rise to the actual thermodynamical stratification in the surface layers of stars. Two intrinsically distinct regimes for the transport of energy can be identified at the boundaries of late-type stars: one convective, where the hydrodynamic equations govern the physics, and another radiative, which is described by the radiative transfer equation.
The main goal of modeling the stellar atmosphere is to calculate an emergent flux of a star for a given temperature, surface gravity and chemical composition. Such models can then be used to compare with observations and ultimately to determine relevant properties of the star. The models allow us to go from observable quantities, e.g. stellar fluxes, spectral energy distributions, and photometric magnitudes, to physical parameters of stars, such as the effective temperature $T_{\rm eff}$, the surface gravity g, the metallicity [Fe/H], abundances, rotation and turbulent velocities [1]...

I will overview in this chapter the basics of the theory of radiative transfer in the first Section 2.1, where I will outline the general approach used in modeling the radiative contribution to the stellar flux. In the second Section 2.2, I will describe the non-Local thermodynamic equilibrium approach to solving the radiative transfer problem. In the third Section 2.3, I will describe briefly the hydrostatic and hydrodynamic approaches to describe the radiative and convective stratification of the stellar atmosphere, in which physical parameters such as temperature, density, micro- and macro- turbulent velocities are expressed as a function of optical or geometric depths.
Unless specified otherwise, what follows is mainly from the work of Rutten (2003), Mihalas (1978) & Gray (2008), in addition to the exhaustive reading and help of the PhD dissertation of Thibault Merle (Merle, 2012).

2.1 Radiative transfer

The dominant mechanism of energy transport throughout the surface layers of a star is radiation, in addition to convection which comes into play in some stars (giants, cool dwarfs and metal-poor stars). Radiation is not only a probe of the physical state of the atmosphere,

[1] Turbulent velocities include macro- and micro- turbulent velocities which correspond to both non-thermal components of the gas velocity which can cause broadening of the stellar spectral lines (explained in Sec. 2.3)

Figure 2.1: Temperature distribution in Kelvin as a function of geometrical height above a zero-point where $\tau_{5000} = 1$ (in kilometers) in the outer layers of the Sun, adapted from Vernazza et al. (1973).

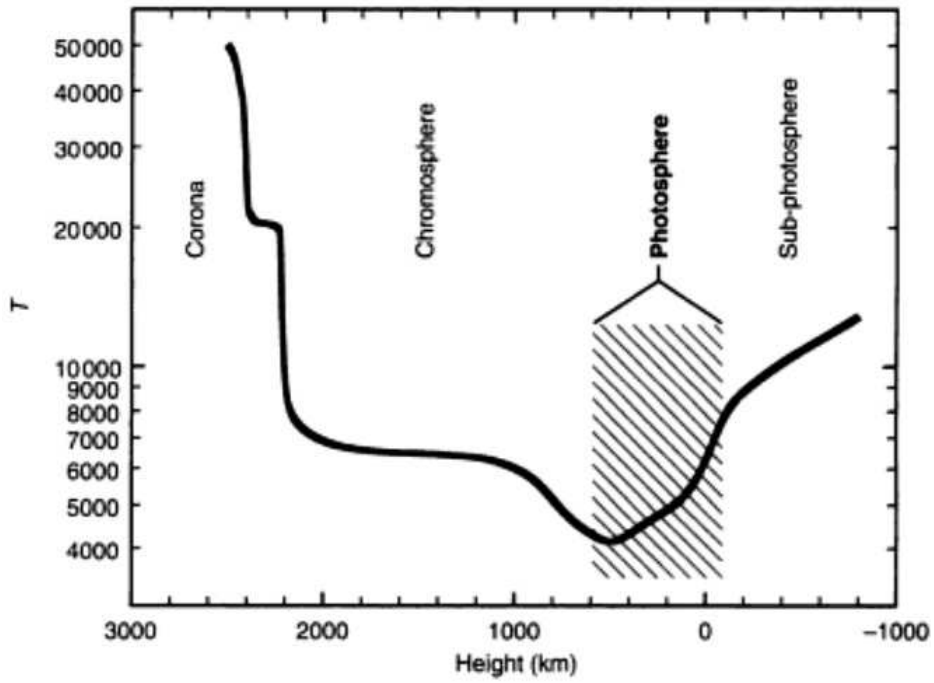

but in fact determines its structure. Thus the knowledge of the processes of interaction between the radiation and the gas in the stellar atmosphere allows us to better understand the physical properties of the medium through which light travels. Hence, we should define some basic physical quantities which help us demonstrate this interaction, leading us to the derivation of the radiative transfer equation which may be viewed as the kinetic equation for photons.

2.1.1 Intensity and Flux

If we consider a radiating surface of area dA of a star (Fig. 2.2), situated at position $\vec{r}$, we can define the specific intensity $I(\vec{r},\vec{k},\nu,t)$ (hereafter denoted I_ν)[2] traveling in direction $\vec{k}$ as the radiative energy transported through this surface per frequency interval dν, per solid angle dΩ, per unit time dt as:

$$I_\nu = \frac{\mathrm{d}E_\nu}{\mathrm{d}A\cos\theta\,\mathrm{d}\Omega\,\mathrm{d}\nu\,\mathrm{d}t} \tag{2.1}$$

where θ is the angle of propagation of the light with the normal $\vec{n}$ to the surface dA.
I_ν represents the energy transported by a bunch of identical photons along a single "ray of light". Thus it is the basic macroscopic quantity to use in formulating radiative transfer.
Equation 2.1 describes the monochromatic intensity emitted from the surface dA at a frequency ν. The intensity emitted in the full spectral range is:

$$I = \int_0^\infty I_\nu\,\mathrm{d}\nu = \int_0^\infty I_\lambda\,\mathrm{d}\lambda \tag{2.2}$$

[2]expressed in units of erg $\cdot$ s^{-1} $\cdot$ cm^{-2} $\cdot$ rad^{-2} $\cdot$ Hz^{-1}

From the specific intensity, other useful quantities can be calculated. The mean intensity J_ν[3] is defined as the directional average of I_ν:

$$J_\nu = \frac{1}{4\pi}\int I_\nu \,\mathrm{d}\Omega = \frac{1}{4\pi}\int_0^{2\pi}\int_0^{\pi} I_\nu \sin\theta \,\mathrm{d}\theta\mathrm{d}\phi \tag{2.3}$$

where $\mathrm{d}\Omega = \sin\theta \;\mathrm{d}\theta \;\mathrm{d}\phi$ in spherical coordinates (See Fig. 2.2). It is interesting to use when only the presence of the radiation is of interest, regardless of its origin, i.e. when calculating the radiative ionization and excitation of atoms in the atmosphere (explained explicitly in Sec. 2.1.4.1).

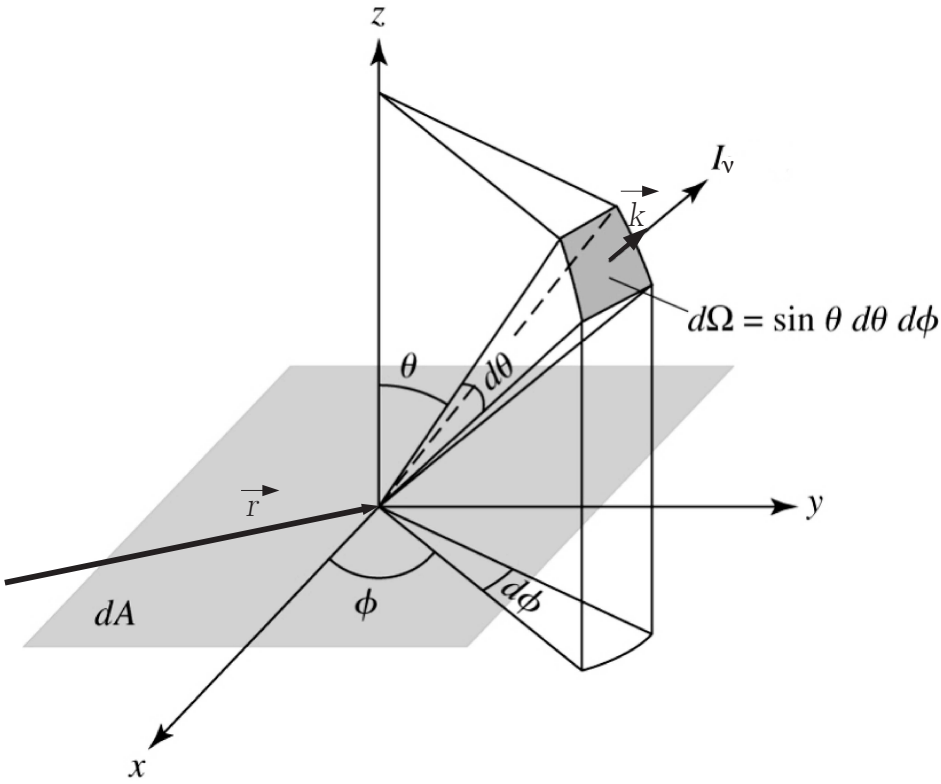

Figure 2.2: A radiation beam of specific intensity I_ν traversing a surface area $\mathrm{d}A$ within a solid angle $\mathrm{d}\Omega$ and with an angle θ to the normal of the surface.

Another quantity of interest is the monochromatic flux F_ν[4], which describes the net flow of energy across the area $\mathrm{d}A$, over a time $\mathrm{d}t$, in a spectral range $\mathrm{d}\nu$, which can be written as:

$$F_\nu = \oint \frac{\mathrm{d}E_\nu}{\mathrm{d}A\mathrm{d}t\mathrm{d}\nu} = \int I_\nu \cos\theta \,\mathrm{d}\Omega = \int_0^{2\pi}\int_0^{\pi} I_\nu \cos\theta \sin\theta \,\mathrm{d}\theta\mathrm{d}\phi \tag{2.4}$$

It is to be noted that while I_ν is independent on the distance from the source, F_ν obeys the standard inverse square law with respect to distance. Specific intensity can only be directly measured if we can resolve the radiating surface (which is usually not the case for stars other than the Sun).

Setting μ=$\cos\theta$, and assuming axial symmetry about the z-axis (i.e. plane-parallel geometry) (Fig. 2.2), the monochromatic flux can be written as:

$$F_\nu = 2\pi \int_{-1}^{1} I_\nu \,\mu \,\mathrm{d}\mu. \tag{2.5}$$

[3]expressed in units of erg $\cdot$ s^{-1} $\cdot$ cm^{-2} $\cdot$ Hz^{-1}
[4]expressed in units of erg $\cdot$ s^{-1} $\cdot$ cm^{-2} $\cdot$ Hz^{-1}

Electromagnetic radiation has a momentum equal to its energy divided by the velocity of light c. The component of momentum, normal to the surface dA, thus transferred by the beam of light, per unit time, per unit frequency is called the radiation pressure [5], which can be written as:

$$p_\nu = \frac{1}{c} \int I_\nu \cos^2\theta \, \mathrm{d}\Omega \tag{2.6}$$

2.1.2 Absorption and emission coefficients

The radiative transfer equation describes the change in the radiation field due to its interaction with matter in the atmosphere. To illustrate this interaction, phenomenological quantities which define the absorption and emission in the layers of the stellar atmosphere must be introduced.

The radiation can be absorbed by an amount dI_ν due to the interaction with charged particles, atoms, ions, molecules or dust particles present in the atmosphere, and can be expressed as:

$$\mathrm{dI}_\nu = -\kappa_\nu \rho I_\nu \mathrm{d}x \tag{2.7}$$

where κ_ν is the monochromatic absorption coefficient[6] per unit mass, referred to as *opacity*, ρ is the density of the gas and dx the geometrical path length along the beam.

In addition photons can be emitted into the direction being considered. This can be expressed as:

$$\mathrm{d}I_\nu = j_\nu \rho \mathrm{d}x \tag{2.8}$$

where j_ν is the monochromatic emission coefficient[7].
The ratio of the emission to the absorption is called the source function S_ν[8]:

$$S_\nu = \frac{j_\nu}{\kappa_\nu} \tag{2.9}$$

2.1.3 Transport equation

Using the above definitions, we can write the radiation transfer equation representing the absorption, emission and scattering along a geometrical path dx in the propagation direction as:

$$\frac{\mathrm{d}I_\nu}{\mathrm{d}x} = j_\nu \rho - \kappa_\nu \rho I_\nu \tag{2.10}$$

Eqn. 2.10 can also be written as:

$$\frac{\mathrm{d}I_\nu}{\kappa_\nu \rho \mathrm{d}x} = S_\nu - I_\nu \tag{2.11}$$

Hence it is appropriate to define the monochromatic *optical thickness* τ_ν (unitless) as a measure of the "optical transparency" of the medium, as:

$$\mathrm{d}\tau_\nu = \kappa_\nu \rho \mathrm{d}x \tag{2.12}$$

[5] expressed in units of dyne $\cdot$ cm^2 $\cdot$ Hz^{-1}
[6] expressed in cm^2 $\cdot$ g^{-1}
[7] expressed in erg $\cdot$ s^{-1} $\cdot$ rad^2 $\cdot$ Hz^{-1} $\cdot$ g^{-1}
[8] expressed in same units as I_ν, and is proportional to the number of photons emitted per unit optical depth interval.

and the monochromatic optical thickness of a medium of total path length (thickness) L as:

$$\tau_\nu(L) = \int_0^L \kappa_\nu \rho \, \mathrm{d}x \tag{2.13}$$

And so the radiative transfer (RT) equation can finally be written in terms of the optical thickness of the medium as:

$$\frac{\mathrm{d}I_\nu}{\mathrm{d}\tau_\nu} = S_\nu - I_\nu \tag{2.14}$$

The concept of optical depth (thickness):
In reality, the definition of the "border" of a star is not trivial at all, and so there is no definitive way to determine the actual extent of the stellar atmosphere. Going from the center of the star outwards, the density of the gas decreases and eventually reaches values as low as the surrounding interstellar medium. At some point in the stellar atmosphere, the density becomes low enough that photons can escape and be observed by our instruments. Therefore, using the term "radial optical depth" is then a reasonable approach to defining different regions in the stellar atmosphere, which can be defined at a given geometrical position z_0 as:

$$\tau_\nu(z_0) = \int_{z_0}^{\infty} \kappa_\nu \rho \mathrm{d}z \tag{2.15}$$

which measures the optical depth along the radial line of sight with $\mu = 1$ at z_0, from $\tau_\nu = 0$ which is the optical depth at the observer's eye located at $z = \infty$. This can be helpful to allow us to answer the question: From which atmospheric depth does the radiation come from?
In order to answer that, we first have to define a solution to the (RT) equation to better understand the propagation of radiation throughout the stellar atmosphere.

2.1.4 Solution of the radiative transfer equation

In order to simplify the solution to the (RT) equation, we assume that the radiation is monochromatic, and that our atmosphere is static (time-independent) and plane parallel which is a valid assumption as long as the atmospheric thickness is much smaller than the stellar radius $R_\star$[9]. The geometric distance traveled by the beam between two consecutive parallel shells $\mathrm{d}z$ apart in the atmosphere, is then:

$$\mathrm{d}x = \frac{\mathrm{d}z}{\cos\theta} \tag{2.16}$$

Hence the (RT) equation can then be written in the standard form in terms of the optical depth as:

$$\mu \frac{\mathrm{d}I_\nu}{\mathrm{d}\tau_\nu} = I_\nu - S_\nu \tag{2.17}$$

The solution to Eqn. 2.17 can be expressed by:

$$\begin{aligned} I_\nu^-(\tau_\nu, \mu) &= -\int_0^{\tau_\nu} S_\nu(\tau'_\nu)\, e^{-(\tau'_\nu - \tau_\nu)/\mu}\, \mathrm{d}\tau'_\nu/\mu \qquad (\mu < 0) \\ I_\nu^+(\tau_\nu, \mu) &= +\int_{\tau_\nu}^{\infty} S_\nu(\tau'_\nu)\, e^{-(\tau'_\nu - \tau_\nu)/\mu}\, \mathrm{d}\tau'_\nu/\mu \qquad (\mu > 0) \end{aligned} \tag{2.18}$$

[9] i.e. the physical variables such as temperature, density, etc., depend on the vertical geometric or optical depth only. A good approximation for stars with photospheres relatively thin with respect to the stellar diameter. For giant stars, however, the assumption of spherical atmospheres is more appropriate, due to their extended atmospheres.

which represent the sums of source functions S_ν originating at points τ'_ν, and exposed to absorption through the optical thickness (τ_ν-τ'_ν) by a factor $e^{-(\tau_\nu - \tau'_\nu)}$, for the cases of inward ($\mu < 0$) and outward ($\mu > 0$) directed intensities respectively.

2.1.4.1 Special case

- **Local Thermodynamic Equilibrium (LTE) approximation:** It is the approximation widely and most often used in the description of emitted radiation field from stellar atmospheres and in the interpretation of stellar spectra, as it vastly simplifies the calculations as will be demonstrated below. The basic criteria for the LTE approximation to hold, is to have a finite volume in the stellar atmosphere with a uniform temperature T, in which the gas material is assumed to be in equilibrium with the radiation field. Hence, the majority of the interaction between photons and gas particles can be viewed as occurring between particles in *thermodynamic equilibrium*. This state allows the properties of the gas to be determined by the *local* temperature T of this volume alone and is known as **Local Thermodynamic Equilibrium** (LTE).

  – **Radiation in LTE:**
  Under the LTE approximation, it is required that as much energy be emitted as is absorbed and this can be expressed by Kirchhoff-Planck's law as:

  $$\mathrm{j}_\nu = \kappa_\nu B_\nu(T) \tag{2.19}$$

  where $B_\nu(T)$ is the Planck function which describes the photon distribution as a function of temperature only.
  From Eqn. 2.19 and under the LTE assumption, the source function of radiation is then equal to the Planck function:

  $$[S_\nu]_{\mathrm{LTE}} = B_\nu(T) = \frac{2h\nu^3}{c^2}\frac{1}{e^{h\nu/k_\mathrm{B}T} - 1} \tag{2.20}$$

  where h is the Planck constant and k_B is the Boltzmann constant.

  – **Matter in LTE:**

    * **Maxwell velocity distribution:**
    Which describes the velocity distribution of gas particle species of mass m:

    $$f(v)\mathrm{d}v = \left[\frac{\mathrm{N}(v)}{\mathrm{N}_{\mathrm{total}}}\mathrm{d}v\right]_{\mathrm{LTE}} = \left(\frac{m}{2\pi k_\mathrm{B}T}\right)^{3/2} 4\pi v^2\, e^{-(1/2)mv^2/k_\mathrm{B}T}\mathrm{d}v \tag{2.21}$$

    where $\mathrm{N}(v)$ is the number of gas particles, per unit volume, of velocity v. $\mathrm{N}_{\mathrm{total}}$ is the total particles density per unit volume. The left-hand-side of the equation is evaluated under LTE conditions, where the kinetic local electron temperature T_e is estimated as equal to all other material temperatures (T=T_e). The most probable velocity of the particles can be evaluated at $v_\mathrm{p} = \sqrt{2k_\mathrm{B}T/m}$.

* **Energy level populations: The Boltzmann distribution**
The fraction of atoms excited to the ith level is:

$$\mathrm{N}_i = g_i \frac{e^{-\chi_i/k_\mathrm{B}T}}{u(T)} \tag{2.22}$$

where g_i=2J+1 is the statistical weight of the level i, in which J is the total quantum angular momentum, χ_i is the energy [10] of level i and

$$u(T) = \sum g_i e^{-\chi_i/k_\mathrm{B}T} \tag{2.23}$$

is the partition function of the level i.

Hence the Boltzmann distribution gives the ratio of populations between two levels j and i:

$$\frac{\mathrm{N}_i}{\mathrm{N}_j} = \frac{g_i}{g_j} e^{-\Delta\chi/k_\mathrm{B}T} \tag{2.24}$$

where $\Delta\chi$ = χ_i-χ_j

* **Ionization fraction distribution: The Saha Equation**
For collisionally dominated gas, the ionized to neutral species ratio N_1/N_0 is described by the Saha equation as:

$$\left[\frac{N_1}{N_0}P_e\right]_\mathrm{LTE} = \frac{(2\pi m_\mathrm{e})^{3/2}(k_\mathrm{B}T)^{5/2}}{h^3}\frac{2u_1(T)}{u_0(T)}e^{-\chi_0^\infty/k_\mathrm{B}T} \tag{2.25}$$

where P_e is the electron gas pressure, m_e is the electron mass, χ_0^∞ is the ionization energy of the ground neutral state.

* **Saha-Boltzmann distribution:** The combination of the two distribution equations above (Boltzmann and Saha) allows to calculate the ratio of the population n_i of a level i in a neutral atom to the number n_c of ions in an ionized state c:

$$\left[\frac{n_c}{n_i}\right]_\mathrm{LTE} = \frac{1}{N_\mathrm{e}}\frac{2g_c}{g_i}\left(\frac{2\pi m_\mathrm{e}k_\mathrm{B}T}{h^2}\right)^{3/2} e^{-\chi_{ci}/k_\mathrm{B}T} \tag{2.26}$$

where N_e is the electron density and χ_{ci} is the ionization energy from level i to c.

2.1.4.2 Breakdown of LTE:

The assumption of LTE is valid in the interior of the stellar atmosphere where the gas particle density is large enough to induce thermodynamic equilibrium, however in the upper reaches of the atmosphere, the density decreases to such a point that collisions between gas particles will be insufficient for the establishment of LTE. Also, as we move outwards, the photon mean free path becomes large, i.e. larger than the scale height of material, and thus the decoupling between radiation and matter increases, radiation becomes non-local, anisotropic, and strongly non-Planckian.
The radiative excitation and ionization rates dominate over collisional ones, and thus the assumption of LTE fails.

[10] Also denoted excitation potential (measured in eV).

In order to quantify the deviation of the populations from those calculated under the LTE assumption using the Saha-Boltzmann distributions, it is convenient to introduce the departure coefficient $b_i \equiv n_i/n_i^{\rm LTE}$ where n_i is the actual population density of energy level i and $n_i^{\rm LTE}$ is the corresponding population density under LTE.

Therefore, when LTE conditions break down, it is necessary to solve for level populations and line strengths using non-Local Thermodynamic Equilibrium approach (hereafter non-LTE) where all possible radiative and collisional transitions are treated in the line formation analysis.

2.2 Non-Local Thermodynamic equilibrium:

The non-LTE level population densities are calculated under the assumption of statistical equilibrium (SE) where the sum of all transition rates to and out of an atomic energy level must be equal to zero. This assumption is valid when considering a time-independent atmosphere, where the radiation field and level populations do not vary with time. The term "*population equations*" introduced earlier under the LTE assumption are more conveniently replaced by the term "*rate equations*". The statistical equilibrium rate equation for a level i can then be written as:

$$\frac{{\rm d}n_i}{{\rm d}t} = \sum_{j\neq i}^{N} n_j P_{ji} - n_i \sum_{j\neq i}^{N} P_{ij} = 0 \tag{2.27}$$

where n_i is the population of a particular level i, P_{ij} is the transition probability of a transition from level i to j, and N is the total number of levels which can be coupled through transitions to level i. The transition rates P_{ij} and P_{ji} are the sum of radiative R_{ij} and collisional C_{ij} processes rates per particle that contribute to the transitions from and to level i respectively:

$$P_{ij} = R_{ij} + C_{ij} \tag{2.28}$$

The following important continuous and line absorption and emission processes that may contribute to these rates will be considered in our calculations:

- **Radiative processes:**
  - **bound-bound radiative processes**, which are due to electron excitation and de-excitation transitions by photon emission or absorption.
  - **bound-free radiative processes**, i.e. photoionization where an atom or ion loses an electron due to a photon absorption, and its counterpart photorecombination.
  - **free-free radiative processes**[11], which are due to accelerating electrons passing close to ions, thus emitting radiation.
- **Collisional processes**
  - **bound-bound collisional processes** which correspond to electron excitation and de-excitation in atoms and ions due to collisions with e^-, atoms or ions.

[11] Also denoted as Bremsstrahlung, important at high temperatures where the plasma is highly ionized.

– **bound-free collisional processes** which correspond to the ionization of an atom or ion, or its recombination with an electron, due to collisions with e^-, atoms or ions.

Figure 2.3: A schematic energy diagram for possible atomic transition processes.

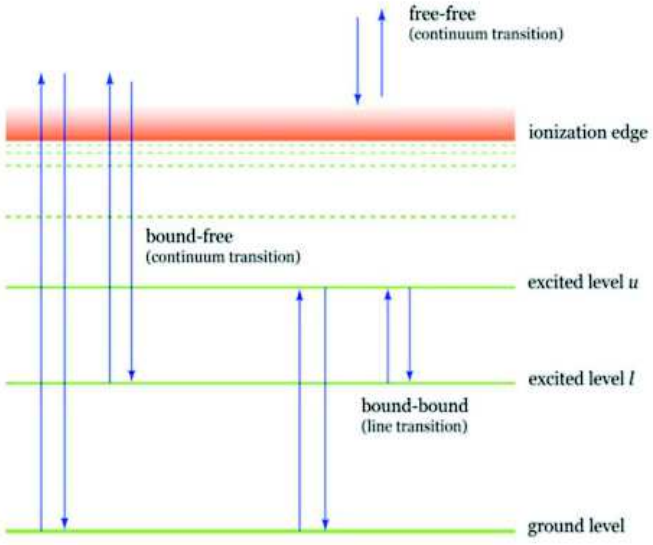

To correctly reproduce the emergent stellar spectrum from a star, the radiative and collisional rates from all the processes that have the ability to populate and depopulate the energy levels of the atoms and ions present in the stellar atmosphere have to be included in the calculation of the level populations.

2.2.1 Radiative rates:

The ***bound-bound*** radiative rates can be due to ***radiative excitation*** (absorption), ***spontaneous radiative de-excitation*** and ***stimulated radiative de-excitation*** (emission).

- The rate of ***spontaneous radiative de-excitations*** per atom from an upper level j to a level i per atom is A_{ji}, where A_{ji} is the Einstein coefficient for spontaneous emission and is defined as the probability per second per atom that an electron in level j will spontaneously decay to level i.
- The probability to have a ***radiative excitation*** transition from level i to level j per atom per second in a radiation field of mean intensity $\bar{J}_\nu$ is equal to $4\pi\bar{J}_\nu B_{ij}$, where B_{ij} is the Einstein coefficient for excitation, and $\nu = E_{ji}/h$ where $E_{ji} = E_j - E_i$ is the energy difference between levels i and j. Here $\bar{J}_\nu = \int_0^\infty J_\nu \phi(\nu) \mathrm{d}\nu$, where $\phi(\nu)$ is the line profile function which represents the probability that a photon is absorbed at frequency ν within the line, and which is normalized[12] to 1 (See Appendix A for details on the line profile function).
- Similarly, the probability of a ***stimulated radiative de-excitation*** from a level j to a level i is $4\pi\bar{J}_\nu B_{ji}$.

[12] $\int_0^\infty \phi(\nu)\,\mathrm{d}\nu = 1$

The Einstein coefficients are coupled by the Einstein relations:

$$\frac{B_{ij}}{B_{ji}} = \frac{g_j}{g_i} \qquad \frac{A_{ji}}{B_{ji}} = \frac{2h\nu^3}{c^2} \tag{2.29}$$

The Einstein coefficients are calculated using quantum mechanics by solving for the wave function of the lower and upper levels $|\psi_i\rangle$ and $|\psi_j\rangle$ respectively. In spectroscopic analysis, it is customary to introduce the dimensionless oscillator strength f_{ij} to describe the probability of a given radiative absorption transition which is related to the absorption Einstein coefficient by:

$$\frac{h\nu}{4\pi} B_{ij} = \frac{\pi e^2}{m_e c} f_{ij} \tag{2.30}$$

The oscillator strength of a given transition line is usually combined with the lower level statistical weight value g_i to give a "gf-value", a product which is commonly used to define the effective transition probability which is needed to calculate the line extinction and emission coefficients.

To express the radiative rates of radiative transitions in terms of Einstein coefficients, we first have to express the source function S_ν in terms of these latter. Assuming complete redistribution, the number of spontaneous emissions per unit time, volume and frequency is $n_j A_{ji} \phi(\nu)$. Since each emission coefficient contributes an energy equal to $h\nu$ over a solid angle 4π, the line emission coefficient is:

$$j_\nu^l = (h\nu/4\pi) n_j A_{ji} \phi(\nu) \tag{2.31}$$

Similarly, the line extinction coefficient per unit path length $\alpha_\nu = \kappa_\nu \rho$ can be expressed as:

$$\begin{aligned} \alpha_\nu^l &= \frac{h\nu}{4\pi}\left[n_i B_{ij}\phi(\nu) - n_j B_{ji}\phi(\nu)\right] \\ &= \frac{h\nu}{4\pi} n_i B_{ij}\phi(\nu)\left[1 - \frac{n_j g_i}{n_i g_j}\right] \end{aligned} \tag{2.32}$$

Hence the line source function S_ν^l can be written using the Einstein relations (Eqn. 2.29) as:

$$\begin{aligned} S_\nu^l &= \frac{j_\nu^l}{\alpha_\nu^l} \\ &= \frac{n_j A_{ji}}{n_i B_{ij} - n_j B_{ji}} \\ &= \frac{2h\nu^3}{c^2} \frac{1}{\frac{g_j n_i}{g_i n_j} - 1} \end{aligned} \tag{2.33}$$

The radiative rates for radiative transitions can then be written as:

- **Bound-bound radiative excitation rate per unit volume:**

$$\begin{aligned} n_i R_{ij} &= n_i B_{ij} \bar{J}_\nu \\ &= n_i \int_0^\infty B_{ij} J_\nu \phi(\nu)\, \mathrm{d}\nu \\ &= 4\pi n_i \int_0^\infty \frac{\sigma_\nu^l}{h\nu} J_\nu \, \mathrm{d}\nu \end{aligned} \tag{2.34}$$

  where $\sigma_\nu^l = \frac{h\nu}{4\pi} B_{ij}\phi(\nu)$ is introduced as the line extinction coefficient per particle.

- **Bound-bound radiative de-excitation rate per unit volume:**

$$\begin{aligned} n_j R_{ji} &= n_j A_{ji} + n_j B_{ji} \bar{J}_\nu \\ &= n_j \int_0^\infty A_{ji} \phi(\nu)\, \mathrm{d}\nu + n_j \int_0^\infty B_{ji} J_\nu \phi(\nu)\, \mathrm{d}\nu \\ &= n_j \frac{g_i}{g_j} \int_0^\infty B_{ij} \phi(\nu) \left(\frac{2h\nu^3}{c^2} + J_\nu \right) \mathrm{d}\nu \\ &= 4\pi n_j \frac{g_i}{g_j} \int_0^\infty \frac{\sigma_\nu^l}{h\nu} \left(\frac{2h\nu^3}{c^2} + J_\nu \right) \mathrm{d}\nu \end{aligned} \tag{2.35}$$

- **Bound-free photoionization rate per unit volume:**
  Similarly the photoionization rate of an electron in an energy level i to a continuum level c can be expressed in terms of the mean radiation field J_ν and the bound-free frequency dependent extinction coefficient per particle (photoionization cross-section) $\sigma_{ic}(\nu)$ as:

$$n_i R_{ic} = 4\pi n_i \int_{\nu_0}^\infty \frac{\sigma_{ic}(\nu)}{h\nu} J_\nu \, \mathrm{d}\nu \tag{2.36}$$

  where ν_0 is the threshold frequency corresponding to the ionization energy of level i equal to $h\nu_0$. As the photoionization cross-sections become more difficult to calculate for complicated atomic systems (atoms and ions with a large number of electrons, Fe-like atoms), a semi-classical approximation, Kramer's law (Travis and Matsushima, 1968), can be used to calculate the photoionization cross-section for Hydrogen like atoms:

$$\sigma_\nu^{ic} = \sigma_{\nu 0}^{ic} \left(\frac{\nu}{\nu_0} \right)^{-3} \tag{2.37}$$

  where ν_0 and $\sigma_{\nu 0}^{ic}$ are respectively the threshold frequency and cross-section (in cm^{-2}) and where:

$$\sigma_{\nu 0}^{ic} = 7.91 \times 10^{-22} \frac{n}{Z^2} g_{\mathrm{rad}}^{ic} \tag{2.38}$$

  where Z is the atomic number of the element in consideration, n is the principal quantum number of the level i from which the level is ionized. g_{rad}^{ic} is called the Gaunt factor and is a correction factor of the order unity. For complex atoms, the cross-sections are shown from laboratory calculations not to a have a simple ν^{-3} dependence but instead possess "resonance" peaks caused by other electrons in the same shell.

- **Bound-free radiative recombination rate per cm^3:**
  Under thermal equilibrium each process is balanced by its reverse counterpart (detailed balance):

$$[n_c R_{ci}]_{\mathrm{TE}} = [n_i R_{ic}]_{\mathrm{TE}} \tag{2.39}$$

  The recombination rate can then be deduced from the photoionization rate assuming the velocity distribution of free electrons to be Maxwellian (Eqn. 2.21). The (single) continuum level can then be considered to be in thermal equilibrium (TE), i.e. n_c can be calculated under the assumption of LTE. Using the Boltzmann distribution equation (Eqn. 2.24), the radiative recombination rate can be written as:

$$n_c R_{ci} = 4\pi n_c \left[\frac{n_i}{n_c} \right]_{[\mathrm{LTE}]} \int_{\nu_0}^\infty \frac{\sigma_{ic}(\nu)}{h\nu} \left(\frac{2h\nu^3}{c^2} + J_\nu \right) e^{-h\nu/k_{\mathrm{B}}T} \, \mathrm{d}\nu \tag{2.40}$$

note:
The rates P_{ij} and P_{ji} in Eqn. 2.27 depend on $\bar{J}_\nu$ which in turn depends on I_ν in all directions, whereas the source function S_ν depends on the populations n_i and n_j of the lower and upper levels involved in the transition at frequency ν. These populations may depend on other transitions and therefore on other populations as well, which are in turn dependent on the radiation fields at other frequencies. Thus a given transition may be influenced by many other transitions in other atoms and molecules which possess transitions at overlapping frequencies. This coupling between populations and radiation is thus non-linear and non-local!

2.2.2 Collisional rates:

The collision of a free particle p of mass m_p and velocity v_p with kinetic energy $E_p^k = 1/2 m_p v_p^2$ greater than the excitation energy of an electron between two bound levels i and j may excite the atom or ion. Considering a Maxwellian velocity distribution for the free colliding particles, the collisional excitation rate per unit volume can be expressed by:

$$n_i C_{ij} = n_i N_p \int_{v_0}^{\infty} \sigma_{ij}^p(v_p) v_p f(v_p)\, \mathrm{d}v_p = n_i N_p \langle \sigma_{ij}^p v_p \rangle \tag{2.41}$$

where C_{ij} is the collisional excitation rate, which is equal to the number of collisional excitations from level i to level j per second, N_p is the free colliding particle density, $\sigma_{ij}^p(v)$ is the particle collisional cross-section, which is a property of the particles, $f(v)$ is the normalized Maxwell velocity distribution, and v_0 is the threshold velocity of the particle equal to $\sqrt{2E_{ij}/m_p}$
The Einstein coefficients for excitation and de-excitation are related by the Einstein relation:

$$\frac{C_{ji}}{C_{ij}} = \frac{g_i}{g_j} e^{E_{ji/k_\mathrm{B}T}} \tag{2.42}$$

which holds in the case of "detailed balance"[13]. This is true since the particles velocity distribution in the stellar atmospheres is considered Maxwellian (Eqn. 2.21).
In the solar atmosphere, Plaskett (1955) considered that the two main candidates to consider in collisional rates are inelastic[14] collisions with electrons and neutral hydrogen atoms in their ground state. The importance of electron collisions arises from the fact that electrons are the most abundant charged particles in the stellar atmosphere and have a much higher thermal velocity than atoms. In terms of atoms, neutral hydrogen is the most abundant perturbers in cool stars as it outnumbers helium by a 10:1 ratio. In hot stars, the H atoms will be almost completely ionized and thus electrons will be the dominant perturbers. Very cool dwarf atmospheres, on the other hand, are mostly rich with H_2 molecules (Lambert, 1993). In this thesis, we are mostly interested by cool stars, and thus we will only consider inelastic collisions with electrons and neutral hydrogen in our calculations.

Electron e^- impact collisional rates:

In calculating the electron impact excitation or ionization collisional cross section, Hebb and Menzel (1940) conveniently introduced the dimensionless *collision strength*[15] Ω_{ij}, which under

[13] Each transition from level i to level j is balanced by its opposite from j to i.
[14] Inelastic collisions are those with transfer of energy to the target atom/ion and are more important to spectral line formation than elastic collisions (Pradhan and Nahar, 2011).
[15] Given its name by M.J. Seaton (1953)

the assumption of detailed balancing is symmetric with respect to the initial and final states ($\Omega_{ij} = \Omega_{ji}$) and is related to the collisional cross-section as follows:

$$\sigma_{ij}^{e} = \frac{\pi a_0^2}{E_e g_i} \Omega_{ij} \tag{2.43}$$

Where a_0 is the Bohr radius and E_e is the electron impact energy in Rydberg (Ry). Being inversely proportional to the electron energy (E_e), Ω_{ij} varies slowly with energy making it easier to compare values for different transitions within an atom/ion, or between different atoms/ions.

Seaton (1953) defined the Maxwellian averaged collision strength (or effective collision strength) $\Upsilon_{ij}^{e}(T)$ as a function of the local temperature of the electrons T_e, which does not vary as strongly with resonances[16] as Ω_{ij} (Fig. 2.4):

$$\Upsilon_{ij}^{e} = \int_0^{\infty} \Omega_{ij}(E) e^{-E/k_{\rm B}T} \, \mathrm{d}\left(\frac{E}{k_{\rm B}T}\right) \tag{2.44}$$

where $E \equiv E_e$. The electron excitation/ionization rate per unit volume can finally be expressed as:

$$\begin{aligned} n_i C_{ij} &= n_i N_e \pi a_0^2 \left(\frac{8(\chi_{\rm H}^{\infty})^2}{\pi m_e k_{\rm B}}\right)^{1/2} \frac{1}{g_i T^{1/2}} \Upsilon_{ij}^{e} e^{-E_{ji}/k_{\rm B}T} \\ &= n_i N_e \frac{8.63 \times 10^{-6}}{g_i T^{1/2}} \Upsilon_{ij}^{e} e^{-E_{ji}/k_{\rm B}T} \end{aligned} \tag{2.45}$$

On the other hand, the collision of an atom with an electron of any energy may cause the de-excitation or re-combination of the atomic electron from a higher to a lower energy level. Using the Einstein relation for collisions, $n_i C_{ij} = n_j C_{ji}$, the de-excitation collision rate by electrons can be expressed as:

$$n_j C_{ji} = n_j N_e \frac{8.63 \times 10^{-6}}{g_j T^{1/2}} \Upsilon_{ji}^{e} \tag{2.46}$$

[16]Resonances result from incident electrons with insufficient energy to re-escape the atom's potential well, that become 'bound' in a doubly excited resonant state.

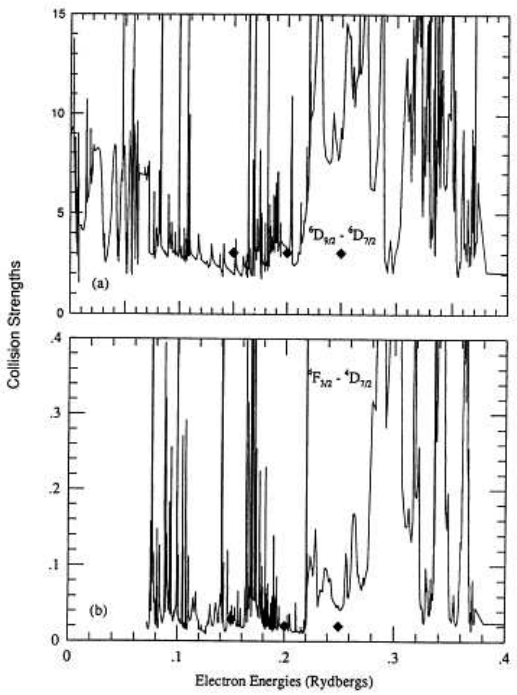

Figure 2.4: Collision strength for FeII bound-bound transition $^6D_{9/2}$ - $^6D_{7/2}$ (upper panel) and $^4F_{3/2}$ - $^4D_{7/2}$ (lower panel) at T=10000 K showing strong resonance peaks (Pradhan and Zhang, 1993).

The inverse process of electron impact ionization is the three-body recombination (2 electrons and ion). It has a low rate, except at high plasma densities, as it scales as n_e^2 (Pradhan and Nahar, 2011).
Theoretically, the study of bound-free impact collisions is more complicated than the bound-bound impact, since the two outgoing final electrons must be accounted for in the presence of the residual atom/ion, which makes calculations much more difficult. Fortunately, experimental measurements of the total ionization impact cross-sections are easier to carry out than the excitation/de-excitations ones, since the latter requires information on both the initial and final states.

In the past few decades, considerable progress has been made in theoretical calculations of the collision cross-sections and effective collision strengths for electron impact transitions (the IRON project collaboration [17], Hummer et al. (1993)). However large-scale calculations involving many atomic states are complex and require extensive computing resources and effort. Quantum mechanically, the basic problem is to describe the electron-atom-photon system with (i) a wave-function expansion and (ii) a Hamiltonian that includes the dominant interactions. The wave-function expansion is a quantum superposition of the possible pathways or channels for a given process or reaction. Practical calculations aim at limited, though sufficient, completeness and convergence using different methods developed from atomic collision theory that have been employed in a number of computer codes used to generate vast quantities of atomic data. The most commonly used approximation to calculate impact cross-sections is the ***close coupling*** (CC) approximation in which the ***R-matrix*** method is implemented.

The CC approximation (Percival and Seaton, 1957) has been a standard method for treating low-energy electron-atom interactions. It is based upon the expansion of the total wave function of the system in terms of products of eigenstates of the atomic Hamiltonian and to-be-determined functions describing the motion of the projectile. These are determined from

[17] http://www.usm.uni-muenchen.de/people/ip/iron-project.html

the solution of coupled integro-differential equations. The detailed description of the quantum theory of collision is beyond the scope of this thesis, however, when available for our relevant iron energy levels, they have been included in our model atom (see Chapter 4).
In non-LTE, it is of paramount importance to have collisional data for all transitions. In the absence of quantum calculations, especially for multi-electronic systems, they are replaced by classical and semi-classical approximation recipes.

For electron collisional excitation/de-excitation and ionization, the most commonly used semi-classical estimates are those by van Regemorter (1962) and the impact approximation of Seaton (1962a,b) which are explained below.

Classical approach for excitation/de-excitation transitions: van Regemorter(1962)

van Regemorter (1962) expressed the electron impact excitation cross sections for allowed transitions in terms of the electric-dipole radiative oscillator strength f_{ij} of the corresponding radiative transition, and the effective Gaunt factor $\bar{g}(E_i)$ as a function of the lower level energy. His formula became widely used in the modeling of high temperature plasmas. For an electron impact excitation from level i to an upper level j, he expressed the corresponding collision cross section (in cm^2) as:

$$\sigma_{ij}^{e} = \frac{8\pi}{\sqrt{3}} \frac{1}{E_e} \frac{f_{ij}}{E_{ij}} \bar{g}(E_i) \pi a_0^2 \tag{2.47}$$

where E_e and E_{ij} are expressed in Ry. Using Eqn. 2.43, the van Regemorter collision strength can be expressed as:

$$\Omega_{ij} = \frac{8\pi}{\sqrt{3}} \frac{g_i f_{ij}}{E_{ij}} \bar{g}(E_i) \tag{2.48}$$

Eqn. 2.47 can be applied only to allowed transitions[18] for which a radiative oscillator strength value exists. In addition, van Regemorter assumed that $\bar{g}$ can be expressed as a function of the impact electron energy in threshold units (E_e) as $\varepsilon = E_i/E_{ij}$. For very high energies for which $\varepsilon >> 1$, $\bar{g}$ is given by:

$$\bar{g} = \frac{\sqrt{3}}{2\pi} \ln\varepsilon \tag{2.49}$$

For low energies, however, van Regemorter chose $\bar{g}$ such that Eqn. 2.47 gave good agreement with available theoretical and experimental results for H, He and Na. For the region $\varepsilon \leq 3$, which is usually the most important energy region in stellar plasmas, he simply used the value $\bar{g} = 0.2$ for positive ions.
Zhang et al. (1991) tested the accuracy of the van Regemorter formula on heavier elements (Ni-like elements), and found out that it is frequently a poor approximation for $\Delta n \geq 1$ transitions, where Δn is the difference in principal quantum number corresponding to levels i and j. They found it to be a better approximation for the $\Delta n = 0$ transitions if a larger $\bar{g}$ was used than the initially recommended one.

Since the publication of van Regemorter, some attempts have been made to infer reasonably accurate Gaunt factors for various classes of transitions (e.g. Crandall (1983); Sobelman et al. (1981)). Fisher et al. (1996) tried fitting the experimental data for 11 different atoms (H,He,Li,O,N,Na,Mg,K,Rb,Cs,Ba) from different reference sources to derive a relation between

[18] transitions which are observed in the laboratory and which obey the quantum selection rules, unlike the forbidden transitions which violate it and whose probabilities of occurance are much smaller than allowed ones (Garstang, 1961)

the effective Gaunt factor and the electron/atom relative energy $x = E_e/E_{ij}$. The fits for all the atoms were shown to be Δn dependent:

$$g(x) = \begin{cases} 0.33 - 0.3x^{-1} + 0.08x^{-2} & \Delta n = 0 \\ (0.276 - 0.18x^{-1})\ln x & \Delta n \geq 0 \end{cases} \tag{2.50}$$

which was found to fit the experimental data with 82% accuracy.

Impact parameter method approach for excitation/de-excitation transitions: Seaton(1962a)

A better alternative to van Regemorter's semi-empirical approximation which does not well reproduce the quantum cross-sections for most cases, is Seaton's semi-classical impact parameter approximation for allowed transitions. It starts from the quantum Born approximation (Born, 1926) for excitation of an atomic electron from level i to level j by an impact electron (described by plane-waves, of weak coupling and with no electron exchange with the target atom) of characteristic impact parameter R_i (Fig. 2.5). The collisional transition cross-section σ_{ij} can be described by:

$$\sigma_{ij}^{e} = \int_0^\infty P_{ij}(R_i)\, 2\pi R_i \mathrm{d}R_i \tag{2.51}$$

where $P_{ij}(R_i)$ is the probability of the transition at an impact parameter R_i.

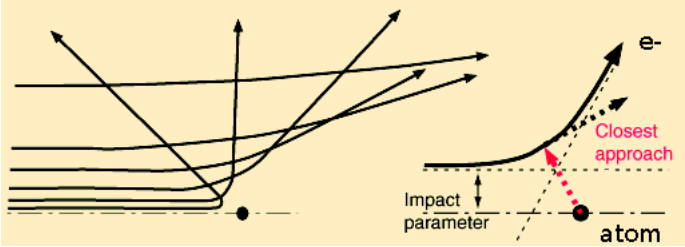

Figure 2.5: Closest approach of an electron-atom impact, at which the impact parameter R is calculated.

The Born approximation is valid for large values of R_i whereas it overestimates the cross sections at smaller R_i. Seaton thus introduced a cutoff value R_0 beyond which the Born approximation may be correctly applied, and he used a semi-classical approach to calculate P_{ij} which at high energies is in good agreement with the quantum Bethe approximation (Seaton, 1955). For weak transition coupling, Eqn. 2.51 can thus be replaced by:

$$\sigma_{ij}^{0} = \int_{R_0}^\infty P_{ji}(R_i)\, 2\pi R_i \mathrm{d}R_i \tag{2.52}$$

whereas for strong transition coupling, Seaton introduced another cutoff parameter R_1 such that $P_{ij}(R_1) = \frac{1}{2}$, and the cross-section would be written as:

$$\sigma_{ij}^{1} = \frac{1}{2}\pi R_1^2 + \int_{R_1}^\infty P_{ij}(R_i)\, 2\pi R_i \mathrm{d}R_i \tag{2.53}$$

For an impact electron with initial and final energies before and after impact $\epsilon = \frac{1}{2}mv^2$ and $\epsilon' = \frac{1}{2}mv'^2$ respectively, Seaton introduced two methods to calculate the cross sections in Eqns.

2.52 and 2.53. The first method is to consider the initial state i to be that with a smaller mean radius r_i of the atom (hereafter referred to as case 1), in which the cross section can be written:

$$\sigma_{ij} = 8\left(\frac{\chi_{\rm H}^{\infty}}{\epsilon}\right)\left(\frac{\chi_{\rm H}^{\infty}}{E_{ij}}f_{ij}\right)\phi(\beta_0)\pi a_0^2 \tag{2.54}$$

where $E_{ij} = |\epsilon - \epsilon'|$ is the transition energy, $\chi_{\rm H}^{\infty} = \frac{me^4}{2\hbar} = 13.6$ eV is the hydrogen ionization potential and $\phi(\beta_0) = \beta_0^2 K_0(\beta_0)K_1(\beta_0)$ is calculated by solving the zeroth and first order modified Bessel functions K_0 and K_1 respectively, where β_0 is dependent of the cutoff radius R_0, and which have been tabulated by Seaton.

The second method is by taking the initial state i to be the one with the smaller statistical weight g_i (hereafter referred to as case 2). In this case, the cross section can be written as:

$$\sigma_{ij} = 8\left(\frac{\chi_{\rm H}^{\infty}}{\epsilon}\right)\left(\frac{\chi_{\rm H}^{\infty}}{E_{ij}}f_{ij}\right)\left\{\frac{1}{2}\zeta(\beta_1) + \phi(\beta_1)\right\}\pi a_0^2 \tag{2.55}$$

where $\zeta(\beta_1) = \beta_0^2\{K_0^2(\beta_1) + K_1^2(\beta_1)\}$, and β_i can be calculated as follows:

$$\beta_i = \left(\frac{\epsilon}{\chi_{\rm H}^{\infty}}\right)^{1/2}\frac{E_{ij}}{(\epsilon+\epsilon')}\frac{R_i}{a_0} \tag{2.56}$$

where $R_i = R_0$ for case 1 and $R_i = R_1$ for case 2. Neglecting the exchange of energy between the perturber and the target at low ϵ allows the use the reciprocity condition, from which the inverse process cross-section can be calculated using:

$$\epsilon\, g_i\sigma_{ij} = \epsilon'\, g_j\sigma_{ji} \tag{2.57}$$

The best cross section is taken to be the smaller between the two cases. A drawback of Seaton's impact method for electron impact excitation is the requirement of the knowledge of the radiative oscillator f_{ij} strength of the transition, which can be prone to large experimental errors, and of the cutoff radii R_0 and R_1. In addition, the close coupling relation neglects the higher states in the wave-function which leads to various distortion and resonance effects, whose total contribution can be important, in particular for forbidden lines excitation (Bely and van Regemorter, 1970).

For forbidden transitions, Seaton (1962b) suggested the calculation of the excitation cross-section using:

$$\sigma_{ij} = \frac{h^2}{4\pi m_e^2}\frac{\Omega_{ij}}{g_i v_e^2} \tag{2.58}$$

where Ω_{ij} is taken to be equal to 1 for forbidden transitions (Allen, 1973).

Therefore, in the lack of quantum theoretical calculations or experimental determinations, it is more appropriate to use the Seaton impact parameter method to calculate the excitation and de-excitation collisional cross-sections. The van Regemorter approximations, since the latter overestimates the cross-sections at low energies (Fig. 2.6). A recent study by Osorio et al. (2015) showed that the impact parameter method was able to reproduce the Mg IR emission lines, whereas the van Regemorter approximation failed to do so.

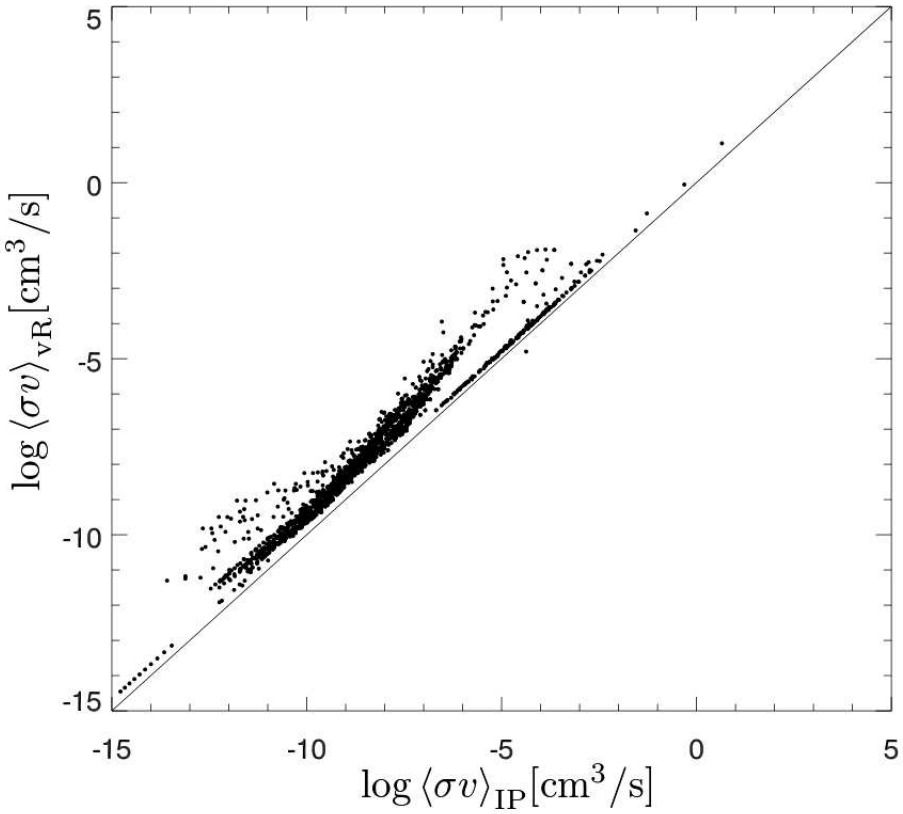

Figure 2.6: Collisional rates calculated using the van Regemorter (vR) classical approximation versus those calculated using Seaton semi-classical impact approximation (IP) on a log-log scale (Osorio et al., 2015).

Impact approximation for ionization transitions: Bely & van Regemorter (1970)

Bely and van Regemorter (1970) formulated an approach to calculating the electron impact ionization cross-section, referred to as Seaton's dipole impact parameter approximation. As presented in Allen (1973), the cross-section can be calculated as a function of the electron energy ϵ before impact (in Ry) to the atomic ionization energy $I_i^{\rm Ry}$ of an atomic electron on level i (also in Ry) as:

$$\sigma_{ic} = 1.63 \times 10^{-14}\, n \left(\frac{1}{I_i^{\rm eV}}\right) \left(\frac{I_i^{\rm Ry}}{\epsilon}\right) F(Y, \epsilon/I_i^{\rm Ry}) \tag{2.59}$$

where n is the number of optical electrons (i.e. the number of electrons in the outermost shell in the electronic configuration) and $I_i^{\rm eV}$ is the ionization energy of level i in eV. The product $q(Y, \epsilon/I_i^{\rm Ry}) = \frac{I_i^{\rm Ry}}{\epsilon} F(Y, \epsilon/I_i^{\rm Ry})$ is referred to as the reduced cross-section, where Y is the charge of the ionized atom (i.e. $Y = 1$ for the ionization of a neutral atom, and $Y = 2$ for the ionization of a singly ionized atom, etc..). Experimental determination of q for H are tabulated

in Table 2.1 for different Y and $\frac{I_i^{\rm Ry}}{\epsilon}$ values which are determined from experimental results of Fite and Brackmann (1958). This approach to the ionization cross-section is a generalized form of Thomson (1912) classical two electron collision approach, which neglects any interaction between the ionizing electron and the atomic nucleus which renders Eqn. 2.59 as:

$$\sigma_{ic}^{\rm classical} = 4n\pi a_0^2 \frac{1}{I_i^{\rm Ry}\epsilon}\left(1 - \frac{I_i^{\rm Ry}}{\epsilon}\right) \tag{2.60}$$

$\epsilon/I_i^{\rm Ry}$	1.0	1.2	1.5	2.0	3.0	5.0	10.0
q (classical)	0.00	0.56	0.89	1.00	0.89	0.64	0.36
q (1,$\epsilon/I_i^{\rm Ry}$)	0.00	0.26	0.52	0.80	0.97	0.92	0.64
q (2,$\epsilon/I_i^{\rm Ry}$)	0.00	0.44	0.78	1.01	1.09	0.94	0.64
q (∞,$\epsilon/I_i^{\rm Ry}$)	0.00	0.62	1.03	1.28	1.28	1.00	0.64

Table 2.1: Reduced cross-section q values for H as a function of ionizing electron energy to ionization energy ratio for the Bely and van Regemorter (1970) approximation, in addition to the Thomson (1912) classical values, from Fite and Brackmann (1958).

The study of inelastic collisions with neutral Hydrogen atoms is the main goal of this PhD dissertation and thus will be discussed in details in Chapter 3.

2.3 Stratification of the stellar atmosphere

In order to reproduce stellar spectra, one also needs theoretical or semi-empirical models of the atmospheric layers. In the case of late-type stars, the theoretical modeling of stellar atmospheres is complicated by the presence of turbulent convective motions as well as of magnetic fields in their envelopes (Nordlund and Stein, 2009). Convection can significantly affect both the atmospheric stratification and the emergent spectral energy distribution of these stars.

One-Dimensional (1D) models:

One dimensional (1D) model atmospheres are commonly used and can be calculated using many public codes such as MARCS (Gustafsson et al., 1975, 2008), ATLAS (Castelli and Kurucz, 2004; Kurucz, 1979), PHOENIX (Hauschildt et al., 1997), and MAFAGS (Grupp, 2004) . These line-blanketed 1D models assume hydrostatic equilibrium, flux constancy, and LTE. The first 1D model atmosphere codes usually assumed a plane-parallel geometry for the atmospheric stratification, which was later improved by allowing for spherical symmetry (Gustafsson et al., 2008; Plez, 1992). That led to lower temperatures in the upper layers, in particular for giant stars, due to the dilution of the radiation field with increasing radius. Line blanketing was included first by means of opacity distribution functions (ODF) (Gustafsson et al., 1975; Strom and Kurucz, 1966) with a few hundred ODF's covering the entire spectrum. These were eventually replaced by opacity sampling (OS) including thousands of wavelength points (Johnson and Krupp, 1976). Nowadays, thousands of ODF's or hundreds of thousands of OS points are used, which result in more accurate models.

The assumption of hydrostatic equilibrium can be written as:

$$\nabla P_{\rm tot} = -\rho\frac{GM_r}{r^2} \tag{2.61}$$

where ρ is the gas density, G is Newton's constant of gravity and M_r is the stellar mass inside radius r (one can usually neglects the mass of the atmosphere as compared to the stellar mass, i.e. M_r is considered the stellar mass). The contribution to the total pressure is distributed among the gas, radiative and turbulent pressures.

$$\nabla P_{\rm tot} = \nabla P_{gas} + \nabla P_{rad} + \nabla P_{turb} \tag{2.62}$$

The radiative pressure is given by Eqn. 2.6, while the turbulent pressure is usually expressed in 1D atmospheres as:

$$P_{turb} = \beta \rho v_t^2 \tag{2.63}$$

where β is a parameters depending on the (an)isotropy of the medium and v_t is the mean turbulent velocity, which characterizes the motion of the gas in the atmosphere, whether due to convection or other turbulent gas motions. The gas pressure can be written for an ideal gas as:

$$P_g = \frac{\mathcal{R}\rho T}{\mu_{mol}} \tag{2.64}$$

where $\mathcal{R}$ is the ideal gas constant and μ_{mol} is the mean molecular weight of the gas. The net stellar energy flux, for a plane-parallel model, is the sum of both radiative and convective fluxes:

$$F_{\rm tot} = F_{\rm rad} + F_{\rm conv} = \sigma_{\rm SB} T_{\rm eff}^4 \tag{2.65}$$

For a spherical model, Eqn. 2.65 can be written as:

$$r^2 \, F_{\rm tot} = \sigma_{\rm SB} T_{\rm eff}^4 \, R^2 \tag{2.66}$$

where r is the radius of a spherical layer and R is the stellar radius.

For modeling convective energy transport, 1D atmospheric codes employ the mixing-length theory (Böhm-Vitense, 1958), which is characterized by 1 to 3 free parameters. Henyey et al. (1965) expressed the convective energy flux using the mixing length theory as:

$$F_{\rm conv} = \frac{1}{2} \, \rho \, c_{\rm p} \, T \, v_{\rm conv} \alpha_{\rm MLT} \delta \Delta \tag{2.67}$$

where $c_{\rm p}$ is the specific heat capacity at constant pressure, T is the temperature, $v_{\rm conv}$ is the convective velocity and $\alpha_{\rm MLT} = \frac{l_m}{H_{\rm p}}$ is the free mixing length parameter. $\alpha_{\rm MLT}$ sets the distance l_m in units of the local pressure scale height $H_{\rm p} = \frac{P}{g\rho}$ over which energy is transported through convection. The factor $\delta\Delta$ is a constant which depends on the adiabatic temperature gradient in the atmosphere, and

$$v_{\rm conv} = \alpha_{\rm MLT} \sqrt{\frac{GM}{r^2} H_{\rm p} \, \mathcal{Q} \, \delta \Delta \, / \nu} \tag{2.68}$$

with $\mathcal{Q} = -\frac{T}{\rho} \left(\frac{\partial \rho}{\partial T} \right)_{\rm p}$. $y = 0.076$ is the radiative heat loss term, and $\nu = 8$ the turbulent viscosity term are free parameters whose values were suggested by Henyey et al. (1965). Hence, in the convective modeling of 1D atmospheres there is a total of 3 free parameters (l_m, y and ν) which need to be calibrated based on observations or their effect on synthetic spectra. Usually $\alpha_{\rm MLT}$ is calibrated to reproduce selected lines (Barklem et al., 2002; Fuhrmann et al., 1993).

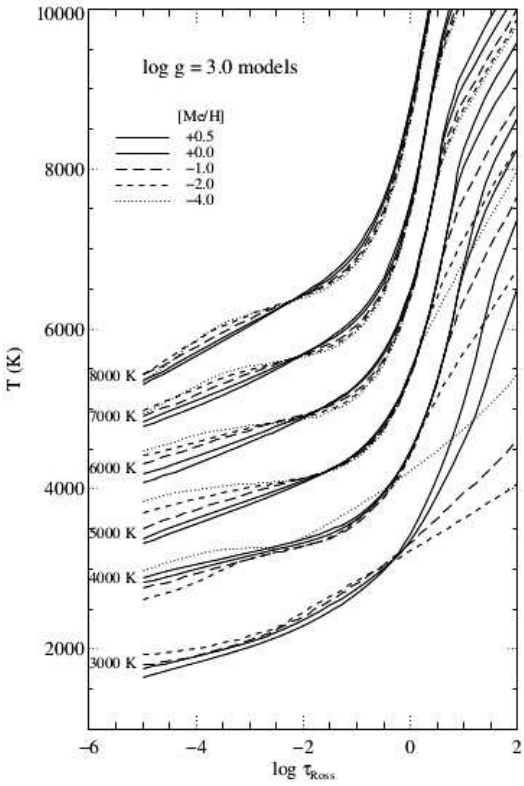

Figure 2.7: Temperature stratification as a function of Rosseland mean opacity of MARCS atmosphere models at logg=3 (cgs) at different $T_{\rm eff}$ and different metallicities [Me/H] (Gustafsson et al., 2008)

Three-Dimensional (3D) models:

Constructing more realistic models to reproduce all observed properties accurately, however, requires to abandon the 1D approximation, since stellar convection is an inherently 3D, time-dependent, non-local and turbulent phenomenon. For late-type metal-poor stars, Asplund et al. (1999a,b) showed that the assumption of pure radiative equilibrium in the convectively stable photospheric layers of classical hydrostatic models is generally insufficient: the temperature structure in the upper layers of the photosphere is determined in 1D atmosphere models by radiative cooling and heating, whereas in reality, the radiative heating is balanced by expansion cooling of upwelling gas and spectral from the above granules (Magic et al., 2013a). This requires 3D modeling to be reproduced (Collet et al., 2006). Hydrodynamical models (Nordlund, 1982) revealed that stellar surface convection requires a different modeling approach than the MLT, since instead of homogeneous convective elements, they display highly asymmetrical motions with slow broad up-flows interspersed with fast narrow turbulent down-drafts (Stein and Nordlund, 1998). These inadequacies in the 1D models, can lead to overestimation of the effective temperatures at very low metallicities, which can lead to severe systematic errors in abundance determinations (Asplund, 2005; Collet et al., 2009).

3D simulations are calculated by solving the time-dependent hydrodynamic equations for mass, momentum, and energy conservation, coupled with 3D radiative transfer equations (Magic et al., 2013a,b), from which convective motions and flow patterns emerge which exhibit the surface granulation pattern that is observed. Several 3D magneto-hydrodynamic codes have been developed to model stellar surface convection, such as the STAGGER-code (Nordlund and Galsgaard, 1995) and CO^{5}BOLD (Freytag et al., 2012), which require parallelization techniques, high computational power and large timescales.

To minimize the large amount of data from the full 3D atmospheric models, temporally and spatially averaged models $\langle 3D \rangle$ have been calculated (Magic et al., 2013b; Stein and Nordlund, 1998). Fig. 2.8 shows the comparison in temperature stratifications of Rosseland-mean optical depth averaged 3D models $\langle 3D \rangle_{\rm Ross}$ as compared to 1D models with $\alpha_{\rm MLT} = 1.5$ at different atmospheric parameters. It can be noticed that in the continuum forming layers, around $-1.0 < log\tau_{\rm Ross} < 0.5$, the difference between $\langle 3D \rangle$ and 1D models are rather small. At lower optical depths, on the other hand, more significant differences can be observed depending on the model, more pronouncedly for lower metallicities, and higher $T_{\rm eff}$ and log g.

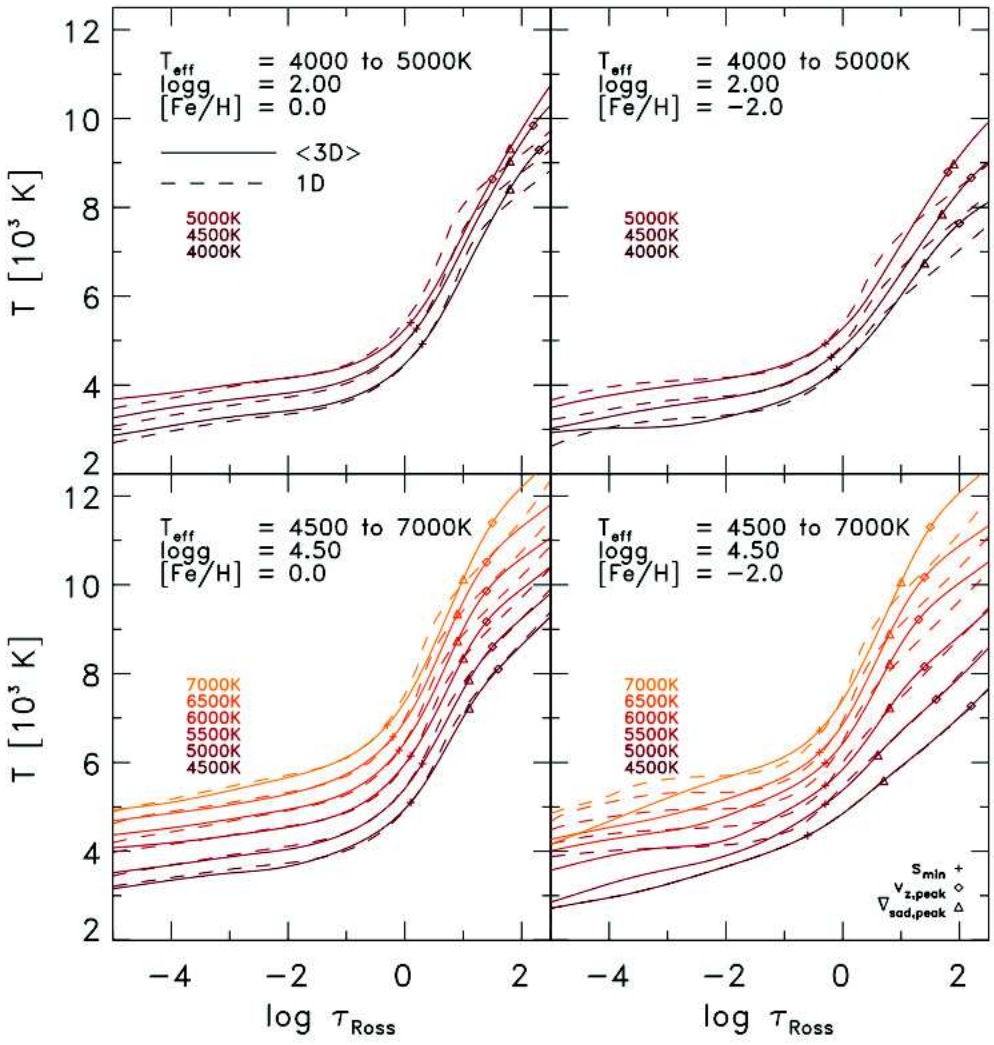

Figure 2.8: $\langle 3D \rangle_{\rm Ross}$ temperature stratification as a function of Rosseland mean optical depth $\tau_{\rm Ross}$ (solid lines), compared to 1D models with $\alpha_{\rm MLT} = 1.5$ (dashed lines) for different atmospheric parameters (Magic et al., 2013b).

Even though 1D atmospheric models depend on assumptions and free parameters, they have demonstrated high predictive capabilities owing to major improvements in the atomic and molecular data, such as new linelists from VALD [19], see e.g. VALD & VALD3 (Kupka et al., 2000; Kurucz, 1993; Piskunov et al., 1995; Ryabchikova et al., 2011). Another advantage of using 1D atmospheric models is the presence of large homogeneous grids of models covering a wide

[19] http://vald.astro.uu.se/

range of stellar atmospheric parameters like the MARCS grid [20] (Gustafsson et al., 2008) and the ATLAS grid[21]. They have proven to be successful in spectroscopic studies when compared with observations and are thus widely applied in astronomy today. Moreover, the radiation fields in 1D models are precisely described by using ODF or OS with $\sim 10^5$ frequency points, while only about ~ 10 points are used in 3D models.

[20] http://marcs.astro.uu.se/
[21] http://www.oact.inaf.it/castelli/

3 The curious case of Hydrogen Collisions

A common problem for calculating non-LTE abundance corrections is that they can be subject to errors from uncertainties in the underlying atomic data. Of these uncertainties, inelastic hydrogen collisions remain a very significant source of uncertainty for stellar abundance analysis. This is due to the difficulty of determining accurate cross section data, especially for low-energy atomic collisions either experimentally or theoretically: there exist very few reliable cross-sections. In the Sun, the ratio of neutral hydrogen to electrons densities $n_{\rm H}/n_e$ varies from 10^4 to 10^6 between optical depths at 5000Å, $\tau_{5000} = 1$ and -1 respectively, and it can reach up to 10^5 at lower metallicities (Asplund, 2005; Lambert, 1993).

Most early non-LTE calculations did not include inelastic collisions with hydrogen at all. This assumption was based on the fact that hydrogen contribution to the collisional rates as compared to that of electrons is reduced by the ratio of their corresponding thermal velocities[1] ($v_{\rm H}/v_e = (m_e/m_{\rm H})^{1/2}$=1/43). In addition, according to the Massey criterion (Massey, 1949), the hydrogen excitation cross-section is expected to be much less than that of electrons. His argument was also discussed by Anderson (1981), who stated that the characteristic time-scale of a collision is proportional to the ratio of the effective range to the relative velocity between the impact perturber and the atom, i.e. $t_c \sim r/v$. From the classical and quantum mechanical points of view, the cross section for excitation and de-excitation is expected to be small unless $1/t \sim \nu$ (or $t\,\nu \leq 1$), where $\nu = \Delta E/h$ is the frequency corresponding to the transition energy ΔE. Lambert (1993) looked closely at this ratio for both electrons and neutral hydrogen atoms and found that for a typical optical transition of $\Delta E \sim 3$eV, $T = 5000$ K, and $r \sim 1$Å, the product $t\,\nu \sim 1/6$ for electrons and ~ 7 for hydrogen. For complex atoms with many high energy lying excitation states (such as Fe, Mg, Ca, Na, ..) where term to term and fine-structure transition energies can be much less than 1 eV, the product $t\,\nu < 1$ and thus the excitation and de-excitation transitions by hydrogen atoms must be considered. This stresses the importance of including hydrogen collisions in solving the non-LTE problem, as it may dominate the collisional processes especially in cool and metal poor stars, where $n_{\rm H}/n_e \sim 10^6$.

In this chapter, I will review the history of classical hydrogen collision treatment in spectroscopic studies and non-LTE abundance analyses in Sect. 3.1. In Sect. 3.2, I will briefly describe the quantum approach to collision cross-section calculations and compare the commonly used classical approaches to recent quantum calculations for some elements which have been treated accordingly. In Sect. 3.3, I will describe the approach to hydrogen collisions used in this work stressing the importance of charge exchange. This will lead us to semi-empirical calibration of hydrogen collision rates in Chapters 6 and 7.

[1] Starting from the assumption that all particles (electrons and hydrogen atoms included) can be described by a single local kinetic energy T, i.e. $\frac{1}{2}m_e v_e^2 = \frac{1}{2}m_{\rm H} v_{\rm H}^2 = k_{\rm B}T$

3.1 Hydrogen collisions: The classical approach

Because of the expectation that neutral hydrogen collision excitation would be negligible as explained above, and because of the almost lack of any reliable calculated or experimental data for H-atom collisions, most early non-LTE studies of cool stars (1960-1970s) neglected the inclusion of neutral H collisions. The first classical approach to H-atom excitation and ionization cross-section calculation was done by Drawin (1968, 1969) whose formulation of the problem is discussed below.

3.1.1 The Drawin Approximation

The classical recipe proposed by Drawin (1968, 1969) was described as a *modified Thomson formula* for calculating excitation cross-section for like-atoms collisions. Drawin started from Thomson (1912) electron-atom ionization cross section for the process: $\mathbf{e + A \longrightarrow 2e + A^-}$ (Eqn. 2.60). Thomson's theory assumes that the bound electron in the target atom is a stationary free classical electron. The Coulomb interaction between the incident electron and the atomic electron is considered by calculating the impact parameter for which the deflection of the incident electron results in an energy transfer between electrons corresponding to the ionization potential. The cross-section can then be calculated easily as all collisions inside this impact parameter will have a larger energy transfer and thus lead to ionization.
Thomson's theory is able to make qualitative predictions regarding the ionization cross-sections and their dependence on the impact energy (Rudge, 1968), however, quantitatively it was found to provide only an order of magnitude precision (Seaton, 1962a). Fig. 3.1 (from Barklem et al. (2011)) compares experimental results for electron collisional ionization cross-sections with Thomson's classical formula for the ground-state for some elements (H, O, Mg and Fe).

The classical formula is shown to overestimate the cross-sections by a factor of $\sim$5 at low energies, particularly for O which seems to differ by a factor of $\sim$20 near the threshold thus showing that the Thomson formula is able to provide only a rough order of magnitude estimate of the cross-sections.

This classical formula of Thomson's was then adapted by Drawin for like-atoms excitation $\mathbf{A + A}_i \longrightarrow \mathbf{A + A}_j$ and ionization $\mathbf{A + A \longrightarrow A + A^+ + }e^-$ collisions. He replaced the ionization potential of the atom **A**, $I_i^{\rm A}$, by the excitation potential from level i to level j ($\Delta E_{ij}^{\rm A} = E_j^{\rm A} - E_i^{\rm A}$). To convert from Eqn. 2.60 to its corresponding $\sigma_{\rm AA}$ for like-atoms collisions, he formulated a conversion between laboratory and center-of-mass coordinates for energy.
In laboratory coordinates, a collision between two atoms **A** and **B** includes a projectile **B** hitting a stationary target **A**, with a kinetic energy $E_{\rm B}^{\rm LAB}$. In center-of-mass coordinates, the total kinetic energy of the collision is expressed as:

$$E_{\rm AB}^{\rm COM} = \frac{m_{\rm A}}{m_{\rm A} + m_{\rm B}} E_{\rm B}^{\rm LAB} \tag{3.1}$$

The excitation of the atomic electron of **A** requires the condition $E_{\rm AB}^{\rm COM} \geq \Delta E_{ij}^{\rm A}$.
For electron excitation collisions ($\mathbf{e^- + A_i \longrightarrow A_j + e^-}$), Drawin introduced the variable:

$$U_{ij}^{\rm eA} = \frac{(\Delta E_{ij}^{\rm A} + \Delta E_e^{\rm LAB})}{\Delta E_{ij}^{\rm A}} \tag{3.2}$$

where $\Delta E_e^{\rm LAB}$ is the electron's projectile energy. At threshold $U_{ij}^{\rm Ae}$=1 when $U_e^{\rm LAB}$=0.

Figure 3.1: Comparison of the classical Thomson (1912) ionization collisional cross-sections for H, O, Mg and Fe to experimental results by Shah et al. (1987), Thompson et al. (1995), McCallion et al. (1992) and Shah et al. (1993) respectively. The plot shows the ratio of the experimental values to the classical ones as a function of the incident electron energy E scaled by the ionization potential I (Barklem et al., 2011).

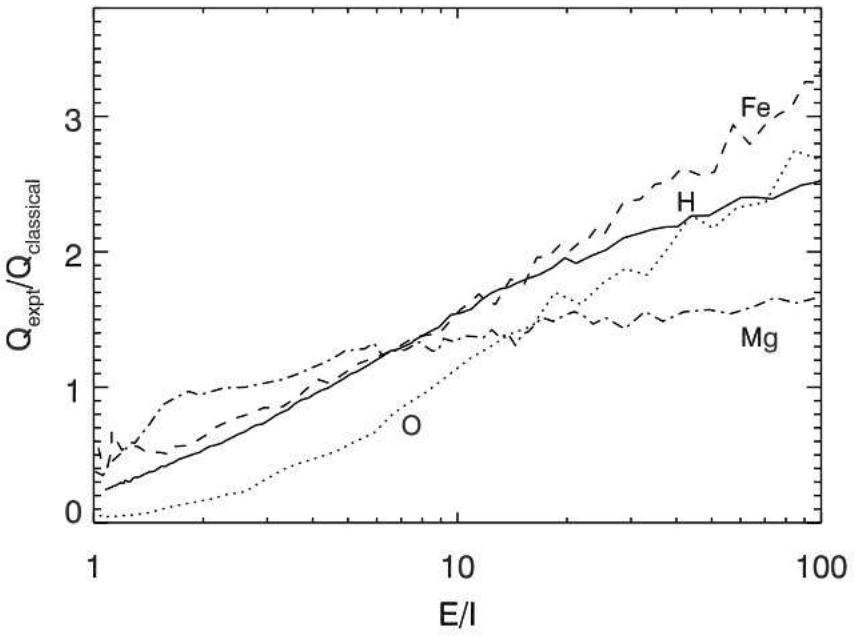

Similarly for like-atoms collisions **A** + $\mathbf{A}_i \longrightarrow$ **A** + $\mathbf{A}_j$, Drawin rewrote Eqn. 3.2 as:

$$W_{ij}^{\mathrm{AA}} = \frac{\Delta E_{ij}^{\mathrm{A}} + \Delta E_{\mathrm{A}}^{\mathrm{LAB}}}{\Delta E_{ij}^{\mathrm{A}}} \tag{3.3}$$

where $E_{\mathrm{A}}^{\mathrm{LAB}}$ is the projectile's kinetic energy above threshold which is attained at $E_{\mathrm{A}}^{\mathrm{LAB}} = 2E_{\mathrm{A}}^{\mathrm{COM}} = 2\Delta E_{ij}^{\mathrm{A}}$. The relation between Eqns. 3.2 and 3.3 stemmed from considering the collision in both cases to occur between the projectile and the atom's "free" electron, and that both types of collisions are equally efficient at equal energies above the threshold in the center-of-mass coordinates, thus allowing for writing:

$$\frac{m_e}{m_e + m_e}\Delta E_e^{\mathrm{LAB}} = \frac{m_e}{m_e + m_{\mathrm{A}}}\Delta E_{\mathrm{A}}^{\mathrm{LAB}} \tag{3.4}$$

which allows to relate $U_{ij}^{e\mathrm{A}}$ and W_{ij}^{AA} as follows:

$$U_{ij}^{e\mathrm{A}} = 1 + \frac{2m_e}{m_e + m_{\mathrm{A}}}(W_{ij}^{\mathrm{AA}} - 1) \tag{3.5}$$

Drawin then substituted Eqn. 3.5 above in Eqn. 2.60 to get the collisional cross-section for **A+A** collisions:

$$\sigma_{\mathrm{AA}} = 4\pi a_0^2 \left(\frac{I^{\mathrm{H}}}{\Delta E_{ij}^{\mathrm{A}}}\right)^2 \frac{m_{\mathrm{A}}}{m_{\mathrm{H}}} f_{ij} \frac{2m_e}{m_e + m_{\mathrm{A}}} \Phi(W_{ij}) \tag{3.6}$$

where

$$\Phi(W_{ij}) = \frac{W_{ij} - 1}{\left[1 + \frac{2m_e}{m_e + m_{\mathrm{A}}}(W_{ij} - 1)\right]^2} \tag{3.7}$$

and

$$W_{ij} = \frac{(E_{\rm A}^{\rm LAB} - \Delta E_{ij}^{\rm A})}{\Delta E_{ij}^{\rm A}} \tag{3.8}$$

where the oscillator strength f_{ij} was introduced to account for allowed transitions as compared to the forbidden, motivated by an analogy with the Bethe approximation for inelastic collisions with electrons. $m_{\rm A}/m_e$ is a fudge factor introduced to ensure a better fit with measurements of He-He and N_2-N_2 collisions.
The main physical assumption in Drawin's classical approach is neglecting the nuclei of the perturbing atoms, thus rendering the problem as a two electrons interaction. Even though Drawin found an agreement within a factor of 2 between his formula and experimental values for ionization collisions between light atoms, Fleischmann and Dehmel (1972) found only order of magnitude agreement with more recent experimental rates which become larger for heavier elements.

3.1.2 A little bit of history

The H-atom collisional rate can be calculated similarly to that of e^--atom collisions starting from Eqn. 2.45 where N_e is replaced by $N_{\rm H}$ and m_e by $m_{\rm H}$, thus allowing for expressing the H collisional rate (per unit volume) for a collisional excitation from level i to level j in terms of the effective collisional strength $\Upsilon_{ij}^{\rm H}$ as

$$n_i C_{ij}^{\rm H} = 2.014 \times 10^{-7} n_i N_{\rm H} \frac{\Upsilon_{ij}^{\rm H}}{g_i\sqrt{T}} e^{-E_{ji}/k_{\rm B}T} \tag{3.9}$$

where $N_{\rm H}$ is the H atom density, and

$$\Upsilon_{ij}^{\rm H} = 4.965 \times 10^6 g_i \sqrt{T} \langle \sigma_{ij} \nu \rangle. \tag{3.10}$$

$\langle \sigma_{ij}\nu \rangle$ is the Maxwellian averaged collisional rate. The earliest work to include neutral hydrogen collisions in their non-LTE spectroscopic calculations was Gehren (1975), in his solar study of Na lines, who stated his using Drawin's classical equation for calculating the collisional cross-sections without specifying on how the formula was extended from like-atoms to H + atom collisions. His study however, found that the H atom collisions were relatively unimportant (less than 50% of the contribution of electrons). Gehren deduced that the influence of atom + H collisions on the kinetic equilibrium was negligible under solar conditions.

Nine years later, Steenbock and Holweger (1984) included H-atom collisions in their Li study. They also started from Drawin's cross-section formula (Eqn. 3.6), substituting $m_{\rm A}$ by $m_{\rm H}$ and removing the fudge factor $m_{\rm A}/m_e$. They expressed the Maxwell-averaged cross-section of a particle species **A** by inelastic collisions with neutral H atom as:

$$\langle \sigma\nu \rangle = 16\pi a_0^2 \left(\frac{2k_{\rm B}T}{\pi\mu}\right)^{1/2} Q \frac{m_{\rm A}}{m_{\rm H}} \frac{m_e}{m_e + m_{\rm H}} \Psi(W) \tag{3.11}$$

where $\mu = \frac{m_{\rm A} m_{\rm H}}{m_{\rm A}+m_{\rm H}}$ is the reduced mass of the **A-H** system. The variable Q was defined differently for the excitation and ionization cases:

$$Q = \begin{cases} \left(\frac{\chi_{\rm H}^{\infty}}{\Delta E_{ij}^{\rm A}}\right)^2 f_{ij} & \text{with } W = \frac{\Delta E_{ij}^{\rm A}}{k_{\rm B}T} \text{ for excitation} \\ \left(\frac{\chi_{\rm H}^{\infty}}{I_i^{\rm A}}\right)^{1/2} f_i \xi_i & \text{with } W = \frac{I_i^{\rm A}}{k_{\rm B}T} \text{ for ionization,} \end{cases} \tag{3.12}$$

where $\chi_{\rm H}^{\infty}$ is the hydrogen ionization potential, $I_i^{\rm A}$ is the ionization energy of level i, f_i is the effective oscillator strength for ionization, and ξ_i is the number of equivalent electrons[2]. The function $\Psi(W)$ was defined as:

$$\Psi(W) = \left(1 + \frac{2}{W}\right) \frac{e^{-W}}{1 + \frac{2m_e}{(m_e + m_{\rm H})W}}. \tag{3.13}$$

Lambert (1993) then reviewed the two previous approaches to Drawin's approximation for the H + atom collisional cross-sections. He re-derived an expression for the rate coefficients from Drawin's approach differing from Steenbock and Holweger (1984) by a negligible factor of $m_{\rm A}/(m_{\rm A} + m_{\rm H})$ of order unity, and expressed it as:

$$\langle \sigma\nu \rangle = 16\pi a_0^2 \left(\frac{2k_{\rm B}T}{\pi\mu}\right)^{1/2} f_{ij} \left(\frac{\chi_{\rm H}^{\infty}}{\Delta E_{ij}^{\rm A}}\right)^2 \frac{m_e(m_{\rm A} + m_{\rm H})}{m_{\rm H}(m_e + m_{\rm H})} \Psi(W_{ij}), \tag{3.14}$$

with

$$\Psi(W_{ij}) = e^{-W_{ij}} \left(1 + \frac{2}{W_{ij}}\right) \text{ and } W_{ij} = \frac{\Delta E_{ij}^{\rm A}}{k_{\rm B}T}. \tag{3.15}$$

3.2 Hydrogen collisions: The Quantum scattering approach

According to the first Born approximation "perturbation theory" (Landau and Lifshitz, 1965), valid for high-energy collisions between electrons and atoms, the Coulomb interaction U is considered between the impact electron and the target atom and includes interactions with the atomic nucleus and atomic electrons $U_{\rm e-nuc}$ and $U_{\rm e-e}$ respectively ($U = U_{\rm e-nuc} + U_{\rm e-e}$). The direct scattering probability amplitude for the excitation of an atom A from level i to level j is expressed as:

$$P^{ij} = -\frac{1}{2\pi} \langle \phi_j^{\rm A}(\mathbf{r}) | \exp(i\mathbf{qR}) U | \phi_i^{\rm A}(\mathbf{r}) \rangle, \tag{3.16}$$

where $\phi_{i/j}^{\rm A}(\mathbf{r})$ denote initial/final wave functions, **r** represents a set of coordinates of the atomic electrons, **R** denotes the impact electron coordinate, **q**=**k**$_i$-**k**$_j$ is the momentum transfer during the transition between the two levels and i is the imaginary complex number.

The collisional cross-section is proportional to the square of the scattering probability amplitude and is shown in Bransden and Joachain (2003) to be proportional to the quantity:

$$\mathcal{F}_{ij} = \frac{2(\Delta E_{ij})}{\rm q^2} |\langle \phi_j^{\rm A}(\mathbf{r}) | \sum \exp(i\mathbf{qR}) U | \phi_i^{\rm A}(\mathbf{r}) \rangle|_{\mathbf{r}}^2, \tag{3.17}$$

which is called the generalized oscillator strength. In Eqn. 3.17, and according to the first Born approximation, the integration over the impact electron coordinate **R** and the orthogonality of the wave functions, has lead to removing the interaction with the nucleus, leaving only the interaction between the incident and atomic electrons. This allows for a bridge between the quantum and the classical Drawin approach which both relate the allowed collisional transitions to their radiative counterparts through the oscillator strength.

The Born approximation, however, is valid only for high-energy electron-atom and electron-molecule collisions. It gives poor results for low-energy collisions, such as inelastic H-atom collisions, which are interesting in the atmospheres of cool stars and are relevant for this thesis

[2]Electrons in an atom which have the same principal and orbital quantum numbers, but not necessarily the same magnetic orbital and magnetic spin quantum numbers (see Chapter 4).

work. In the latter case, the Born-Oppenheimer approach should be used which requires full quantum treatment of the total wave functions of the entire collisional system.

Although the understanding of H-atom collisions has increased in the past 30 years, there are still a lot of experimental difficulties, especially for complex atoms. Fleck et al. (1991) performed an experimental study of the **Na(3s) + H $\longrightarrow$ Na(3p) + H** excitation transition. They could not, however, go below the threshold values of 2.1 eV (the relevant temperature regime for stellar atmospheres) due to experimental complications. Fig. 3.2 shows these experimental cross-section results as compared to quantum theoretical calculations (Belyaev et al., 1999) and to those calculated using Lambert's approach of Drawin's approximation. It can be seen that the quantum theoretical calculations fit well to experimental data, while Drawin's approximation overestimates them by many orders of magnitude. In addition, it does not provide cross-sections for forbidden transitions. It can also be markedly seen that the deviation from quantum calculations varies from one transition to another. This is shown in Fig. 3.3, where the quantum scattering rate coefficients, the Drawin approximation rate coefficients and corresponding ratios are shown for Li+H and Na+H collisions. The Drawin to quantum ratio is specifically shown to overestimate the collisional rates, especially for higher energies which correspond to transitions from low-lying to high-lying energy levels, while the quantum scattering calculations show decreasing rates with increasing transition energies down to negligible values.

Figure 3.2: Calculations for Na(3s) + H $\longrightarrow$ Na(3p) +H collisional excitation cross-sections as a function of the H collision energy. The solid line represents the quantum scattering calculations (Belyaev et al., 1999), while the circles represent Fleck et al. (1991) experimental data. The dashed line represents the cross-sections calculated using the Drawin approximation which overestimates the experimental data by orders of magnitude (Barklem et al., 2011)

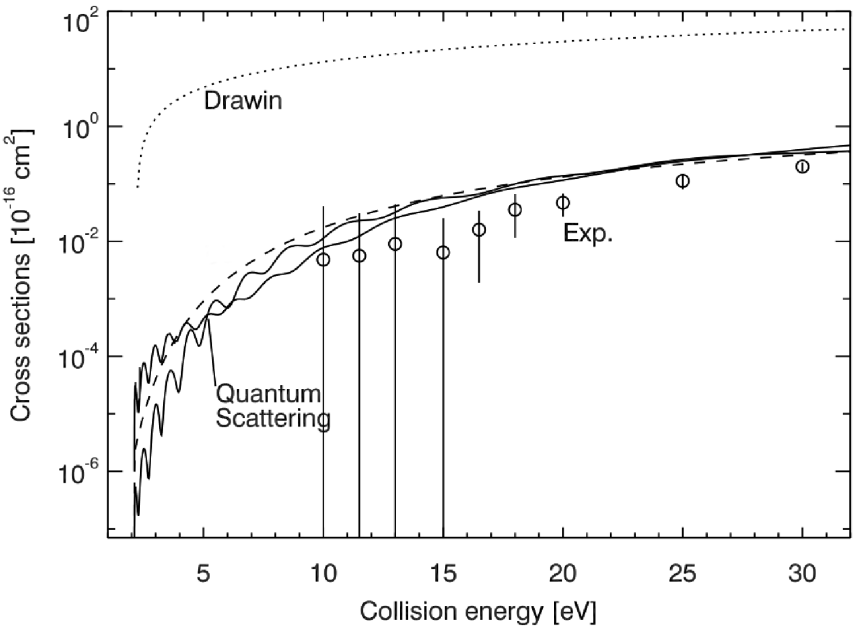

It can be deduced that at low energies, the Drawin approximation does not hold the essential physics behind collisional excitation by H atoms. It is in error by orders of magnitude, well beyond the estimated uncertainties of the quantum calculations (Barklem et al., 2010).

Figure 3.3: Li+H (upper left panel) and Na+H (upper right panel) quantum scattering H-collision rate coefficients calculation for excitation transitions (Barklem et al., 2003) and Barklem et al. (2010) respectively for different initial energy states. Different symbols denote different transition energies. Lower left and right panels show the corresponding rate coefficients calculated using the Drawin approximation for Li+H and Na+H respectively. The dotted lines in all panels show the linear fit to the quantum calculations. The smaller panels show the Drawin to quantum ratios which demonstrates the overestimation of the rates as a function of transition energies. Adapted from Barklem et al. (2011).

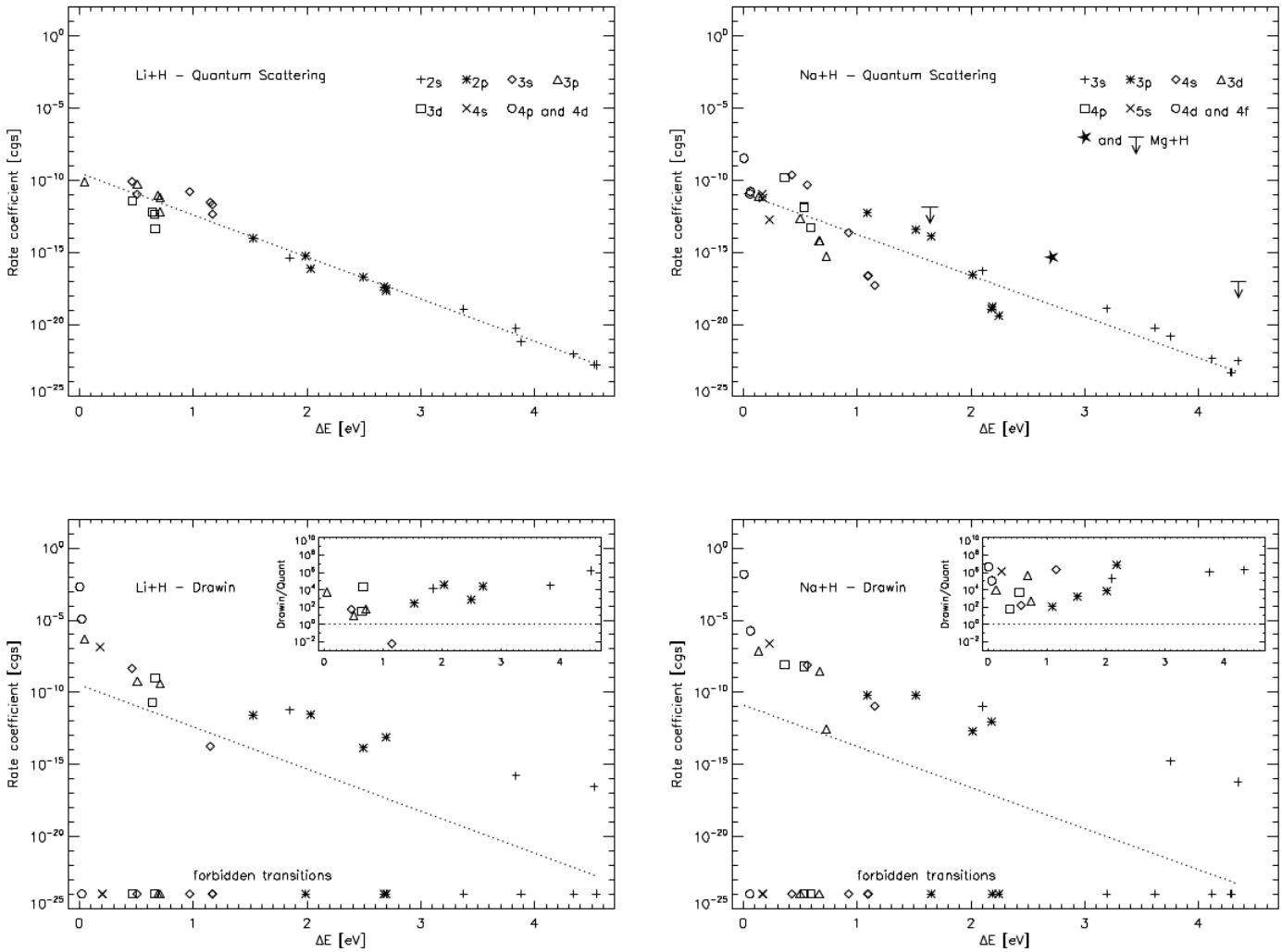

In the lack of quantum calculations and experimental data for most elements, and in an attempt to correct the Drawin H-collisional rates, a multiplicative fudge scaling factor S_H has been introduced for the Drawin rates, a method which has been used exhaustively in most non-LTE studies. The S_H values have been calibrated with different means whether on solar or benchmark star observations.

Several non-LTE studies of iron have included H-Fe collisions by using the Drawin approximation of Steenbock and Holweger (1984) and Lambert (1993). However, many different scaling factors S_H have been used in each study. Thévenin and Idiart (1999) found a best fit upon using a value of S_H=1, and found no important effects whether including the H collisions or not, while finding significant non-LTE effects in their study. Gratton et al. (1999) derived a value of S_H=30 using RR-Lyrae stars, and found very little non-LTE effects, as increasing the

collisions to large values leads to LTE conditions. It is to be noted that the former two studies used rather incomplete FeI/FeII model atoms which did not include all the necessary levels and lines. In addition, they did not include the high-lying FeI levels which induce important coupling with FeII ground levels (details discussed in Chapter 4). Another study by Gehren et al. (2001) found a best fit when adopting a value of $\mathbf{S_H}$=3. Two more recent studies, which used a rather more complete FeI/II model atoms, are those of Mashonkina et al. (2011) and Bergemann et al. (2012) which included a large number of levels, including the theoretical high-lying levels and lines in their studies, and who both used FeI/FeII excitation balance to determine metallicity dependent values of $\mathbf{S_H}$=0.1 and $\mathbf{S_H}$=1.

Another attempt was to scale the Drawin approximation on an energy basis which was adopted by Zhao and Gehren (2000), who tried to scale $\mathbf{S_H}$, with an exponential factor of the upper level energy E_n (applied for Mg) using the formulation:

$$\mathbf{S_H} = 1000 \times \ e^{nE_n/2} \tag{3.18}$$

where n is the principal quantum number of the level n.

Figure 3.4: S_H timeline diagram showing the different S_H values adopted by different references in the literature in the past few years.

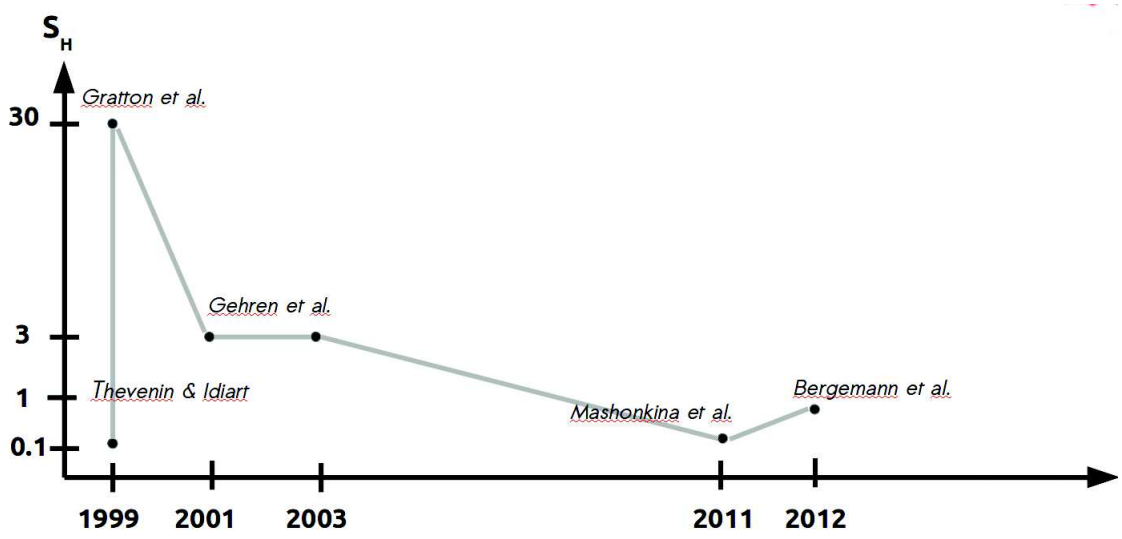

Thus different input model atoms and different calibration techniques (as well as different input stellar parameters) deliver different $\mathbf{S_H}$ scaling factors. This calls for a further investigation of the curious case of H-collisions that will be made in Chapters 6 and 7.

3.3 Charge Transfer

In addition to the importance of H-atom excitation and ionization collisional processes in the atmospheres of cool stars, it has been shown recently (Barklem et al., 2010, 2012; Belyaev, 2013; Belyaev and Barklem, 2003; Belyaev et al., 2014; Lind et al., 2011; Osorio et al., 2015) that the charge exchange (transfer) processes can be equally important and even dominate over the other collisional processes.

An interpretation of this process is that at certain separations during the collisions between a neutral hydrogen atom and an atomic element **A**, an **AH** quasi-molecule is formed momentarily and the optical electron associated with **A** may tunnel into the H atom, thus leading to the ionization of the element into $\mathbf{A}^+$, and producing a negative $\mathbf{H}^-$ ion. This process is referred to as an **ion-pair production**.
During an $\mathbf{H}^- + \mathbf{A}^+$ collision, an electron may tunnel towards the atom **A**. This process corresponds to the inverse of the former one and is referred to as **mutual neutralization**.

The charge transfer collisional rate (per unit volume) for ion-pair production between an initial level i and a continuum level c can be expressed as:

$$n_i C_{ic} = n_i N_{\mathrm{H}} \langle \sigma^{\mathrm{ic}} \nu \rangle \tag{3.19}$$

whereas the inverse rate for the corresponding mutual neutralization rate can be written as:

$$n_c C_{ci} = n_c N_{\mathrm{H^-}} \langle \sigma^{\mathrm{ci}} \nu \rangle \tag{3.20}$$

where $N_{\mathrm{H^-}}$ is the ionized H^- density.

Barklem et al. (2003) first included charge transfer cross-sections into their non-LTE calculations for Li. Their cross-sections were calculated by Belyaev and Barklem (2003) using the quantum scattering method. Their Li+H rate coefficients show higher cross-sections for charge exchange than those of excitation from the same initial levels, thus showing that the former are dominant in thermalizing Li, whereas the latter are relatively unimportant.

Similar results have been found in non-LTE studies for late type stars, for Na+H (Lind et al., 2011), Mg+H (Barklem et al., 2012), Al+H (Belyaev, 2013) and Si+H (Belyaev et al., 2014) where charge-exchange rates dominated for most transitions over those of collisional excitation and ionization.
Fig. 3.5 shows the domination of the ion-pair production transitions (circled symbols) over their corresponding excitation transitions (un-circled symbols) from the same initial levels.

In the absence of an approximation for calculating charge transfer rates, we expanded Lambert's Drawin approximation for **A + H** collisional rate coefficients to those of charge transfer using Eqn. 3.14, replacing ΔE_{ij} by $\Delta E_{ic} - I_{\mathrm{H^-}}$ where $I_{\mathrm{H^-}} = 0.754$ eV is the ionization energy of H^-. The oscillator strength f_{ij} in Eqn. 3.14 is set to 1, thus allowing to calculate the rate coefficients for both optically allowed and forbidden transitions. This approach was motivated and justified by the following reasons:

- Steenbock (1985), upon studying the FeI/FeII statistical equilibrium in Pollux and the Sun, set the Q-factor in Eqn. 3.12 for excitation transitions with unknown f-values equal to 1.

- A similar approach to removing the f value from the classical approximations, was used by Collet et al. (2005) with the Van Regemorter equation (Eqn. 2.47) for electron collisions by setting a constant $f = 10^{-3}$ for all transitions, thus avoiding the problem of forbidden transitions.

- Recent quantum calculations found large H-collisional rates for Mg and other elements for forbidden transitions, which were found to be roughly equal to the allowed transitions (Feautrier et al., 2014).

Figure 3.5: Mg+H rate coefficients calculated via the quantum scattering method as a function of transition energies. Different symbols denote transitions of different initial energy states, while circled symbols denote ion pair production (IPP) transitions from the same initial states (Barklem et al., 2012).

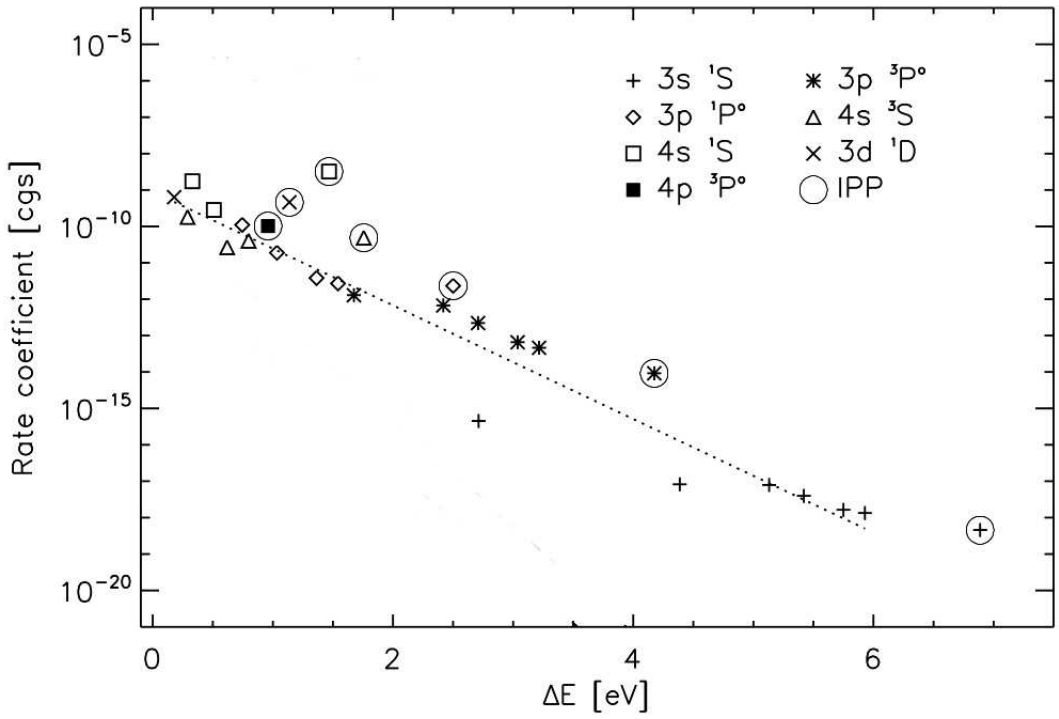

Removing the f dependence allows to compute the rates for all transitions (allowed and forbidden), and for a better comparison with the quantum rates and hence keeping only the ΔE dependence which can help to reveal the differences in both methods lying in the quantum chemistry of the atom.

Figs. 3.6 - 3.9 show the charge transfer and de-excitation rate coefficients for H collisions with Al, Mg, Na and Si respectively, calculated via the quantum scattering method (upper panels) and compared to those of the same transitions calculated via Lambert's Drawin's approximation (middle and lower panels) as explained above.

The plots show the dependence of the collisional rate coefficients on the transition energies ΔE for de-excitation and charge transfer (mutual neutralization) processes respectively. It can be seen that for the four atoms, the charge exchange rate coefficients (filled triangles) calculated using the quantum scattering method exceed the de-excitation rates (empty circles) by up to two orders of magnitude. For de-excitation collisions, a decrease in collisional rates as a function of increasing transition energies ΔE can be seen, which correspond to transitions between the low-lying levels (ground and first ionized) with those of the higher-lying levels. As for charge exchange, it can be observed that similar behavior exists as a function of ΔE peaking between 1.2 & 1.8 eV for all the atoms.

Middle panels show collisional rate coefficients for the same processes corresponding to the same transitions calculated using the Drawin's approximation, that show a decreasing behavior with ΔE for both de-excitation and charge exchange processes.

The quantum to Drawin ratios (lower panels) clearly show that the Drawin approximation over-estimates all the de-excitation rates by several orders of magnitude. For charge transfer, the ratio is < 1 for most transitions. In addition, it can be observed that the quantum rates behavior with transition energies is not at all reproduced in the Drawin approximation. The estimated uncertainties in the rate coefficients from the quantum mechanical data are not sufficient to explain the differences with the Drawin approximation (Barklem et al., 2010).

It can thus be generally concluded that charge-exchange processes dominate over the hydrogen collisions for atoms, for which reliable quantum data exist. We can only assume that this is the case for other atoms, including iron, which is at the heart of this work. To test this assumption, we constructed a new iron model atom (see Chapter 4) and adopted different methods for coupling all the levels in our model with H-collisions, including for charge exchange. The details and results of these methods will be presented in Chapters 6 and 7.

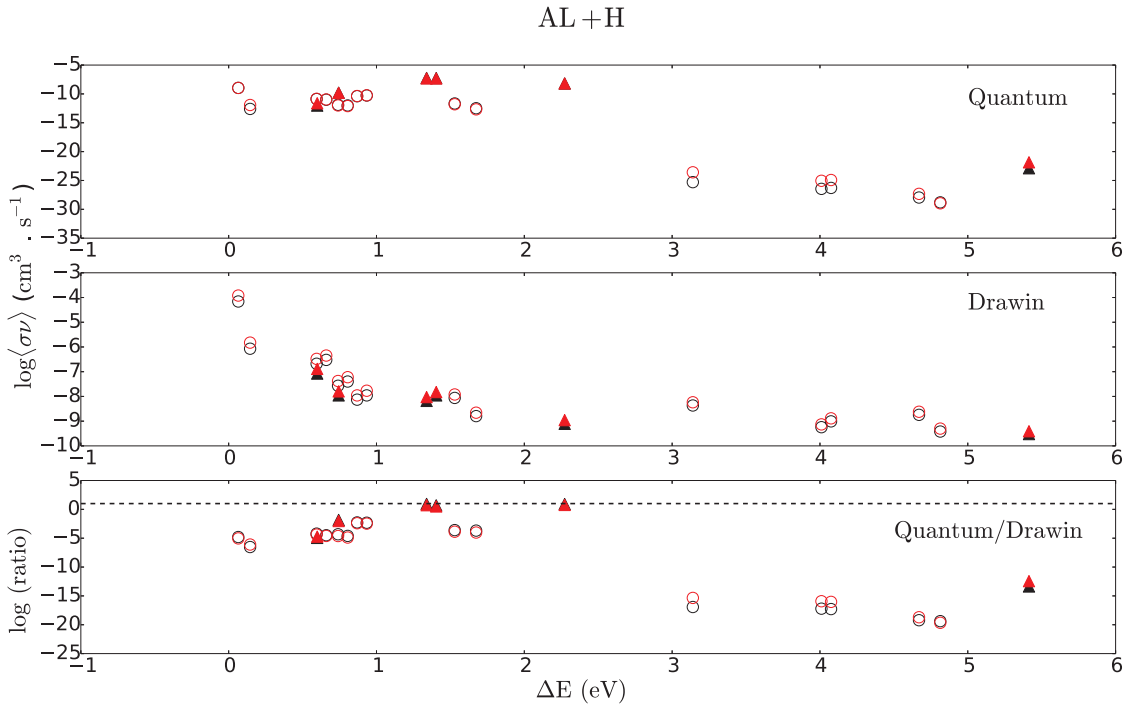

Figure 3.6: Al+H rate coefficients at T=4000K (black) and T=6000K (red) calculated via the quantum scattering method (upper panel) as a function of the transition energies ΔE from Belyaev (2013) for de-excitation and charge exchange (mutual neutralization). Open circles represent de-excitation rates, while filled triangles represent charge exchange rates. The middle panel shows the corresponding rate coefficients of the same transitions calculated via Lambert (1993) approach to Drawin's approximation (using $f = 1$). The lower panel shows the ratios of the quantum/Drawin rates. The dotted line corresponds to log(ratio)=1.

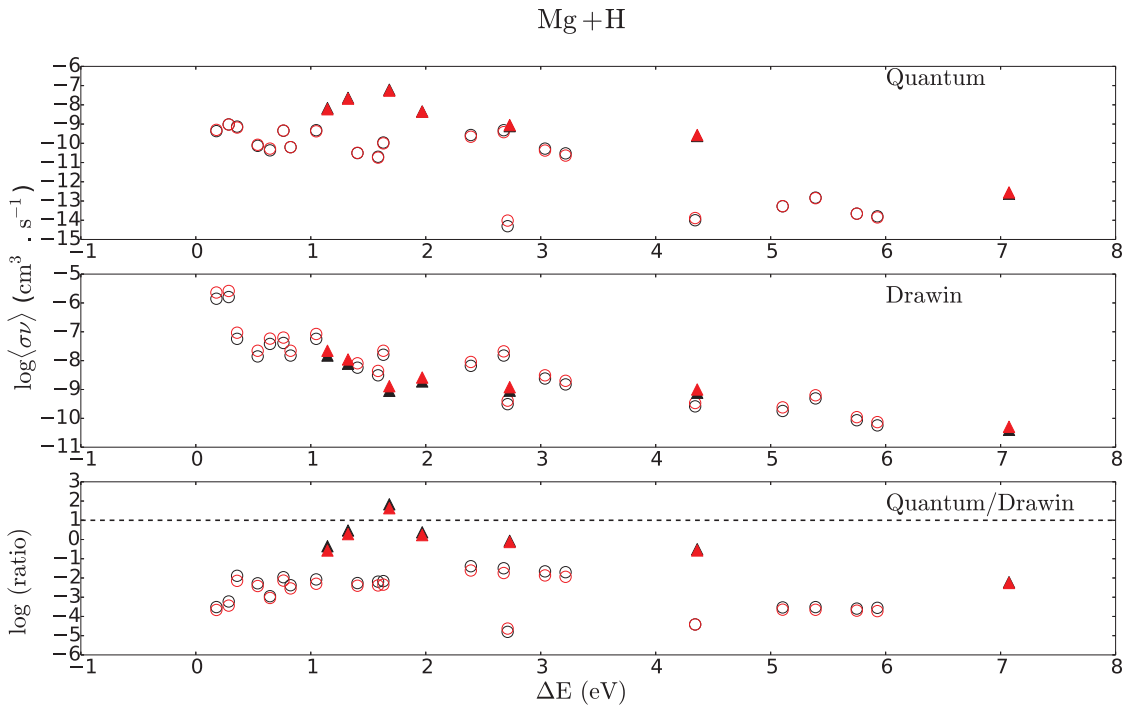

Figure 3.7: Mg+H rate coefficients at T=4000K (black) and T=6000K (red) as a function of the transition energies ΔE from Belyaev et al. (2012). Panels and symbols represent the same information as in Fig. 3.6 .

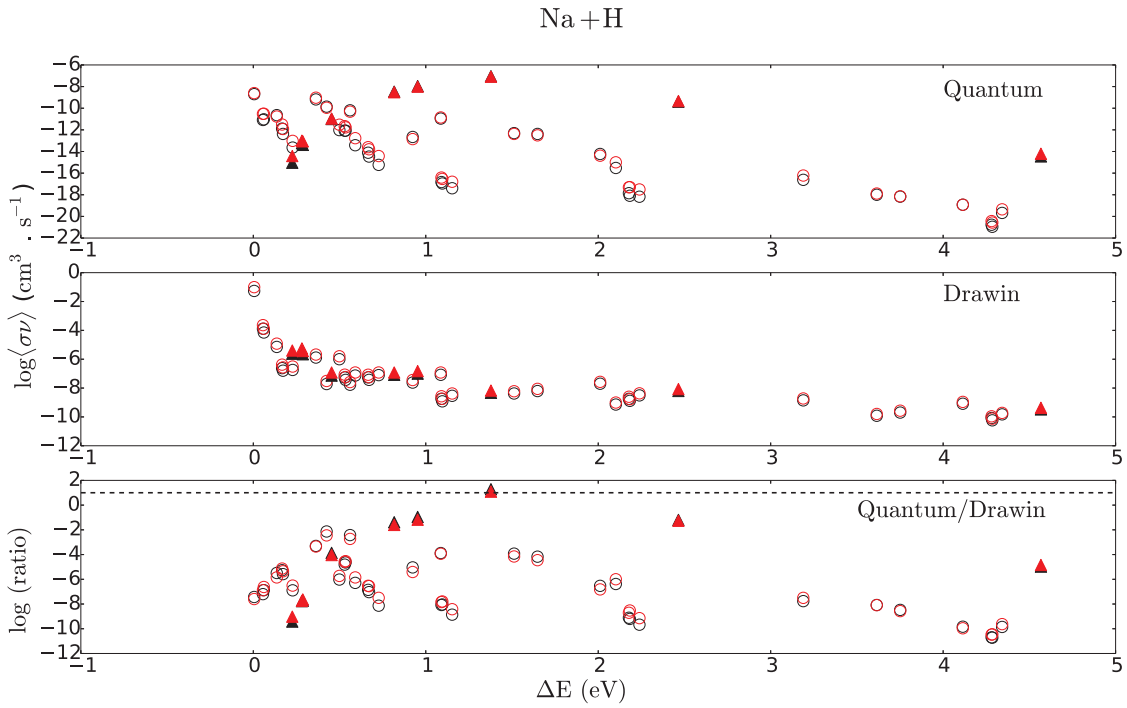

Figure 3.8: Na+H rate coefficients at T=4000K (black) and T=6000K (red) as a function of the transition energies ΔE from Barklem et al. (2010). Panels and symbols represent the same information as in Fig. 3.6 .

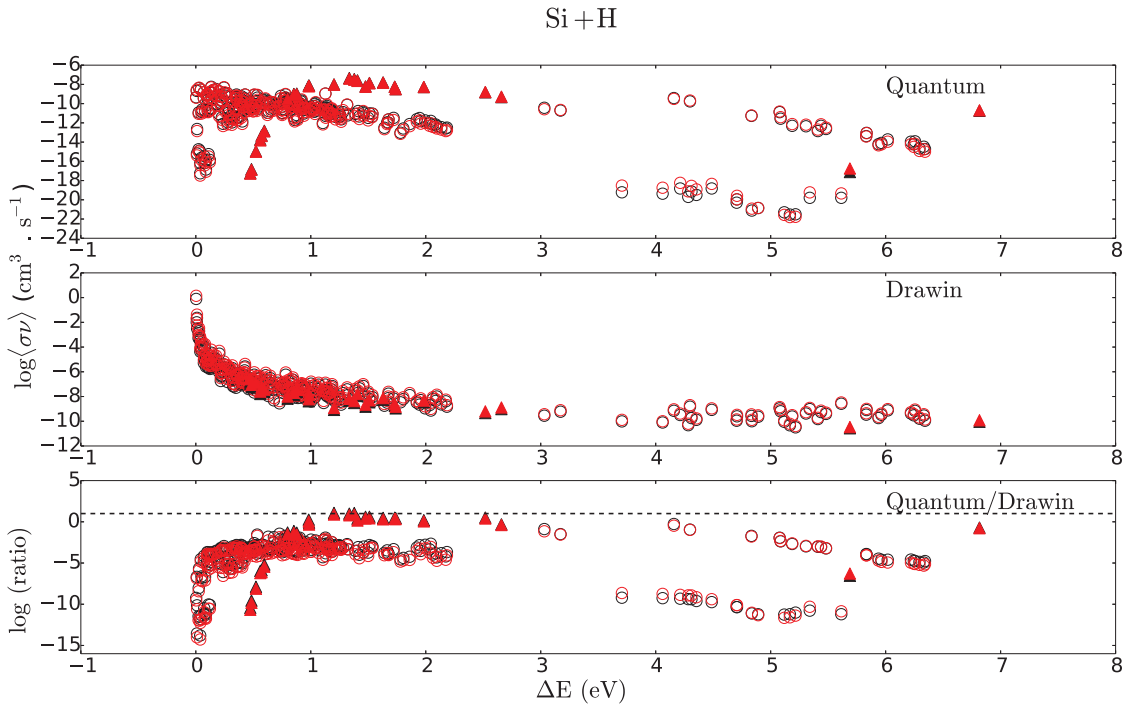

Figure 3.9: Si+H rate coefficients at T=4000K (black) and T=6000K (red) as a function of the transition energies ΔE from Belyaev et al. (2014). Panels and symbols represent the same information as in Fig. 3.6 .

4 | Iron model atom construction

Solving the non-LTE problem of a multi-level atom, as described explicitly in Annex B, requires the build up of the grand matrix which must include all the radiative and collisional rates for all transitions between the energy levels of the atom.
In cool stars (T_{eff} between 3000K and 7000 K), lines of neutral iron (Fe I) dominate the absorption spectrum (Peterson and Kurucz, 2015) even though iron is almost completely ionized throughout the atmosphere of these stars. Fig. 4.1 shows the ionization fractions for iron as function of the optical depths in the Solar atmosphere and that of the metal-poor sub-giant HD140283. A minority species like Fe I is particularly sensitive to non-LTE effects because any small change in the ionization fraction changes their populations by a large amount. In the non-LTE treatment of iron, it is essential to include all important Fe I and Fe II lines and levels.

The number of levels and discrete radiative transitions in Fe is enormous. Recent calculations of Kurucz[1] predict $\sim$ 37 000 theoretical energy levels below and above the first ionization threshold of Fe I, as well as 6 025 000 radiatively permitted transitions between them. Such huge numbers of lines and levels are not treatable by current non-LTE codes. To reduce the amount of computing time, as well as memory requirements, it is important to decrease the size of the rate matrix by including the important levels and lines and combining them into superlevels and superlines respectively as described in the sections below.

In this chapter, the construction of the iron model atom, referred to hereafter as the "Iron model atom", used in the non-LTE calculations with the **MULTI2.3** code (Annex B) is described explicitly. The model atom includes the Fe I and Fe II energy levels and the Fe III ground state, and their combination into super levels described in Section 4.1, and their corresponding radiative (Section 4.2) and collisional (Section 4.3) bound-bound and bound-free transitions. In Section 4.5, a comparison of our model with the iron model atoms available in the literature is presented.

4.1 Energy levels

The first step in constructing a model atom is to identify the important energy levels. The energies of these states are predicted through quantum mechanics, or are experimentally measured. Four quantum numbers are used to describe the orbitals in which electrons can be found. These are namely:

- the principal quantum number n
- the orbital angular quantum number l whose values can range from $0\ to\ (n-1)$
- the magnetic quantum number m_l whose values can range from $(l-1)\ to\ (l+1)$

[1] http://kurucz.harvard.edu/atoms.html

Figure 4.1: Ionization fraction of Fe I and Fe II in the Sun (left panel) and in the metal poor halo subgiant HD140283 (right panel, [Fe/H]=-2.40, $T_{\rm eff}$=5522 K, log g=3.58) as a function of atmospheric optical depth at 5000Å τ_{5000}.

- the electron spin m_s which according to Hund's law can have the values of +1/2 or -1/2 respectively

These numbers describe the size, shape, and orientation in space of the orbitals of an atom. Orbitals that have the same value of n form a shell which can accommodate $2n^2$ electrons, while orbitals within a shell are divided into sub-shells l which can accommodate $2(2l+1)$ electrons. These sub-shells are labeled according to their corresponding values of l as shown in table below for the first 10 values of l:

l	0	1	2	3	4	5	6	7	8	9	10
label	s	p	d	f	g	h	i	k	l	m	n

In addition, the sub-shells might be further split through the coupling between two close electrons resulting in the formation of a Russel-Saunders **LS** spectroscopic term coupling denoted by $^{\mathbf{2S+1}}\mathbf{L_J}$ ($2\mathbf{S}+1$ also referred to as multiplicity or degeneracy), where $\mathbf{S}$ is the total electrons spin $\mathbf{S}=\sum_{\mathbf{i}}\mathbf{m_{si}}$ and $\mathbf{L}$ is the total orbital angular momentum of the electrons $\mathbf{L}=\sum_{\mathbf{i}}\mathbf{l_i}$, which can have the same labels as l depending on the values of $\mathbf{L}$, i.e. term labels $\mathbf{S},\mathbf{P},\mathbf{D},\mathbf{F}..$ correspond to $\mathbf{L}=0,1,2,3..$ respectively. On the other hand, farther electrons can also couple via **JJ** coupling, where $\mathbf{J}=\mathbf{L}+\mathbf{S}$ is the total angular momentum of the electrons. Thus each energy level state is defined by a standard set of notations depending on the positions and coupling of their valence electrons. For example the FeI and FeII ground state electron

configurations, starting by the outermost sub-shells, can be written as:

$$\textbf{Fe I}\,(\textbf{groundstate}) : [\mathrm{Ar}]\, 3d^6\ 4s^2\ -\ a^5\mathrm{D}$$
$$\textbf{Fe II}\,(\textbf{groundstate}) : [\mathrm{Ar}]\, 3d^6\ 4s - a^6\mathrm{D}$$

where $[\mathrm{Ar}]$ is the inert gas Argon configuration: $^{18}\mathrm{Ar} : 1s^2\ 2s^2\ 2p^6\ 3s^2\ 3p^6$. The integers preceding the labels s, p and d correspond to the principal quantum numbers n, while the integer superscripts correspond to the number of electrons occupying the respective sub-shells. The terms $a^5\mathrm{D}$ and $a^6\mathrm{D}$ correspond to the **LS** coupling spectroscopic terms of the corresponding levels. In addition, each respective energy state is further split into close fine structure splittings corresponding to each value of **J**.
Finally, the **LS** and **JJ** coupling terms may have an odd or even parity determined by the number of electrons occupying the odd orbitals:

- An odd number of electrons in the odd orbitals will give an odd term denoted by a superscript 'o' or '*', such as $z^7\mathrm{D}^*$.
- An even number of electrons in the odd orbitals will give an even term denoted with no superscript, such as $a^5\mathrm{P}$.

The National Institute of Standards and Technology (NIST)[2] in its 5^{th} version provides several online atomic spectroscopic databases widely used in astrophysics (Ralchenko et al., 2006; Reader et al., 2002). The data include wavelengths, energy levels, and oscillator strengths which are regularly updated for a large number of atoms and molecules.

The iron model atom was built up using all the Fe I energy levels extracted from the NIST database (846 levels) from the experimental analysis of Nave et al. (1994), up to 7.815 eV. The model also includes the predicted high lying Fe I levels (66 levels) from Peterson and Kurucz (2015), up to 8.392 eV. The coupling between these latter high-lying levels and the low-lying levels correspond to important UV transitions, which is important for the determination of abundances for in individual stars from their UV spectra (Peterson, 2011, 2013). The coupling between the high-lying levels themselves corresponds to the important IR transitions which are vital for infrared spectroscopic iron abundances determination in luminous red giants in dust-obscured regions like the bulge, bar, and disk of the Milky Way (Majewski, 2010).
The main NLTE mechanism for Fe I is the over-ionization of low-excitation levels by ultraviolet radiation (Asplund, 2005; Bergemann and Nordlander, 2014). Thus, the role of these high-excitation levels is to compensate, in part, for population losses via collisional coupling to the large continuum reservoir, with subsequent spontaneous transitions down to low-excitation levels (Mashonkina, 2009).

The model atom was completed with all Fe II levels from Nave and Johansson (2013), with 1027 levels up to 19.83 eV, corresponding to 189 spectroscopic terms. Only the ground level of Fe III was included.

4.1.1 Superlevels

To reduce the amount of computing time, as well as memory requirements, it is helpful to reduce the number of levels by using the **superlevel algorithm**, in which the number of individual atomic levels is reduced by combining a set of actual levels into a superlevel.

[2] http://www.nist.gov/pml/data/asd.cfm

A superlevel I consists of a set of actual levels $i \in I$, so that each level is included in exactly one super level, and there is no overlap between two superlevels. The total population density of a super level is necessarily the sum of the population densities of all included levels:

$$n_I = \sum_i n_i \tag{4.1}$$

Also, all levels of a super level share the same departure coefficient $b_I = b_i = n_i/n_i^{\mathrm{LTE}} = n_I/n_I^{\mathrm{LTE}}$.

However, combining levels into superlevels means that not all actual levels and transitions are treated in full non-LTE. Only the populations of the combined levels are fully calculated via the non-LTE approach, while the populations of the actual levels constituting a super level are then populated according to their statistical weights by redistributing the super level population using the Boltzmann equation. This approach can be justified if levels combined are close in energies and are thus closely coupled via collisions. Hence the closer the combined levels are in energies, the better is the LTE assumption is within a superlevel, and the closer to full non-LTE calculations will the results be.

In our iron model atom, the energy levels for Fe I and Fe II were combined using the code `FORMATO` (Merle et al., in prep) as follows:

- The fine structure levels of the ground and first ionized states for each of FeI and FeII were included.
- All other fine structure levels were combined into mean levels according to their statistical weights. Thus the excitation potential of each mean level is a weighted mean of the excitation potential of the corresponding fine structure levels:

$$E_I = \frac{\sum_{i=1}^{N} E_i g_i}{\sum_{i=1}^{N} g_i} \tag{4.2}$$

- All mean levels above 5 eV and lying within an energy interval of 0.0124 eV (100 cm^{-1}) were combined into superlevels. The excitation energy of each super level is a weighted mean of the statistical weights and excitation energies of the corresponding mean levels.

The final number of levels in our iron model is 203 Fe I levels, 189 Fe II levels and, 1 Fe III level (Fig. 4.2 and Fig. 4.3), each defined with an excitation energy relative to the neutral ground state, a statistical weight $g = 2\mathbf{J} + 1$, a configuration, a spectroscopic term ID, and an ionization stage (1 for neutral, 2 for first ionized, etc ..), as shown in Table 4.1 for a few levels in the model.

4.2 Radiative transitions

4.2.1 Bound-bound transitions

Calculation of the radiative bound-bound rates requires computing the input of Einstein coefficient B_{ij}, which can be related to the transitional oscillator strength f_{ij} though Eqn. 2.30.
The bound-bound radiative input data in our iron model includes both allowed and forbidden transitions between the available energy levels in the model. The allowed transitions should obey the selection rules:

E (cm^{-1})	g	Configuration	term ID	Ion
0.000	9.0	$3d^6\ 4s^2$	a^5D	1
6928.268	11.0	$3d^6$ (^{4}F) 4s	a^5F	1
11976.239	9.0	$3d^6$ (^{4}F) 4s	a^3F	1
⋮				
63737.704	10.0	$3d^6$ (^{5}D) 4s	a^6D	2
65610.304	10.0	$3d^7$	a^4F	2
71693.023	8.0	$3d^6$ (^{5}D) 4s	a^4D	2
⋮				
194393.104	9.0	$3d^6$	^{5}D	3

Table 4.1: Excitation energies relative to the neutral ground state, statistical weight g, level configuration & term ID and ionization stage (ion) of the first few levels of FeI and FeII and that of the ground FeIII levels in the FeI/FeII model.

- $\Delta\mathbf{J} = 0, \pm 1$ ($\mathbf{J} = 0 \leftrightarrow \mathbf{J}$=0 not allowed)
- $\Delta\mathbf{L} = 0, \pm 1$ ($\mathbf{L} = 0 \leftrightarrow \mathbf{L}$=0 not allowed)
- $\Delta\mathbf{S} = 0$
- Parity must change

Transitions not obeying one of these rules are referred to as forbidden, while those only violating the $\Delta\mathbf{S} = 0$ rule are referred to as semi-forbidden. In our model, the transitions are described by their wavelengths, oscillator strengths f, and their radiative and hydrogen collisional broadening coefficients γ^r from Kurucz (2009) & $\Gamma_{\rm H}^{\rm col}$ from Anstee and O'Mara (1995); Barklem et al. (1998); Barklem and O'Mara (1997) ABO theory calculations when available and using Unsold (1955) approximation otherwise (See Appendix A).

Radiative line transitions can be collected from several available databases, namely that of NIST, Kurucz, the FERRUM project (Johansson et al., 2000) and VALD (versions 1,2, and 3) (Kupka et al., 2000; Kurucz, 1993; Piskunov et al., 1995; Ryabchikova et al., 2011) which is a collection of atomic and molecular transition parameters. These parameters include the oscillator strengths and broadening coefficients of the transitions regularly updated from the most up-to-date references. For our iron model atom, we used the VALD3 interface database to extract all the Fe I and Fe II radiative bound-bound transition accounting to 79594 Fe I lines and 113964 Fe II lines. The UV and IR lines (1568 lines) corresponding to transitions from and to the predicted high lying levels (Peterson and Kurucz, 2015) have also been included in the model, thus increasing the total number of Fe I lines to 81162.

4.2.1.1 Superlines

Individual transitions belonging to levels that have been combined to superlevels have also been combined into superlines (super transitions). The radiative rate of each super transition between two super levels I and J is calculated by summing over the rates of all existing transitions between all levels belonging to both super levels. The superline total oscillator

E_{low} (cm^{-1})	E_{up} (cm^{-1})	f	γ^{rad} (s^{-1})	$\Gamma^{H} = \sigma_{H}^{br} \cdot \alpha$	λ_{vac} (Å)
0.000	19624.0673	2.679×10^{-5}	5.36×10^{5}	204.59	5113.682
415.933	31566.8014	3.925×10^{-4}	3.34×10^{7}	270.26	3216.729
24565.1648	37043.8386	1.488×10^{-6}	5.70×10^{8}	389.24	7741.293
⋮					

Table 4.2: A few transitions from our iron superlevels atom with their lower and upper level energies, their oscillator strength f, their radiative broadening coefficient, the hydrogen Van der Waals collisional broadening cross-section σ_{H}^{br} (the integer part of the number, in Bohr radii squared units) and its velocity parameter α (the decimal part of the number), and their vacuum wavelength.

strength is a weighted average of gf-values of individual transitions and can be computed using the relation from Martin et al. (1988):

$$f_{IJ} = \frac{1}{\bar{\nu} \sum_i g_i} \sum_{i \in I} \sum_{j \in J} g_i \, \nu_{ij} \, f_{ij} \tag{4.3}$$

where $\bar{\nu}$ is the mean frequency of all the individual transition frequencies ν_{ij} belonging to the super transition from I to J.

Our final iron model includes 9816 FeI transitions and 16745 FeII transitions combined from the individual lines (Fig. 4.4 and Fig. 4.5). An example of a few transitions and their parameters is shown in table 4.2. The line broadening and line profiles are calculated as explained in Appendix A.

4.2.2 Bound-free transitions

Calculation of radiative bound-free photoionization and recombination rates requires the input of full cross-section tables as a function of the photon energies. The TOPBASE[3] (The Opacity Project (OP) collaboration, Cunto et al., 1993) database includes photoionization cross-section tables for a large number of atoms and ions. For Fe I levels, the photoionization cross-section tables calculated by Bautista (1997), and those for Fe II calculated by Nahar and Pradhan (1994) using the ab initio **R-*matrix*** close coupling (CC) approximation, were extracted from the NORAD[4] database (as they were not extractable from the TOPBASE website directly). These tables correspond to calculations for 52 LS Fe I terms (for $n \leq 10$ and $l \leq 9$) of spin multiplicities $\mathbf{2S+1}$=1,3,5 & 7, and for 83 Fe II LS terms of spin multiplicities $\mathbf{2S+1}$=2,4,6 & 8, coupled through photoionization to the ground Fe II and Fe III levels respectively.

The theoretical threshold ionization energies (expressed in Rydberg energy units)[5] in the former TOPBASE tables are, however, shifted from those in NIST (Verner et al., 1994), and thus also from our iron model energy levels. Thus, all the photoionization energies from TOPBASE for each level in the model were shifted to match the threshold ionization energies in NIST. In addition, the TOPBASE calculations of the cross-sections (in Mega-barn Mb) reproduce many

[3] http://cdsweb.u-strasbrg.fr/OP.htx
[4] http://www.astronomy.ohio-state.edu/∼csur/NORAD/norad.html
[5] The threshold energy of an atomic level is the minimum energy required for ionization.

auto-ionization resonances near the ionization thresholds (Fig. 4.6). These resonances are important for calculating the photoionization rate produced by radiation in spectral lines whose frequency positions coincide with the autoionization resonances. The sharp reasonances in the photoionization tables were smoothed and resampled in our iron model up to a maximum of 200 frequency points, as follows:

- The first 30 frequency point cross-sections corresponding to the photon energies closest to the threshold were all included in the tables.
- The remaining points were smoothed using a box smoothing method (moving average) over windows of 7 frequency points each, and then re-sampled depending on the standard deviation variation relative to the average of the cross-sections in frequency intervals as follows:

  1- The cross-sections were divided into intervals of 10 consecutive frequency points each.

  2- The average of the cross-sections of each interval was calculated.

  3- The standard deviation $\sigma_{\rm sd}$ relative to this average was also calculated.

  4- If $\sigma_{\rm sd}$ is less than 0.1 Mbarn, only the first and last points of each interval were chosen.

  5- If $\sigma_{\rm sd}$ is greater than 0.1 Mbarn, the intervals were further divided into two equal parts of 5 frequency points each.

  6- Steps 2,3 and 4 were repeated on each interval. If $\sigma_{\rm sd}$ is greater than 0.1 Mbarn, the $1^{\rm st}$, $3^{\rm rd}$ and $5^{\rm th}$ points of each interval were chosen.

Figure 4.6: Photoionization cross-section (in Mbarn) as a function of photon energy (in Ry) for the Fe I ground level, showing resonance peaks from TOPBASE data (solid black line). The smoothed re-sampled cross-sections (see Sect. 4.2.2) are shown (dashed red line), in addition to those calculated using Kramer's ν^{-3} hydrogenic approximation (Eqn. 2.37, dashed blue line).

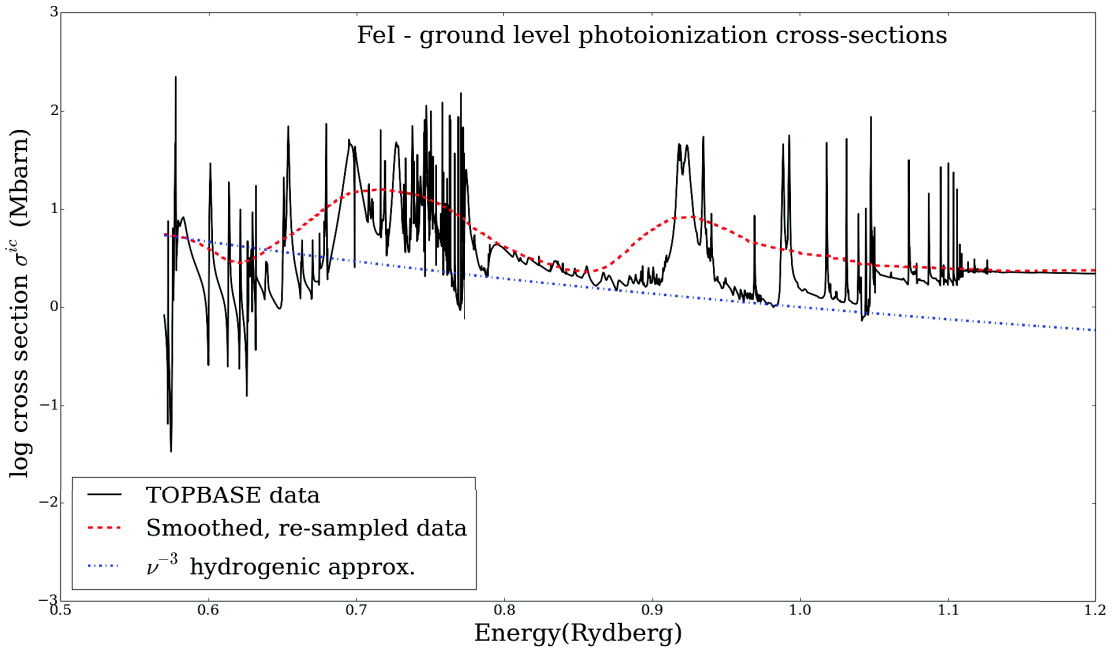

The bound-free radiative rate between a superlevel and the continuum is the summation over the bound-free rates of individual levels belonging to the superlevel to that continuum. Since the TOPBASE calculations do not include photoionization cross-section tables for fine structure transitions, the cross-sections of these latter were included as g-weighted average of their corresponding mean level cross-sections at each photon energy:

$$\sigma_i^{fs} = \frac{\sigma_i^{ml}\, g_{fs}}{g_{ml}} \tag{4.4}$$

where g_{fs}, σ_i^{fs}, g_{ml}, and σ_i^{ml} are the statistical weights and photoionization cross-sections for the fine structure and mean levels respectively.

Cross-section tables from TOPBASE were available for 158 levels of our iron model. For the remaining levels, Kramer's hydrogenic approximation was used. Table 4.3 shows part of the smoothed, re-sampled photoionization table for the Fe I ground state included in our iron model.

Ionizing wavelength (Å)	Photoionization cross-section (cm^2)
1598.75	2.68×10^{-20}
1571.63	4.06×10^{-18}
1545.42	9.88×10^{-19}
1520.06	2.00×10^{-18}
1495.53	5.33×10^{-19}
1305.84	1.33×10^{-19}
⋮	⋮

Table 4.3: Sample of the photoionization cross-sections (in cm^2) for the ground Fe I level as a function of the photon ionizing wavelengths (in Å) in our iron model. The first value is the cross-section at the threshold wavelength.

4.3 Collisional transitions

The calculation of the rates for collisional excitation and de-excitation as per Eqn. 2.41 requires the input of the collisional cross-sections as a function of the collisional perturber's temperature. Levels in our model atom are coupled via collisional with electrons and neutral hydrogen atoms. As has been explained in Chapter 3, the scarcity of the *ab initio* calculations for the Fe + e^- and Fe + H collisional cross-sections calls for the use of different classical or semi-classical approximations for each process as explained below.

4.3.1 electron Collisions

For Fe I, quantum electron-impact excitation rates have not yet been calculated for most transitions. Pelan and Berrington (1997) calculated effective excitation collisional strengths for the fine-structure transitions involving the ground term and the first excited term using the

R-matrix method. In our model atom, these results were included for the corresponding transitions, while for all other transitions, the excitation cross-sections were estimated using Seaton (1962a) impact parameter approximation for allowed transitions and that of Seaton (1962b) for forbidden transitions. The cross-sections were then averaged over a Maxwellian velocity distribution to obtain the rate coefficients $\langle \sigma \nu \rangle^{e-}$.

For Fe II, the situation is better, as Zhang and Pradhan (1995), and Bautista and Pradhan (1996) calculated rate coefficients for 10011 excitation transitions among 142 fine structure levels, using the ***R-matrix*** method. These calculations were also included in our model atom, and the impact parameter approximation of Seaton (1962a) was used for all other transitions. For bound-free transitions, Bely and van Regemorter (1970) approximation was used to calculate the collisional cross-sections for both Fe I and Fe II.

As for radiative rates, the collisional rate for a transition between two superlevels is calculated by summing the collisional rates of the transitions between individual levels belonging to these superlevels.

4.3.2 Hydrogen Collisions

For collisions with neutral H atom, being the main aim of this PhD dissertation, various recipes have been adopted which will be detailed in Chapters 6 and 7.

4.4 Background Opacities

Background line opacities are important to include in non-LTE calculations (Collet et al., 2005), as a large number of metals contribute to the UV "line haze" typically encountered in the spectra of cool stars.

`MULTI2.3` allows for the inclusion of background line opacities in addition to its built-in continuous opacities. Thus, opacity sampling tables were extracted using the MARCS code (Gustafsson et al., 2008) including all atomic and molecular lines, except for iron. The opacity sampling tables were calculated as function of the star's metallicity (See Chapter 5).

4.5 Comparison with published models

There have been a few different atomic models of iron built for the study of cool stars in recent years, namely that of Collet et al. (2005), Mashonkina et al. (2011) and Bergemann et al. (2012). It is thus interesting to compare these models to ours.

Collet et al. (2005) adopted an updated version of the iron model atom by Thévenin and Idiart (1999). Their model included energy levels extracted from the NIST database with fine structure multiplets (334 Fe I, 189 Fe II and 1 Fe III). The $gf-$values of their lines (3466 Fe I & 3440 Fe II) were adopted from Nave et al. (1994) and Kurucz and Bell (1995). Photoionization rates for the levels were included from the calculations of Bautista (1997) (TOPBASE) when available, and using the hydrogenic approximation for the rest. The levels were coupled with electrons & neutral hydrogen collisions using different recipes as shown in Table 4.4. For the H-collisions, they adopted different values of 0.001 & 1 for S_H using Steenbock and Holweger (1984) approach to Drawin's approximation in order to determine upper and lower limits of

non-LTE abundance corrections respectively.

Mashonkina et al. (2011) built a more complete iron model atom using the superlevel and supertransition algorithm, with all the experimental atomic levels and lines from NIST, in addition to predicted ones from Kurucz (2009)[6]. Ignoring all fine structures, their Fe I levels belong to 233 terms, which where combined into superlevels whenever their energy difference was less than 150 cm^{-1} for levels below 60 000 cm^{-1}, and whenever the difference was less than 210 cm^{-1} for levels above 60 000 cm^{-1}. Photoionization transitions were included using the cross-section tables from Bautista (1997) when available, and using Kramer's hydrogenic approximation when not. When available, quantum calculations for electron bound-bound transitions were adopted in their model from Pelan and Berrington (1997) for Fe I and from Zhang and Pradhan (1995) and Bautista and Pradhan (1996) for Fe II. Otherwise, the van Regemorter approximation was used. For forbidden e^- transitions, they adopted effective collisional strength values of Υ^e=1. Mashonkina generalized this assumption from the result of Pelan and Berrington (1997) for the FeI forbidden transition "$a^5D - a^5F$" at T=4000 K (Υ^e=0.98). For H collisions, they also used Steenbock and Holweger (1984) approximation of Drawin's formula multiplied by S_H=0, 0.1 and 1, calibrated on benchmark stars as a function of metallicity. For forbidden transitions, the Takeda (1994) approximation was used, which relates the H-collisional rates to their corresponding e^- - collisional rates using the formulation: $C_{\rm H} = C_{e^-}\sqrt{(m_e/m_{\rm H})}\,N_{\rm H}/N_{e^-}$, where $C_{\rm H}$ and C_{e^-} are the H and e^- - collisional rates respectively, $N_{\rm H}$ and N_{e^-} are H and e^- number densities.

Most recently, Bergemann et al. (2012) built another complete iron model atom, also using the super level algorithm and adopting a large number of levels and radiative lines from the NIST and Kurucz (2009) databases. Fine structure in their model were neglected for all levels except Fe I and Fe II ground levels. Their levels were combined into superlevels whenever they had the same parity and lied within an energy difference of 10 cm^{-1} below 54 000 cm^{-1}. Above this value all levels lying within 1000 cm^{-1} were combined into superlevels. In addition to the photoionization data from Bautista (1997), they claimed to have included more recent data from private communication with him. Their e^- and H-collisional transitions were calculated using different recipes specified in Table 4.4. They also adopted different S_H values (0.1 & 1) by calibrating their lines on different benchmark stars. For forbidden H-collisional transitions, they similarly adopted the Takeda (1994) approximation.

The comparison of the different recipes used in our model as compared to those of Collet et al. (2005), Mashonkina et al. (2011) and Bergemann et al. (2012) are tabulated in Table 4.4, along with all the corresponding references.

[6]http://kurucz.harvard.edu/atoms/2600/

Table 4.4: Atomic data and their references adopted in the FeI/FeII models of Collet et al. (2005) (COL05), Mashonkina et al. (2011) (MAS11) & Bergemann et al. (2012) (BER12). References denoted by letters in the table refer to: [a] Nave et al. (1994); [b] Kurucz (2009); [c] Peterson and Kurucz (2015) ; [d] Johansson et al. (2000); [e] Kurucz (1993); [f] Nave and Johansson (2013), [g] VALD3; [h] Bautista (1997); [i] Travis and Matsushima (1968); [j] NORAD (Nahar & Collaboration); [k] van Regemorter (1962); [l] Seaton (1962a); [m] cox (2000); [n] Steenbock and Holweger (1984); [o] Pelan and Berrington (1997); [p] Zhang and Pradhan (1995); [q] Bautista and Pradhan (1996); [r] Takeda (1994) ;[s] Seaton (1962b); [t] Lambert (1993); [u] Allen (1973)

Model	COL05	MAS11	BER12	Our iron model	notes
superlevels	no	yes	yes	yes	
Fe I levels	334 [1] [a]	233 terms [2] [a] [b]	296 terms [3] [a]	203 terms [a] [c] [4]	[1] up to 6.91 eV above ground FeI; [2] up to 7.89 eV above ground FeI; [3] 0.03 eV below ionization limit; [4] up to 8.392 above ground FeI
Fe II levels	189 [5] [d]	89 terms [6] [e]	112 terms [7] [d]	189 terms [8] [f]	[5] up to 16.5 eV above ground FeI; [6] up to 10 eV above ground FeII; [7] 2.72 below ionization limit; [8] up to 19.83 eV above ground FeI
Fe I radiative bound-bound transitions	3466 [a]	11958 [a] [b]	13888 [a]	9816 [c] [g]	
Fe II radiative bound-bound transitions	3440 [d]	1525 [e]	2316 [d]	16745 [g]	
Fe I radiative bound-free transitions	[h]	[h]	[h] [i]	[h] [j] [i]	
Fe II radiative bound-free transitions	[h]	[i]	[h] [i]	[h] [j] [i]	
Fe I e^- collisional bound-bound transitions (allowed)	[k] [9]	[k] [o]	[k]	[l] [o]	[9] all f values set to 10^{-3}
Fe II e^- collisional bound-bound transitions (allowed)	[k] [9]	[k] [p] [q]	[k]	[l] [p] [q]	
Fe I e^- collisional bound-bound transitions (forbidden)		Γ=1	[u]	[u]	
Fe II e^- collisional bound-bound transitions (forbidden)		Γ=1	[u]	[u]	
Fe I H collisional bound-bound transitions (allowed)	[n] [10]	[n] [12]	[n] [12]	[t] [11]	[10] S_H =0.001 & 1; [11] f=1; [12] S_H =0, 0.1 & 1
Fe II H collisional bound-bound transitions (allowed)	[n] [10]	[n] [12]	[n] [12]	[t] [11]	
Fe I H collisional bound-bound transitions (forbidden)		[r]	[r]	[t] [11]	
Fe II H collisional bound-bound transitions (forbidden)		[r]	[r]	[t] [11]	
Fe I e^- collisional bound-free transitions	[m]	[s] [13]	[s]	[s]	[13] Gaunt factor $\bar{g}$=0.1
Fe I H collisional bound-free transitions	[n]	[n]	[n]	[t]	
Fe II e^- collisional bound-free transitions	[m]	[s] [14]	[s]	[s]	[14] Gaunt factor $\bar{g}$=0.2
Fe II H collisional bound-free transitions	[n]	[n]	[n]	[t]	
Fe I H collisional charge transfer transitions				[t] [15]	[15] extended in this work to charge transfer process
Fe II H collisional charge transfer transitions				[t] [15]	

Figure 4.2: Grotrian diagram of FeI levels in our final model atom. The energies of the levels (y-axis, in eV) are displayed as a function of their spectroscopic terms (x-axis). Cyan colored solid lines correspond to fine structure levels of the ground and first ionized levels, black solid lines below 5 eV correspond to mean levels, while those above 5 eV correspond to superlevels. Only labels of the levels below 6 eV are included to avoid crowding.

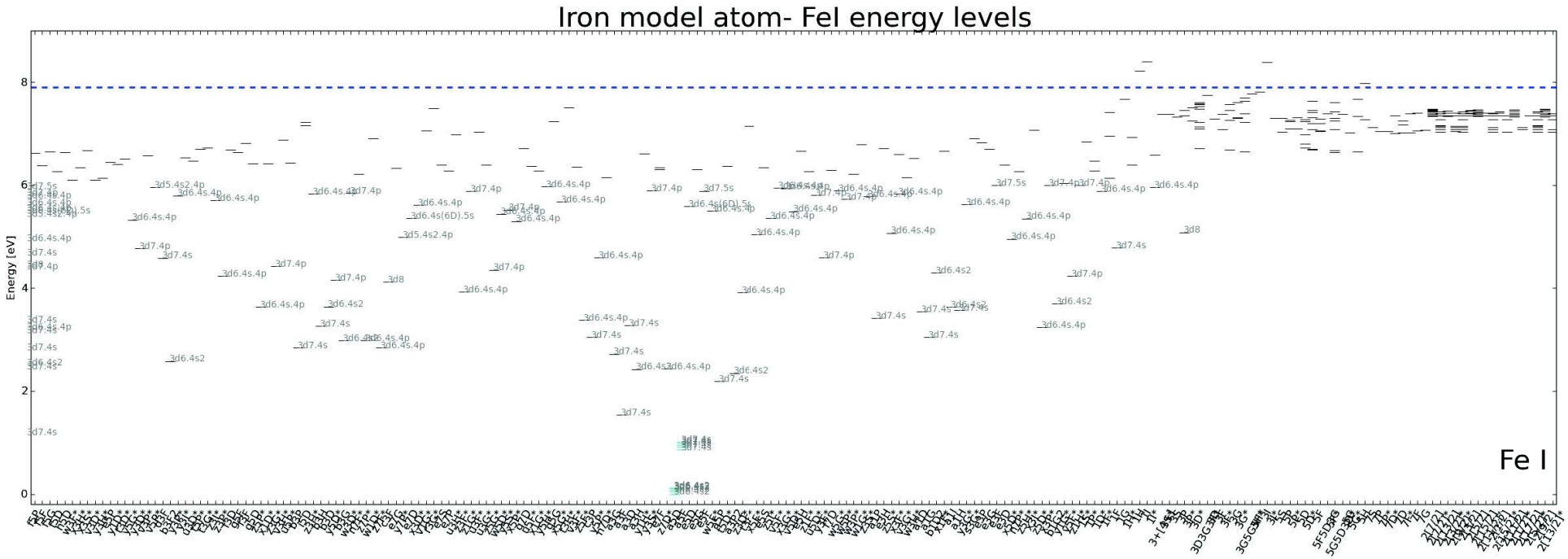

Figure 4.3: Grotrian diagram of FeII levels in our final model atom. The energies of the levels relative to the FeII ground state at 0eV (y-axis, in eV) are displayed as a function of their spectroscopic terms (x-axis). Colors have the same meaning as those in Fig. 5.2. Only labels of the levels below 12 eV are included to avoid crowding.

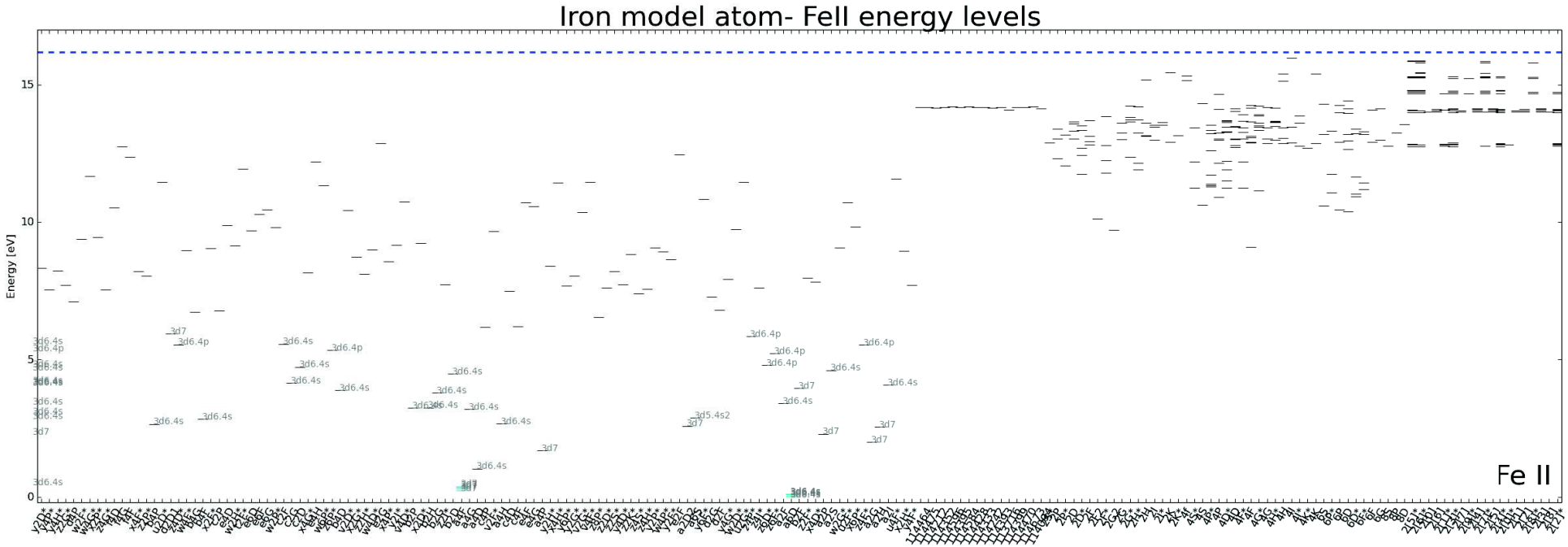

Figure 4.4: Grotrian diagram for allowed FeI bound-bound radiative transitions in our final model atom. Gray lines display super transitions between different super levels.

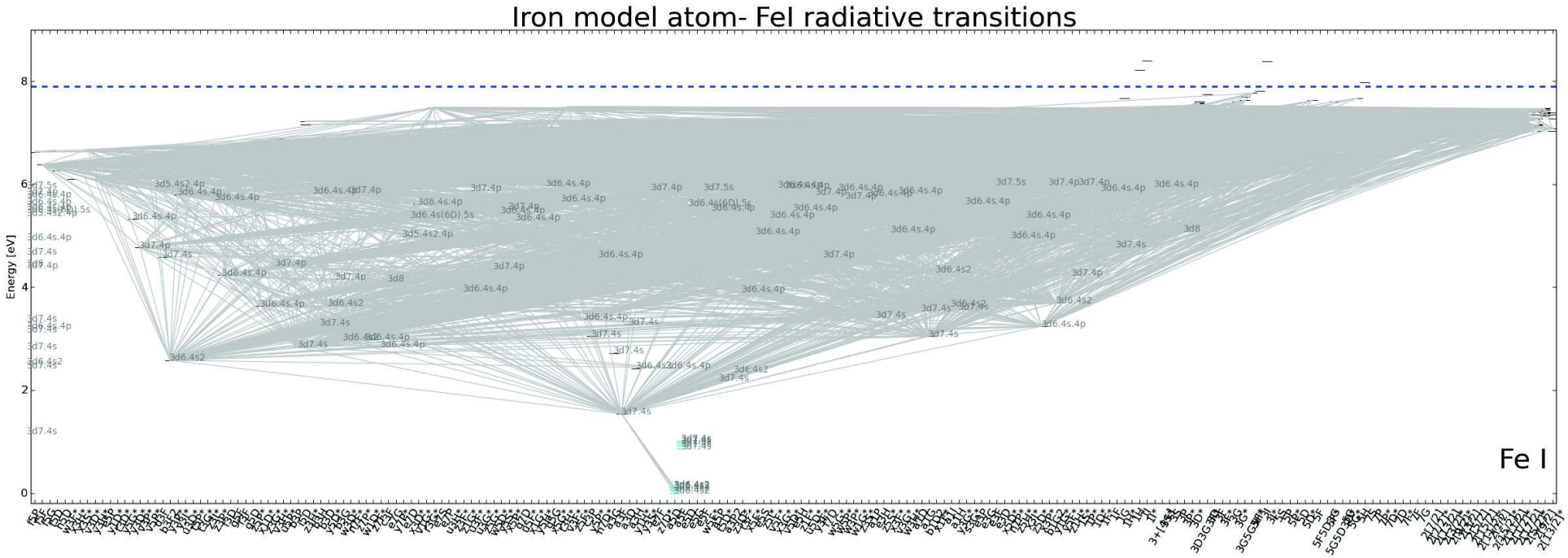

Figure 4.5: Grotrian diagram of allowed FeII bound-bound radiative transitions in our final model atom. Colors have the same meaning as in Fig. 5.2 & Fig. 5.4.

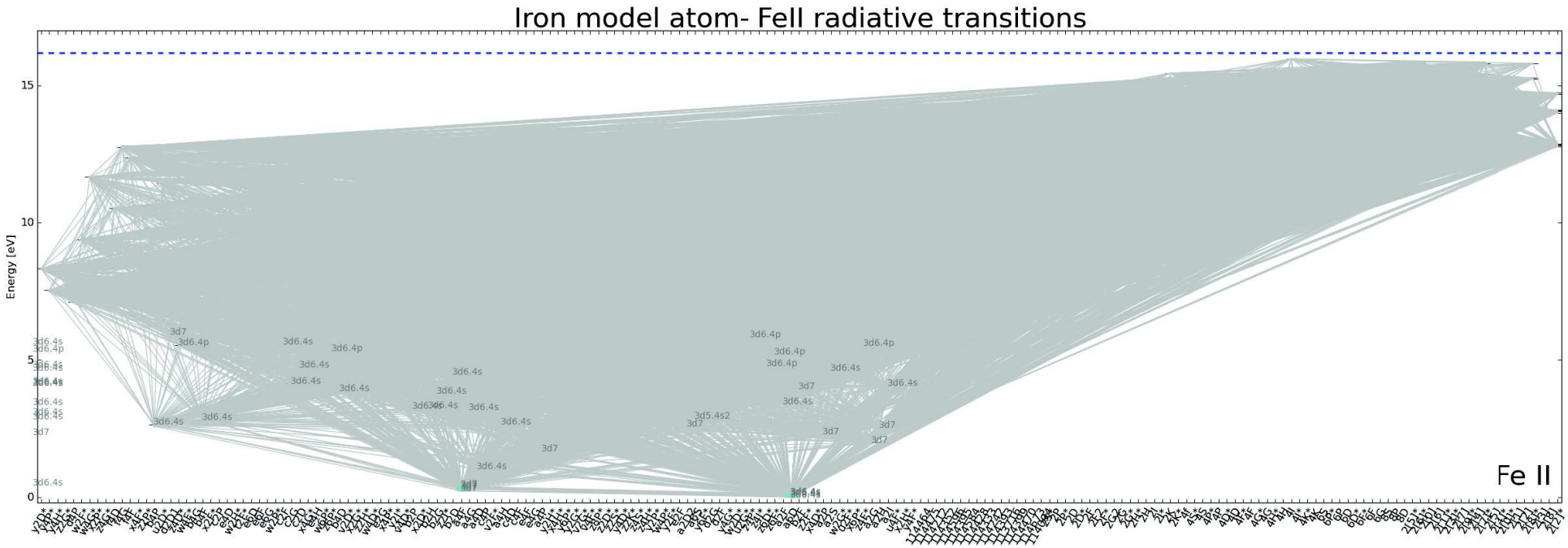

5 Benchmark stars as probes of spectroscopic studies

The state of a given star is set by a handful of fundamental parameters such as its mass, age, and its hydrogen, helium & metal content. These quantities, not directly observable, can be linked to secondary stellar properties comprising generally the effective temperature, luminosity, surface gravity, and the metallicity (or its proxy [Fe/H], which denotes the iron content relative to hydrogen) through well-defined relations, in addition to dynamic properties such as its projected rotational velocity (ν sin$i$) [1]

The main aim of the present dissertation work is to reduce the uncertainties in Fe abundance determinations to a limit which places useful constraints on stellar and Galactic evolutionary models. Thus an essential part of the method we apply, is to start from accurate stellar parameters for these stars, which can be provided by different methods discussed in the few sections below. With the good knowledge of these parameters, the spectroscopic determination of the abundances of iron will allow precise calibration of the non-LTE calculations independently of most parameter assumptions.

An example of a good set of cool stars, for which well-known and well-determined parameters exist, is the Gaia-ESO survey **FGK-Benchmark stars** (Heiter et al., 2015a; Jofré et al., 2014) which present a common set of bright (V magnitudes ranging between 0 and 8) calibration stars, covering different regions of the HR diagram and spanning a wide range in metallicity, temperature and surface gravities. This makes them an ideal set for testing our method.

In this chapter, a brief description of the methods used to derive the fundamental atmospheric parameters of cool stars will be presented in 5.1, followed by presenting a sample of Benchmark (standard/reference) stars with well-determined parameters in 5.2, upon which our calculations, methods and calibrations were tested (for the method and results see chapters 6 and 7).

5.1 Stellar parameters

The input effective temperature $T_{\rm eff}$ and surface gravity g of the star, in addition to the metallicity [Fe/H] and micro-turbulent velocity ξ_t (hereafter referred to as atmospheric fundamental parameters, or AFP), are the prerequisites to any detailed abundance or spectral synthesis analysis. In the following sections, some common methods used to determine the AFP of cool stars are briefly explained for $T_{\rm eff}$, log g and [Fe/H].

[1] ν sin$i$ is referred to as the line of sight rotational velocity of the star, where ν is the rotational velocity at the equator of the star and i is the angle of inclination between its axis of inclination and the line of sight toward the Earth.

5.1.1 Effective temperature $T_{\rm eff}$

5.1.1.1 Angular diameter

The effective temperature $T_{\rm eff}$ of a star is defined to be the temperature of a black body emitting the same total radiative flux $F_{\rm bol}$, defined by the Stefan-Boltzmann law:

$$F_{\rm bol} = \sigma_{\rm SB} T_{\rm eff}^4 \tag{5.1}$$

where $\sigma_{\rm SB}$ is the Stefan-Boltzmann constant. This relation is commonly written in terms of the luminosity of the star $L_\star$ as:

$$L_\star = 4\pi R_\star^2\, \sigma_{\rm SB} T_{\rm eff}^4 \tag{5.2}$$

where $R_\star$ is the radius of the star. It is possible to link $T_{\rm eff}$ to the angular diameter of the star $\theta_{\rm D\star}$, a measurable quantity using interferometry, by making use of the concept that the flux at the stellar surface of radius R$_\star$ and that at the Earth, $f_{\rm bol}$ [2] at a distance d from the star, satisfy the relation: $F_{\rm bol} R_\star^2 = f_{\rm bol} d^2$. Plugging this relation into Eqn. 5.2, ignoring interstellar absorption, allows to write $T_{\rm eff}$ in terms of the measurable quantities $\theta_{D\star}$ and $F_{\rm bol}$ such as:

$$T_{\rm eff} = \left(\frac{f_{\rm bol}}{\sigma_{\rm SB}}\right)^{1/4} \left(\frac{\theta_{\rm D\star}}{2}\right)^{1/2} \tag{5.3}$$

where $\theta_{\rm D\star} = 2R_\star/d$.
This method, challenging due to the small apparent sizes of stars in the sky, has been improving rapidly due to measurements by CHARA [3] and other interferometers such as the VLTI[4] (Kervella and Fouqué, 2008) which have provided angular diameters with unprecedented quality for many giants and dwarf stars (McAlister et al., 2005), in addition to the available $f_{\rm bol}$ measurements of a large number of these stars from the integration of their observed spectral energy distribution (SED).

5.1.1.2 IRFM

The Infra-Red Flux Method (hereafter IRFM) was introduced by Blackwell et al. (1979). The basic idea is to compare the ratio $\mathcal{R}_{\rm obs}$ of the bolometric flux $f_{\rm bol}$ to the (IR) flux obtained at Earth $f_{\rm IR}$ to that ratio obtained at the surface of the star denoted $\mathcal{R}_{\rm theo}$, which is determined theoretically for a set of input parameters ($T_{\rm eff}$, log g and [Fe/H]). In this manner, the $T_{\rm eff}$ input is varied and the method is iterated until $\mathcal{R}_{\rm obs} = \mathcal{R}_{\rm theo}$. $T_{\rm eff}$ is then calculated using Stefan-Boltzmann Eqn. 5.2:

$$T_{\rm eff} = \left(\frac{f_{\rm bol}\, F_{\rm IR}({\rm theo})}{\sigma_{\rm SB}\, f_{\rm IR}}\right)^{1/4} \tag{5.4}$$

where $F_{\rm IR}$(theo) and $f_{\rm IR}$ are respectively the (IR) theoretical flux at the surface of the star and that observed at Earth.

This method is argued to be almost model independent (Casagrande et al., 2006) and useful to measure the effective temperature for large sample of stars since for those with $T_{\rm eff}$ greater than 4500 K, the (IR) SED in the Rayleigh-Jeans tail of the Plank function
(at $\lambda > 1.2\mu m$) determined via photometry is largely dominated by the continuum and are thus linearly related to $T_{\rm eff}$ (Casagrande et al., 2010).

The advantage for using the IRFM is the availability of the (IR) photometric data for a very large number of stars provided by the 2MASS [5] telescope with all-sky coverage. In addition,

[2] The term $f_{\rm bol}$ refers to the bolometric flux which is the total radiative flux from the star received at the Earth.
[3] Center for High Angular Resolution Astronomy: http://www.chara.gsu.edu/
[4] The Very Large Telescope Interferometer: https://www.eso.org/sci/facilities/paranal/telescopes/vlti.html
[5] The Two Micron All Sky Survey at IPAC: http://www.ipac.caltech.edu/2mass/

it has been shown that its results have a high internal accuracy, and are independent from non-LTE effects and granulation (Asplund and García Pérez, 2001; Casagrande, 2009). On the other hand, inaccurate reddening and absolute flux calibrations can induce errors as large as 100K (Casagrande et al., 2006).

Casagrande et al. (2010) used this method to compare $\theta_{\rm D}$ determined from the IRFM to those measured via interferometry (Eqn. 5.3) and found a good agreement for most stars, though a difference of up to 10% can be found for some.

5.1.1.3 Excitation equilibrium

This method is based on the idea that if local thermodynamical equilibrium (LTE) conditions are attained (Sec. 2.1.4.1), then the fraction of ionized to neutral species (specifically iron FeII/FeI) is given by the ionization equilibrium (See Saha equation in Sec. 2.25), and that the FeI and FeII energy level populations are governed by the Boltzmann equation 2.24. Consequently, the abundances derived from a set of lines, should not depend on the ionization stage, or on the excitation energy of the lines. Therefore the $T_{\rm eff}$ is determined iteratively by the absence of trend in abundances of FeI and FeII lines with their corresponding excitation potentials [6].

While this method is found to yield good results for a sample of Solar twins with similar properties (Ramírez et al., 2009), it is highly model-dependent and is prone to non-LTE effects (sec. 2.1.4.2) and inhomogeneities which can lead to serious under- or over- estimation of $T_{\rm eff}$ in some stars especially metal-poor ones.

5.1.2 Surface gravity log g

The surface gravity of a star of radius $R_\star$ and mass $M_\star$ is:

$$g = \left(G \frac{M_\star}{R_\star^2} \right) \tag{5.5}$$

most often denoted in logarithmic form as log g. Different methods are used to determine the surface gravities of stars, from which we briefly describe the spectroscopic ionization equilibrium and the asteroseimic methods below.

5.1.2.1 Ionization equilibrium

The most commonly used method to determine log g is the ionization equilibrium of FeI/FeII lines as a function of measured equivalent width (a measurement of the strength of the line). This is based on the fact that increasing gravity increases gas and electron pressures, which cause a change in the ratio of the line absorbers to the continuous opacity, which in turn affects the line strengths (by changing the ionization equilibrium of FeII/FeI). Thus the line strengths are sensitive to log g, and this dependence is used to determine log g of the model by varying its input values until there is agreement between FeI and FeII abundance with the equivalent widths.

A significant contribution to the uncertainty of this method is due to the correlation between log g and $T_{\rm eff}$ in the spectral analysis of the equivalent widths, and in which the abundance

[6] Excitation potential (EP) of an absorption line is the energy of its lower level.

calculations can also be prone to non-LTE and 3D atmospheric model effects. These uncertainties can result in a difference of log g up to 0.2 dex (Hekker and Meléndez, 2007; Morel and Miglio, 2012).

5.1.2.2 Asteroseismology

In the past decade, asteroseismology has become possible for stars other than the Sun, and has revolutionized our understanding of stellar interiors. The concept is that stars show pulsation variabilities which support standing waves whose frequencies and amplitudes depend on the stellar structure. Two types of modes have been identified: acoustic *p-mode* waves, in which the restoring force is pressure and buoyancy, *g-mode* waves, where the restoring force is gravity, and whose excitation origin is believed to be turbulent convections.
p-modes are the primary observable modes propagating in the envelopes of solar-like stars which give rise to displacements at the stellar surface, resulting in changes in the brightness which can be detected via photometric methods, or radial velocity shifts in spectral lines that can be detected via spectroscopic methods.

The patterns of the waves at the surface of the star can be described by the spherical wave equation:

$$\nabla^2\psi = \frac{1}{c^2}\frac{\mathrm{d}^2\psi}{\mathrm{d}t^2} \tag{5.6}$$

whose eigenvalues are known as the radial order n (the number of nodes seen from the center to the surface radially), the angular degree, l, and the azimuthal order, m. Modes of low angular degrees, l, propagate more deeply into the stellar interior, while modes of higher degrees propagate closer to the stellar surface (see Fig. 5.1). In this manner, each mode samples the conditions at a different depth in the star, and with enough modes, we can invert the problem and determine the stellar sound speed profiles, which in turn depends on pressure, density, and composition (See, for e.g., Christensen-Dalsgaard, 1991).
Moreover, the spacing between adjacent radial orders and the spacing between modes of different angular degrees in a power-frequency spectrum (Fig. 5.2) can be related to the fundamental parameters of the star. The spacing between adjacent radial orders of the same angular degree is termed the large frequency spacing, $\Delta\nu_{n,l}$, and is defined as:

$$\Delta\nu_{n,l} = \nu_{n,l} - \nu_{n-1,l} \tag{5.7}$$

The small frequency spacing, $\delta\nu_{n,l}$ is that between the pairs of even and odd modes, which is defined as:

$$\delta\nu_{n,l} = \nu_{n,l} - \nu_{n-1,l+2} \tag{5.8}$$

Scaling relations with stellar parameters
The average large frequency separation $\Delta\nu_\star$ of a star undergoing solar-like oscillations is directly proportional to the square root of its density $\sqrt{\rho_\star}$) (Kjeldsen and Bedding, 1995), which can be compared to the well known solar value[7] to determine the mass $M_\star$ and radius $R_\star$ of the star via:

$$\begin{aligned}\Delta\nu_\star &\propto \sqrt{\rho_\star} \\ &\propto \left(\frac{M_\star}{R_\star^3}\right)^{1/2} \\ &= \frac{(M_\star/M_\odot)^{1/2}}{(R\star/R_\odot)^{3/2}}\,\Delta\nu_\odot\end{aligned} \tag{5.9}$$

[7]The large frequency spacing for the Sun varies with both n and l, but is in general around 135.229 μHz (Bazot et al., 2011).

Figure 5.1: Examples of oscillatory surface displacements (i.e. angular components) for a number of modes with different values of m and l.

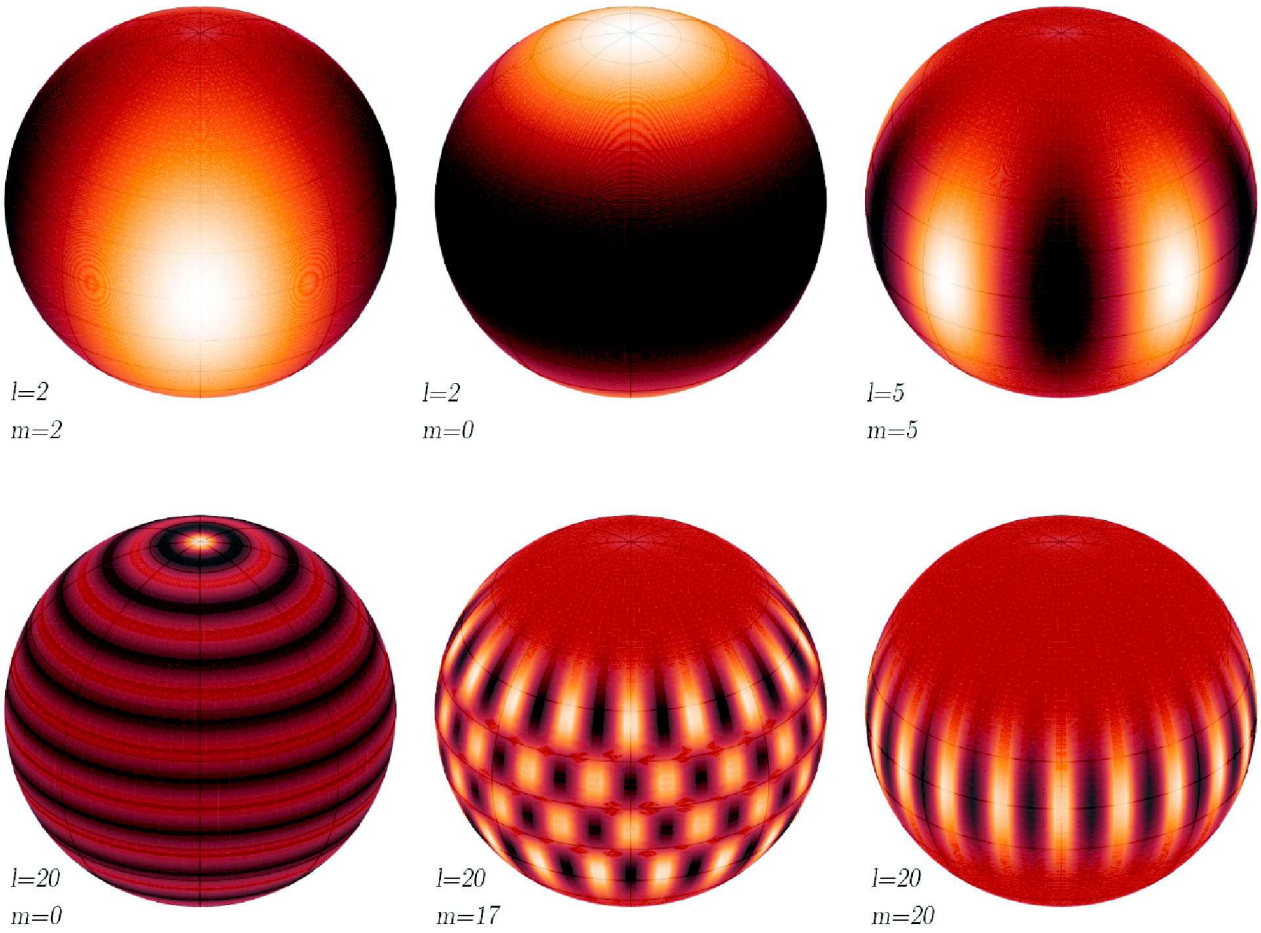

where $M_\odot$, $R_\odot$ and $\Delta\nu_\odot$ are the solar values for mass, radius and large frequency separation respectively.

In addition, for a given value of effective temperature $T_{\rm eff}$ of the star, the frequency at maximum power $\nu_{\rm max}$ of the oscillations is also related to $M_\star$ & $R_\star$ (Belkacem et al., 2011; Brown et al., 1991), such that:

$$\nu_{\rm max\star} \simeq \frac{M_\star/M_\odot}{(R_\star/R_\odot)^2\,(T_{\rm eff\star}/T_{\rm eff\odot})^{1/2}}\,\nu_{\rm max\odot} \tag{5.10}$$

where $\nu_{\rm max\odot} = 3100\,\mu$Hz (Mosser et al., 2013) is the solar maximum power frequency and $T_{\rm eff\odot} = 5777$ K is the solar effective temperature.

Thus the correlation between $\Delta\nu$, $\nu_{\rm max}$ and $T_{\rm eff}$ allows the determination of the mass and radius of the star from which the surface gravity can be calculated.

Two methods are generally used to determine $\log g$: either directly from $\nu_{\rm max} \propto g/\sqrt{T_{\rm eff}}$, where a 0.4% change in $\log g$ is obtained upon a 1% change in $\nu_{\rm max}$ (Hekker et al., 2011), or indirectly by using grid-based modeling, which is based on searching for the "best model" among a large grid of models for a given set of observables ($\Delta\nu$, $\nu_{\rm max}$, $T_{\rm eff}$ and metallicity [Fe/H]) (Gai et al., 2011). The advantage of using asteroseismic $\log g$ as input for spectral synthesis models is that it is not prone to non-LTE and 3D effects, and is not correlated with $T_{\rm eff}$ as is the case

Figure 5.2: Solar power-frequency spectrum showing angular degrees l=0,1,2,3 and their respective small and large frequency separations. Taken from BiSON dataset (Asteroseismology of red giant stars, Neil James Tarrant, PhD dissertation, 2010)

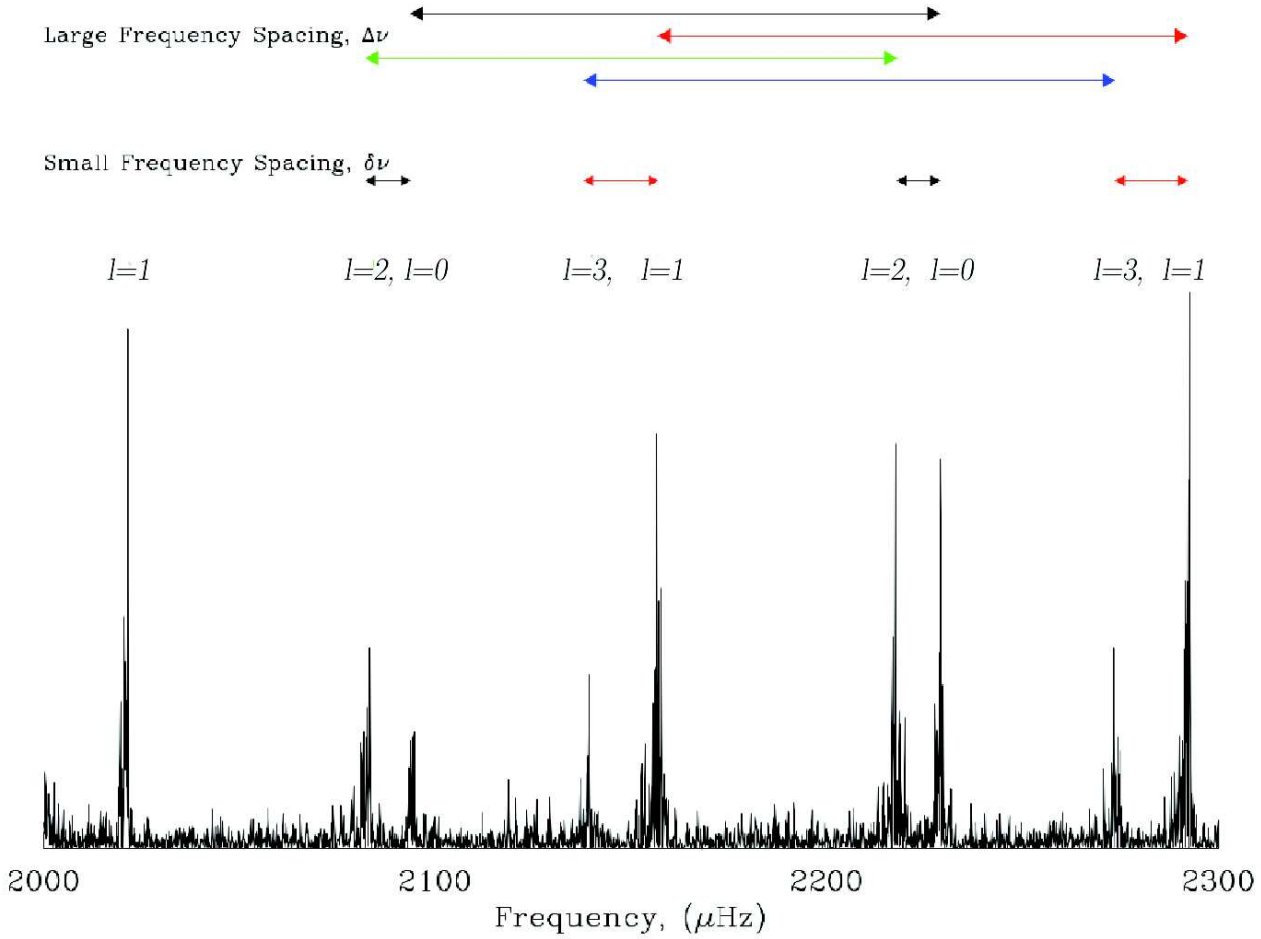

in spectroscopic models, where quoted uncertainties of the asteroseismic log g are often an order of magnitude lower than those quoted in spectroscopic analyses, indicating more precise values (Gai et al., 2011).
Brogaard et al. (2015), tested the accuracy of asteroseismic log g by comparing to those determined from detached eclipsing binaries in open clusters in the *Kepler* & *CoRoT* fields (NGC 6791, NGC 6819, ...) and found an accordance up to 0.01 dex.

Over the past few years the number of stars with detected solar-like oscillations has increased considerably, from a few to over ten thousand thanks to missions like *Kepler* [8] and *CoRoT* [9] (Convection, Rotation and planetary Transits) (NASA's and CNES[10]-ESA missions respectively).

[8]http://kepler.nasa.gov/Mission
[9]http://sci.esa.int/corot/
[10]https://cnes.fr/fr

5.1.3 Metallicity [Fe/H]

By metals, we denote all chemical elements except hydrogen and helium. The Solar chemical composition comprises $\sim$ 73% hydrogen, $\sim$ 25% helium and $\sim$ 2% metals (Asplund et al., 2009).
A star's metallicity can be indirectly determined from the star's spectral line features. It is generally defined to be equal to the abundance of iron (Fe) compared to its hydrogen (H) abundance, normalized to the solar abundance on a logarithmic scale:

$$[\mathrm{Fe/H}] = \log(\mathrm{n_{Fe}/n_H}) - \log(\mathrm{n_{Fe}/n_H})_\odot \tag{5.11}$$

where $\mathrm{n_{Fe}}$ and $\mathrm{n_H}$ are the number densities of Fe and H respectively. Iron is chosen as a proxy of the total metal content due to the wealth of iron lines in most stars spectra, thus making them easily measurable as compared to other metals.

Abundance determination:
The absolute abundance of a chemical element species A is often defined on the following scale:

$$\log \varepsilon(A) = \log(\mathrm{n_A/n_H}) + 12 \tag{5.12}$$

One method of determining the abundances is by using a curve of growth (cog) method, which provides a relation between the chemical abundance of an element and the line equivalent width which is defined as:

$$\mathrm{W}_\lambda = \int_0^\infty \frac{I_\lambda - I_{\mathrm{cont}}}{I_{\mathrm{cont}}}\,\mathrm{d}\lambda \tag{5.13}$$

where I_λ and I_{cont} are the respective intensities of the spectral line at a wavelength λ and at the continuum, which can also be defined as the width of a rectangle of length I_{cont} and has the same area as that beneath the corresponding spectral line (Fig. 5.3). Another commonly used abundance determination method is the iterative spectral fitting, which will not be discussed in depth as it was not used in this dissertation.

The curve of growth thus provides a relation between the equivalent width of the spectral line and the number of absorbing atoms $\log A$ of a chemical species. This relation W_λ/λ vs. $\log A$ depends on the strength of the spectral line which is demonstrated in Fig. 5.4. It can generally be divided into 3 parts:

- a linear part which corresponds to weak lines (small W_λ): the equivalent width is proportional to $\log A$
- a "plateau" part where the central depth of the line approaches its maximum value due to saturation, and the line strength grows asymptotically towards a constant value.
- a damping part which corresponds to strong lines: the equivalent width is proportional to $\sqrt{\log A}$.

The elemental abundance is then calculated using the (cog) method by computing synthetic equivalent widths using spectral synthesis codes[11] for different inputs of log(A), and then the actual abundance is interpolated to the measured equivalent width value of the line.

[11] In this dissertation, **MULTI2.3** (Carlsson, 1986) was used for spectral synthesis and equivalent width calculations. See appendix B for details on the code and chapter 2 for details on the theory of stellar atmospheres employed by the code.

Figure 5.3: Equivalent width of a spectral line and its equivalent area.

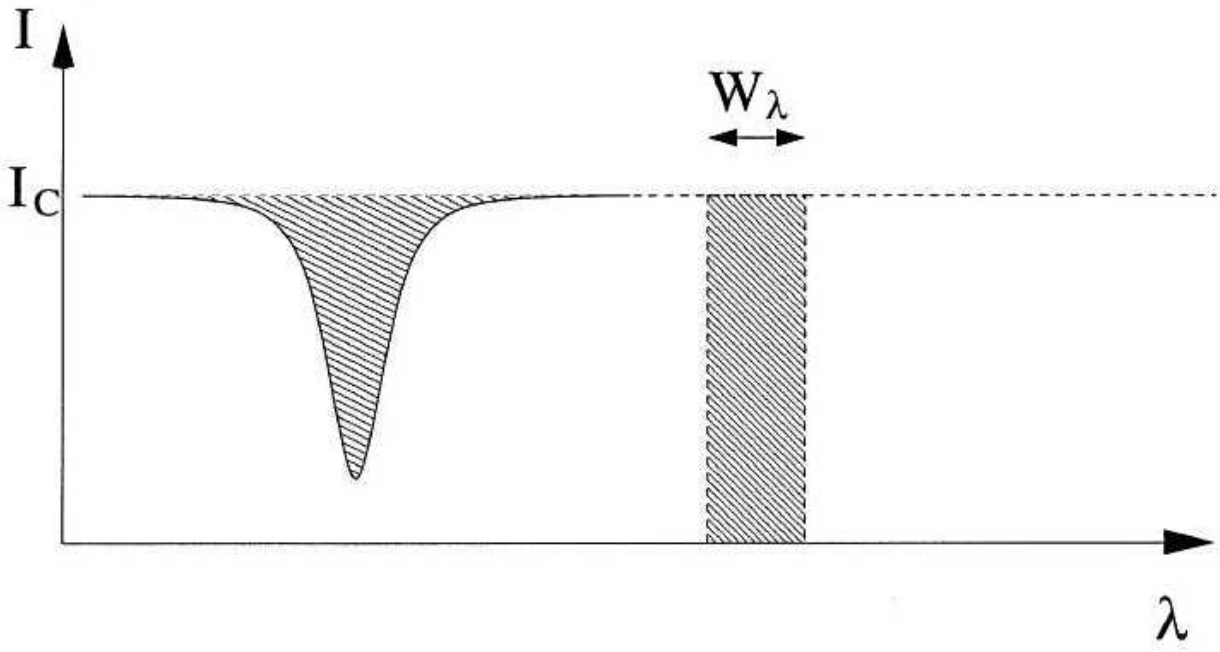

The effect of microturbulence ξ_t:
The observed equivalent widths of spectral lines are found to be greater than predicted by models when calculated using just thermal and damping broadening parameters in the calculations of the synthetic spectral lines (equivalent widths) (see appendix A). This difference is due to the micro-turbulent velocity which is an ad-hoc free parameter which has to be added to the calculations. Its values typically range between 0.5 and 5 km/sec. The micro-turbulent velocity is determined to be the value of ξ_t that makes the strong FeI line abundances independent of W_λ.

5.2 Benchmark stars

The determination and calibration of stellar abundances through spectral line synthesis in the light of the present work, requires minimizing the inaccuracies from input data in the calculations. As demonstrated in the previous sections, these calculations are highly affected by the input AFP and their determination methods which alter the atmospheric thermal structure of the models, and can lead to serious inaccuracies in abundance determination and calibration.

This calibration also requires a set of reference stars spanning over a large parameter space to homogenize and validate the method we are proposing and using. For these reasons, the FGK *Gaia*-ESO Benchmark stars (GBS) proposed by Heiter et al. (2015a), Blanco-Cuaresma et al. (2014) & Jofré et al. (2014) have been adopted as test benchs of our methods and in our calculations. Most of them will be observed by *Gaia*[12] (Perryman et al., 2001; Turon et al., 2005), which has the goal of providing parallaxes and proper motions of exquisite precision for 1 billion stars of our Galaxy. It is complemented by a large set of ground-based spectroscopic and spectrophotometric observations which are led and analyzed by international team collaborations such as the *Gaia*-ESO survey (Gilmore et al., 2012a,b), RAVE (Steinmetz et al.,

[12]http://sci.esa.int/gaia/

Figure 5.4: Curve of growth: showing the relation between W_λ/λ and the abundance (number of absorbing atoms) $\log A$ of the corresponding species (upper panel) for different line strengths (lower panel) from Gray (2008).

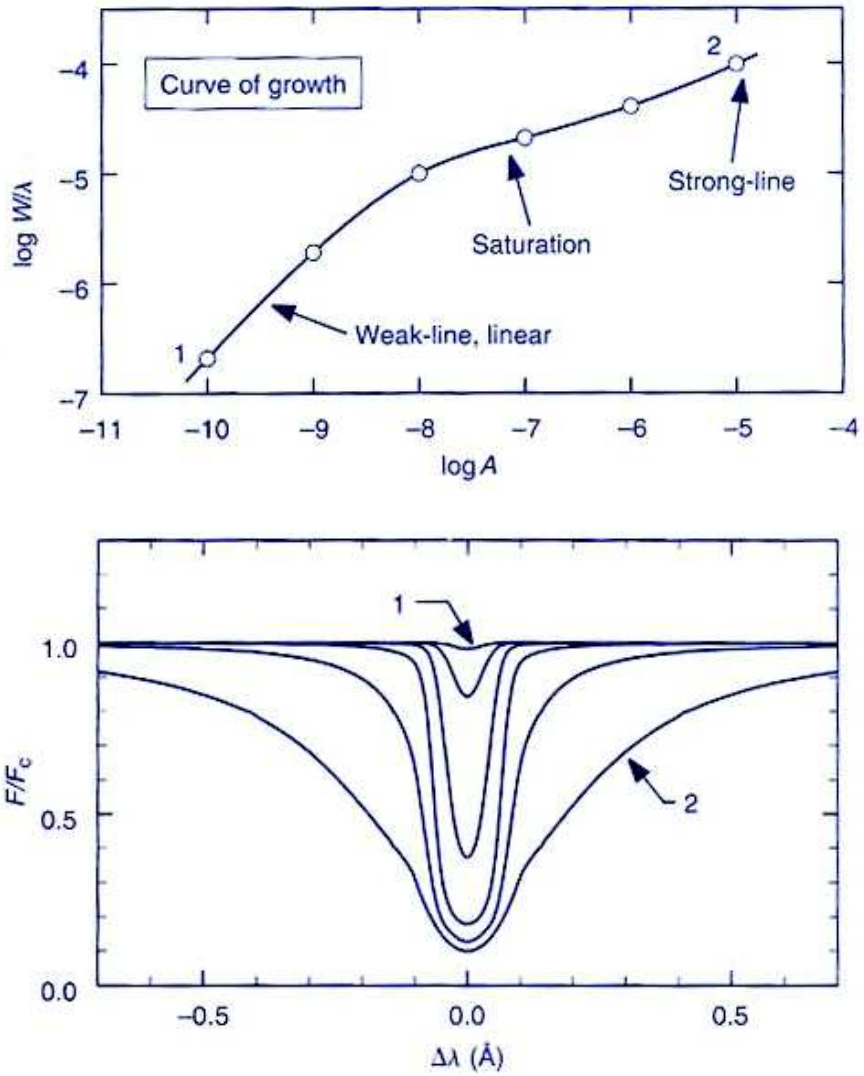

2006), APOGEE (Allende Prieto et al., 2008) and GALAH (De Silva et al., 2015).

5.2.1 General description and selection criteria

The GBS stars are reference objects for the calibration of all the observed *Gaia* stars. They are therefore carefully studied from the ground. In addition, they will also serve to calibrate the different methods and input data used in the afore-mentioned complementary spectroscopic ground-based surveys to *Gaia*.

They have been chosen such that their AFP values cover a wide range of $T_{\rm eff}$, log g and [Fe/H] parameter space and thus representing different stellar types and populations. In addition, they were selected to have well-determined angular diameters $\theta_{\rm D}$ and bolometric fluxes $f_{\rm bol}$, from which $T_{\rm eff}$ was calculated, and homogeneous mass determinations from stellar-evolution models from which their log g were determined, or for which asteroseismic log g from *Kepler* and *CoRoT* existed, thus assuring AFP values as independent from spectroscopic methods as possible.

Another criterion for choosing these stars, is whether they have been subjected to frequent spectroscopic investigation, which allowed for the comparison of their parameters determined via different methods.
Their V magnitudes range from 0 to 8 mag, and their positions are evenly distributed along the celestial equator, with declinations within $\pm 30^{\circ}$.

The list of stars used in this work consisted of 30 stars out of 34 suggested FGK GBS from the Heiter et al. (2015a) paper, for which we had available spectra from the *Gaia*-ESO collaboration. The spectra were collected using the UVES [13] spectrograph at the VLT [14]. The sources of the UVES spectra are from the Advanced Data Products collection of the ESO Science Archive Facility, which were reduced by the standard UVES pipeline version 3.2 (Ballester et al., 2000), and from the UVES Paranal Observatory Project UVES-POP library which were reduced with tools written especially for that library (Bagnulo et al., 2003).
Table 5.1 lists their names and IDs, right ascensions ($\alpha_{\rm RA}$), declinations ($\delta_{\rm DEC}$) and spectral types extracted from the SIMBAD[15] database, and their V magnitudes extracted from GCPD [16] (General Catalog of Photometric Data).

5.2.2 $T_{\rm eff}$ determination

The stars $T_{\rm eff}$ values were determined using Eqn. 5.3, where $\theta_{\rm D}$ and $\rm F_{bol}$ were extracted from the literature when available, from interferometric measurements and absolute flux measurements respectively (see Heiter et al. (2015a) for more details on the sources).

For μ Leo and HD107328, the angular diameters were indirectly determined by Cohen et al. (1999), by scaling their (IR) photometry to absolute flux calibrations in the (IR) of reference stars with similar types (using Arcturus for μ Leo and β Gem for HD107283). For HD22879, HD84937, ϵ For and μ Ara the surface-brightness relations by Kervella et al. (2004) were used to estimate the angular diameters, in which the interstellar extinction was considered negligible since these stars lie within 40 pc, where interstellar reddening 3D maps show negligible values (Lallement et al., 2014).

Indirect measurements of $f_{\rm bol}$ were derived using the V magnitudes and the bolometric corrections in the visible $\rm BC_V$ of the stars using the relation:

$$f_{\rm bol} = \frac{1}{4\pi(10pc)^2} L_0 \, 10^{-0.4(V+BC_V)} \tag{5.14}$$

where $L_0 = 3.055 \times 10^{28}$ W is the zero-point luminosity (Andersen, 1999). The $\rm BC_V$ used were adopted from Alonso et al. (1999) with an uncertainty of 0.05 mag.

[13] http://www.eso.org/sci/facilities/paranal/instruments/uves.html
[14] http://www.eso.org/public/teles-instr/vlt/
[15] http://simbad.u-strasbg.fr/simbad/
[16] http://obswww.unige.ch/gcpd/gcpd.html (Mermilliod et al., 1997)

Star name (ID)	$\alpha_{\rm RA}$ (J2000)	$\delta_{\rm DEC}$ (J2000)	Spectral Type	$V_{\rm mag}$
18 Sco	16 15 37.269	-08 22 09.99	G2Va	5.5
61 Cyg B	21 06 55.264	+38 44 31.40	K7V	6.0
α Cen A	14 39 36.494	-60 50 02.37	G2V	0.0
α Cet	03 02 16.773	+04 05 23.06	M1.5IIIa	2.5
α Tau	04 35 55.239	+16 30 33.49	K5III	0.9
Arcturus	14 15 39.672	+19 10 56.67	K1.5III	-0.1
β Ara	17 25 17.988	-55 31 47.59	K3IB-II	2.8
β Gem	07 45 18.950	+28 01 34.32	K0IIIb	1.1
β Hyi	00 25 45.070	-77 15 15.29	G0V	2.8
β Vir	11 50 41.718	+01 45 52.99	F9V	3.6
δ Eri	03 43 14.901	-60 45 48.21	K1III-IV	3.5
ϵ Eri	03 32 55.845	-09 27 29.73	K2Vk:	3.7
ϵ For	03 01 37.637	-28 05 29.60	K2VFe-1.3CH-08	5.9
ϵ Vir	13 02 10.598	+10 57 32.94	G8III	2.8
η Boo	13 54 41.079	+18 23 51.79	G0IV	2.8
γ Sge	19 58 45.429	+19 29 31.73	M0III	3.5
HD 107328	12 20 20.981	+03 18 45.26	K0IIIb	5.0
HD 122563	14 02 31.845	+09 41 09.95	F8IV	6.2
HD 140283	15 43 03.097	-10 56 00.60	sdF3	7.2
HD 220009	23 20 20.583	+05 22 52.70	K2III	5.0
HD 22879	03 40 22.064	-03 13 01.12	F9V	6.7
HD 49933	06 50 49.832	-00 32 27.17	F2V	5.8
HD 84937	09 48 56.098	+13 44 39.32	sdF5	8.3
ξ Hya	11 33 00.115	-31 51 27.44	G7III	3.5
μ Ara	17 44 08.701	-51 5 02.59	G3IV-V	5.1
μ Leo	09 52 45.817	+26 00 25.03	K2III	3.9
Procyon	07 39 18.119	+05 13 29.96	F5IV-V	0.4
ψ Phe	01 53 38.741	-46 18 09.60	M4III	4.4
Sun				
τ Cet	01 44 04.083	-15 56 14.93	G8.5V	3.5

Table 5.1: *Gaia* Benchmark stars adopted in our study: General information including their names, right ascension $\alpha_{\rm RA}$, declination $\delta_{\rm DEC}$ spectral types and visual magnitudes V.

5.2.3 log g determination

The log g values were determined using Eqn. 5.5. The stellar radii were measured using the angular diameters and their distances which were determined from their parallaxes π. The distances to the stars can be thus calculated using the relation $d = 1/\pi$, where d is measured in parsecs (pc) and π in arc seconds (arc-sec).
The parallaxes for the benchmark stars were determined from the HIPPARCOS[17] measurements (Söderhjelm, 1999; van Leeuwen, 2007; VandenBerg et al., 2014).

The stellar masses were determined using asteroseismic relations (Sec. 5.1.2.2), where the large frequency separation values from Bruntt et al. (2010) & Kallinger et al. (2010) were adopted. For stars which are part of binary systems, their masses were derived from combined dynamic astrometric and spectroscopic observations (α Cen A, Pourbaix et al., 2002), from astrometric observations (61 Cyg B, Gorshanov et al., 2006 ,μ Cas, Drummond et al., 1995 and

[17]http://sci.esa.int/hipparcos/

Procyon, Girard et al., 2000).
For single stars, and in the case of the absence of asterosismic data, the masses were determined by interpolation in grids of evolutionary tracks using the *Padova* and the *Yonsei-Yale* (Yi et al., 2003) stellar evolution models, using $T_{\rm eff}$, luminosity and [Fe/H] constraints. The adopted masses are the averages of the values obtained from both evolutionary model grids. The difference between the latter is that the *Yonsei-Yale* models take the helium diffusion into account while the *Padova* models don't.
For most stars, seismic masses agree with those determined from stellar models within $\pm 0.1 M_{\odot}$.

The log g determinations of the stars using their masses and radii as explained above, compare well to the seismic log g calculated using Eqn. 5.10 from the $\nu_{\rm max}$ measurements of Morel and Miglio (2012), and lie within Δlog g = log g(Heiter et al.)-log g(asteroseismology) = 0.06 dex (15%). Larger deviations were found for Procyon (-0.08 dex), τ Cet (+0.08 dex) and Arcturus (-0.2 dex). These deviations are due to large uncertainties in $\nu_{\rm max}$ measurement for Procyon, and the uncertain evolutionary-models mass for τ Cet (which was found unreasonable corresponding to its age). Regarding Arcturus, its evolutionary-model mass was found inconsistent with its seismic mass due to uncertain $\Delta\nu$ values resulting from irregularities found in its p-mode oscillations (Retter et al., 2003).

5.2.4 [Fe/H] determination

The metallicities of the stars were calculated starting from the non-spectroscopic $T_{\rm eff}$ and log g as described above, as inputs to calculating synthetic spectra and equivalent widths for FeI and FeII lines (Jofré et al., 2014). FeI and FeII abundances were calculated for the set of *Gaia*-ESO survey linelist, version v3 (GES-v3) (Heiter et al., 2015b), by 7 different methods all starting from the same parameters and using the same 1D MARCS model atmospheres (Gustafsson et al., 2008) (see Sect. 2.3 for more details on the models) to provide non-biased and non-model dependent results which are averaged to calculate the metallicity for each star (see below).

The lines were selected as to lie on the linear part of curve of growth (i.e. log $(W_\lambda/\lambda) \leq$ -4.8). This avoided using saturated and strong lines which can be strongly affected by turbulent velocities or damping parameters. The abundances calculated by each method and for each line were then chosen such that the agreement between different methods lies within 2σ of the mean abundance. Excitation balance was then checked as a function of excitation potential (EP) and equivalent widths for all the stars. For FeI lines, non-LTE corrections were applied individually to each lines from the calculations of Bergemann et al. (2012). Finally the metallicities were computed by averaging the abundances of these final list of lines and by using an absolute abundance of 7.45 for the Sun (Grevesse et al., 2007).

The list of stars adopted in this work along with their fundamental parameters whose determination methods have been discussed above, including their angular diameters $\theta_{\rm D}$, bolometric fluxes $f_{\rm bol}$, masses, parallaxes, $T_{\rm eff}$, log g, [Fe/H], and their corresponding uncertainties are listed in Table 5.2.

Table 5.2: *Gaia* Benchmark stars adopted in our study: fundamental parameters including the adopted angular diameters $\theta_{\rm D}$, bolometric Fluxes $F_{\rm bol}$, $T_{\rm eff}$ and their uncertainties $\sigma\ T_{\rm eff}$, masses M, parallaxes π, log g and their uncertainties σlog g, [Fe/H] and their uncertainties σ[Fe/H] and their microturbulent velocities ξ_t. The last column shows the method used to determine the stellar mass: Seis. (Asteroseismology), Evol. (Evolutionary tracks), Bin. (Binary system).

Star name (ID)	$\theta_{\rm D}$ (mas)	$F_{\rm bol}$ (10^{-9} W m^{-2})	$T_{\rm eff}$ (K)	$\sigma\ T_{\rm eff}$ (K)	M ($M_\odot$)	π (mas)	log g	σlog g	[Fe/H]	σ[Fe/H]	ξ_t (Km·s^{-1})	
18 Sco	0.676	0.1734	5810	80	1.02	71.93	4.44	0.03	+0.03	0.01	1.2	Seis.
61 Cyg B	1.581	0.2228	4044	32	0.61	285.89	4.67	0.04	-0.38	0.03	1.1	Bin.
α Cen A	8.511	27.160	5792	16	1.11	747.10	4.31	0.01	+0.26	0.01	1.2	Seis.
α Cet	12.2	10.3	3796	65	1.76	13.10	0.68	0.23	-0.45	0.05	1.4	Bin.
α Tau	20.58	33.57	3927	40	0.96	48.92	1.11	0.19	-0.37	0.02	1.4	Evol.
Arcturus	21.050	49.8	4286	35	1.03	88.83	1.64	0.09	-0.52	0.01	1.3	Seis.
β Ara	5.997	3.7179	4197	50	8.21	4.54	1.05	0.15	-0.05	0.04	1.5	Evol.
β Gem	7.98	11.82	4858	60	2.30	96.52	2.90	0.08	+0.13	0.01	1.1	Seis.
β Hyi	2.257	2.0191	5873	45	1.15	134.07	3.98	0.02	-0.04	0.01	1.3	Seis.
β Vir	1.450	0.9590	6083	41	1.34	91.50	4.10	0.02	+0.24	0.01	1.4	Seis.
δ Eri	2.394	1.150	4954	30	1.13	110.62	3.76	0.02	+0.06	0.01	1.2	Seis.
ϵ Eri	2.126	1.0	5076	30	0.80	310.95	4.61	0.03	-0.09	0.01	1.1	Evol.
ϵ For	0.788	0.1425	5132	78	0.91	31.05	3.52	0.08	-0.60	0.01	1.2	Evol.
ϵ Vir	3.28	2.21	4983	61	3.02	29.75	2.77	0.02	+0.15	0.01	1.1	Evol.
η Boo	2.189	2.21	6099	28	1.64	87.77	3.79	0.02	+0.32	0.01	1.4	Seis.
γ Sge	6.060	2.57	3807	49	1.11	12.61	1.05	0.32	-0.17	0.04	1.4	Evol.
HD 107328	1.74	0.4122	4496	59	1.41	10.60	2.09	0.13	-0.33	0.01	1.2	Evol.
HD 122563	0.94	0.1303	4587	60	0.86	4.22	1.61	0.07	-2.64	0.01	1.3	Evol.
HD 140283	0.353	0.0386	5522	105	0.68	17.18	3.58	0.11	-2.36	0.02	1.3	Evol.
HD 220009	2.045	0.4409	4217	60	0.83	7.55	1.43	0.12	-0.74	0.01	1.3	Evol.
HD 22879	0.382	0.0577	5868	89	0.75	39.13	4.27	0.04	-0.86	0.01	1.2	Evol.
HD 49933	0.445	0.1279	6635	91	1.17	33.68	4.20	0.03	-0.41	0.01	1.9	Seis.
HD 84937	0.153	0.0127	6356	97	0.75	12.24	4.06	0.04	-2.03	0.02	1.5	Evol.
ξ Hya	2.386	1.228	5044	40	2.84	25.14	2.87	0.02	+0.16	0.01	1.1	Seis.
μ Ara	0.763	0.2354	5902	66	1.19	64.48	4.30	0.03	+0.35	0.01	1.2	Seis.
μ Leo	2.93	1.1458	4474	60	1.69	26.27	2.51	0.11	+0.25	0.02	1.1	Evol.
Procyon	5.39	17.86	6554	84	1.50	284.52	4.00	0.02	+0.01	0.01	1.8	Seis.
ψ Phe	8.13	3.2	3472	92	1.00	9.54	0.51	0.18	-1.24	0.24	1.5	Evol.
Sun			5777	1			4.4380	0.0002	+0.03	0.01	1.2	
τ Cet	2.015	1.162	5414	21	0.71	273.96	4.49	0.02	-0.49	0.01	1.1	Seis.

6 Non-LTE calculations using the Drawin approximation

This chapter presents the results of tests on the role of hydrogen collisions in non-LTE line formation using the Drawin approximation (see Sect. 3.1.1). For that purpose, a silicon model atom was constructed to test our different approximations for the H-collisional rates, as quantum calculation for H+Si excitation and charge transfer processes are available from Belyaev et al. (2014). Our aim is thus to scale the Drawin approximation in order to reproduce the H+Si quantum rates, and if possible, apply this scaling recipe on iron for which no quantum data have been published yet. This chapter is divided as follows: In Section 6.1, the Si model atom construction is described. In Sections 6.2 and 6.3, the non-LTE calculations for silicon and iron using the Drawin approximation, with various scaling factors S_H are presented.

6.1 Testing our method: Silicon atoms

The silicon model atom was built in a similar manner to the iron model atom described in Chapter 4.

6.1.1 Energy levels

The Si I energy levels and the Si II ground level were extracted from the NIST database (Martin and Zalubas, 1983). The total number of Si I fine structure levels used in our model is 296. The same number of levels was used by Shchukina et al. (2012) in their non-LTE, 3D-model atmosphere study of the silicon abundance in the Solar photosphere. Fig. 6.1 shows the grotrian diagram of our Si atom, showing the distribution of the levels as a function of their term IDs and energies.

6.1.2 Radiative transitions

Line data for transitions between our model energy levels were extracted from the VALD3 (Ryabchikova et al., 2011) database. The total number of transitions is 8674, shown in the grotrian diagram of Fig 6.2. The oscillator strengths, the radiative damping coefficients and the wavelengths are from the Kurucz database (Kurucz and Bell, 1995).
The Van der Waals hydrogen collisional broadening coefficients were calculated using the ABO theory (see Sec. A.2) by Barklem et al. (2015).

Line profiles were calculated using a Voigt profile function with a maximum of 80 frequency points. In `MULTI2.3`, the Doppler core and the Lorentzian wings of the line are controlled by two input parameters in the model atom, Q_0 and Q_{max} defined as:

- Q_0 is the transition from Doppler Core to Lorentzian wings, hence it is the distance from the line center (in Doppler widths) at which the transition from Doppler core to Lorentzian wings occurs.

- Q_{max} is the distance from the line center (in Doppler widths) to which the line wings are calculated.

Based upon these parameters, the quadrature points (Q) of the line profile and their corresponding weights (ΔQ) are calculated based on the trapezoidal rule depending on the position of the frequency point with respect to the central wavelength. i.e.: for $Q < Q_0$, the trapezoidal rule is applied on a linear mapping of Q while for $Q > Q_0$, the trapezoidal rule is applied on a logarithmic (10log) mapping of Q. The input values of Q_0 and Q_{max} were determined line-by-line based on the values of the damping parameter a (See Sec. A.4).

In addition to the bound-bound transitions, all the levels in the Si model were coupled to the Si II ground level via bound-free transitions. The bound-free photoionization tables were calculated by Nahar (1993) using the close-coupling approximation and the R-matrix method, and are extracted from the NORAD database. They include photoionization cross-sections for 264 Si I LS-coupling terms of multiplicities 1 and 3, up to n=10 and l=8. The photoionization cross-sections for the mean levels were distributed onto the fine structure levels using their corresponding statistical weights. Due to the large number of points in the tables and the sharp resonance peaks in the data, the cross-sections were smoothed and re-sampled as described for iron in Sec. 4.2.2.
For terms of multiplicity 5 and for JJ-coupling terms for which no photoionization tables exist, Kramer's approximation was used to calculate the cross-sections (Eqn. 2.37).

6.1.3 Collisional transitions

All levels in the Si model are coupled via inelastic collisions with electrons and neutral hydrogen atoms.

For allowed electron collisional bound-bound transitions, the Seaton (1962a) impact parameter approximation was used (Eqn. 2.51) to calculate the effective collisional strengths Υ^{e-}. For forbidden transitions, Seaton (1962b) approximation as listed in Allen (1973) is used with a collisional strength $\Omega = 1$ (Eqn. 2.58).
All the levels were coupled to the Si II ground level through electron collisional ionization using Bely and van Regemorter (1970) dipole impact approximation (Eqn. 2.59).

The neutral H+Si collisional rates were calculated using the Drawin approximation via the Lambert (1993) derivation (Eqn. 3.14), using an oscillator strength $f = 1$, which allows to calculate the collisional rates for both allowed and forbidden transitions.
All the energy levels in the Si model were coupled via H-collisional bound-bound, bound-free and charge transfer transitions as described in Chapter 4. In order to test the effect of hydrogen collisions, different model atoms were created with different H+Si collisional rates, by applying a scaling factor for the excitation, ionization and charge exchange processes. In the following sections and hereafter, we introduce two different scaling factors such as:

- ⋆ **S_H**: scaling factor for excitation, de-excitation, and ionization transitions.

- ⋆ **S_H(CE)**: scaling factor for charge exchange processes: ion-pair production, and mutual neutralization transitions.

Star	Sun	HD140283	α Cent A	Procyon	Arcturus	μ Leo
log ε(Si)	7.549	5.303	7.799	7.516	7.287	8.071
σ log ε(Si)	0.016	0.094	0.028	0.065	0.051	0.093

Table 6.1: Adopted values for Si abundances in our calculations and their σ values.

For comparison, a reference Si model was created using the quantum data of Belyaev et al. (2014) for the H+Si collisional rates for the bound-bound and charge transfer processes. The collisional rates of the mean levels were distributed on the fine structure levels according to their statistical weights.

6.2 Silicon non-LTE calculations using the Drawin approximation

6.2.1 Method

Using the Si atomic data described above, several modified Si model atoms were created by varying the values of S_H and S_H(CE) as follows:

- S_H was varied between 0.0001 and 10 in multiplicative steps of 10.
- S_H(CE) was varied between 0.1 and 10 in multiplicative steps of 10, in addition to the S_H(CE) = 0 value.

Using MARCS model atmospheres as input, non-LTE calculations were performed for the previously described Si model atoms for all the combinations of S_H and S_H(CE) as described above. They are hereafter referred to as the Drawin models. The calculations performed with the reference Si model are hereafter referred to as the quantum model. The calculations were performed for 6 benchmark stars, namely, the Sun, the metal poor halo subgiant HD140283, the metal rich main sequence star α Centauri A, Procyon, and two red giant benchmark stars: Arcturus and μ Leo. Background line opacity files excluding Si lines were included in the calculations, thus accounting for line blanketing effects. The opacity files were calculated for each star's metallicity and microturbulent velocity. $T_{\rm eff}$ and log g are from the GBS values in Table 5.2. The Solar Si abundance value adopted in the calculations is taken from the non-LTE, 3D calculations of Shchukina et al. (2012), while those for the other stars are from Jofré et al. (2015) where line-by-line abundance analyses of Gaia benchmark stars were performed. The abundance values and their corresponding uncertainties are shown in Table 6.1.

6.2.2 Results

The calculated non-LTE equivalent widths for the Drawin models (EW_{Drawin}) were compared to the reference values (EW_{QM}) for different values of S_H and S_H(CE) through the computation of a χ^2_{QM} using chosen equivalent widths corresponding to lines of transition energies lying between 1eV and 4eV ($1\mathrm{eV} < \Delta E < 4\mathrm{eV}$):

$$\chi^2_{\mathrm{QM}} = \sum_{\mathrm{N_{lines}}} \frac{(\mathrm{EW_{Drawin}} - \mathrm{EW_{Quantum}})^2}{\mathrm{EW_{Quantum}}} \tag{6.1}$$

Figs. 6.3, 6.4, 6.5, 6.6, 6.7 and 6.8 show the comparison of the calculated equivalent widths for all the models as compared to those of the reference model, for the 6 stars. Table 6.2 shows the obtained χ^2_{QM} for each corresponding model.

The results obtained for each star are summarized below:

Sun: The best-fit Drawin model is obtained for S_H=0.01 and S_H(CE)=0.1. It can be seen from Table 6.2, that as the S_H value increases, thus increasing the excitation and de-excitation H+Si collisional rates, the Drawin models deviate from the reference calculations.

HD140283: The best-fit Drawin model to reproduce the reference calculations is obtained for S_H=1.0 and S_H(CE)=0.1. The χ^2_{QM} values behavior with S_H is, however, opposite to those obtained for the Sun, as the deviation from the reference calculations is increasing with decreasing S_H (i.e. with decreasing Si+H excitation rates).

α Cent A & Procyon: The best-fit model for both stars is obtained for S_H =10 and S_H(CE)=0.1. The χ^2_{QM} behavior with S_H for both is similar to that of HD140283. For these two metal rich stars, high collisional excitation rates are required to reproduce the reference calculations.

Arcturus & μ Leo: The best-fit obtained model is for S_H=0.0001 and S_H(CE)=1. For both red giant stars, small excitation rates for small values of S_H are required for better fitting the reference calculations. For high charge exchange rates at S_H(CE) = 10, larger χ^2_{QM} values are obtained.

For all the stars, it can be observed that no clear trend is obtained with S_H(CE), which is less constrained than S_H.

Figure 6.3: non-LTE calculated equivalent widths using the Drawin Si models vs. the quantum Si model for different scaling factors S_H and S_H(CE) for the Sun.

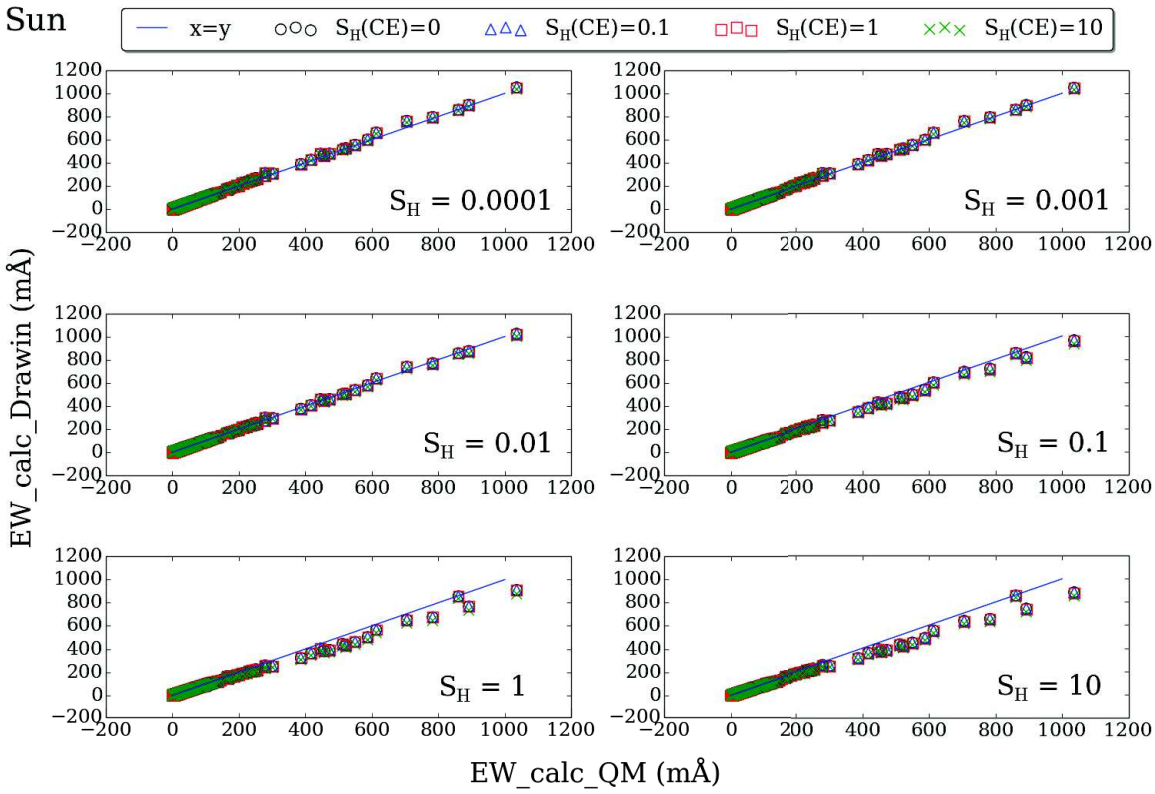

Figure 6.4: non-LTE calculated equivalent widths using the Drawin Si models vs. the quantum Si model for different scaling factors S_H and S_H(CE) for HD140283.

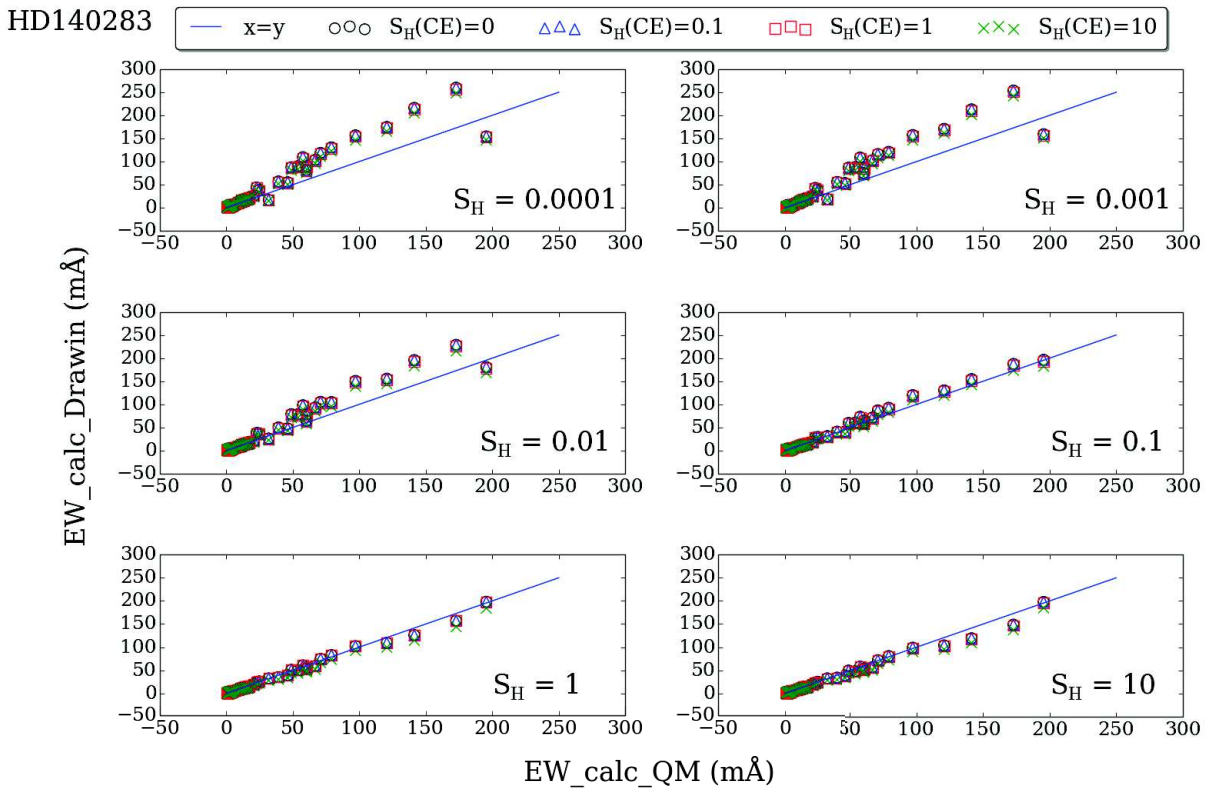

Figure 6.5: non-LTE calculated equivalent widths using the Drawin Si models vs. the quantum Si model for different scaling factors S_H and S_H(CE) for the α Cent A.

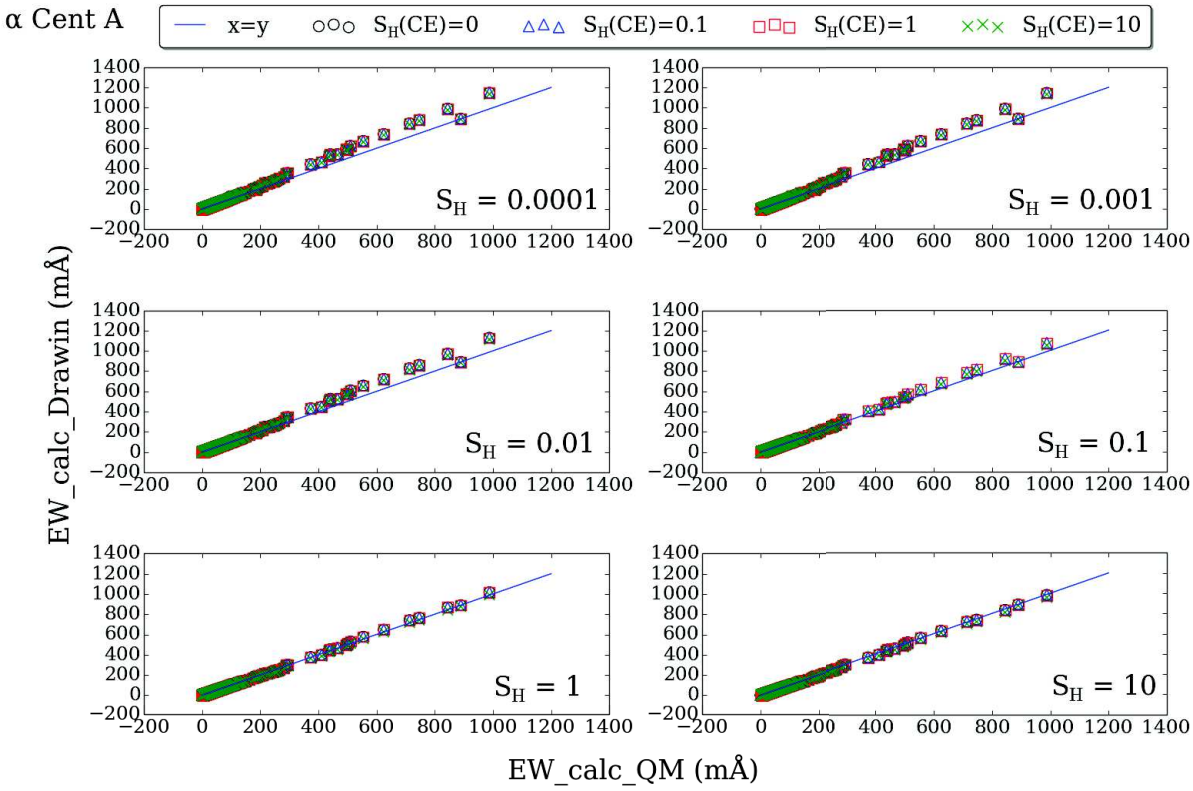

Figure 6.6: non-LTE calculated equivalent widths using the Drawin Si models vs. the quantum Si model for different scaling factors S_H and S_H(CE) for the Procyon.

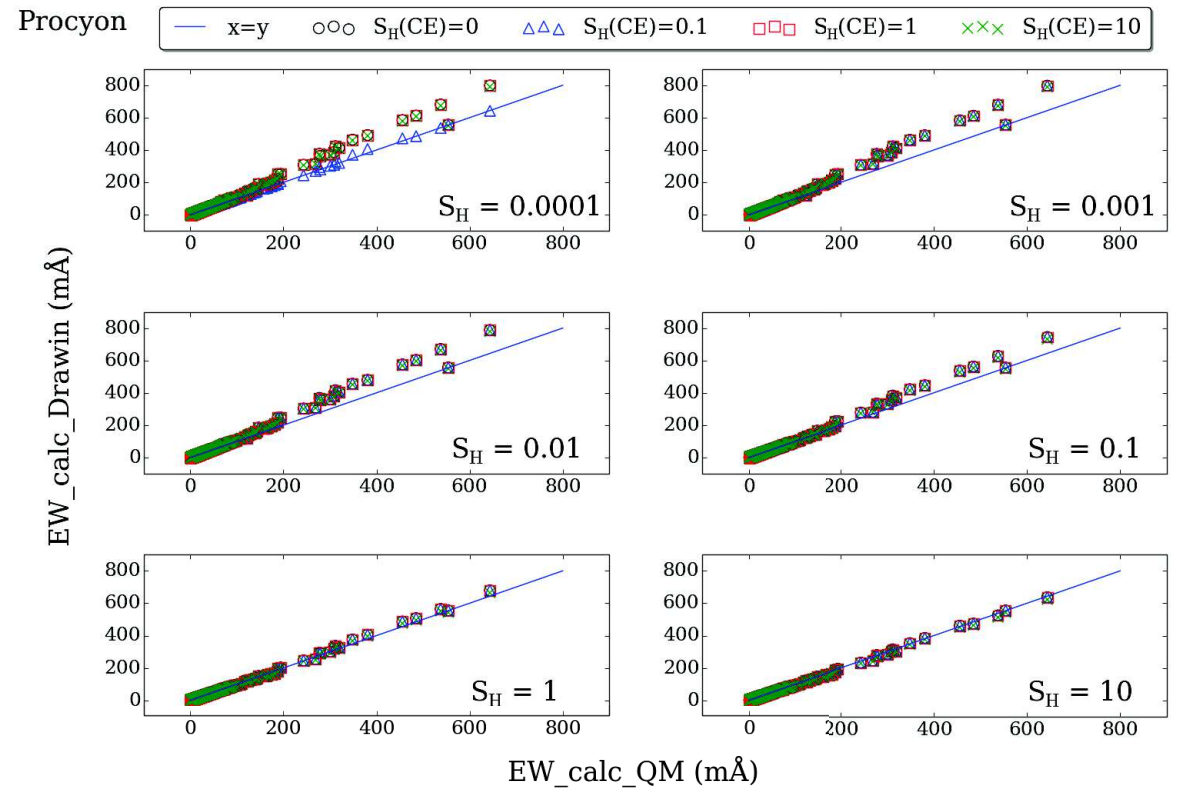

Figure 6.7: non-LTE calculated equivalent widths using the Drawin Si models vs. the quantum Si model for different scaling factors S_H and S_H(CE) for the Arcturus.

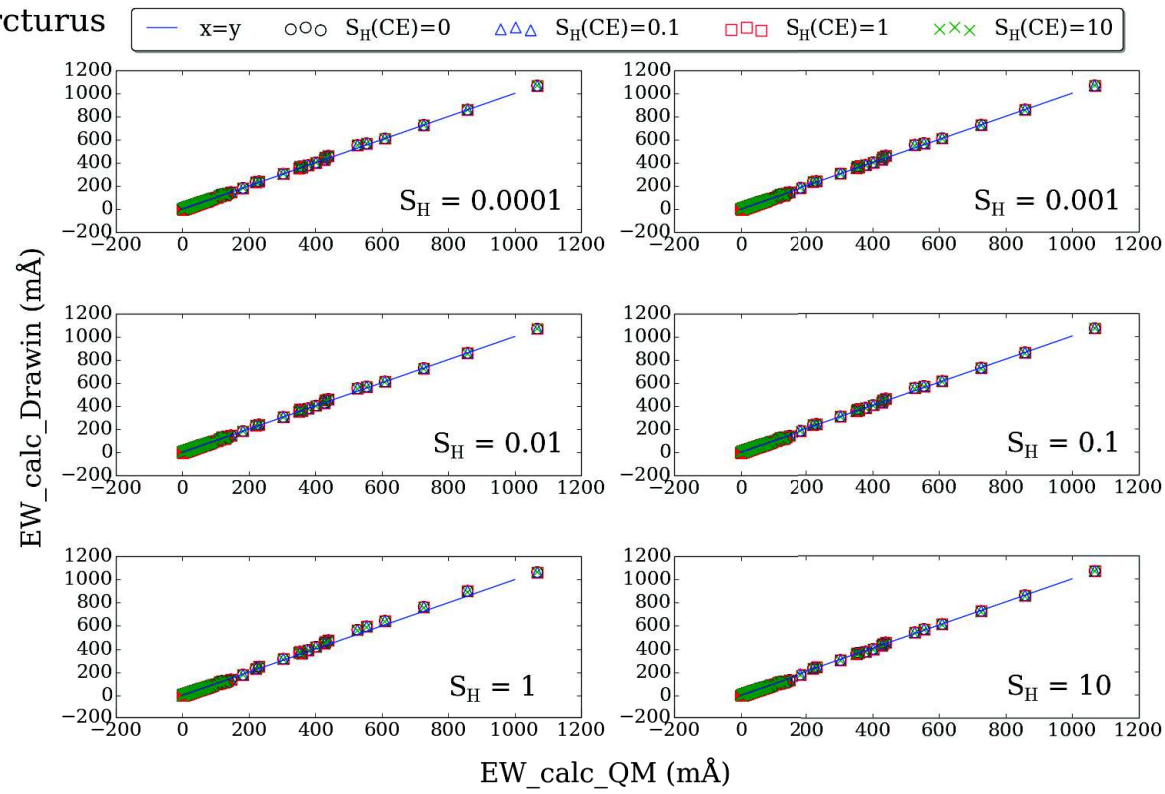

Figure 6.8: non-LTE calculated equivalent widths using the Drawin Si models vs. the quantum Si model for different scaling factors S_H and S_H(CE) for the μ Leo.

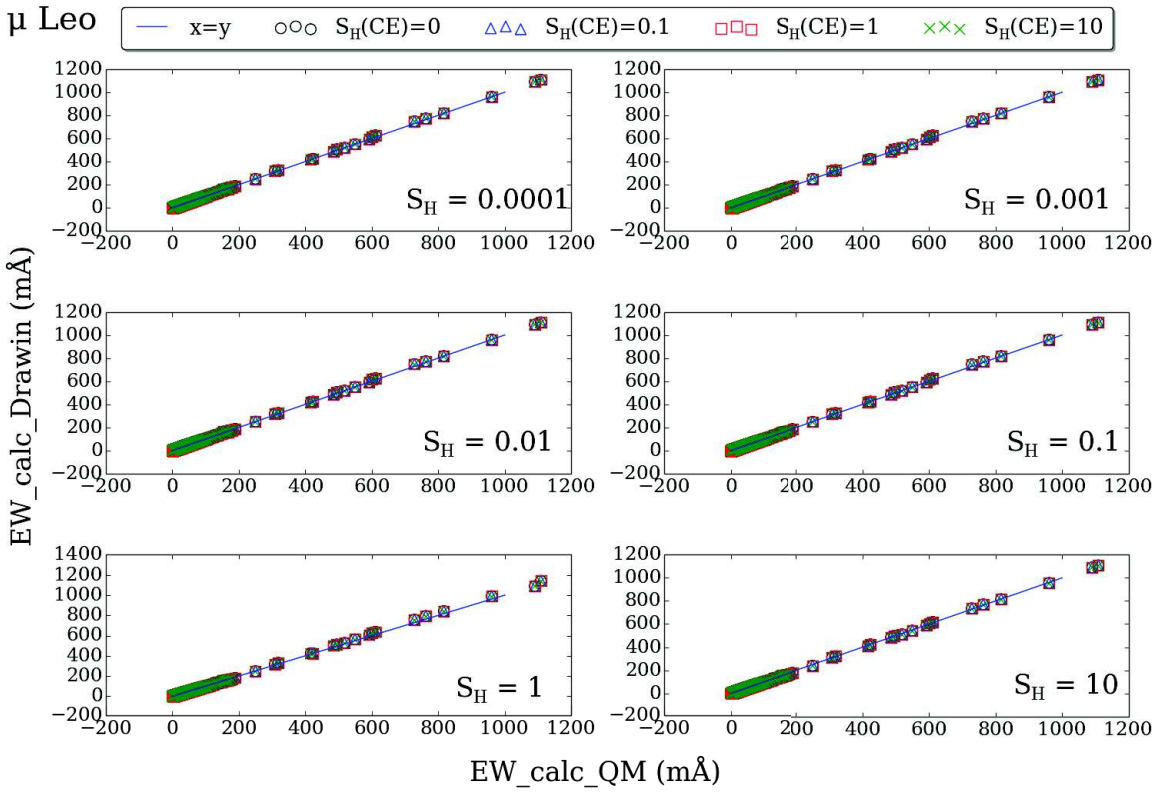

			S_H					
			0.0001	0.001	0.01	0.1	1.0	10.0
Sun	S_H(CE)	0	57.099	45.776	13.237	107.358	252.183	317.127
		0.1	55.986	44.733	<u>13.080</u>	110.062	256.387	321.084
		1.0	48.388	37.731	13.585	135.332	294.636	356.922
		10.0	28.972	24.723	62.607	364.666	618.549	667.761
HD140283	S_H(CE)	0	461.176	402.107	210.132	28.148	11.202	17.052
		0.1	454.951	396.229	206.158	27.314	<u>10.816</u>	17.519
		1.0	416.261	359.931	180.655	21.909	15.181	21.758
		10.0	309.631	260.832	116.140	22.805	50.366	58.479
α Cent A	S_H(CE)	0	493.696	468.430	318.271	88.562	14.430	12.405
		0.1	491.336	466.030	315.833	80.484	14.434	<u>12.049</u>
		1.0	472.496	446.885	296.302	71.530	16.282	17.002
		10.0	373.565	347.512	205.985	78.745	110.670	123.594
Procyon	S_H(CE)	0	667.085	651.198	519.893	176.539	26.969	21.773
		0.1	660.543	649.948	518.630	175.687	26.901	<u>21.570</u>
		1.0	658.249	639.322	507.840	168.514	26.649	23.885
		10.0	585.439	567.263	434.940	128.584	46.495	62.300
Arcturus	S_H(CE)	0	11.081	12.408	13.766	17.760	46.172	35.676
		0.1	11.028	12.371	13.747	17.800	46.133	35.776
		1.0	<u>10.885</u>	12.329	13.769	18.307	46.0759	37.581
		10.0	15.145	18.840	20.7029	29.708	59.122	64.602
μ Leo	S_H(CE)	0	4.829	5.265	5.603	7.325	20.080	17.456
		0.1	4.801	5.243	5.588	7.341	20.077	17.559
		1.0	<u>4.777</u>	5.260	5.597	7.580	20.214	18.631
		10.0	11.182	11.912	11.576	14.822	30.209	36.403

Table 6.2: Calculated $\chi^2_{\rm QM}$ values for the Drawin models with different S_H and S_H(CE) scaling factors, compared to the reference calculations for the Sun, HD140283, α Cent A, Procyon, Arcturus and μ Leo. The least $\chi^2_{\rm QM}$ value for each star is underlined.

6.2.3 Conclusions

Assuming that the quantum model calculations are the correct ones to reproduce the observed Si line profiles, it has been shown that they could be quite well reproduced using the Drawin models by employing different recipes for the excitation and charge transfer rates through the scaling factors S_H and $S_H(CE)$. These recipes are, however, found to be star dependent!

6.3 Iron non-LTE calculations using The Drawin approximation

In this section, an attempt is made to better reproduce the observed measured equivalent widths (see Sect. 6.3.1.3 below), and improve the accuracy by which iron abundances are determined.
The possibility of scaling the Drawin approximation for iron with a set of analogous scaling factors S_H and $S_H(CE)$ for all of the *Gaia* benchmark stars is tested.

Iron non-LTE calculations were performed for the *Gaia* benchmark stars introduced in Chapter 5, using the iron model atom developed in Chapter 4, and were compared to the observed equivalent widths of the stars. The H+Fe collisional rates for excitation, ionization and charge transfer were treated using the Drawin approximation. The method and results are presented below.

6.3.1 Method

6.3.1.1 Model atoms

Modified versions of the iron model atom described in Chapter 4 were constructed by varying the Fe I+H and Fe II+H excitation, ionization and charge exchange rates by varying the scaling fudge factors S_H and $S_H(CE)$ as follows:

- S_H was varied between 0.0001 and 10 in multiplicative steps of 10.
- $S_H(CE)$ was varied between 0.1 and 10 in multiplicative steps of 10 for each value of S_H, in addition to the $S_H(CE) = 0$ models.

6.3.1.2 Model Atmospheres

For each of the GBS stars, 1D MARCS model atmospheres were interpolated to the AFP values of the star (Table 5.2), using the MARCS interpolation routine `interpol_marcs.f` [1] written by Thomas Masseron. According to the available models extracted from the MARCS database, spherical models were used for stars with log g values smaller than 3 cgs, while plane-parallel models were used for log g values greater than that. For the Sun, a special MARCS model calculated at the exact AFP parameters is used.

Background opacity files were also included in the non-LTE calculations for each star, and were calculated as a function of the star's metallicity and microturbulent velocity.

[1] http://marcs.astro.uu.se/software.php

6.3.1.3 Linelists and measured equivalent widths

The Fe I and Fe II linelist chosen in the analysis of the non-LTE calculations is a subset of the *Gaia*-ESO survey "golden" linelist `version 4` (v4) (Heiter et al., 2015b).

The observed equivalent widths were measured from the UVES spectra using the code `Robospect`[2] (Automated Equivalent Width Measurement) (Waters and Hollek, 2013). The subset linelist was chosen based on the measurements made on the Sun as follows:

- Blended lines were removed.
- Lines with measured equivalent widths > 150 mÅ and < 10 mÅ were removed.
- Lines with relative errors on measured equivalent width larger than 3% were removed.
- Lines whose relative differences with non-LTE calculated equivalent widths $\Delta \mathrm{W}_\lambda\,(\mathrm{rel}) > 0.3$ were removed, where:

$$\Delta \mathrm{W}_\lambda(\mathrm{rel}) = \frac{|\mathrm{W}_\lambda(\mathrm{non-LTE}) - \mathrm{W}_\lambda(\mathrm{obs})|}{\mathrm{W}_\lambda(\mathrm{obs})} \tag{6.2}$$

  Non-LTE calculations for the Sun were performed for $\mathrm{S_H}$=0.0001 and $\mathrm{S_H}$(CE)=0.1 (See Table 6.3 below).

The final subset linelist (hereafter referred to as linelist), includes 160 Fe I and 22 Fe II lines, is listed in Annex D. Equivalent widths were measured for these lines with `Robospect` for all the GBS stars. All blended lines were again removed for each star.

Non-LTE calculations were performed for each of the modified model atoms described above, thus resulting in 24 calculated models for each star.

6.3.2 Results

For convenience, the GBS were grouped into five categories according to their different spectral types:

- **metal-poor**, including HD122563, HD140283 & HD 84937.
- **FG dwarfs**, including δ Eri, ϵ For, τ Cet, 18 Sco, Sun, HD 22879, α Cen A, μ Ara, β Hyi, β Vir, η Boo , Procyon & HD 49933.
- **FGK giants**, including Arcturus, HD 220009, μ Leo, HD 107328, β Gem, ϵ Vir & ξ Hya.
- **M giants**, including ψ Phe, α Cet, γ Sge, α Tau & β Ara.
- **K dwarfs**, including 61 Cyg B & ϵ Eri.

The calculated equivalent widths were compared to the observed measured equivalent width using a χ^2 test:

$$\chi^2 = \frac{1}{\mathrm{N_{lines}}} \sum_{\mathrm{lines}} \left(\frac{\mathrm{EW(calc)} - \mathrm{EW(obs)}}{\sigma \mathrm{EW(obs)}} \right)^2 \tag{6.3}$$

where $\mathrm{N_{lines}}$ is the total number of lines used in the χ^2 test, and $\sigma \mathrm{EW(obs)}$ is the uncertainty on each measured equivalent width (presented in Annex D for each star).

[2] http://www.ifa.hawaii.edu/users/watersc1/robospect/

The scaling factors S_H and S_H(CE) at which the smallest χ^2 was obtained for the GBS are listed in Table 6.3. The LTE χ^2, calculated from the LTE equivalent widths, are included in the table for comparison. The plots of the variation of χ^2 as a function of S_H and S_H(CE) are presented in Figs. 6.9, 6.10, 6.11, 6.12 and 6.13 for the metal-poor, the FG dwarfs, the FGK giants, the M giants and K dwarfs respectively. The LTE χ^2 values are also shown on the plots (dotted black lines)

Metal-poor stars: For the three very metal-poor stars, the least χ^2 is obtained for small excitation rates (smaller values of S_H) and larger values for charge exchange (larger values of S_H(CE))

FG Dwarfs: For most stars (except ϵ For, τ Cet and Procyon), charge exchange rates play an important role for small values of S_H ($<$0.1), where very large values of χ^2 were obtained upon excluding charge exchange rates at S_H(CE)=0. For $S_H \geq 0.1$, small differences were obtained for different values of S_H(CE). The least χ^2 are obtained for larger excitation rates.

FGK Giants: For the giant stars, the results show that excluding the charge exchange rates from the calculations gave better fits to the observations.

M giants & K Dwarfs: For the M giants and K dwarfs, the results show that while the best-fit are obtained for S_H(CE)=0, varying the scaling factors S_H and S_H(CE) do not play a major effect on χ^2 which varies very slightly between the different models, even compared to LTE.

6.3.3 Conclusions

The non-LTE calculations for the GBS with different scaling factors have shown that including the charge exchange rates play an important role for metal-poor stars and most FG dwarfs. For the giant stars, however, removing the charge transfer rates is more important for a better fit with the observations. It has to be well noted that while the collisional rates are expected to be an atomic quality, it can be observed that using the Drawin approximation with different scaling factors to calculate the rates, no single set of values for S_H and S_H(CE) has been found for all the stars upon which the best-fits are obtained. As expected, the non-LTE results do provide better fits with the observations as compared to those of LTE, especially for metal poor stars and FGK giants. This is not the case, however, for the M giants and K dwarfs where no significant differences were found between the different models, even with LTE.

Our results are consistent with previous non-LTE studies of iron, in the sense that no single value of S_H is able to reproduce the observations of different types of stars. Even within a given spectral type, no single prescription can be given. This shows that the Drawin approximation should definitely NOT be used!
This failure of the Drawin approximation to reproduce the correct H+Fe collisional rates is well expected due to its lack of proper physical assumptions in describing the collisions (see Barklem et al., 2010).

We thus introduce an alternative method for computing the hydrogen collisional rates based on a semi-empirical fitting of existing collisional rates. This is described in the following chapter.

Star name (ID)	S_H	S_H(CE)	Non-LTE χ^2	LTE χ^2
Metal-poor				
HD 122563	0.001	0.1	86.904	156.253
HD 140283	0.0001	1.0	65.929	266.129
HD 84937	0.0001	1.0	34.177	171.124
FG dwarfs				
δ Eri	0.0001	10.0	58.986	59.716
ϵ For	0.01	0.0	145.396	410.611
τ Cet	0.01	0.0	94.156	161.470
18 Sco	0.001	0.1	59.406	68.976
Sun	0.0001	0.1	40.326	65.082
HD 22879	0.0001	1.0	59.048	142.106
α Cen A	0.01	10	18.929	21.041
μ Ara	0.0001	10.0	46.231	46.445
β Hyi	1.0	0.1	139.732	146.391
β Vir	0.0001	0.1	66.936	101.372
η Boo	1.0	0.1	154.691	155.076
Procyon	0.01	0.0	50.795	210.385
HD 49933	1.0	0.1	126.86	134.536
FGK giants				
Arcturus	0.0001	0.0	66.337	122.966
HD 220009	0.0001	0.0	162.848	343.342
μ Leo	0.001	0.0	91.011	117.479
HD 107328	0.1	0.0	87.007	148.616
β Gem	0.001	0.0	35.949	65.209
ϵ Vir	0.001	0.0	104.27	347.575
ξ Hya	0.0001	0.0	163.191	356.553
M giants				
ψ Phe	0.001	0.1	28.333	28.699
α Cet	0.0001	0.1	15.467	15.781
γ Sge	0.01	0.1	53.661	53.471
α Tau	0.0001	0.1	26.888	27.910
β Ara	0.001	0.1	129.565	130.145
K dwarfs				
61 Cyg B	0.0001	0.1	34.831	34.853
ϵ Eri	0.0001	10.0	164.23	175.01

Table 6.3: *Gaia* Benchmark stars calculated non-LTE smallest χ^2 and their corresponding scaling factors. The LTE χ^2 is also included for comparison.

Figure 6.9: $\chi^2_{\rm nLTE}$ obtained for different S_H and S_H(CE) recipes for the metal poor GBS. The dotted lines represents the $\chi^2_{\rm LTE}$.

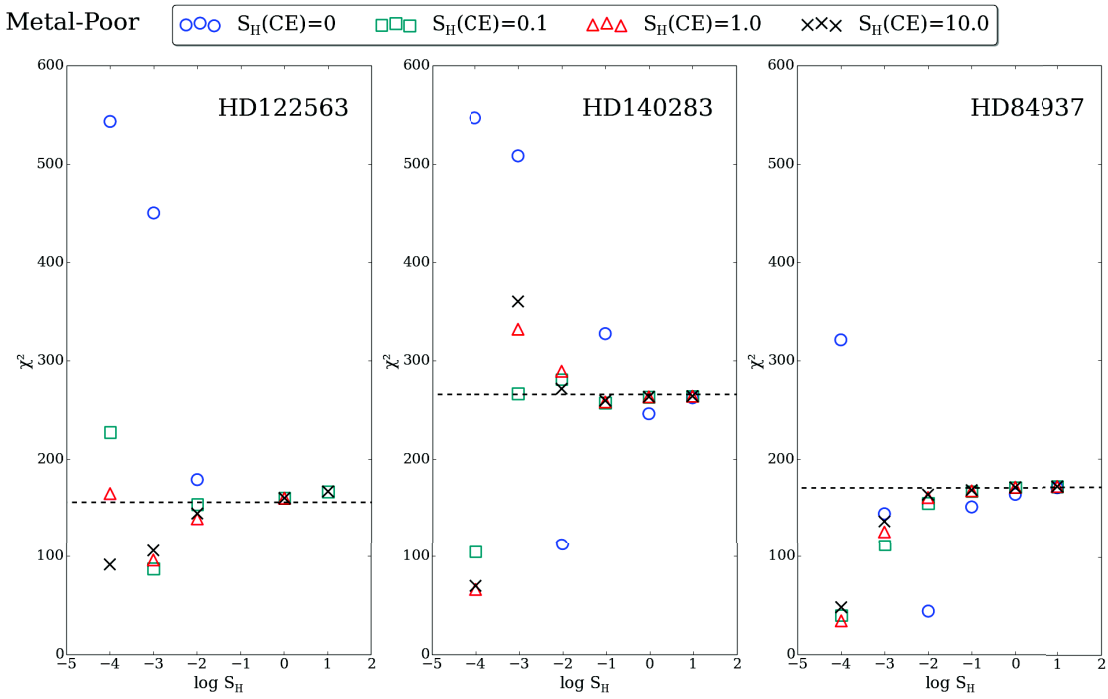

Figure 6.10: $\chi^2_{\rm nLTE}$ obtained for different S_H and S_H(CE) recipes for the FG dwarf GBS. The dotted lines represents $\chi^2_{\rm LTE}$.

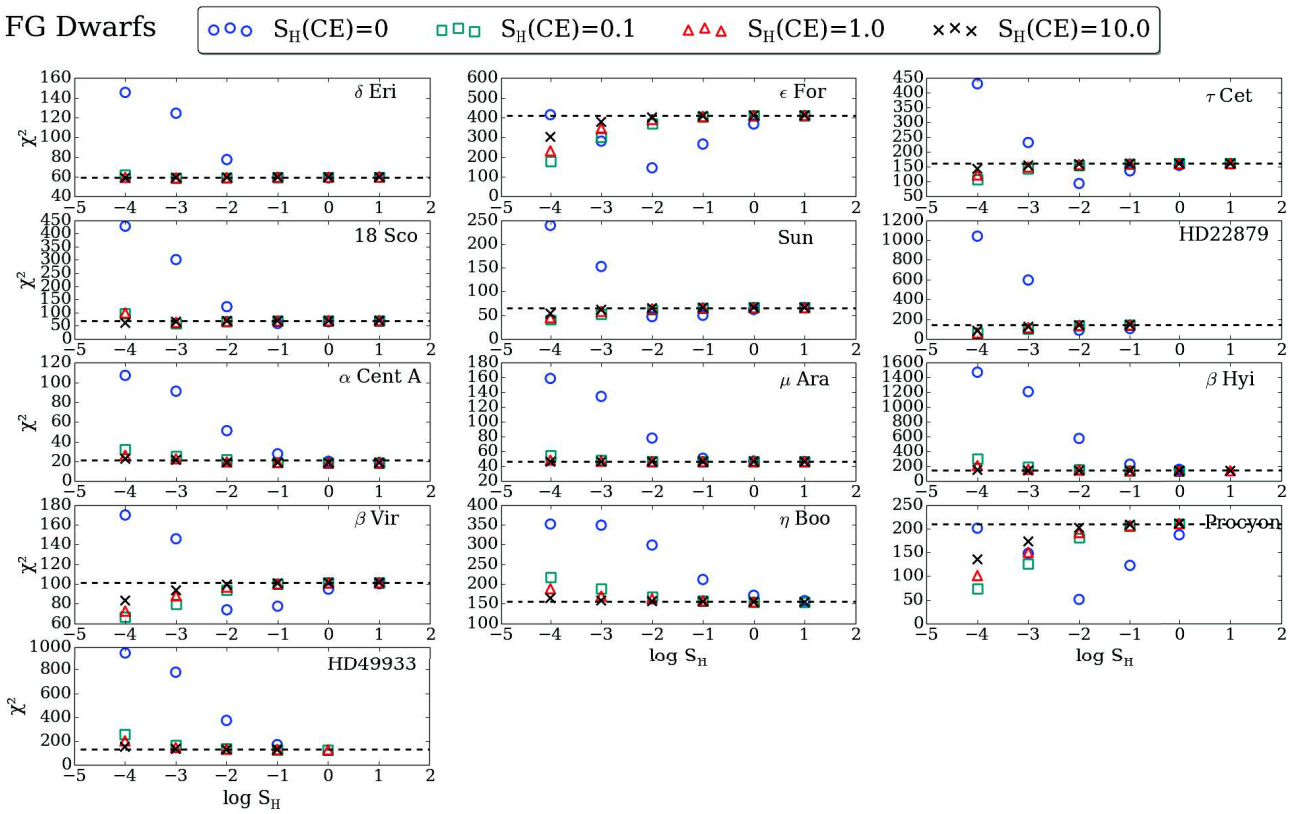

Figure 6.11: $\chi^2_{\rm nLTE}$ obtained for different S_H and S_H(CE) recipes for the FGK giant GBS. The dotted lines represents $\chi^2_{\rm LTE}$.

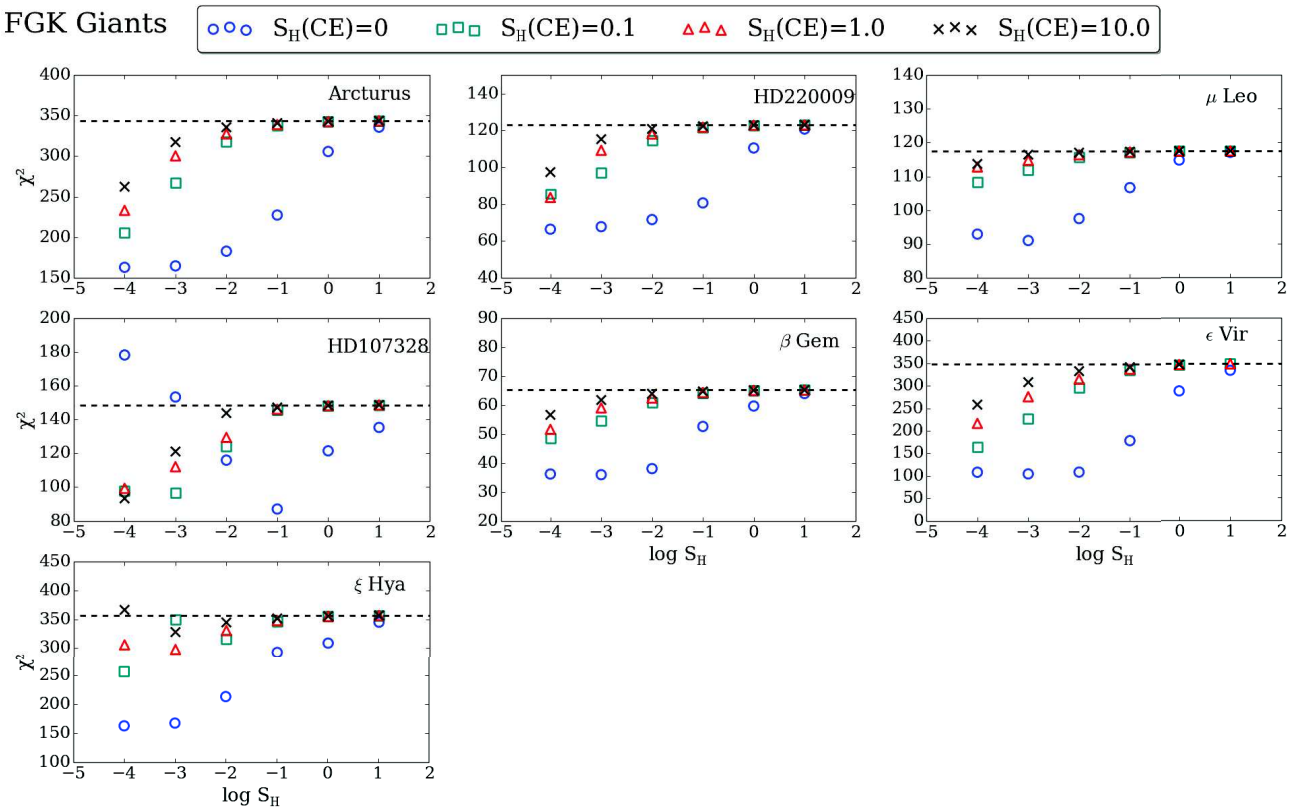

Figure 6.12: $\chi^2_{\rm nLTE}$ obtained for different S_H and S_H(CE) recipes for the M giant GBS. The dotted lines represents $\chi^2_{\rm LTE}$.

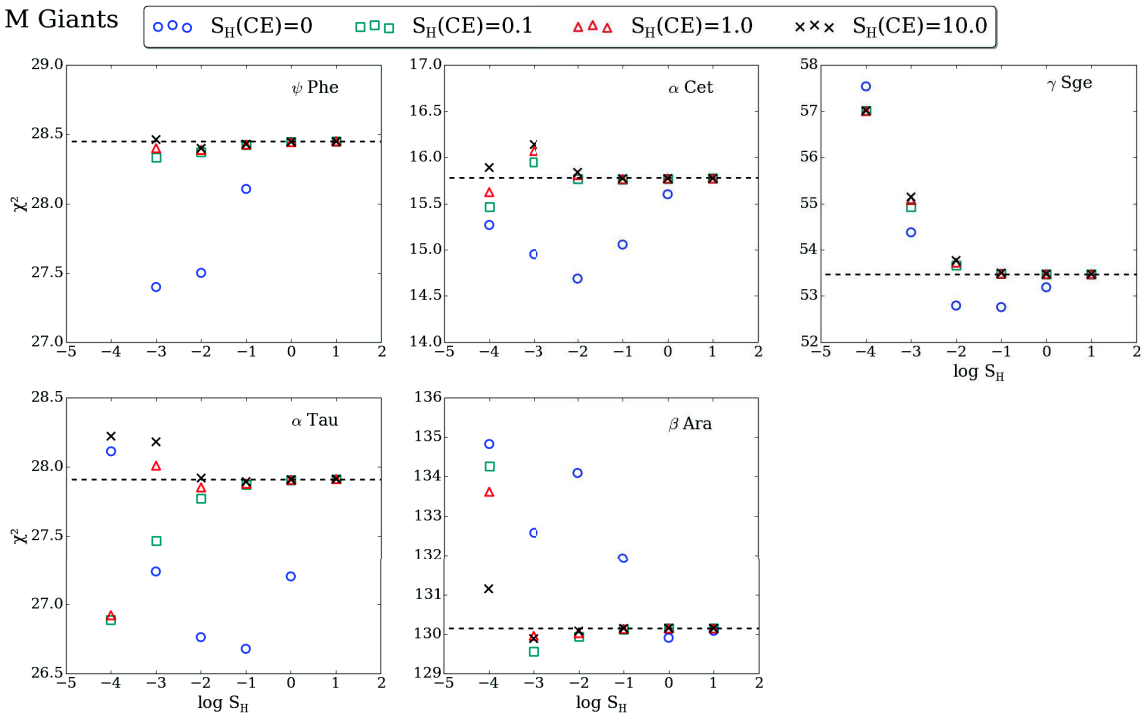

Figure 6.13: $\chi^2_{\rm nLTE}$ obtained for different S_H and S_H(CE) recipes for the K dwarf GBS. The dotted lines represents $\chi^2_{\rm LTE}$.

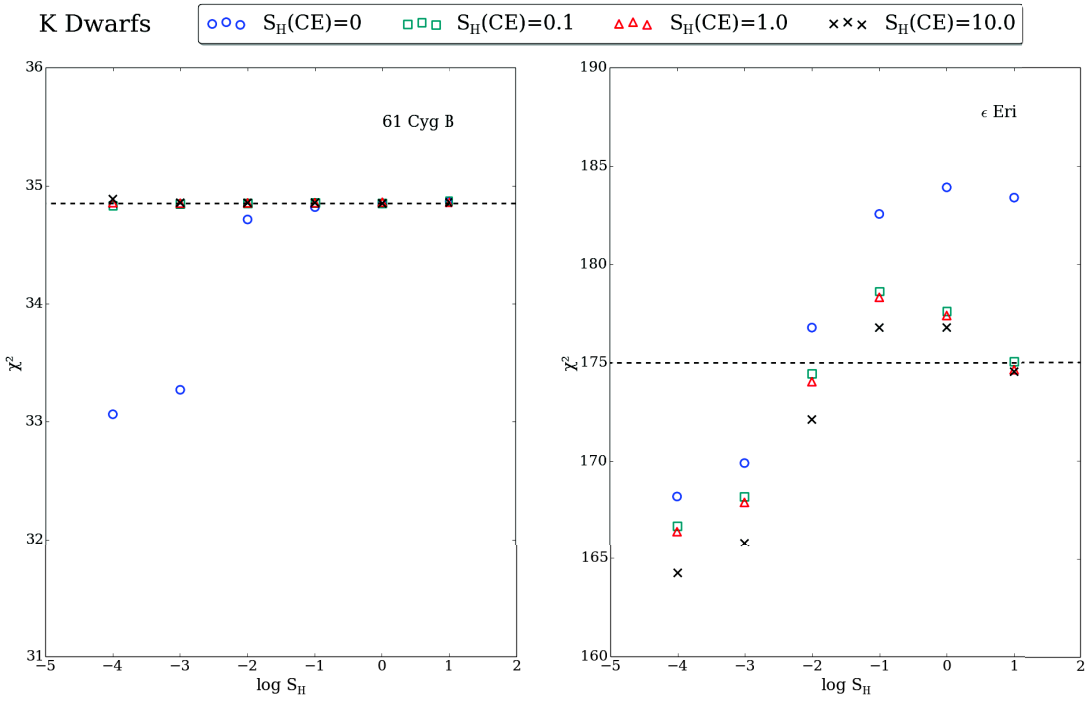

Figure 6.1: Grotrian diagram of SiI levels. Only labels of the levels below 7 eV are included to avoid crowding.

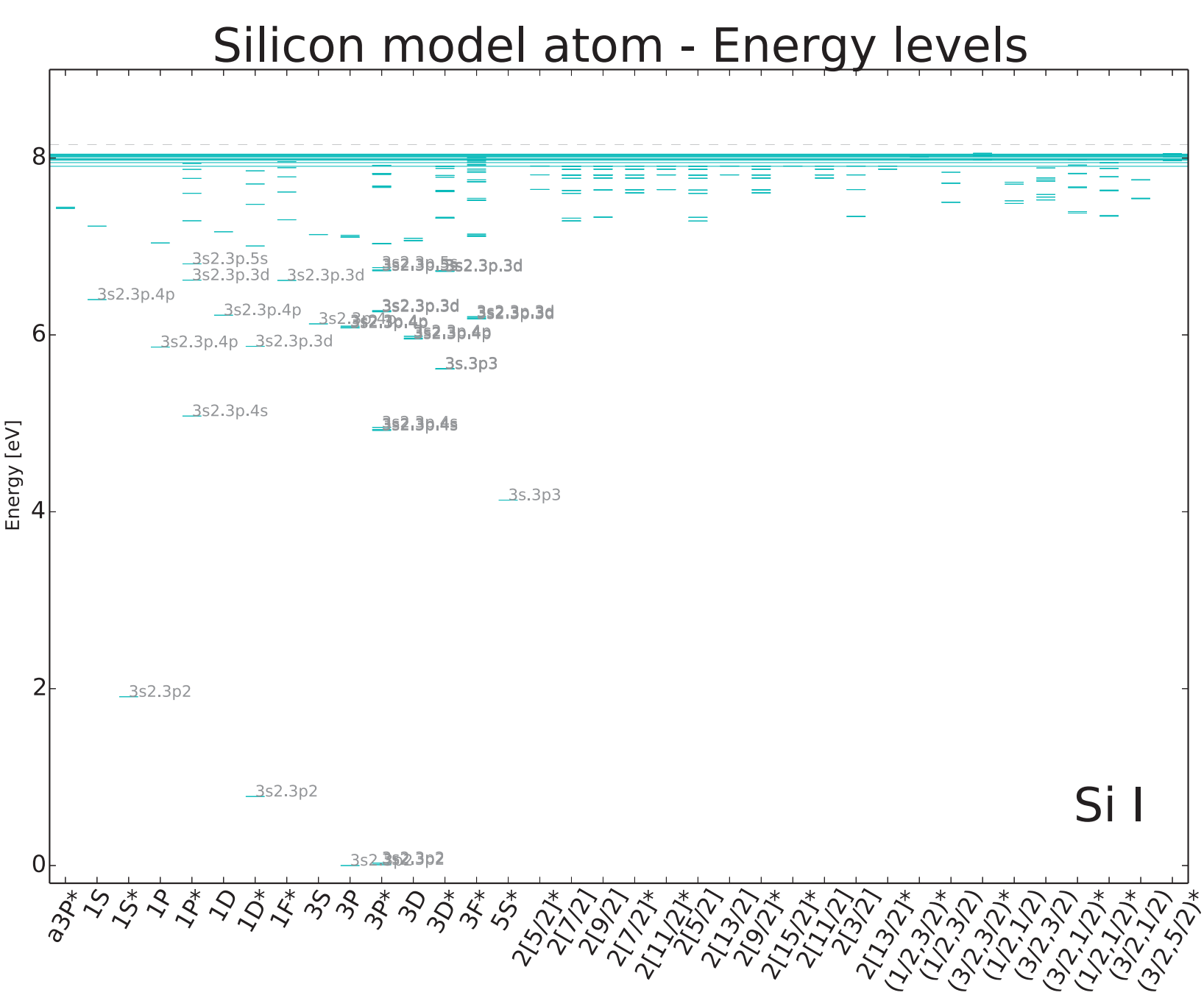

Figure 6.2: Grotrian diagram for allowed SiI bound-bound radiative transitions. Gray lines display transitions between the different fine structure levels.

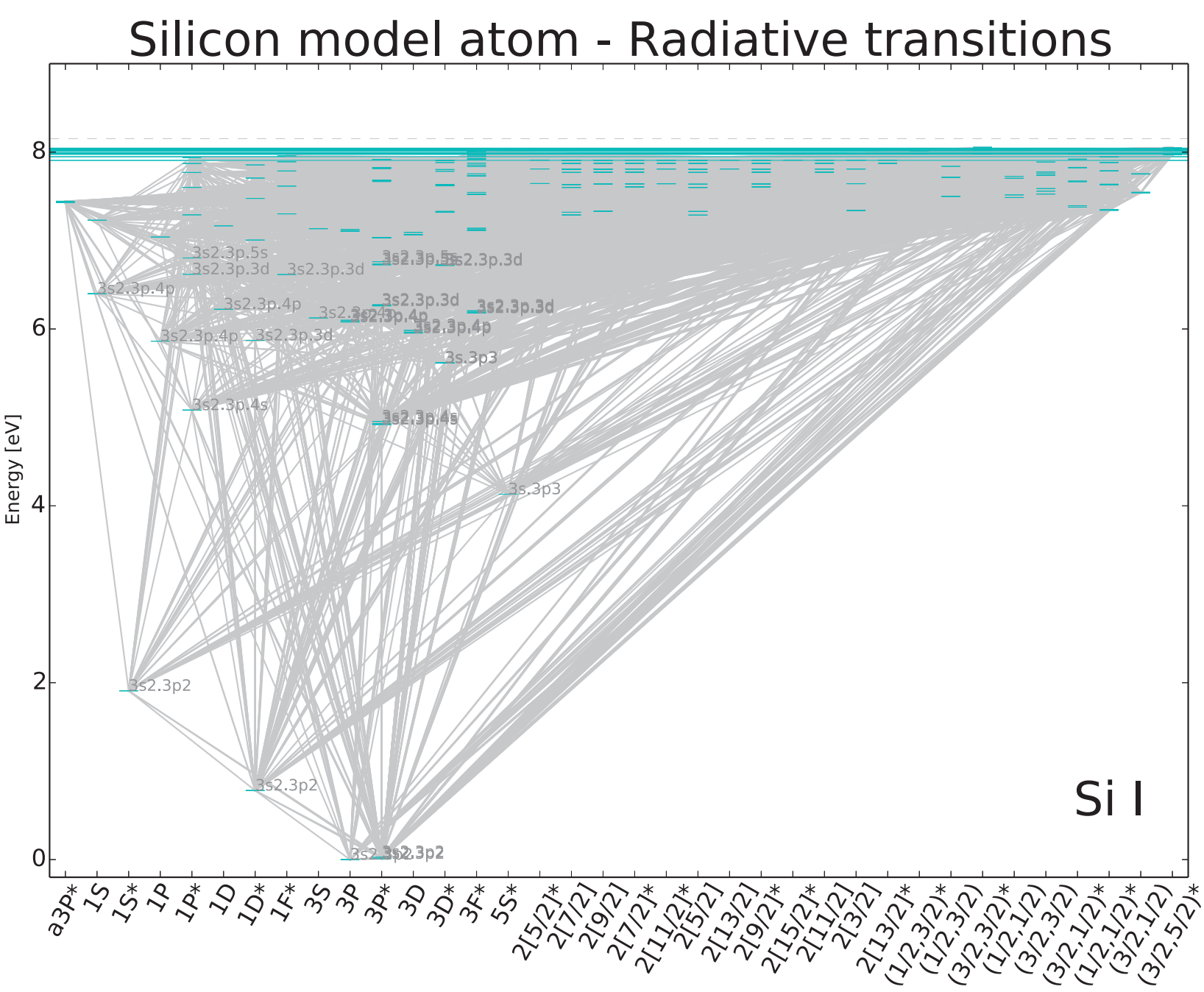

7 | Introducing the quantum fitting method (QFM)

It has been well established so far, in the course of this dissertation and throughout the literature, that the commonly used Drawin approximation, in the lack of quantum calculations for H collisions, is not able to correctly describe the rates for both excitation and charge transfer. Upon comparison with quantum calculations for Na, Mg, Al and Si (Figs. 3.8, 3.7, 3.6, and 3.9 respectively), it has been shown that not only does the Drawin approximation overestimate the magnitude of the rates by several orders of magnitude for most transitions, it also does not reproduce the correct behavior of the rates with transition energies. While the Drawin approximation adopted in this work depends solely on transition energy, it can be seen that the Drawin collisional rates decrease exponentially with ΔE, while the existing charge transfer quantum rates peak at ΔE between 1eV and 2eV. For Si, it can also be seen that the excitation/de-excitations rates behavior with ΔE is opposite to that predicted by Drawin's approximation: a peak is observed in the quantum rates for $\Delta E < 1$ eV (transitions between high lying Si levels).

In the light of these discrepancies, I thus introduce a semi-empirical method to determine the H collision rates for excitation / de-excitation, and charge transfer processes, which is based on fitting the H-collisional rates of Na, Mg, Al and Si. This approach was motivated by the analogous behavior of these rates as a function of energies for all these element.

7.1 Fitting the quantum data

7.1.1 Charge Transfer rates

Investigation of the charge transfer rates for Na, Mg, Al and Si shows similar behaviors with ΔE. As presented in Figs. 7.1, 7.2, 7.3 and 7.4, where the logarithmic mutual-neutralization (downward charge transfer) rates are plotted as a function of the inverse transition energies, a maximum peak occurs between 0.5 and 1 eV^{-1} for all four elements. In an attempt to fit the quantum data, we divided the rates into two linear parts intersecting at the maximum rate. By ignoring the rates whose value is less than 10^{-4} the maximum rate (thus assuring a better fit for dominant values), we were able to describe the rate coefficients $Q = \langle \sigma\nu \rangle$ as a function of $1/\Delta E$ for all the elements using the following general equations:

$$\log Q = \begin{cases} a_1 \left(\frac{1}{\Delta E} - \frac{1}{\Delta E_0} \right) + \log Q_{\max} & \textit{for} \quad \frac{1}{\Delta E} < \frac{1}{\Delta E_0} \\ a_2 \left(\frac{1}{\Delta E} - \frac{1}{\Delta E_0} \right) + \log Q_{\max} & \textit{for} \quad \frac{1}{\Delta E} > \frac{1}{\Delta E_0} \end{cases} \tag{7.1}$$

where a_1 and a_2 are respectively the positive and negative slopes of the linear fits, and $Q_{\max}$ is the maximum rate at $\frac{1}{\Delta E_0}$. For each element, the mutual-neutralization charge transfer rates,

at T=6000K, can be expressed as:

Na:

$$\log Q = \begin{cases} 7.03\left(\frac{1}{\Delta E} - 0.72\right) - 7.13 & \textit{for} \quad \frac{1}{\Delta E} < \frac{1}{\Delta E_0} \\ -2.60\left(\frac{1}{\Delta E} - 0.72\right) - 7.13 & \textit{for} \quad \frac{1}{\Delta E} > \frac{1}{\Delta E_0} \end{cases} \tag{7.2}$$

Mg:

$$\log Q = \begin{cases} 5.99\left(\frac{1}{\Delta E} - 0.63\right) - 7.34 & \textit{for} \quad \frac{1}{\Delta E} < \frac{1}{\Delta E_0} \\ -3.42\left(\frac{1}{\Delta E} - 0.63\right) - 7.34 & \textit{for} \quad \frac{1}{\Delta E} > \frac{1}{\Delta E_0} \end{cases} \tag{7.3}$$

Al:

$$\log Q = \begin{cases} 3.4\left(\frac{1}{\Delta E} - 0.73\right) - 7.2 & \textit{for} \quad \frac{1}{\Delta E} < \frac{1}{\Delta E_0} \\ -4.9\left(\frac{1}{\Delta E} - 0.73\right) - 7.2 & \textit{for} \quad \frac{1}{\Delta E} > \frac{1}{\Delta E_0} \end{cases} \tag{7.4}$$

Si:

$$\log Q = \begin{cases} 4.39\left(\frac{1}{\Delta E} - 0.75\right) - 7.44 & \textit{for} \quad \frac{1}{\Delta E} < \frac{1}{\Delta E_0} \\ -3.52\left(\frac{1}{\Delta E} - 0.75\right) - 7.44 & \textit{for} \quad \frac{1}{\Delta E} > \frac{1}{\Delta E_0} \end{cases} \tag{7.5}$$

Figure 7.1: Na+H mutual-neutralization rate fits as a function of $1/\Delta E$ at T=6000K.

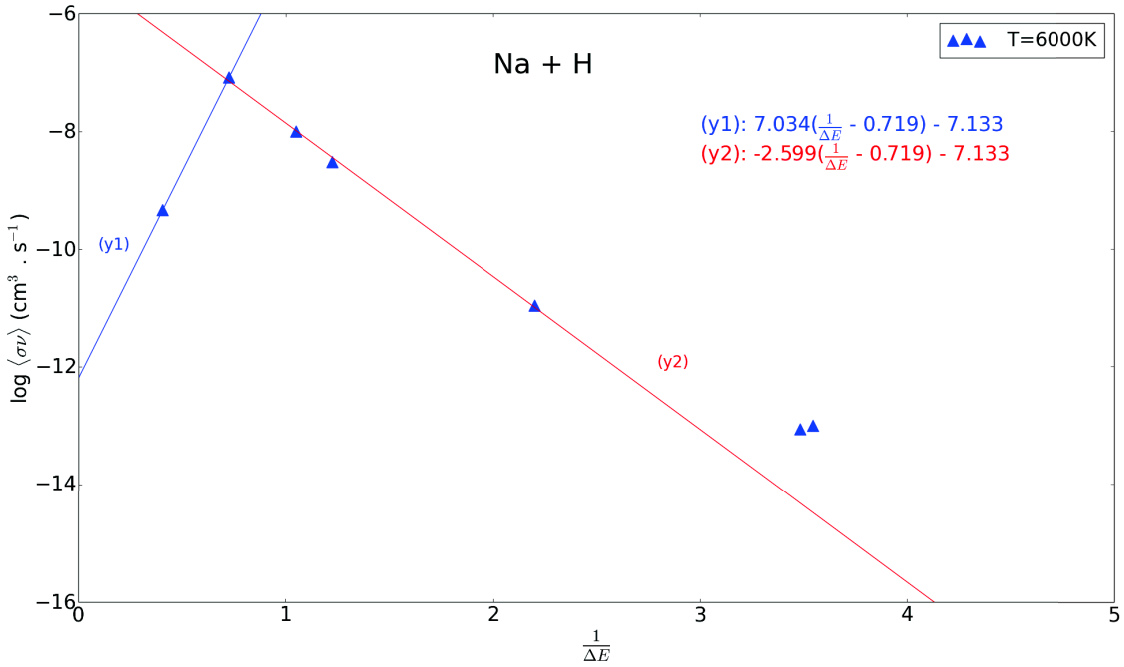

Figure 7.2: Mg+H mutual-neutralization rate fits as a function of $1/\Delta E$ at T=6000K.

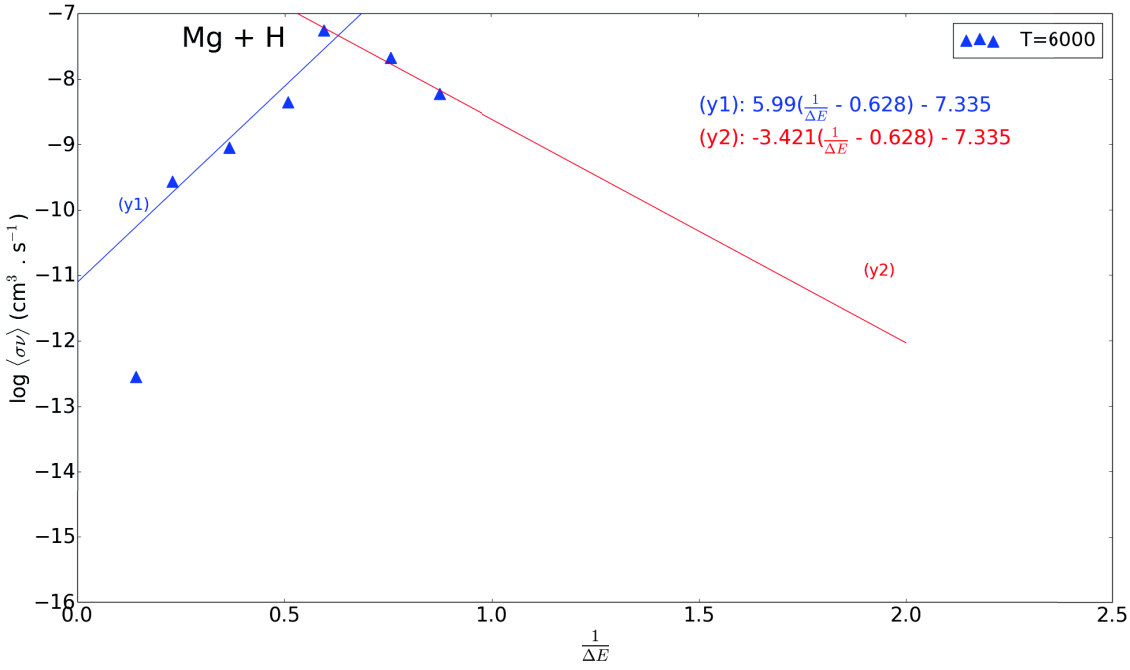

Figure 7.3: Al+H mutual-neutralization rate fits as a function of $1/\Delta E$ at T=6000K.

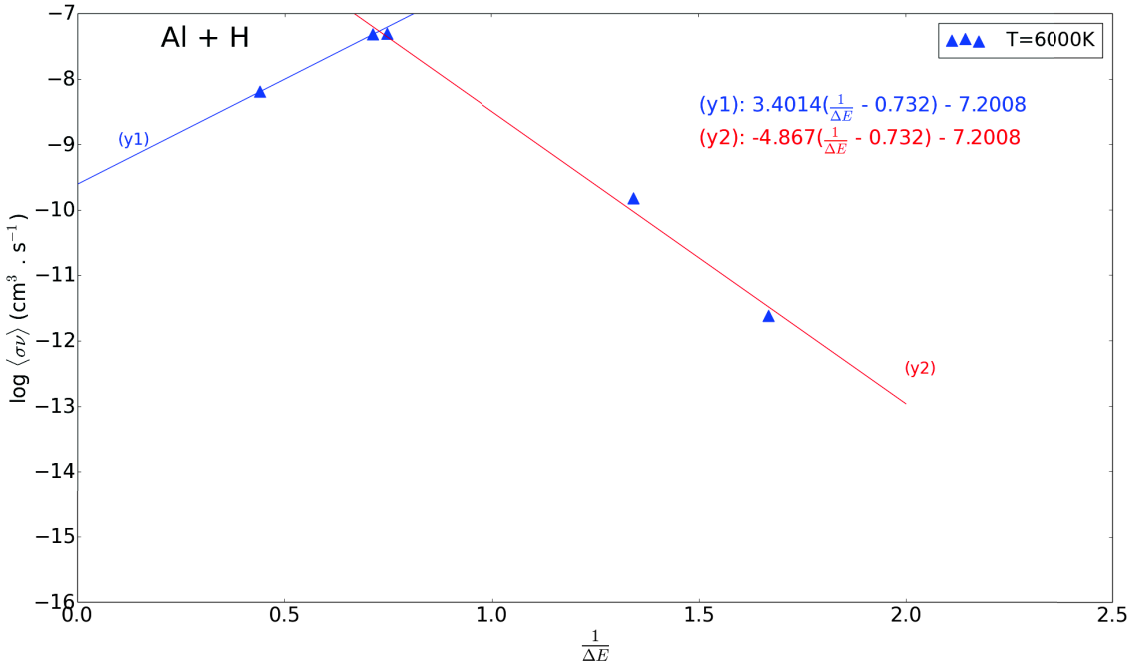

Figure 7.4: Si+H mutual-neutralization rate fits as a function of $1/\Delta E$ at T=6000K.

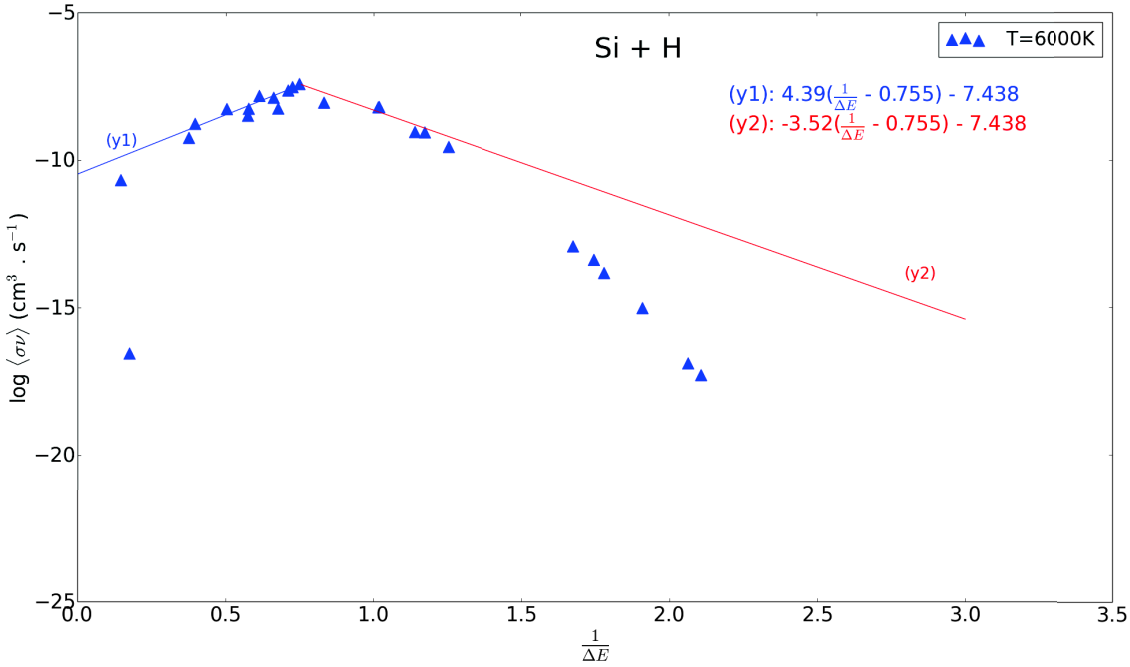

We see that $\log Q_{\max} \simeq -7.2 \pm 0.3$ cm$^3 \cdot$s^{-1} and $\frac{1}{\Delta E_0} \simeq 0.7 \pm 0.07$ eV^{-1} for all four elements.

Temperature dependence plots of the fitting parameters, a_1, a_2, $\frac{1}{\Delta E_0}$ and log $Q_{\max}$, for all four chemical elements (Figs. 7.5, 7.6, 7.7 and 7.8) show that a_1 depends roughly linearly on T, $\log Q_{\max}$ depends linearly on log T, while a_2 and $\frac{1}{\Delta E_0}$ do not vary significantly with temperature, except a_2 for Al. It follows that a_1 and $\log Q_{\max}$ can be generally written as:

$$\begin{cases} a_1 = a_{11}\left(\frac{T}{10^4}\right) + a_{10} \\ Q_{\max} = T^{\alpha} \times 10^{y_0} \end{cases} \tag{7.6}$$

which for the different elements are found to be:

Na:

$$\begin{cases} a_1 = -1.50\left(\frac{T}{10^4}\right) + 7.92 \\ Q_{\max} = T^{-0.37} \times 10^{-5.71} \end{cases} \tag{7.7}$$

Mg:

$$\begin{cases} a_1 = -2.12\left(\frac{T}{10^4}\right) + 7.36 \\ Q_{\max} = T^{-0.35} \times 10^{-6.01} \end{cases} \tag{7.8}$$

Al:

$$\begin{cases} a_1 = -7.46\left(\frac{T}{10^4}\right) + 3.74 \\ Q_{\max} = T^{-0.56} \times 10^{-5.71} \end{cases} \tag{7.9}$$

Si:

$$\begin{cases} a_1 = -1.20\left(\frac{T}{10^4}\right) + 4.90 \\ Q_{\max} = T^{-0.34} \times 10^{-6.19} \end{cases} \tag{7.10}$$

where similar values of $\alpha \simeq -0.34 \pm 0.03$ and $y_0 \simeq -6.0 \pm 0.3$ are obtained for all elements, except for Al where $\alpha = -0.56$. For $T \in [3000, 7000]$ (temperature range of interest in cool stellar atmospheres), a_1 varies within $< 20\%$ while $Q_{\max}$ varies within less than a factor of 5.

Figure 7.5: Na+H charge transfer fitting parameters temperature dependence.

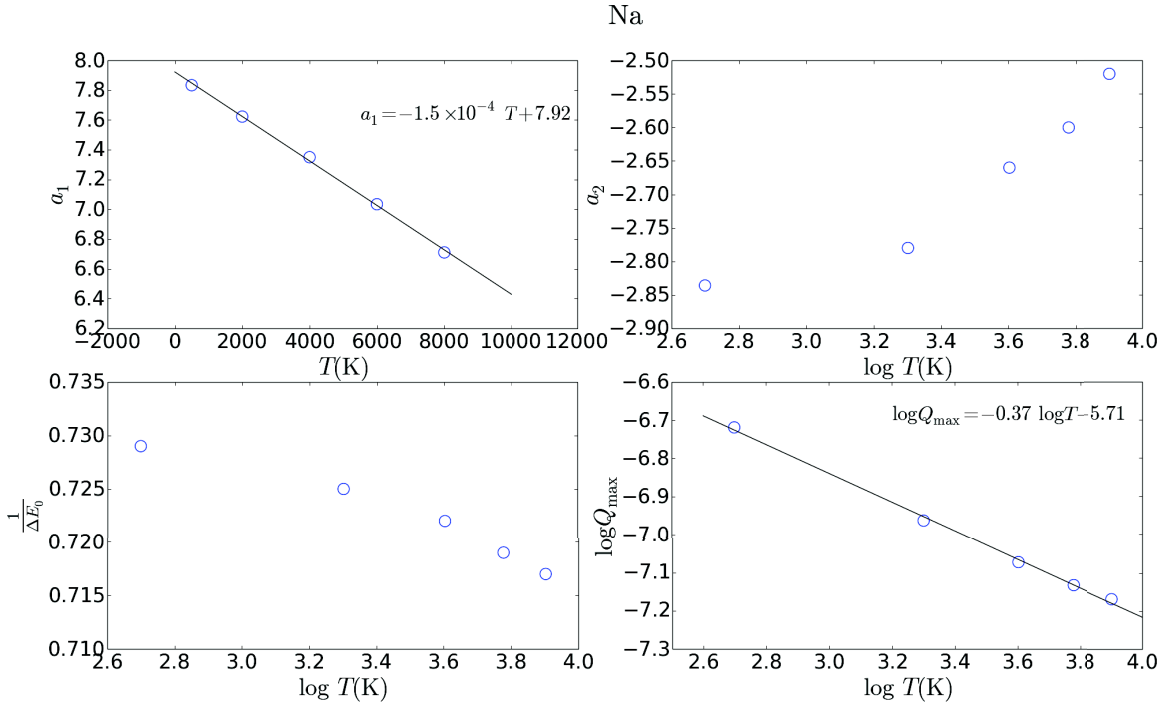

Figure 7.6: Mg+H charge transfer fitting parameters temperature dependence.

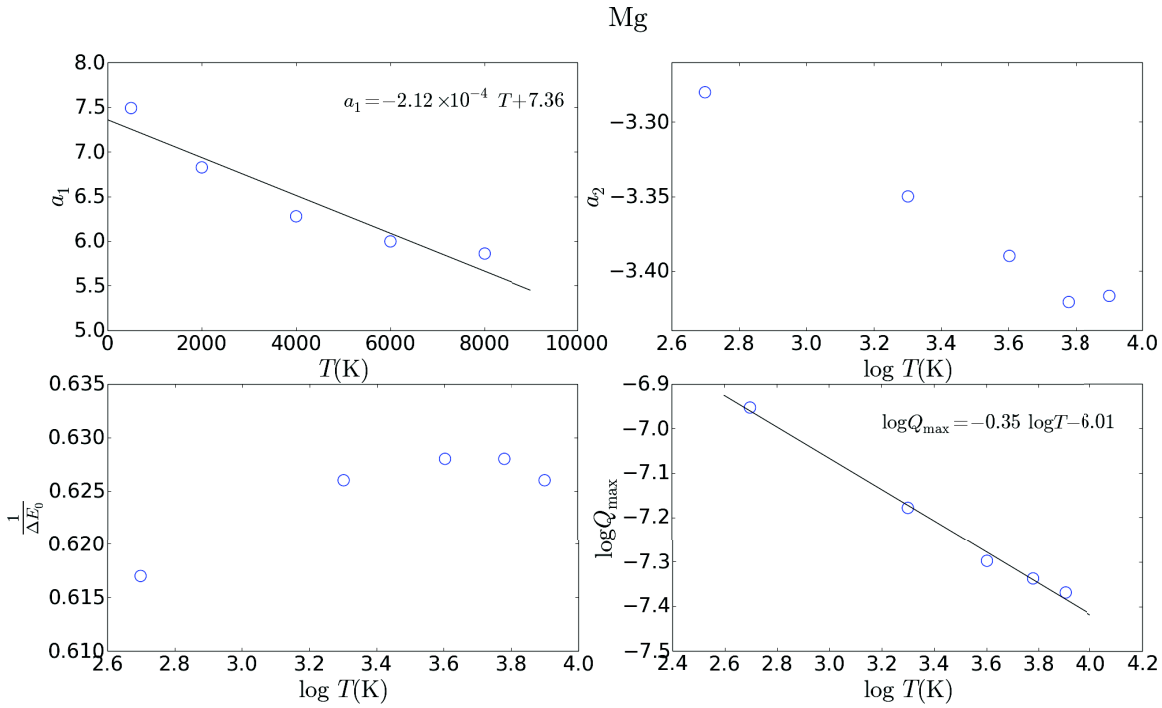

Figure 7.7: Al+H charge transfer fitting parameters temperature dependence.

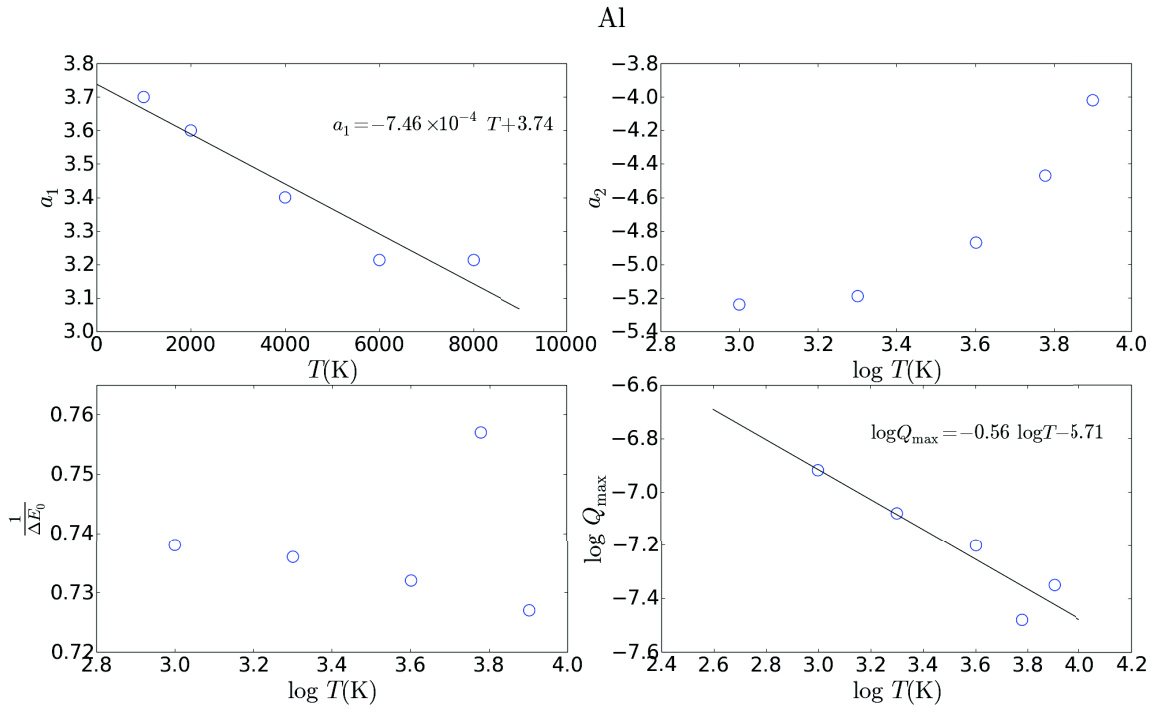

Figure 7.8: Si+H charge transfer fitting parameters temperature dependence.

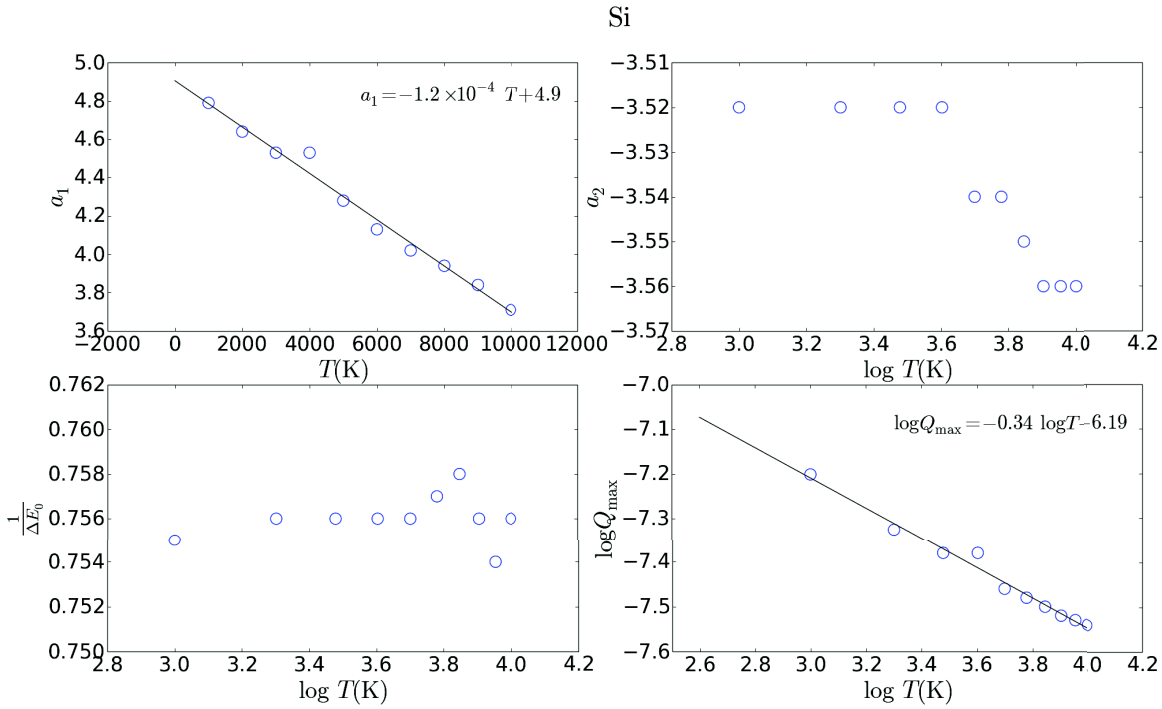

7.1.2 De-excitation rates

The quantum de-excitation rates for all four atoms show larger scatter than charge transfer rates as more transitions are included, and a decreasing behavior with increasing transition energies with large variations in magnitudes between the maximum and minimum rates (up to 10 orders of magnitude). The rates are best fit as a function of ΔE using a third degree polynomial fit, i.e.:

$$\log Q = b_3 \Delta E^3 + b_2 \Delta E^2 + b_1 \Delta E + b_0 \tag{7.11}$$

The de-excitation rates and their respective fits are shown in Figs. 7.9, 7.10, 7.11, and 7.12 for Na, Mg, Al and Si respectively.
The rates can be written for the different species,at T=6000K, as follows:

Na:

$$\log Q = -0.23\,\Delta E^3 + 1.74\,\Delta E^2 - 5.39\,\Delta E - 9.84 \tag{7.12}$$

Mg:

$$\log Q = -0.08\,\Delta E^3 - 0.57\,\Delta E^2 - 1.38\,\Delta E - 9.05 \tag{7.13}$$

Al:

$$\log Q = 0.324\,\Delta E^3 - 2.72\,\Delta E^2 + 2.00\,\Delta E - 10.87 \tag{7.14}$$

Si:

$$\log Q = -0.07\,\Delta E^3 - 0.68\,\Delta E^2 - 1.85\,\Delta E - 9.45 \tag{7.15}$$

The obtained fitting parameters b_3, b_2 and b_1 vary from one element to the other, while b_0 which is the scaling coefficient of log$Q$ varies between $\simeq$ -9.0 and $\simeq$ -11.0. For Mg and Si, similar values are obtained for $b_3 \simeq -0.1$, $b_2 \simeq 0.6$, $b_1 \simeq -1.5$ and $b_0 \simeq -9.5$ respectively. In addition, b_3, b_2 and b_1 are linearly dependent on $\log T$, while b_0 does not vary much with temperature as is shown in Fig. 7.13 for Si for e.g.

This allows the de-excitation fitting parameters to be written as:

$$\begin{cases} b_3 = b_{31}\ \log T + b_{30} \\ b_2 = b_{21}\ \log T + b_{20} \\ b_1 = b_{11}\ \log T + b_{10} \\ b_0 = \text{constant} \end{cases} \tag{7.16}$$

where for Si, they can be written as:

$$\begin{cases} b_3 = -0.08\ \log T + 0.233 \\ b_2 = 0.69\ \log T - 2.047 \\ b_1 = -1.356\ \log T + 3.511 \\ b_0 \simeq -9.75 \end{cases} \tag{7.17}$$

Figure 7.9: Na+H de-excitation rates fit as a function of ΔE.

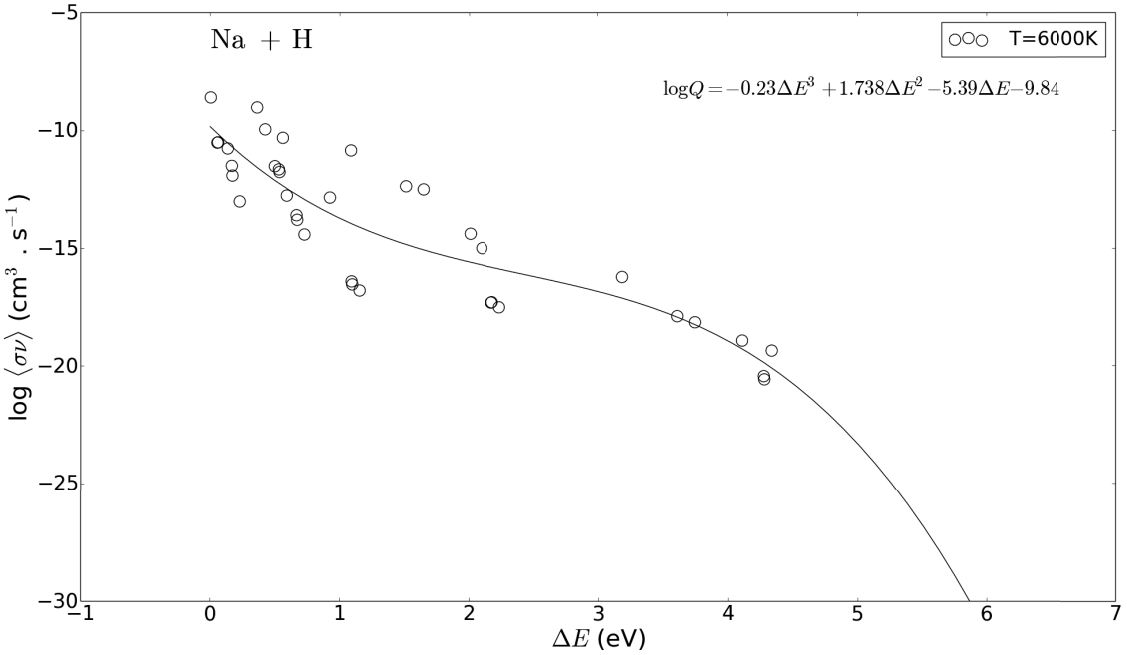

Figure 7.10: Mg+H de-excitation rates fit as a function of ΔE.

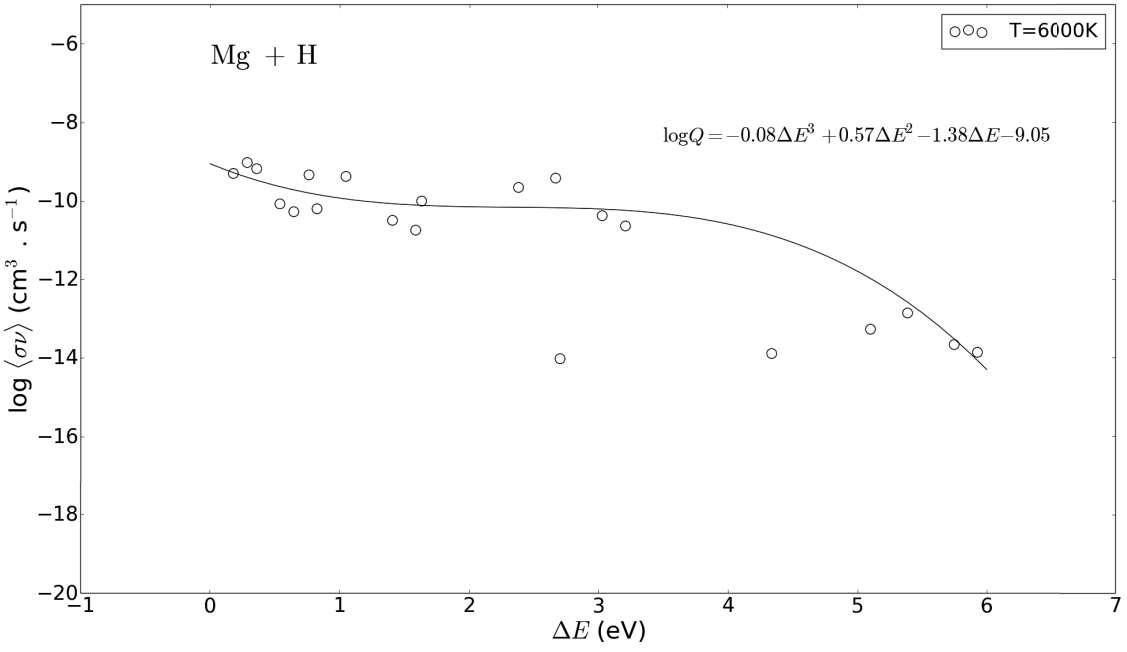

Figure 7.11: Al+H de-excitation rates fit as a function of ΔE.

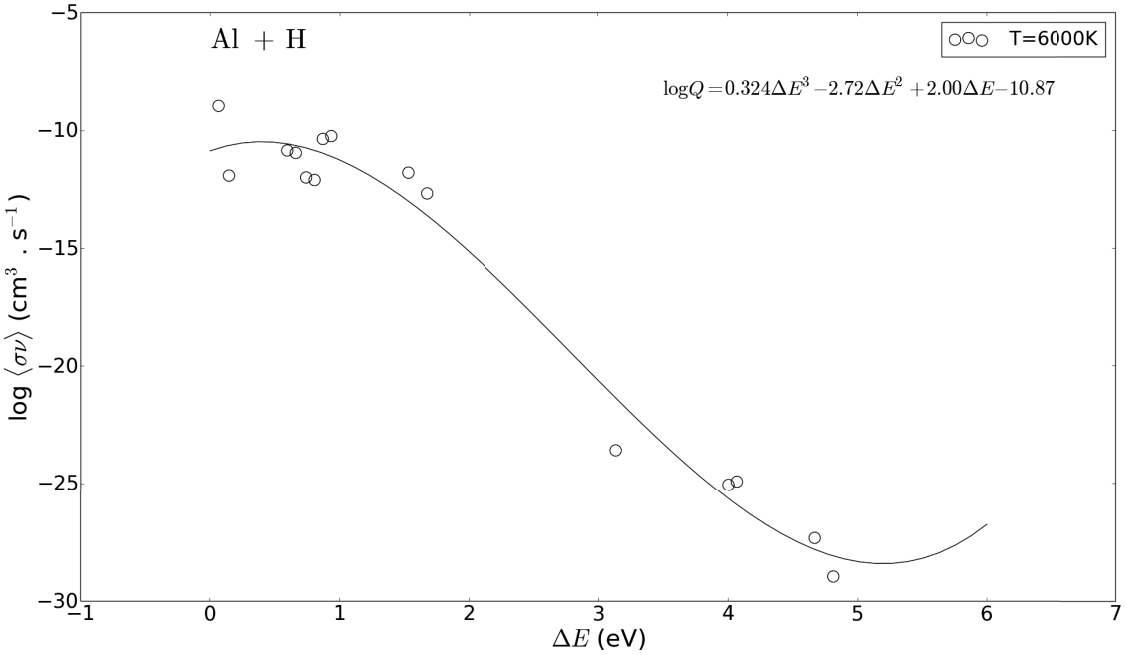

Figure 7.12: Si+H de-excitation rates fit as a function of ΔE.

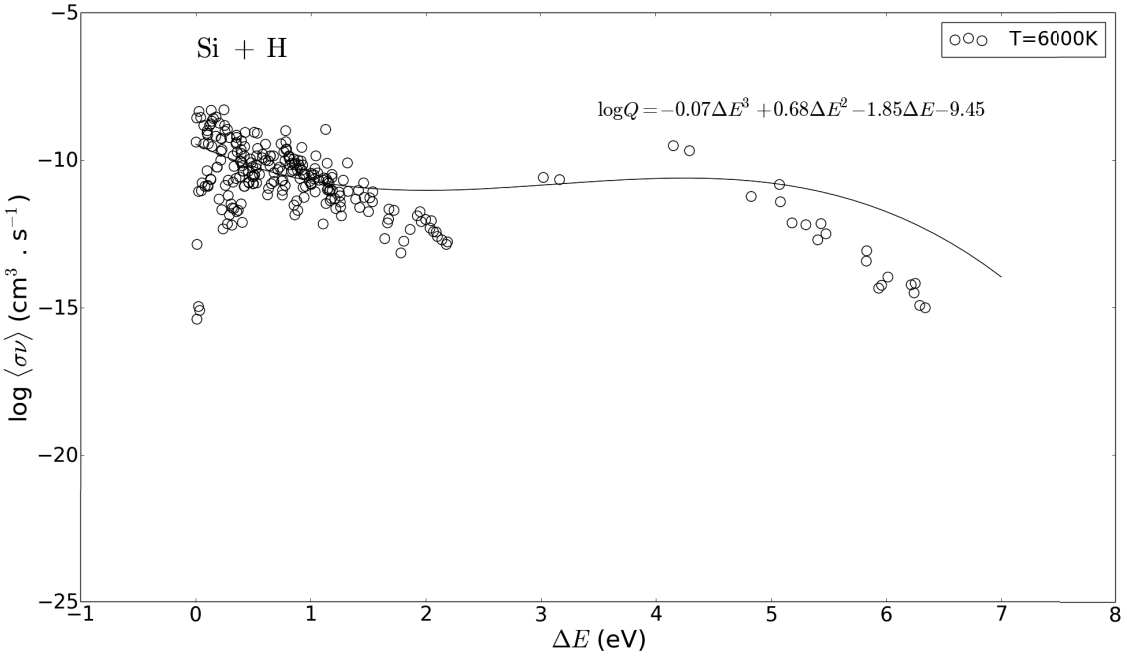

Figure 7.13: Si+H de-excitation fitting parameters temperature dependence.

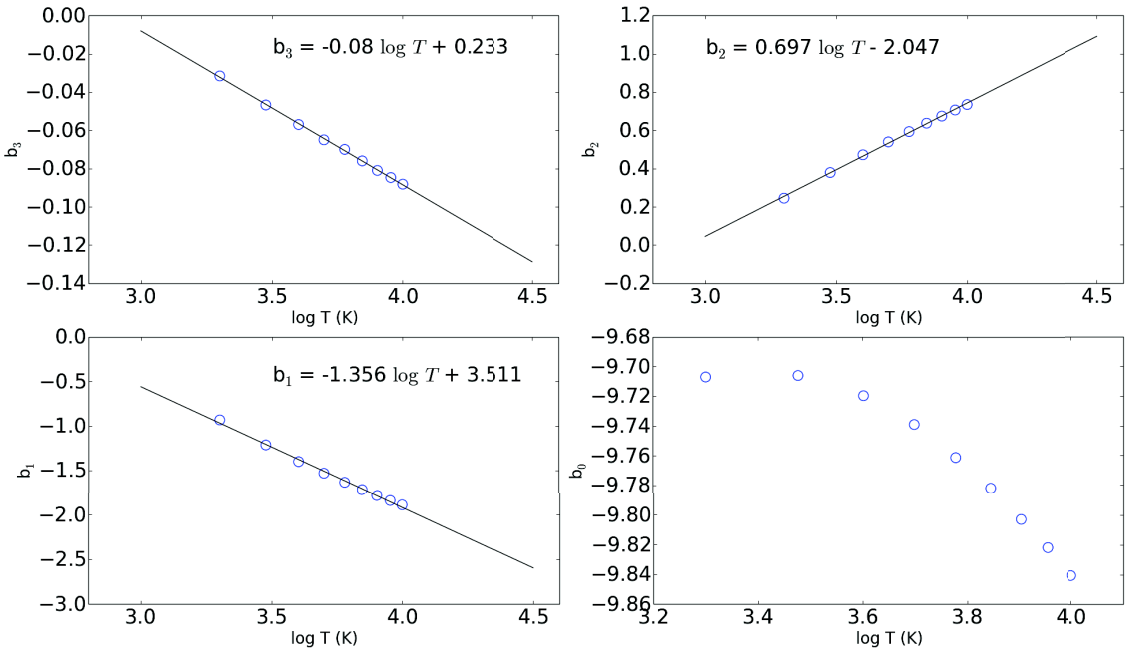

7.2 Silicon non-LTE calculations using the quantum fitting method

To test the effects of using the QFM as compared to the real quantum data on the non-LTE calculations, a modified Si model atom (described in Sect. 6.1) was built using the Si quantum fitting parameters described in Eqns. 7.5 and 7.15 for the calculation of the charge transfer and excitation rates, and taking into account the temperature dependence of the parameters from Eqns. 7.10 & 7.17. The Si model atoms were used to compute non-LTE EW. The tests were performed on three benchmark stars: the Sun, Arcturus and HD140283. Results are shown in Fig. 7.14, where the QFM $\mathrm{EW_{fit}}$ are compared to the reference $\mathrm{EW_{QM}}$ (calculated using the real quantum data), for lines whose transition energies are between 1 eV and 4 eV (lines between $2000\text{Å} \leq \lambda \leq 10000\text{Å}$).
To quantify the differences, we define the average relative difference $\overline{Y_{\mathrm{rel}}}$ between $\mathrm{EW_{fit}}$ and $\mathrm{EW_{QM}}$ as:

$$\overline{Y_{\mathrm{rel}}} = \frac{1}{\mathrm{N_{lines}}} \sum_{i=1}^{\mathrm{nlines}} \frac{\mathrm{EW}^i_{\mathrm{fit}} - \mathrm{EW}^i_{\mathrm{QM}}}{\mathrm{EW}^i_{\mathrm{QM}}} \tag{7.18}$$

The non-LTE calculations made using the QFM for Si+H collisions are able to well-reproduce those using the quantum data within negligible differences, where $\overline{Y_{\mathrm{rel}}}$ obtained for the three stars was $\leq 3\%$ (0.0384 for the Sun, 0.0056 for Arcturus, and 0.0035 for HD140283).

This also shows that ignoring rates whose magnitudes are 4 orders of magnitude smaller than the maximum rate in the fit as shown in Fig. 7.4, is acceptable and does not propagate onto the computed equivalent widths.

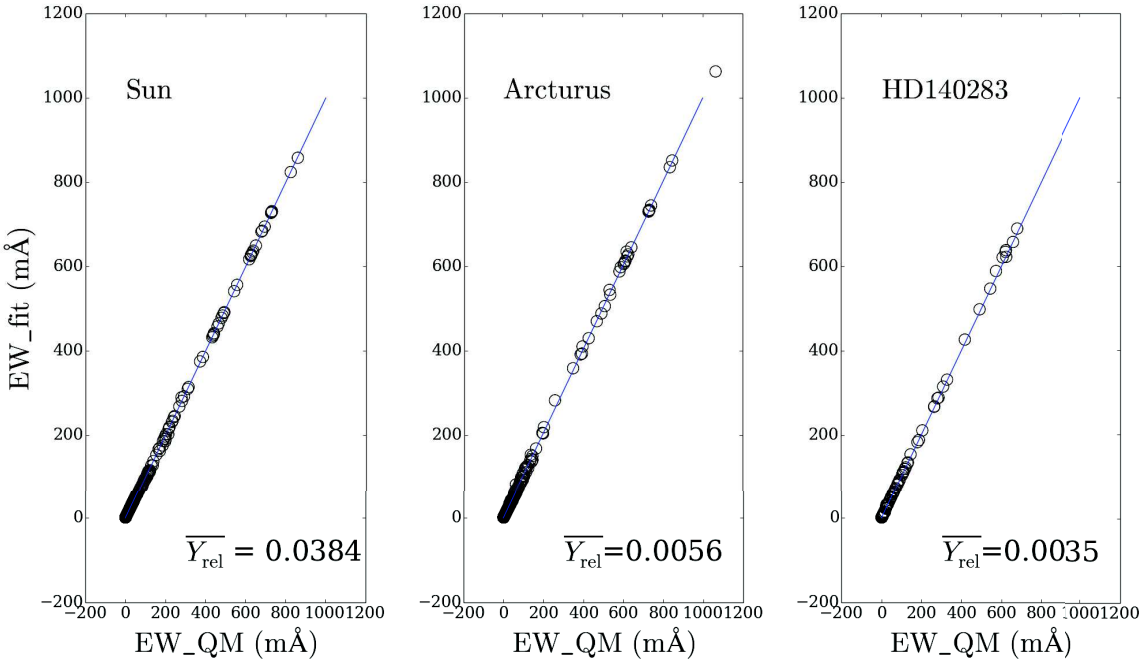

Figure 7.14: Si non-LTE EW calculated using the QMF ($\mathrm{EW_{fit}}$) vs. real quantum rates ($\mathrm{EW_{QM}}$) for the Sun, Arcturus, and HD140283.

7.2.1 Testing the effects of the QFM parameters

To test the effects of varying the different fitting parameters on the calculated EW, modified Si model atoms were used where the Si fitting parameters for charge transfer and de-excitation were varied around their nominal values from Eqns. 7.5 & 7.15 (hereafter denoted reference fit). Each parameter was respectively decreased and increased from its reference value as shown in Table 7.1. a_{11} and α are kept to their reference values of -1.2 and -0.35 respectively, to avoid larger number of fitting parameters. Changing one parameter at a time, non-LTE Si calculations were performed for each model for the Sun and the metal poor star HD140283. Calculated $\mathrm{EW_{mod}}$ for each model, are compared to those obtained by the reference fit (Figs. 7.16, 7.17, 7.18 and 7.19).

To quantify the difference, the relative difference standard deviation $\sigma\, Y_{\rm rel} = \sqrt{\mathrm{var}\, Y_{\rm rel}}$ was calculated for each model from the variance, where:

$$\mathrm{var}\, Y_{\rm rel} = \frac{1}{\mathrm{N_{lines}} - 1} \sum_{i=1}^{\rm nlines} \left(\frac{\mathrm{EW}^i_{\rm mod} - \mathrm{EW}^i_{\rm ref}}{\mathrm{EW}^i_{\rm ref}} \right)^2 \tag{7.19}$$

is the relative difference variance. Table 7.1 shows $\sigma\, Y_{\rm rel}$ obtained for each model for the two stars.

It is shown that varying the charge transfer fitting parameters a_{10}, a_2, and $\frac{1}{\Delta E_0}$ within $\pm 50\%$ of their reference values, results in a small percentage of variation in the computed $\mathrm{EW_{mod}}$ ($Y_{\rm rel} < 0.1$, i.e. $< 10\%$) and a small scatter (dotted lines show $\sigma\, Y < 0.01$ for a_1 and a_2, and $\sigma\, Y_{\rm rel} < 0.03$ for $\frac{1}{\Delta E_0}$), for the two stars.
Varying y_0 within ± 1 order of magnitude from its reference value, shows slightly larger scatter ($\sigma\, Y_{\rm rel} < 0.05$) than other parameters with relative differences $Y_{\rm rel} < 0.1$. This shows that y_0 plays an expected important role in shifting the computed $\mathrm{EW_{mod}}$, as it scales and shifts the

rates by orders of magnitudes from their nominal values.

Varying the de-excitation fitting parameters within $\pm 50\%$ and b_0 within $\pm$ 1 order of magnitude from their respective reference values, results in a relative difference up to 0.1 (i.e. 10%), with a scatter $\sigma\, Y < 0.05$ for all models and both stars (See Table 7.1 for detailed numbers).
The results thus show that a variation in the fit within $\pm 50\%$ from its reference value, as presented in Fig. 7.15 for the variation of a_1 and a_2 (dark and light gray shaded areas respectively), propagates onto a relative difference of $< 10\%$ and a scatter of $\sigma\, Y < 5\%$ in the computed $\mathrm{EW}_{\mathrm{mod}}$. This means that the acceptable range of variation around the optimal values is quite broad.

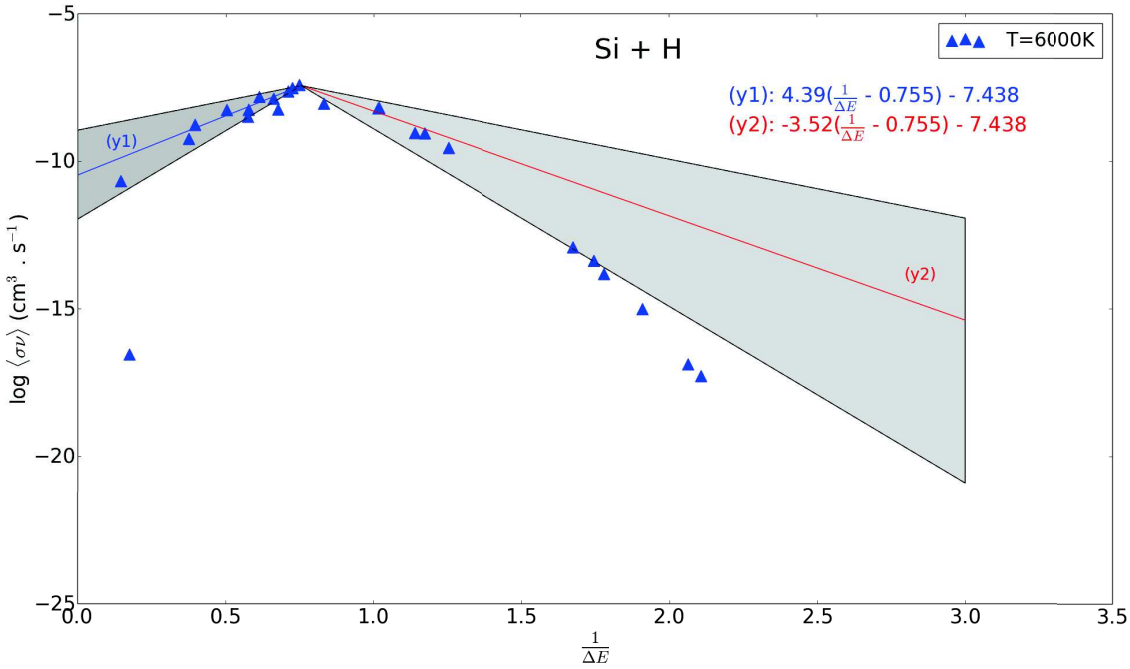

Figure 7.15: Si+H mutual neutralization rates fits as a function of $1/\Delta E$ at T=6000K, also showing the range of variation of a_1 between [2,6] (dark gray shaded area) and a_2 between [-6,-2] (light gray shaded area).

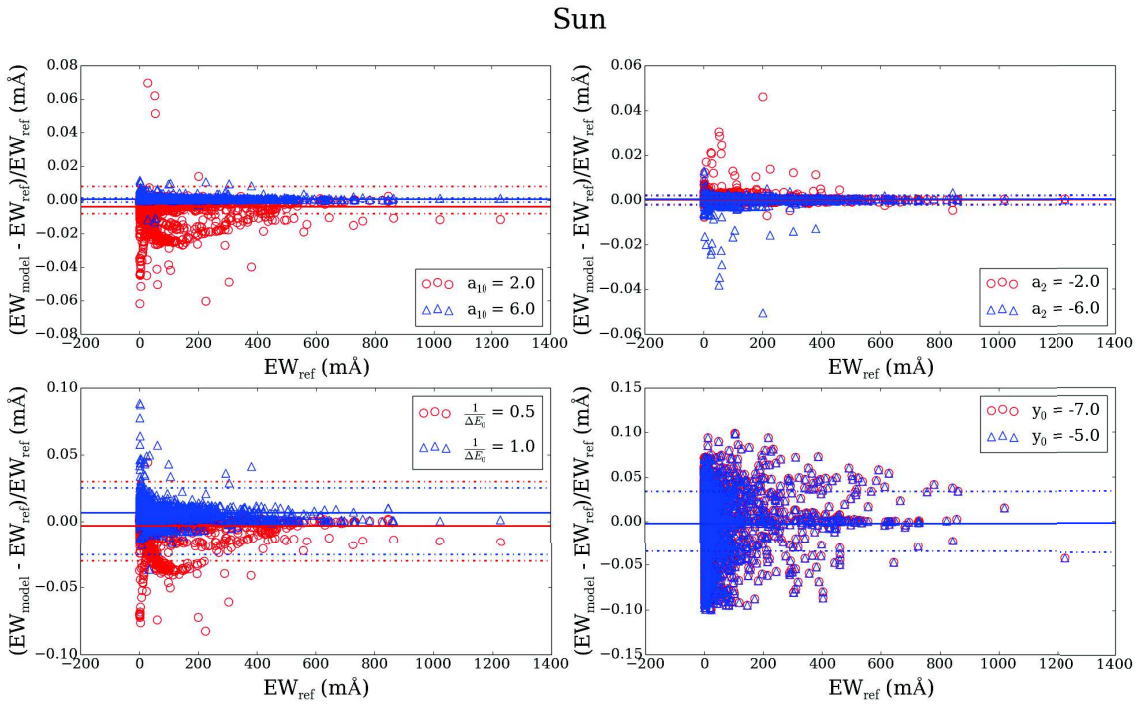

Figure 7.16: Si+H charge transfer fitting parameter variation effects on the calculated non-LTE EW as compared to the reference fit for the Sun. Solid and dotted lines show the relative difference average $\overline{Y_{\rm rel}}$, and its standard deviation $\sigma\, Y$ for each corresponding model.

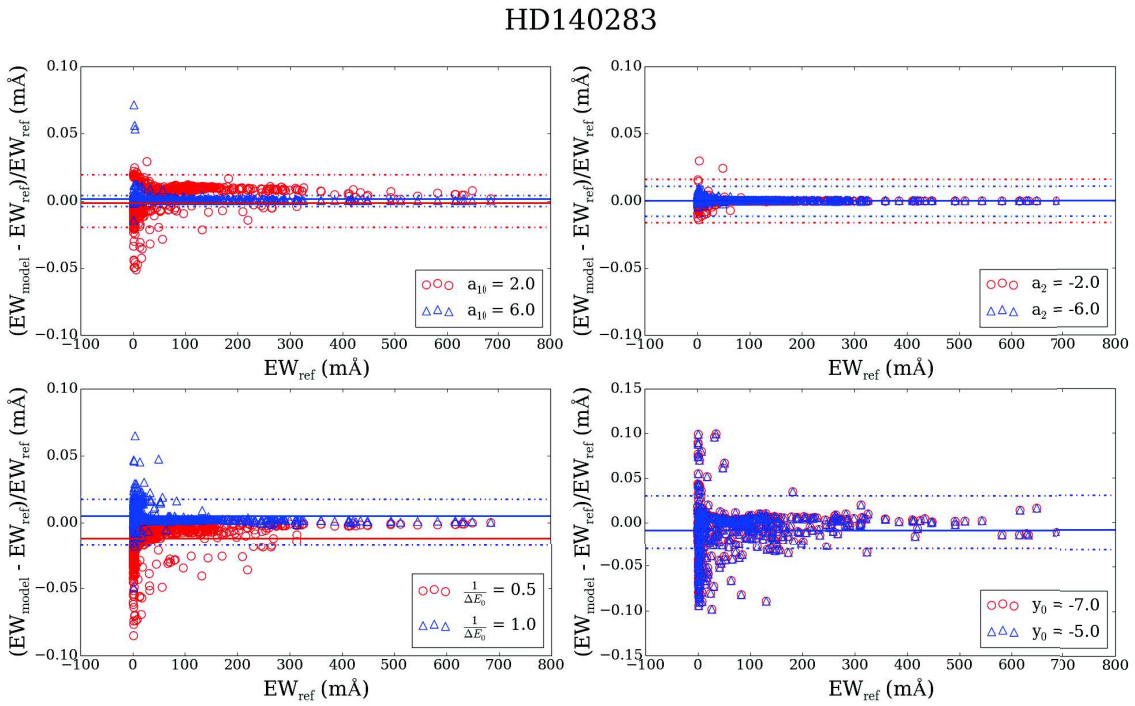

Figure 7.17: Si+H charge transfer fitting parameter variation effects on the calculated non-LTE EW as compared to the reference fit for HD140283. Solid and dotted lines represent the same thing as in Fig. 7.16.

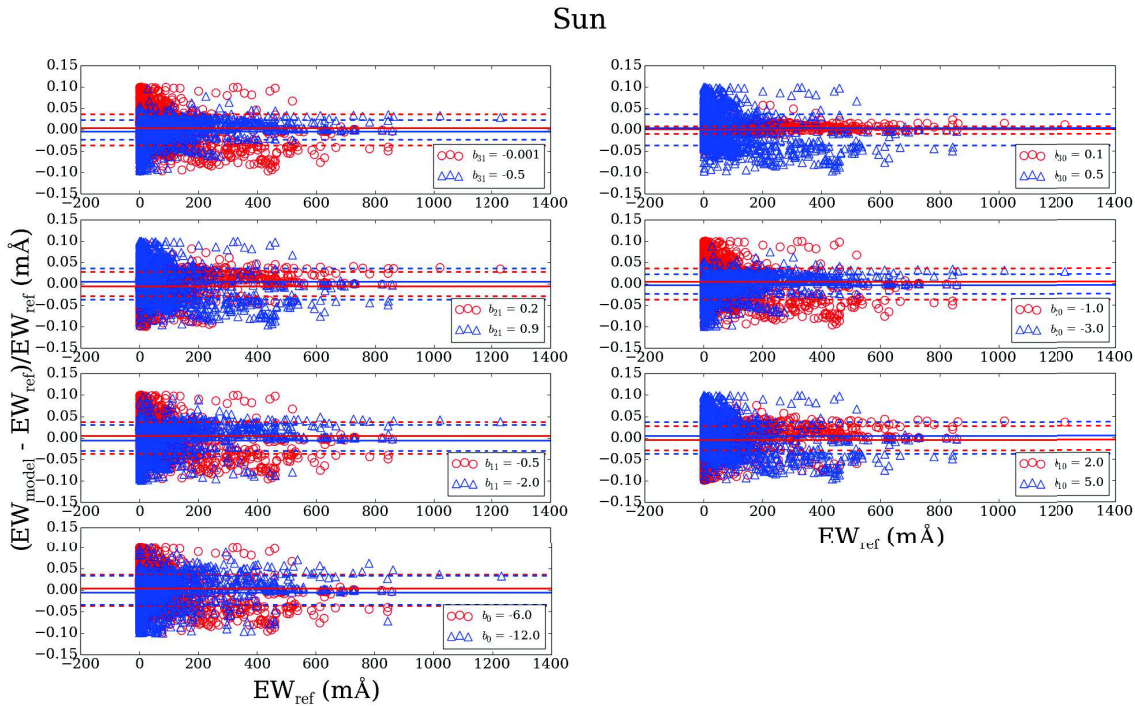

Figure 7.18: Si+H de-excitation fitting parameter variation effects on the calculated non-LTE EW as compared to the reference fit for the Sun. Solid and dotted lines represent the same thing as in Fig. 7.16.

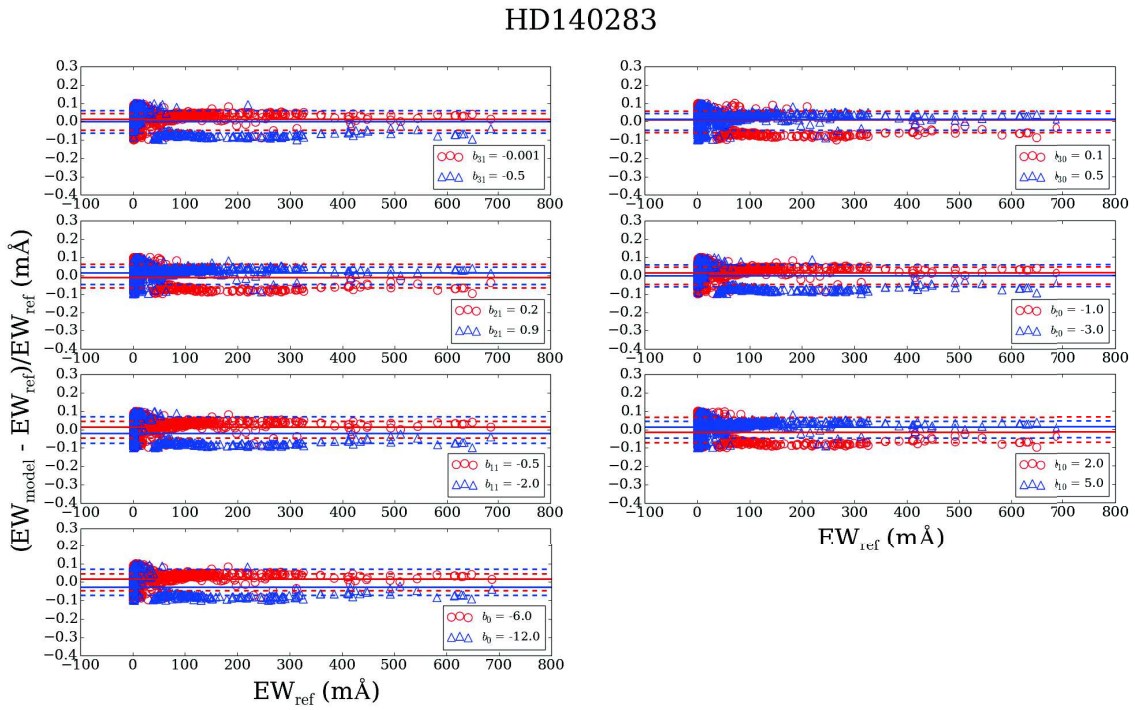

Figure 7.19: Si+H de-excitation fitting parameter variation effects on the calculated non-LTE EW as compared to the reference fit for HD140283. Solid and dotted lines represent the same thing as in Fig. 7.16.

fitting parameter	reference value	value	$\sigma\, Y_{\rm rel}$		value	$\sigma\, Y_{\rm rel}$	
			Sun	HD140283		Sun	HD140283
Mutual-neutralization rate parameters							
a_1	4.9	2	7.98×10^{-3}	1.94×10^{-2}	7	1.09×10^{-3}	4.26×10^{-2}
a_2	-3.52	-2	1.88×10^{-3}	1.62×10^{-2}	-6	2.16×10^{-3}	1.23×10^{-2}
$\frac{1}{\Delta E_0}$	0.75	0.5	1.02×10^{-2}	1.78×10^{-2}	1.00	1.29×10^{-2}	1.75×10^{-2}
y_0	-6.0	-5.0	4.41×10^{-2}	1.55×10^{-2}	-7.0	4.79×10^{-2}	3.51×10^{-2}
De-excitation rate parameters							
b_{31}	-0.08	-0.001	3.57×10^{-2}	8.72×10^{-2}	-0.5	2.62×10^{-3}	9.85×10^{-2}
b_{30}	0.233	0.1	9.41×10^{-3}	9.375×10^{-2}	0.5	3.57×10^{-2}	8.72×10^{-2}
b_{21}	0.69	0.2	4.01×10^{-2}	9.87×10^{-2}	0.9	9.92×10^{-2}	8.72×10^{-2}
b_{20}	-2.047	-1.0	9.75×10^{-2}	8.73×10^{-2}	-3.0	2.71×10^{-2}	9.70×10^{-2}
b_{11}	-1.35	-0.5	1.88×10^{-2}	8.62×10^{-2}	-2.0	7.59×10^{-2}	9.95×10^{-2}
b_{10}	3.5	2.0	5.73×10^{-2}	9.50×10^{-2}	5.0	1.87×10^{-2}	8.64×10^{-2}
b_0	-9.75	-8.0	9.88×10^{-2}	8.52×10^{-2}	-11.0	9.52×10^{-2}	9.80×10^{-2}

Table 7.1: Si+H rates fitting parameters variations from the reference values for which non-LTE calculations were performed.

7.3 Iron non-LTE calculations using the QFM

The similarity in the behavior of the mutual neutralization and de-excitation quantum rates as a function of transition energies for the different chemical species, and the similar values obtained for the fitting parameters, especially for charge transfer rates, has motivated us to apply the QFM recipe to iron, instead of using Drawin approximation. The aim in this section, is therefore to calibrate the iron fitting parameters using the benchmark stars (Chapter 5).

7.3.1 Method

We implement collisional rates in our iron model atom using Eqns. 7.1 and 7.11 to calculate Fe I+H charge transfer rates and Fe I+H excitation rates respectively. For the Fe I+H ionization rates and Fe II+H rates, Lambert's version of the Drawin approximation was used since no quantum data for the other chemical species have been calculated for these processes, and thus the QFM can only be applied for the charge transfer and bound-bound transitions for neutral iron. It can be stated though, that using the Drawin approximation to calculate the Fe II+H collisional rates should be acceptable since it is well established in all previous iron non-LTE studies, that Fe II species, being the dominant in cool stars, are not subject to non-LTE effects (Bergemann et al., 2012; Lind et al., 2011; Mashonkina et al., 2011; Thévenin and Idiart, 1999). On the other hand, using the Drawin approximation to calculate Fe I+H ionization rates, for the lack of an alternative, can be acceptable under the assumption that ionization collisions are higher-energy collisions than excitations, that can be well described by the Born approximation, which is the basis of the Drawin approximation (Barklem et al., 2010).

7.3.2 Charge transfer fitting

The best fitting parameters for Fe I+H charge transfer rates are determined starting with the fitting parameters for Si, and calculating a grid of non-LTE models defined by varying the fitting parameters a_{11}, a_2, $\frac{1}{\Delta E_0}$ and y_0 between the values shown in Table 7.2, while keeping the de-excitation rates constant. The different models were tested on 3 types of benchmark stars: a dwarf (Sun), a giant (Arcturus) and a metal-poor star (HD140283). Hence, a total of 72

models were calculated for each star. The calculated EW_{mod} of each model were compared to the measured EW_{obs} using the χ^2 defined in Eqn. 6.3. The results for the different models are shown in Figs. 7.20, 7.21 and 7.22 for the Sun, Arcturus and HD140283 respectively. Missing symbols for Arcturus and HD140283 correspond to models where no numerical convergence could be obtained.

parameter	values range	step
a_{10}	[2.0,6.0]	$\Delta = 2.0$
a_2	[-6.0,-2.0]	$\Delta = 2.0$
$\frac{1}{\Delta E_0}$	[0.5,1.0]	$\Delta = 0.25$
y_0	[-11.0,-3.0]	$\Delta = 1$

Table 7.2: Fe I+H charge transfer rates fitting parameters range of values, for which non-LTE calculations were performed.

For the 3 stars (Figs. 7.20, 7.21 and 7.22), a clear flat minimum is obtained around $y_0 \simeq -9.0$ which is independent of other parameters, within the range of variation.
For the Sun, a_2 does not play an important role: negligible χ^2 differences are obtained for all the models. For Arcturus and HD140283, χ^2 decreases slightly with increasing a_2.
Increasing a_{11} and $\frac{1}{\Delta E_0}$ also induces a decrease in χ^2 for all values of y_0. While increasing values of a_{11}, a_2 and $\frac{1}{\Delta E_0}$ give general decreasing χ^2 values, it can be seen that y_0 plays the most important role in the χ^2 variation. We find a single set of best fitting parameters for Fe I+H charge transfer fits for all 3 stars: $\boxed{a_{10} = 6.0}$, $\boxed{a_2 = -6.0}$, $\boxed{\frac{1}{\Delta E_0} = 0.75}$ and $\boxed{y_0 = -9.0}$.

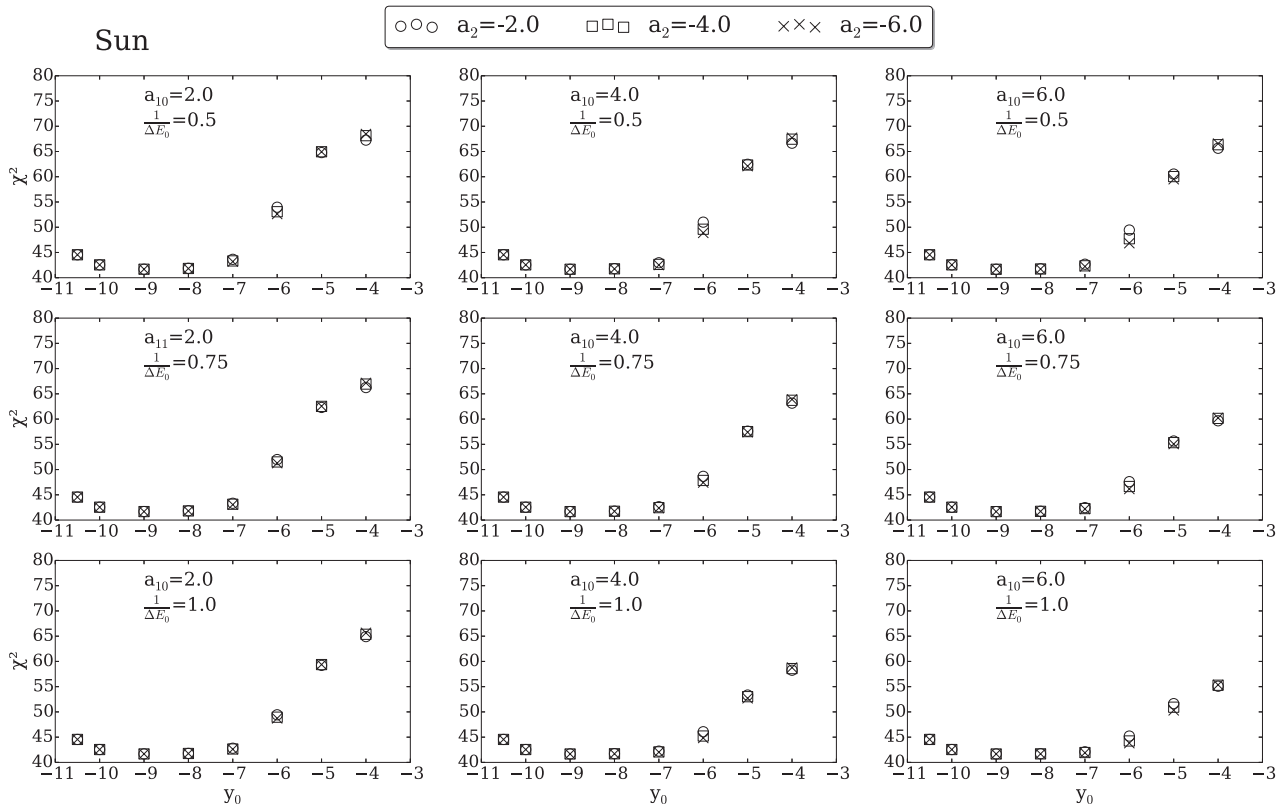

Figure 7.20: χ^2 variation as a function of Fe I+H charge transfer fitting parameters for the Sun.

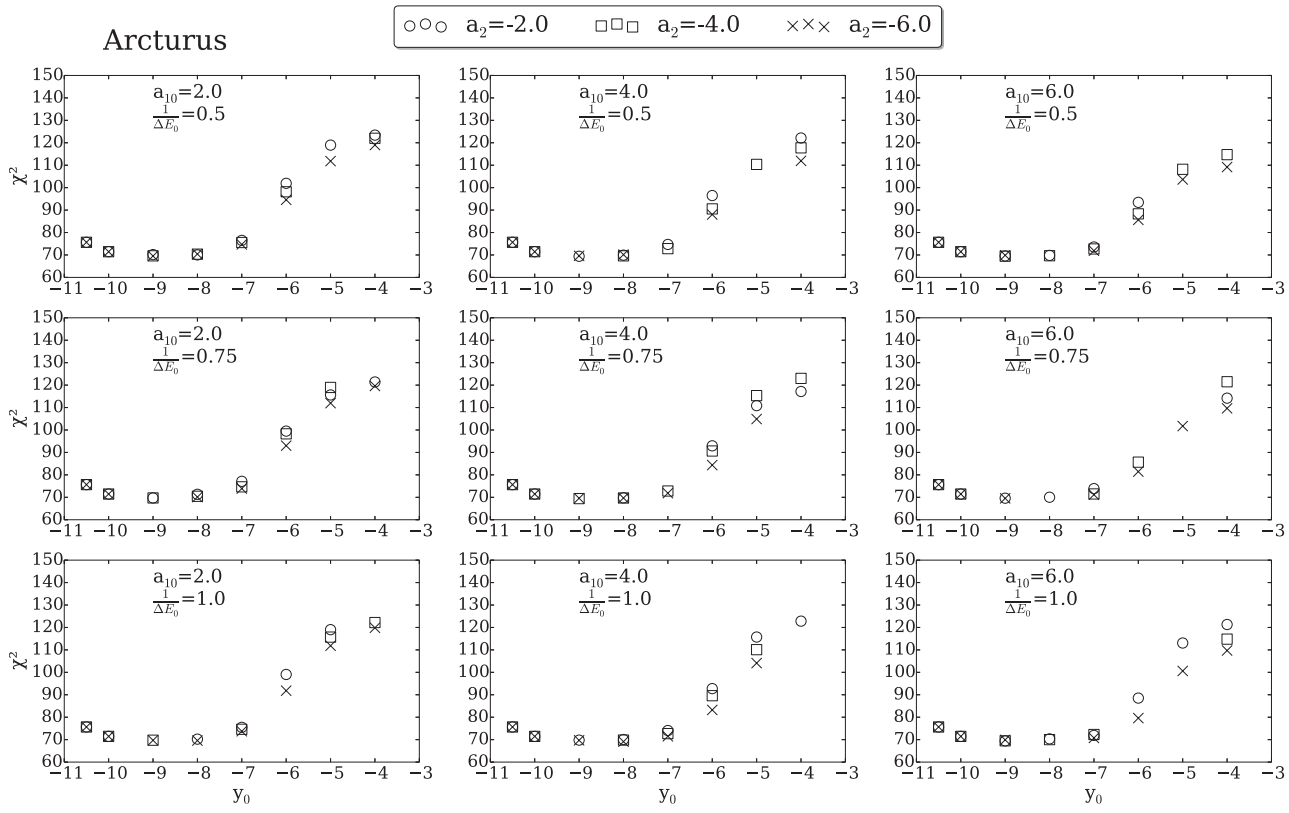

Figure 7.21: χ^2 variation as a function of Fe I+H charge transfer fitting parameters for Arcturus.

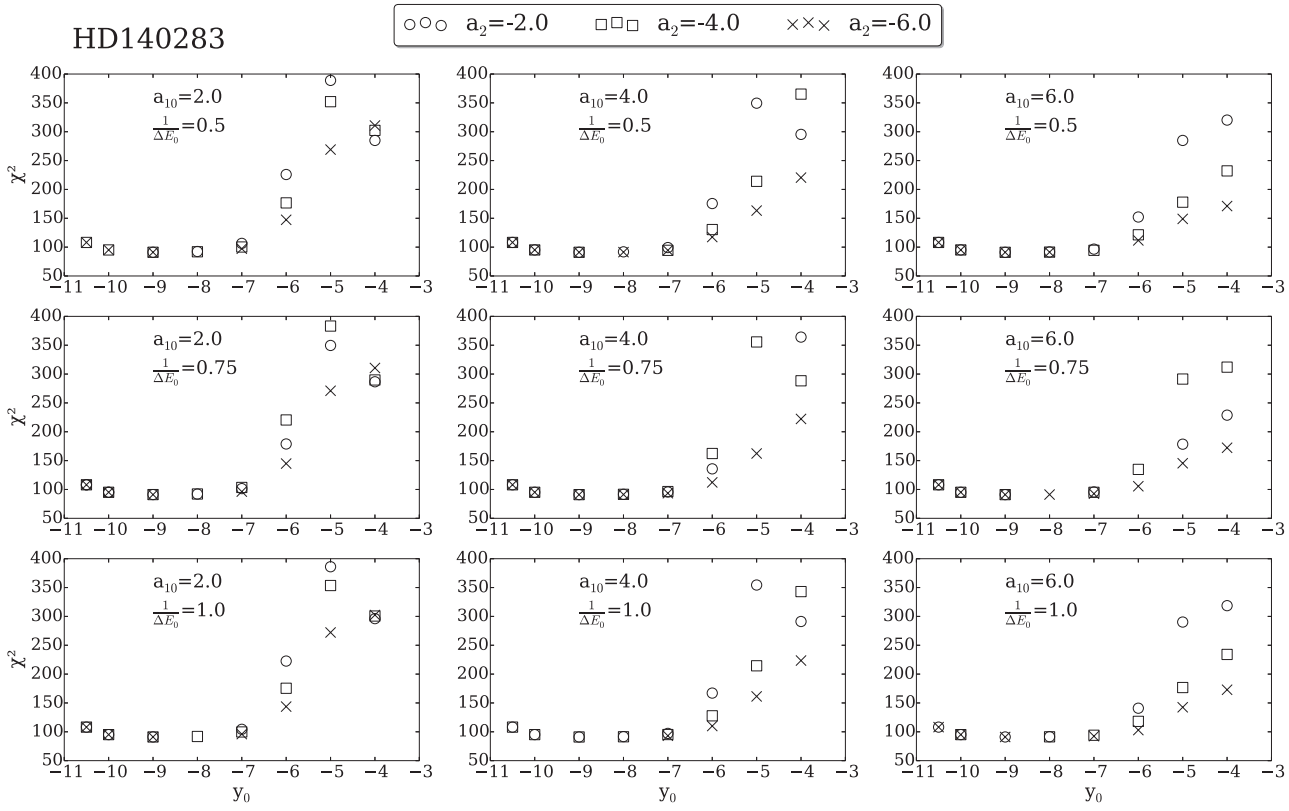

Figure 7.22: χ^2 variation as a function of Fe I+H charge transfer fitting parameters for HD140283.

7.3.3 De-excitation fitting

To find the best fitting parameters for the de-excitation rates, the fitting parameters from Eqn. 7.15 are varied for the values shown in Table 7.3. The charge transfer rates were kept constant at the best fitting values discussed in Sect. 7.3.2. The calculated EW_{calc} were compared to the measured EW_{obs} for the Sun, Arcturus and HD140283 using the χ^2 in Eqn. 6.3. The fitting parameter b_0 is found to play the most important role in varying the calculated EW_{calc}. Table 7.4 shows the χ^2 values obtained for different values of b_0 for the three stars. It can be seen that for $b_0 = -12$ & $b_0 = -6$, EW_{calc} are driven away from their corresponding EW_{obs} with χ^2 increasing to large values. The best fit obtained for the 3 types of stars is at $\boxed{b_{31} = -0.1}$, $\boxed{b_{30} = 0.2}$, $\boxed{b_{21} = 0.7}$, $\boxed{b_{20} = -2.0}$, $\boxed{b_{11} = -1.5}$, $\boxed{b_{10} = 3.5}$ and $\boxed{b_0 = -9.0}$.

parameter	values range	step
b_{31}	[-0.30,-0.10]	Δ = 0.10
b_{30}	[0.1,0.3]	Δ = 0.1
b_{21}	[0.5,0.9]	Δ = 0.2
b_{20}	[-3.0,-1.0]	Δ = 1.0
b_{11}	[-2.0,-1.0]	Δ = 0.5
b_{10}	[2.5,4.5]	Δ = 1.0
b_0	[-12.0,-6.0]	Δ = 1.0

Table 7.3: Fe I+H de-excitation rates fitting parameters range of values for which non-LTE calculations were performed.

Star	y_0	b_0	χ^2
HD140283	-9.0	-6.0	241.158
	-9.0	-9.0	61.481
	-9.0	-12.0	258.817
Arcturus	-9.0	-6.0	110.171
	-9.0	-9.0	64.452
	-9.0	-12.0	160.835
Sun	-9.0	-6.0	60.940
	-9.0	-9.0	40.571
	-9.0	-12.0	86.432

Table 7.4: χ^2 obtained for different b_0 fitting parameters used in the Fe I+H calculations.

7.4 Iron abundance determinations for GBS

Using the best fit model, for the best Fe I+H fitting parameters described in Sect. 7.3.2 & 7.3.3 (hereafter denoted our final iron model atom), non-LTE iron abundances were determined for the *Gaia* benchmark stars. The abundances are calculated using MARCS model atmospheres, and are normalized to the Solar Fe abundance $\varepsilon(\mathrm{Fe})_{\odot} = 7.45$ from Asplund et al. (2000).

The χ^2_{NLTE} and χ^2_{LTE} were calculated using Eqn. 6.3 for all the stars. Fe I and Fe II average iron abundances were derived from individual Fe I and Fe II lines. The [Fe I/H] and [Fe II/H] abundances and their corresponding standard deviation together with the non-LTE and LTE metallicities ([Fe/H] and [Fe/H]$_{\mathrm{LTE}}$ respectively), calculated by averaging abundances from all Fe I and Fe II lines, and their standard deviations are shown in Table 7.5. The non-LTE effect defined by the difference between non-LTE and LTE total metallicity, Δ[Fe/H] = [Fe/H] - [Fe/H]$_{\mathrm{LTE}}$, was calculated for each star as well. The number of Fe I and Fe II lines used in the abundance analyses of the stars are also included. The results are categorized into the different stellar types defined in Sect. 6.3.2. No numerical convergence was obtained for most M giants (to be investigated in future work), which were thus removed from the GBS list.

7.4.1 Results and analysis

The non-LTE Fe I and Fe II abundances for the different types of stars are plotted as a function of excitation potential and measured observed equivalent widths in Fig. 7.23 for the metal poor stars, Figs. 7.25, 7.26 and 7.27 for the FG dwarfs, Figs. 7.28 & 7.29 for the FGK giants and Fig. 7.30 for the K dwarfs.

Metal poor stars
The non-LTE iron abundances for the metal poor stars HD122563, HD140283 and HD84937 show excellent agreement between Fe I and Fe II lines, in addition to very small dispersion in the Fe I lines abundances. Fig. 7.24 represents the corresponding LTE abundances for the same stars. The comparison between the LTE and non-LTE abundances shows that the difference between Fe I and Fe II abundances is ≤ 0.05 in non-LTE for all three stars (0.019 dex for HD122563, 0.028 dex for HD140283 and 0.052 dex for HD84937), while it is > 0.12 dex in LTE (0.198 dex for HD122563, 0.154 dex for HD140283 and 0.124 dex for HD84937).

It has to be noted that Fe II lines also show small dispersion and are not affected by non-LTE, as already noted in previous non-LTE studies (Bergemann et al., 2012; Mashonkina et al., 2011; Thévenin and Idiart, 1999).

FG dwarfs
The dispersion of Fe I non-LTE and LTE line abundances is small ($\sigma < 0.1$ dex) in all stars. The results also show good agreement between Fe I and Fe II lines, with differences between Fe I and Fe II abundances less than 0.1 dex for most stars, except ϵ For (0.154 dex) and α Cen A (0.012 dex). All stars in this category display small non-LTE effects (≤ 0.05 dex), except ϵ For and HD49933 with slightly larger non-LTE corrections (0.061 and 0.072 dex respectively). Although no significant differences are found between LTE and non-LTE abundances for these stars, the χ^2_{NLTE} are smaller than χ^2_{LTE} for most stars. Again FeII lines are not affected by non-LTE.

Table 7.5: Non-LTE iron abundance calculations using the final iron model for the *Gaia* benchmark stars. The columns correspond to the calculated $\chi^2_{\rm NLTE}$ and $\chi^2_{\rm LTE}$, the Fe I average abundances and their standard deviations, the FeII average abundances and their standard deviations, the non-LTE and LTE total iron abundances and their standard deviations, the non-LTE effects, in addition to the number of Fe I and Fe II lines used in the analyses respectively.

Star name (ID)	$\chi^2_{\rm NLTE}$	$\chi^2_{\rm LTE}$	[FeI/H]	σ[FeI/H]	[FeII/H]	σ[FeII/H]	[Fe/H]$_{\rm NLTE}$	σ[Fe/H]$_{\rm NLTE}$	[Fe/H]$_{\rm LTE}$	σ[Fe/H]$_{\rm LTE}$	Δ[Fe/H]	N Fe I	N Fe II
Metal-poor													
HD 122563	58.15	261.861	-2.611	0.022	-2.592	0.018	-2.610	0.022	-2.773	0.130	0.163	110	10
HD 140283	60.66	248.545	-2.347	0.047	-2.378	0.035	-2.348	0.041	-2.522	0.087	0.174	63	3
HD 84937	29.48	352.243	-2.025	0.068	-2.077	0.035	-2.028	0.067	-2.191	0.093	0.163	68	4
FG dwarfs													
δ Eri	62.16	79.10	0.100	0.096	0.013	0.096	0.093	0.098	0.071	0.098	0.022	165	14
ϵ For	68.49	74.98	-0.577	0.065	-0.731	0.074	-0.593	0.080	-0.654	0.072	0.061	150	17
τ Cet	79.68	84.76	-0.524	0.081	-0.552	0.057	-0.525	0.077	-0.559	0.080	0.034	175	12
18 Sco	98.36	124.97	0.033	0.066	0.028	0.080	0.033	0.067	-0.009	0.076	0.042	174	18
Sun	40.64	65.00	-0.010	0.071	-0.051	0.086	-0.015	0.073	-0.062	0.074	0.047	154	16
HD 22879	61.75	144.31	-0.853	0.054	-0.888	0.072	-0.857	0.057	-0.918	0.058	0.061	130	17
α Cen A	30.06	31.36	0.347	0.069	0.235	0.079	0.333	0.079	0.308	0.081	0.025	183	22
μ Ara	46.63	45.87	0.388	0.079	0.319	0.095	0.381	0.083	0.352	0.085	0.029	180	19
β Hyi	112.89	147.25	0.017	0.066	-0.018	0.083	0.014	0.068	-0.038	0.083	0.052	180	18
β Vir	77.57	145.28	0.203	0.079	0.227	0.089	0.206	0.081	0.165	0.072	0.041	217	27
η Boo	85.97	81.78	0.406	0.086	0.437	0.114	0.408	0.089	0.366	0.101	0.041	171	17
Procyon	62.43	84.17	0.013	0.033	0.030	0.046	0.015	0.035	-0.027	0.046	0.042	136	20
HD 49933	101.59	109.37	-0.363	0.092	-0.370	0.081	-0.363	0.091	-0.435	0.091	0.072	125	14
FGK giants													
Arcturus	35.17	48.36	-0.482	0.076	-0.558	0.126	-0.490	0.085	-0.535	0.092	0.045	148	17
HD 220009	92.25	110.21	-0.680	0.093	-0.866	0.076	-0.693	0.102	-0.787	0.126	0.094	177	13
μ Leo	38.55	47.97	0.245	0.192	0.192	0.164	0.241	0.121	0.229	0.124	0.012	160	14
HD 107328	63.60	121.98	-0.242	0.053	-0.389	0.085	-0.259	0.074	-0.328	0.082	0.069	96	13
β Gem	18.13	21.66	0.082	0.094	0.036	0.096	0.079	0.094	0.035	0.106	0.044	150	12
ϵ Vir	75.86	88.68	0.204	0.077	0.159	0.115	0.198	0.084	0.122	0.093	0.076	128	21
ξ Hya	104.08	213.84	0.116	0.098	0.044	0.107	0.108	0.102	-0.001	0.137	0.109	133	17
K dwarfs													
61 Cyg B	33.28	33.31	-0.426	0.110			-0.426	0.109	-0.427	0.109	0.001	107	0
ϵ Eri	79.03	91.92	-0.108	0.077	-0.085	0.077	-0.107	0.077	-0.102	0.078	-0.005	153	10

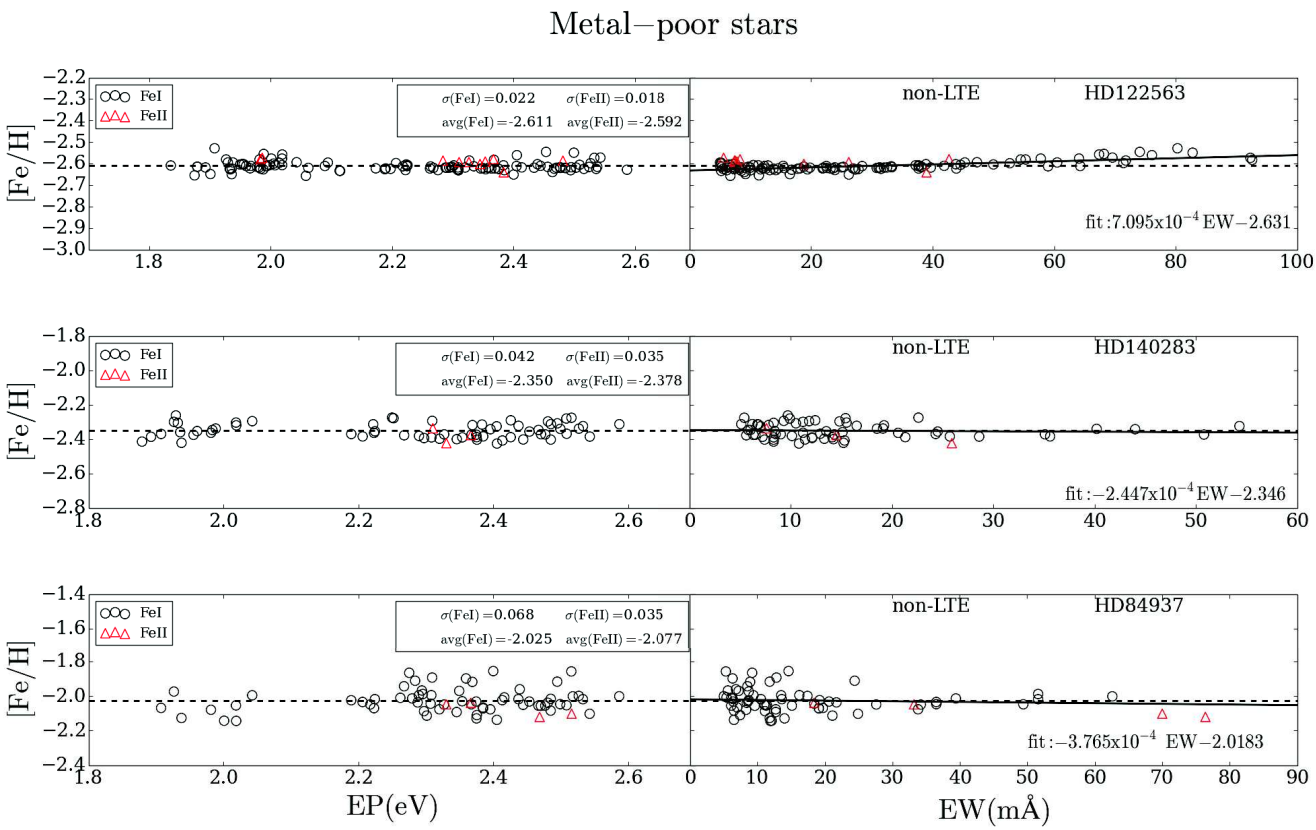

Figure 7.23: Non-LTE iron abundance determination for the metal-poor stars using our final iron model. Total line abundance average [Fe/H] is presented by the dotted lines. Solid lines represent the abundance fits as a function of EW.

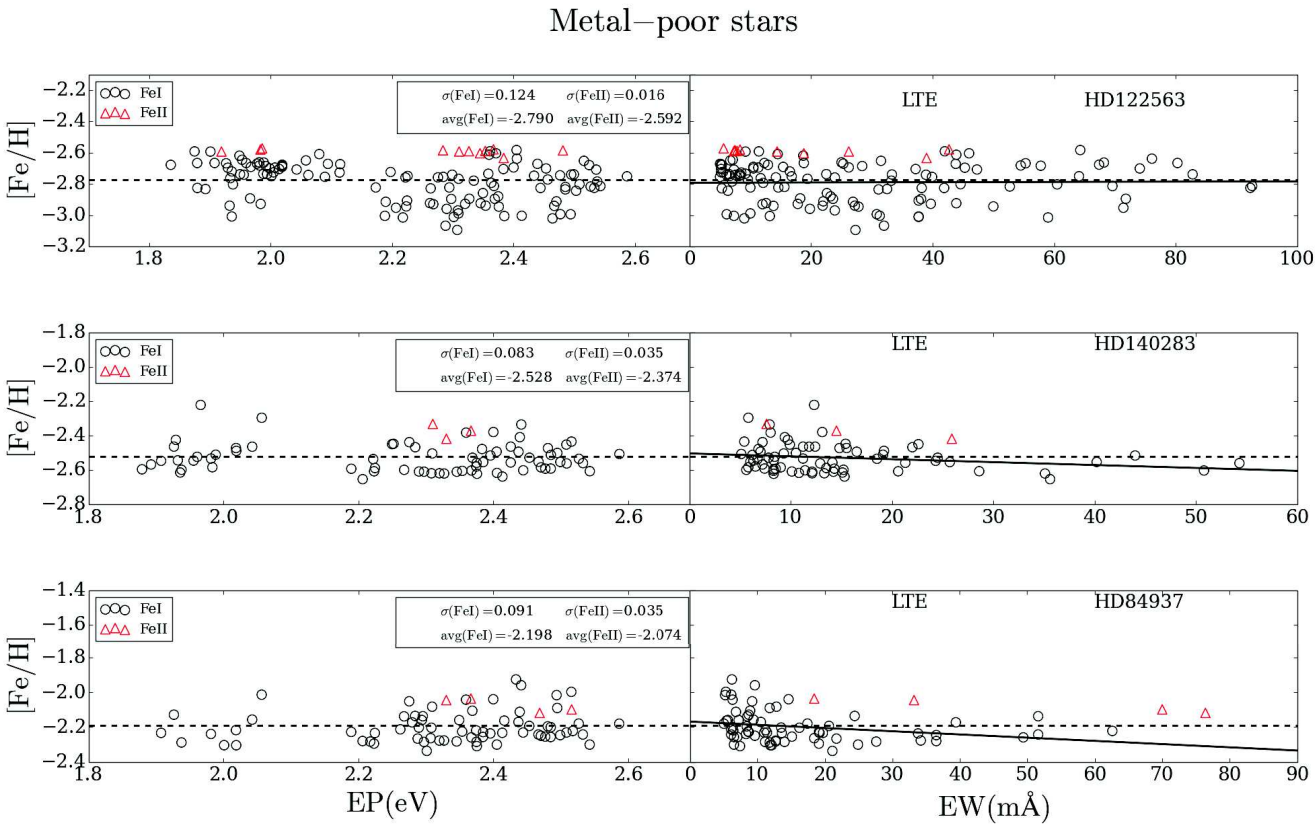

Figure 7.24: LTE iron abundance determination for the metal-poor stars.

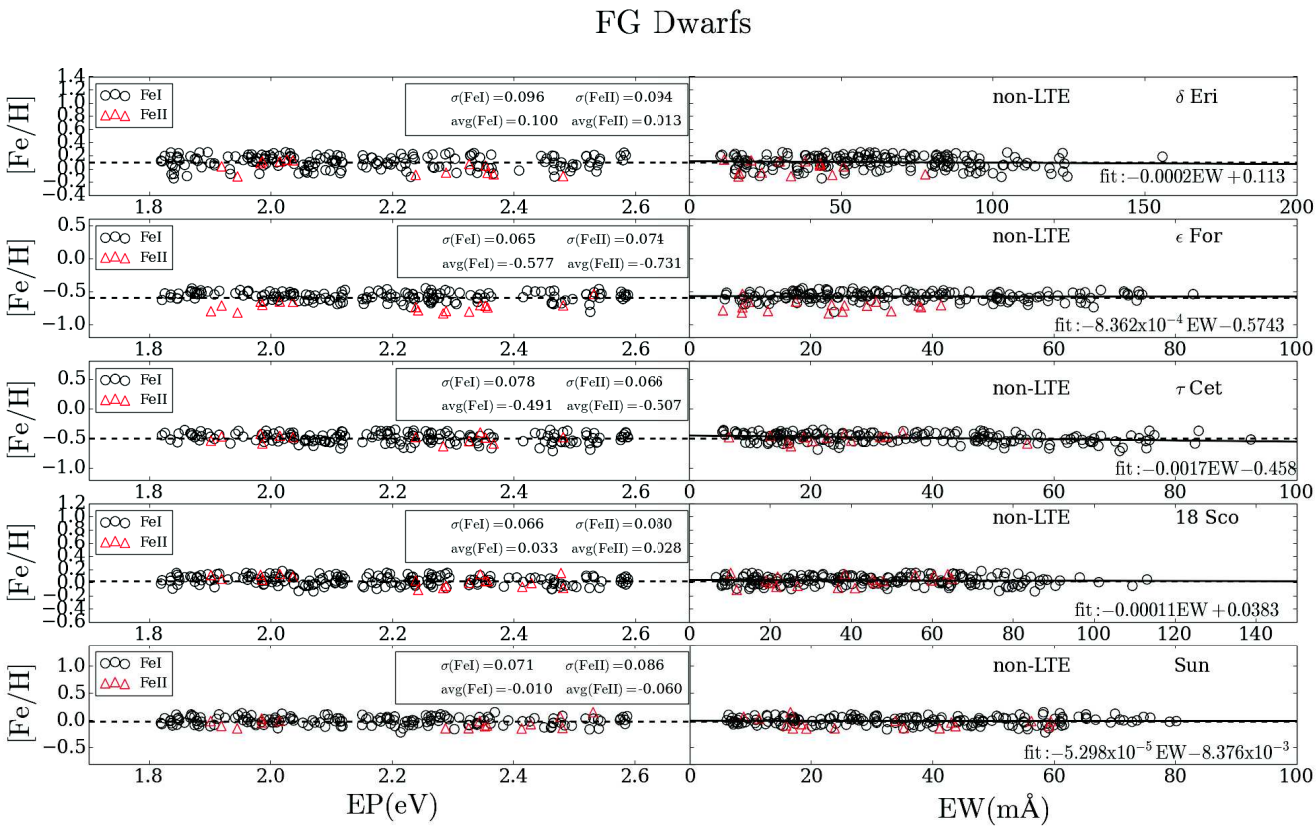

Figure 7.25: Non-LTE iron abundance determination for the FG dwarfs stars δ Eri, ϵ For, τ Cet, 18 Sco and the Sun using our final iron model.

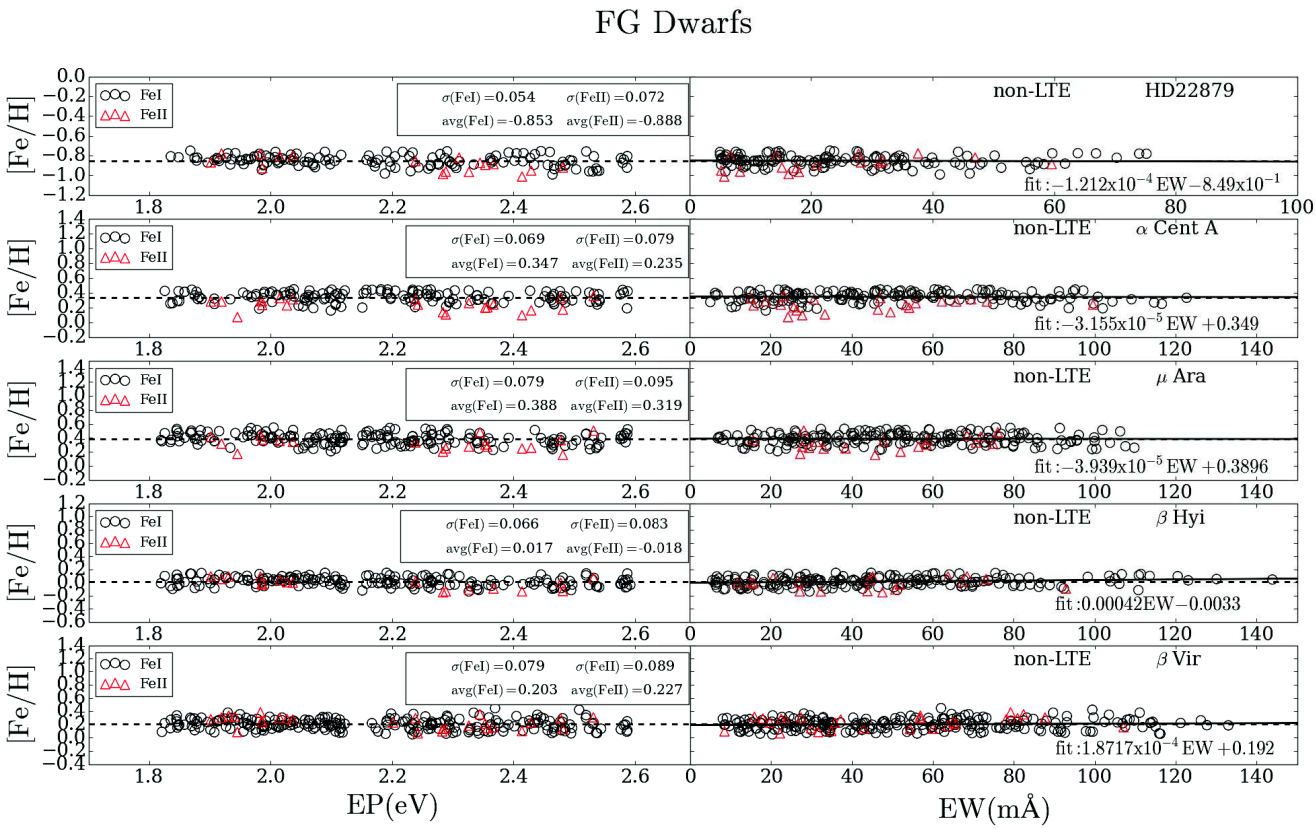

Figure 7.26: Non-LTE iron abundance determination for the FG dwarfs stars HD22879, α Cent A, μ Ara, β Hyi and the β Vir using our final iron model.

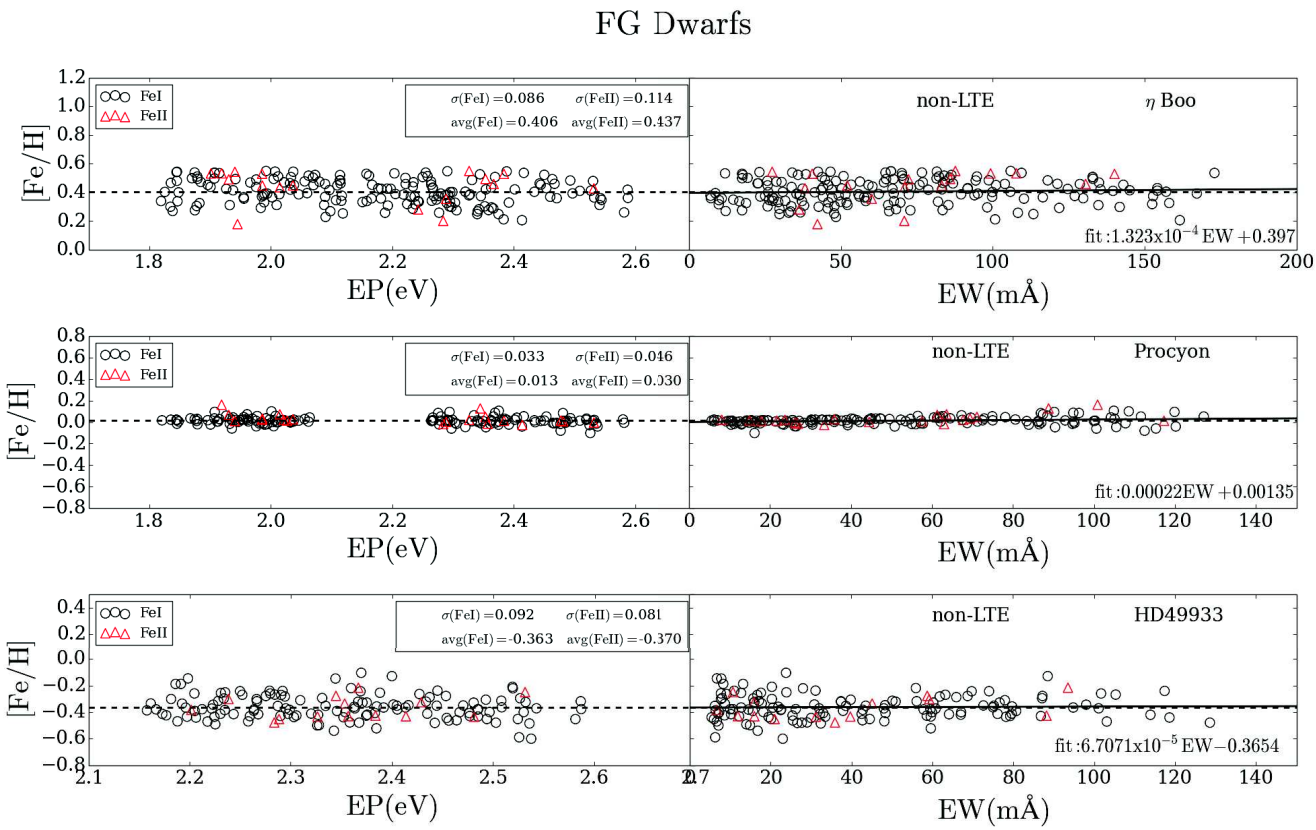

Figure 7.27: Non-LTE iron abundance determination for the FG dwarfs stars η Boo, Procyon and HD49933 using our final iron model.

FGK Giants

The stars in this category also show small scatter in FeI lines (≤ 0.1 dex) and good agreement between FeI and FeII, i.e. ≤ 0.07 dex for most stars except HD220009 (0.186 dex) and HD107328 (0.147) which show larger differences. The possible explanations for these larger differences for the two stars is that the AFP for HD220009 calculated by Heiter et al. (2015a) and Jofré et al. (2014), were found to be inconsistent with the previous literature studies, which they explained as due to erroneous calibrations of $T_{\rm eff}$, and thus rendering its parameters less reliable than others. In addition, the fundamental log g used in this work for HD107328 was found to be 30% smaller than the spectroscopic one by Heiter et al. (2015a). The values obtained for these two stars are however, lower than the non-LTE ionization imbalance of 0.2 dex found by Jofré et al. (2014) for the FGK giants. Also a slightly smaller scatter is found in non-LTE than in LTE for all the stars, whereas smaller χ^2_{NLTE} are found than the χ^2_{LTE} for all stars.

K dwarfs

The two stars in this category show larger FeI dispersion for 61 Cyg B (σ [FeI/H] = 0.11 dex) than stars in other categories. While no FeII lines could be measured for 61 Cyg B (due to blends with molecular bands). The agreement is good between Fe I and Fe II for ϵ Eri and the Fe I dispersion is small (σ[FeI/H] = 0.077 dex).

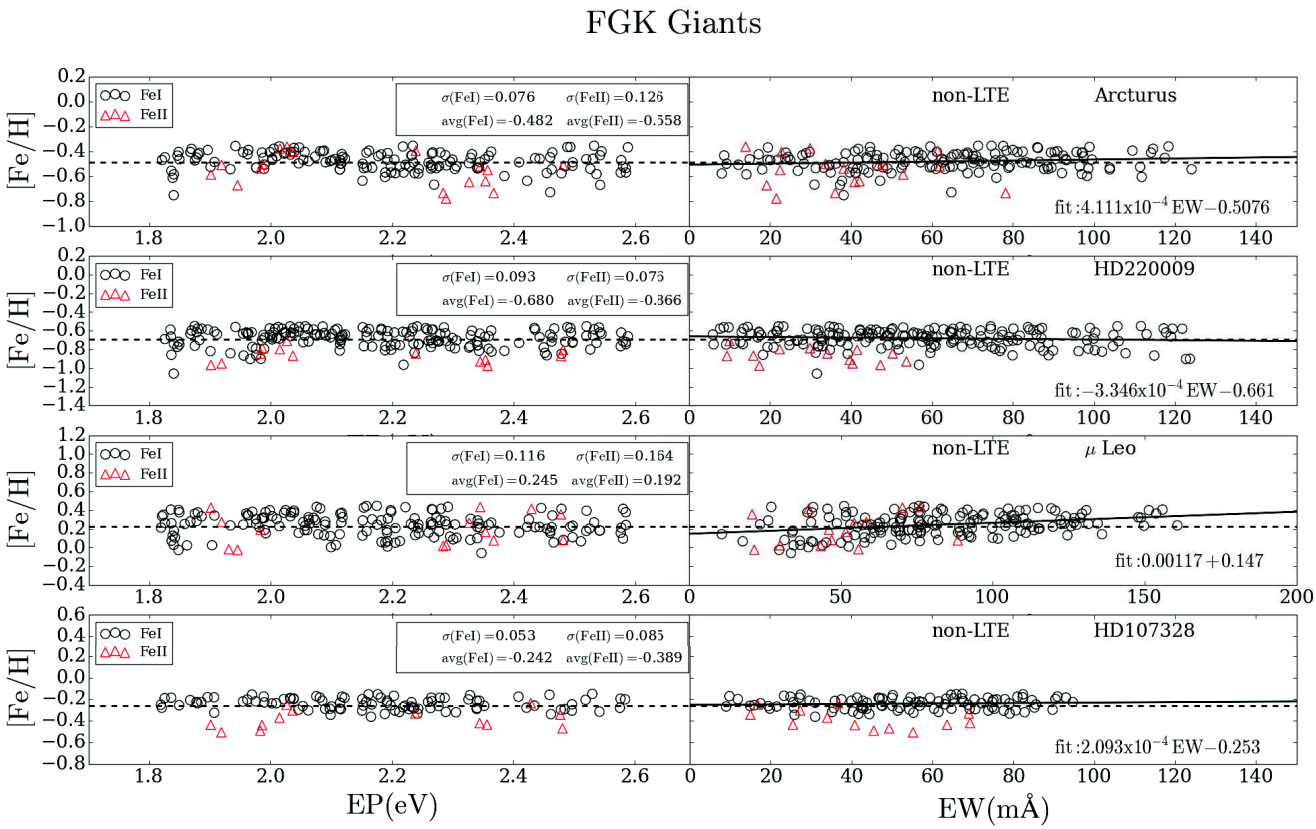

Figure 7.28: Non-LTE iron abundance determination for the FGK giant stars Arcturus, HD220009, μ Leo and HD107328 using our final iron model.

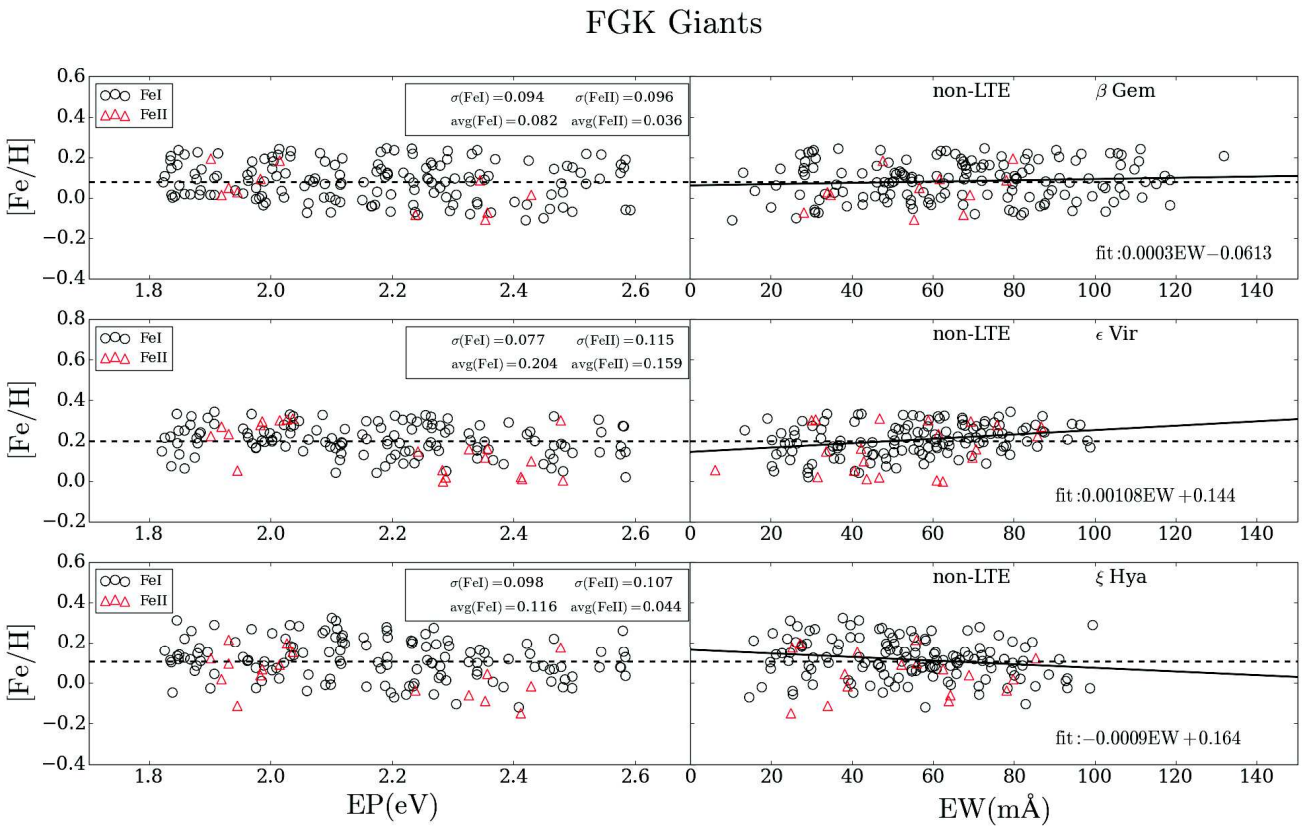

Figure 7.29: Non-LTE iron abundance determination for the FGK giant stars β Gem, ϵ Vir and ξ Hya using our final iron model.

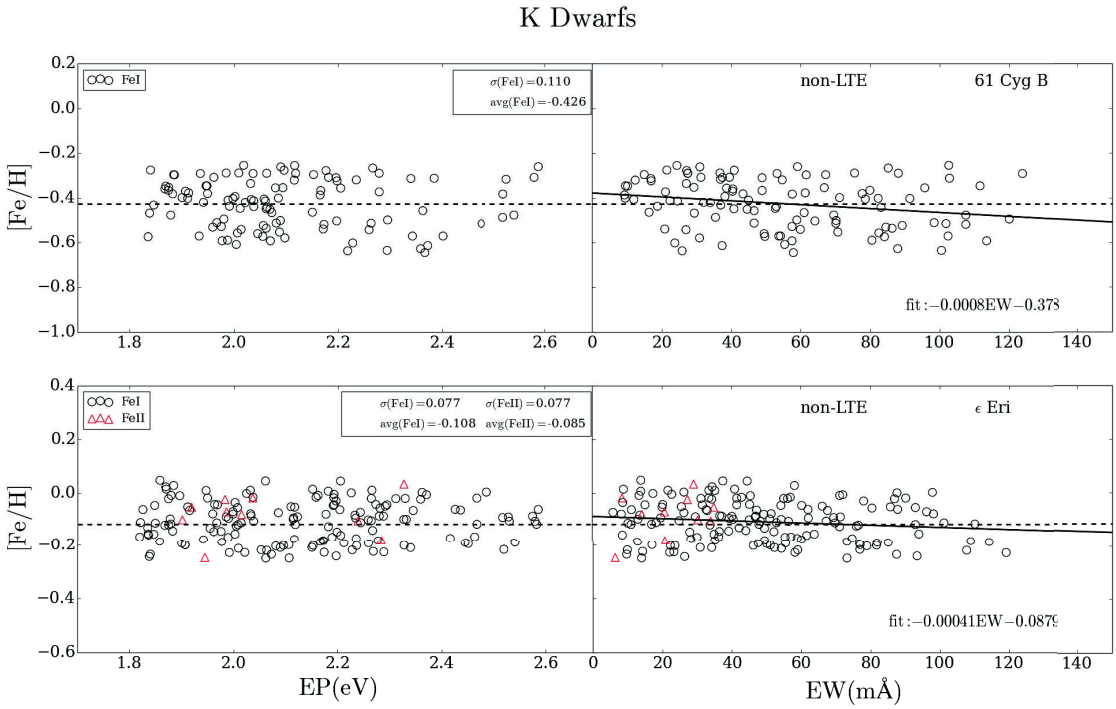

Figure 7.30: Non-LTE iron abundance determination for the K dwarfs stars 61 Cyg B and ϵ Eri using our final iron model.

7.4.1.1 3D effects

The dispersion in Fe I line abundances obtained in the Giants and K dwarfs may be due to 3D effects, which are not taken care of in 1D models. In order to test for this effect, we calculated an average $\langle 3D \rangle$ non-LTE corrections for the Sun using the published $\langle 3D \rangle$ Solar model from the Stagger 3D model grid[1] (Magic et al., 2013b). We used the $\tau_{\rm Rosseland}$ averaged model as recommended by Magic et al. (2013b). The results of the calculations are shown in Fig. 7.31. While the 1D, non-LTE calculations gave a dispersion of 0.071 dex for Fe I and 0.086 for Fe II lines, the $\langle 3D \rangle$ model gives a smaller dispersion of 0.069 and 0.070 dex for Fe I and Fe II respectively. In addition, while the difference obtained between [FeI/H] and [FeII/H] is 0.05 in the 1D model, a difference of 0.008 is obtained using the $\langle 3D \rangle$ model. The absolute Solar iron abundance obtained with the $\langle 3D \rangle$ model is 7.456 dex, which is equal to that obtained from the full 3D hydrodynamical model for the Sun and the meteoritic value (Asplund et al., 2000). The abundance obtained with the 1D model is 7.435 in non-LTE, and 7.398 in LTE.

[1]https://staggergrid.wordpress.com/

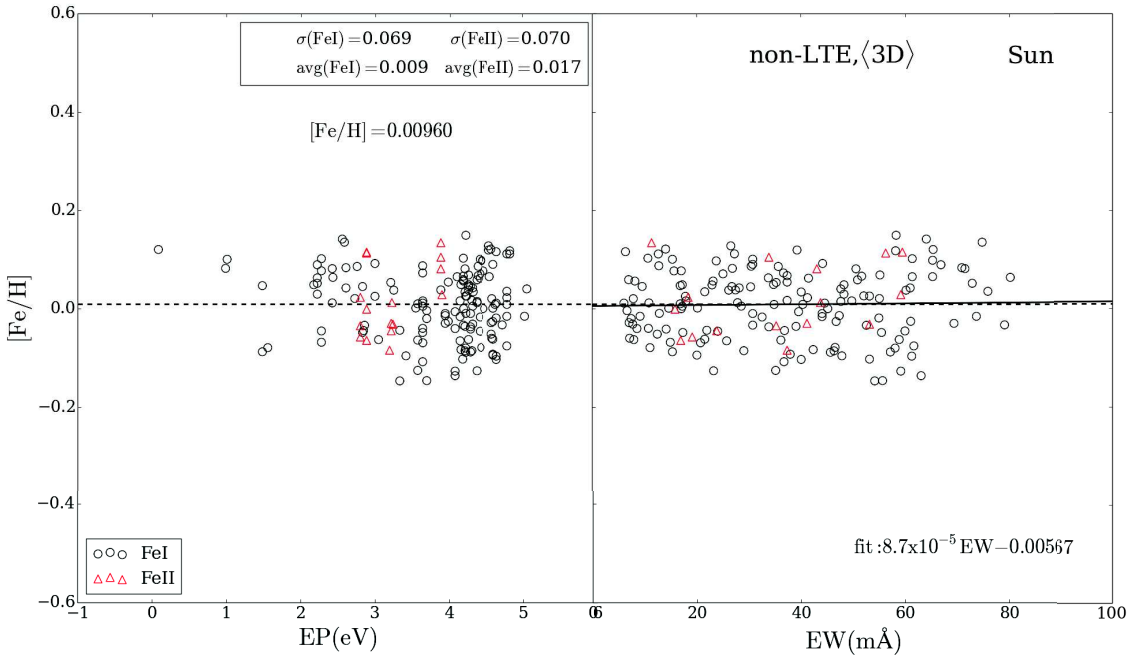

Figure 7.31: ⟨3D⟩, non-LTE iron abundance determination for the Sun with our final iron model.

7.4.2 Comparison with the literature abundances

We compared our non-LTE Fe I and Fe II abundances with the results of 1D and ⟨3D⟩ calculations by Bergemann et al. (2012) (hereafter BER12), and 1D calculations by Mashonkina et al. (2011) (hereafter MAS11) for 5 stars in common: the Sun, Procyon, HD84937, HD140283 and HD122563. They used $S_{\rm H} = 1$ with the Drawin recipe, and did not include any charge transfer collisional rates. Details of the atomic models used in these studies can be found in Sect. 4.5. The results of the determined abundances by the different studies are listed in Table 7.6.

MAS11 determined Solar 1D abundances of 7.54 and 7.56 for Fe I and Fe II respectively. Smaller values of 7.44 and 7.41 were found by BER12, and this work. Our ⟨3D⟩ Solar abundances agree very well with BER12, with no difference obtained between Fe I and Fe II as compared to a 0.02 dex difference by BER12.

For Procyon, a 0.1 dex abundance difference is found between Fe I and Fe II by MAS11, which agrees well with the 1D BER12 determinations within uncertainties (though a smaller difference of 0.03 dex was found by BER12). Larger values, though, are determined in this work with a difference of 0.02 dex, which are in better agreement with the ⟨3D⟩ results of BER12. It has to be noted that while the input $T_{\rm eff}$ in the three studies agree within uncertainties, the log g used in this work is slightly larger by 0.04 dex.

1D abundance determinations for HD84937 agree well between the three studies within uncertainties, with the results in this work closer to the ⟨3D⟩ values by BER12. For HD140283, our abundances are only compared to BER12 (no calculations for this star by MAS11) which agree well, though smaller dispersions are obtained by us ($\sigma \leq 0.05$). Again, our results for this star agree well with ⟨3D⟩ determinations of BER12, although a 0.12 cgs difference in log g is present between both studies.

Object		$T_{\rm eff}$	log g	1D Fe I	1D Fe II	⟨3D⟩ Fe I	⟨3D⟩ Fe II
Sun	MAS11	5777	4.44	7.54±0.09	7.56±0.05		
	BER12	5777	4.44	7.44±0.05	7.44±0.04	7.45±0.04	7.47±0.04
	This work	5777	4.44	7.44±0.07	7.41±0.08	7.46±0.07	7.46±0.07
Procyon	MAS11	6510±49	3.96±0.02	7.32±0.07	7.42±0.05		
	BER12	6543±84	3.94±0.02	7.37±0.04	7.40±0.04	7.43±0.04	7.43±0.04
	This work	6554±84	4.00±0.02	7.46±0.03	7.48±0.04		
HD84937	MAS11	6350±37	4.09±0.05	5.32±0.07	5.37±0.04		
	BER12	6408±66	4.13±0.09	5.39±0.07	5.33±0.04	5.45±0.06	5.38±0.03
	This work	6356±97	4.06±0.04	5.42±0.06	5.38±0.04		
HD140283	BER12	5777±80	3.70±0.08	5.07±0.09	5.01±0.04	5.05±0.05	5.09±0.04
	This work	5522±102	3.58±0.11	5.10±0.05	5.07±0.04		
HD122563	MAS11	4600±61	1.60±0.07	4.98±0.10	4.89±0.07		
	BER12	4665±61	1.64±0.16	4.87±0.12	4.95±0.05	4.85±0.08	5.01±0.05
	This work	4587±60	1.61±0.07	4.84±0.02	4.86±0.02		

Table 7.6: This work's non-LTE Fe I and Fe II abundance results compared to those of Mashonkina et al. (2011) (MAS11) and Bergemann et al. (2012) (BER12) for the Sun, Procyon, HD84937, HD140283 and HD122563

An interesting case of comparison is the well studied very metal-poor star HD122563 ([Fe/H]$<$ 2.50 dex). Our Fe I abundance (4.84±0.02 dex) is lower than those obtained by MAS11 and BER12 (4.98±0.10 dex and 4.87±0.12 dex respectively), and is in excellent agreement with the ⟨3D⟩ value (4.85±0.08 dex). In addition, while a 0.1 dex difference was found between Fe I and Fe II by both MAS11 and BER12, an excellent agreement with a 0.02 dex difference is obtained in this work.

7.5 Comparison with preliminary quantum calculations

We have very recently obtained Fe I+H quantum calculations from private communication with Paul Barklem. The plots of the charge transfer rates (Fig. 7.32) as a function of $\frac{1}{\Delta E}$ shows the same behavior as those obtained for Mg, Na, Al and Si, with a peak observed between 0.5 and 1 eV^{-1}. The fits of these rates at $T = 6000$ K also shown on the figure and compared to those we obtained: an excellent agreement is found!.

The de-excitation rates as a function of ΔE at 6000 K are plotted in Fig. 7.33. The rates show a decreasing trend with transition energies. The fits to the data are shown in blue solid line, while those obtained with our QFM method are shown with a red dotted line. The fits agree well for ΔE <4 eV, i.e. for rates $> 10^{-15}$ cm$^3 \cdot$ s^{-1}.

Although the data from Paul Barklem are preliminary, and further comparisons are to be made in future work with calculations with the actual quantum data, they validate our method and show that our proposed QFM is able to reproduce the quantum data. This could be extended to other atoms where no quantum data have yet been published.

Figure 7.32: Fe I+H charge transfer rates calculated by Paul Barklem (private communication) and their fits as a function of $1/\Delta E$ Our best fits obtained using the QFM are also shown (black dotted lines).

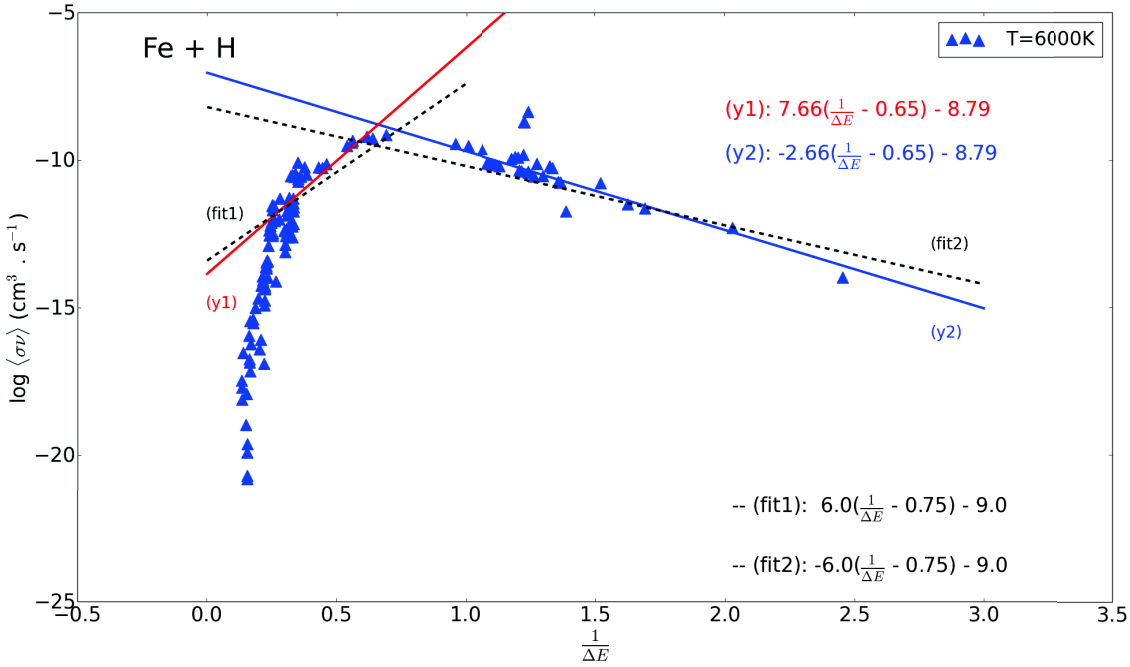

Figure 7.33: Fe I+H de-excitation rates (private communication P. Barklem) and their fits as a function of ΔE. The data fits with a third degree polynomial are shown in blue solid line, while best fits obtained in this work using the QFM are also shown (red dotted line).

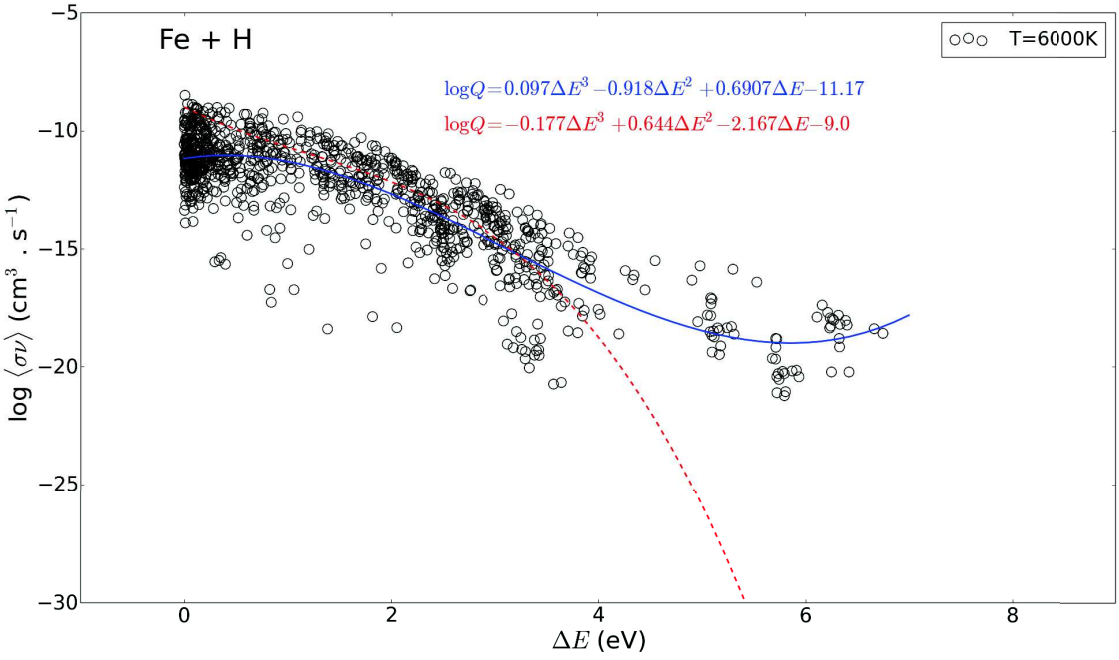

8 | Conclusions and Perspectives

The work in this dissertation shed the light on the role of hydrogen collisions in non-LTE iron modeling in cool stellar atmospheres, which is usually modeled with the semi-classical Drawin approximation.
In the first part of this work, the commonly used Drawin approximation to calculate the hydrogen collisional rates was put to test:

The Drawin approximation was extended and used to calculate charge transfer collisional rates, in addition to excitation and ionization rates. It was shown that Drawin approximation over estimates, and predicts the rates with a completely different behavior with transition energies. A silicon test model atom was developed and utilized to compare non-LTE calculations using the Drawin approximation rates to those using the quantum data. The results showed that different sets of multiplicative scaling factors for different stars are required to reproduce the reference calculations made with the quantum data.

The Drawin approximation was then tested on iron, using a newly developed, rather complete, model atom. Non-LTE calculations using the Drawin approximation were compared to observed equivalent widths for 30 *Gaia*-ESO benchmark stars of different spectral types with well determined atmospheric parameters. The results have shown once again that no single set of scaling factors for excitation and charge transfer could be used for all the stars to produce a best fit of the observations. Even within same spectral type categories no single recipe could be found.

In the light of these results, we deduce that the Drawin approximation is unreliable and should not be used to calculate collisional rates.

In the second part, we introduce a new method to calculate hydrogen collisional rates, which we call the Quantum Fitting Method (QFM), which is based on fitting the existing quantum calculations of a few elements, namely, Na, Mg, Al and Si. We show that a general fitting recipe for charge transfer rates can be used for all four elements. A different recipe is adopted for de-excitation rates as well.

The fitting recipes are first tested on Si, where non-LTE calculations using the QFM are shown to reproduce the equivalent width calculations using the real quantum data within a scatter of $< 1\%$. Our calculations also demonstrate that a variation in the fitting parameters within $\pm 50\%$ from their reference values, only alters the results of the calculations within $< \pm 10\%$.

The QFM was then extended to iron, for which no quantum data existed. The general form of the excitation and charge transfer collisional rate fits obtained for other elements were conserved and used. The fitting parameters for each of charge transfer and excitation rates were varied at once, thus creating a multidimensional grid of parameters for which non-LTE calculations were computed. A best fit minimum was found at the same set of parameters for

three stars of different stellar types.

The best fit model was used to determine 1D, non-LTE and LTE Fe I and Fe II abundances for the benchmark stars. The non-LTE iron abundances demonstrated much smaller scatter than the LTE, especially for metal-poor stars and FGK giants. An excellent agreement was also found between Fe I and Fe II abundances, within ≤ 0.05 dex. Larger non-LTE effects were determined for metal-poor stars, as expected. 3D effects were tested on the Sun using an average $\langle$3D$\rangle$ Solar model, and an excellent agreement was found between Fe I and Fe II lines ($\log \varepsilon$(Fe I) = $\log \varepsilon$(Fe II) = 7.46 dex), with a dispersion of $\sigma < 0.01$. These values are in agreement with the full 3D results and the meteoritic values by Asplund et al. (2000). Our results also agree well with the most recent iron abundance calculations from the literature (Bergemann et al., 2012; Mashonkina et al., 2011), with less scatter obtained in this work.

We thus deduce that our proposed QFM method is able to reproduce the observations with high accuracy. Luckily, we were able to compare our method to recent preliminary iron quantum collisional rates (private communication from Paul Barklem). Our determined best fits show very good agreement with the fits of quantum data. This strengthens the validity of our method and suggests it could be extended to other elements when no quantum calculations exist.

In future work, we aim to implement the iron quantum data into our model atom and compare the calculations to this work's results.

As we find slightly more consistent results using a $\langle$3D$\rangle$ model for the Sun, we plan to extend the $\langle$3D$\rangle$ calculations to the whole sample of stars.

As part of the GES-CoRoT collaboration, which is an ongoing international collaboration whose objective is to derive the best stellar parameters using the seismic constraints (surface gravity) from the CoRoT satellite, combined with high resolution spectroscopic data, we plan to determine non-LTE corrections on the fundamental atmospheric parameters of a sample of 700 stars with high resolution spectra (obtained with UVES and GIRAFFE).

Another future interest is to utilize our QFM in non-LTE calculations for other elements prone to non-LTE effects in cool stars, e.g. B I, O I, S I, K I, Sc I, Ti I, Co I, Sr I, ... (See e.g. review by Bergemann and Nordlander, 2014).

A priority of ours is to provide a line-by-line non-LTE corrections grid for a large parameter space, that would be accessible through the world wide web.

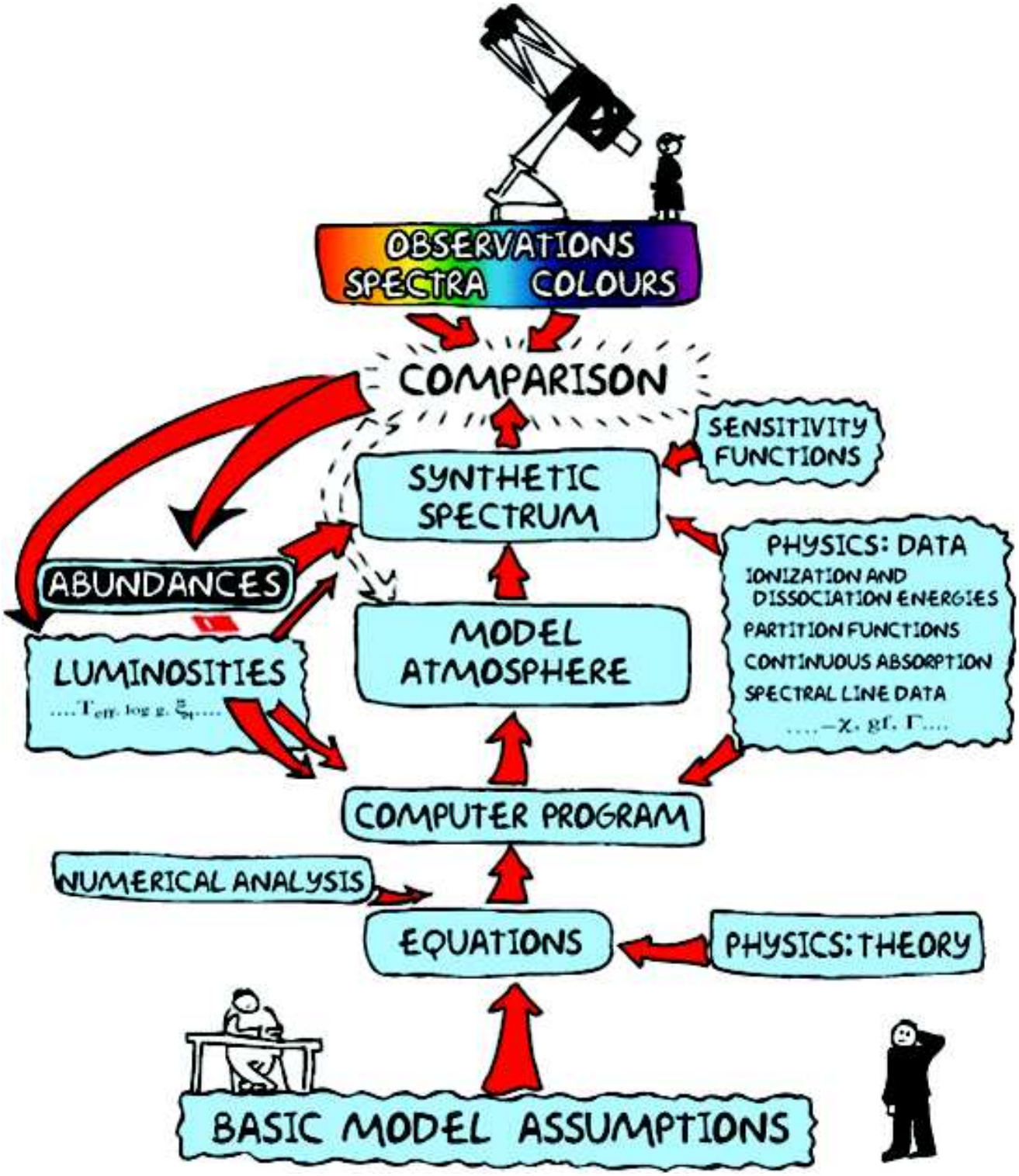

Figure 8.1: Abundance determination journey through essential steps of spectroscopic modeling (Bengt Gustafsson, 2009).

A Spectral line formation and Broadening Coefficients

Observed spectral lines are not delta-like functions (infinitely narrow) in the continuum, but are rather broadened due to several mechanisms. In what follows I will explain the microscopic processes responsible for broadening spectral emission and absorption lines.

A.1 Natural (radiative) broadening

Due to the Heisenberg uncertainty principle, an electron in an atom lying at an energy level of energy E above the ground state, and of a lifetime Δt on that state has an uncertainty in energy:

$$\Delta E \Delta t \sim \hbar \tag{A.1}$$

hence a photon emitted in a transition from this level to another level will have a range of possible frequencies

$$\Delta\nu \sim \frac{\Delta E}{h} \sim \frac{1}{2\pi\Delta t} \tag{A.2}$$

The sum of all spontaneous (natural) decay rates (in s^{-1}) of an electron in an atomic energy state j to all possible lower energy states i is:

$$\gamma_i^{\rm rad} = \sum_i A_{ji} \tag{A.3}$$

then the line emission profile (can be considered the same for absorption under detailed balancing) due to natural broadening (damping) is called a Lorentzian or natural line profile (for derivation see Bransden and Joachain (2003)) and is of the form:

$$\phi^{\rm rad}(\nu - \nu_0) = \frac{\gamma^{\rm rad}/4\pi^2}{(\nu - \nu_0)^2 + (\gamma^{\rm rad}/4\pi)^2} \tag{A.4}$$

where ν_0 is the central frequency around which the line is broadened. The classical value for $\gamma^{\rm rad}$ for a damped harmonic oscillator is:

$$\gamma_{rad} = \frac{8\pi e^2 \nu_0^2}{3 m_e c^3} = 2.47 \times 10^{-22} \nu_0^2 \tag{A.5}$$

A.2 Collisional (pressure) broadening

The presence of collisional perturbers in the neighborhood of atoms, mainly electrons and neutral hydrogen atoms for late-type cool stars, whose charges affect the radiating atom through Coulomb's interactions and therefore affects the frequency of the photons of the bound-bound

transitions, by further decreasing the lifetime of the energy states than the radiative broadening and thus further broadening the spectral lines. HI atoms in particular have large polarization due to bad shielding of the proton by the single electron in the atom. They are thus important spectral line broadeners in cool atmospheres.

The commonly classical description of collisional broadening is to distinguish between the different interactions based on the different closest seperation distances $r^{\rm p}$ between the absorbing atom and the corresponding pertuber. Hence starting from Heisenberg's uncertainty principle again, one can write:

$$\Delta\nu = \frac{\Delta E}{h} \equiv \frac{C_n}{r_n^{\rm p}} \tag{A.6}$$

where C_n is the interaction constant and the index n defines the type of possible interactions. In this thesis we will consider the relevant broadening interaction contributions in late-type cool stars, namely from electrons and neutral hydrogen atoms.

Stark effect (n=4)
This defines the collisional broadening due to interaction of atoms with free electrons. The spatial dependence of this type of broadening is r^{-4} in which the electrons at large speeds cause a momentary disruption of the radiation emitted by the atom. Similar to the natural broadening, electron Stark effect contributes to the Lorentzian line profile by $\Gamma_e^{\rm col}$. Electron broadening dominates in atmospheres of hot stars where electron density is high (Griem, 1974).

Van der Waals broadening (n=6)
Neutral hydrogen atoms dominate in cools stars (See Appendix B for details) which make them the dominant broadeners of spectral lines there. The classical approach to calculating the hydrogen broadening coefficient $\Gamma_{\rm H}^{\rm col}$ (commonly called the Van der Waals damping coefficient, also denoted γ_6) was described by Unsold (1955), where he formulated the latter coefficient as:

$$\gamma_6 = \log\Gamma_{\rm H}^{\rm col} \approx 6.33 + 0.4\log\overline{r^2} + \log P_g - 0.7\log T \tag{A.7}$$

where $\overline{r^2}$ is the mean square radius (in atomic units) between the upper and lower levels of the atom, extended from the hydrogenic approximation by **?** to non-hydrogenic atoms of ionization stage Z as:

$$\overline{r^2} = \frac{n^{*2}}{2Z^2}\left(5n^{*2} + 1 - 3l(l+1)\right) \tag{A.8}$$

where l is the angular quantum number of the corresponding level and n^* is its effective principal quantum number given by:

$$n^{*2} = R\frac{Z^2}{E_\infty - E_n} \tag{A.9}$$

with R=13.6eV is the Rydberg constant and $E_\infty - E_n$ is the ionization energy from the corresponding level. For non-hydrogenic lines, the observed line profiles from cool stars seem to suffer more damping than the values estimated from Unsöld's approximation, and thus it is common to apply an enhancement fudge factor to the Van der Waals damping coefficient which ranges between 2 to 5 depending on the atom and ionization stage.

Anstee, Barklem and O'Mara (ABO) theory The ABO theory (Anstee and O'Mara, 1995; Barklem et al., 1998; Barklem and O'Mara, 1997) has been originally developed by Anstee and O'Mara (1995) as a universal theory for the hydrogen broadening of atomic and ionic lines which is more intricate than the r^{-6} dependence formulated by Unsöld. The ABO theory

presented results of the variation of the hydrogen broadening cross-sections $\sigma_{\rm H}^{\rm br}$ as a function of collisional speed of hydrogen atoms v, and found to be a power law dependent on a velocity parameter α such as:

$$\sigma_{\rm H}^{\rm br} \propto v^{-\alpha} \tag{A.10}$$

The damping coefficient can then be calculated using:

$$\gamma_6 = 2\left(\frac{4}{\pi}\right)^{\alpha/2}\Gamma\frac{4-\alpha}{2}\bar{v}\,\sigma_{\rm H}^{\rm br}\,n_{\rm H} \tag{A.11}$$

where Γ is Euler's Gamma function, $\bar{v} = (8k_{\rm B}T/\pi\mu)^{1/2}$, and μ is the reduced mass of the two atoms in contact and $v_0 = 10^4 m/s$ the relative collisional speed.

The ABO theory has been implemented in most spectral synthesis codes used nowadays (LTE & non-LTE) which will provide $\sigma_{\rm H}^{\rm br}$ and α for large grids of lines calculated for different elements and their ions useful in many astrophysical approximations. This allowed for much better improvement of spectral lines synthesis which resulted in better fits with the observed lines, that allowed for more reliable derivations of stellar parameters.

A.3 Thermal broadening

Individual atoms in a stellar atmospheric gas of temperature T have random motions away or toward the observer (or observation instrument), leading to red- or blue-wards Doppler frequency shifting. Considering a Maxwell velocity distribution of an atom of mass m, the line of sight mean kinetic energy can be written as $\frac{1}{2}m\langle V^2\rangle = \frac{3}{2}k_{\rm B}T$, where the thermal light of sight velocity (Doppler velocity) is $v_D \equiv \sqrt{\frac{2k_{\rm B}T}{m}}$. In addition, small-scale mass motions characterized with a mean micro-turbulent velocity ξ also produce Doppler shifts analogous to the ones produces by thermal motions and thus should also be added to the broadening coefficient.
Hence Doppler width shift in frequency can be written as:

$$\Delta\nu_{\rm D} = \nu_0\frac{v_D}{c} = \frac{\nu_0}{c}\sqrt{\frac{2k_{\rm B}T}{m} + \xi^2} \tag{A.12}$$

and the thermally broadened cross-section calculated from the integrating over the absorption coefficient of the atoms moving at velocity v at Maxwell velocity distribution

$$\sigma_\nu^{\rm th} \propto \frac{1}{\Delta\nu_{\rm D}}e^{-\left(\frac{\nu-\nu_0}{\Delta\nu_D}\right)^2} \tag{A.13}$$

Thermal broadening causes a Gaussian (or Doppler) shaped profile.

A.4 Line profile

The final line profile is a convolution of the profiles for all the broadening processes, i.e. of a Lorentzian profile (from radiative and collisional broadening) and a Gaussian profile (from thermal broadening) $f_{\rm V}(\nu) = f_{\rm L}(\nu)\bigotimes f_{\rm D}(\nu)$ which results in a Voigt profile.

$$\phi^V(\nu) = \frac{\sqrt{\pi}}{\Delta\nu_{\rm D}}H(a,x) \tag{A.14}$$

where H(a,x) is called the Hjerting function (Hjerting, 1938),

$$H(a,x) = \frac{a}{\pi}\int_{-\infty}^{+\infty} \frac{e^{-y^2}}{(x-y)^2+a^2}\,\mathrm{d}y \tag{A.15}$$

with a the damping parameter, determined by:

$$a = \frac{\gamma^{\mathrm{tot}}}{4\pi}\frac{1}{\Delta\nu_{\mathrm{D}}} \quad \text{and} \quad x = \frac{\nu-\nu_0}{\Delta\nu_{\mathrm{D}}}$$

where $\gamma^{\mathrm{tot}} = \gamma^{rad} + \gamma_4 + \gamma_6$ is the total broadening coefficient.

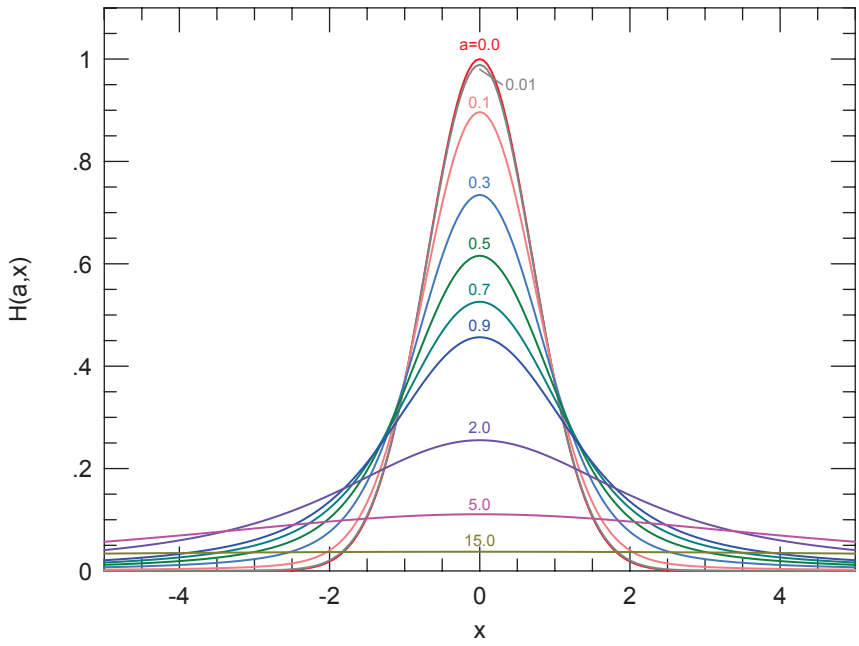

Figure A.1: Hjerting function line profile variation as a function of its parameters a and x.

As is shown in Fig. (A.1), for small values of a the line profile is close to that of a Gaussian, and the wings grow with increasing a.

B Numerical Solution to the multi-level non-LTE problems (MULTI2.3)

The non-linear coupling between the radiative transfer equation (Eqn. 3.15) and the statistical equilibrium rate equation (Eqn. 3.36) and the complexity introduced by many different atomic processes asks for a non-analytical numerical solution to the non-LTE problem.

B.1 Approximate Lambda Iteration (ALI)

In this thesis, I used the fortran77 numerical code **MULTI2.3** (Carlsson, 1986, 1992) to solve for the non-LTE equations, which uses the Approximate Lambda Iteration (ALI) method and the Newton-Raphson iterative scheme to solve for non-LTE populations. The coupling of eqns (3.15), (3.36) and that of the particle conservation equation $\sum_{j=1}^{N} n_j = n_{\rm tot}$ can be written as:

$$\mathbf{\Lambda}[\mathbf{n}] = \mathbf{b} \tag{B.1}$$

where $\mathbf{\Lambda}$ is called the Lambda operator containing the radiative and collisional rates (A matrix of dimensions $(N_{\rm lev} \times N_{\rm depth})^2$ where $N_{\rm lev}$ is the number of levels in the considered atom and $N_{\rm depth}$ is the number of optical depth points in the considered model atmosphere), and $\mathbf{n}$ is a 1D array containing the populations of each level at each atmospheric depth point.

Supposing that an estimate of the population numbers $\mathbf{n}^{(i)}$ for a certain iteration i produces an error $\mathbf{e}^{(i)}$, equation (B.1) can then be expressed as:

$$\mathbf{\Lambda}[\mathbf{n}^{(i)}] = \mathbf{b} + \mathbf{e}^{(i)} \tag{B.2}$$

and if a correction $\delta^{(i)}\mathbf{n}$ is needed to obtain the required solution $\mathbf{n}$, this gives:

$$\mathbf{\Lambda}[\mathbf{n}^{(i)} + \delta^{(i)}\mathbf{n}] = \mathbf{b} + \mathbf{e}^{(i)} \tag{B.3}$$

An approximate lambda operator $\mathbf{\Lambda}^*$ can be defined such that:

$$\mathbf{\Lambda}^{*(i)}[\delta^{(i)}\mathbf{n}] \approx \mathbf{\Lambda}[\mathbf{n}^{(i)} + \delta^{(i)}\mathbf{n}] - \mathbf{\Lambda}[\mathbf{n}^{(i)}] \tag{B.4}$$

Subtracting eqns. (B.2) from (B.3) we obtain

$$\mathbf{\Lambda}^{*(i)}[\delta^{(i)}\mathbf{n}] \approx -\mathbf{e}^{(i)} \tag{B.5}$$

Si Thus an iterative procedure can be constructed from the equations above to determine the populations at each iteration until convergence is obtained:

$$\begin{cases} \mathbf{e}^{(i)} = \mathbf{\Lambda}[\mathbf{n}^{(i)}] - \mathbf{b} \\ \delta\mathbf{n}^{(i)} = \mathbf{\Lambda}^{*(i)-\mathbf{1}}[-\mathbf{e}^{(i)}] \\ \mathbf{n}^{i+1} = \mathbf{n}^{i} + \delta\mathbf{n}^{(i)} \end{cases} \tag{B.6}$$

The construction of the approximate Lambda operator $\mathbf{\Lambda}^{*(i)}$ is of fundamental importance, which should be chosen to contain all the important interactions and to be useful, in the terms that it could be easily assembled and inverted within possible computational effort.

In **MULTI2.3**, $\mathbf{\Lambda}^*$ is constructed by making use of Scharmer's operator (Scharmer, 1981) to represent the radiative interactions and corresponding to the coefficient matrix (denoted the **Grand Matrix**) of a set of linear equations in the code which determine the relative corrections of $\delta\mathbf{n}^{(i)}/\mathbf{n}^{(i)}$ at each iteration. Different elements of the Grand Matrix demonstrate different physical properties:

- Each row in the Grand Matrix corresponds to the statistical equilibrium equation for one atomic level at one depth point in the atmosphere.

- The grand matrix itself then consists of smaller matrices each of size $N_{\rm lev} \times N_{\rm lev}$, where each corresponds to the influence from changes of the population numbers at one depth in the atmosphere on the population numbers at another depth.

- Each element in each small matrix corresponds to the influence from changing the population number of one specific atomic level on the population number of another level.

- Diagonal element matrices correspond to the local interactions while all non-diagonal blocks correspond to the non-local interactions through the radiative transfer in the lines.

B.2 Starting Approximation

The use of the iterative correction method which depends on its previous approximation at each iteration, requires a good starting approximation which can have notable effect on the actual, the divergence or the slow convergence of the solution. The standard procedure is to start from LTE populations and then perform one or two Lambda iterations Auer et al. (1972). In **MULTI2.3** , I have started from zero radiation field and continued by solving the statistical equilibrium equations until convergence is obtained. In the case of divergence of the latter, I started from LTE populations and performed several Lambda iterations until convergence was obtained. A slower convergence is observed for when starting from LTE population as compared to when starting from zero populations (see Fig. B.1).

B.3 Properties of MULTI2.3

The code **MULTI2.3** is a useful program to use for solving non-LTE radiative transfer problems in 1D, plane parallel, semi-infinite atmospheres of cool stars for its many interesting properties:

- A local approximate lambda operator option is implemented (Rybicki and Hummer, 1991), which is much less memory demanding thus makes it possible to solve problems with very large model atoms (more than 100 levels)
- The model atom of the considered element can contain many atomic levels and several ionization stages which can be treated in details simultaneously, thus making it ideal for the non-LTE study of FeI/II atom.

- The bound-bound lines are assumed to be formed with complete redistribution over the profile function which is assumed to be a Voigt profile.

- The code is relatively efficient. The CPU time scales almost linearly with the number of frequencies points and angles making it useful for solving problems including velocity fields.

- The code, written in FORTRAN77, is highly portable and well commented, thus facilitating changes and additions.

- It is possible to go through the formal solution with a new set of atomic levels and transitions in which the converged populations are redistributed to the new levels, done proportionally to their statistical weights. This is ideal for the use of superlevels and superlines (described in sections 4.1.1 & 4.2.1.1 respectively) in the case of complex large atoms such as FeI/FeII.

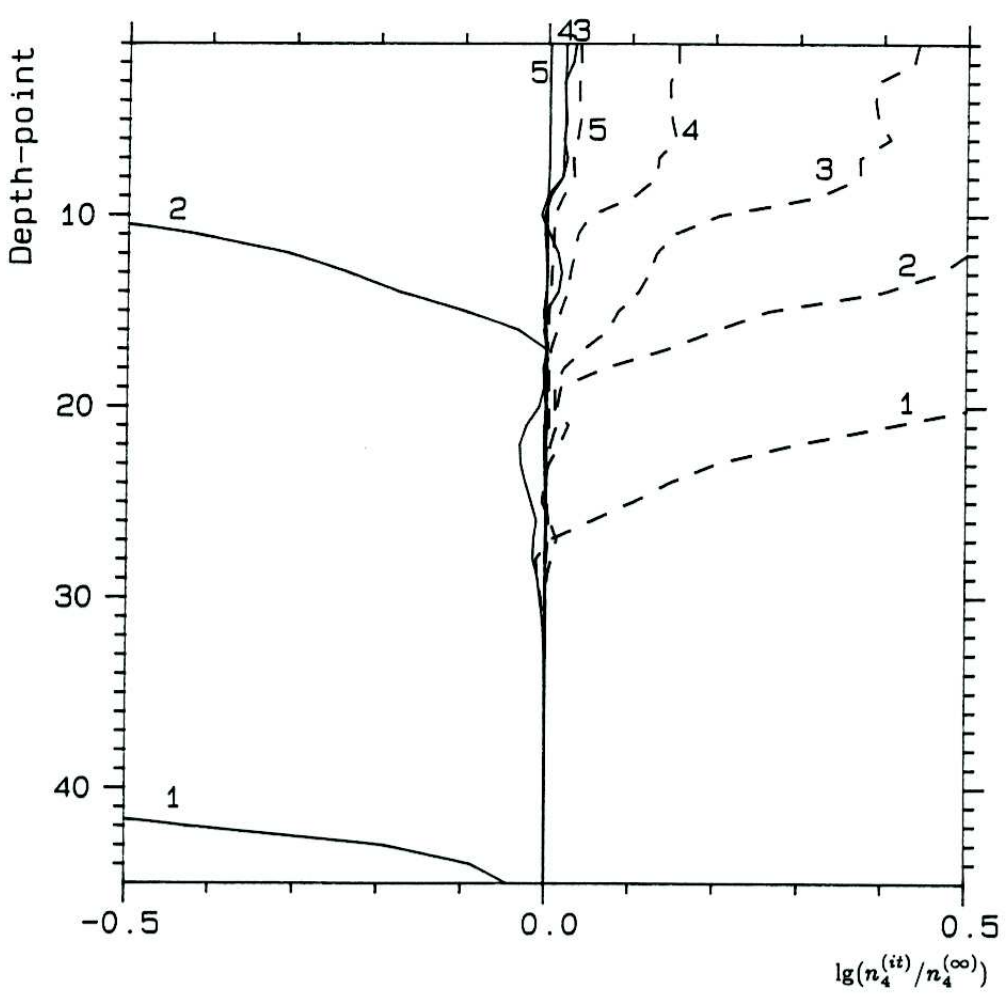

Figure B.1: Convergence of the populations of an atomic level four in a five level CaII atom plus continuum calculations for different iteration numbers. The lines show the log of the ratio of the populations to that of the global final populations at that level, $\log(n_4^{it}/n_4^{\infty})$ as a function of depth points (depth point 1 is at the top of the atmosphere) for iteration numbers $it = 1 - 5$. Dashed lines represent relative populations at different iterations when starting from LTE populations, while the solid lines for when starting from zero populations and solving the statistical equilibrium equations (Carlsson, 1986).

C | Physical Constants & Conversion of units

Below, I present the values of the physical constants utilized in this thesis, the conversion of units commonly used, and the Solar fundamental parameters values. Values adopted in sections C.1 and C.2 are from the 2014 values of the CODATA measurements of the Physical Measurement Laboratory of the National Institute of Standards and Technology (NIST)[1], while the Solar parameters are adopted from the "Sun fact sheet" [2] by Williams, D.R. (2013).

C.1 Physical constants

Newtonian constant of Gravitation G	=	$6.674\,08 \times 10^{-11}$ m$^3 \cdot$ kg$^{-1} \cdot$ s^{-1}
Planck constant h	=	$6.626\,070\,040 \times 10^{-34}$ J $\cdot$ s
speed of light (vacuum) c	=	299 792 458 m $\cdot$ s^{-1}
elementary charge e^-	=	$1.602\,176\,6208 \times 10^{-19}$ C
electron mass m_e	=	$9.109\,383\,56 \times 10^{-31}$ kg
proton mass m_p	=	$1.672\,621\,898 \times 10^{-27}$ kg
Bohr radius a_0	=	$0.529\,177\,210\,67 \times 10^{-10}$ m
Rydberg constant R_∞	=	10 973 731.568 508 m^{-1}
Boltzmann constant k_B	=	$1.380\,648\,52 \times 10^{-23}$ J $\cdot$ K^{-1}
Stefan-Boltzmann constant σ_SB	=	$5.670\,367 \times 10^{-8}$ W $\cdot$ m$^{-2} \cdot$ K^{-4}

C.2 Conversion of units

1 electron Volts (eV)	=	1.60210×10^{-19} Joules (J)
1 electron Volts (eV)	=	8065.73 cm^{-1}
1 Rydberg energy unit (Ry)	=	13.60569172 eV
1 Rydberg energy unit (Ry)	=	109737.31568 cm^{-1}
1 Mega-barn (Mb)	=	1×10^{-16} cm^2
1 parsec (pc)	=	$3.08567758 \times 10^{16}$ m
1 dyne	=	1 g $\cdot$ cm $\cdot$ s^{-2}
1 light year (ly)	=	9.46053×10^{15} m

[1] http://physics.nist.gov/cuu/Constants/index.html
[2] http://nssdc.gsfc.nasa.gov/planetary/factsheet/sunfact.html

C.3 Solar fundamental parameters

Equatorial Solar Radius $R_\odot$	=	6.9599×10^8 m
Solar mass $M_\odot$	=	1.989×10^{30} kg
Solar luminosity $L_\odot$	=	3.846×10^{26} W

D | Linelist, EW and iron abundances

Sun												
						EW_{obs} (mÅ)		EW_{calc} (mÅ)			ε_{Fe} (dex)	
element	λ (air)	EP (eV)	loggf	$\Gamma^{H} = \sigma_{H}^{br} \cdot \alpha$	γ_{rad}	EW	σEW	1D,nLTE	1D,LTE	$\langle$3D$\rangle$,nLTE	1D,nLTE	$\langle$3D$\rangle$,nLTE
Fe I	4787.827	2.998	-2.604	818.227	9.55E+07	36.86	0.25	40.609	42.791	39.860	7.525	7.542
Fe I	4794.354	2.424	-3.950	426.249	4.47E+08	10.90	0.48	10.752	11.725	10.652	7.456	7.461
Fe I	4799.406	3.640	-2.130	353.241	9.12E+07	31.24	0.49	33.867	35.838	33.375	7.511	7.522
Fe I	4808.148	3.252	-2.690	297.274	1.58E+08	23.68	0.24	25.222	26.918	24.744	7.474	7.487
Fe I	4809.938	3.573	-2.620	301.271	1.02E+08	16.90	0.43	16.856	18.086	16.602	7.451	7.460
Fe I	4869.463	3.547	-2.420	246.248	3.39E+07	20.21	0.02	20.718	22.158	20.151	7.434	7.451
Fe I	4875.877	3.332	-1.900	848.231	8.13E+07	54.27	1.21	62.245	64.637	62.152	7.295	7.303
Fe I	4877.604	2.998	-3.050	795.230	9.55E+07	17.33	0.20	17.395	18.745	17.126	7.466	7.475
Fe I	4892.859	4.218	-1.290	1015.278	2.95E+08	52.12	0.22	50.494	53.152	50.636	7.480	7.476
Fe I	4905.133	3.929	-1.730	930.278	8.71E+07	32.50	0.20	40.308	42.474	39.812	7.283	7.325
Fe I	4962.572	4.178	-1.182	905.278	2.40E+08	53.31	0.22	58.570	61.266	59.027	7.349	7.347
Fe I	4986.223	4.218	-1.290	950.279	2.95E+08	42.27	1.88	50.534	53.138	50.508	7.357	7.361
Fe I	4999.112	4.186	-1.640	-7.600	1.02E+08	30.80	2.60	32.805	34.825	32.246	7.404	7.416
Fe I	5023.498	4.313	-1.670	1051.281	1.48E+08	23.52	4.06	26.861	28.667	26.407	7.481	7.492
Fe I	5029.618	3.415	-1.950	230.261	3.24E+07	47.44	0.68	53.473	55.876	52.480	7.333	7.354
Fe I	5031.914	4.371	-1.570	1119.288	1.55E+08	23.21	0.21	28.946	30.892	28.498	7.313	7.323
Fe I	5054.643	3.640	-1.921	353.313	3.39E+07	34.21	0.32	42.466	44.607	41.380	7.318	7.342
Fe I	5088.153	4.154	-1.680	810.278	2.95E+08	34.92	1.16	33.081	35.081	32.529	7.487	7.499
Fe I	5104.438	4.283	-1.590	960.279	2.40E+08	30.10	2.54	31.737	33.799	31.236	7.429	7.440
Fe I	5129.631	3.943	-1.670	718.235	1.51E+08	44.62	8.05	45.108	47.532	44.616	7.430	7.440
Fe I	5180.056	4.473	-1.160	1152.293	1.35E+08	45.24	0.04	45.430	48.278	45.186	7.445	7.450
Fe I	5197.936	4.301	-1.540	925.279	2.40E+08	29.79	1.13	33.485	35.660	32.929	7.352	7.364
Fe I	5228.376	4.220	-1.190	809.278	2.40E+08	56.16	1.45	50.487	53.088	50.104	7.598	7.599
Fe I	5243.776	4.256	-1.050	842.278	2.40E+08	58.89	0.77	62.141	65.001	62.511	7.389	7.387
Fe I	5247.050	0.087	-4.949	206.253	4.27E+03	65.21	0.81	64.279	68.309	60.922	7.478	7.570
Fe I	5253.021	2.279	-3.840	368.253	1.66E+08	17.80	0.25	15.266	16.648	14.910	7.512	7.527
Fe I	5267.270	4.371	-1.596	973.280	2.09E+08	27.84	0.67	27.945	29.856	27.379	7.448	7.462
Fe I	5285.127	4.435	-1.660	1046.282	1.41E+08	24.84	0.15	22.854	24.521	22.345	7.507	7.520
Fe I	5293.959	4.143	-1.770	290.250	1.74E+08	25.80	0.32	29.134	31.060	28.401	7.368	7.384
Fe I	5294.547	3.640	-2.760	394.237	1.17E+08	11.25	0.28	11.902	12.881	11.663	7.400	7.410
Fe I	5295.312	4.415	-1.590	1014.281	2.09E+08	25.12	0.32	26.475	28.316	25.916	7.390	7.404
Fe I	5320.036	3.642	-2.440	-7.700	2.45E+08	17.46	2.46	17.968	19.362	17.510	7.451	7.466
Fe I	5322.041	2.279	-2.802	341.236	1.20E+08	59.47	0.32	64.077	66.956	61.931	7.359	7.404
Fe I	5326.143	3.573	-2.071	-7.820	3.63E+07	36.93	0.76	40.044	42.330	39.016	7.364	7.386
Fe I	5361.625	4.415	-1.330	975.280	2.14E+08	41.62	1.12	38.933	41.418	38.357	7.501	7.512
Fe I	5379.574	3.695	-1.514	363.249	7.08E+07	57.98	0.33	63.953	66.687	63.339	7.286	7.303
Fe I	5401.267	4.320	-1.820	836.278	2.19E+08	21.27	0.19	20.897	22.422	20.381	7.469	7.484
Fe I	5409.133	4.371	-1.200	895.279	2.09E+08	50.06	0.57	48.233	50.932	47.721	7.500	7.508
Fe I	5417.033	4.415	-1.580	944.280	2.04E+08	30.99	0.34	27.021	28.930	26.427	7.536	7.550
Fe I	5441.339	4.313	-1.630	807.278	2.04E+08	28.56	0.25	29.031	30.983	28.375	7.439	7.455
Fe I	5452.088	3.640	-2.802	395.238	3.09E+07	12.75	0.29	11.061	11.997	10.821	7.525	7.537
Fe I	5472.708	4.209	-1.495	752.215	1.02E+08	40.69	1.44	39.371	41.707	38.501	7.465	7.484
Fe I	5473.163	4.191	-2.040	929.278	2.82E+08	16.23	1.04	17.533	18.873	17.094	7.435	7.450
Fe I	5491.832	4.186	-2.188	-7.690	1.23E+08	10.01	0.27	8.952	9.699	8.722	7.539	7.552
Fe I	5522.446	4.209	-1.450	744.215	1.05E+08	40.36	0.30	41.700	44.127	40.780	7.395	7.414
Fe I	5539.280	3.642	-2.560	383.260	3.24E+07	17.00	0.07	17.597	18.983	17.145	7.440	7.455
Fe I	5543.936	4.218	-1.040	742.238	3.02E+08	59.97	0.25	62.668	65.552	62.375	7.360	7.370
Fe I	5546.506	4.371	-1.210	825.278	2.04E+08	47.09	0.94	47.575	50.238	46.923	7.452	7.464
Fe I	5549.949	3.695	-2.810	373.316	3.80E+07	7.39	1.59	8.001	8.697	7.808	7.418	7.430
Fe I	5560.211	4.435	-1.090	895.278	1.91E+08	48.96	0.40	51.347	54.221	50.873	7.360	7.371
Fe I	5567.391	2.609	-2.568	372.252	1.58E+08	62.74	3.26	61.653	64.491	59.138	7.435	7.492
Fe I	5577.025	5.033	-1.543	-7.390	7.59E+08	9.27	0.19	9.832	10.840	9.486	7.416	7.434
Fe I	5584.765	3.573	-2.220	296.271	1.74E+08	36.89	1.35	42.208	44.665	40.897	7.301	7.324
Fe I	5618.632	4.209	-1.255	732.214	1.55E+08	47.68	0.19	51.625	54.285	50.612	7.343	7.364
Fe I	5619.595	4.387	-1.600	808.277	2.04E+08	30.84	0.54	27.497	29.409	26.804	7.519	7.536
Fe I	5636.696	3.640	-2.510	368.310	4.07E+07	17.9	1.68	19.434	20.964	18.900	7.386	7.401

Sun												
						EW_{obs} (mÅ)		EW_{calc} (mÅ)			ε_{Fe} (dex)	
element	λ (air)	EP (eV)	loggf	$\Gamma^{H} = \sigma_{H}^{br} \cdot \alpha$	γ_{rad}	EW	σEW	1D,nLTE	1D,LTE	$\langle$3D$\rangle$,nLTE	1D,nLTE	$\langle$3D$\rangle$,nLTE
Fe I	5651.469	4.473	-1.900	898.278	1.86E+08	15.66	0.37	13.997	15.116	13.602	7.511	7.526
Fe I	5652.317	4.260	-1.850	754.210	1.02E+08	23.53	0.29	21.873	23.469	21.267	7.480	7.498
Fe I	5679.023	4.652	-0.820	1106.291	1.62E+08	55.18	0.36	56.258	59.785	56.105	7.427	7.431
Fe I	5680.240	4.186	-2.480	-7.770	4.90E+07	8.59	0.80	7.503	8.155	7.306	7.493	7.506
Fe I	5691.497	4.301	-1.450	746.231	2.34E+08	37.01	0.88	37.543	39.982	36.624	7.446	7.466
Fe I	5717.833	4.284	-0.990	758.209	1.51E+08	57.6	2.82	62.341	65.347	61.891	7.349	7.362
Fe I	5731.762	4.256	-1.200	727.232	2.40E+08	55.38	1.80	52.633	55.287	51.704	7.501	7.518
Fe I	5741.848	4.256	-1.672	725.232	2.95E+08	30.62	0.54	29.359	31.366	28.539	7.474	7.494
Fe I	5760.344	3.642	-2.390	386.250	7.76E+07	21.69	1.56	23.955	25.758	23.237	7.363	7.380
Fe I	5848.126	4.608	-1.056	-7.520	2.14E+08	38.96	0.66	43.193	46.048	42.508	7.342	7.357
Fe I	5849.683	3.695	-2.890	379.305	6.03E+07	6.61	0.45	6.925	7.560	6.752	7.434	7.446
Fe I	5855.076	4.608	-1.478	962.279	2.14E+08	20.85	0.35	24.201	26.051	23.530	7.339	7.355
Fe I	5858.778	4.220	-2.160	786.278	3.02E+08	12.05	0.12	13.513	14.624	13.128	7.425	7.440
Fe I	5861.108	4.283	-2.304	854.279	2.40E+08	6.98	0.16	9.019	9.782	8.769	7.481	7.495
Fe I	5873.212	4.256	-2.040	712.228	2.40E+08	16.78	0.42	16.277	17.559	15.824	7.483	7.498
Fe I	5881.280	4.608	-1.740	950.279	2.14E+08	14.77	0.72	15.121	16.365	14.669	7.434	7.451
Fe I	5909.972	3.211	-2.587	716.243	1.62E+08	30.49	0.92	34.123	36.456	32.930	7.475	7.503
Fe I	5927.789	4.652	-0.990	984.281	2.09E+08	40.96	0.49	46.237	49.451	45.535	7.332	7.346
Fe I	5987.065	4.796	-0.429	-7.420	2.00E+08	73.56	2.03	73.824	78.872	74.750	7.448	7.434
Fe I	6034.035	4.313	-2.312	710.223	1.95E+08	7.44	0.31	8.563	9.308	8.315	7.404	7.418
Fe I	6093.643	4.608	-1.400	866.274	2.14E+08	29.58	1.33	27.674	29.789	26.908	7.521	7.540
Fe I	6096.664	3.984	-1.830	963.250	5.62E+07	36.54	0.96	35.822	38.149	34.809	7.482	7.504
Fe I	6127.906	4.143	-1.399	290.250	1.00E+08	46.87	1.05	50.155	53.074	48.963	7.443	7.466
Fe I	6151.617	2.176	-3.295	277.263	1.95E+08	48.14	0.78	48.761	51.873	46.162	7.440	7.498
Fe I	6157.728	4.076	-1.160	-7.790	7.76E+07	60.59	1.65	67.274	70.518	66.406	7.304	7.323
Fe I	6165.360	4.143	-1.473	380.250	1.00E+08	44.51	0.32	46.108	48.947	44.903	7.410	7.434
Fe I	6170.506	4.796	-0.440	1057.288	2.00E+08	75.93	6.79	72.969	77.544	73.505	7.496	7.485
Fe I	6173.334	2.223	-2.880	281.266	2.04E+08	66.38	1.29	66.428	69.924	63.025	7.460	7.539
Fe I	6180.203	2.728	-2.591	335.259	1.62E+08	53.63	4.97	56.992	60.055	54.165	7.409	7.470
Fe I	6187.989	3.943	-1.620	903.244	5.62E+07	47.2	0.98	48.133	49.115	49.435	7.411	7.436
Fe I	6200.312	2.609	-2.433	350.235	1.20E+08	70.01	1.76	70.332	73.723	67.105	7.462	7.533
Fe I	6226.734	3.884	-2.120	845.244	6.76E+07	27.7	0.52	26.751	28.734	25.938	7.467	7.488
Fe I	6229.226	2.845	-2.805	350.250	1.58E+08	36.12	2.39	40.734	43.426	38.822	7.366	7.405
Fe I	6270.224	2.858	-2.470	350.249	1.58E+08	52.28	2.08	56.839	59.894	54.120	7.360	7.416
Fe I	6271.278	3.332	-2.703	720.247	1.66E+08	22.87	0.60	24.413	26.335	23.580	7.386	7.406
Fe I	6293.924	4.835	-1.717	-7.420	2.00E+08	11.79	0.17	10.585	11.543	10.202	7.542	7.561
Fe I	6297.792	2.223	-2.737	278.264	1.95E+08	72.6	0.86	74.222	78.046	70.556	7.421	7.501
Fe I	6311.500	2.832	-3.141	344.250	1.58E+08	26.57	4.32	26.141	28.261	25.077	7.466	7.495
Fe I	6380.743	4.186	-1.375	380.250	7.59E+07	50.03	0.55	49.506	52.554	48.230	7.491	7.516
Fe I	6436.406	4.186	-2.580	-7.810	3.02E+07	8.74	0.29	6.368	6.975	6.190	7.495	7.509
Fe I	6469.192	4.835	-0.730	982.286	2.51E+08	55.84	5.13	52.155	55.900	51.378	7.557	7.567
Fe I	6481.870	2.279	-2.981	308.243	1.95E+08	61.08	2.91	60.234	63.740	56.894	7.475	7.551
Fe I	6569.214	4.733	-0.380	835.271	2.57E+08	79.59	4.17	80.894	85.241	81.377	7.422	7.417
Fe I	6574.227	0.990	-5.004	227.254	1.66E+04	26.41	0.17	24.832	27.622	23.783	7.501	7.532
Fe I	6581.209	1.485	-4.679	254.245	1.78E+07	17.51	0.27	18.627	20.697	17.935	7.343	7.362
Fe I	6591.313	4.593	-2.081	276.262	1.66E+08	7.61	0.13	8.401	9.181	8.132	7.374	7.390
Fe I	6593.870	2.433	-2.420	321.247	1.02E+08	80.04	0.22	80.939	85.020	77.169	7.434	7.513
Fe I	6597.559	4.796	-0.970	893.276	2.51E+08	40.31	0.19	40.946	43.886	39.950	7.439	7.458
Fe I	6608.025	2.279	-3.930	306.242	2.00E+08	15.97	0.23	17.558	19.295	16.915	7.362	7.381
Fe I	6609.110	2.559	-2.691	335.245	9.77E+07	63.49	5.94	61.122	64.543	57.812	7.514	7.591
Fe I	6625.021	1.011	-5.336	-7.830	1.15E+04	14.05	1.34	13.221	14.922	12.798	7.531	7.550
Fe I	6627.544	4.549	-1.590	754.209	2.14E+08	26.56	0.48	22.461	24.230	21.743	7.556	7.577
Fe I	6703.566	2.759	-3.060	320.264	1.20E+08	35.58	0.76	33.668	36.202	32.034	7.494	7.536
Fe I	6710.318	1.485	-4.764	252.246	1.86E+07	16.67	0.69	16.131	17.983	15.556	7.475	7.496
Fe I	6716.236	4.580	-1.836	274.260	6.61E+07	14.96	1.23	11.578	12.626	11.201	7.553	7.571
Fe I	6739.521	1.557	-4.794	256.244	1.74E+07	11.78	0.34	13.327	14.891	12.885	7.354	7.370
Fe I	6745.956	4.076	-2.500	-7.820	3.09E+07	8.57	1.52	9.603	10.495	9.319	7.395	7.409
Fe I	6750.151	2.424	-2.618	335.241	4.90E+06	71.84	1.07	71.564	75.331	67.831	7.448	7.531
Fe I	6752.707	4.638	-1.204	778.274	2.63E+08	34.53	1.04	35.569	38.123	34.507	7.435	7.458
Fe I	6786.858	4.191	-1.970	962.248	2.51E+08	24.59	6.36	21.121	21.842	21.805	7.486	7.506
Fe I	6810.262	4.607	-0.986	873.275	2.63E+08	46.55	1.04	49.358	52.564	48.150	7.401	7.424
Fe II	4993.350	2.807	-3.684	172.220	3.09E+08	35.3	1.15	41.347	41.019	36.689	7.307	7.415
Fe II	5100.654	2.807	-4.197	173.221	3.47E+08	18.4	0.48	20.671	20.507	17.705	7.378	7.473
Fe II	5132.661	2.807	-4.094	172.219	3.47E+08	19.2	0.59	24.368	24.175	21.028	7.298	7.392
Fe II	5256.931	2.891	-4.182	174.210	3.47E+08	15.9	0.42	18.672	18.524	15.925	7.355	7.449
Fe II	5264.802	3.230	-3.130	186.300	3.63E+08	43.8	0.44	48.492	48.155	43.280	7.342	7.462
Fe II	5284.103	2.891	-3.195	174.209	3.47E+08	59.5	1.62	60.230	59.811	54.614	7.433	7.565
Fe II	5325.552	3.221	-3.160	179.252	2.95E+08	41.2	0.54	47.577	47.246	42.418	7.303	7.420
Fe II	5414.069	3.221	-3.580	185.303	3.63E+08	23.9	0.41	29.452	29.218	25.481	7.302	7.405
Fe II	6149.245	3.889	-2.841	186.269	3.16E+08	33.9	0.51	34.319	34.080	29.842	7.439	7.554
Fe II	6238.385	3.889	-2.600	186.271	3.16E+08	43.1	0.82	44.894	44.582	39.734	7.408	7.531
Fe II	6239.942	3.889	-3.573	186.271	3.16E+08	11.4	0.29	10.749	10.674	8.799	7.481	7.584
Fe II	6369.459	2.891	-4.110	169.204	2.95E+08	17.0	0.31	21.747	21.574	18.906	7.300	7.385
Fe II	6456.379	3.903	-2.185	185.276	3.16E+08	59.2	0.38	64.144	63.761	57.909	7.345	7.478
Fe II	6516.076	2.891	-3.310	169.203	2.95E+08	56.3	1.19	56.997	56.601	51.335	7.435	7.563

HD122563

		EW_{obs} (mÅ)		EW_{calc} (mÅ)		ε_{Fe} (dex)	
el	λ (air)	EW	σEW	nLTE	LTE	nLTE	LTE
Fe I	4789.6509	16.800	1.1300	12.034	21.48	4.821	4.698
Fe I	4872.1377	69.600	0.8500	61.694	77.99	4.878	4.636
Fe I	4882.1431	7.000	0.4700	5.396	9.82	4.835	4.665
Fe I	4891.4922	92.300	1.1500	86.383	101.15	4.877	4.624
Fe I	4903.3101	52.700	0.5800	46.477	62.13	4.852	4.633
Fe I	4924.7695	31.500	0.3900	21.712	32.50	4.825	4.797
Fe I	4938.8140	44.600	0.5600	38.634	53.80	4.844	4.647
Fe I	4950.1055	6.300	0.5900	5.329	9.72	4.831	4.606
Fe I	4957.2979	82.800	1.3000	73.649	87.67	4.901	4.710
Fe I	4966.0884	33.300	0.4200	25.428	39.54	4.833	4.709
Fe I	4967.8970	6.100	0.4800	5.763	11.27	4.819	4.455
Fe I	4985.2529	15.600	0.4400	11.967	22.03	4.829	4.630
Fe I	4985.5469	31.100	0.5200	27.814	41.20	4.830	4.614
Fe I	5001.8633	30.800	0.5600	27.876	46.00	4.830	4.456
Fe I	5002.7920	8.400	0.3800	6.067	10.95	4.833	4.704
Fe I	5014.9424	22.000	0.5900	18.627	32.85	4.831	4.538
Fe I	5022.2354	13.800	0.3000	12.198	22.50	4.826	4.509
Fe I	5028.1260	9.000	0.5000	8.942	16.55	4.811	4.429
Fe I	5044.2109	9.600	0.3500	7.754	13.07	4.835	4.678
Fe I	5049.8198	74.100	0.7500	64.330	77.41	4.904	4.748
Fe I	5068.7656	41.900	0.8200	36.853	52.20	4.839	4.623
Fe I	5079.2227	43.800	0.5800	33.027	46.25	4.847	4.778
Fe I	5090.7729	8.200	0.4000	5.411	10.73	4.831	4.702
Fe I	5133.6880	31.300	0.7000	28.161	46.70	4.832	4.446
Fe I	5150.8394	76.100	0.7900	60.815	76.01	4.889	4.811
Fe I	5151.9106	64.300	0.6300	43.117	59.22	4.839	4.866
Fe I	5162.2725	26.200	0.5500	16.164	29.60	4.799	4.755
Fe I	5195.4717	13.200	0.4100	12.427	22.97	4.819	4.444
Fe I	5198.7109	37.200	0.5300	29.090	41.85	4.842	4.744
Fe I	5215.1802	27.800	0.3600	25.638	41.08	4.825	4.504
Fe I	5217.3892	23.200	0.6300	20.737	33.55	4.827	4.570
Fe I	5229.8447	23.600	0.5900	20.532	34.56	4.828	4.554
Fe I	5232.9399	92.600	0.9500	87.507	101.28	4.867	4.636
Fe I	5242.4907	12.100	0.4300	9.002	16.82	4.827	4.656
Fe I	5253.4619	9.200	0.2900	6.361	11.73	4.830	4.714
Fe I	5263.3062	27.200	0.4400	25.270	40.30	4.824	4.510
Fe I	5273.1636	22.600	0.4600	19.118	32.18	4.829	4.590
Fe I	5281.7896	43.900	0.4400	41.602	57.94	4.827	4.526
Fe I	5307.3608	33.200	0.7100	28.839	41.43	4.837	4.670
Fe I	5324.1787	71.800	0.8200	65.971	83.82	4.864	4.554
Fe I	5339.9292	39.700	0.4800	36.511	53.85	4.832	4.522
Fe I	5364.8711	19.400	0.6000	13.335	25.11	4.823	4.682
Fe I	5365.3989	10.000	0.4500	9.386	17.70	4.818	4.461
Fe I	5367.4658	23.900	0.3500	20.673	36.91	4.832	4.480
Fe I	5369.9614	27.300	0.4100	25.798	44.47	4.823	4.355
Fe I	5383.3687	37.700	0.7100	32.958	54.11	4.842	4.438
Fe I	5393.1670	38.100	0.5300	34.608	51.12	4.833	4.553
Fe I	5400.5010	10.000	0.3900	7.307	14.64	4.831	4.626
Fe I	5410.9097	19.800	0.3900	17.020	31.40	4.831	4.490
Fe I	5415.1987	32.000	0.6200	29.161	49.34	4.831	4.382
Fe I	5445.0420	14.200	0.5100	9.390	18.52	4.820	4.691
Fe I	5463.2754	12.000	0.4600	10.054	19.67	4.830	4.520
Fe I	5476.5640	12.600	0.6300	10.356	20.46	4.827	4.527
Fe I	5567.3911	6.600	0.4000	5.073	8.71	4.843	4.700
Fe I	5569.6182	37.700	0.7900	32.505	51.10	4.838	4.543
Fe I	5572.8423	50.000	0.4600	44.752	64.76	4.846	4.506
Fe I	5586.7554	59.000	0.9800	55.838	75.867	4.837	4.435
Fe I	5615.6440	71.400	0.9100	66.769	85.821	4.852	4.497
Fe I	5658.8164	26.900	0.6500	24.155	39.213	4.827	4.535
Fe I	5662.5161	7.300	0.3700	6.491	13.523	4.824	4.445
Fe I	5701.5444	14.600	0.4700	13.083	20.933	4.828	4.626
Fe I	6065.4819	47.300	0.3700	37.824	52.171	4.856	4.742
Fe I	6136.6147	67.400	0.5800	55.458	69.846	4.892	4.772
Fe I	6136.9937	10.500	0.3500	7.325	12.168	4.843	4.758
Fe I	6137.6914	57.800	0.6100	46.269	60.960	4.873	4.766
Fe I	6173.3345	11.300	0.3700	7.969	13.216	4.842	4.754
Fe I	6191.5576	64.100	0.8600	56.317	70.750	4.873	4.698
Fe I	6200.3125	10.500	0.3700	7.513	12.439	4.843	4.749
Fe I	6213.4292	22.500	0.3000	17.848	27.757	4.839	4.712
Fe I	6219.2803	28.400	0.3700	20.694	31.594	4.838	4.763
Fe I	6230.7222	68.200	0.7100	55.223	69.814	4.895	4.786
Fe I	6232.6401	8.200	0.4500	5.168	10.483	4.823	4.714
Fe I	6246.3179	17.800	0.4100	15.594	28.047	4.826	4.521
Fe I	6252.5547	54.500	0.4700	43.118	57.644	4.869	4.767
Fe I	6254.2578	25.000	0.3300	17.015	26.544	4.832	4.787
Fe I	6265.1323	25.300	0.4200	17.609	27.386	4.835	4.779
Fe I	6297.7925	15.400	1.1500	10.911	17.713	4.839	4.758
Fe I	6301.5000	18.200	0.3900	14.939	27.665	4.828	4.557
Fe I	6322.6851	12.300	0.3800	8.108	13.357	4.838	4.783

HD122563

		EW_{obs} (mÅ)		EW_{calc} (mÅ)		ε_{Fe} (dex)	
el	λ (air)	EW	σEW	nLTE	LTE	nLTE	LTE
Fe I	6335.3301	38.900	0.4000	32.017	45.739	4.847	4.708
Fe I	6393.6006	60.500	0.6700	55.222	69.990	4.855	4.646
Fe I	6400.0005	37.700	0.4400	35.195	54.736	4.827	4.441
Fe I	6400.3169	16.500	0.3600	10.415	20.145	4.801	4.729
Fe I	6408.0176	11.700	0.5700	7.916	15.583	4.823	4.686
Fe I	6411.6479	21.900	0.3500	19.126	33.851	4.827	4.510
Fe I	6421.3501	45.300	0.3800	35.420	49.538	4.855	4.753
Fe I	6430.8452	55.300	0.4800	42.672	57.509	4.869	4.781
Fe I	6494.9805	80.300	0.8400	67.353	81.938	4.921	4.783
Fe I	6546.2383	32.500	0.3900	29.516	43.026	4.832	4.616
Fe I	6592.9126	38.200	0.4700	34.707	48.883	4.835	4.624
Fe I	6593.8696	18.800	0.5000	12.660	20.288	4.836	4.783
Fe I	6750.1514	12.900	0.3900	8.729	14.428	4.841	4.771
Fe II	4993.3501	7.500	0.3600	5.153	5.057	4.864	4.863
Fe II	5197.5674	39.000	0.4100	39.011	38.548	4.809	4.815
Fe II	5234.6226	42.700	0.4900	34.641	34.230	4.870	4.870
Fe II	5264.8022	7.800	0.4000	5.868	5.764	4.859	4.860
Fe II	5284.1030	18.800	0.5200	11.974	11.774	4.848	4.845
Fe II	5325.5522	7.300	0.3100	5.663	5.563	4.857	4.859
Fe II	5362.8613	26.200	0.5000	19.547	19.239	4.857	4.856
Fe II	5425.2485	7.400	0.6000	5.313	5.219	4.864	4.864
Fe II	6247.5571	8.300	0.3900	5.193	5.101	4.870	4.869

HD140283

		EW_{obs} (mÅ)		EW_{calc} (mÅ)		ε_{Fe} (dex)	
el	λ (air)	EW	σEW	nLTE	LTE	nLTE	LTE
Fe I	4872.1377	28.600	0.69	29.760	40.216	5.066	4.843
Fe I	4891.4922	54.300	0.90	52.212	64.143	5.127	4.890
Fe I	4903.3101	18.500	0.34	17.706	24.973	5.112	4.915
Fe I	4938.8140	12.900	0.24	13.116	18.791	5.082	4.888
Fe I	4939.6865	9.900	0.21	8.240	11.908	5.171	4.998
Fe I	4957.2979	40.200	0.73	39.098	49.806	5.110	4.897
Fe I	4966.0884	10.500	0.19	9.314	13.901	5.143	4.949
Fe I	4985.2529	6.200	0.11	5.526	8.528	5.138	4.938
Fe I	4985.5469	7.400	0.15	8.157	11.908	5.048	4.859
Fe I	4994.1294	14.800	0.27	12.906	18.203	5.154	4.978
Fe I	5001.8633	14.300	0.20	14.657	21.975	5.078	4.858
Fe I	5014.9424	9.000	0.12	9.213	14.066	5.080	4.866
Fe I	5022.2354	6.000	0.10	5.800	8.964	5.104	4.898
Fe I	5049.8198	24.500	0.34	24.283	31.618	5.095	4.922
Fe I	5068.7656	11.400	0.25	12.484	18.093	5.049	4.849
Fe I	5083.3384	16.500	0.26	15.233	20.953	5.128	4.957
Fe I	5107.4473	12.400	0.26	10.600	15.143	5.160	4.986
Fe I	5107.6406	14.100	0.26	14.921	20.136	5.062	4.894
Fe I	5133.6880	15.300	0.20	16.823	25.072	5.043	4.812
Fe I	5150.8394	10.800	0.18	12.489	17.640	5.025	4.833
Fe I	5151.9106	7.000	0.12	6.438	9.223	5.125	4.957
Fe I	5171.5962	44.000	0.60	43.086	51.050	5.109	4.935
Fe I	5194.9414	25.700	0.36	26.706	34.064	5.067	4.896
Fe I	5198.7109	6.800	0.16	6.120	8.706	5.136	4.972
Fe I	5215.1802	8.300	0.10	9.154	14.040	5.048	4.828
Fe I	5216.2739	21.300	0.25	22.386	29.186	5.062	4.892
Fe I	5217.3892	6.500	0.13	6.708	10.241	5.077	4.871
Fe I	5229.8447	7.800	0.30	7.051	11.034	5.132	4.922
Fe I	5232.9399	50.800	0.63	51.509	62.816	5.078	4.847
Fe I	5263.3062	8.300	0.16	8.877	13.594	5.061	4.845
Fe I	5281.7896	14.200	0.22	15.439	22.311	5.051	4.840
Fe I	5324.1787	35.100	0.29	35.677	48.082	5.079	4.830
Fe I	5339.9292	13.300	0.14	14.401	21.430	5.053	4.831
Fe I	5364.8711	9.300	0.13	7.987	12.441	5.157	4.946
Fe I	5367.4658	12.100	0.18	12.872	19.773	5.061	4.831
Fe I	5393.1670	12.100	0.14	13.000	19.345	5.057	4.840
Fe I	5410.9097	10.100	0.14	10.565	16.431	5.070	4.841
Fe I	5463.2754	5.600	0.17	5.827	9.279	5.073	4.851
Fe I	5501.4648	15.400	0.16	12.911	18.083	5.172	5.003
Fe I	5506.7788	22.600	0.26	19.119	26.119	5.176	5.000
Fe I	5569.6182	13.500	0.14	13.306	20.598	5.097	4.862
Fe I	5572.8423	20.600	0.25	20.707	30.768	5.087	4.843
Fe I	5576.0889	6.700	0.14	5.968	9.657	5.137	4.914
Fe I	5615.6440	35.600	0.33	36.833	50.318	5.067	4.797
Fe I	5658.8164	8.500	0.21	8.689	13.555	5.081	4.858
Fe I	6065.4819	11.800	0.18	10.240	14.443	5.155	4.986
Fe I	6136.6147	19.200	0.14	17.746	23.884	5.131	4.961
Fe I	6137.6914	15.500	0.15	13.785	19.014	5.147	4.978
Fe I	6230.7222	19.100	0.23	18.288	24.614	5.113	4.939
Fe I	6246.3179	5.800	0.15	5.601	9.273	5.104	4.866
Fe I	6252.5547	11.200	0.20	11.257	15.613	5.088	4.917
Fe I	6318.0181	8.400	0.17	8.255	11.676	5.098	4.927
Fe I	6335.3301	6.300	0.20	6.511	9.275	5.076	4.905
Fe I	6393.6006	15.200	0.17	17.145	23.138	5.030	4.852
Fe I	6400.0005	15.100	0.25	15.057	23.712	5.091	4.836
Fe I	6411.6479	8.300	0.28	7.253	12.048	5.145	4.907
Fe I	6421.3501	9.700	0.16	7.786	11.044	5.189	5.025
Fe I	6430.8452	11.200	0.21	9.802	13.709	5.152	4.986
Fe I	6494.9805	24.300	1.12	24.668	32.162	5.081	4.903
Fe I	6546.2383	7.200	0.22	7.635	11.001	5.064	4.882
Fe I	6592.9126	8.300	0.23	9.358	13.274	5.037	4.854
Fe II	5234.6226	14.500	0.18	14.928	14.810	5.074	5.079
Fe II	5316.6089	25.900	0.60	28.472	28.302	5.028	5.032
Fe II	5362.8613	7.600	0.11	7.227	7.170	5.114	5.118

HD84937

		EW_{obs} (mÅ)		EW_{calc} (mÅ)		ε_{Fe} (dex)	
el	λ (air)	EW	σEW	nLTE	LTE	nLTE	LTE
Fe I	4872.1377	24.900	0.89	28.151	37.736	5.347	5.149
Fe I	4891.4922	51.600	1.16	50.917	62.398	5.432	5.207
Fe I	4903.3101	17.400	0.27	16.351	22.647	5.451	5.270
Fe I	4920.5024	62.600	1.17	60.877	72.129	5.449	5.228
Fe I	4938.8140	11.400	0.33	11.979	16.801	5.397	5.219
Fe I	4957.2979	36.500	1.33	37.361	47.412	5.404	5.204
Fe I	4966.0884	11.800	0.55	9.175	13.259	5.534	5.360
Fe I	4985.2529	6.300	0.21	6.094	8.988	5.435	5.249
Fe I	4985.5469	6.500	0.26	7.358	10.452	5.366	5.193
Fe I	4994.1294	8.400	0.30	8.558	11.739	5.412	5.254
Fe I	5001.8633	15.100	0.30	15.888	22.860	5.395	5.195
Fe I	5014.9424	9.600	0.27	10.154	14.823	5.394	5.200
Fe I	5022.2354	6.100	0.21	6.461	9.529	5.395	5.207
Fe I	5049.8198	20.600	0.51	20.654	26.963	5.419	5.257
Fe I	5068.7656	11.000	0.36	11.494	16.280	5.400	5.218
Fe I	5079.2227	6.800	0.22	5.802	8.070	5.490	5.338
Fe I	5083.3384	10.500	0.21	10.218	13.827	5.433	5.279
Fe I	5127.3594	5.400	0.25	5.121	7.152	5.443	5.287
Fe I	5133.6880	19.200	0.41	18.959	27.123	5.427	5.217
Fe I	5150.8394	6.500	0.29	8.317	11.472	5.313	5.149
Fe I	5162.2725	14.600	0.33	10.046	14.861	5.595	5.411
Fe I	5171.5962	33.800	0.63	36.058	43.707	5.374	5.213
Fe I	5194.9414	19.100	0.43	20.618	26.673	5.379	5.221
Fe I	5195.4717	7.000	0.31	7.589	11.210	5.384	5.193
Fe I	5215.1802	7.400	0.26	8.882	13.217	5.340	5.140
Fe I	5216.2739	14.000	0.30	17.038	22.389	5.321	5.165
Fe I	5217.3892	6.400	0.21	6.421	9.499	5.419	5.231
Fe I	5229.8447	8.900	0.18	6.858	10.375	5.533	5.344
Fe I	5232.9399	49.400	0.80	50.387	61.149	5.403	5.191
Fe I	5263.3062	8.600	0.29	8.597	12.774	5.420	5.224
Fe I	5273.1636	7.200	0.31	6.251	9.414	5.481	5.290
Fe I	5281.7896	12.700	0.26	14.487	20.520	5.358	5.167
Fe I	5324.1787	34.200	0.52	35.157	46.876	5.401	5.173
Fe I	5339.9292	12.700	0.32	14.007	20.329	5.374	5.172
Fe I	5364.8711	12.800	0.33	9.531	14.162	5.558	5.368
Fe I	5367.4658	16.200	0.36	15.110	22.155	5.455	5.246
Fe I	5369.9614	18.400	0.24	18.882	27.565	5.406	5.186
Fe I	5383.3687	21.100	0.28	24.381	35.081	5.337	5.112
Fe I	5393.1670	11.100	0.27	12.559	18.228	5.363	5.165
Fe I	5397.1279	51.600	0.94	49.334	56.511	5.462	5.313
Fe I	5410.9097	13.500	0.30	12.568	18.675	5.455	5.247
Fe I	5415.1987	21.700	0.33	21.943	31.894	5.414	5.183
Fe I	5424.0679	24.400	0.34	19.705	28.851	5.539	5.314
Fe I	5434.5234	39.400	0.81	38.526	46.194	5.437	5.277
Fe I	5445.0420	9.200	0.21	6.311	9.606	5.585	5.399
Fe I	5463.2754	8.500	0.24	6.984	10.582	5.507	5.312
Fe I	5476.5640	6.100	0.35	5.818	8.965	5.440	5.237
Fe I	5569.6182	13.600	0.24	13.246	19.919	5.432	5.216
Fe I	5572.8423	19.100	0.31	20.606	29.951	5.380	5.155
Fe I	5586.7554	27.600	0.33	28.449	39.845	5.402	5.166
Fe I	5615.6440	36.500	0.48	36.706	49.536	5.416	5.169
Fe I	5658.8164	8.700	0.13	8.577	12.956	5.426	5.222
Fe I	6065.4819	9.400	0.22	8.710	12.097	5.455	5.293
Fe I	6136.6147	11.900	0.86	15.022	20.110	5.306	5.145
Fe I	6137.6914	11.200	0.30	11.775	16.064	5.396	5.232
Fe I	6191.5576	12.100	0.24	15.229	20.332	5.307	5.146
Fe I	6252.5547	8.300	0.35	9.242	12.660	5.371	5.210
Fe I	6393.6006	11.800	0.40	14.397	19.325	5.323	5.161
Fe I	6430.8452	8.700	0.34	7.680	10.608	5.477	5.322
Fe I	6494.9805	19.700	0.64	21.126	27.580	5.382	5.217
Fe II	4923.9214	70.000	1.46	73.108	72.962	5.348	5.352
Fe II	5018.4355	76.400	1.93	80.312	80.232	5.330	5.332
Fe II	5234.6226	18.400	0.32	18.677	18.584	5.412	5.414
Fe II	5316.6089	33.200	0.82	33.994	33.859	5.402	5.405

δ Eri

		EW_{obs} (mÅ)		EW_{calc} (mÅ)		ε_{Fe} (dex)	
el	λ (air)	EW	σEW	nLTE	LTE	nLTE	LTE
Fe I	4794.3540	38.500	1.14	32.624	34.233	7.653	7.613
Fe I	4799.4058	61.200	1.22	54.013	55.569	7.693	7.652
Fe I	4802.8799	82.100	2.41	79.223	80.840	7.578	7.540
Fe I	4809.9385	41.500	1.59	35.942	37.323	7.646	7.611
Fe I	4874.3530	42.500	3.21	38.961	40.458	7.599	7.561
Fe I	4875.8770	85.000	2.35	82.352	83.862	7.567	7.534
Fe I	4882.1431	103.300	1.90	103.754	105.334	7.502	7.476
Fe I	4885.4302	92.300	2.48	97.827	99.317	7.407	7.379
Fe I	4892.8589	74.100	1.74	67.277	69.215	7.658	7.616
Fe I	4905.1328	59.800	1.00	58.354	59.912	7.546	7.507
Fe I	4907.7319	87.200	2.34	88.531	89.971	7.483	7.455
Fe I	4917.2300	85.300	1.59	79.097	81.125	7.636	7.594
Fe I	4918.0127	74.400	1.43	68.250	70.216	7.642	7.600
Fe I	4950.1055	103.600	2.13	103.789	105.477	7.507	7.479
Fe I	4961.9136	52.400	1.76	52.147	53.704	7.516	7.478
Fe I	4962.5718	73.000	1.51	74.767	76.606	7.473	7.435
Fe I	4969.9175	96.000	1.63	101.992	104.500	7.413	7.374
Fe I	4986.2227	65.300	1.61	67.270	69.137	7.467	7.428
Fe I	4999.1123	51.400	1.67	50.012	51.665	7.544	7.504
Fe I	5002.7920	106.600	1.44	107.965	109.721	7.488	7.460
Fe I	5022.2354	124.600	2.29	139.486	141.898	7.330	7.302
Fe I	5023.1860	54.600	1.68	53.406	55.171	7.538	7.497
Fe I	5023.4976	49.800	1.07	44.170	45.772	7.641	7.602
Fe I	5025.3027	27.600	1.36	30.656	31.967	7.432	7.401
Fe I	5029.6177	77.400	3.73	71.943	73.637	7.648	7.604
Fe I	5048.4355	95.600	4.13	90.930	92.597	7.604	7.571
Fe I	5054.6426	61.500	2.42	60.029	61.631	7.552	7.506
Fe I	5067.1494	90.700	1.65	83.920	85.808	7.642	7.605
Fe I	5143.7227	51.200	1.96	54.537	56.574	7.421	7.371
Fe I	5236.2021	51.300	1.09	56.845	58.603	7.378	7.339
Fe I	5242.4907	118.700	2.32	122.347	124.717	7.459	7.426
Fe I	5243.7764	84.900	3.74	77.506	79.412	7.662	7.623
Fe I	5253.0210	39.200	1.67	41.222	43.164	7.460	7.415
Fe I	5285.1274	43.700	1.28	39.044	40.629	7.618	7.580
Fe I	5288.5249	81.000	1.09	82.138	83.986	7.485	7.445
Fe I	5293.9590	45.900	2.73	46.814	48.462	7.488	7.449
Fe I	5294.5474	27.500	1.57	28.187	29.515	7.492	7.459
Fe I	5295.3120	37.800	2.20	43.165	44.870	7.386	7.351
Fe I	5307.3608	123.000	2.15	114.325	118.226	7.687	7.606
Fe I	5315.0698	54.000	1.36	47.105	48.763	7.668	7.628
Fe I	5320.0356	42.600	1.04	37.041	38.544	7.645	7.607
Fe I	5321.1079	63.000	0.78	66.930	69.000	7.426	7.384
Fe I	5322.0405	93.200	1.74	87.414	90.304	7.649	7.578
Fe I	5373.7085	80.200	1.10	87.046	89.553	7.386	7.342
Fe I	5379.5737	85.300	1.87	81.253	83.166	7.600	7.557
Fe I	5401.2666	44.900	0.95	37.187	38.696	7.691	7.653
Fe I	5412.7837	35.500	0.95	36.657	38.184	7.482	7.448
Fe I	5417.0332	50.800	1.44	43.834	45.518	7.669	7.629
Fe I	5441.3389	45.100	0.91	46.397	48.030	7.480	7.443
Fe I	5460.8726	24.700	0.64	26.439	27.831	7.463	7.427
Fe I	5466.3960	97.300	0.80	99.370	101.502	7.477	7.442
Fe I	5466.9873	59.300	0.44	53.255	54.959	7.665	7.620
Fe I	5487.1450	56.100	1.87	50.974	52.768	7.626	7.585
Fe I	5539.2798	40.100	0.54	36.657	38.224	7.594	7.555
Fe I	5543.9355	83.100	1.05	77.526	79.270	7.631	7.594
Fe I	5546.5059	70.700	1.34	63.529	65.426	7.670	7.626
Fe I	5573.1021	61.800	1.23	66.428	68.201	7.407	7.368
Fe I	5577.0249	18.700	0.89	18.223	19.616	7.526	7.481
Fe I	5584.7646	66.400	2.87	62.316	64.177	7.611	7.564
Fe I	5594.6553	85.400	3.13	86.735	89.418	7.486	7.440
Fe I	5595.0601	15.200	0.40	11.209	12.079	7.675	7.634
Fe I	5624.0220	52.300	1.98	49.966	51.725	7.563	7.523
Fe I	5636.6958	43.100	1.26	39.069	40.697	7.607	7.567
Fe I	5638.2622	95.900	2.38	95.697	97.253	7.514	7.485
Fe I	5650.7056	44.600	1.68	44.051	47.469	7.523	7.450
Fe I	5653.8652	44.200	2.79	42.714	44.355	7.544	7.506
Fe I	5680.2402	15.500	0.35	17.512	18.453	7.440	7.410
Fe I	5691.4971	56.400	0.56	54.032	55.876	7.567	7.522
Fe I	5696.0894	31.600	0.68	31.417	32.897	7.515	7.479
Fe I	5701.5444	111.300	1.23	109.831	113.462	7.535	7.473
Fe I	5717.8325	81.900	1.45	77.020	78.914	7.615	7.575
Fe I	5720.8862	40.000	1.46	35.365	36.915	7.618	7.581
Fe I	5742.9600	18.700	0.30	19.971	21.000	7.470	7.439
Fe I	5754.4023	38.800	1.54	35.328	36.915	7.594	7.555
Fe I	5759.2622	14.800	0.62	11.360	12.021	7.652	7.622
Fe I	5760.3438	44.100	1.31	44.454	46.210	7.501	7.460
Fe I	5849.6831	19.200	1.06	18.158	19.174	7.544	7.511
Fe I	5853.1484	29.700	1.36	28.110	30.258	7.550	7.496
Fe I	5855.0757	35.700	1.48	39.579	41.314	7.420	7.384
Fe I	5858.7778	32.500	0.71	27.516	28.813	7.637	7.602

δ Eri

		EW_{obs} (mÅ)		EW_{calc} (mÅ)		ε_{Fe} (dex)	
el	λ (air)	EW	σEW	nLTE	LTE	nLTE	LTE
Fe I	5859.5864	94.600	1.86	102.821	105.349	7.382	7.343
Fe I	5873.2124	38.200	0.53	31.944	33.344	7.654	7.620
Fe I	5879.4868	16.100	1.24	14.387	15.176	7.574	7.544
Fe I	5881.2798	29.300	0.53	28.121	29.477	7.540	7.506
Fe I	5883.8164	91.500	1.36	88.418	90.222	7.566	7.533
Fe I	5898.2153	25.500	0.59	23.270	24.546	7.571	7.536
Fe I	5905.6714	73.000	1.40	77.824	80.563	7.418	7.367
Fe I	5909.9722	64.500	0.78	57.946	60.048	7.667	7.614
Fe I	5927.7886	57.500	1.29	61.429	63.856	7.428	7.380
Fe I	5929.6763	55.600	1.24	50.531	52.418	7.623	7.580
Fe I	5952.7178	86.800	2.09	82.089	83.936	7.600	7.565
Fe I	5969.5620	10.900	0.37	8.086	8.566	7.660	7.631
Fe I	5976.7769	92.300	1.28	90.864	92.435	7.536	7.508
Fe I	5984.8149	100.100	1.04	109.203	113.047	7.381	7.329
Fe I	5987.0649	84.900	0.82	86.849	90.846	7.476	7.411
Fe I	6003.0112	108.200	1.79	105.589	107.197	7.551	7.526
Fe I	6007.9595	80.000	1.06	80.373	82.859	7.503	7.455
Fe I	6008.5557	113.900	2.18	115.477	117.117	7.488	7.464
Fe I	6015.2437	21.200	0.42	25.493	27.236	7.391	7.349
Fe I	6024.0576	123.200	1.45	132.149	135.122	7.406	7.372
Fe I	6027.0508	84.400	1.53	88.924	91.204	7.426	7.385
Fe I	6034.0352	19.100	0.34	19.116	20.122	7.509	7.479
Fe I	6056.0044	90.300	1.41	98.789	102.160	7.377	7.326
Fe I	6078.4912	95.600	1.59	94.859	98.504	7.522	7.465
Fe I	6079.0078	65.000	0.97	60.132	62.248	7.612	7.567
Fe I	6093.6431	48.600	0.72	43.302	45.200	7.630	7.585
Fe I	6096.6641	61.800	0.89	55.813	57.480	7.642	7.605
Fe I	6098.2441	32.400	0.56	25.522	26.781	7.685	7.649
Fe I	6120.2466	30.800	0.42	23.304	25.581	7.699	7.637
Fe I	6127.9063	70.400	1.33	67.783	69.879	7.566	7.521
Fe I	6151.6172	81.300	1.98	76.019	79.352	7.642	7.557
Fe I	6157.7280	83.700	0.98	84.440	86.694	7.496	7.452
Fe I	6165.3599	65.600	0.99	64.006	66.122	7.545	7.499
Fe I	6180.2026	87.900	1.18	80.480	83.485	7.685	7.611
Fe I	6187.3979	15.700	0.66	12.848	13.756	7.620	7.583
Fe I	6187.9893	72.900	0.77	69.003	70.772	7.592	7.555
Fe I	6199.5063	17.400	0.45	13.411	14.405	7.655	7.615
Fe I	6219.2803	123.600	2.06	122.495	127.732	7.527	7.447
Fe I	6221.6719	10.400	0.42	7.978	8.944	7.643	7.586
Fe I	6226.7344	51.300	0.82	46.983	48.738	7.607	7.567
Fe I	6229.2261	68.300	0.90	65.234	67.670	7.587	7.525
Fe I	6232.6401	110.600	2.20	111.283	113.438	7.500	7.467
Fe I	6240.6460	81.500	1.88	75.770	79.009	7.661	7.573
Fe I	6253.8286	36.100	1.07	42.212	44.063	7.373	7.336
Fe I	6265.1323	121.900	1.94	115.919	121.127	7.609	7.522
Fe I	6270.2236	81.200	1.33	79.495	82.293	7.551	7.485
Fe I	6271.2778	50.000	1.32	47.475	49.505	7.569	7.521
Fe I	6290.5430	16.600	0.19	15.332	16.451	7.555	7.515
Fe I	6293.9243	25.600	0.31	20.144	21.294	7.665	7.629
Fe I	6297.7925	107.300	1.42	101.484	105.933	7.624	7.536
Fe I	6311.4995	58.000	0.64	51.843	54.116	7.661	7.603
Fe I	6315.8110	64.500	0.71	59.600	61.634	7.621	7.574
Fe I	6338.8760	58.800	0.56	55.491	57.924	7.581	7.528
Fe I	6380.7432	72.900	0.87	67.012	69.227	7.636	7.588
Fe I	6408.0176	119.300	2.14	130.152	132.673	7.371	7.340
Fe I	6411.1055	15.200	0.89	17.103	18.060	7.442	7.410
Fe I	6421.3501	155.900	4.37	146.453	151.765	7.633	7.563
Fe I	6495.7412	59.800	1.32	60.274	62.982	7.500	7.447
Fe I	6496.4658	80.900	0.96	79.867	82.678	7.529	7.478
Fe I	6518.3657	85.900	1.40	84.831	88.090	7.533	7.464
Fe I	6533.9282	56.500	0.43	47.938	49.883	7.700	7.654
Fe I	6569.2139	92.900	0.93	95.349	98.096	7.471	7.428
Fe I	6581.2090	59.500	0.56	51.965	55.223	7.695	7.611
Fe I	6591.3130	19.200	0.49	17.410	18.423	7.569	7.535
Fe I	6597.5591	60.200	0.63	55.728	57.990	7.603	7.556
Fe I	6608.0249	49.200	0.72	45.497	48.043	7.597	7.536
Fe I	6633.7485	84.300	1.09	77.528	79.843	7.638	7.594
Fe I	6653.8511	23.300	0.27	30.089	31.507	7.338	7.308
Fe I	6667.4180	23.400	0.23	23.509	25.170	7.507	7.463
Fe I	6699.1411	18.400	0.24	16.409	17.382	7.578	7.544
Fe I	6703.5659	67.100	0.83	59.972	62.601	7.686	7.616
Fe I	6710.3179	53.800	0.87	48.664	51.881	7.633	7.554
Fe I	6713.0459	44.000	0.33	39.562	41.210	7.614	7.575
Fe I	6725.3560	35.700	0.28	37.855	39.473	7.461	7.426
Fe I	6732.0649	15.100	0.51	19.162	20.256	7.370	7.339
Fe I	6739.5205	43.200	0.52	43.724	46.714	7.498	7.432
Fe I	6745.9556	17.200	0.23	21.855	23.078	7.365	7.333
Fe I	6746.9536	16.400	0.16	16.040	17.247	7.523	7.481
Fe I	6750.1514	104.800	1.15	96.362	100.587	7.696	7.600
Fe I	6752.7065	55.800	0.64	50.645	52.536	7.627	7.584

δ Eri

		EW_{obs} (mÅ)		EW_{calc} (mÅ)		ε_{Fe} (dex)	
el	λ (air)	EW	σEW	nLTE	LTE	nLTE	LTE
Fe I	6786.8584	45.800	0.18	39.691	41.345	7.644	7.606
Fe I	6804.2710	28.500	0.33	26.595	28.024	7.561	7.522
Fe I	6810.2622	67.600	0.70	64.655	66.861	7.571	7.525
Fe II	4993.3501	33.600	2.00	39.756	39.168	7.337	7.351
Fe II	5234.6226	77.800	1.05	84.402	83.155	7.364	7.390
Fe II	5256.9321	16.500	0.85	19.801	19.489	7.388	7.398
Fe II	5264.8022	43.100	0.64	43.559	42.915	7.497	7.515
Fe II	5325.5522	43.100	0.49	42.730	42.099	7.520	7.538
Fe II	5414.0698	24.000	1.02	27.746	27.336	7.390	7.402
Fe II	5534.8379	47.200	2.18	53.063	52.176	7.357	7.377
Fe II	6084.1016	20.500	0.28	18.665	18.335	7.576	7.590
Fe II	6113.3193	11.600	0.57	10.130	9.961	7.588	7.598
Fe II	6149.2461	29.900	0.34	28.311	27.893	7.560	7.574
Fe II	6238.3857	38.300	0.53	36.476	35.902	7.562	7.580
Fe II	6247.5571	43.300	0.40	42.476	41.766	7.532	7.553
Fe II	6369.4590	16.300	0.37	21.228	20.771	7.332	7.345
Fe II	6456.3794	50.900	0.43	51.878	50.961	7.485	7.508

ϵ For

		EW_{obs} (mÅ)		EW_{calc} (mÅ)		ε_{Fe} (dex)	
el	λ (air)	EW	σEW	nLTE	LTE	nLTE	LTE
Fe I	4787.8267	41.200	0.83	39.084	42.253	6.897	6.827
Fe I	4793.9614	9.100	0.29	8.850	10.000	6.864	6.803
Fe I	4794.3540	13.400	0.24	12.308	13.986	6.895	6.827
Fe I	4799.4058	31.400	0.40	28.791	31.500	6.912	6.848
Fe I	4802.8799	55.200	1.38	55.937	59.318	6.833	6.755
Fe I	4808.1479	26.800	0.43	23.225	25.663	6.943	6.879
Fe I	4809.9385	14.600	0.48	14.188	15.835	6.865	6.806
Fe I	4869.4634	19.800	0.76	17.842	19.824	6.911	6.849
Fe I	4874.3530	18.200	1.42	16.477	18.431	6.906	6.843
Fe I	4875.8770	56.000	0.97	56.041	59.303	6.849	6.779
Fe I	4877.6045	21.400	0.89	16.972	18.963	6.984	6.921
Fe I	4892.8589	42.900	0.63	38.964	42.491	6.934	6.859
Fe I	4896.4385	28.500	0.55	27.772	30.418	6.868	6.804
Fe I	4907.7319	55.800	1.15	60.775	64.041	6.744	6.675
Fe I	4917.2300	52.800	0.67	50.387	54.238	6.901	6.820
Fe I	4918.0127	42.300	0.66	39.781	43.334	6.904	6.828
Fe I	4962.5718	45.600	0.57	46.496	49.996	6.831	6.759
Fe I	4986.2227	37.300	0.57	39.157	42.562	6.810	6.739
Fe I	4999.1123	21.800	0.62	24.834	27.380	6.767	6.704
Fe I	5023.1860	27.200	0.80	26.489	29.302	6.868	6.799
Fe I	5023.4976	22.900	0.66	19.072	21.191	6.959	6.897
Fe I	5025.3027	8.900	0.63	10.788	12.135	6.754	6.694
Fe I	5029.6177	44.600	1.02	48.412	51.833	6.765	6.691
Fe I	5031.9141	17.800	0.33	20.328	22.612	6.773	6.710
Fe I	5036.9214	24.900	1.13	21.304	23.724	6.947	6.881
Fe I	5067.1494	59.000	0.61	54.573	58.304	6.943	6.865
Fe I	5088.1533	28.900	0.50	25.019	27.524	6.946	6.883
Fe I	5115.7769	17.100	0.65	14.002	15.680	6.959	6.898
Fe I	5129.6309	36.500	1.20	36.009	39.183	6.861	6.793
Fe I	5243.7764	49.900	0.64	48.964	52.649	6.870	6.793
Fe I	5253.0210	20.200	0.31	17.899	20.294	6.920	6.847
Fe I	5267.2695	19.800	0.59	19.657	21.865	6.854	6.791
Fe I	5285.1274	17.000	0.32	15.500	17.357	6.901	6.838
Fe I	5293.9590	19.900	0.45	22.034	24.482	6.788	6.722
Fe I	5294.5474	9.800	0.29	9.745	11.011	6.853	6.791
Fe I	5295.3120	17.900	0.52	18.297	20.421	6.837	6.774
Fe I	5320.0356	16.000	0.19	14.891	16.713	6.889	6.826
Fe I	5361.6250	31.300	0.66	28.026	31.037	6.927	6.856
Fe I	5373.7085	50.100	0.54	54.777	59.218	6.755	6.670
Fe I	5379.5737	52.500	0.91	55.554	59.226	6.783	6.705
Fe I	5401.2666	17.300	0.44	14.577	16.305	6.944	6.883
Fe I	5412.7837	12.700	0.26	14.059	15.779	6.796	6.734
Fe I	5417.0332	22.800	0.30	18.699	20.916	6.967	6.902
Fe I	5436.2949	27.700	0.20	25.000	27.685	6.918	6.850
Fe I	5441.3389	20.800	0.17	20.856	23.173	6.848	6.784
Fe I	5452.0884	10.000	0.28	9.043	10.241	6.900	6.838
Fe I	5460.8726	8.700	0.23	9.028	10.294	6.832	6.766
Fe I	5466.3960	64.400	0.59	64.756	69.036	6.843	6.759
Fe I	5466.9873	27.000	0.26	28.481	31.401	6.813	6.744
Fe I	5470.0928	15.800	0.21	13.894	15.646	6.919	6.855
Fe I	5472.7085	35.500	0.22	30.302	33.372	6.970	6.898
Fe I	5473.1626	11.100	0.29	12.520	14.083	6.788	6.726
Fe I	5473.9004	65.300	0.55	69.199	72.995	6.768	6.685
Fe I	5481.2432	50.800	0.65	47.696	51.508	6.916	6.835
Fe I	5483.0986	36.000	0.46	37.732	41.102	6.811	6.738
Fe I	5487.1450	24.400	0.40	24.167	26.852	6.856	6.788
Fe I	5494.4624	18.700	0.54	14.403	16.147	6.995	6.933

ϵ For

		EW_{obs} (mÅ)		EW_{calc} (mÅ)		ε_{Fe} (dex)	
el	λ (air)	EW	σEW	nLTE	LTE	nLTE	LTE
Fe I	5522.4463	32.800	0.19	32.349	35.509	6.861	6.788
Fe I	5539.2798	13.900	0.31	14.566	16.385	6.825	6.760
Fe I	5543.9355	50.800	0.32	50.813	54.638	6.850	6.767
Fe I	5546.5059	38.300	0.22	35.718	39.036	6.907	6.834
Fe I	5546.9907	19.900	0.33	18.208	20.321	6.902	6.838
Fe I	5554.8945	66.600	0.65	74.392	79.991	6.708	6.607
Fe I	5560.2114	39.100	0.21	38.243	41.841	6.868	6.792
Fe I	5567.3911	64.400	1.58	61.816	65.902	6.912	6.815
Fe I	5577.0249	6.200	0.30	5.256	6.184	6.929	6.851
Fe I	5584.7646	32.200	0.85	36.924	40.310	6.742	6.672
Fe I	5594.6553	51.300	1.39	53.845	58.400	6.799	6.712
Fe I	5618.6323	41.900	0.54	41.233	44.818	6.865	6.787
Fe I	5636.6958	17.800	0.47	16.150	18.146	6.905	6.839
Fe I	5638.2622	66.100	0.96	66.151	70.001	6.849	6.767
Fe I	5652.3174	13.200	0.90	15.636	17.529	6.758	6.695
Fe I	5653.8652	22.600	0.65	18.108	20.232	6.981	6.916
Fe I	5655.1763	29.400	0.25	28.577	33.345	6.871	6.762
Fe I	5679.0229	43.700	0.51	40.011	44.211	6.928	6.840
Fe I	5691.4971	32.700	1.01	28.133	31.190	6.959	6.885
Fe I	5717.8325	50.600	1.09	49.968	53.903	6.864	6.779
Fe I	5731.7617	46.100	0.29	41.711	45.240	6.945	6.869
Fe I	5741.8477	21.800	0.31	21.612	24.067	6.855	6.788
Fe I	5742.9600	5.900	0.26	6.159	6.991	6.830	6.769
Fe I	5754.4023	11.500	0.61	13.704	15.467	6.758	6.693
Fe I	5760.3438	19.500	0.44	20.061	22.440	6.833	6.766
Fe I	5838.3716	18.300	0.60	14.720	16.521	6.970	6.907
Fe I	5848.1265	28.100	0.35	30.866	34.372	6.783	6.705
Fe I	5849.6831	6.100	0.27	5.529	6.312	6.897	6.834
Fe I	5853.1484	11.700	0.31	9.684	11.433	6.946	6.862
Fe I	5855.0757	15.900	0.28	15.755	17.742	6.855	6.789
Fe I	5859.5864	61.900	1.15	66.185	71.090	6.768	6.675
Fe I	5873.2124	9.300	0.39	11.253	12.687	6.755	6.693
Fe I	5883.8164	57.300	0.75	56.906	60.797	6.858	6.781
Fe I	5905.6714	44.600	0.69	46.179	51.027	6.817	6.721
Fe I	5909.9722	29.900	0.26	31.603	34.920	6.810	6.737
Fe I	5927.7886	32.100	0.40	32.102	35.908	6.850	6.766
Fe I	5934.6543	72.200	0.98	69.017	72.803	6.911	6.838
Fe I	5952.7178	50.700	0.93	51.501	55.318	6.834	6.758
Fe I	5976.7769	60.700	0.60	58.965	62.729	6.884	6.810
Fe I	5984.8149	64.500	0.71	68.329	74.432	6.779	6.671
Fe I	5987.0649	51.300	0.58	51.942	57.713	6.837	6.728
Fe I	6003.0112	72.300	0.87	70.316	74.095	6.888	6.815
Fe I	6007.9595	48.400	0.53	50.267	54.817	6.811	6.719
Fe I	6020.1685	74.600	1.12	71.841	77.165	6.900	6.804
Fe I	6027.0508	55.800	0.83	58.230	62.479	6.801	6.716
Fe I	6056.0044	59.100	0.70	61.505	67.072	6.804	6.701
Fe I	6078.4912	59.200	0.52	57.970	63.773	6.874	6.765
Fe I	6079.0078	34.200	0.25	31.101	34.557	6.920	6.842
Fe I	6082.7100	39.700	0.48	36.780	40.821	6.915	6.826
Fe I	6093.6431	20.200	0.25	18.265	20.592	6.909	6.839
Fe I	6096.6641	29.600	0.37	28.023	30.930	6.887	6.819
Fe I	6098.2441	10.000	0.21	8.386	9.519	6.937	6.875
Fe I	6127.9063	40.300	0.44	39.361	43.112	6.870	6.791
Fe I	6136.9937	71.600	1.54	67.464	72.698	6.946	6.826
Fe I	6151.6172	53.300	1.22	52.785	57.500	6.862	6.760
Fe I	6157.7280	52.800	0.62	54.673	58.915	6.811	6.726
Fe I	6165.3599	36.800	0.44	35.894	39.487	6.870	6.793
Fe I	6173.3345	71.700	1.03	68.738	73.991	6.921	6.798
Fe I	6180.2026	57.700	0.86	56.762	61.166	6.871	6.775
Fe I	6187.9893	38.600	0.37	39.974	43.450	6.821	6.750
Fe I	6200.3125	74.000	0.94	69.811	74.664	6.948	6.835
Fe I	6226.7344	22.800	0.26	21.029	23.470	6.899	6.832
Fe I	6229.2261	38.000	0.42	40.561	44.475	6.793	6.712
Fe I	6232.6401	73.700	0.93	75.847	80.007	6.809	6.728
Fe I	6240.6460	54.400	0.64	53.271	57.966	6.876	6.773
Fe I	6271.2778	22.800	0.66	21.896	24.575	6.875	6.803
Fe I	6311.4995	30.800	0.24	26.432	29.599	6.955	6.878
Fe I	6315.8110	36.300	0.43	32.184	35.562	6.942	6.866
Fe I	6338.8760	28.400	0.23	26.963	30.467	6.885	6.801
Fe I	6355.0283	67.800	1.09	62.624	67.193	6.968	6.863
Fe I	6380.7432	41.700	0.23	38.427	42.320	6.920	6.837
Fe I	6469.1919	40.100	0.31	35.250	39.607	6.955	6.860
Fe I	6496.4658	49.700	0.80	47.168	52.119	6.901	6.803
Fe I	6533.9282	25.400	0.20	21.762	24.507	6.947	6.873
Fe I	6569.2139	63.200	0.49	59.084	64.222	6.928	6.831
Fe I	6574.2266	41.900	0.41	36.611	41.937	6.964	6.849
Fe I	6581.2090	28.500	0.55	25.974	29.993	6.912	6.815
Fe I	6593.8696	83.000	0.95	80.525	86.586	6.906	6.774
Fe I	6597.5591	30.600	0.21	27.043	30.351	6.935	6.856
Fe I	6608.0249	20.200	0.25	20.469	23.420	6.842	6.761

ϵ For

		EW_{obs} (mÅ)		EW_{calc} (mÅ)		ε_{Fe} (dex)	
el	λ (air)	EW	σEW	nLTE	LTE	nLTE	LTE
Fe I	6609.1099	65.200	0.36	61.594	66.588	6.933	6.820
Fe I	6625.0215	27.000	0.69	21.481	25.331	6.992	6.890
Fe I	6627.5439	17.900	0.28	14.869	16.801	6.953	6.886
Fe I	6633.7485	51.100	0.57	46.776	51.177	6.938	6.848
Fe I	6653.8511	10.900	0.70	10.378	11.753	6.875	6.811
Fe I	6703.5659	37.100	0.16	34.253	38.059	6.914	6.829
Fe I	6710.3179	22.400	0.18	22.865	26.587	6.837	6.744
Fe I	6713.0459	16.000	0.27	16.196	18.321	6.843	6.773
Fe I	6750.1514	74.100	0.64	72.065	77.656	6.898	6.772
Fe I	6752.7065	24.600	0.61	24.368	27.349	6.856	6.780
Fe I	6786.8584	17.600	0.17	15.585	17.551	6.917	6.852
Fe I	6804.2710	8.400	0.32	8.969	10.262	6.818	6.750
Fe II	4893.8125	8.800	0.63	7.822	7.691	6.909	6.918
Fe II	4993.3501	25.600	0.77	29.791	29.351	6.735	6.746
Fe II	5256.9321	8.800	0.20	11.606	11.412	6.705	6.713
Fe II	5264.8022	29.300	0.28	33.826	33.359	6.730	6.741
Fe II	5284.1030	41.500	0.84	46.060	45.379	6.739	6.754
Fe II	5325.5522	25.300	0.32	33.000	32.544	6.642	6.652
Fe II	5414.0698	13.000	0.26	18.257	17.969	6.650	6.659
Fe II	5425.2485	23.000	0.25	31.534	31.068	6.614	6.625
Fe II	5525.1172	5.600	0.51	8.211	8.082	6.660	6.668
Fe II	5534.8379	38.200	0.26	43.903	43.297	6.709	6.723
Fe II	6084.1016	9.900	0.21	11.111	10.904	6.788	6.798
Fe II	6149.2461	17.600	0.28	19.199	18.915	6.793	6.803
Fe II	6238.3857	23.500	0.56	27.035	26.635	6.745	6.755
Fe II	6247.5571	30.800	0.32	33.001	32.513	6.791	6.803
Fe II	6456.3794	37.800	0.29	42.470	41.842	6.734	6.748
Fe II	6516.0767	33.300	0.56	41.715	40.937	6.647	6.663

τ Cet

		EW_{obs} (mÅ)		EW_{calc} (mÅ)		ε_{Fe} (dex)	
el	λ (air)	EW	σEW	nLTE	LTE	nLTE	LTE
Fe I	4787.8267	32.200	0.49	31.918	33.179	6.967	6.926
Fe I	4788.7568	57.900	1.11	57.426	58.898	6.971	6.916
Fe I	4793.9614	7.900	0.31	6.698	7.110	7.041	7.010
Fe I	4794.3540	10.400	0.45	8.731	9.298	7.050	7.015
Fe I	4799.4058	26.400	0.27	24.406	25.529	7.013	6.977
Fe I	4802.8799	50.000	1.17	49.699	51.183	6.967	6.914
Fe I	4808.1479	18.900	0.72	18.474	19.405	6.974	6.939
Fe I	4809.9385	10.700	0.45	11.562	12.196	6.919	6.889
Fe I	4875.8770	50.700	0.97	50.859	52.378	6.957	6.912
Fe I	4882.1431	66.500	1.10	70.740	72.405	6.886	6.843
Fe I	4885.4302	62.300	1.02	66.734	68.445	6.874	6.823
Fe I	4892.8589	40.600	0.53	36.923	38.502	7.036	6.994
Fe I	4896.4385	23.400	0.46	23.732	24.798	6.951	6.914
Fe I	4905.1328	21.200	0.34	28.815	30.047	6.758	6.726
Fe I	4907.7319	51.900	0.89	56.749	58.324	6.865	6.823
Fe I	4917.2300	51.100	0.55	49.252	51.091	6.995	6.950
Fe I	4918.0127	42.200	0.63	37.845	39.463	7.048	7.006
Fe I	4950.1055	66.200	0.68	70.489	72.222	6.885	6.841
Fe I	4962.5718	41.800	0.42	44.434	46.046	6.907	6.866
Fe I	4969.9175	64.900	0.62	70.862	73.205	6.863	6.815
Fe I	4979.5859	11.500	0.29	9.165	9.698	7.076	7.046
Fe I	4986.2227	33.400	0.41	36.900	38.438	6.884	6.846
Fe I	4993.6797	37.600	0.81	33.312	34.736	7.053	7.014
Fe I	4999.1123	19.500	0.57	22.022	23.084	6.884	6.850
Fe I	5002.7920	70.200	0.68	73.943	75.684	6.897	6.853
Fe I	5023.1860	24.400	0.59	24.429	25.661	6.959	6.924
Fe I	5023.4976	19.200	0.59	17.314	18.225	7.019	6.987
Fe I	5029.6177	39.000	1.05	41.555	43.018	6.899	6.852
Fe I	5031.9141	15.500	0.42	18.717	19.723	6.855	6.824
Fe I	5036.9214	20.400	0.44	16.415	17.315	7.091	7.055
Fe I	5044.2109	67.800	0.74	66.368	68.000	6.989	6.933
Fe I	5054.6426	28.700	0.62	30.866	32.085	6.898	6.853
Fe I	5067.1494	57.300	0.81	53.913	55.753	7.023	6.976
Fe I	5072.6719	51.900	0.82	61.993	63.976	6.781	6.737
Fe I	5088.1533	25.300	0.55	22.379	23.458	7.038	7.004
Fe I	5129.6309	30.400	0.89	33.127	34.543	6.900	6.865
Fe I	5235.3867	63.400	1.15	63.254	65.210	6.963	6.907
Fe I	5242.4907	75.300	0.98	86.731	88.773	6.781	6.732
Fe I	5243.7764	47.700	0.69	47.395	49.165	6.966	6.921
Fe I	5253.0210	14.200	0.27	12.630	13.450	7.025	6.987
Fe I	5285.1274	15.000	0.32	14.184	14.994	6.990	6.958
Fe I	5288.5249	44.700	0.61	51.417	53.062	6.816	6.768
Fe I	5293.9590	16.500	0.49	19.286	20.301	6.867	6.833
Fe I	5295.3120	15.300	0.50	16.790	17.711	6.909	6.877

τ Cet

		EW_{obs} (mÅ)		EW_{calc} (mÅ)		ε_{Fe} (dex)	
el	λ (air)	EW	σEW	nLTE	LTE	nLTE	LTE
Fe I	5315.0698	19.500	0.24	19.403	20.424	6.963	6.930
Fe I	5320.0356	12.500	0.23	12.164	12.858	6.975	6.941
Fe I	5322.0405	54.700	0.59	53.117	54.816	7.002	6.925
Fe I	5326.1426	27.100	0.26	29.416	30.706	6.898	6.857
Fe I	5361.6250	27.900	1.16	26.343	27.700	6.998	6.960
Fe I	5373.7085	50.000	0.49	56.626	58.863	6.844	6.798
Fe I	5379.5737	47.600	1.05	50.429	52.042	6.899	6.849
Fe I	5398.2793	57.400	0.48	63.125	65.482	6.864	6.815
Fe I	5401.2666	13.800	0.24	13.051	13.781	6.990	6.959
Fe I	5409.1333	39.500	0.60	34.270	35.810	7.070	7.029
Fe I	5417.0332	19.700	0.37	17.161	18.121	7.039	7.005
Fe I	5436.2949	25.300	0.23	23.106	24.297	7.017	6.982
Fe I	5441.3389	18.200	0.27	18.872	19.865	6.939	6.906
Fe I	5466.3960	64.700	0.60	67.026	69.313	6.922	6.873
Fe I	5466.9873	22.200	0.28	23.484	24.616	6.922	6.883
Fe I	5470.0928	14.500	0.25	12.681	13.433	7.031	6.999
Fe I	5472.7085	30.400	0.20	27.093	28.399	7.044	7.003
Fe I	5473.1626	9.300	0.30	10.967	11.605	6.876	6.844
Fe I	5473.9004	66.700	0.80	67.419	69.361	6.947	6.892
Fe I	5481.2432	46.900	0.32	43.974	45.664	7.022	6.973
Fe I	5483.0986	32.000	0.42	33.863	35.311	6.915	6.872
Fe I	5487.1450	21.700	0.25	22.415	23.595	6.940	6.904
Fe I	5494.4624	15.100	0.27	12.385	13.092	7.068	7.035
Fe I	5522.4463	29.600	0.26	28.982	30.316	6.976	6.934
Fe I	5539.2798	10.100	0.19	11.953	12.662	6.872	6.839
Fe I	5543.1470	48.000	0.97	43.476	44.960	7.079	7.014
Fe I	5543.9355	48.600	0.40	47.360	49.129	6.987	6.935
Fe I	5546.5059	37.200	0.21	33.698	35.212	7.036	6.995
Fe I	5546.9907	17.000	0.33	16.014	16.892	6.994	6.960
Fe I	5554.8945	71.400	1.46	83.768	86.896	6.788	6.737
Fe I	5560.2114	37.500	0.28	36.766	38.418	6.975	6.933
Fe I	5567.3911	53.800	1.08	50.049	51.704	7.057	6.985
Fe I	5584.7646	24.700	0.24	31.246	32.616	6.790	6.752
Fe I	5594.6553	52.200	1.13	55.760	58.083	6.898	6.851
Fe I	5600.2241	23.800	0.43	28.159	29.517	6.844	6.805
Fe I	5618.6323	37.000	0.16	37.416	38.975	6.950	6.903
Fe I	5619.5952	22.100	0.21	17.569	18.513	7.094	7.060
Fe I	5636.6958	11.200	0.21	13.278	14.051	6.869	6.835
Fe I	5638.2622	62.800	0.48	64.107	66.022	6.935	6.880
Fe I	5641.4341	48.500	0.28	43.667	45.392	7.065	7.013
Fe I	5650.7056	21.100	0.42	18.646	20.071	7.031	6.986
Fe I	5651.4688	9.300	0.23	8.244	8.742	7.020	6.989
Fe I	5652.3174	15.100	0.20	13.785	14.572	7.011	6.977
Fe I	5655.1763	35.300	1.03	30.121	32.319	7.070	7.016
Fe I	5661.3447	13.000	0.14	15.670	16.547	6.856	6.823
Fe I	5679.0229	43.800	0.30	40.608	42.655	7.021	6.975
Fe I	5691.4971	26.700	0.26	25.388	26.696	6.995	6.953
Fe I	5701.5444	75.800	0.77	70.351	72.527	7.076	6.999
Fe I	5717.8325	47.200	0.53	46.822	48.621	6.968	6.915
Fe I	5741.8477	21.000	0.22	19.167	20.197	7.016	6.980
Fe I	5760.3438	14.500	0.31	16.600	17.529	6.883	6.848
Fe I	5838.3716	13.400	0.45	12.685	13.423	6.989	6.957
Fe I	5848.1265	24.900	0.25	29.262	30.835	6.849	6.809
Fe I	5853.1484	7.600	0.24	6.135	6.668	7.065	7.022
Fe I	5855.0757	13.500	0.17	14.745	15.620	6.913	6.879
Fe I	5858.7778	9.000	0.32	8.260	8.769	7.003	6.972
Fe I	5859.5864	59.300	0.66	70.752	73.394	6.779	6.728
Fe I	5861.1084	5.900	0.16	5.347	5.688	7.007	6.977
Fe I	5873.2124	10.400	0.19	10.030	10.636	6.978	6.948
Fe I	5883.8164	54.400	0.60	55.538	57.433	6.940	6.894
Fe I	6098.2441	9.000	0.19	7.669	8.159	7.039	7.007
Fe I	6127.9063	35.700	0.49	36.570	38.253	6.941	6.897
Fe I	6151.6172	44.100	0.94	40.176	41.981	7.063	6.992
Fe I	6157.7280	49.100	0.53	52.346	54.357	6.897	6.847
Fe I	6165.3599	32.800	0.30	33.048	34.642	6.954	6.912
Fe I	6180.2026	48.400	0.34	45.689	47.444	7.028	6.960
Fe I	6187.9893	34.400	0.24	36.641	38.208	6.912	6.872
Fe I	6213.4292	76.600	1.01	74.567	77.352	7.002	6.915
Fe I	6219.2803	83.900	1.02	78.114	81.031	7.075	6.985
Fe I	6226.7344	18.600	0.15	18.231	19.251	6.972	6.937
Fe I	6229.2261	29.100	0.25	31.796	33.294	6.888	6.840
Fe I	6232.6401	74.100	1.23	74.664	76.736	6.951	6.900
Fe I	6240.6460	42.900	0.61	40.750	42.581	7.017	6.947
Fe I	6271.2778	16.500	0.21	17.727	18.759	6.918	6.882
Fe I	6338.8760	27.500	0.24	26.809	28.460	6.977	6.934
Fe I	6364.3638	17.100	0.37	13.866	14.798	7.073	7.036
Fe I	6380.7432	38.800	0.27	35.827	37.555	7.024	6.978

τ Cet

		EW_{obs} (mÅ)		EW_{calc} (mÅ)		ε_{Fe} (dex)	
el	λ (air)	EW	σEW	nLTE	LTE	nLTE	LTE
Fe I	6408.0176	83.300	0.83	90.338	92.654	6.861	6.813
Fe I	6469.1919	38.400	0.38	36.066	38.165	7.007	6.958
Fe I	6496.4658	48.100	0.90	49.258	51.742	6.939	6.886
Fe I	6518.3657	49.300	0.53	48.706	50.577	6.974	6.907
Fe I	6533.9282	22.900	0.17	20.339	21.546	7.033	6.993
Fe I	6569.2139	63.800	1.22	62.412	65.080	6.983	6.928
Fe I	6574.2266	27.800	0.22	24.008	25.843	7.068	7.003
Fe I	6581.2090	16.000	0.25	17.245	18.583	6.915	6.865
Fe I	6597.5591	28.200	0.24	26.623	28.172	6.998	6.957
Fe I	6608.0249	14.700	0.24	14.541	15.569	6.966	6.923
Fe I	6625.0215	14.300	0.18	13.394	14.606	6.997	6.944
Fe I	6627.5439	15.500	0.58	13.597	14.434	7.032	6.997
Fe I	6633.7485	49.500	0.36	45.782	47.889	7.033	6.980
Fe I	6703.5659	28.800	0.24	26.288	27.730	7.029	6.979
Fe I	6710.3179	13.100	0.14	15.044	16.264	6.881	6.833
Fe I	6752.7065	21.700	0.43	22.841	24.170	6.927	6.886
Fe I	6786.8584	16.100	0.32	13.891	14.731	7.039	7.006
Fe I	6804.2710	8.900	0.37	8.222	8.775	7.000	6.965
Fe II	4993.3501	18.900	0.68	18.679	18.494	6.968	6.968
Fe II	5234.6226	55.700	0.45	59.952	59.535	6.861	6.847
Fe II	5264.8022	22.700	0.33	22.691	22.489	6.960	6.958
Fe II	5284.1030	35.200	1.46	32.062	31.776	7.049	7.041
Fe II	5325.5522	20.300	0.33	22.024	21.828	6.902	6.900
Fe II	5425.2485	16.800	0.37	20.843	20.657	6.815	6.816
Fe II	5534.8379	31.500	0.75	31.149	30.871	6.970	6.965
Fe II	6084.1016	6.600	0.23	6.512	6.435	6.967	6.971
Fe II	6149.2461	13.400	0.20	12.743	12.629	6.990	6.991
Fe II	6238.3857	16.200	0.42	18.779	18.611	6.861	6.861
Fe II	6247.5571	25.600	0.15	23.633	23.422	7.023	7.020
Fe II	6456.3794	32.500	0.19	31.777	31.494	6.981	6.976
Fe II	6516.0767	26.700	0.39	28.424	28.087	6.909	6.908
Fe II	5898.2153	7.800	0.23	6.851	7.312	7.022	6.990
Fe II	5905.6714	43.400	0.37	47.554	49.952	6.882	6.833
Fe II	5909.9722	23.100	0.26	25.776	27.076	6.886	6.848
Fe II	5927.7886	28.600	0.29	31.634	33.404	6.891	6.849
Fe II	5930.1797	75.200	1.28	79.205	82.334	6.903	6.850
Fe II	5934.6543	66.000	0.56	69.558	71.562	6.902	6.856
Fe II	5940.9912	12.000	0.15	11.259	11.927	6.994	6.961
Fe II	5952.7178	47.300	0.57	49.485	51.333	6.919	6.874
Fe II	5976.7769	55.500	0.63	57.432	59.331	6.925	6.880
Fe II	5984.8149	67.400	0.61	77.166	80.549	6.821	6.767
Fe II	5987.0649	53.000	0.59	56.644	59.625	6.900	6.846
Fe II	6003.0112	72.800	0.75	70.578	72.536	6.996	6.949
Fe II	6007.9595	47.100	0.56	49.852	52.038	6.906	6.852
Fe II	6020.1685	75.800	0.95	78.597	81.532	6.920	6.866
Fe II	6024.0576	92.500	1.37	95.073	98.216	6.928	6.877
Fe II	6027.0508	53.500	0.78	56.528	58.578	6.903	6.854
Fe II	6056.0044	59.400	0.69	67.436	70.392	6.835	6.783
Fe II	6078.4912	62.000	0.75	63.914	66.996	6.930	6.876
Fe II	6079.0078	31.200	0.26	30.308	31.937	6.980	6.939
Fe II	6082.7100	30.000	0.45	26.960	28.439	7.044	6.990
Fe II	6093.6431	18.600	0.19	17.167	18.205	7.006	6.970
Fe II	6096.6641	25.100	0.16	25.023	26.285	6.962	6.926

18 Sco

		EW_{obs} (mÅ)		EW_{calc} (mÅ)		ε_{Fe} (dex)	
el	λ (air)	EW	σEW	nLTE	LTE	nLTE	LTE
Fe I	4793.9614	9.000	0.25	10.113	10.957	7.421	7.380
Fe I	4794.3540	13.400	0.22	11.904	12.967	7.542	7.497
Fe I	4799.4058	37.700	0.66	35.638	37.672	7.525	7.481
Fe I	4802.8799	62.400	1.49	64.148	66.613	7.441	7.388
Fe I	4808.1479	28.000	0.69	26.966	28.748	7.506	7.462
Fe I	4809.9385	17.800	0.94	18.260	19.571	7.465	7.425
Fe I	4869.4634	21.700	1.23	22.155	23.670	7.467	7.424
Fe I	4875.8770	58.100	1.60	63.680	66.058	7.369	7.324
Fe I	4892.8589	54.800	0.87	52.175	54.863	7.531	7.479
Fe I	4896.4385	39.000	0.95	35.724	37.723	7.553	7.508
Fe I	4907.7319	64.200	1.08	70.085	72.552	7.367	7.321
Fe I	4917.2300	67.400	0.82	65.018	68.010	7.525	7.469
Fe I	4918.0127	57.100	0.96	53.249	55.993	7.554	7.501
Fe I	4950.1055	78.300	0.87	83.807	86.399	7.383	7.338
Fe I	4962.5718	55.900	0.61	60.085	62.850	7.400	7.350
Fe I	4986.2227	48.300	0.75	52.194	54.883	7.404	7.354
Fe I	4999.1123	32.300	0.70	34.446	36.528	7.431	7.385
Fe I	5002.7920	81.900	0.62	87.224	89.829	7.389	7.345
Fe I	5023.1860	36.500	0.98	37.845	40.133	7.452	7.405

18 Sco

		EW_{obs} (mÅ)		EW_{calc} (mÅ)		ε_{Fe} (dex)	
el	λ (air)	EW	σEW	nLTE	LTE	nLTE	LTE
Fe I	5023.4976	29.000	0.40	28.555	30.442	7.490	7.447
Fe I	5025.3027	15.500	0.66	16.935	18.190	7.431	7.391
Fe I	5029.6177	49.000	0.98	54.794	57.256	7.354	7.304
Fe I	5031.9141	25.300	0.59	30.692	32.721	7.352	7.310
Fe I	5036.9214	24.800	0.44	23.619	25.342	7.511	7.466
Fe I	5048.4355	73.800	3.77	76.689	79.388	7.423	7.369
Fe I	5067.1494	71.000	0.84	70.089	73.009	7.497	7.444
Fe I	5088.1533	36.900	0.48	34.835	36.901	7.525	7.480
Fe I	5104.4375	35.100	1.68	33.495	35.633	7.515	7.469
Fe I	5129.6309	46.000	0.32	47.050	49.526	7.460	7.413
Fe I	5151.9106	96.500	1.94	94.521	98.768	7.527	7.428
Fe I	5180.0557	49.400	0.37	47.258	50.221	7.521	7.465
Fe I	5197.9360	31.100	1.49	35.267	37.518	7.388	7.343
Fe I	5243.7764	61.700	0.81	63.609	66.537	7.444	7.390
Fe I	5247.0503	67.700	1.41	65.270	69.362	7.546	7.437
Fe I	5250.6455	101.200	1.16	102.581	106.744	7.456	7.385
Fe I	5253.0210	17.000	0.63	16.744	18.240	7.489	7.440
Fe I	5267.2695	29.500	1.49	29.650	31.644	7.477	7.432
Fe I	5285.1274	27.700	0.35	24.432	26.186	7.560	7.516
Fe I	5293.9590	28.300	0.51	30.784	32.784	7.420	7.375
Fe I	5294.5474	12.300	0.67	13.015	14.070	7.450	7.409
Fe I	5295.3120	27.100	0.86	28.152	30.109	7.455	7.410
Fe I	5307.3608	88.400	1.14	87.905	91.759	7.492	7.401
Fe I	5320.0356	19.800	0.23	19.386	20.845	7.493	7.449
Fe I	5322.0405	63.900	0.65	65.432	68.372	7.443	7.376
Fe I	5326.1426	38.800	0.47	41.805	44.145	7.413	7.363
Fe I	5401.2666	24.000	0.38	22.402	24.011	7.523	7.480
Fe I	5409.1333	56.000	0.39	49.946	52.686	7.596	7.542
Fe I	5412.7837	18.500	0.23	22.351	23.982	7.369	7.327
Fe I	5417.0332	33.100	0.47	28.714	30.710	7.578	7.532
Fe I	5436.2949	40.300	0.25	36.619	38.915	7.556	7.508
Fe I	5441.3389	30.800	0.18	30.753	32.786	7.481	7.436
Fe I	5452.0884	13.400	0.39	12.112	13.122	7.533	7.491
Fe I	5466.3960	78.900	0.71	84.959	88.499	7.383	7.328
Fe I	5466.9873	35.800	0.23	34.556	36.723	7.508	7.459
Fe I	5470.0928	25.700	0.38	22.217	23.864	7.570	7.526
Fe I	5472.7085	43.200	0.31	40.982	43.367	7.528	7.476
Fe I	5473.1626	17.500	0.43	18.905	20.328	7.436	7.394
Fe I	5473.9004	81.300	1.20	84.920	87.818	7.415	7.362
Fe I	5481.2432	65.300	0.40	59.914	62.803	7.586	7.528
Fe I	5483.0986	46.700	0.54	48.879	51.452	7.434	7.382
Fe I	5487.1450	36.200	0.52	35.833	38.120	7.488	7.440
Fe I	5522.4463	43.100	0.33	43.280	45.751	7.476	7.424
Fe I	5536.5801	8.100	0.26	9.455	10.333	7.403	7.358
Fe I	5539.2798	17.300	0.20	19.048	20.526	7.424	7.381
Fe I	5543.9355	62.700	0.43	63.873	66.743	7.456	7.400
Fe I	5546.5059	52.200	0.65	49.253	51.955	7.538	7.485
Fe I	5546.9907	26.000	0.56	26.512	28.355	7.467	7.422
Fe I	5549.9487	8.800	0.34	8.787	9.551	7.481	7.439
Fe I	5552.6919	6.700	0.29	6.020	6.637	7.531	7.485
Fe I	5560.2114	52.900	0.19	53.046	55.956	7.477	7.423
Fe I	5567.3911	67.000	1.47	62.721	65.608	7.580	7.512
Fe I	5577.0249	9.500	0.39	10.666	11.760	7.421	7.373
Fe I	5594.6553	69.600	2.20	73.750	77.632	7.410	7.349
Fe I	5600.2241	37.800	0.49	42.477	44.997	7.379	7.328
Fe I	5618.6323	51.600	0.38	53.005	55.736	7.450	7.395
Fe I	5636.6958	19.900	0.32	20.969	22.572	7.449	7.404
Fe I	5641.4341	65.100	0.54	60.066	62.896	7.582	7.524
Fe I	5651.4688	16.700	0.56	15.159	16.353	7.533	7.492
Fe I	5652.3174	24.600	0.35	23.379	25.058	7.512	7.468
Fe I	5655.1763	53.600	1.16	47.434	52.011	7.597	7.508
Fe I	5661.3447	22.600	0.27	26.197	28.048	7.385	7.340
Fe I	5679.0229	60.200	0.49	58.046	61.685	7.519	7.454
Fe I	5691.4971	42.600	1.09	39.171	41.671	7.554	7.499
Fe I	5698.0200	14.900	0.30	18.639	20.129	7.354	7.311
Fe I	5701.5444	82.500	0.53	84.232	87.742	7.443	7.373
Fe I	5717.8325	62.300	1.04	63.577	66.573	7.454	7.396
Fe I	5731.7617	59.200	0.44	54.021	56.685	7.586	7.531
Fe I	5741.8477	33.200	0.30	31.006	33.055	7.531	7.483
Fe I	5754.4023	15.100	0.59	17.996	19.434	7.381	7.338
Fe I	5760.3438	22.800	0.40	25.647	27.548	7.404	7.358
Fe I	5838.3716	21.800	0.28	20.868	22.463	7.506	7.462
Fe I	5848.1265	42.800	0.30	44.939	47.858	7.436	7.379
Fe I	5849.6831	8.900	0.25	7.626	8.316	7.556	7.514
Fe I	5855.0757	24.500	0.31	25.808	27.751	7.447	7.401
Fe I	5858.7778	16.000	0.29	14.660	15.849	7.528	7.485
Fe I	5861.1084	9.900	0.18	9.858	10.680	7.482	7.442
Fe I	5873.2124	19.500	0.24	17.637	19.005	7.536	7.494

18 Sco

		EW_{obs} (mÅ)		EW_{calc} (mÅ)		ε_{Fe} (dex)	
el	λ (air)	EW	σEW	nLTE	LTE	nLTE	LTE
Fe I	5879.4868	9.000	0.38	7.332	7.961	7.580	7.540
Fe I	5880.0273	14.000	0.20	14.767	15.964	7.451	7.410
Fe I	5881.2798	16.300	0.49	16.341	17.666	7.479	7.435
Fe I	5883.8164	69.200	0.89	71.398	74.450	7.442	7.390
Fe I	5909.9722	39.700	0.34	36.090	38.475	7.557	7.506
Fe I	5927.7886	45.500	0.61	48.055	51.286	7.431	7.373
Fe I	5934.6543	79.800	0.83	85.945	89.062	7.382	7.333
Fe I	5940.9912	20.500	0.44	19.330	20.830	7.515	7.470
Fe I	5952.7178	65.700	1.55	65.204	68.205	7.489	7.436
Fe I	5956.6938	54.800	1.24	49.974	53.735	7.591	7.503
Fe I	5976.7769	70.700	1.08	73.484	76.466	7.432	7.381
Fe I	5984.8149	85.400	0.83	97.179	102.726	7.316	7.247
Fe I	5987.0649	71.800	0.68	75.725	80.903	7.417	7.341
Fe I	6003.0112	86.700	0.98	86.880	89.938	7.477	7.429
Fe I	6007.9595	64.700	0.66	68.290	72.036	7.414	7.349
Fe I	6008.5557	90.500	0.97	95.763	98.929	7.402	7.355
Fe I	6024.0576	109.500	2.03	116.169	121.009	7.400	7.343
Fe I	6034.0352	8.300	0.26	9.383	10.188	7.420	7.379
Fe I	6056.0044	76.600	0.84	87.058	92.027	7.322	7.254
Fe I	6078.4912	80.100	1.10	83.598	88.745	7.427	7.354
Fe I	6079.0078	49.100	0.64	46.624	49.600	7.527	7.471
Fe I	6082.7100	36.900	0.49	34.728	37.382	7.529	7.469
Fe I	6093.6431	32.900	0.31	29.361	31.537	7.559	7.510
Fe I	6096.6641	40.300	0.32	37.770	40.138	7.532	7.483
Fe I	6098.2441	17.100	0.22	14.366	15.548	7.575	7.532
Fe I	6127.9063	51.500	0.63	51.892	54.854	7.472	7.416
Fe I	6136.9937	72.200	1.75	65.835	69.373	7.625	7.541
Fe I	6151.6172	52.400	1.04	50.500	53.666	7.522	7.453
Fe I	6157.7280	64.300	0.72	68.797	72.114	7.397	7.339
Fe I	6165.3599	47.200	0.54	47.892	50.733	7.466	7.412
Fe I	6170.5059	81.300	1.01	74.815	79.506	7.584	7.508
Fe I	6173.3345	70.000	0.93	67.467	71.018	7.539	7.457
Fe I	6180.2026	59.200	0.66	58.363	61.435	7.499	7.432
Fe I	6187.9893	50.100	0.44	51.322	54.080	7.457	7.405
Fe I	6200.3125	76.200	0.81	71.296	74.734	7.590	7.512
Fe I	6219.2803	91.600	1.11	91.616	96.134	7.480	7.392
Fe I	6226.7344	31.000	0.21	28.574	30.626	7.536	7.488
Fe I	6229.2261	40.300	0.31	42.586	45.304	7.429	7.373
Fe I	6232.6401	86.700	1.24	90.553	93.837	7.418	7.365
Fe I	6240.6460	51.100	0.67	51.358	54.520	7.474	7.406
Fe I	6265.1323	87.500	1.13	86.575	90.940	7.500	7.411
Fe I	6271.2778	25.000	0.56	26.233	28.238	7.449	7.401
Fe I	6293.9243	14.100	0.56	11.500	12.527	7.586	7.541
Fe I	6297.7925	77.800	1.06	75.163	79.036	7.539	7.454
Fe I	6311.4995	30.800	0.24	28.044	30.252	7.546	7.493
Fe I	6315.8110	43.600	0.46	42.945	45.638	7.493	7.439
Fe I	6322.6851	78.100	0.73	72.912	76.428	7.595	7.516
Fe I	6338.8760	44.800	0.33	42.840	46.015	7.518	7.457
Fe I	6380.7432	53.900	0.38	51.259	54.357	7.531	7.471
Fe I	6421.3501	113.100	2.42	112.114	117.274	7.497	7.411
Fe I	6469.1919	59.800	0.44	53.970	57.784	7.585	7.515
Fe I	6481.8696	65.900	0.72	61.596	65.181	7.577	7.495
Fe I	6495.7412	42.600	0.87	47.835	51.325	7.380	7.321
Fe I	6496.4658	69.400	1.86	68.399	72.610	7.497	7.427
Fe I	6518.3657	62.200	1.09	62.150	65.421	7.481	7.414
Fe I	6533.9282	38.100	0.40	33.642	36.097	7.575	7.521
Fe I	6569.2139	83.100	2.72	82.756	87.112	7.485	7.420
Fe I	6574.2266	30.500	0.14	27.130	30.111	7.561	7.489
Fe I	6581.2090	18.400	0.27	20.530	22.786	7.415	7.354
Fe I	6593.8696	84.400	0.76	81.791	86.005	7.536	7.447
Fe I	6597.5591	45.000	0.18	42.783	45.806	7.523	7.465
Fe I	6608.0249	18.700	0.20	19.256	21.137	7.463	7.408
Fe I	6625.0215	16.200	0.16	14.815	16.702	7.529	7.463
Fe I	6633.7485	67.500	0.81	64.023	67.606	7.543	7.478
Fe I	6667.7104	9.400	0.19	8.492	9.281	7.531	7.486
Fe I	6699.1411	8.600	0.18	8.552	9.346	7.483	7.439
Fe I	6703.5659	38.300	0.22	35.673	38.317	7.538	7.480
Fe I	6710.3179	16.000	0.31	17.878	19.909	7.417	7.357
Fe I	6713.0459	29.700	1.32	26.177	28.178	7.566	7.516
Fe I	6716.2363	15.600	0.34	12.571	13.694	7.595	7.550
Fe I	6750.1514	74.700	0.52	72.556	76.375	7.528	7.444
Fe I	6752.7065	37.000	0.34	37.230	39.861	7.475	7.420
Fe I	6804.2710	15.500	0.28	15.378	16.733	7.484	7.438
Fe I	6810.2622	48.700	0.52	51.062	54.321	7.434	7.374
Fe II	4993.3501	36.800	1.05	41.429	41.223	7.368	7.372
Fe II	5000.7305	10.300	0.26	8.179	8.122	7.596	7.599
Fe II	5100.6548	20.000	0.21	21.198	21.072	7.443	7.447
Fe II	5132.6611	21.600	0.30	24.870	24.722	7.386	7.389

18 Sco

		EW_{obs} (mÅ)		EW_{calc} (mÅ)		ε_{Fe} (dex)	
el	λ (air)	EW	σEW	nLTE	LTE	nLTE	LTE
Fe II	5256.9321	19.000	0.56	19.188	19.074	7.474	7.478
Fe II	5264.8022	48.000	0.42	48.293	48.053	7.473	7.479
Fe II	5284.1030	63.900	1.89	59.728	59.431	7.577	7.585
Fe II	5325.5522	46.000	0.42	47.415	47.179	7.446	7.452
Fe II	5414.0698	26.800	0.30	29.803	29.655	7.400	7.404
Fe II	5425.2485	41.000	0.44	45.798	45.570	7.366	7.371
Fe II	5525.1172	11.800	0.29	15.220	15.129	7.338	7.341
Fe II	5534.8379	59.900	1.28	59.808	59.510	7.482	7.489
Fe II	6084.1016	21.900	0.23	19.947	19.828	7.540	7.543
Fe II	6149.2461	38.500	0.43	34.449	34.278	7.579	7.584
Fe II	6238.3857	45.300	0.52	44.758	44.535	7.493	7.498
Fe II	6247.5571	55.900	0.69	52.040	51.781	7.567	7.573
Fe II	6456.3794	64.900	0.55	63.568	63.252	7.509	7.516
Fe II	6516.0767	60.500	0.80	56.720	56.382	7.563	7.571

HD22879

		EW_{obs} (mÅ)		EW_{calc} (mÅ)		ε_{Fe} (dex)	
el	λ (air)	EW	σEW	nLTE	LTE	nLTE	LTE
Fe I	4788.7568	30.700	0.26	28.456	31.202	6.644	6.578
Fe I	4789.6509	51.300	0.61	54.423	58.206	6.527	6.448
Fe I	4799.4058	7.500	0.22	7.192	8.163	6.610	6.549
Fe I	4802.8799	22.300	0.55	22.784	25.287	6.577	6.510
Fe I	4875.8770	17.100	0.51	20.266	22.518	6.495	6.433
Fe I	4882.1431	30.000	0.51	34.317	37.464	6.496	6.429
Fe I	4885.4302	32.800	0.46	35.980	39.322	6.519	6.446
Fe I	4892.8589	14.400	0.19	13.017	14.742	6.643	6.577
Fe I	4896.4385	5.900	0.24	7.333	8.323	6.488	6.425
Fe I	4907.7319	20.500	0.18	24.268	26.845	6.490	6.426
Fe I	4917.2300	23.800	0.28	20.072	22.527	6.691	6.624
Fe I	4950.1055	30.400	0.19	34.060	37.224	6.510	6.443
Fe I	4962.5718	17.500	0.24	17.247	19.357	6.598	6.533
Fe I	4969.9175	35.000	0.24	34.407	38.061	6.603	6.526
Fe I	4985.2529	56.900	0.62	58.477	62.676	6.558	6.471
Fe I	4986.2227	12.100	0.15	13.117	14.838	6.549	6.483
Fe I	4993.6797	11.300	0.30	11.384	12.907	6.586	6.521
Fe I	5002.7920	34.300	0.36	36.562	39.828	6.542	6.474
Fe I	5022.2354	56.000	0.50	59.829	64.194	6.513	6.423
Fe I	5023.1860	6.900	0.42	7.569	8.650	6.546	6.481
Fe I	5028.1260	41.200	0.41	47.620	51.315	6.458	6.382
Fe I	5044.2109	32.300	0.29	33.853	36.757	6.555	6.491
Fe I	5067.1494	27.500	0.26	23.287	26.019	6.694	6.626
Fe I	5088.1533	7.900	0.20	6.771	7.703	6.663	6.602
Fe I	5090.7729	44.500	0.29	46.235	50.641	6.557	6.473
Fe I	5104.4375	6.800	0.46	6.298	7.206	6.626	6.562
Fe I	5127.3594	63.900	0.77	60.646	63.704	6.674	6.595
Fe I	5129.6309	10.600	0.35	10.575	11.990	6.591	6.528
Fe I	5151.9106	59.700	0.93	56.423	59.455	6.672	6.596
Fe I	5159.0576	27.300	0.25	27.004	30.206	6.597	6.523
Fe I	5180.0557	12.700	0.23	10.599	12.141	6.681	6.613
Fe I	5198.7109	57.300	0.88	57.741	60.973	6.580	6.509
Fe I	5225.5259	34.500	0.38	31.989	35.269	6.649	6.572
Fe I	5235.3867	33.600	0.64	33.213	36.699	6.599	6.521
Fe I	5242.4907	48.200	0.28	48.720	52.557	6.579	6.500
Fe I	5243.7764	19.700	0.19	19.335	21.749	6.601	6.532
Fe I	5247.0503	27.700	0.30	26.347	29.372	6.624	6.549
Fe I	5307.3608	47.800	0.44	49.104	52.238	6.559	6.486
Fe I	5361.6250	8.500	0.21	8.474	9.718	6.591	6.524
Fe I	5373.7085	21.900	0.17	24.468	27.554	6.524	6.449
Fe I	5379.5737	20.400	0.20	22.026	24.610	6.544	6.475
Fe I	5389.4790	39.300	0.14	40.571	44.929	6.565	6.480
Fe I	5398.2793	28.900	0.19	28.864	32.395	6.591	6.512
Fe I	5400.5010	55.400	1.14	55.802	60.919	6.583	6.491
Fe I	5409.1333	14.700	0.20	12.054	13.729	6.692	6.626
Fe I	5417.0332	5.400	0.23	5.019	5.782	6.624	6.558
Fe I	5436.2949	8.400	0.20	7.189	8.244	6.664	6.599
Fe I	5441.3389	5.200	0.29	5.590	6.411	6.557	6.491
Fe I	5445.0420	61.800	0.66	63.098	68.585	6.568	6.473
Fe I	5466.3960	33.900	0.18	32.055	35.736	6.630	6.551
Fe I	5472.7085	8.400	0.27	9.060	10.378	6.553	6.484
Fe I	5473.9004	34.300	0.21	36.400	40.132	6.544	6.463
Fe I	5483.0986	10.700	0.25	12.375	14.078	6.516	6.448
Fe I	5522.4463	8.800	0.30	9.961	11.397	6.529	6.460
Fe I	5543.9355	20.500	0.23	20.960	23.630	6.577	6.503
Fe I	5546.5059	14.200	0.18	11.903	13.557	6.681	6.615
Fe I	5554.8945	36.700	0.66	41.720	46.459	6.492	6.405
Fe I	5560.2114	14.800	0.36	13.347	15.236	6.644	6.574

HD22879

		EW_{obs} (mÅ)		EW_{calc} (mÅ)		ε_{Fe} (dex)	
el	λ (air)	EW	σEW	nLTE	LTE	nLTE	LTE
Fe I	5587.5742	7.600	0.23	6.175	7.098	6.687	6.623
Fe I	5618.6323	12.900	0.23	14.595	16.585	6.525	6.454
Fe I	5619.5952	5.800	0.17	5.185	5.960	6.642	6.577
Fe I	5638.2622	31.500	0.23	33.772	37.441	6.539	6.458
Fe I	5641.4341	18.400	0.33	18.451	20.896	6.588	6.515
Fe I	5655.1763	13.000	0.38	10.696	12.525	6.690	6.609
Fe I	5691.4971	8.700	0.18	8.393	9.669	6.607	6.537
Fe I	5701.5444	40.300	0.28	40.901	44.027	6.577	6.508
Fe I	5705.4644	9.200	0.29	10.187	11.696	6.540	6.469
Fe I	5717.8325	20.500	0.34	20.659	23.317	6.585	6.511
Fe I	5731.7617	16.700	0.25	14.976	17.018	6.649	6.579
Fe I	5741.8477	6.000	0.32	5.819	6.704	6.604	6.537
Fe I	5883.8164	23.300	0.23	23.074	25.926	6.596	6.524
Fe I	5905.6714	18.300	0.24	19.267	22.121	6.561	6.481
Fe I	5909.9722	7.700	0.31	7.335	8.345	6.613	6.551
Fe I	5927.7886	11.200	0.20	10.976	12.718	6.600	6.525
Fe I	5930.1797	44.200	1.12	39.182	43.877	6.687	6.596
Fe I	5956.6938	14.800	0.26	13.758	15.634	6.629	6.560
Fe I	5976.7769	22.200	0.23	24.471	27.434	6.532	6.459
Fe I	5984.8149	35.400	0.42	37.212	41.953	6.553	6.462
Fe I	5987.0649	23.300	0.30	24.084	27.588	6.570	6.486
Fe I	6003.0112	35.300	0.33	33.412	37.001	6.629	6.555
Fe I	6008.5557	38.800	0.36	39.214	43.140	6.582	6.504
Fe I	6027.0508	25.100	0.23	25.228	28.378	6.587	6.510
Fe I	6056.0044	29.300	0.28	31.330	35.481	6.545	6.459
Fe I	6065.4819	74.000	0.98	70.249	73.791	6.669	6.594
Fe I	6078.4912	30.400	0.23	28.736	32.692	6.627	6.541
Fe I	6079.0078	10.600	0.45	10.447	12.091	6.597	6.523
Fe I	6093.6431	6.000	0.18	5.169	6.017	6.659	6.589
Fe I	6096.6641	7.800	0.17	7.509	8.621	6.608	6.541
Fe I	6127.9063	13.500	0.24	13.056	14.955	6.607	6.535
Fe I	6136.9937	25.700	0.33	24.481	27.051	6.622	6.556
Fe I	6151.6172	13.800	0.30	13.925	15.646	6.585	6.522
Fe I	6157.7280	21.900	0.24	22.560	25.520	6.572	6.496
Fe I	6165.3599	11.600	0.18	11.322	13.014	6.602	6.530
Fe I	6170.5059	27.800	0.18	23.833	27.207	6.686	6.604
Fe I	6173.3345	28.000	0.32	26.264	28.957	6.633	6.567
Fe I	6200.3125	30.800	0.34	29.083	31.854	6.631	6.565
Fe I	6213.4292	43.700	0.57	44.171	47.496	6.580	6.508
Fe I	6219.2803	50.200	0.55	47.511	50.868	6.649	6.575
Fe I	6229.2261	9.400	0.40	10.024	11.352	6.558	6.494
Fe I	6232.6401	35.600	0.17	37.497	41.342	6.551	6.472
Fe I	6240.6460	12.400	0.19	14.525	16.284	6.507	6.444
Fe I	6252.5547	75.200	0.90	71.598	75.366	6.668	6.586
Fe I	6265.1323	45.700	0.57	43.166	46.465	6.646	6.573
Fe I	6280.6172	22.500	0.51	20.697	23.255	6.641	6.569
Fe I	6297.7925	33.700	0.27	32.626	35.618	6.615	6.546
Fe I	6311.4995	5.400	0.23	5.166	5.884	6.611	6.549
Fe I	6322.6851	31.400	0.27	30.322	33.139	6.615	6.550
Fe I	6335.3301	58.300	0.61	59.542	63.141	6.563	6.484
Fe I	6344.1479	18.000	0.79	17.699	19.731	6.600	6.536
Fe I	6355.0283	24.100	0.29	23.686	26.230	6.601	6.535
Fe I	6380.7432	15.000	0.22	12.753	14.692	6.674	6.601
Fe I	6400.3169	22.300	0.56	21.528	24.162	6.611	6.540
Fe I	6408.0176	46.300	0.30	47.950	52.290	6.559	6.476
Fe I	6421.3501	66.900	0.77	63.252	66.863	6.672	6.591
Fe I	6430.8452	70.300	0.69	68.586	72.501	6.627	6.543
Fe I	6469.1919	13.500	0.34	13.360	15.481	6.595	6.517
Fe I	6475.6240	14.300	0.15	13.664	15.336	6.614	6.552
Fe I	6481.8696	22.200	0.15	20.950	23.304	6.625	6.560
Fe I	6496.4658	21.100	0.32	20.628	23.710	6.603	6.520
Fe I	6533.9282	6.200	0.16	6.371	7.443	6.577	6.502
Fe I	6593.8696	39.900	0.22	38.162	41.346	6.629	6.558
Fe I	6597.5591	9.200	0.17	9.028	10.485	6.599	6.525
Fe I	6609.1099	22.900	0.28	21.592	23.938	6.626	6.562
Fe I	6633.7485	23.100	0.46	19.160	22.023	6.699	6.619
Fe I	6703.5659	8.100	0.29	7.419	8.412	6.632	6.571
Fe I	6750.1514	32.200	0.23	29.984	32.913	6.642	6.573
Fe II	4993.3501	15.200	0.33	16.898	16.831	6.529	6.531
Fe II	5100.6548	5.200	0.26	6.300	6.269	6.498	6.500
Fe II	5132.6611	5.700	0.22	7.811	7.772	6.437	6.440
Fe II	5234.6226	59.600	0.60	60.708	60.526	6.563	6.568
Fe II	5264.8022	20.900	0.27	22.030	21.942	6.556	6.558
Fe II	5284.1030	31.200	0.30	31.719	31.593	6.577	6.580
Fe II	5325.5522	18.000	0.11	21.350	21.265	6.483	6.486
Fe II	5362.8613	47.000	0.73	45.395	45.259	6.629	6.632
Fe II	5414.0698	8.300	0.20	10.153	10.102	6.487	6.490

HD22879

		EW_{obs} (mÅ)		EW_{calc} (mÅ)		ε_{Fe} (dex)	
el	λ (air)	EW	σEW	nLTE	LTE	nLTE	LTE
Fe II	5425.2485	16.300	0.15	20.131	20.051	6.463	6.465
Fe II	5534.8379	31.800	0.28	31.643	31.517	6.594	6.597
Fe II	6149.2461	14.200	0.15	12.890	12.839	6.644	6.647
Fe II	6238.3857	17.600	0.23	19.601	19.523	6.523	6.525
Fe II	6247.5571	27.800	0.32	25.078	24.978	6.666	6.669
Fe II	6456.3794	37.600	0.47	34.362	34.225	6.671	6.675
Fe II	6516.0767	28.200	0.30	28.551	28.437	6.581	6.584

α Cen A

		EW_{obs} (mÅ)		EW_{calc} (mÅ)		ε_{Fe} (dex)	
el	λ (air)	EW	σEW	nLTE	LTE	nLTE	LTE
Fe I	4787.8267	51.700	2.62	47.462	49.595	7.873	7.821
Fe I	4789.6509	102.000	2.77	110.343	113.172	7.642	7.600
Fe I	4799.4058	45.600	1.86	42.002	44.120	7.856	7.805
Fe I	4802.8799	72.300	2.00	67.367	69.666	7.891	7.834
Fe I	4809.9385	26.300	1.75	24.080	25.672	7.830	7.787
Fe I	4874.3530	23.000	2.49	23.992	25.660	7.742	7.697
Fe I	4875.8770	66.600	2.83	66.966	69.180	7.762	7.712
Fe I	4877.6045	26.600	1.90	24.266	25.981	7.833	7.786
Fe I	4882.1431	81.800	2.16	85.798	87.998	7.694	7.651
Fe I	4885.4302	83.100	1.60	85.191	87.375	7.728	7.684
Fe I	4892.8589	61.500	1.61	58.281	60.900	7.839	7.783
Fe I	4905.1328	46.600	1.16	48.228	50.448	7.731	7.680
Fe I	4907.7319	77.100	0.78	73.046	75.228	7.856	7.810
Fe I	4950.1055	91.200	2.77	85.766	88.055	7.872	7.829
Fe I	4962.5718	64.300	1.42	65.260	67.908	7.750	7.695
Fe I	4985.2529	114.700	2.45	118.264	121.048	7.721	7.682
Fe I	4986.2227	59.800	1.47	58.285	60.840	7.803	7.748
Fe I	4992.7852	12.800	1.24	13.093	14.078	7.758	7.719
Fe I	4999.1123	43.100	1.49	41.491	43.675	7.809	7.757
Fe I	5002.7920	94.700	1.55	88.978	91.259	7.874	7.832
Fe I	5022.2354	116.600	2.27	121.648	124.639	7.703	7.662
Fe I	5023.1860	41.900	1.76	45.151	47.527	7.696	7.646
Fe I	5023.4976	38.900	1.07	36.113	38.255	7.834	7.785
Fe I	5025.3027	21.900	1.94	23.333	24.902	7.729	7.687
Fe I	5029.6177	60.500	1.69	58.899	61.226	7.810	7.752
Fe I	5031.9141	37.700	0.89	38.379	40.656	7.754	7.704
Fe I	5036.9214	29.900	1.31	29.376	31.318	7.783	7.735
Fe I	5048.4355	84.500	4.21	79.777	82.160	7.870	7.820
Fe I	5054.6426	50.600	2.39	49.300	51.515	7.805	7.746
Fe I	5072.6719	79.800	1.66	82.352	85.162	7.723	7.671
Fe I	5104.4375	45.800	3.23	40.984	43.232	7.879	7.826
Fe I	5180.0557	56.000	1.19	54.184	57.277	7.809	7.744
Fe I	5197.9360	40.400	1.66	42.796	45.143	7.716	7.666
Fe I	5236.2021	45.600	1.26	48.255	50.688	7.707	7.653
Fe I	5242.4907	99.700	2.24	103.500	106.372	7.708	7.662
Fe I	5253.0210	24.400	1.13	21.096	22.906	7.864	7.811
Fe I	5267.2695	37.000	1.75	37.277	39.488	7.764	7.714
Fe I	5288.5249	69.300	1.25	69.668	72.195	7.762	7.705
Fe I	5293.9590	37.400	0.97	37.953	40.119	7.757	7.706
Fe I	5294.5474	19.500	1.20	17.936	19.307	7.820	7.776
Fe I	5295.3120	37.700	1.25	35.823	38.029	7.814	7.763
Fe I	5320.0356	24.500	0.82	25.442	27.211	7.744	7.698
Fe I	5326.1426	52.100	1.76	47.527	49.871	7.884	7.824
Fe I	5373.7085	75.000	1.28	78.911	82.457	7.698	7.636
Fe I	5379.5737	73.800	1.60	68.823	71.393	7.884	7.824
Fe I	5386.3330	42.700	0.90	42.770	45.068	7.768	7.717
Fe I	5398.2793	83.300	0.89	85.414	88.880	7.733	7.675
Fe I	5401.2666	27.700	1.31	29.561	31.481	7.722	7.676
Fe I	5406.7749	39.600	1.12	36.428	38.589	7.843	7.793
Fe I	5412.7837	25.700	0.85	29.695	31.658	7.668	7.623
Fe I	5441.3389	40.600	1.23	38.345	40.577	7.822	7.771
Fe I	5452.0884	17.800	0.90	16.779	18.100	7.805	7.760
Fe I	5466.3960	87.500	1.01	89.551	92.607	7.736	7.685
Fe I	5473.1626	27.800	0.92	25.509	27.253	7.830	7.784
Fe I	5473.9004	95.200	2.20	88.403	90.763	7.896	7.853
Fe I	5483.0986	56.400	0.91	55.059	57.533	7.801	7.744
Fe I	5487.1450	48.800	1.12	43.517	45.952	7.887	7.832
Fe I	5491.8315	16.000	1.03	14.193	15.311	7.837	7.795
Fe I	5522.4463	54.600	1.17	49.865	52.269	7.881	7.824
Fe I	5524.2495	6.900	0.91	6.118	6.636	7.828	7.789
Fe I	5525.5435	68.600	0.91	65.850	68.451	7.832	7.773
Fe I	5536.5801	10.400	1.01	12.812	13.987	7.659	7.613
Fe I	5539.2798	25.100	0.76	25.061	26.861	7.771	7.723
Fe I	5543.9355	73.000	0.75	68.674	71.239	7.865	7.808
Fe I	5546.5059	61.400	0.88	55.772	58.461	7.894	7.833

α Cen A

		EW_{obs} (mÅ)		EW_{calc} (mÅ)		ε_{Fe} (dex)	
el	λ (air)	EW	σEW	nLTE	LTE	nLTE	LTE
Fe I	5546.9907	38.200	0.88	33.806	35.849	7.875	7.825
Fe I	5554.8945	104.400	1.98	107.073	111.767	7.733	7.671
Fe I	5560.2114	60.200	1.21	59.578	62.385	7.783	7.725
Fe I	5577.0249	15.800	0.85	15.998	17.619	7.763	7.708
Fe I	5584.7646	51.500	1.24	49.668	52.172	7.814	7.754
Fe I	5618.6323	63.400	0.98	58.677	61.186	7.880	7.821
Fe I	5636.6958	27.900	0.80	27.204	29.126	7.788	7.739
Fe I	5638.2622	85.700	1.69	85.718	88.097	7.770	7.724
Fe I	5650.7056	47.100	0.94	41.369	45.361	7.896	7.805
Fe I	5651.4688	23.600	1.12	21.326	22.882	7.835	7.790
Fe I	5652.3174	34.000	0.97	30.485	32.431	7.857	7.808
Fe I	5679.0229	71.000	1.15	64.528	68.139	7.898	7.824
Fe I	5680.2402	14.700	0.88	12.116	13.113	7.874	7.832
Fe I	5717.8325	74.200	1.87	68.556	71.264	7.893	7.833
Fe I	5741.8477	41.500	1.00	38.331	40.519	7.845	7.793
Fe I	5742.9600	17.400	1.26	14.019	15.139	7.892	7.848
Fe I	5754.4023	26.800	1.20	23.862	25.631	7.849	7.801
Fe I	5760.3438	27.600	0.77	32.230	34.360	7.652	7.604
Fe I	5838.3716	32.200	1.11	27.542	29.425	7.883	7.836
Fe I	5848.1265	54.900	1.31	52.111	55.086	7.832	7.766
Fe I	5855.0757	29.200	0.67	33.638	35.938	7.662	7.614
Fe I	5858.7778	20.900	0.90	20.417	21.954	7.785	7.739
Fe I	5861.1084	14.600	0.60	14.359	15.490	7.779	7.737
Fe I	5873.2124	27.000	0.80	24.214	25.925	7.842	7.797
Fe I	5880.0273	18.300	0.53	20.944	22.520	7.688	7.644
Fe I	5881.2798	20.600	0.66	22.930	24.629	7.702	7.658
Fe I	5883.8164	78.600	1.66	75.877	78.629	7.822	7.769
Fe I	5898.2153	23.500	0.64	19.208	20.788	7.894	7.846
Fe I	5902.4731	18.800	0.81	24.093	25.934	7.612	7.567
Fe I	5905.6714	72.200	0.79	71.645	75.416	7.780	7.710
Fe I	5909.9722	46.300	0.83	42.194	44.697	7.865	7.806
Fe I	5927.7886	55.900	0.61	55.471	58.762	7.779	7.713
Fe I	5934.6543	89.300	1.31	89.675	92.258	7.764	7.720
Fe I	5940.9912	28.600	0.55	25.869	27.697	7.842	7.793
Fe I	5976.7769	80.300	0.86	77.917	80.493	7.815	7.766
Fe I	5984.8149	93.600	1.26	102.352	107.626	7.645	7.574
Fe I	5987.0649	82.400	1.47	81.481	86.682	7.786	7.700
Fe I	6003.0112	97.200	1.31	90.489	93.000	7.882	7.840
Fe I	6007.9595	76.800	1.03	74.102	77.594	7.822	7.755
Fe I	6008.5557	100.800	1.47	99.039	101.683	7.797	7.756
Fe I	6015.2437	9.800	1.08	10.315	11.436	7.744	7.691
Fe I	6024.0576	122.700	1.94	121.511	125.788	7.784	7.734
Fe I	6027.0508	76.900	1.27	77.616	80.682	7.756	7.698
Fe I	6034.0352	11.400	0.83	13.805	14.924	7.668	7.627
Fe I	6056.0044	86.600	1.21	92.440	97.203	7.678	7.607
Fe I	6078.4912	91.400	2.04	89.249	94.344	7.804	7.725
Fe I	6079.0078	60.500	1.20	54.258	57.174	7.899	7.837
Fe I	6093.6431	40.400	0.95	37.351	39.820	7.839	7.783
Fe I	6096.6641	47.900	0.85	44.997	47.415	7.833	7.780
Fe I	6098.2441	24.000	1.00	20.401	21.984	7.873	7.826
Fe I	6120.2466	6.400	0.63	5.803	6.655	7.817	7.751
Fe I	6127.9063	62.200	1.22	58.108	61.038	7.858	7.794
Fe I	6157.7280	75.900	1.29	73.517	76.580	7.818	7.757
Fe I	6165.3599	56.900	1.11	54.439	57.304	7.824	7.761
Fe I	6187.3979	5.100	0.74	5.588	6.181	7.726	7.678
Fe I	6187.9893	62.200	1.04	57.529	60.114	7.869	7.813
Fe I	6199.5063	6.300	0.64	5.337	5.923	7.849	7.799
Fe I	6226.7344	39.900	1.05	35.745	38.027	7.864	7.811
Fe I	6229.2261	50.600	0.89	47.694	50.523	7.840	7.772
Fe I	6232.6401	94.000	1.37	93.517	96.409	7.778	7.729
Fe I	6253.8286	31.400	1.13	37.119	39.615	7.637	7.587
Fe I	6270.2236	64.300	0.84	61.762	64.876	7.833	7.756
Fe I	6271.2778	34.100	1.35	32.609	34.913	7.806	7.751
Fe I	6293.9243	17.700	0.58	16.969	18.405	7.795	7.747
Fe I	6315.8110	51.900	0.62	49.741	52.469	7.818	7.758
Fe I	6338.8760	54.900	1.06	50.817	54.061	7.855	7.787
Fe I	6408.0176	109.100	2.17	109.494	112.532	7.764	7.721
Fe I	6495.7412	52.300	0.82	55.747	59.368	7.700	7.632
Fe I	6496.4658	75.000	1.14	74.866	78.889	7.772	7.701
Fe I	6569.2139	89.000	1.11	89.100	93.103	7.768	7.706
Fe I	6581.2090	25.500	0.97	24.553	27.160	7.795	7.728
Fe I	6591.3130	13.600	1.02	13.634	14.836	7.769	7.722
Fe I	6597.5591	55.600	0.86	50.981	54.063	7.865	7.801
Fe I	6608.0249	25.700	0.75	23.970	26.225	7.817	7.756
Fe I	6625.0215	21.900	1.12	17.802	20.070	7.894	7.822
Fe I	6667.4180	12.000	1.04	9.989	11.074	7.865	7.812
Fe I	6667.7104	15.100	1.03	12.708	13.828	7.865	7.818

α Cen A

		EW_{obs} (mÅ)		EW_{calc} (mÅ)		ε_{Fe} (dex)	
el	λ (air)	EW	σEW	nLTE	LTE	nLTE	LTE
Fe I	6699.1411	12.100	0.99	12.794	13.937	7.740	7.694
Fe I	6703.5659	45.700	0.92	41.274	44.143	7.874	7.805
Fe I	6710.3179	20.800	0.50	21.656	24.089	7.745	7.678
Fe I	6739.5205	16.600	0.71	18.316	20.442	7.712	7.649
Fe I	6752.7065	42.300	1.42	45.032	47.703	7.708	7.650
Fe I	6786.8584	35.500	1.01	30.831	32.939	7.877	7.827
Fe II	4893.8125	23.300	1.29	22.036	21.948	7.808	7.811
Fe II	4993.3501	46.500	1.66	51.989	51.833	7.625	7.629
Fe II	5000.7305	15.100	1.07	14.766	14.707	7.783	7.785
Fe II	5100.6548	26.400	0.92	32.052	31.924	7.615	7.618
Fe II	5132.6611	27.800	1.65	36.078	35.934	7.550	7.553
Fe II	5234.6226	99.600	2.18	103.804	103.597	7.692	7.696
Fe II	5256.9321	25.700	1.72	29.798	29.679	7.655	7.658
Fe II	5264.8022	54.200	0.87	58.815	58.639	7.650	7.654
Fe II	5325.5522	55.800	1.04	58.049	57.875	7.712	7.716
Fe II	5414.0698	33.400	0.82	41.449	41.284	7.560	7.563
Fe II	5425.2485	49.600	0.87	56.620	56.451	7.590	7.594
Fe II	5525.1172	22.500	1.26	25.104	25.004	7.692	7.694
Fe II	5534.8379	69.500	2.20	69.725	69.516	7.764	7.770
Fe II	6084.1016	30.700	0.83	30.934	30.811	7.764	7.767
Fe II	6113.3193	15.800	0.89	18.241	18.150	7.682	7.685
Fe II	6149.2461	47.100	1.05	46.686	46.500	7.781	7.785
Fe II	6238.3857	53.400	0.82	56.740	56.570	7.687	7.691
Fe II	6239.9429	18.800	0.66	19.729	19.650	7.738	7.741
Fe II	6247.5571	62.300	0.65	63.704	63.513	7.736	7.741
Fe II	6369.4590	24.300	0.71	33.478	33.311	7.524	7.527
Fe II	6456.3794	73.400	0.82	74.987	74.763	7.734	7.739
Fe II	6516.0767	65.800	1.46	67.274	67.006	7.735	7.741

μ Ara

		EW_{obs} (mÅ)		EW_{calc} (mÅ)		ε_{Fe} (dex)	
el	λ (air)	EW	σEW	nLTE	LTE	nLTE	LTE
Fe I	4787.8267	59.100	0.85	51.888	53.603	7.973	7.931
Fe I	4788.7568	82.200	1.46	77.713	79.461	7.906	7.865
Fe I	4793.9614	15.600	0.28	15.973	16.974	7.787	7.752
Fe I	4794.3540	22.100	0.27	18.165	19.407	7.918	7.879
Fe I	4799.4058	49.600	1.09	45.998	47.716	7.884	7.843
Fe I	4802.8799	73.800	1.86	72.067	73.764	7.841	7.801
Fe I	4808.1479	40.300	0.90	36.901	38.519	7.880	7.841
Fe I	4809.9385	28.500	1.34	27.146	28.485	7.835	7.800
Fe I	4869.4634	33.600	1.59	31.599	33.053	7.851	7.814
Fe I	4875.8770	69.400	2.10	71.749	73.363	7.749	7.714
Fe I	4882.1431	86.800	1.73	91.030	92.510	7.722	7.694
Fe I	4885.4302	85.300	1.66	90.358	91.827	7.702	7.672
Fe I	4892.8589	66.500	1.14	62.595	64.598	7.881	7.839
Fe I	4905.1328	47.400	0.57	52.350	54.081	7.688	7.651
Fe I	4907.7319	76.000	1.52	77.997	79.508	7.759	7.727
Fe I	4917.2300	79.800	1.07	74.235	76.373	7.911	7.868
Fe I	4918.0127	68.600	1.34	63.642	65.678	7.903	7.860
Fe I	4950.1055	91.800	1.88	91.078	92.653	7.813	7.784
Fe I	4962.5718	67.300	1.20	69.801	71.812	7.749	7.708
Fe I	4986.2227	59.600	1.30	62.633	64.637	7.737	7.696
Fe I	4999.1123	47.700	1.12	45.330	47.072	7.855	7.814
Fe I	5002.7920	95.600	1.05	94.423	96.056	7.821	7.792
Fe I	5023.1860	48.200	1.58	49.082	50.915	7.781	7.742
Fe I	5023.4976	41.100	0.71	39.685	41.382	7.832	7.794
Fe I	5025.3027	24.000	1.12	26.119	27.436	7.744	7.712
Fe I	5028.1260	99.400	1.71	106.025	107.859	7.690	7.658
Fe I	5029.6177	62.300	1.68	63.548	65.379	7.770	7.727
Fe I	5031.9141	38.100	1.27	42.041	43.884	7.714	7.677
Fe I	5036.9214	33.100	1.20	33.129	34.799	7.799	7.760
Fe I	5054.6426	53.100	1.44	53.634	55.407	7.786	7.742
Fe I	5067.1494	81.600	1.31	79.179	81.126	7.847	7.809
Fe I	5088.1533	53.300	1.21	45.965	47.682	7.963	7.923
Fe I	5180.0557	60.800	0.66	58.392	60.825	7.850	7.799
Fe I	5197.9360	43.000	1.92	46.702	48.597	7.720	7.681
Fe I	5236.2021	46.900	0.53	52.417	54.318	7.676	7.636
Fe I	5243.7764	72.800	1.29	73.297	75.254	7.790	7.751
Fe I	5253.0210	26.100	1.05	24.493	26.140	7.843	7.799
Fe I	5267.2695	41.400	1.94	40.927	42.721	7.811	7.771
Fe I	5285.1274	40.600	0.54	35.313	36.977	7.918	7.879
Fe I	5288.5249	69.900	0.91	74.618	76.531	7.697	7.655
Fe I	5293.9590	40.800	1.06	41.739	43.523	7.778	7.738
Fe I	5294.5474	20.600	0.87	20.479	21.671	7.804	7.769
Fe I	5295.3120	38.300	1.39	39.395	41.165	7.776	7.737

μ Ara

		EW_{obs} (mÅ)		EW_{calc} (mÅ)		ε_{Fe} (dex)	
el	λ (air)	EW	σEW	nLTE	LTE	nLTE	LTE
Fe I	5320.0356	30.800	0.35	28.691	30.169	7.853	7.815
Fe I	5322.0405	76.900	0.90	72.664	75.222	7.909	7.842
Fe I	5326.1426	53.500	0.52	51.908	53.791	7.838	7.793
Fe I	5379.5737	73.000	1.36	73.793	75.763	7.783	7.739
Fe I	5401.2666	34.000	0.88	32.827	34.374	7.828	7.791
Fe I	5406.7749	47.000	0.74	40.074	41.787	7.951	7.912
Fe I	5409.1333	69.400	0.50	60.953	63.033	7.975	7.931
Fe I	5412.7837	30.100	0.60	32.940	34.565	7.733	7.697
Fe I	5417.0332	46.000	0.67	40.096	41.854	7.929	7.888
Fe I	5436.2949	52.400	0.43	48.202	50.054	7.890	7.850
Fe I	5441.3389	43.500	0.48	42.110	43.865	7.831	7.792
Fe I	5460.8726	13.600	0.64	16.466	17.573	7.694	7.659
Fe I	5466.9873	49.600	0.41	45.061	46.939	7.907	7.862
Fe I	5470.0928	36.800	0.34	32.820	34.439	7.891	7.853
Fe I	5472.7085	59.200	0.68	51.938	53.766	7.965	7.923
Fe I	5473.1626	27.600	0.77	28.556	29.996	7.776	7.741
Fe I	5473.9004	94.000	1.57	93.920	95.350	7.801	7.775
Fe I	5483.0986	58.000	0.79	59.576	61.419	7.765	7.725
Fe I	5487.1450	48.600	0.87	47.468	49.343	7.824	7.784
Fe I	5491.8315	18.500	0.57	16.165	17.124	7.878	7.845
Fe I	5494.4624	38.200	0.79	30.625	32.135	7.980	7.941
Fe I	5522.4463	54.300	0.76	54.150	55.940	7.803	7.763
Fe I	5539.2798	28.300	0.30	28.297	29.818	7.800	7.763
Fe I	5543.9355	74.300	0.56	73.592	75.402	7.815	7.777
Fe I	5546.5059	63.700	1.04	60.161	62.214	7.875	7.831
Fe I	5546.9907	40.500	0.79	37.411	39.051	7.871	7.833
Fe I	5549.9487	14.300	0.48	14.407	15.327	7.796	7.762
Fe I	5552.6919	10.600	0.43	10.699	11.517	7.795	7.757
Fe I	5554.8945	107.600	2.28	112.860	116.231	7.730	7.686
Fe I	5560.2114	63.800	0.57	64.099	66.150	7.794	7.753
Fe I	5577.0249	16.000	0.59	18.015	19.392	7.732	7.691
Fe I	5594.6553	79.900	2.28	84.174	86.957	7.726	7.679
Fe I	5600.2241	52.000	0.63	53.497	55.380	7.766	7.725
Fe I	5618.6323	63.000	0.55	63.290	65.180	7.794	7.751
Fe I	5619.5952	48.600	0.47	40.539	42.316	7.976	7.934
Fe I	5636.6958	28.800	0.54	30.617	32.228	7.755	7.717
Fe I	5641.4341	79.200	0.85	70.132	71.930	7.993	7.956
Fe I	5650.7056	49.300	0.32	45.171	48.467	7.887	7.816
Fe I	5651.4688	25.700	0.75	23.938	25.224	7.847	7.812
Fe I	5652.3174	36.300	0.52	33.872	35.431	7.857	7.820
Fe I	5655.1763	67.100	1.53	59.621	64.109	7.950	7.855
Fe I	5661.3447	33.800	0.32	37.059	38.724	7.724	7.687
Fe I	5679.0229	70.900	0.49	69.145	71.876	7.833	7.782
Fe I	5680.2402	16.700	0.15	13.853	14.706	7.904	7.871
Fe I	5691.4971	53.900	0.95	50.325	52.313	7.881	7.836
Fe I	5698.0200	23.800	0.47	27.819	29.345	7.695	7.659
Fe I	5701.5444	96.100	0.90	91.713	94.745	7.892	7.828
Fe I	5717.8325	76.600	1.67	73.519	75.482	7.864	7.824
Fe I	5731.7617	71.300	0.69	64.490	66.212	7.949	7.912
Fe I	5741.8477	46.000	0.37	42.172	43.883	7.887	7.848
Fe I	5742.9600	20.100	0.40	15.986	16.952	7.934	7.900
Fe I	5754.4023	25.900	1.02	27.020	28.532	7.771	7.733
Fe I	5759.2622	11.800	0.38	10.003	10.653	7.885	7.853
Fe I	5760.3438	33.800	0.74	36.010	37.786	7.748	7.709
Fe I	5838.3716	33.700	0.50	30.882	32.439	7.866	7.829
Fe I	5848.1265	58.700	0.66	56.434	58.724	7.849	7.799
Fe I	5849.6831	12.500	0.35	12.666	13.518	7.793	7.758
Fe I	5853.1484	15.200	0.49	11.196	12.303	7.962	7.912
Fe I	5855.0757	36.500	0.46	37.107	38.937	7.786	7.747
Fe I	5858.7778	24.800	0.49	23.045	24.335	7.848	7.812
Fe I	5861.1084	16.000	0.46	16.344	17.314	7.788	7.755
Fe I	5873.2124	30.600	0.31	27.167	28.567	7.883	7.848
Fe I	5880.0273	19.800	0.42	23.519	24.809	7.694	7.662
Fe I	5881.2798	25.400	0.31	25.657	27.036	7.793	7.758
Fe I	5883.8164	83.700	1.29	81.140	83.050	7.847	7.812
Fe I	5898.2153	23.100	0.34	21.574	22.878	7.843	7.806
Fe I	5902.4731	21.700	0.75	26.920	28.457	7.659	7.624
Fe I	5905.6714	73.200	1.25	76.534	79.310	7.740	7.689
Fe I	5909.9722	51.800	0.51	46.706	48.805	7.913	7.865
Fe I	5927.7886	58.400	1.08	59.874	62.434	7.771	7.721
Fe I	5934.6543	92.800	1.26	95.428	97.078	7.757	7.729
Fe I	5940.9912	32.900	0.74	28.988	30.514	7.896	7.857
Fe I	5952.7178	81.300	2.45	75.320	77.251	7.913	7.877
Fe I	5969.5620	7.200	0.29	6.331	6.749	7.862	7.831
Fe I	5976.7769	85.800	1.14	83.332	85.033	7.844	7.814
Fe I	5984.8149	100.400	1.54	108.225	112.034	7.693	7.643
Fe I	5987.0649	85.900	0.81	86.722	90.713	7.787	7.724
Fe I	6003.0112	99.900	1.49	96.344	97.911	7.857	7.832

μ Ara

		EW_{obs} (mÅ)		EW_{calc} (mÅ)		ε_{Fe} (dex)	
el	λ (air)	EW	σEW	nLTE	LTE	nLTE	LTE
Fe I	6007.9595	77.800	1.17	79.276	81.728	7.773	7.727
Fe I	6008.5557	103.800	1.75	105.138	106.631	7.780	7.757
Fe I	6027.0508	79.900	1.31	82.999	85.215	7.742	7.701
Fe I	6034.0352	13.100	0.43	15.735	16.686	7.701	7.670
Fe I	6056.0044	90.800	1.37	98.038	101.489	7.691	7.640
Fe I	6078.4912	94.200	1.41	94.757	98.500	7.792	7.736
Fe I	6079.0078	62.100	0.76	58.673	60.864	7.868	7.824
Fe I	6082.7100	51.600	0.98	44.583	47.078	7.963	7.902
Fe I	6093.6431	44.700	0.79	41.059	43.039	7.879	7.835
Fe I	6096.6641	53.200	0.74	49.327	51.169	7.881	7.842
Fe I	6098.2441	25.600	0.56	22.943	24.253	7.872	7.835
Fe I	6127.9063	65.000	0.93	62.843	65.055	7.845	7.799
Fe I	6151.6172	63.800	1.61	59.676	62.553	7.899	7.829
Fe I	6157.7280	77.900	1.03	78.810	81.080	7.783	7.739
Fe I	6165.3599	59.900	0.81	59.056	61.261	7.818	7.772
Fe I	6180.2026	75.600	0.84	67.310	70.042	7.998	7.928
Fe I	6187.3979	7.600	0.26	6.646	7.200	7.865	7.826
Fe I	6187.9893	64.600	0.65	62.361	64.290	7.846	7.806
Fe I	6199.5063	7.000	0.20	6.388	6.943	7.844	7.804
Fe I	6219.2803	106.300	1.75	99.114	103.244	7.943	7.859
Fe I	6226.7344	43.300	0.50	39.698	41.525	7.878	7.838
Fe I	6229.2261	55.600	0.55	52.677	55.101	7.868	7.811
Fe I	6232.6401	100.000	1.15	99.745	101.677	7.804	7.773
Fe I	6240.6460	64.500	1.03	60.329	63.172	7.903	7.831
Fe I	6265.1323	101.900	1.50	94.129	98.153	7.963	7.875
Fe I	6271.2778	37.000	0.79	36.629	38.597	7.808	7.765
Fe I	6290.5430	9.000	0.34	7.494	8.146	7.891	7.849
Fe I	6293.9243	22.200	0.29	19.109	20.307	7.891	7.854
Fe I	6297.7925	91.400	1.27	83.060	86.701	7.990	7.903
Fe I	6311.4995	44.500	0.47	38.181	40.360	7.943	7.891
Fe I	6315.8110	58.000	0.74	54.255	56.398	7.880	7.834
Fe I	6338.8760	58.000	0.83	55.076	57.611	7.859	7.808
Fe I	6380.7432	68.200	0.55	62.412	64.743	7.919	7.870
Fe I	6408.0176	109.800	2.26	116.307	118.318	7.709	7.680
Fe I	6469.1919	73.800	0.79	65.980	68.873	7.947	7.892
Fe I	6495.7412	60.400	2.31	60.238	63.076	7.803	7.750
Fe I	6496.4658	80.300	1.00	80.022	82.924	7.805	7.755
Fe I	6518.3657	73.700	1.15	71.406	74.381	7.852	7.785
Fe I	6533.9282	52.200	0.49	45.627	47.727	7.939	7.893
Fe I	6569.2139	95.600	2.61	94.942	97.677	7.810	7.769
Fe I	6574.2266	43.400	0.49	36.178	39.239	7.960	7.889
Fe I	6581.2090	32.300	0.57	28.901	31.346	7.881	7.822
Fe I	6591.3130	14.300	0.61	15.506	16.531	7.755	7.719
Fe I	6597.5591	57.000	0.46	55.343	57.709	7.833	7.786
Fe I	6608.0249	29.300	0.27	27.844	29.908	7.836	7.786
Fe I	6625.0215	26.300	0.19	21.507	23.712	7.928	7.866
Fe I	6627.5439	41.900	0.29	35.024	36.713	7.955	7.915
Fe I	6633.7485	82.600	0.81	75.809	78.154	7.924	7.881
Fe I	6667.7104	15.900	0.33	14.479	15.436	7.852	7.817
Fe I	6699.1411	14.600	0.19	14.574	15.537	7.801	7.766
Fe I	6703.5659	51.400	0.45	46.142	48.622	7.919	7.861
Fe I	6710.3179	28.600	0.52	25.674	27.967	7.874	7.815
Fe I	6713.7427	32.400	0.21	25.100	26.589	7.978	7.937
Fe I	6716.2363	26.000	0.53	20.470	21.753	7.954	7.915
Fe I	6746.9536	8.300	0.26	7.942	8.642	7.822	7.780
Fe I	6752.7065	48.800	0.88	49.252	51.251	7.790	7.747
Fe I	6786.8584	39.900	0.56	34.442	36.141	7.918	7.880
Fe I	6804.2710	24.400	0.41	24.317	25.787	7.802	7.763
Fe I	6810.2622	64.200	0.71	63.218	65.579	7.819	7.773
Fe II	4893.8125	28.200	0.88	22.745	22.654	7.954	7.957
Fe II	4993.3501	45.800	1.92	53.455	53.295	7.607	7.610
Fe II	5000.7305	15.700	0.41	15.264	15.203	7.816	7.819
Fe II	5100.6548	29.500	0.73	32.967	32.836	7.708	7.711
Fe II	5132.6611	33.100	0.75	37.084	36.936	7.697	7.701
Fe II	5256.9321	27.800	0.83	30.620	30.498	7.724	7.727
Fe II	5264.8022	58.500	0.55	60.306	60.126	7.754	7.759
Fe II	5284.1030	76.100	2.37	70.831	70.619	7.931	7.936
Fe II	5325.5522	56.500	0.57	59.512	59.334	7.724	7.729
Fe II	5414.0698	38.500	0.47	42.454	42.327	7.700	7.703
Fe II	5425.2485	52.100	0.60	58.032	57.858	7.653	7.656
Fe II	5534.8379	70.700	2.08	71.425	71.211	7.782	7.788
Fe II	6084.1016	31.300	0.30	31.600	31.474	7.792	7.795
Fe II	6149.2461	47.800	0.69	47.535	47.393	7.807	7.810
Fe II	6238.3857	58.800	0.74	57.812	57.639	7.824	7.828
Fe II	6247.5571	68.500	1.50	64.932	64.738	7.883	7.889
Fe II	6369.4590	27.300	0.37	34.228	34.058	7.621	7.625
Fe II	6456.3794	74.900	0.81	76.396	76.092	7.767	7.774
Fe II	6516.0767	71.900	0.89	68.949	68.674	7.868	7.875

β Hyi

		EW_{obs} (mÅ)		EW_{calc} (mÅ)		ε_{Fe} (dex)	
el	λ (air)	EW	σEW	nLTE	LTE	nLTE	LTE
Fe I	4779.4390	41.600	1.10	41.387	44.550	7.415	7.342
Fe I	4787.8267	37.100	0.29	33.393	36.297	7.498	7.429
Fe I	4788.7568	66.600	0.95	59.486	62.683	7.588	7.507
Fe I	4789.6509	86.200	1.18	87.506	91.152	7.385	7.313
Fe I	4793.9614	6.700	0.25	7.178	8.120	7.376	7.316
Fe I	4794.3540	9.600	0.36	8.269	9.418	7.485	7.420
Fe I	4799.4058	29.000	0.64	27.852	30.506	7.439	7.373
Fe I	4802.8799	57.000	1.28	53.743	57.052	7.490	7.409
Fe I	4808.1479	21.200	0.59	20.436	22.631	7.433	7.369
Fe I	4809.9385	14.000	0.57	13.554	15.127	7.428	7.368
Fe I	4875.8770	50.400	1.54	51.757	54.944	7.379	7.309
Fe I	4882.1431	67.100	1.13	68.031	71.162	7.390	7.322
Fe I	4885.4302	68.000	1.06	68.580	71.887	7.397	7.321
Fe I	4892.8589	46.700	0.75	41.658	45.231	7.521	7.442
Fe I	4896.4385	31.600	0.64	28.320	30.951	7.493	7.426
Fe I	4907.7319	57.200	0.82	57.043	60.235	7.413	7.343
Fe I	4917.2300	60.600	0.74	52.429	56.315	7.590	7.503
Fe I	4918.0127	49.400	0.60	42.548	46.148	7.560	7.480
Fe I	4962.5718	48.900	0.51	48.491	52.141	7.419	7.340
Fe I	4966.0884	110.800	1.96	116.250	119.599	7.336	7.290
Fe I	4969.9175	72.600	1.39	69.513	73.950	7.472	7.383
Fe I	4985.2529	91.800	1.14	93.091	96.869	7.387	7.316
Fe I	4986.2227	41.300	0.42	41.779	45.264	7.399	7.325
Fe I	4993.6797	43.600	0.40	38.394	41.642	7.527	7.453
Fe I	4999.1123	25.500	0.48	27.180	29.901	7.365	7.299
Fe I	5002.7920	73.800	0.79	70.504	73.749	7.480	7.411
Fe I	5022.2354	92.400	0.43	95.142	99.106	7.362	7.289
Fe I	5023.4976	20.700	0.96	21.952	24.337	7.373	7.309
Fe I	5028.1260	79.900	1.15	80.418	83.944	7.399	7.325
Fe I	5029.6177	42.700	1.89	44.993	48.328	7.356	7.281
Fe I	5044.2109	66.800	0.19	65.400	68.770	7.443	7.364
Fe I	5048.4355	67.600	3.46	63.906	67.411	7.495	7.414
Fe I	5067.1494	64.100	0.26	56.620	60.427	7.572	7.489
Fe I	5074.7480	103.900	0.15	99.862	104.897	7.468	7.396
Fe I	5088.1533	29.600	0.94	27.237	29.898	7.470	7.403
Fe I	5090.7729	84.100	0.15	83.534	88.116	7.420	7.339
Fe I	5104.4375	27.600	0.79	26.041	28.743	7.450	7.382
Fe I	5129.6309	37.600	0.81	36.858	40.063	7.427	7.357
Fe I	5180.0557	40.000	0.25	37.030	40.827	7.477	7.392
Fe I	5198.7109	88.900	0.49	88.801	93.573	7.412	7.318
Fe I	5229.8447	106.100	0.31	104.765	108.565	7.431	7.372
Fe I	5242.4907	81.800	0.18	82.373	86.074	7.399	7.324
Fe I	5243.7764	54.800	1.09	51.419	55.230	7.484	7.401
Fe I	5253.4619	69.800	0.20	69.634	73.068	7.414	7.339
Fe I	5288.5249	51.200	0.42	54.422	58.019	7.336	7.257
Fe I	5293.9590	22.000	0.65	24.046	26.629	7.352	7.285
Fe I	5294.5474	8.400	0.43	9.478	10.710	7.350	7.288
Fe I	5295.3120	21.600	0.50	21.624	24.053	7.409	7.342
Fe I	5315.0698	26.600	0.29	24.521	27.125	7.465	7.397
Fe I	5320.0356	14.000	0.19	14.446	16.213	7.393	7.329
Fe I	5322.0405	56.300	0.21	55.215	58.927	7.437	7.346
Fe I	5326.1426	29.600	0.39	33.447	36.554	7.315	7.246
Fe I	5361.6250	37.900	0.21	31.960	35.237	7.548	7.469
Fe I	5379.5737	54.000	0.17	53.619	57.224	7.419	7.337
Fe I	5398.2793	64.400	0.44	64.193	68.951	7.414	7.320
Fe I	5400.5010	106.700	0.14	95.463	100.699	7.576	7.500
Fe I	5406.7749	28.600	0.71	22.145	24.578	7.579	7.511
Fe I	5436.2949	31.900	0.27	28.620	31.555	7.490	7.418
Fe I	5441.3389	24.000	0.25	23.809	26.367	7.415	7.348
Fe I	5452.0884	11.200	0.14	8.785	9.949	7.533	7.471
Fe I	5466.3960	70.500	0.15	67.958	72.296	7.460	7.375
Fe I	5466.9873	28.600	0.78	27.004	29.806	7.451	7.380
Fe I	5470.0928	18.300	0.25	16.880	18.924	7.457	7.390
Fe I	5472.7085	35.500	0.47	32.778	35.941	7.476	7.400
Fe I	5473.1626	13.000	0.49	14.239	15.963	7.361	7.298
Fe I	5473.9004	73.700	0.18	70.137	73.828	7.486	7.407
Fe I	5481.2432	54.000	0.89	48.986	52.844	7.522	7.435
Fe I	5483.0986	38.500	0.15	39.706	43.112	7.382	7.307
Fe I	5487.1450	29.200	0.44	27.952	30.886	7.441	7.370
Fe I	5494.4624	20.500	1.08	15.748	17.635	7.565	7.499
Fe I	5506.7788	113.600	0.19	107.149	112.551	7.551	7.432
Fe I	5522.4463	35.700	0.38	34.790	38.022	7.432	7.356
Fe I	5539.2798	12.600	0.19	14.114	15.876	7.349	7.285
Fe I	5543.9355	55.800	1.27	52.686	56.469	7.481	7.395
Fe I	5546.5059	44.400	0.24	39.290	42.846	7.525	7.444
Fe I	5546.9907	19.900	0.52	20.464	22.763	7.393	7.327

β Hyi

		EW_{obs} (mÅ)		EW_{calc} (mÅ)		ε_{Fe} (dex)	
el	λ (air)	EW	σEW	nLTE	LTE	nLTE	LTE
Fe I	5554.8945	80.300	0.89	79.395	85.463	7.426	7.321
Fe I	5560.2114	43.800	0.37	42.325	46.106	7.443	7.361
Fe I	5567.3911	58.500	0.11	52.425	56.130	7.559	7.467
Fe I	5594.6553	59.700	3.98	58.481	63.360	7.435	7.338
Fe I	5618.6323	44.000	0.24	43.376	46.995	7.424	7.342
Fe I	5619.5952	27.400	0.15	22.510	25.039	7.540	7.470
Fe I	5636.6958	14.300	0.35	15.620	17.551	7.361	7.296
Fe I	5638.2622	69.600	0.22	67.624	71.409	7.452	7.370
Fe I	5641.4341	56.100	0.82	49.390	53.165	7.562	7.476
Fe I	5650.7056	28.300	0.18	25.207	29.209	7.492	7.388
Fe I	5651.4688	12.200	0.28	11.364	12.812	7.447	7.384
Fe I	5652.3174	18.400	0.45	17.907	19.985	7.426	7.361
Fe I	5655.1763	44.800	0.97	36.727	42.508	7.598	7.457
Fe I	5679.0229	50.500	0.20	45.672	50.300	7.514	7.414
Fe I	5680.2402	6.500	0.32	6.012	6.832	7.448	7.386
Fe I	5691.4971	32.400	0.32	31.155	34.387	7.441	7.363
Fe I	5701.5444	75.900	0.25	71.292	75.441	7.521	7.421
Fe I	5717.8325	54.000	0.19	52.315	56.253	7.448	7.360
Fe I	5731.7617	50.800	0.17	44.198	47.730	7.560	7.479
Fe I	5741.8477	25.100	0.19	24.217	26.848	7.434	7.364
Fe I	5742.9600	9.500	0.34	7.101	8.051	7.554	7.492
Fe I	5760.3438	16.900	0.32	19.365	21.685	7.330	7.263
Fe I	5838.3716	15.700	0.40	15.515	17.413	7.417	7.352
Fe I	5848.1265	33.700	0.39	35.924	39.739	7.357	7.274
Fe I	5849.6831	6.400	0.29	5.463	6.243	7.486	7.422
Fe I	5855.0757	20.100	0.27	19.729	22.143	7.421	7.351
Fe I	5858.7778	11.600	0.44	10.920	12.339	7.442	7.377
Fe I	5859.5864	69.800	0.83	70.917	76.010	7.389	7.292
Fe I	5873.2124	15.300	0.55	13.101	14.737	7.494	7.430
Fe I	5881.2798	15.700	0.35	12.289	13.886	7.543	7.477
Fe I	5883.8164	60.900	0.77	57.007	60.905	7.490	7.410
Fe I	5905.6714	52.400	0.82	51.870	56.937	7.421	7.318
Fe I	5909.9722	30.300	0.41	27.624	30.591	7.476	7.403
Fe I	5929.6763	36.100	0.40	28.161	31.255	7.597	7.520
Fe I	5930.1797	83.800	0.89	76.990	82.874	7.529	7.426
Fe I	5934.6543	71.100	0.84	68.573	72.411	7.459	7.384
Fe I	5952.7178	56.500	0.64	51.954	55.805	7.505	7.424
Fe I	5976.7769	62.500	0.79	58.849	62.605	7.485	7.408
Fe I	5984.8149	76.400	1.19	74.937	81.542	7.436	7.321
Fe I	5987.0649	63.000	0.58	58.749	65.132	7.495	7.370
Fe I	6003.0112	77.400	0.93	69.421	73.152	7.564	7.493
Fe I	6007.9595	56.300	0.68	55.422	60.176	7.429	7.329
Fe I	6008.5557	81.300	0.94	76.029	79.779	7.507	7.439
Fe I	6024.0576	98.300	1.21	90.092	95.639	7.536	7.451
Fe I	6027.0508	63.000	0.69	59.065	63.307	7.493	7.404
Fe I	6054.0732	7.200	0.30	5.820	6.614	7.513	7.451
Fe I	6056.0044	67.100	0.73	67.851	73.912	7.396	7.285
Fe I	6065.4819	110.900	1.57	102.632	107.468	7.561	7.471
Fe I	6078.4912	70.600	0.66	64.870	71.207	7.519	7.399
Fe I	6079.0078	40.500	0.33	36.758	40.572	7.493	7.408
Fe I	6082.7100	29.000	0.41	26.039	29.192	7.486	7.405
Fe I	6093.6431	27.100	0.34	22.602	25.339	7.530	7.455
Fe I	6096.6641	32.300	0.31	29.143	32.131	7.486	7.414
Fe I	6098.2441	13.700	0.28	10.747	12.185	7.538	7.472
Fe I	6127.9063	44.100	0.61	41.292	45.128	7.472	7.388
Fe I	6136.6147	123.100	1.47	118.443	124.024	7.484	7.396
Fe I	6137.6914	120.500	1.50	112.063	117.221	7.547	7.463
Fe I	6151.6172	44.200	0.72	40.266	44.200	7.501	7.410
Fe I	6157.7280	58.900	0.57	55.568	59.815	7.481	7.391
Fe I	6165.3599	40.900	0.36	37.903	41.606	7.478	7.395
Fe I	6180.2026	51.700	0.44	47.948	51.892	7.498	7.406
Fe I	6187.9893	43.400	0.42	40.501	44.023	7.473	7.397
Fe I	6213.4292	79.100	1.02	74.421	79.340	7.520	7.405
Fe I	6226.7344	23.800	0.19	21.568	24.071	7.472	7.403
Fe I	6229.2261	32.800	0.24	33.404	36.829	7.395	7.317
Fe I	6230.7222	130.100	1.47	123.490	129.174	7.504	7.423
Fe I	6232.6401	78.000	0.53	72.898	76.897	7.510	7.432
Fe I	6240.6460	43.100	0.40	41.162	45.084	7.455	7.365
Fe I	6252.5547	111.400	1.36	102.514	108.137	7.581	7.471
Fe I	6270.2236	46.600	0.36	47.795	51.726	7.382	7.295
Fe I	6271.2778	20.100	0.30	19.470	21.876	7.429	7.359
Fe I	6311.4995	23.100	0.25	20.798	23.395	7.476	7.402
Fe I	6315.8110	37.300	0.36	33.777	37.240	7.492	7.411
Fe I	6318.0181	103.600	2.01	96.339	101.838	7.553	7.444
Fe I	6338.8760	36.800	0.36	33.383	37.383	7.489	7.397
Fe I	6364.3638	23.000	0.23	19.109	21.690	7.524	7.446
Fe I	6380.7432	46.800	0.41	40.678	44.652	7.545	7.456

β Hyi

		EW_{obs} (mÅ)		EW_{calc} (mÅ)		ε_{Fe} (dex)	
el	λ (air)	EW	σEW	nLTE	LTE	nLTE	LTE
Fe I	6408.0176	86.700	0.74	84.847	88.938	7.443	7.370
Fe I	6430.8452	105.000	1.01	99.645	105.893	7.514	7.393
Fe I	6436.4058	6.700	0.27	5.064	5.821	7.543	7.477
Fe I	6469.1919	49.600	1.20	42.329	47.137	7.566	7.460
Fe I	6494.9805	143.900	4.37	136.945	144.153	7.496	7.407
Fe I	6495.7412	35.300	0.78	37.382	41.814	7.363	7.272
Fe I	6496.4658	58.100	0.70	54.005	59.346	7.494	7.385
Fe I	6518.3657	52.500	0.46	51.223	55.376	7.439	7.346
Fe I	6533.9282	29.800	0.47	26.149	29.282	7.503	7.423
Fe I	6569.2139	75.500	2.23	65.555	70.947	7.595	7.494
Fe I	6581.2090	13.600	0.44	13.926	16.231	7.397	7.314
Fe I	6597.5591	35.900	0.40	33.481	37.284	7.466	7.380
Fe I	6608.0249	12.400	0.29	13.452	15.462	7.366	7.292
Fe I	6627.5439	24.300	0.41	18.385	20.681	7.583	7.511
Fe I	6633.7485	60.000	0.54	51.575	56.182	7.586	7.488
Fe I	6667.7104	6.900	0.28	6.260	7.187	7.457	7.390
Fe I	6699.1411	6.400	0.37	6.304	7.246	7.417	7.350
Fe I	6703.5659	31.200	0.32	27.096	30.275	7.512	7.432
Fe I	6710.3179	11.700	0.36	11.964	14.009	7.398	7.315
Fe I	6713.0459	23.500	0.89	20.189	22.710	7.506	7.432
Fe I	6713.7427	15.900	0.30	11.851	13.513	7.569	7.499
Fe I	6716.2363	11.200	0.44	9.358	10.707	7.503	7.433
Fe I	6752.7065	28.800	0.29	29.387	32.725	7.395	7.315
Fe I	6786.8584	22.200	0.55	17.533	19.722	7.550	7.481
Fe I	6810.2622	42.100	0.41	40.729	44.905	7.440	7.350
Fe II	4893.8125	20.600	0.24	17.198	17.129	7.520	7.522
Fe II	4993.3501	43.900	0.74	47.487	47.345	7.321	7.324
Fe II	5000.7305	11.800	0.30	11.035	10.991	7.446	7.448
Fe II	5132.6611	27.200	0.41	30.774	30.651	7.316	7.320
Fe II	5234.6226	92.900	0.19	95.269	95.079	7.359	7.363
Fe II	5325.5522	50.800	0.20	53.415	53.255	7.345	7.349
Fe II	5414.0698	32.400	0.50	36.130	36.022	7.316	7.319
Fe II	5425.2485	47.600	1.25	51.952	51.797	7.303	7.307
Fe II	5534.8379	67.300	0.21	65.034	64.839	7.466	7.471
Fe II	6084.1016	27.000	0.22	25.600	25.498	7.448	7.451
Fe II	6113.3193	15.100	0.35	13.944	13.875	7.455	7.458
Fe II	6149.2461	44.400	0.41	41.190	41.067	7.489	7.492
Fe II	6238.3857	51.900	0.32	51.420	51.266	7.422	7.425
Fe II	6239.9429	15.800	0.27	14.989	14.929	7.441	7.443
Fe II	6247.5571	63.800	0.74	58.349	58.174	7.540	7.545
Fe II	6416.9189	45.200	0.35	26.897	30.221	7.541	7.544
Fe II	6416.9189	45.200	0.35	39.812	39.693	7.541	7.544
Fe II	6456.3794	73.200	0.53	69.131	68.924	7.504	7.509
Fe II	6516.0767	68.500	1.36	62.793	62.605	7.544	7.549

β Vir

		EW_{obs} (mÅ)		EW_{calc} (mÅ)		ε_{Fe} (dex)	
el	λ (air)	EW	σEW	nLTE	LTE	nLTE	LTE
Fe I	4787.8267	34.600	1.16	40.589	43.226	7.560	7.509
Fe I	4788.7568	69.100	1.31	68.735	71.524	7.699	7.634
Fe I	4793.9614	8.700	0.29	9.465	10.447	7.648	7.599
Fe I	4799.4058	33.100	0.73	35.348	37.846	7.639	7.586
Fe I	4808.1479	21.800	0.82	26.140	28.290	7.576	7.526
Fe I	4869.4634	18.700	0.57	22.216	24.095	7.586	7.538
Fe I	4892.8589	50.900	1.02	51.648	54.828	7.675	7.611
Fe I	4896.4385	35.000	0.75	36.291	38.772	7.661	7.607
Fe I	4907.7319	61.500	0.89	66.632	69.264	7.583	7.527
Fe I	4917.2300	67.900	0.78	63.006	66.392	7.791	7.721
Fe I	4918.0127	55.700	0.64	52.638	55.820	7.753	7.688
Fe I	4939.6865	99.400	1.80	92.630	96.995	7.873	7.753
Fe I	4962.5718	54.400	0.72	58.846	62.008	7.599	7.537
Fe I	4969.9175	79.200	1.51	81.318	85.061	7.650	7.579
Fe I	4986.2227	47.200	0.60	51.791	54.922	7.596	7.536
Fe I	4993.6797	50.700	0.67	48.086	50.993	7.745	7.684
Fe I	4994.1294	102.400	1.84	102.422	106.912	7.689	7.579
Fe I	4999.1123	30.000	0.55	35.437	38.023	7.565	7.513
Fe I	5002.7920	80.800	1.98	80.854	83.527	7.689	7.635
Fe I	5023.1860	33.800	0.96	38.456	41.218	7.589	7.534
Fe I	5023.4976	26.300	0.43	29.481	31.837	7.613	7.561
Fe I	5036.9214	22.900	0.59	22.393	24.447	7.704	7.649
Fe I	5048.4355	72.500	3.03	74.875	77.752	7.639	7.575
Fe I	5056.8413	25.600	0.32	23.596	25.592	7.742	7.690
Fe I	5067.1494	70.900	0.95	67.586	70.845	7.757	7.691
Fe I	5074.7480	113.800	1.77	114.582	118.492	7.680	7.626
Fe I	5079.2227	103.500	0.97	98.428	102.316	7.797	7.715
Fe I	5083.3384	108.600	1.32	106.939	111.395	7.730	7.624

β Vir

		EW_{obs} (mÅ)		EW_{calc} (mÅ)		ε_{Fe} (dex)	
el	λ (air)	EW	σEW	nLTE	LTE	nLTE	LTE
Fe I	5088.1533	34.800	0.27	35.508	38.017	7.674	7.621
Fe I	5090.7729	90.000	1.18	96.796	100.411	7.579	7.516
Fe I	5104.4375	33.100	0.43	34.331	36.915	7.662	7.607
Fe I	5107.6406	109.700	4.28	108.846	113.028	7.709	7.615
Fe I	5127.3594	93.100	1.75	93.342	97.843	7.684	7.569
Fe I	5129.6309	39.600	0.71	46.061	48.949	7.559	7.506
Fe I	5151.9106	93.100	1.53	89.739	94.165	7.777	7.663
Fe I	5159.0576	69.600	0.76	73.111	76.959	7.622	7.549
Fe I	5180.0557	45.000	0.45	47.077	50.620	7.647	7.579
Fe I	5197.9360	32.300	0.88	36.085	38.801	7.606	7.551
Fe I	5216.2739	121.200	3.81	122.077	126.505	7.673	7.586
Fe I	5225.5259	66.100	1.11	65.170	69.850	7.713	7.602
Fe I	5228.3760	62.000	0.65	51.945	55.026	7.897	7.832
Fe I	5229.8447	111.800	1.32	117.220	120.226	7.610	7.564
Fe I	5243.7764	60.300	0.91	62.223	65.429	7.651	7.586
Fe I	5247.0503	57.400	0.95	59.285	63.954	7.647	7.547
Fe I	5250.6455	99.700	1.66	96.429	100.657	7.756	7.671
Fe I	5267.2695	25.000	1.13	30.684	33.172	7.553	7.502
Fe I	5285.1274	29.600	0.65	25.593	27.818	7.788	7.732
Fe I	5293.9590	26.100	0.52	31.763	34.264	7.554	7.503
Fe I	5295.3120	26.100	0.64	29.258	31.699	7.613	7.559
Fe I	5307.3608	89.700	1.28	84.326	88.392	7.828	7.722
Fe I	5320.0356	16.200	0.18	19.343	21.140	7.590	7.539
Fe I	5361.6250	43.500	1.45	41.380	44.447	7.735	7.671
Fe I	5379.5737	59.600	0.69	63.610	66.747	7.604	7.538
Fe I	5397.6177	20.200	0.72	20.102	21.969	7.693	7.640
Fe I	5398.2793	71.500	0.50	76.426	80.364	7.598	7.524
Fe I	5401.2666	22.000	0.48	23.428	25.465	7.651	7.599
Fe I	5406.7749	32.900	0.47	29.861	32.247	7.760	7.705
Fe I	5409.1333	54.500	0.33	50.012	53.261	7.782	7.715
Fe I	5417.0332	31.100	0.45	29.868	32.325	7.719	7.662
Fe I	5436.2949	37.100	0.22	37.546	40.329	7.680	7.622
Fe I	5441.3389	27.300	0.31	31.770	34.272	7.585	7.533
Fe I	5452.0884	11.600	0.35	12.025	13.258	7.671	7.620
Fe I	5466.3960	77.800	0.58	80.513	84.043	7.641	7.575
Fe I	5466.9873	33.200	0.34	34.392	37.060	7.663	7.605
Fe I	5470.0928	23.600	0.19	23.434	25.527	7.694	7.641
Fe I	5472.7085	41.100	0.40	41.961	44.830	7.671	7.611
Fe I	5473.1626	16.500	0.44	19.718	21.503	7.589	7.539
Fe I	5473.9004	80.300	1.02	82.323	85.132	7.650	7.591
Fe I	5483.0986	44.300	0.40	49.587	52.584	7.579	7.520
Fe I	5487.1450	34.400	0.82	36.830	39.602	7.637	7.580
Fe I	5494.4624	24.500	0.74	21.493	23.438	7.772	7.718
Fe I	5501.4648	105.600	1.37	105.942	110.818	7.682	7.568
Fe I	5522.4463	41.300	0.17	44.214	47.136	7.627	7.567
Fe I	5543.1470	64.600	1.42	59.446	62.641	7.809	7.735
Fe I	5543.9355	61.800	0.37	63.662	66.872	7.651	7.584
Fe I	5546.5059	48.200	0.53	49.446	52.658	7.664	7.600
Fe I	5560.2114	48.300	0.62	52.954	56.274	7.596	7.533
Fe I	5567.3911	62.900	1.46	60.816	64.288	7.737	7.659
Fe I	5577.0249	12.200	0.27	12.067	13.620	7.696	7.632
Fe I	5587.5742	33.500	0.95	33.407	36.077	7.692	7.634
Fe I	5618.6323	51.200	0.51	53.618	56.739	7.639	7.574
Fe I	5619.5952	32.700	0.52	30.319	32.813	7.745	7.687
Fe I	5635.8223	28.100	1.05	23.178	25.221	7.815	7.761
Fe I	5641.4341	62.700	2.95	60.242	63.413	7.742	7.675
Fe I	5650.7056	32.700	0.48	34.668	38.909	7.645	7.561
Fe I	5653.8652	29.600	0.77	28.772	31.172	7.710	7.654
Fe I	5655.1763	47.500	0.51	47.886	53.744	7.682	7.572
Fe I	5701.5444	76.700	0.59	81.054	84.962	7.594	7.511
Fe I	5717.8325	62.500	1.14	63.439	66.778	7.670	7.601
Fe I	5838.3716	20.000	0.41	21.077	23.010	7.659	7.607
Fe I	5855.0757	23.700	0.30	27.242	29.708	7.600	7.545
Fe I	5858.7778	14.700	0.58	15.385	16.888	7.665	7.614
Fe I	5859.5864	78.300	0.92	84.264	88.420	7.586	7.510
Fe I	5861.1084	11.200	0.49	10.466	11.526	7.725	7.675
Fe I	5873.2124	17.600	0.40	18.334	20.037	7.667	7.616
Fe I	5879.4868	9.100	0.22	8.082	8.930	7.749	7.699
Fe I	5881.2798	17.300	0.28	17.634	19.336	7.679	7.627
Fe I	5883.8164	65.600	0.97	68.029	71.309	7.643	7.581
Fe I	5898.2153	13.000	0.18	14.528	16.071	7.631	7.577
Fe I	5905.6714	60.000	0.76	63.792	68.227	7.617	7.535
Fe I	5909.9722	32.700	0.27	34.614	37.461	7.647	7.588
Fe I	5916.2471	52.000	0.62	48.521	52.005	7.765	7.690
Fe I	5929.6763	40.300	0.65	37.333	40.273	7.753	7.691
Fe I	5930.1797	90.300	0.98	91.208	96.008	7.675	7.597
Fe I	5934.6543	75.700	0.85	80.465	83.470	7.604	7.547
Fe I	5940.9912	22.700	0.30	20.120	22.013	7.764	7.709

β Vir

		EW_{obs} (mÅ)		EW_{calc} (mÅ)		ε_{Fe} (dex)	
el	λ (air)	EW	σEW	nLTE	LTE	nLTE	LTE
Fe I	5952.7178	64.800	1.76	62.682	65.981	7.731	7.667
Fe I	5956.6938	42.700	0.70	43.479	47.832	7.674	7.587
Fe I	5976.7769	65.600	0.75	70.060	73.132	7.605	7.546
Fe I	5987.0649	69.800	0.94	71.561	77.363	7.658	7.557
Fe I	6003.0112	82.400	0.90	81.331	84.194	7.709	7.657
Fe I	6005.5415	17.800	0.29	16.990	18.878	7.716	7.657
Fe I	6007.9595	64.100	1.00	67.693	71.785	7.620	7.541
Fe I	6008.5557	86.900	1.11	88.450	91.280	7.663	7.613
Fe I	6024.0576	108.000	1.57	105.709	110.114	7.722	7.660
Fe I	6027.0508	68.500	0.80	70.511	74.144	7.651	7.581
Fe I	6056.0044	76.400	0.82	81.401	86.689	7.603	7.514
Fe I	6065.4819	113.700	1.47	114.732	119.017	7.672	7.597
Fe I	6078.4912	79.300	0.85	78.307	83.930	7.707	7.611
Fe I	6079.0078	47.800	0.60	47.380	50.782	7.698	7.631
Fe I	6082.7100	29.600	0.33	31.349	34.374	7.649	7.584
Fe I	6093.6431	30.800	0.37	30.818	33.534	7.690	7.629
Fe I	6096.6641	35.200	0.46	37.631	40.420	7.638	7.582
Fe I	6098.2441	15.300	0.33	15.495	17.046	7.683	7.630
Fe I	6127.9063	49.000	0.71	51.441	54.900	7.640	7.573
Fe I	6136.6147	127.700	1.43	130.969	135.719	7.639	7.565
Fe I	6136.9937	65.900	1.39	62.960	67.050	7.754	7.666
Fe I	6137.6914	126.200	2.35	124.695	129.218	7.714	7.643
Fe I	6151.6172	43.000	0.92	47.191	50.962	7.602	7.531
Fe I	6157.7280	62.900	0.62	66.772	70.435	7.614	7.542
Fe I	6165.3599	44.400	0.45	47.720	51.092	7.622	7.557
Fe I	6173.3345	66.000	0.63	64.734	68.866	7.718	7.628
Fe I	6180.2026	54.300	0.69	56.352	60.077	7.646	7.571
Fe I	6187.9893	45.100	0.43	50.311	53.409	7.586	7.529
Fe I	6200.3125	72.400	0.72	68.972	72.909	7.767	7.679
Fe I	6213.4292	81.200	0.95	84.258	88.974	7.624	7.528
Fe I	6219.2803	88.100	1.04	87.320	92.110	7.707	7.606
Fe I	6226.7344	25.700	0.30	28.526	30.973	7.621	7.566
Fe I	6230.7222	133.000	1.48	136.803	141.618	7.637	7.570
Fe I	6232.6401	80.500	0.83	84.783	87.949	7.611	7.551
Fe I	6240.6460	42.500	0.52	48.246	51.989	7.569	7.500
Fe I	6252.5547	114.300	1.33	114.282	119.542	7.690	7.594
Fe I	6265.1323	84.800	0.98	82.799	87.525	7.734	7.632
Fe I	6271.2778	20.900	0.43	25.209	27.611	7.575	7.520
Fe I	6293.9243	13.500	0.27	12.745	14.130	7.721	7.666
Fe I	6301.5000	115.000	3.35	120.189	123.144	7.619	7.577
Fe I	6311.4995	24.600	0.44	26.121	28.704	7.651	7.590
Fe I	6315.8110	40.800	0.56	43.033	46.272	7.643	7.579
Fe I	6318.0181	106.900	1.36	108.064	113.156	7.668	7.575
Fe I	6322.6851	73.200	0.58	70.492	74.516	7.750	7.662
Fe I	6338.8760	43.200	0.48	43.801	47.558	7.678	7.603
Fe I	6355.0283	68.800	0.69	63.512	67.351	7.806	7.721
Fe I	6364.3638	28.600	0.23	26.789	29.438	7.734	7.670
Fe I	6380.7432	51.900	0.32	50.898	54.495	7.710	7.639
Fe I	6400.3169	58.900	0.82	56.140	61.022	7.750	7.647
Fe I	6408.0176	91.500	0.68	97.849	100.979	7.584	7.529
Fe I	6421.3501	111.100	1.59	104.220	109.131	7.829	7.729
Fe I	6430.8452	107.500	1.17	111.293	117.151	7.619	7.514
Fe I	6436.4058	8.100	0.21	7.338	8.181	7.738	7.685
Fe I	6469.1919	55.300	0.41	53.864	58.231	7.718	7.634
Fe I	6475.6240	48.000	0.66	47.530	51.218	7.700	7.624
Fe I	6481.8696	59.100	0.52	58.688	62.835	7.699	7.613
Fe I	6496.4658	65.700	0.82	66.624	71.256	7.673	7.588
Fe I	6533.9282	34.900	0.35	35.049	38.055	7.687	7.623
Fe I	6569.2139	83.200	2.37	79.436	83.882	7.754	7.678
Fe I	6581.2090	14.000	0.28	16.456	18.700	7.603	7.534
Fe I	6593.8696	79.200	0.64	78.598	83.261	7.703	7.604
Fe I	6597.5591	42.300	0.33	44.009	47.577	7.655	7.586
Fe I	6608.0249	13.200	0.19	16.682	18.702	7.565	7.504
Fe I	6609.1099	62.300	0.47	60.027	64.063	7.740	7.653
Fe I	6625.0215	9.700	0.27	10.995	12.726	7.627	7.554
Fe I	6627.5439	27.100	0.20	25.544	27.856	7.729	7.672
Fe I	6633.7485	66.900	0.60	63.710	67.633	7.751	7.676
Fe I	6667.7104	8.500	0.16	9.277	10.319	7.647	7.593
Fe I	6699.1411	8.500	0.19	9.345	10.406	7.643	7.589
Fe I	6703.5659	30.900	0.25	33.387	36.528	7.634	7.568
Fe I	6710.3179	12.000	0.27	14.172	16.178	7.603	7.535
Fe I	6713.0459	28.100	0.90	27.878	30.368	7.695	7.636
Fe I	6713.7427	20.400	0.17	17.262	19.074	7.787	7.729
Fe I	6716.2363	14.700	0.23	13.625	15.105	7.731	7.675
Fe I	6750.1514	71.300	0.37	69.883	74.265	7.721	7.627
Fe I	6752.7065	34.600	0.42	38.983	42.098	7.594	7.532
Fe I	6786.8584	23.300	0.43	24.024	26.227	7.671	7.616
Fe II	4893.8125	27.400	0.39	24.794	24.720	7.758	7.760

β Vir

		EW_{obs} (mÅ)		EW_{calc} (mÅ)		ε_{Fe} (dex)	
el	λ (air)	EW	σEW	nLTE	LTE	nLTE	LTE
Fe II	4993.3501	54.300	1.12	59.041	58.923	7.579	7.582
Fe II	5000.7305	18.000	0.32	16.503	16.454	7.740	7.742
Fe II	5100.6548	35.800	0.75	36.411	36.338	7.676	7.677
Fe II	5132.6611	34.900	0.43	41.064	40.982	7.550	7.551
Fe II	5234.6226	107.100	1.27	111.295	111.184	7.609	7.611
Fe II	5256.9321	29.900	0.58	33.917	33.849	7.594	7.595
Fe II	5264.8022	65.700	0.77	66.827	66.694	7.663	7.666
Fe II	5284.1030	82.400	2.56	77.581	77.426	7.805	7.809
Fe II	5325.5522	63.600	0.58	66.025	65.893	7.633	7.636
Fe II	5414.0698	42.900	0.29	47.586	47.491	7.584	7.586
Fe II	5425.2485	60.000	0.34	64.509	64.380	7.586	7.589
Fe II	5427.8159	8.500	0.32	11.065	11.054	7.546	7.546
Fe II	5525.1172	22.200	0.47	28.800	28.714	7.517	7.519
Fe II	5534.8379	80.900	1.39	78.569	78.412	7.744	7.748
Fe II	5627.4888	19.700	0.81	20.029	19.969	7.680	7.682
Fe II	6084.1016	37.200	0.39	35.691	35.584	7.725	7.727
Fe II	6113.3193	22.500	0.49	20.952	20.889	7.735	7.737
Fe II	6149.2461	56.800	0.55	54.132	54.024	7.750	7.753
Fe II	6238.3857	65.000	0.51	65.246	65.116	7.685	7.687
Fe II	6239.9429	23.700	0.25	23.044	22.975	7.709	7.711
Fe II	6247.5571	79.200	1.08	72.728	72.583	7.833	7.837
Fe II	6369.4590	31.700	0.28	38.484	38.369	7.536	7.538
Fe II	6383.7222	15.900	0.19	13.983	13.955	7.766	7.767
Fe II	6416.9189	56.900	0.36	36.237	39.474	7.783	7.786
Fe II	6416.9189	56.900	0.36	52.707	52.602	7.783	7.786
Fe II	6456.3794	87.700	0.99	84.591	84.422	7.756	7.760
Fe II	6516.0767	78.100	1.37	76.303	76.151	7.729	7.733

η Boo

		EW_{obs} (mÅ)		EW_{calc} (mÅ)		ε_{Fe} (dex)	
el	λ (air)	EW	σEW	nLTE	LTE	nLTE	LTE
Fe I	4787.8267	47.100	1.00	45.070	47.896	7.812	7.754
Fe I	4788.7568	78.800	3.22	74.494	77.276	7.868	7.805
Fe I	4799.4058	36.700	1.09	39.488	42.188	7.710	7.655
Fe I	4869.4634	26.400	1.20	25.306	27.417	7.798	7.745
Fe I	4872.9072	7.200	0.53	6.626	7.281	7.810	7.765
Fe I	4875.8770	65.600	3.39	65.985	68.663	7.762	7.706
Fe I	4892.8589	58.600	2.01	56.378	59.596	7.815	7.750
Fe I	4896.4385	48.400	0.81	40.666	43.308	7.929	7.875
Fe I	4903.3101	154.200	2.66	146.807	147.842	7.862	7.849
Fe I	4938.8140	139.600	2.70	133.346	134.693	7.861	7.841
Fe I	4962.5718	67.400	0.78	63.815	66.962	7.843	7.779
Fe I	4969.9175	94.400	1.31	85.777	89.258	7.933	7.870
Fe I	5014.9424	129.800	1.46	127.101	129.168	7.810	7.780
Fe I	5022.2354	121.300	1.52	112.906	115.093	7.910	7.879
Fe I	5029.6177	67.300	1.46	59.187	62.237	7.942	7.878
Fe I	5036.9214	27.400	0.73	25.394	27.692	7.819	7.763
Fe I	5049.8198	154.200	1.78	145.762	149.807	7.880	7.827
Fe I	5056.8413	35.900	0.85	26.767	28.969	7.972	7.921
Fe I	5068.7656	143.000	1.34	133.666	134.880	7.903	7.886
Fe I	5072.6719	86.900	5.48	79.589	82.476	7.913	7.859
Fe I	5090.7729	105.800	1.13	100.685	103.585	7.854	7.808
Fe I	5127.3594	109.500	1.57	101.061	105.712	7.986	7.865
Fe I	5133.6880	161.600	1.82	174.234	176.887	7.656	7.630
Fe I	5159.0576	83.300	0.86	78.011	81.601	7.871	7.803
Fe I	5180.0557	51.900	1.01	51.455	55.150	7.779	7.706
Fe I	5187.9141	66.500	0.86	55.452	58.617	7.996	7.932
Fe I	5198.7109	100.800	2.78	106.581	111.022	7.662	7.581
Fe I	5217.3892	113.400	2.70	117.678	119.228	7.699	7.670
Fe I	5229.8447	132.900	1.35	120.556	122.641	7.957	7.928
Fe I	5236.2021	45.700	0.73	47.244	50.313	7.738	7.676
Fe I	5242.4907	98.200	1.24	99.474	102.129	7.746	7.692
Fe I	5243.7764	73.100	1.22	67.386	70.414	7.884	7.825
Fe I	5253.4619	83.500	1.23	85.644	88.202	7.727	7.673
Fe I	5263.3062	135.500	4.90	128.378	130.201	7.871	7.847
Fe I	5267.2695	33.700	1.17	34.463	37.137	7.753	7.696
Fe I	5281.7896	152.800	1.10	148.320	149.215	7.824	7.813
Fe I	5285.1274	38.500	1.55	28.941	31.389	7.976	7.921
Fe I	5288.5249	68.200	0.81	69.994	73.063	7.733	7.668
Fe I	5293.9590	33.400	0.99	35.776	38.510	7.718	7.660
Fe I	5295.3120	29.800	1.13	32.915	35.545	7.699	7.643
Fe I	5315.0698	44.800	0.74	36.656	39.373	7.936	7.879
Fe I	5322.0405	72.400	0.69	69.396	73.125	7.836	7.754
Fe I	5326.1426	49.300	0.63	46.423	49.491	7.829	7.766
Fe I	5339.9292	157.100	2.67	149.730	150.938	7.855	7.841
Fe I	5373.7085	72.900	0.89	75.220	79.096	7.725	7.650

η Boo

		EW_{obs} (mÅ)		EW_{calc} (mÅ)		ε_{Fe} (dex)	
el	λ (air)	EW	σEW	nLTE	LTE	nLTE	LTE
Fe I	5379.5737	69.600	1.09	69.198	72.307	7.778	7.713
Fe I	5389.4790	99.900	1.43	95.057	98.301	7.852	7.798
Fe I	5393.1670	141.800	0.97	143.490	144.939	7.748	7.729
Fe I	5397.6177	26.100	1.60	22.895	24.995	7.852	7.798
Fe I	5398.2793	82.000	0.85	81.166	84.724	7.786	7.718
Fe I	5401.2666	25.900	0.77	26.609	28.860	7.752	7.699
Fe I	5406.7749	36.600	1.23	33.635	36.206	7.834	7.778
Fe I	5409.1333	66.500	0.83	54.869	58.124	7.998	7.934
Fe I	5410.9097	158.100	3.92	157.467	162.505	7.776	7.727
Fe I	5417.0332	36.400	1.30	33.614	36.261	7.830	7.773
Fe I	5434.5234	167.200	1.11	162.444	166.098	7.842	7.787
Fe I	5441.3389	32.900	0.91	35.711	38.358	7.709	7.654
Fe I	5445.0420	127.000	0.87	122.883	125.905	7.825	7.785
Fe I	5452.0884	14.600	0.86	13.817	15.234	7.799	7.747
Fe I	5461.5493	25.100	0.86	22.991	24.990	7.825	7.773
Fe I	5466.3960	91.800	0.64	85.664	88.587	7.880	7.830
Fe I	5466.9873	44.100	0.50	38.630	41.538	7.883	7.822
Fe I	5470.0928	27.500	0.57	26.616	28.899	7.791	7.737
Fe I	5472.7085	53.400	0.62	46.758	49.743	7.904	7.844
Fe I	5473.1626	28.800	0.81	22.526	24.511	7.925	7.873
Fe I	5487.1450	50.900	1.04	41.087	43.990	7.963	7.906
Fe I	5494.4624	34.000	1.24	24.506	26.666	7.988	7.935
Fe I	5506.7788	132.900	0.82	124.388	129.167	7.957	7.852
Fe I	5522.4463	49.900	0.89	49.167	52.139	7.785	7.725
Fe I	5525.5435	67.500	0.56	66.554	69.617	7.789	7.726
Fe I	5536.5801	9.800	0.53	9.854	10.986	7.767	7.712
Fe I	5539.2798	23.500	0.39	21.600	23.632	7.821	7.767
Fe I	5543.9355	77.000	0.60	69.504	72.400	7.920	7.866
Fe I	5546.5059	60.400	0.60	54.336	57.498	7.891	7.828
Fe I	5546.9907	29.800	0.59	31.283	33.746	7.736	7.681
Fe I	5554.8945	99.800	1.64	96.822	101.384	7.819	7.743
Fe I	5569.6182	152.500	0.79	152.610	153.841	7.769	7.755
Fe I	5576.0889	128.700	0.78	119.544	121.488	7.908	7.882
Fe I	5577.0249	19.300	0.74	13.918	15.727	7.951	7.884
Fe I	5584.7646	51.500	1.27	48.281	51.472	7.835	7.771
Fe I	5618.6323	62.500	0.90	59.095	62.205	7.839	7.776
Fe I	5622.9453	11.900	0.51	7.711	8.568	7.983	7.933
Fe I	5638.2622	91.700	0.78	86.216	88.336	7.875	7.839
Fe I	5650.7056	37.900	1.79	38.443	43.146	7.758	7.665
Fe I	5653.8652	37.400	2.27	32.473	35.068	7.876	7.819
Fe I	5662.5161	108.300	6.16	112.599	114.663	7.708	7.674
Fe I	5679.0229	67.000	0.54	61.567	65.707	7.876	7.795
Fe I	5680.2402	10.800	0.54	10.016	11.055	7.808	7.758
Fe I	5691.4971	50.300	0.69	44.999	48.127	7.878	7.814
Fe I	5717.8325	75.900	0.94	69.271	72.383	7.902	7.843
Fe I	5720.8862	27.900	1.24	26.323	28.612	7.808	7.753
Fe I	5731.7617	70.200	0.82	60.307	63.083	7.966	7.915
Fe I	5741.8477	37.200	0.56	36.301	38.950	7.789	7.733
Fe I	5742.9600	17.500	0.60	11.749	12.939	7.980	7.932
Fe I	5760.3438	29.400	0.76	28.860	31.404	7.783	7.724
Fe I	5848.1265	47.800	1.15	51.116	54.728	7.704	7.633
Fe I	5853.1484	7.100	0.85	6.305	7.239	7.827	7.761
Fe I	5855.0757	31.700	0.67	30.761	33.436	7.791	7.732
Fe I	5858.7778	22.600	0.95	17.683	19.368	7.913	7.861
Fe I	5859.5864	98.700	0.78	89.112	92.536	7.934	7.881
Fe I	5861.1084	17.700	1.08	12.112	13.310	7.971	7.923
Fe I	5862.3564	118.100	1.60	107.127	110.554	7.934	7.888
Fe I	5873.2124	25.900	0.59	20.941	22.787	7.899	7.849
Fe I	5879.4868	9.900	0.97	9.399	10.363	7.796	7.747
Fe I	5905.6714	65.900	1.10	68.628	72.854	7.719	7.638
Fe I	5909.9722	43.500	0.84	38.732	41.827	7.866	7.803
Fe I	5927.7886	48.400	1.29	53.069	56.941	7.679	7.607
Fe I	5929.6763	44.100	1.10	41.662	44.654	7.819	7.759
Fe I	5930.1797	104.000	1.15	95.389	99.364	7.909	7.848
Fe I	5934.6543	85.400	1.25	85.832	88.123	7.762	7.719
Fe I	5956.6938	56.300	0.67	48.298	53.016	7.925	7.832
Fe I	5976.7769	86.400	0.96	75.505	78.082	7.971	7.930
Fe I	5984.8149	101.100	1.04	93.090	97.989	7.901	7.822
Fe I	5987.0649	85.800	0.82	75.758	81.285	7.953	7.851
Fe I	6007.9595	84.000	0.69	73.419	77.121	7.967	7.903
Fe I	6015.2437	8.700	0.96	7.466	8.465	7.845	7.783
Fe I	6027.0508	84.300	0.72	76.051	79.385	7.927	7.865
Fe I	6056.0044	89.600	0.66	85.765	90.469	7.836	7.755
Fe I	6079.0078	59.100	0.67	52.197	55.588	7.901	7.838
Fe I	6082.7100	46.600	0.95	35.212	38.567	7.994	7.925
Fe I	6093.6431	43.800	0.58	34.665	37.557	7.957	7.895
Fe I	6096.6641	47.000	0.48	41.962	44.783	7.869	7.813
Fe I	6098.2441	22.800	0.82	17.816	19.535	7.914	7.861

η Boo

		EW_{obs} (mÅ)		EW_{calc} (mÅ)		ε_{Fe} (dex)	
el	λ (air)	EW	σEW	nLTE	LTE	nLTE	LTE
Fe I	6127.9063	64.200	0.50	56.473	59.950	7.920	7.853
Fe I	6151.6172	55.800	1.26	52.384	56.448	7.837	7.758
Fe I	6157.7280	82.300	1.47	72.310	75.797	7.961	7.897
Fe I	6165.3599	52.200	0.80	52.603	56.080	7.762	7.695
Fe I	6173.3345	81.600	0.56	71.073	75.449	7.995	7.898
Fe I	6180.2026	70.700	0.68	62.138	66.104	7.944	7.862
Fe I	6187.9893	57.700	0.67	55.318	58.352	7.816	7.757
Fe I	6213.4292	95.100	0.93	91.601	96.422	7.842	7.744
Fe I	6219.2803	105.900	0.88	94.783	99.667	7.999	7.895
Fe I	6226.7344	35.400	0.60	32.152	34.797	7.840	7.783
Fe I	6229.2261	45.900	0.61	45.358	48.930	7.781	7.711
Fe I	6232.6401	94.000	0.74	90.673	93.285	7.830	7.783
Fe I	6240.6460	56.100	1.04	53.538	57.568	7.821	7.741
Fe I	6246.3179	121.900	1.10	123.827	124.826	7.742	7.725
Fe I	6270.2236	70.600	0.99	62.230	66.062	7.940	7.861
Fe I	6271.2778	33.800	1.20	28.493	31.174	7.888	7.827
Fe I	6301.5000	135.000	3.29	124.301	125.938	7.918	7.900
Fe I	6335.3301	110.300	1.00	108.425	113.772	7.806	7.704
Fe I	6336.8232	116.500	0.68	113.502	115.230	7.816	7.790
Fe I	6380.7432	64.900	0.65	55.907	59.602	7.943	7.872
Fe I	6393.6006	145.100	0.87	138.820	143.706	7.865	7.791
Fe I	6411.6479	134.800	0.57	135.470	136.151	7.761	7.752
Fe I	6430.8452	124.700	0.62	118.971	124.577	7.874	7.772
Fe I	6469.1919	70.100	0.96	58.572	62.913	7.984	7.905
Fe I	6494.9805	173.000	3.62	155.444	160.749	7.985	7.922
Fe I	6495.7412	64.700	1.07	53.013	57.311	7.988	7.908
Fe I	6496.4658	81.500	1.47	71.626	75.955	7.947	7.872
Fe I	6518.3657	72.100	1.21	66.182	70.332	7.888	7.805
Fe I	6533.9282	45.900	1.09	39.304	42.445	7.902	7.838
Fe I	6574.2266	30.500	0.82	23.914	27.237	7.922	7.842
Fe I	6581.2090	18.800	0.76	18.625	21.165	7.775	7.703
Fe I	6592.9126	133.000	2.61	122.629	126.683	7.944	7.877
Fe I	6593.8696	94.800	0.70	85.690	90.486	7.960	7.858
Fe I	6597.5591	47.900	0.84	48.668	52.219	7.755	7.687
Fe I	6608.0249	17.500	0.71	18.946	21.240	7.725	7.661
Fe I	6609.1099	76.700	0.74	66.074	70.441	7.988	7.895
Fe I	6625.0215	17.500	0.61	12.453	14.413	7.948	7.873
Fe I	6703.5659	41.400	0.66	37.463	40.943	7.850	7.779
Fe I	6710.3179	16.600	0.93	16.062	18.336	7.788	7.715
Fe I	6713.0459	42.500	0.96	31.650	34.253	7.994	7.939
Fe I	6713.7427	25.800	0.59	19.792	21.797	7.930	7.873
Fe I	6716.2363	23.200	0.66	15.712	17.400	7.991	7.936
Fe I	6739.5205	12.100	0.73	13.323	15.244	7.720	7.650
Fe I	6750.1514	83.600	0.66	76.611	81.156	7.916	7.820
Fe I	6752.7065	42.700	0.72	43.685	46.822	7.750	7.687
Fe I	6786.8584	30.900	0.82	27.266	29.605	7.853	7.799
Fe I	6810.2622	58.200	0.71	57.165	60.749	7.789	7.722
Fe II	4893.8125	38.200	1.40	33.333	33.266	7.878	7.880
Fe II	5197.5674	140.100	4.63	128.236	128.108	7.979	7.981
Fe II	5234.6226	130.600	1.58	123.247	123.124	7.908	7.911
Fe II	5264.8022	86.000	4.38	78.474	78.396	7.944	7.946
Fe II	5414.0698	60.200	2.74	58.589	58.472	7.805	7.807
Fe II	5425.2485	70.900	0.90	76.206	76.130	7.651	7.653
Fe II	5525.1172	36.300	0.55	38.040	37.964	7.731	7.733
Fe II	6084.1016	52.100	0.61	45.931	45.839	7.898	7.900
Fe II	6149.2461	71.000	0.66	65.602	65.536	7.886	7.887
Fe II	6238.3857	83.200	0.71	77.261	77.184	7.897	7.899
Fe II	6239.9429	40.600	0.90	31.185	31.123	7.980	7.981
Fe II	6369.4590	42.300	0.59	49.146	49.048	7.629	7.631
Fe II	6383.7222	27.400	0.60	19.641	19.621	7.994	7.994
Fe II	6416.9189	72.300	0.63	40.571	44.003	7.941	7.944
Fe II	6416.9189	72.300	0.63	64.188	64.060	7.941	7.944
Fe II	6456.3794	107.800	1.28	97.360	97.263	7.983	7.985
Fe II	6516.0767	99.300	2.31	89.161	88.983	7.982	7.986

Procyon

		EW_{obs} (mÅ)		EW_{calc} (mÅ)		ε_{Fe} (dex)	
el	λ (air)	EW	σEW	nLTE	LTE	nLTE	LTE
Fe I	4799.4058	14.900	0.44	16.343	18.488	7.443	7.397
Fe I	4802.8799	44.700	0.41	42.303	46.283	7.475	7.445
Fe I	4882.1431	50.800	0.66	55.135	59.031	7.410	7.339
Fe I	4885.4302	57.800	0.70	59.828	63.987	7.436	7.366
Fe I	4892.8589	34.000	0.43	30.102	33.671	7.471	7.462
Fe I	4896.4385	17.700	0.52	17.568	19.806	7.461	7.435
Fe I	4905.1328	16.200	0.21	21.846	24.546	7.348	7.248
Fe I	4907.7319	39.200	0.36	43.013	46.804	7.422	7.358

Procyon

		EW_{obs} (mÅ)		EW_{calc} (mÅ)		ε_{Fe} (dex)	
el	λ (air)	EW	σEW	nLTE	LTE	nLTE	LTE
Fe I	4917.2300	46.100	0.37	41.283	45.566	7.482	7.464
Fe I	4918.0127	34.700	0.33	31.004	34.641	7.471	7.460
Fe I	4938.8140	100.300	1.46	100.089	102.132	7.463	7.430
Fe I	4962.5718	35.900	0.33	36.973	40.899	7.451	7.404
Fe I	4969.9175	61.900	0.72	59.063	64.199	7.487	7.432
Fe I	4979.5859	5.600	0.26	5.419	6.236	7.464	7.438
Fe I	4985.2529	83.400	1.18	83.454	87.754	7.459	7.384
Fe I	4985.5469	86.300	1.32	86.853	89.910	7.452	7.399
Fe I	4986.2227	28.300	1.16	30.239	33.787	7.443	7.391
Fe I	4993.6797	27.200	0.45	27.046	30.253	7.461	7.429
Fe I	4994.1294	86.900	1.22	82.157	86.572	7.534	7.466
Fe I	5001.8633	112.500	1.58	120.580	124.953	7.370	7.300
Fe I	5002.7920	55.000	0.45	57.455	61.449	7.433	7.370
Fe I	5014.9424	95.200	1.12	96.478	100.708	7.442	7.365
Fe I	5023.1860	17.600	0.31	19.517	22.103	7.438	7.385
Fe I	5028.1260	68.700	1.04	70.104	74.420	7.441	7.366
Fe I	5049.8198	111.600	1.34	108.907	112.857	7.501	7.439
Fe I	5056.8413	10.600	0.18	10.180	11.634	7.464	7.442
Fe I	5068.7656	100.000	1.05	99.974	102.014	7.460	7.428
Fe I	5088.1533	16.200	0.23	17.269	19.491	7.449	7.408
Fe I	5090.7729	72.500	0.68	71.977	77.146	7.466	7.392
Fe I	5127.3594	74.900	0.70	71.523	76.169	7.504	7.440
Fe I	5133.6880	120.200	1.96	124.939	129.470	7.409	7.345
Fe I	5151.9106	69.600	1.26	66.971	71.627	7.491	7.431
Fe I	5159.0576	52.300	0.46	50.853	55.882	7.472	7.419
Fe I	5180.0557	23.400	0.54	26.384	30.050	7.427	7.355
Fe I	5187.9141	32.700	0.29	29.397	32.883	7.472	7.459
Fe I	5194.9414	105.100	1.37	103.974	108.194	7.481	7.398
Fe I	5197.9360	19.500	0.75	17.806	20.234	7.466	7.454
Fe I	5198.7109	75.000	0.69	74.546	79.220	7.466	7.394
Fe I	5215.1802	95.000	1.29	95.372	98.627	7.455	7.402
Fe I	5216.2739	104.900	2.18	99.299	103.652	7.555	7.483
Fe I	5217.3892	83.900	0.75	86.289	89.511	7.426	7.365
Fe I	5225.5259	30.400	0.56	32.074	36.740	7.447	7.382
Fe I	5229.8447	94.900	0.92	88.294	92.165	7.537	7.499
Fe I	5235.3867	62.000	0.88	57.318	62.100	7.501	7.459
Fe I	5242.4907	71.200	0.67	71.575	76.063	7.455	7.383
Fe I	5243.7764	41.500	0.33	40.419	44.613	7.468	7.428
Fe I	5247.0503	23.000	0.25	25.706	29.821	7.433	7.355
Fe I	5263.3062	90.400	0.94	94.358	97.679	7.402	7.335
Fe I	5273.1636	86.200	0.91	86.308	89.811	7.459	7.402
Fe I	5281.7896	107.800	1.44	109.340	110.780	7.439	7.415
Fe I	5293.9590	14.200	0.51	14.867	16.952	7.453	7.413
Fe I	5295.3120	14.300	0.24	13.573	15.530	7.465	7.444
Fe I	5307.3608	67.300	1.44	61.613	66.251	7.513	7.473
Fe I	5315.0698	15.400	0.31	15.648	17.802	7.458	7.424
Fe I	5339.9292	105.500	1.95	109.663	112.015	7.404	7.360
Fe I	5373.7085	45.700	0.41	48.152	53.443	7.434	7.352
Fe I	5379.5737	39.200	0.31	41.038	45.246	7.443	7.384
Fe I	5389.4790	67.500	0.52	66.512	72.139	7.471	7.395
Fe I	5393.1670	100.600	1.39	105.530	108.125	7.390	7.338
Fe I	5398.2793	53.500	0.35	53.705	59.016	7.458	7.388
Fe I	5400.5010	90.200	1.19	81.749	87.526	7.544	7.494
Fe I	5406.7749	14.100	0.54	13.842	15.801	7.462	7.435
Fe I	5409.1333	33.000	0.36	28.799	32.358	7.472	7.464
Fe I	5417.0332	16.700	0.16	13.893	15.914	7.462	7.465
Fe I	5434.5234	127.100	1.58	124.681	128.009	7.502	7.443
Fe I	5436.2949	19.500	0.19	18.928	21.485	7.464	7.438
Fe I	5441.3389	13.000	0.22	14.974	17.035	7.428	7.370
Fe I	5445.0420	96.300	1.40	89.159	94.951	7.534	7.478
Fe I	5463.2754	92.900	1.32	92.448	98.349	7.465	7.380
Fe I	5466.3960	61.300	0.08	57.470	62.467	7.492	7.447
Fe I	5466.9873	17.800	0.77	15.486	17.678	7.466	7.461
Fe I	5470.0928	10.200	0.23	10.236	11.779	7.460	7.427
Fe I	5472.7085	22.800	0.15	22.193	25.134	7.464	7.435
Fe I	6003.0112	60.500	0.75	56.182	60.541	7.493	7.460
Fe I	6008.5557	62.100	0.95	62.625	66.979	7.454	7.394
Fe I	6027.0508	49.500	0.54	47.061	51.772	7.478	7.436
Fe I	6056.0044	57.300	0.54	57.008	63.696	7.463	7.372
Fe I	6079.0078	30.200	0.31	26.691	30.331	7.472	7.459
Fe I	6082.7100	10.800	0.32	11.179	12.984	7.454	7.412
Fe I	6093.6431	15.200	0.25	14.657	16.905	7.464	7.436
Fe I	6096.6641	16.600	0.37	17.826	20.234	7.446	7.400

Procyon

		EW_{obs} (mÅ)		EW_{calc} (mÅ)		ε_{Fe} (dex)	
el	λ (air)	EW	σEW	nLTE	LTE	nLTE	LTE
Fe I	6098.2441	6.200	0.24	6.314	7.325	7.457	7.419
Fe I	6127.9063	30.400	0.45	29.057	32.796	7.468	7.436
Fe I	6136.9937	36.100	0.88	34.948	39.179	7.467	7.430
Fe I	6157.7280	42.200	0.53	43.331	48.039	7.450	7.386
Fe I	6165.3599	24.600	0.55	25.894	29.358	7.448	7.395
Fe I	6170.5059	56.500	0.33	48.102	54.291	7.508	7.479
Fe I	6173.3345	37.700	0.58	37.309	41.686	7.463	7.418
Fe I	6180.2026	26.100	0.30	30.158	33.962	7.412	7.333
Fe I	6187.9893	26.100	0.24	27.217	30.512	7.451	7.405
Fe I	6191.5576	108.600	1.18	102.390	107.103	7.550	7.484
Fe I	6200.3125	44.900	0.89	43.123	47.650	7.473	7.432
Fe I	6213.4292	56.000	0.76	58.508	63.596	7.430	7.349
Fe I	6219.2803	64.500	0.74	62.112	67.221	7.485	7.424
Fe I	6226.7344	10.400	0.38	12.080	13.869	7.426	7.364
Fe I	6232.6401	57.300	0.52	59.335	63.939	7.438	7.366
Fe I	6246.3179	87.000	0.86	88.230	91.525	7.445	7.392
Fe I	6253.8286	13.100	0.51	14.603	16.863	7.437	7.377
Fe I	6265.1323	62.700	0.73	57.023	62.117	7.506	7.466
Fe I	6270.2236	26.500	0.49	30.621	34.444	7.411	7.331
Fe I	6271.2778	9.800	0.30	9.626	11.128	7.462	7.432
Fe I	6290.9653	40.100	0.38	34.415	39.152	7.482	7.467
Fe I	6311.4995	9.200	0.34	9.445	10.983	7.456	7.415
Fe I	6315.8110	25.600	0.36	22.024	25.113	7.469	7.463
Fe I	6318.0181	87.400	1.68	82.725	87.818	7.522	7.454
Fe I	6322.6851	47.400	0.42	44.440	49.051	7.480	7.444
Fe I	6335.3301	78.100	1.08	75.307	80.628	7.496	7.422
Fe I	6336.8232	80.600	0.74	79.319	83.494	7.474	7.419
Fe I	6344.1479	31.200	0.83	27.097	30.757	7.473	7.463
Fe I	6355.0283	38.900	0.48	37.579	41.894	7.469	7.430
Fe I	6364.3638	11.800	0.39	12.363	14.460	7.452	7.402
Fe I	6380.7432	30.300	0.31	28.531	32.422	7.470	7.439
Fe I	6393.6006	104.200	1.01	101.942	106.857	7.494	7.416
Fe I	6400.0005	115.300	1.21	121.295	122.893	7.391	7.359
Fe I	6400.3169	25.500	1.08	24.074	27.863	7.468	7.437
Fe I	6408.0176	72.900	1.12	70.687	75.199	7.483	7.429
Fe I	6411.6479	94.700	0.79	96.792	99.683	7.434	7.386
Fe I	6430.8452	88.500	0.82	84.948	90.466	7.510	7.429
Fe I	6469.1919	40.700	0.80	32.351	37.185	7.477	7.480
Fe I	6475.6240	21.400	0.83	21.937	25.042	7.455	7.411
Fe I	6481.8696	29.900	0.24	30.580	34.593	7.455	7.404
Fe I	6494.9805	119.900	1.11	113.679	118.787	7.545	7.477
Fe I	6496.4658	47.200	0.79	43.742	49.482	7.484	7.436
Fe I	6518.3657	30.500	0.36	33.628	37.742	7.427	7.357
Fe I	6533.9282	18.500	0.27	17.244	19.912	7.468	7.443
Fe I	6592.9126	86.500	0.71	88.485	93.142	7.430	7.345
Fe I	6593.8696	54.700	0.43	52.537	57.606	7.479	7.426
Fe I	6597.5591	24.100	0.34	24.027	27.554	7.461	7.417
Fe I	6609.1099	36.200	0.43	32.936	37.048	7.476	7.453
Fe I	6633.7485	45.000	0.57	40.896	45.899	7.484	7.451
Fe I	6703.5659	12.600	0.23	12.935	14.988	7.456	7.414
Fe I	6713.0459	15.400	0.43	12.838	14.859	7.467	7.465
Fe I	6713.7427	11.200	0.32	7.255	8.495	7.435	7.465
Fe I	6716.2363	6.200	0.27	5.409	6.356	7.473	7.456
Fe I	6750.1514	44.400	0.34	42.743	47.440	7.472	7.428
Fe I	6804.2710	7.100	0.36	6.781	7.950	7.466	7.435
Fe II	4893.8125	26.200	0.25	20.073	20.053	7.446	7.446
Fe II	4993.3501	57.600	0.63	57.897	57.839	7.457	7.457
Fe II	5000.7305	15.000	0.35	12.665	12.640	7.464	7.464
Fe II	5132.6611	33.400	0.33	36.918	36.881	7.424	7.424
Fe II	5197.5674	117.300	1.31	117.181	117.181	7.462	7.462
Fe II	5256.9321	26.900	0.43	29.415	29.386	7.435	7.436
Fe II	5264.8022	71.100	0.64	67.882	67.814	7.498	7.499
Fe II	5284.1030	88.800	1.89	79.170	79.091	7.577	7.578
Fe II	5325.5522	67.700	0.79	66.943	66.876	7.470	7.470
Fe II	5414.0698	44.500	0.33	45.514	45.469	7.451	7.451
Fe II	5425.2485	63.000	0.54	65.150	65.085	7.431	7.432
Fe II	6084.1016	35.900	0.45	32.263	32.231	7.476	7.476
Fe II	6113.3193	21.700	0.23	17.457	17.422	7.463	7.463
Fe II	6129.6948	8.100	0.37	6.502	6.489	7.472	7.471
Fe II	6149.2461	63.600	0.62	54.924	54.869	7.522	7.522
Fe II	6238.3857	69.400	0.53	67.509	67.442	7.483	7.484
Fe II	6239.9429	23.700	0.54	20.506	20.486	7.471	7.471
Fe II	6383.7222	17.900	0.24	13.343	13.330	7.460	7.460
Fe II	6416.9189	61.300	0.48	53.302	53.249	7.516	7.517

HD49933

		EW_{obs} (mÅ)		EW_{calc} (mÅ)		ε_{Fe} (dex)	
el	λ (air)	EW	σEW	nLTE	LTE	nLTE	LTE
Fe I	4788.7568	26.200	0.82	24.949	28.096	7.072	6.992
Fe I	4789.6509	56.100	1.97	51.799	56.303	7.131	7.036
Fe I	4799.4058	6.000	0.31	6.568	7.628	6.997	6.924
Fe I	4872.1377	101.100	1.13	98.773	100.584	7.078	7.049
Fe I	4885.4302	32.400	0.33	35.739	39.754	6.964	6.877
Fe I	4892.8589	16.000	0.22	13.683	15.818	7.126	7.046
Fe I	4896.4385	7.300	0.29	7.154	8.299	7.050	6.976
Fe I	4903.3101	87.100	0.99	81.111	83.448	7.154	7.114
Fe I	4907.7319	20.100	0.83	21.578	24.410	6.998	6.921
Fe I	4917.2300	28.000	0.23	20.812	23.840	7.229	7.146
Fe I	4918.0127	20.300	0.74	14.210	16.409	7.240	7.163
Fe I	4938.8140	75.000	0.93	72.729	75.523	7.086	7.029
Fe I	4939.6865	50.100	0.84	45.822	49.969	7.136	7.043
Fe I	4950.1055	27.700	0.30	30.662	34.221	6.970	6.891
Fe I	4962.5718	18.200	0.30	17.886	20.465	7.050	6.971
Fe I	4967.8970	44.500	0.47	46.525	51.867	6.998	6.890
Fe I	4969.9175	39.800	0.32	35.104	39.621	7.143	7.044
Fe I	4985.2529	59.500	0.76	58.004	62.911	7.072	6.966
Fe I	4985.5469	59.600	0.76	60.738	64.137	7.016	6.942
Fe I	4986.2227	14.500	0.47	13.748	15.894	7.069	6.989
Fe I	4994.1294	60.200	1.22	56.726	60.670	7.121	7.029
Fe I	5001.8633	86.800	0.68	88.107	93.334	7.020	6.933
Fe I	5002.7920	33.000	0.29	32.893	36.548	7.042	6.961
Fe I	5014.9424	72.600	0.57	69.638	74.639	7.100	6.996
Fe I	5022.2354	59.900	0.62	59.482	64.444	7.049	6.942
Fe I	5028.1260	42.700	0.35	45.132	49.541	6.988	6.895
Fe I	5044.2109	25.500	0.39	27.657	30.902	6.986	6.909
Fe I	5048.4355	30.000	0.38	31.441	35.248	7.006	6.918
Fe I	5049.8198	87.200	0.80	81.128	84.596	7.171	7.098
Fe I	5067.1494	31.100	0.31	24.139	27.462	7.212	7.128
Fe I	5068.7656	75.200	0.49	72.289	75.066	7.098	7.043
Fe I	5072.6719	26.600	1.15	29.542	33.419	6.968	6.881
Fe I	5083.3384	65.900	0.64	60.753	64.425	7.162	7.075
Fe I	5088.1533	7.000	0.28	7.030	8.165	7.038	6.964
Fe I	5090.7729	50.900	0.30	46.552	51.782	7.129	7.022
Fe I	5104.4375	9.100	0.26	6.745	7.889	7.186	7.112
Fe I	5127.3594	48.300	0.55	45.523	49.643	7.102	7.010
Fe I	5133.6880	94.800	0.51	91.866	97.522	7.084	6.996
Fe I	5150.8394	57.800	0.45	56.506	60.434	7.070	6.979
Fe I	5151.9106	43.500	0.39	40.888	44.932	7.098	7.009
Fe I	5159.0576	30.800	0.40	28.009	31.974	7.107	7.013
Fe I	5162.2725	88.500	0.51	72.415	78.118	7.321	7.230
Fe I	5180.0557	12.700	0.21	11.673	13.733	7.084	6.998
Fe I	5187.9141	17.600	0.18	13.277	15.403	7.195	7.116
Fe I	5194.9414	79.700	1.02	77.538	81.192	7.092	7.003
Fe I	5195.4717	59.600	0.85	65.481	71.021	6.927	6.815
Fe I	5198.7109	48.400	0.71	48.276	52.531	7.043	6.953
Fe I	5215.1802	67.000	0.36	67.504	71.660	7.030	6.944
Fe I	5216.2739	76.600	0.53	73.215	76.987	7.122	7.031
Fe I	5217.3892	58.600	0.72	59.440	63.369	7.023	6.941
Fe I	5225.5259	15.900	0.51	13.683	16.155	7.122	7.031
Fe I	5228.3760	23.800	0.52	13.838	15.979	7.346	7.274
Fe I	5229.8447	69.700	0.42	61.265	65.735	7.207	7.122
Fe I	5232.9399	128.600	0.74	134.523	134.658	6.970	6.967
Fe I	5235.3867	37.400	0.32	33.576	37.811	7.127	7.031
Fe I	5242.4907	48.000	0.41	46.219	50.790	7.078	6.981
Fe I	5243.7764	21.900	0.28	20.177	23.165	7.090	7.005
Fe I	5250.6455	55.900	0.29	47.033	51.178	7.231	7.142
Fe I	5253.4619	29.000	0.23	31.933	35.679	6.972	6.889
Fe I	5263.3062	67.100	0.70	66.638	70.741	7.049	6.965
Fe I	5267.2695	5.400	0.35	5.747	6.737	7.011	6.934
Fe I	5281.7896	80.700	0.38	79.707	82.088	7.058	7.012
Fe I	5288.5249	16.800	0.34	21.093	24.134	6.909	6.829
Fe I	5307.3608	38.600	0.33	36.093	40.059	7.096	7.008
Fe I	5315.0698	8.000	0.26	6.299	7.376	7.156	7.080
Fe I	5322.0405	14.900	0.30	17.481	20.001	6.951	6.874
Fe I	5324.1787	113.900	0.37	114.694	116.915	7.030	6.998
Fe I	5326.1426	7.100	0.26	8.567	10.008	6.949	6.871
Fe I	5339.9292	79.600	0.43	79.687	83.007	7.038	6.973
Fe I	5364.8711	77.900	0.28	72.171	79.483	7.139	7.012
Fe I	5373.7085	25.400	0.24	26.026	30.018	7.024	6.927
Fe I	5379.5737	19.500	0.33	20.426	23.397	7.012	6.929
Fe I	5389.4790	42.800	0.29	41.530	46.874	7.067	6.956
Fe I	5393.1670	76.100	0.25	76.292	79.720	7.036	6.967
Fe I	5398.2793	32.000	0.32	30.388	34.769	7.078	6.978
Fe I	5400.5010	61.800	0.34	55.273	61.346	7.167	7.049
Fe I	5405.7744	117.400	0.66	108.990	110.875	7.209	7.172

HD49933

		EW_{obs} (mÅ)		EW_{calc} (mÅ)		ε_{Fe} (dex)	
el	λ (air)	EW	σEW	nLTE	LTE	nLTE	LTE
Fe I	5409.1333	16.700	0.55	12.944	15.069	7.179	7.098
Fe I	5410.9097	79.200	1.06	80.402	88.451	7.020	6.883
Fe I	5417.0332	6.200	0.21	5.508	6.495	7.096	7.017
Fe I	5424.0679	105.300	0.74	95.011	101.943	7.182	7.089
Fe I	5434.5234	101.700	0.42	95.094	97.833	7.190	7.129
Fe I	5436.2949	11.000	0.69	7.814	9.161	7.210	7.134
Fe I	5445.0420	68.700	0.24	61.715	68.043	7.171	7.053
Fe I	5463.2754	64.100	0.54	64.442	70.971	7.034	6.909
Fe I	5466.3960	37.400	0.19	33.278	37.730	7.131	7.033
Fe I	5466.9873	7.700	0.24	6.152	7.221	7.148	7.072
Fe I	5472.7085	10.000	0.23	9.397	11.029	7.071	6.989
Fe I	5473.9004	37.900	0.21	37.017	41.499	7.060	6.961
Fe I	5483.0986	12.200	0.43	12.699	14.732	7.019	6.938
Fe I	5487.1450	6.700	0.36	7.595	8.914	6.980	6.900
Fe I	5501.4648	63.200	0.33	57.069	60.971	7.180	7.091
Fe I	5506.7788	74.000	0.48	66.981	70.730	7.207	7.119
Fe I	5522.4463	10.200	0.36	10.314	12.077	7.034	6.952
Fe I	5543.1470	23.900	0.31	18.440	21.293	7.199	7.114
Fe I	5543.9355	22.500	0.26	21.605	24.891	7.065	6.975
Fe I	5546.5059	15.700	0.31	12.758	14.835	7.153	7.072
Fe I	5553.5771	12.700	0.23	9.412	11.047	7.193	7.114
Fe I	5554.8945	42.500	0.39	42.672	48.712	7.036	6.915
Fe I	5560.2114	17.100	0.30	14.444	16.854	7.134	7.048
Fe I	5567.3911	14.000	0.25	16.271	18.724	6.958	6.879
Fe I	5569.6182	78.200	0.30	79.662	83.591	7.014	6.937
Fe I	5572.8423	98.000	1.54	93.725	97.225	7.105	7.053
Fe I	5576.0889	60.800	0.21	58.938	63.648	7.076	6.982
Fe I	5586.7554	103.100	0.63	107.512	109.930	6.979	6.936
Fe I	5600.2241	10.700	0.40	10.058	11.805	7.072	6.988
Fe I	5615.6440	118.600	3.19	121.160	123.005	7.009	6.983
Fe I	5618.6323	15.600	0.25	15.082	17.497	7.059	6.975
Fe I	5619.5952	7.700	0.25	5.628	6.613	7.190	7.115
Fe I	5638.2622	33.500	0.35	34.589	38.995	7.015	6.917
Fe I	5641.4341	20.600	0.22	19.166	22.183	7.083	6.994
Fe I	5650.7056	8.700	0.32	7.512	9.286	7.113	7.007
Fe I	5653.8652	8.300	0.26	5.202	6.127	7.262	7.189
Fe I	5662.5161	48.100	0.36	51.260	56.516	6.980	6.879
Fe I	5667.5181	13.200	0.38	8.517	9.996	7.262	7.186
Fe I	5679.0229	20.300	0.26	16.873	19.921	7.148	7.051
Fe I	5691.4971	8.600	0.29	8.858	10.446	7.025	6.941
Fe I	5701.5444	32.200	0.22	32.369	36.166	7.036	6.950
Fe I	5717.8325	22.600	0.28	21.540	24.787	7.070	6.980
Fe I	5731.7617	17.800	0.30	15.598	18.074	7.115	7.031
Fe I	5741.8477	6.400	0.26	6.097	7.165	7.063	6.985
Fe II	4893.8125	10.700	0.22	7.785	7.769	7.200	7.202
Fe II	4993.3501	31.200	1.18	32.266	32.234	7.015	7.016
Fe II	5100.6548	15.900	0.61	13.660	13.633	7.124	7.125
Fe II	5132.6611	16.000	0.35	16.626	16.593	7.018	7.019
Fe II	5197.5674	88.200	0.67	88.966	88.877	7.023	7.025
Fe II	5234.6226	93.500	0.75	85.000	84.915	7.234	7.235
Fe II	5256.9321	11.900	0.31	12.374	12.349	7.019	7.020
Fe II	5264.8022	45.100	0.75	41.750	41.708	7.114	7.115
Fe II	5284.1030	58.700	0.23	52.698	52.645	7.172	7.174
Fe II	5325.5522	39.700	0.27	40.778	40.737	7.016	7.017
Fe II	5414.0698	21.000	0.25	22.477	22.432	6.998	6.999
Fe II	5425.2485	35.900	0.22	38.965	38.926	6.971	6.972
Fe II	5534.8379	59.200	0.32	54.287	54.233	7.148	7.150
Fe II	5627.4888	6.700	0.29	6.347	6.334	7.066	7.067

Arcturus

		EW_{obs} (mÅ)		EW_{calc} (mÅ)		ε_{Fe} (dex)	
el	λ (air)	EW	σEW	nLTE	LTE	nLTE	LTE
Fe I	4787.8267	86.000	3.18	79.676	82.395	7.081	7.020
Fe I	4793.9614	35.000	1.41	37.414	40.712	6.879	6.809
Fe I	4794.3540	52.500	2.00	53.288	57.115	6.914	6.837
Fe I	4802.8799	88.500	3.30	88.628	91.653	6.927	6.850
Fe I	4808.1479	63.100	2.39	60.846	64.251	6.978	6.905
Fe I	4809.9385	41.100	3.04	43.589	46.971	6.878	6.807
Fe I	4869.4634	55.900	2.85	50.149	53.578	7.049	6.979
Fe I	4873.7510	37.300	2.79	44.613	48.126	6.779	6.708
Fe I	4874.3530	57.500	3.17	53.237	56.756	7.018	6.946
Fe I	4885.4302	97.000	4.35	99.810	101.951	6.867	6.809
Fe I	4892.8589	74.700	7.62	66.937	71.210	7.093	7.009
Fe I	4896.4385	62.400	2.22	59.604	62.873	6.990	6.919
Fe I	4905.1328	63.200	1.18	64.198	67.719	6.908	6.828
Fe I	4918.0127	70.300	2.28	67.651	71.893	6.986	6.895

Arcturus

		EW_{obs} (mÅ)		EW_{calc} (mÅ)		ε_{Fe} (dex)	
el	λ (air)	EW	σEW	nLTE	LTE	nLTE	LTE
Fe I	4961.9136	62.700	1.73	61.240	64.667	6.961	6.887
Fe I	4962.5718	75.300	1.82	75.173	78.551	6.933	6.856
Fe I	4969.9175	98.900	3.01	91.839	96.368	7.084	6.990
Fe I	4979.5859	44.700	1.59	37.020	40.371	7.084	7.018
Fe I	4986.2227	67.500	1.47	67.592	71.602	6.928	6.839
Fe I	4999.1123	50.000	3.03	52.727	56.513	6.873	6.791
Fe I	5029.6177	89.400	3.92	84.737	87.901	7.040	6.967
Fe I	5031.9141	43.200	1.42	44.412	48.485	6.904	6.818
Fe I	5036.9214	64.800	2.47	61.378	64.950	7.002	6.927
Fe I	5048.4355	92.100	4.79	94.554	97.278	6.875	6.803
Fe I	5072.6719	90.500	3.44	87.788	90.972	6.989	6.919
Fe I	5088.1533	56.600	2.71	53.487	57.022	6.994	6.921
Fe I	5115.7769	37.800	3.50	43.473	46.998	6.813	6.740
Fe I	5143.7227	83.300	2.97	81.928	85.520	6.961	6.878
Fe I	5196.0591	98.300	2.36	102.314	106.800	6.851	6.750
Fe I	5243.7764	82.400	2.07	76.968	80.426	7.046	6.975
Fe I	5253.0210	70.100	2.14	66.049	69.967	7.013	6.933
Fe I	5267.2695	46.400	2.99	43.751	47.607	6.985	6.905
Fe I	5285.1274	38.200	2.15	36.711	40.431	6.962	6.882
Fe I	5288.5249	89.500	2.37	90.028	93.197	6.918	6.842
Fe I	5293.9590	49.000	1.51	49.887	53.816	6.912	6.830
Fe I	5294.5474	33.300	1.14	33.866	37.215	6.918	6.846
Fe I	5295.3120	40.500	2.06	41.231	45.160	6.915	6.831
Fe I	5315.0698	50.900	0.94	46.108	49.954	7.026	6.949
Fe I	5320.0356	48.000	0.80	44.618	48.340	6.997	6.923
Fe I	5326.1426	72.800	0.80	71.690	75.305	6.954	6.874
Fe I	5373.7085	79.200	1.54	79.264	83.789	6.929	6.827
Fe I	5379.5737	88.700	1.81	89.680	92.933	6.908	6.830
Fe I	5389.4790	99.500	1.73	96.893	100.930	6.983	6.898
Fe I	5398.2793	86.500	1.32	84.784	89.246	6.966	6.869
Fe I	5412.7837	34.700	1.32	34.399	37.968	6.937	6.859
Fe I	5417.0332	46.400	1.40	41.998	45.950	7.019	6.939
Fe I	5436.2949	56.600	2.06	51.032	54.932	7.040	6.964
Fe I	5441.3389	46.500	1.20	46.486	50.201	6.930	6.854
Fe I	5452.0884	31.300	1.92	32.049	35.296	6.914	6.843
Fe I	5460.8726	31.000	0.63	38.048	41.674	6.782	6.709
Fe I	5466.3960	97.200	1.38	91.552	94.971	7.041	6.978
Fe I	5466.9873	64.400	1.02	64.645	68.407	6.925	6.844
Fe I	5470.0928	38.700	1.32	33.901	37.668	7.031	6.952
Fe I	5473.1626	34.600	2.55	34.209	37.634	6.938	6.865
Fe I	5473.9004	98.600	2.69	99.502	101.636	6.911	6.860
Fe I	5483.0986	70.200	1.30	68.845	72.392	6.957	6.884
Fe I	5522.4463	61.000	0.71	62.071	65.684	6.909	6.831
Fe I	5524.2495	8.100	0.56	9.137	10.359	6.871	6.807
Fe I	5539.2798	41.200	0.48	43.964	47.683	6.874	6.799
Fe I	5543.9355	82.200	0.97	80.868	84.150	6.957	6.886
Fe I	5546.5059	71.400	1.69	63.325	67.082	7.093	7.022
Fe I	5549.9487	28.000	0.60	24.349	27.115	7.017	6.951
Fe I	5552.6919	8.700	0.65	7.299	9.147	7.016	6.905
Fe I	5560.2114	65.100	0.95	65.316	69.338	6.926	6.840
Fe I	5577.0249	12.200	0.66	11.944	14.986	6.941	6.819
Fe I	5584.7646	71.600	0.94	74.095	77.831	6.878	6.796
Fe I	5587.5742	59.600	0.91	51.586	55.529	7.087	7.013
Fe I	5600.2241	60.000	0.94	60.222	64.066	6.926	6.845
Fe I	5618.6323	68.800	0.70	71.580	75.110	6.874	6.793
Fe I	5622.9453	22.000	0.55	20.096	22.580	6.982	6.914
Fe I	5636.6958	44.300	0.41	46.867	50.667	6.879	6.802
Fe I	5638.2622	96.500	1.31	96.570	98.742	6.929	6.879
Fe I	5651.4688	28.900	0.43	24.556	27.406	7.035	6.966
Fe I	5652.3174	41.700	0.55	39.179	42.679	6.981	6.910
Fe I	5661.3447	39.700	0.86	42.166	45.833	6.879	6.802
Fe I	5662.5161	111.800	2.57	116.721	118.982	6.844	6.793
Fe I	5679.0229	68.000	0.64	63.313	68.669	7.024	6.916
Fe I	5691.4971	60.100	2.36	56.029	60.117	7.010	6.930
Fe I	5717.8325	78.900	1.76	79.564	83.139	6.917	6.836
Fe I	5731.7617	78.400	1.71	72.118	75.123	7.055	7.001
Fe I	5741.8477	47.900	0.44	48.363	52.059	6.921	6.845
Fe I	5742.9600	23.900	1.82	19.880	22.262	7.038	6.973
Fe I	5754.4023	41.600	3.26	42.432	46.172	6.913	6.838
Fe I	5759.2622	9.300	0.69	8.940	10.300	6.949	6.878
Fe I	5760.3438	47.200	1.57	53.152	57.091	6.813	6.734
Fe I	5838.3716	44.100	0.87	41.035	44.410	6.991	6.924
Fe I	5849.6831	24.500	0.62	21.628	24.247	7.004	6.936
Fe I	5853.1484	66.200	2.56	60.917	65.927	7.026	6.935
Fe I	5855.0757	36.300	0.92	35.331	39.213	6.951	6.867
Fe I	5858.7778	28.400	0.89	27.530	30.521	6.951	6.880
Fe I	5859.5864	93.200	1.90	90.694	94.670	6.978	6.899
Fe I	5861.1084	18.100	0.36	18.972	21.269	6.903	6.835
Fe I	5862.3564	103.900	2.73	105.286	108.879	6.904	6.827
Fe I	5883.8164	93.000	2.30	90.113	92.329	6.987	6.944

Arcturus

		EW_{obs} (mÅ)		EW_{calc} (mÅ)		ε_{Fe} (dex)	
el	λ (air)	EW	σEW	nLTE	LTE	nLTE	LTE
Fe I	5898.2153	20.100	0.63	18.502	21.218	6.978	6.897
Fe I	5905.6714	71.700	0.91	69.594	75.318	6.971	6.853
Fe I	5927.7886	57.200	0.90	55.605	61.037	6.961	6.852
Fe I	5934.6543	109.500	2.51	102.964	103.899	7.055	7.046
Fe I	5940.9912	41.000	1.29	35.150	38.499	7.049	6.982
Fe I	5952.7178	91.000	2.45	84.851	87.206	7.051	7.011
Fe I	5976.7769	97.400	2.19	93.392	94.718	7.007	6.987
Fe I	6007.9595	77.700	1.57	75.636	80.550	6.969	6.871
Fe I	6027.0508	95.700	2.27	89.910	93.852	7.044	6.969
Fe I	6034.0352	19.400	0.79	17.687	19.851	6.982	6.917
Fe I	6054.0732	19.500	0.41	14.769	16.632	7.080	7.019
Fe I	6056.0044	84.400	1.13	83.212	88.712	6.953	6.839
Fe I	6078.4912	86.200	1.22	78.556	84.834	7.076	6.958
Fe I	6079.0078	61.200	0.90	55.130	59.729	7.045	6.959
Fe I	6093.6431	44.800	0.57	39.065	43.357	7.046	6.960
Fe I	6096.6641	65.400	0.87	60.480	63.529	7.023	6.968
Fe I	6120.2466	68.800	1.84	62.532	68.416	7.039	6.937
Fe I	6127.9063	75.600	1.68	70.401	74.656	7.031	6.949
Fe I	6151.6172	118.400	2.88	110.305	115.261	7.088	6.993
Fe I	6165.3599	70.900	1.30	66.753	71.014	7.010	6.928
Fe I	6180.2026	114.600	2.26	107.529	111.660	7.069	6.989
Fe I	6187.3979	23.800	0.54	21.445	24.150	6.990	6.921
Fe I	6187.9893	77.200	1.17	74.601	77.227	6.979	6.929
Fe I	6199.5063	29.800	1.60	24.760	27.852	7.043	6.973
Fe I	6226.7344	52.800	0.46	52.172	55.680	6.942	6.874
Fe I	6229.2261	87.700	1.40	88.795	92.785	6.908	6.825
Fe I	6232.6401	117.500	2.24	113.899	116.342	6.996	6.953
Fe I	6240.6460	114.100	4.15	108.994	113.535	7.039	6.942
Fe I	6270.2236	103.900	2.57	104.528	108.432	6.917	6.836
Fe I	6271.2778	59.500	0.95	60.033	64.413	6.920	6.836
Fe I	5638.2622	96.500	1.31	96.570	98.742	6.929	6.879
Fe I	5651.4688	28.900	0.43	24.556	27.406	7.035	6.966
Fe I	5652.3174	41.700	0.55	39.179	42.679	6.981	6.910
Fe I	5661.3447	39.700	0.86	42.166	45.833	6.879	6.802
Fe I	5662.5161	111.800	2.57	116.721	118.982	6.844	6.793
Fe I	5679.0229	68.000	0.64	63.313	68.669	7.024	6.916
Fe I	5691.4971	60.100	2.36	56.029	60.117	7.010	6.930
Fe I	5717.8325	78.900	1.76	79.564	83.139	6.917	6.836
Fe I	5731.7617	78.400	1.71	72.118	75.123	7.055	7.001
Fe I	5741.8477	47.900	0.44	48.363	52.059	6.921	6.845
Fe I	5742.9600	23.900	1.82	19.880	22.262	7.038	6.973
Fe I	5754.4023	41.600	3.26	42.432	46.172	6.913	6.838
Fe I	5759.2622	9.300	0.69	8.940	10.300	6.949	6.878
Fe I	5760.3438	47.200	1.57	53.152	57.091	6.813	6.734
Fe I	5838.3716	44.100	0.87	41.035	44.410	6.991	6.924
Fe I	5849.6831	24.500	0.62	21.628	24.247	7.004	6.936
Fe I	5853.1484	66.200	2.56	60.917	65.927	7.026	6.935
Fe I	5855.0757	36.300	0.92	35.331	39.213	6.951	6.867
Fe I	5858.7778	28.400	0.89	27.530	30.521	6.951	6.880
Fe I	5859.5864	93.200	1.90	90.694	94.670	6.978	6.899
Fe I	5861.1084	18.100	0.36	18.972	21.269	6.903	6.835
Fe I	5862.3564	103.900	2.73	105.286	108.879	6.904	6.827
Fe I	5883.8164	93.000	2.30	90.113	92.329	6.987	6.944
Fe I	5898.2153	20.100	0.63	18.502	21.218	6.978	6.897
Fe I	5905.6714	71.700	0.91	69.594	75.318	6.971	6.853
Fe I	5927.7886	57.200	0.90	55.605	61.037	6.961	6.852
Fe I	5934.6543	109.500	2.51	102.964	103.899	7.055	7.046
Fe I	5940.9912	41.000	1.29	35.150	38.499	7.049	6.982
Fe I	5952.7178	91.000	2.45	84.851	87.206	7.051	7.011
Fe I	5976.7769	97.400	2.19	93.392	94.718	7.007	6.987
Fe I	6007.9595	77.700	1.57	75.636	80.550	6.969	6.871
Fe I	6027.0508	95.700	2.27	89.910	93.852	7.044	6.969
Fe I	6034.0352	19.400	0.79	17.687	19.851	6.982	6.917
Fe I	6054.0732	19.500	0.41	14.769	16.632	7.080	7.019
Fe I	6056.0044	84.400	1.13	83.212	88.712	6.953	6.839
Fe I	6078.4912	86.200	1.22	78.556	84.834	7.076	6.958
Fe I	6079.0078	61.200	0.90	55.130	59.729	7.045	6.959
Fe I	6093.6431	44.800	0.57	39.065	43.357	7.046	6.960
Fe I	6096.6641	65.400	0.87	60.480	63.529	7.023	6.968
Fe I	6120.2466	68.800	1.84	62.532	68.416	7.039	6.937
Fe I	6127.9063	75.600	1.68	70.401	74.656	7.031	6.949
Fe I	6151.6172	118.400	2.88	110.305	115.261	7.088	6.993
Fe I	6165.3599	70.900	1.30	66.753	71.014	7.010	6.928
Fe I	6180.2026	114.600	2.26	107.529	111.660	7.069	6.989
Fe I	6187.3979	23.800	0.54	21.445	24.150	6.990	6.921
Fe I	6187.9893	77.200	1.17	74.601	77.227	6.979	6.929
Fe I	6199.5063	29.800	1.60	24.760	27.852	7.043	6.973
Fe I	6226.7344	52.800	0.46	52.172	55.680	6.942	6.874
Fe I	6229.2261	87.700	1.40	88.795	92.785	6.908	6.825

Arcturus

		EW_{obs} (mÅ)		EW_{calc} (mÅ)		ε_{Fe} (dex)	
el	λ (air)	EW	σEW	nLTE	LTE	nLTE	LTE
Fe I	6232.6401	117.500	2.24	113.899	116.342	6.996	6.953
Fe I	6240.6460	114.100	4.15	108.994	113.535	7.039	6.942
Fe I	6270.2236	103.900	2.57	104.528	108.432	6.917	6.836
Fe I	6271.2778	59.500	0.95	60.033	64.413	6.920	6.836
Fe I	6311.4995	80.000	0.94	73.235	77.415	7.060	6.981
Fe I	6315.8110	68.700	2.72	63.703	67.841	7.026	6.947
Fe I	6338.8760	53.700	1.68	47.931	53.257	7.042	6.939
Fe I	6380.7432	77.600	1.50	69.042	73.527	7.092	7.012
Fe I	6408.0176	124.100	3.11	125.523	128.085	6.906	6.857
Fe I	6495.7412	53.300	2.00	51.564	57.357	6.963	6.849
Fe I	6518.3657	111.400	2.45	111.741	116.155	6.924	6.842
Fe I	6533.9282	51.800	0.82	44.975	49.261	7.059	6.980
Fe I	6581.2090	97.000	1.10	91.500	97.444	7.036	6.921
Fe I	6591.3130	17.200	0.39	14.410	16.525	7.025	6.952
Fe I	6597.5591	52.300	0.50	48.694	53.451	6.999	6.907
Fe I	6608.0249	75.700	1.99	73.155	78.157	6.977	6.885
Fe I	6627.5439	41.800	0.31	34.885	38.293	7.069	7.002
Fe I	6633.7485	81.100	1.17	74.731	78.830	7.043	6.974
Fe I	6699.1411	15.000	0.21	13.503	15.503	6.985	6.912
Fe I	6703.5659	90.300	1.50	84.348	88.787	7.044	6.960
Fe I	6710.3179	92.400	1.75	87.900	93.910	7.015	6.901
Fe I	6732.0649	14.200	0.39	16.048	18.341	6.864	6.787
Fe I	6733.1504	38.200	0.35	50.127	54.605	6.697	6.604
Fe I	6739.5205	75.900	1.16	81.016	86.834	6.837	6.731
Fe I	6746.9536	26.900	0.12	28.562	32.056	6.893	6.817
Fe I	6786.8584	43.800	0.74	40.084	43.381	7.002	6.938
Fe I	6804.2710	25.000	0.69	23.096	26.097	6.979	6.902
Fe II	4993.3501	46.700	2.21	46.386	44.135	6.938	6.997
Fe II	5234.6226	78.200	1.06	87.000	82.700	6.714	6.816
Fe II	5256.9321	22.500	0.91	23.455	22.359	6.899	6.935
Fe II	5264.8022	42.100	0.88	46.712	44.488	6.810	6.865
Fe II	5284.1030	61.900	2.53	61.942	58.546	6.929	7.014
Fe II	5325.5522	40.900	0.64	45.798	43.576	6.802	6.857
Fe II	5414.0698	21.600	0.87	29.769	28.433	6.670	6.704
Fe II	5425.2485	36.100	1.19	44.231	42.005	6.715	6.766
Fe II	6084.1016	22.900	0.60	19.637	18.596	7.043	7.084
Fe II	6238.3857	33.700	0.98	33.112	31.505	6.947	6.997
Fe II	6247.5571	38.200	0.45	38.918	36.924	6.910	6.967
Fe II	6369.4590	19.200	0.39	23.721	22.148	6.777	6.825
Fe II	6456.3794	48.100	0.75	47.714	44.971	6.940	7.012
Fe II	6516.0767	52.900	0.61	55.906	51.574	6.862	6.962

μ Leo

		EW_{obs} (mÅ)		EW_{calc} (mÅ)		ε_{Fe} (dex)	
el	λ (air)	EW	σEW	nLTE	LTE	nLTE	LTE
Fe I	4793.9614	57.100	1.44	57.476	58.470	7.692	7.669
Fe I	4794.3540	76.200	1.99	70.507	71.726	7.828	7.802
Fe I	4802.5234	45.600	2.63	38.213	40.014	7.864	7.821
Fe I	4802.8799	101.700	3.18	108.419	109.073	7.546	7.526
Fe I	4808.1479	77.900	2.73	79.418	80.301	7.664	7.641
Fe I	4809.9385	61.000	3.65	65.081	66.005	7.607	7.584
Fe I	4874.3530	69.000	4.58	71.826	72.772	7.633	7.609
Fe I	4875.8770	109.200	2.46	112.334	112.446	7.633	7.628
Fe I	4892.8589	92.700	3.56	91.748	92.675	7.720	7.701
Fe I	4907.7319	115.100	2.19	117.355	117.121	7.654	7.658
Fe I	4917.2300	108.800	2.11	101.932	102.962	7.845	7.828
Fe I	4918.0127	89.200	2.99	92.680	93.616	7.627	7.604
Fe I	4935.4141	17.700	1.68	23.947	24.637	7.517	7.498
Fe I	4961.9136	81.000	2.50	81.642	82.467	7.685	7.665
Fe I	4962.5718	92.900	2.00	99.646	100.348	7.560	7.541
Fe I	4969.9175	119.800	4.98	121.350	122.576	7.673	7.649
Fe I	4992.7852	31.500	2.72	38.823	39.778	7.532	7.510
Fe I	4999.1123	83.000	3.66	75.880	76.802	7.865	7.847
Fe I	5025.3027	45.200	3.95	54.200	55.250	7.504	7.480
Fe I	5029.6177	107.100	3.91	103.218	103.946	7.793	7.777
Fe I	5031.9141	68.100	1.28	69.527	70.729	7.668	7.640
Fe I	5036.9214	76.300	2.64	79.294	80.338	7.629	7.602
Fe I	5048.4355	115.400	4.29	117.719	117.837	7.652	7.648
Fe I	5067.1494	114.900	1.61	106.577	107.005	7.873	7.872
Fe I	5072.6719	112.800	3.89	114.319	114.663	7.671	7.662
Fe I	5088.1533	75.600	2.81	77.041	77.819	7.668	7.649
Fe I	5109.6519	104.200	4.57	101.728	102.652	7.751	7.733
Fe I	5115.7769	64.000	2.01	65.271	66.265	7.672	7.649
Fe I	5143.7227	91.800	3.25	95.449	96.608	7.611	7.581

μ Leo

		EW_{obs} (mÅ)		EW_{calc} (mÅ)		ε_{Fe} (dex)	
el	λ (air)	EW	σEW	nLTE	LTE	nLTE	LTE
Fe I	5213.8062	34.000	2.79	37.918	38.771	7.612	7.593
Fe I	5243.7764	102.500	3.12	101.668	102.076	7.717	7.709
Fe I	5253.0210	81.600	3.78	81.814	83.144	7.695	7.665
Fe I	5279.6499	33.600	2.83	48.324	49.361	7.391	7.370
Fe I	5285.1274	60.500	2.03	62.276	63.418	7.662	7.636
Fe I	5288.5249	111.600	3.47	111.310	111.869	7.706	7.694
Fe I	5293.9590	75.500	1.99	73.681	74.727	7.740	7.718
Fe I	5294.5474	55.400	0.88	56.868	57.910	7.670	7.648
Fe I	5295.3120	59.800	2.59	66.728	67.951	7.550	7.521
Fe I	5320.0356	69.900	1.74	67.222	68.246	7.757	7.736
Fe I	5321.1079	82.000	1.07	89.930	90.930	7.533	7.505
Fe I	5373.7085	100.000	2.10	107.495	108.471	7.555	7.529
Fe I	5379.5737	110.800	1.77	110.923	111.480	7.697	7.685
Fe I	5386.3330	71.300	3.51	79.011	79.809	7.538	7.516
Fe I	5398.2793	106.900	1.94	114.087	115.123	7.568	7.543
Fe I	5406.7749	77.500	1.77	68.659	69.634	7.885	7.871
Fe I	5412.7837	59.900	0.83	60.058	61.221	7.697	7.672
Fe I	5417.0332	69.500	2.06	67.962	68.997	7.732	7.711
Fe I	5432.9478	105.100	3.18	96.909	97.987	7.866	7.852
Fe I	5436.2949	78.800	1.69	76.660	77.513	7.745	7.728
Fe I	5441.3389	68.100	2.11	71.723	72.594	7.624	7.603
Fe I	5452.0884	58.000	4.84	54.665	55.724	7.769	7.748
Fe I	5460.8726	52.200	1.10	58.969	60.172	7.559	7.533
Fe I	5466.3960	122.500	1.32	122.262	122.384	7.704	7.702
Fe I	5466.9873	91.700	1.27	84.981	85.926	7.855	7.838
Fe I	5470.0928	67.600	1.50	59.764	60.984	7.862	7.840
Fe I	5473.1626	58.700	2.96	59.033	59.993	7.693	7.673
Fe I	5473.9004	126.800	3.54	125.618	124.993	7.722	7.735
Fe I	5483.0986	88.600	1.93	93.014	93.388	7.610	7.598
Fe I	5522.4463	81.300	1.73	85.822	86.167	7.603	7.590
Fe I	5524.2495	23.400	0.65	23.459	24.110	7.698	7.681
Fe I	5525.5435	99.800	1.29	101.728	101.830	7.660	7.655
Fe I	5536.5801	54.600	1.16	60.250	61.480	7.583	7.557
Fe I	5539.2798	69.500	0.81	66.561	67.643	7.763	7.741
Fe I	5543.9355	104.200	1.27	105.046	105.046	7.683	7.682
Fe I	5554.8945	131.500	2.14	131.312	132.505	7.703	7.684
Fe I	5577.0249	40.900	0.55	32.816	34.985	7.882	7.829
Fe I	5600.2241	76.000	6.40	84.592	85.103	7.519	7.499
Fe I	5618.6323	93.200	0.90	95.132	95.418	7.659	7.650
Fe I	5619.2246	50.100	2.35	59.600	60.692	7.502	7.478
Fe I	5636.6958	75.600	2.55	69.384	70.441	7.833	7.813
Fe I	5638.2622	130.800	1.90	122.634	121.903	7.850	7.872
Fe I	5650.7056	64.500	2.29	61.565	66.199	7.761	7.666
Fe I	5651.4688	40.300	3.88	48.785	49.781	7.517	7.495
Fe I	5652.3174	52.600	3.64	64.088	64.866	7.461	7.439
Fe I	5653.8652	63.200	2.71	67.469	68.427	7.612	7.589
Fe I	5655.1763	72.400	1.36	75.461	81.668	7.639	7.524
Fe I	5661.3447	57.800	2.65	67.197	67.944	7.504	7.482
Fe I	5677.6846	40.800	0.41	49.876	50.842	7.510	7.488
Fe I	5679.0229	93.700	0.94	91.565	93.054	7.743	7.713
Fe I	5696.0894	53.100	0.48	53.334	54.534	7.695	7.670
Fe I	5698.0200	75.800	6.13	66.379	67.458	7.896	7.877
Fe I	5717.8325	107.000	2.46	104.402	104.507	7.752	7.753
Fe I	5741.8477	69.500	1.87	73.056	73.719	7.625	7.607
Fe I	5742.9600	51.100	3.18	41.541	42.475	7.894	7.877
Fe I	5754.4023	74.000	3.69	65.422	66.553	7.878	7.858
Fe I	5759.2622	26.100	1.33	24.552	25.364	7.741	7.719
Fe I	5760.3438	69.700	3.38	75.440	76.511	7.578	7.552
Fe I	5849.6831	46.100	1.58	42.417	43.460	7.775	7.754
Fe I	5853.1484	81.600	3.26	75.723	77.506	7.822	7.786
Fe I	5855.0757	62.900	1.37	61.995	63.260	7.718	7.693
Fe I	5859.5864	129.400	3.03	122.514	122.760	7.814	7.816
Fe I	5862.3564	136.000	3.39	143.528	143.672	7.593	7.586
Fe I	5880.0273	36.700	2.36	47.139	48.150	7.477	7.455
Fe I	5902.4731	39.300	2.90	50.796	52.098	7.454	7.427
Fe I	5905.6714	92.300	2.66	98.995	100.197	7.573	7.540
Fe I	5929.6763	76.000	2.24	74.551	75.456	7.729	7.711
Fe I	5930.1797	127.600	2.37	127.998	128.641	7.694	7.683
Fe I	5934.6543	124.600	2.87	131.814	130.380	7.582	7.601
Fe I	5952.7178	119.300	4.22	110.282	109.733	7.869	7.887
Fe I	5961.9180	10.800	0.94	13.227	13.693	7.593	7.574
Fe I	5969.5620	27.100	1.54	20.000	20.619	7.885	7.869
Fe I	5976.7769	122.300	3.42	119.778	118.475	7.745	7.771
Fe I	5984.8149	128.800	3.45	124.377	125.760	7.769	7.750
Fe I	6003.0112	134.600	2.68	134.098	132.639	7.708	7.732

μ Leo

		EW_{obs} (mÅ)		EW_{calc} (mÅ)		ε_{Fe} (dex)	
el	λ (air)	EW	σEW	nLTE	LTE	nLTE	LTE
Fe I	6007.9595	107.700	3.34	105.004	105.744	7.748	7.737
Fe I	6008.5557	147.900	4.42	142.824	141.270	7.775	7.800
Fe I	6015.2437	62.900	1.23	66.114	67.670	7.637	7.606
Fe I	6024.0576	149.800	3.41	151.168	151.168	7.684	7.683
Fe I	6027.0508	113.600	1.93	117.074	117.662	7.638	7.624
Fe I	6034.0352	40.200	0.61	39.121	40.001	7.723	7.704
Fe I	6056.0044	110.900	1.68	116.428	117.485	7.607	7.583
Fe I	6078.4912	120.600	2.25	111.902	113.606	7.846	7.823
Fe I	6079.0078	90.100	2.47	83.551	84.395	7.824	7.814
Fe I	6093.6431	72.700	1.50	66.255	67.538	7.828	7.805
Fe I	6096.6641	89.200	1.80	84.976	84.976	7.784	7.788
Fe I	6120.2466	83.600	2.00	75.941	78.129	7.850	7.808
Fe I	6127.9063	102.200	2.75	95.950	96.821	7.822	7.810
Fe I	6151.6172	125.800	3.40	126.910	128.843	7.679	7.642
Fe I	6165.3599	95.000	1.71	92.174	93.105	7.756	7.739
Fe I	6187.9893	103.600	2.17	99.150	98.853	7.786	7.797
Fe I	6200.3125	151.400	2.68	142.565	143.860	7.850	7.830
Fe I	6220.7798	75.000	2.57	79.862	80.344	7.603	7.590
Fe I	6221.6719	51.700	1.37	44.309	46.252	7.828	7.795
Fe I	6226.7344	73.500	2.54	76.549	77.166	7.639	7.624
Fe I	6229.2261	110.100	2.00	106.897	108.086	7.766	7.743
Fe I	6232.6401	148.800	3.09	144.027	143.883	7.770	7.774
Fe I	6240.6460	126.800	4.34	123.802	125.433	7.766	7.731
Fe I	6253.8286	62.400	1.30	64.049	65.290	7.667	7.641
Fe I	6270.2236	123.600	2.72	123.324	124.444	7.705	7.683
Fe I	6271.2778	84.700	3.04	82.076	83.495	7.753	7.725
Fe I	6290.5430	53.900	1.23	46.677	48.022	7.833	7.809
Fe I	6311.4995	96.700	1.20	92.124	93.432	7.794	7.769
Fe I	6315.8110	93.500	1.50	88.636	89.441	7.797	7.784
Fe I	6322.6851	153.800	2.41	146.690	148.022	7.815	7.795
Fe I	6338.8760	76.700	1.65	76.926	78.256	7.696	7.668
Fe I	6408.0176	160.800	3.04	161.813	161.651	7.687	7.689
Fe I	6496.4658	106.200	1.54	100.939	101.856	7.793	7.782
Fe I	6509.6157	34.500	3.33	45.102	46.211	7.475	7.451
Fe I	6569.2139	124.100	1.74	118.441	118.678	7.784	7.785
Fe I	6591.3130	40.500	0.48	34.623	35.694	7.826	7.804
Fe I	6597.5591	80.200	1.62	78.357	79.389	7.734	7.716
Fe I	6608.0249	96.900	3.00	91.138	92.998	7.812	7.777
Fe I	6633.7485	106.600	1.70	104.863	104.968	7.729	7.729
Fe I	6653.8511	43.900	0.52	55.459	56.189	7.474	7.456
Fe I	6667.4180	62.200	0.99	62.054	63.645	7.703	7.673
Fe I	6699.1411	39.000	0.81	33.103	34.127	7.828	7.806
Fe I	6703.5659	110.900	2.79	103.238	104.810	7.852	7.824
Fe I	6704.4795	29.700	1.15	42.541	43.498	7.424	7.403
Fe I	6725.3560	57.800	1.48	65.229	65.954	7.559	7.541
Fe I	6732.0649	34.200	0.85	37.241	38.314	7.632	7.607
Fe I	6733.1504	66.600	1.22	77.994	78.702	7.480	7.453
Fe I	6739.5205	89.700	1.73	95.866	98.123	7.578	7.532
Fe I	6745.9556	36.500	0.29	44.908	46.059	7.524	7.499
Fe I	6746.9536	48.700	0.37	48.140	49.578	7.710	7.684
Fe I	6750.1514	155.900	2.30	147.586	149.077	7.856	7.833
Fe I	6786.8584	67.400	1.25	66.641	67.178	7.714	7.704
Fe I	6796.1235	70.400	1.72	65.148	66.342	7.801	7.780
Fe I	6804.2710	51.700	0.53	47.430	48.596	7.786	7.764
Fe I	6810.2622	89.000	1.09	91.050	91.416	7.664	7.654
Fe II	4993.3501	47.000	4.03	53.401	52.099	7.531	7.562
Fe II	5000.7305	20.800	1.33	17.982	17.647	7.805	7.819
Fe II	5100.6548	39.400	3.67	33.564	32.809	7.864	7.888
Fe II	5234.6226	88.500	1.01	95.802	93.012	7.527	7.592
Fe II	5264.8022	51.600	1.19	54.799	53.462	7.616	7.650
Fe II	5325.5522	54.400	0.79	53.829	52.465	7.715	7.751
Fe II	5414.0698	30.000	1.01	37.507	36.664	7.475	7.496
Fe II	5425.2485	43.400	2.10	52.149	50.778	7.467	7.500
Fe II	6247.5571	46.100	1.31	48.289	46.974	7.641	7.676
Fe II	6369.4590	21.500	1.33	29.932	28.920	7.427	7.452
Fe II	6416.9189	55.800	0.87	69.523	70.942	7.432	7.396
Fe II	6416.9189	55.800	0.87	31.981	31.231	7.432	7.396
Fe II	6456.3794	58.400	2.00	57.483	55.701	7.723	7.769

HD107328

		EW_{obs} (mÅ)		EW_{calc} (mÅ)		ε_{Fe} (dex)	
el	λ (air)	EW	σEW	nLTE	LTE	nLTE	LTE
Fe I	4793.9614	37.500	0.57	31.188	36.014	7.248	7.150
Fe I	4808.1479	63.400	1.54	56.638	62.308	7.254	7.142
Fe I	4809.9385	42.500	2.30	39.978	45.122	7.170	7.069

HD107328

		EW_{obs} (mÅ)		EW_{calc} (mÅ)		ε_{Fe} (dex)	
el	λ (air)	EW	σEW	nLTE	LTE	nLTE	LTE
Fe I	4873.7510	40.300	1.38	39.586	44.933	7.134	7.031
Fe I	4896.4385	67.400	1.41	58.513	63.879	7.299	7.193
Fe I	4918.0127	75.100	1.37	68.962	75.286	7.243	7.116
Fe I	4961.9136	63.100	1.11	58.994	64.686	7.202	7.088
Fe I	4962.5718	77.600	1.04	76.473	82.229	7.143	7.023
Fe I	4986.2227	70.600	1.28	68.745	74.886	7.157	7.032
Fe I	4999.1123	54.300	1.70	52.643	58.427	7.153	7.039
Fe I	5031.9141	44.400	0.86	44.873	50.761	7.111	6.997
Fe I	5036.9214	64.600	1.28	55.797	61.859	7.290	7.174
Fe I	5088.1533	56.900	1.60	53.300	58.895	7.190	7.081
Fe I	5115.7769	42.400	1.28	39.800	45.176	7.171	7.067
Fe I	5143.7227	81.000	1.75	73.715	80.387	7.273	7.133
Fe I	5267.2695	47.600	1.80	44.142	49.878	7.188	7.076
Fe I	5285.1274	42.800	1.08	37.071	42.464	7.235	7.127
Fe I	5293.9590	51.900	0.94	49.396	55.377	7.168	7.054
Fe I	5294.5474	35.900	0.64	30.416	35.244	7.233	7.133
Fe I	5295.3120	43.700	1.24	41.719	47.462	7.160	7.047
Fe I	5320.0356	50.200	0.55	41.245	46.923	7.287	7.181
Fe I	5326.1426	75.900	0.51	69.670	75.811	7.248	7.122
Fe I	5373.7085	82.800	0.93	82.386	89.550	7.128	6.980
Fe I	5412.7837	35.200	0.67	34.646	39.869	7.132	7.026
Fe I	5417.0332	50.000	0.80	42.558	48.361	7.262	7.151
Fe I	5436.2949	59.400	1.18	51.873	57.894	7.263	7.149
Fe I	5441.3389	50.100	0.64	46.675	52.444	7.186	7.076
Fe I	5466.9873	67.700	0.84	62.039	68.325	7.231	7.108
Fe I	5470.0928	41.400	0.77	34.251	39.597	7.264	7.155
Fe I	5473.1626	35.600	1.42	33.329	38.353	7.167	7.065
Fe I	5483.0986	74.800	0.88	69.349	75.379	7.224	7.108
Fe I	5522.4463	64.700	0.67	62.567	68.604	7.161	7.043
Fe I	5525.5435	79.100	0.56	79.302	85.363	7.116	6.990
Fe I	5539.2798	42.900	0.28	40.606	46.354	7.164	7.055
Fe I	5543.9355	85.200	0.65	82.542	88.469	7.172	7.051
Fe I	5549.9487	25.600	0.58	21.543	25.434	7.222	7.124
Fe I	5552.6919	9.000	0.54	7.939	10.284	7.182	7.054
Fe I	5560.2114	69.200	0.86	67.226	73.713	7.158	7.032
Fe I	5577.0249	14.900	0.28	13.122	17.019	7.189	7.048
Fe I	5584.7646	74.800	0.96	72.030	78.550	7.175	7.045
Fe I	5600.2241	61.500	0.87	60.900	67.144	7.131	7.011
Fe I	5618.6323	73.800	0.52	72.583	78.723	7.144	7.020
Fe I	5622.9453	23.300	0.41	17.421	20.789	7.281	7.185
Fe I	5636.6958	47.400	0.44	43.574	49.516	7.192	7.081
Fe I	5651.4688	29.600	0.38	24.671	28.821	7.235	7.138
Fe I	5652.3174	43.800	0.61	38.801	44.142	7.217	7.113
Fe I	5661.3447	41.700	0.35	42.051	47.677	7.113	7.006
Fe I	5679.0229	73.700	0.51	66.310	74.255	7.264	7.109
Fe I	5691.4971	65.900	1.81	56.650	63.085	7.295	7.174
Fe I	5717.8325	85.600	1.27	81.406	87.722	7.201	7.076
Fe I	5720.8862	31.000	0.76	32.530	37.738	7.087	6.981
Fe I	5731.7617	82.400	0.81	73.301	78.988	7.294	7.189
Fe I	5741.8477	54.000	0.72	48.381	54.300	7.226	7.114
Fe I	5754.4023	42.700	1.94	39.016	44.794	7.191	7.081
Fe I	5759.2622	11.900	0.43	9.146	11.059	7.250	7.157
Fe I	5760.3438	51.400	1.23	50.133	56.520	7.144	7.026
Fe I	5838.3716	46.700	0.59	39.109	44.543	7.263	7.160
Fe I	5849.6831	24.900	0.49	19.025	22.676	7.273	7.175
Fe I	5855.0757	38.300	0.43	36.500	42.245	7.157	7.043
Fe I	5858.7778	31.000	0.52	26.706	31.162	7.217	7.116
Fe I	5861.1084	19.800	0.40	18.368	21.712	7.162	7.067
Fe I	5898.2153	21.500	0.54	19.332	23.180	7.182	7.075
Fe I	5902.4731	25.900	0.79	26.542	31.300	7.104	6.997
Fe I	5905.6714	75.300	1.01	73.136	81.534	7.160	6.998
Fe I	5927.7886	60.400	0.83	58.255	66.124	7.160	7.013
Fe I	5940.9912	40.000	0.77	34.242	39.404	7.235	7.132
Fe I	5952.7178	93.000	1.62	85.305	90.943	7.265	7.161
Fe I	5969.5620	9.800	0.62	7.039	8.501	7.277	7.189
Fe I	6007.9595	80.600	1.02	79.217	86.861	7.146	6.999
Fe I	6034.0352	19.400	0.38	17.208	20.389	7.186	7.092
Fe I	6056.0044	89.700	1.10	87.926	96.728	7.152	6.985
Fe I	6078.4912	90.400	1.01	83.320	92.887	7.251	7.072
Fe I	6079.0078	65.200	0.65	57.763	64.829	7.256	7.127
Fe I	6093.6431	47.600	0.55	40.541	46.814	7.256	7.135
Fe I	6096.6641	67.200	0.71	59.499	65.384	7.259	7.154
Fe I	6127.9063	77.900	1.15	71.012	78.207	7.249	7.114
Fe I	6165.3599	72.100	0.71	67.168	74.301	7.212	7.079
Fe I	6187.9893	79.000	0.95	74.078	79.912	7.210	7.103
Fe I	6226.7344	55.800	0.75	50.304	56.458	7.220	7.108

HD107328

		EW_{obs} (mÅ)		EW_{calc} (mÅ)		ε_{Fe} (dex)	
el	λ (air)	EW	σEW	nLTE	LTE	nLTE	LTE
Fe I	6229.2261	90.900	1.00	82.898	90.500	7.274	7.128
Fe I	6271.2778	61.600	0.64	55.516	62.659	7.230	7.101
Fe I	6290.5430	27.400	0.49	20.243	24.687	7.292	7.182
Fe I	6315.8110	70.400	0.87	63.574	70.559	7.246	7.117
Fe I	6338.8760	56.800	0.46	51.006	58.695	7.228	7.084
Fe I	6495.7412	55.300	1.47	55.086	63.463	7.124	6.972
Fe I	6496.4658	82.300	1.09	74.066	82.663	7.267	7.113
Fe I	6533.9282	54.600	0.44	46.520	53.227	7.268	7.145
Fe I	6569.2139	94.700	1.36	88.570	96.481	7.223	7.088
Fe I	6591.3130	17.500	0.28	14.750	17.836	7.212	7.110
Fe I	6597.5591	57.500	0.46	51.834	59.104	7.223	7.091
Fe I	6633.7485	84.600	0.99	77.610	85.005	7.241	7.113
Fe I	6699.1411	15.900	0.28	13.821	16.753	7.194	7.092
Fe I	6746.9536	27.100	0.36	21.088	25.780	7.263	7.150
Fe I	6786.8584	47.000	0.66	39.451	45.087	7.259	7.155
Fe I	6804.2710	25.800	0.38	23.761	28.287	7.171	7.062
Fe I	6810.2622	68.800	0.92	64.371	71.683	7.198	7.068
Fe II	4993.3501	49.300	1.57	55.600	53.616	6.979	7.020
Fe II	5000.7305	15.000	1.05	15.370	14.822	7.106	7.127
Fe II	5100.6548	36.700	1.73	32.912	31.677	7.212	7.245
Fe II	5256.9321	25.500	0.61	29.432	28.327	7.014	7.041
Fe II	5284.1030	69.300	1.98	73.492	70.597	7.028	7.090
Fe II	5534.8379	69.000	4.23	69.136	66.413	7.117	7.178
Fe II	6084.1016	27.300	0.36	26.380	25.268	7.146	7.178
Fe II	6113.3193	16.800	0.81	14.752	14.144	7.198	7.224
Fe II	6149.2461	34.000	0.42	35.591	34.321	7.079	7.111
Fe II	6238.3857	40.800	0.70	45.468	43.719	7.009	7.048
Fe II	6247.5571	45.500	0.68	52.621	50.549	6.958	7.000
Fe II	6456.3794	55.200	0.75	63.470	60.737	6.942	6.995
Fe II	6516.0767	63.600	2.32	69.014	65.231	7.012	7.086

β Gem

		EW_{obs} (mÅ)		EW_{calc} (mÅ)		ε_{Fe} (dex)	
el	λ (air)	EW	σEW	nLTE	LTE	nLTE	LTE
Fe I	4779.4390	78.900	7.98	87.227	90.111	7.389	7.319
Fe I	4793.9614	30.800	1.74	39.900	42.857	7.391	7.337
Fe I	4794.3540	53.500	4.05	50.459	54.141	7.638	7.568
Fe I	4799.4058	72.000	4.50	71.120	74.161	7.599	7.532
Fe I	4808.1479	67.300	2.44	65.691	68.858	7.614	7.547
Fe I	4809.9385	50.600	4.09	50.968	53.934	7.573	7.514
Fe I	4869.4634	61.000	4.65	57.023	60.024	7.664	7.600
Fe I	4874.3530	54.600	6.03	56.367	59.648	7.544	7.478
Fe I	4917.2300	96.700	2.90	92.561	96.018	7.667	7.595
Fe I	4918.0127	79.700	3.12	82.672	86.027	7.519	7.448
Fe I	4935.4141	13.200	1.48	13.355	14.644	7.574	7.526
Fe I	4961.9136	70.500	1.85	69.559	72.684	7.600	7.533
Fe I	4962.5718	79.900	1.79	89.585	92.738	7.381	7.313
Fe I	4979.5859	46.200	2.74	44.794	47.755	7.608	7.550
Fe I	4992.7852	20.100	1.64	26.972	29.127	7.402	7.355
Fe I	4999.1123	62.800	4.95	65.615	68.779	7.521	7.455
Fe I	5023.1860	68.300	2.86	67.696	70.960	7.593	7.524
Fe I	5031.9141	53.700	2.22	59.320	62.706	7.466	7.401
Fe I	5036.9214	55.100	3.45	64.247	67.700	7.395	7.329
Fe I	5058.4966	26.300	3.08	36.889	39.623	7.349	7.300
Fe I	5109.6519	95.300	3.54	92.663	96.223	7.634	7.561
Fe I	5115.7769	42.700	1.67	50.972	54.110	7.416	7.359
Fe I	5159.0576	95.500	4.26	103.568	107.547	7.430	7.349
Fe I	5228.3760	86.100	4.00	83.108	86.301	7.641	7.576
Fe I	5243.7764	82.500	3.43	92.497	95.555	7.377	7.309
Fe I	5253.0210	61.000	2.66	62.139	66.317	7.558	7.477
Fe I	5267.2695	56.600	3.79	58.614	61.960	7.540	7.473
Fe I	5285.1274	51.000	2.73	51.707	54.949	7.566	7.502
Fe I	5293.9590	54.600	2.16	62.686	66.055	7.418	7.354
Fe I	5294.5474	47.100	2.15	41.564	44.644	7.686	7.626
Fe I	5295.3120	48.800	2.95	56.420	59.830	7.428	7.366
Fe I	5315.0698	65.600	1.36	61.229	64.519	7.667	7.602
Fe I	5320.0356	50.400	3.78	52.911	56.288	7.531	7.467
Fe I	5326.1426	78.200	3.78	79.501	82.986	7.552	7.476
Fe I	5373.7085	92.600	2.44	98.587	102.481	7.465	7.385
Fe I	5379.5737	98.500	1.72	100.102	103.518	7.545	7.471
Fe I	5386.3330	59.600	2.26	68.036	71.391	7.414	7.349
Fe I	5398.2793	94.500	1.84	104.992	108.800	7.385	7.304
Fe I	5406.7749	63.300	2.78	58.078	61.264	7.682	7.620
Fe I	5409.1333	82.800	3.33	79.777	83.101	7.640	7.574
Fe I	5412.7837	42.800	1.07	49.199	52.395	7.453	7.395
Fe I	5417.0332	54.900	2.57	57.509	60.856	7.529	7.465

β Gem

		EW_{obs} (mÅ)		EW_{calc} (mÅ)		ε_{Fe} (dex)	
el	λ (air)	EW	σEW	nLTE	LTE	nLTE	LTE
Fe I	5436.2949	68.100	2.25	66.629	69.915	7.609	7.544
Fe I	5436.5879	106.200	3.09	109.957	115.259	7.500	7.389
Fe I	5460.8726	35.700	1.28	40.948	44.316	7.475	7.413
Fe I	5466.9873	74.000	5.41	72.485	76.060	7.612	7.537
Fe I	5470.0928	46.200	2.00	48.933	52.223	7.526	7.464
Fe I	5473.1626	49.100	3.22	46.837	49.933	7.624	7.564
Fe I	5483.0986	80.600	2.81	82.485	85.565	7.543	7.479
Fe I	5487.1450	63.900	3.29	65.523	68.899	7.548	7.482
Fe I	5491.8315	30.500	2.21	29.715	32.159	7.598	7.544
Fe I	5536.5801	30.900	0.74	40.842	44.345	7.380	7.320
Fe I	5539.2798	47.700	1.32	52.338	55.738	7.490	7.427
Fe I	5543.1470	93.800	2.46	96.241	99.835	7.525	7.442
Fe I	5543.9355	87.500	2.07	95.763	98.623	7.415	7.346
Fe I	5546.5059	83.400	3.66	79.088	82.469	7.668	7.599
Fe I	5549.9487	36.700	1.28	31.246	33.926	7.693	7.637
Fe I	5560.2114	80.700	2.11	82.360	85.702	7.548	7.481
Fe I	5584.7646	82.100	2.08	82.386	86.178	7.574	7.494
Fe I	5622.9453	30.600	1.23	25.910	28.317	7.685	7.630
Fe I	5636.6958	49.500	1.75	55.353	58.886	7.467	7.402
Fe I	5638.2622	102.700	1.55	113.213	115.406	7.381	7.325
Fe I	5650.7056	52.800	1.03	53.568	60.460	7.564	7.438
Fe I	5651.4688	37.500	1.34	37.867	40.630	7.572	7.517
Fe I	5652.3174	52.400	1.28	52.821	55.895	7.572	7.512
Fe I	5655.1763	72.800	1.97	67.314	76.493	7.695	7.512
Fe I	5661.3447	54.900	0.69	56.281	59.431	7.553	7.491
Fe I	5679.0229	83.800	1.50	83.172	87.642	7.592	7.504
Fe I	5680.2402	30.200	0.95	25.969	28.227	7.677	7.624
Fe I	5691.4971	72.500	2.43	70.758	74.170	7.615	7.546
Fe I	5696.0894	37.800	1.49	42.747	45.915	7.480	7.420
Fe I	5698.0200	51.900	9.06	51.896	55.444	7.580	7.513
Fe I	5705.4644	67.500	1.58	75.843	79.003	7.415	7.348
Fe I	5717.8325	86.500	1.02	95.210	98.357	7.408	7.336
Fe I	5720.8862	38.800	1.82	47.501	50.749	7.408	7.350
Fe I	5754.4023	48.100	3.09	50.856	54.391	7.527	7.461
Fe I	5760.3438	54.600	2.96	61.886	65.627	7.439	7.370
Fe I	5849.6831	31.100	2.06	28.150	30.731	7.645	7.588
Fe I	5855.0757	49.200	1.77	52.136	55.701	7.523	7.456
Fe I	5858.7778	36.200	2.25	39.380	42.299	7.515	7.458
Fe I	5859.5864	104.700	3.05	113.539	117.051	7.429	7.358
Fe I	5861.1084	28.400	2.25	29.145	31.542	7.563	7.510
Fe I	5881.2798	32.000	2.54	38.692	41.649	7.439	7.383
Fe I	5883.8164	106.400	3.39	104.640	107.433	7.613	7.560
Fe I	5902.4731	31.000	1.27	40.587	43.830	7.378	7.321
Fe I	5905.6714	83.900	2.40	90.742	95.217	7.453	7.362
Fe I	5929.6763	67.600	1.83	65.014	68.508	7.629	7.563
Fe I	5930.1797	115.200	3.31	119.023	123.340	7.518	7.443
Fe I	5934.6543	111.700	4.32	119.231	121.293	7.451	7.408
Fe I	5952.7178	103.800	4.82	98.955	101.806	7.671	7.619
Fe I	5976.7769	106.000	2.59	107.919	110.121	7.545	7.502
Fe I	5984.8149	112.500	6.45	115.630	120.952	7.529	7.439
Fe I	6003.0112	118.600	2.82	121.088	123.182	7.538	7.499
Fe I	6007.9595	87.700	4.08	96.356	100.371	7.423	7.340
Fe I	6015.2437	31.800	1.95	42.351	46.642	7.376	7.307
Fe I	6027.0508	102.000	3.05	105.889	109.843	7.508	7.432
Fe I	6093.6431	62.000	1.31	56.634	60.442	7.682	7.609
Fe I	6096.6641	77.000	2.40	73.045	76.168	7.655	7.596
Fe I	6120.2466	42.600	2.93	43.112	49.047	7.571	7.469
Fe I	6127.9063	78.500	2.82	85.206	89.221	7.452	7.373
Fe I	6139.6440	16.100	1.26	19.225	21.601	7.484	7.420
Fe I	6151.6172	111.300	4.45	105.749	112.022	7.691	7.566
Fe I	6157.7280	106.600	2.28	102.179	106.215	7.662	7.587
Fe I	6165.3599	80.200	2.62	81.362	85.375	7.558	7.480
Fe I	6180.2026	110.900	4.42	108.347	113.930	7.630	7.520
Fe I	6187.3979	22.400	1.61	21.882	24.395	7.593	7.530
Fe I	6187.9893	91.200	1.54	87.366	90.347	7.652	7.597
Fe I	6220.7798	58.900	1.18	67.157	70.617	7.426	7.363
Fe I	6226.7344	67.000	1.00	63.640	67.202	7.643	7.576
Fe I	6229.2261	87.900	2.44	90.346	95.302	7.531	7.433
Fe I	6232.6401	118.600	2.38	128.719	132.291	7.413	7.348
Fe I	6240.6460	99.400	4.68	105.188	111.192	7.458	7.336
Fe I	6253.8286	48.000	1.39	54.943	58.637	7.448	7.381
Fe I	6270.2236	102.600	2.86	106.659	111.919	7.499	7.394
Fe I	6271.2778	59.200	1.68	66.507	70.903	7.444	7.368
Fe I	6290.5430	28.500	2.17	26.298	29.383	7.629	7.561
Fe I	6293.9243	28.000	0.90	28.007	30.575	7.580	7.522
Fe I	6311.4995	72.100	1.63	74.489	79.244	7.534	7.445
Fe I	6315.8110	76.600	2.65	77.472	81.464	7.563	7.485

β Gem

		EW_{obs} (mÅ)		EW_{calc} (mÅ)		ε_{Fe} (dex)	
el	λ (air)	EW	σEW	nLTE	LTE	nLTE	LTE
Fe I	6338.8760	63.000	4.61	68.803	73.117	7.471	7.389
Fe I	6380.7432	79.600	5.01	84.540	88.803	7.487	7.404
Fe I	6475.6240	105.700	2.03	101.342	107.354	7.669	7.547
Fe I	6481.8696	117.300	1.86	118.459	125.486	7.558	7.430
Fe I	6495.7412	67.300	3.75	73.663	78.532	7.464	7.375
Fe I	6496.4658	91.300	2.52	93.157	97.751	7.547	7.462
Fe I	6518.3657	107.300	4.28	113.624	119.604	7.464	7.356
Fe I	6569.2139	109.800	2.91	109.120	113.195	7.591	7.524
Fe I	6574.2266	89.400	3.18	94.145	102.332	7.487	7.338
Fe I	6581.2090	73.500	5.35	79.649	86.575	7.465	7.347
Fe I	6591.3130	29.300	2.22	25.242	27.647	7.675	7.618
Fe I	6597.5591	67.800	1.61	69.915	73.984	7.542	7.466
Fe I	6608.0249	68.300	2.12	68.928	74.517	7.569	7.470
Fe I	6633.7485	88.600	1.33	95.168	98.927	7.467	7.395
Fe I	6667.4180	33.400	1.65	39.118	43.320	7.469	7.395
Fe I	6667.7104	27.300	1.26	23.830	26.129	7.664	7.608
Fe I	6699.1411	21.300	1.53	23.900	26.206	7.511	7.455
Fe I	6703.5659	90.500	1.51	85.042	90.470	7.686	7.581
Fe I	6710.3179	77.500	3.15	75.721	82.665	7.613	7.488
Fe I	6725.3560	45.800	3.24	52.450	55.857	7.458	7.398
Fe I	6739.5205	62.000	1.92	69.303	75.907	7.451	7.346
Fe I	6745.9556	27.200	2.34	32.357	35.324	7.465	7.405
Fe I	6746.9536	28.200	1.26	27.470	30.761	7.596	7.526
Fe I	6750.1514	131.900	3.75	128.010	134.747	7.656	7.524
Fe I	6752.7065	69.600	13.08	66.635	70.142	7.635	7.570
Fe I	6786.8584	53.100	2.96	54.352	57.699	7.557	7.497
Fe I	6796.1235	50.000	0.76	52.877	56.735	7.526	7.457
Fe II	4993.3501	57.700	3.53	62.180	60.901	7.477	7.505
Fe II	5100.6548	34.800	3.63	39.531	38.718	7.464	7.483
Fe II	5256.9321	28.200	1.81	36.137	35.394	7.377	7.392
Fe II	5264.8022	55.400	3.07	65.875	64.520	7.342	7.367
Fe II	5284.1030	78.200	7.02	80.116	78.238	7.536	7.579
Fe II	5534.8379	67.600	1.52	77.248	75.438	7.366	7.401
Fe II	6149.2461	47.700	1.93	45.433	44.499	7.634	7.658
Fe II	6247.5571	61.700	0.52	63.354	61.869	7.543	7.576
Fe II	6369.4590	34.000	2.28	38.273	37.158	7.478	7.503
Fe II	6416.9189	56.700	1.26	60.976	65.145	7.499	7.422
Fe II	6416.9189	56.700	1.26	43.516	42.579	7.499	7.422
Fe II	6456.3794	69.200	1.61	74.652	72.760	7.464	7.502
Fe II	6516.0767	79.800	5.35	76.680	74.159	7.644	7.699

ϵ Vir

		EW_{obs} (mÅ)		EW_{calc} (mÅ)		ε_{Fe} (dex)	
el	λ (air)	EW	σEW	nLTE	LTE	nLTE	LTE
Fe I	4793.9614	29.300	0.83	35.075	39.103	7.469	7.388
Fe I	4794.3540	43.800	1.14	44.072	49.078	7.594	7.494
Fe I	4799.4058	70.800	1.17	65.594	69.855	7.721	7.622
Fe I	4802.5234	30.300	1.81	25.372	29.163	7.723	7.627
Fe I	4808.1479	60.900	1.62	59.984	64.430	7.620	7.522
Fe I	4809.9385	45.400	1.89	46.221	50.405	7.582	7.495
Fe I	4869.4634	56.300	1.78	52.136	56.363	7.692	7.599
Fe I	4874.3530	50.400	2.46	50.754	55.288	7.592	7.497
Fe I	4877.6045	59.000	4.75	51.748	56.370	7.753	7.656
Fe I	4961.9136	63.600	1.01	64.070	68.524	7.589	7.490
Fe I	4986.2227	77.500	1.56	76.565	81.021	7.620	7.522
Fe I	4992.7852	20.800	1.08	24.504	27.471	7.499	7.426
Fe I	4999.1123	62.500	2.03	60.959	65.407	7.634	7.535
Fe I	5023.1860	64.100	1.42	62.929	67.376	7.626	7.528
Fe I	5023.4976	61.300	0.97	53.377	57.767	7.770	7.676
Fe I	5025.3027	37.100	2.30	38.930	42.827	7.560	7.478
Fe I	5031.9141	51.000	1.24	54.992	59.580	7.514	7.419
Fe I	5036.9214	57.500	1.26	58.242	63.101	7.584	7.480
Fe I	5058.4966	30.200	1.31	33.062	36.817	7.534	7.454
Fe I	5088.1533	63.900	1.05	61.686	65.974	7.648	7.555
Fe I	5104.4375	63.300	0.79	58.934	63.506	7.694	7.596
Fe I	5115.7769	50.100	0.73	46.207	50.610	7.681	7.589
Fe I	5180.0557	75.200	0.76	68.935	74.605	7.740	7.613
Fe I	5197.9360	57.800	1.90	60.925	65.652	7.534	7.436
Fe I	5236.2021	66.400	3.91	68.518	73.203	7.554	7.451
Fe I	5253.0210	55.300	1.22	55.003	60.777	7.606	7.490
Fe I	5267.2695	56.500	2.62	54.380	58.980	7.645	7.548
Fe I	5285.1274	53.900	0.73	47.900	52.407	7.726	7.631
Fe I	5293.9590	58.900	1.33	58.100	62.811	7.617	7.517
Fe I	5294.5474	35.600	1.02	37.360	41.557	7.562	7.477
Fe I	5295.3120	52.400	1.24	52.331	57.005	7.601	7.504

ϵ Vir

		EW_{obs} (mÅ)		EW_{calc} (mÅ)		ε_{Fe} (dex)	
el	λ (air)	EW	σEW	nLTE	LTE	nLTE	LTE
Fe I	5320.0356	50.600	0.60	48.123	52.766	7.651	7.556
Fe I	5326.1426	77.200	1.71	73.488	78.429	7.685	7.572
Fe I	5401.2666	51.600	0.70	46.545	50.925	7.706	7.614
Fe I	5406.7749	61.700	0.85	53.939	58.439	7.760	7.668
Fe I	5412.7837	40.800	0.34	45.548	49.998	7.499	7.412
Fe I	5417.0332	57.800	1.36	53.426	58.009	7.690	7.596
Fe I	5436.2949	68.000	0.54	62.047	66.646	7.724	7.629
Fe I	5441.3389	56.700	0.47	56.714	61.246	7.600	7.506
Fe I	5452.0884	36.600	0.81	35.490	39.654	7.624	7.536
Fe I	5466.9873	72.700	0.45	66.752	71.776	7.732	7.621
Fe I	5470.0928	50.800	0.71	45.334	49.818	7.712	7.620
Fe I	5472.7085	76.300	0.58	68.410	72.854	7.768	7.677
Fe I	5473.1626	45.100	0.83	43.085	47.346	7.642	7.554
Fe I	5483.0986	78.100	0.83	76.994	81.475	7.623	7.527
Fe I	5487.1450	67.300	1.62	61.042	65.707	7.729	7.633
Fe I	5494.4624	55.100	1.46	46.552	51.044	7.776	7.684
Fe I	5522.4463	69.600	0.76	70.781	75.139	7.575	7.479
Fe I	5528.8979	40.700	2.02	33.932	37.702	7.744	7.662
Fe I	5539.2798	44.600	0.32	47.549	52.309	7.539	7.445
Fe I	5549.9487	32.500	0.34	27.869	31.526	7.706	7.622
Fe I	5552.6919	19.200	0.30	14.473	17.209	7.759	7.662
Fe I	5560.2114	76.900	0.71	76.912	81.648	7.600	7.500
Fe I	5577.0249	22.700	0.53	22.840	27.094	7.596	7.487
Fe I	5584.7646	73.200	0.56	76.090	81.380	7.537	7.422
Fe I	5587.5742	67.400	0.89	60.124	64.999	7.753	7.651
Fe I	5600.2241	71.500	0.87	69.684	74.211	7.638	7.541
Fe I	5618.6323	79.100	1.09	80.020	84.498	7.580	7.480
Fe I	5619.5952	62.900	0.53	54.445	59.179	7.773	7.676
Fe I	5622.9453	25.900	0.39	22.905	26.177	7.676	7.593
Fe I	5636.6958	48.500	0.41	50.404	55.328	7.561	7.462
Fe I	5651.4688	37.200	0.68	34.960	38.801	7.649	7.566
Fe I	5652.3174	50.500	0.56	48.915	53.226	7.633	7.544
Fe I	5661.3447	48.500	0.37	52.237	56.656	7.523	7.434
Fe I	5679.0229	83.000	0.60	77.525	83.540	7.713	7.589
Fe I	5691.4971	72.900	1.84	65.971	70.784	7.746	7.646
Fe I	5698.0200	41.800	3.90	47.103	51.990	7.491	7.398
Fe I	5741.8477	60.900	0.81	58.089	62.663	7.658	7.563
Fe I	5742.9600	33.200	1.91	26.814	30.196	7.746	7.667
Fe I	5754.4023	45.100	1.75	46.121	51.019	7.579	7.482
Fe I	5760.3438	60.500	2.35	56.618	61.810	7.680	7.573
Fe I	5838.3716	53.200	0.73	47.832	52.447	7.707	7.615
Fe I	5849.6831	26.500	0.56	25.020	28.529	7.637	7.552
Fe I	5853.1484	42.200	1.27	40.054	46.847	7.642	7.513
Fe I	5855.0757	47.900	0.79	48.527	53.444	7.587	7.488
Fe I	5858.7778	37.300	0.64	36.101	40.157	7.626	7.540
Fe I	5861.1084	24.800	0.33	26.609	29.931	7.554	7.476
Fe I	5880.0273	29.100	1.00	33.836	37.721	7.491	7.411
Fe I	5881.2798	36.500	0.50	35.900	39.978	7.613	7.527
Fe I	5898.2153	32.400	0.70	29.753	33.619	7.662	7.573
Fe I	5905.6714	85.800	1.50	84.749	90.641	7.621	7.500
Fe I	5927.7886	72.500	0.96	70.348	76.299	7.643	7.523
Fe I	5940.9912	52.700	0.61	43.913	48.416	7.777	7.686
Fe I	5969.5620	13.600	0.36	11.177	12.862	7.701	7.629
Fe I	6007.9595	93.300	2.79	90.380	95.945	7.655	7.547
Fe I	6034.0352	25.300	0.55	25.383	28.617	7.598	7.520
Fe I	6054.0732	27.800	0.36	21.957	24.810	7.747	7.673
Fe I	6079.0078	76.500	1.13	70.026	75.216	7.726	7.626
Fe I	6082.7100	87.100	1.33	79.266	86.441	7.771	7.614
Fe I	6093.6431	58.800	0.84	52.814	58.037	7.720	7.615
Fe I	6096.6641	71.900	0.88	67.587	72.208	7.686	7.594
Fe I	6098.2441	41.600	0.72	33.092	37.016	7.779	7.695
Fe I	6120.2466	35.400	0.67	34.347	41.785	7.621	7.479
Fe I	6127.9063	85.400	1.23	79.136	84.819	7.728	7.612
Fe I	6165.3599	78.900	0.93	75.532	81.217	7.669	7.552
Fe I	6187.3979	20.300	0.81	18.490	21.753	7.653	7.560
Fe I	6187.9893	83.300	1.21	80.989	85.612	7.646	7.553
Fe I	6199.5063	22.600	0.36	19.432	23.024	7.687	7.589
Fe I	6226.7344	60.700	0.93	58.512	63.531	7.643	7.544
Fe I	6229.2261	87.200	0.77	82.673	89.376	7.696	7.554
Fe I	6240.6460	98.200	1.87	95.986	103.881	7.649	7.476
Fe I	6270.2236	98.900	1.24	98.103	105.148	7.617	7.469
Fe I	6271.2778	61.100	1.13	60.446	66.497	7.613	7.496
Fe I	6290.5430	23.500	0.32	22.083	26.041	7.637	7.538
Fe I	6293.9243	33.900	0.87	26.075	29.631	7.782	7.695
Fe I	6311.4995	70.700	0.57	67.455	73.964	7.666	7.536
Fe I	6315.8110	76.100	1.13	71.844	77.502	7.687	7.571
Fe I	6338.8760	70.000	0.76	64.471	70.306	7.709	7.594

ϵ Vir

		EW_{obs} (mÅ)		EW_{calc} (mÅ)		ε_{Fe} (dex)	
el	λ (air)	EW	σEW	nLTE	LTE	nLTE	LTE
Fe I	6495.7412	79.200	2.50	69.036	75.614	7.793	7.670
Fe I	6496.4658	94.400	1.50	87.236	93.400	7.733	7.620
Fe I	6533.9282	67.300	0.40	58.832	64.227	7.763	7.660
Fe I	6574.2266	87.600	1.05	83.190	93.682	7.691	7.480
Fe I	6581.2090	74.300	0.78	70.044	79.056	7.684	7.510
Fe I	6591.3130	24.700	0.36	23.278	26.634	7.637	7.552
Fe I	6597.5591	68.900	0.71	65.655	71.287	7.662	7.554
Fe I	6608.0249	59.300	0.46	61.062	68.532	7.566	7.432
Fe I	6627.5439	56.800	0.31	47.998	52.629	7.770	7.681
Fe I	6633.7485	96.400	1.32	89.221	94.714	7.728	7.632
Fe I	6667.4180	29.300	0.15	33.313	38.826	7.513	7.407
Fe I	6667.7104	25.800	0.20	21.965	25.160	7.700	7.616
Fe I	6699.1411	21.400	0.41	22.034	25.268	7.582	7.498
Fe I	6703.5659	82.200	1.10	77.317	84.685	7.699	7.551
Fe I	6710.3179	68.100	1.53	66.152	75.173	7.637	7.471
Fe I	6713.7427	42.400	0.19	33.657	38.031	7.782	7.689
Fe I	6746.9536	20.300	0.19	23.123	27.364	7.524	7.423
Fe I	6752.7065	66.200	1.18	62.572	67.499	7.670	7.574
Fe I	6786.8584	53.500	0.75	50.145	54.984	7.664	7.572
Fe I	6804.2710	34.600	0.77	34.729	39.153	7.597	7.504
Fe II	4993.3501	61.000	1.86	67.052	65.931	7.453	7.478
Fe II	5000.7305	30.100	1.31	24.536	24.102	7.750	7.763
Fe II	5100.6548	43.000	0.36	45.144	44.346	7.548	7.567
Fe II	5132.6611	43.700	0.65	49.575	48.698	7.460	7.479
Fe II	5136.7949	31.600	0.72	36.711	36.062	7.470	7.485
Fe II	5256.9321	42.300	0.72	41.856	41.116	7.611	7.629
Fe II	5264.8022	69.800	1.08	71.181	69.991	7.567	7.595
Fe II	5325.5522	70.700	0.78	70.386	69.209	7.608	7.636
Fe II	5414.0698	46.800	0.74	52.312	51.387	7.468	7.488
Fe II	5425.2485	62.500	0.77	68.937	67.718	7.448	7.474
Fe II	5427.8159	6.300	0.63	7.451	7.429	7.504	7.506
Fe II	5525.1172	33.700	1.09	33.841	33.275	7.596	7.611
Fe II	6084.1016	46.900	0.37	40.092	39.267	7.759	7.781
Fe II	6113.3193	31.100	0.76	25.402	24.904	7.754	7.771
Fe II	6149.2461	58.900	0.62	52.447	51.520	7.750	7.775
Fe II	6238.3857	69.400	0.69	63.038	61.863	7.745	7.775
Fe II	6247.5571	75.900	1.26	70.302	68.924	7.727	7.761
Fe II	6369.4590	40.600	0.52	44.849	43.755	7.502	7.525
Fe II	6416.9189	61.400	0.38	57.238	62.899	7.682	7.570
Fe II	6416.9189	61.400	0.38	50.693	49.748	7.682	7.570
Fe II	6456.3794	86.800	1.08	81.426	79.751	7.719	7.759
Fe II	6516.0767	85.900	1.00	82.555	80.463	7.672	7.721

ξ Hya

		EW_{obs} (mÅ)		EW_{calc} (mÅ)		ε_{Fe} (dex)	
el	λ (air)	EW	σEW	nLTE	LTE	nLTE	LTE
Fe I	4793.9614	28.700	0.92	34.434	38.218	7.485	7.363
Fe I	4794.3540	41.800	1.31	43.459	48.234	7.578	7.429
Fe I	4799.4058	67.900	1.21	68.135	72.330	7.605	7.466
Fe I	4802.5234	29.600	1.87	25.403	28.867	7.710	7.638
Fe I	4808.1479	57.500	1.80	61.647	66.003	7.527	7.372
Fe I	4809.9385	42.600	2.00	46.724	50.732	7.528	7.399
Fe I	4869.4634	53.000	2.15	53.272	57.405	7.605	7.479
Fe I	4874.3530	47.100	2.46	51.336	55.739	7.527	7.380
Fe I	4961.9136	60.000	0.95	66.394	70.707	7.482	7.333
Fe I	4962.5718	78.400	1.41	87.605	91.829	7.424	7.311
Fe I	4986.2227	73.000	1.34	80.208	84.608	7.467	7.329
Fe I	4992.7852	17.700	1.33	24.195	26.913	7.429	7.339
Fe I	4999.1123	59.300	1.69	63.326	67.656	7.529	7.377
Fe I	5023.1860	60.900	1.52	65.496	69.825	7.519	7.371
Fe I	5023.4976	58.100	0.87	55.057	59.329	7.670	7.571
Fe I	5031.9141	49.100	1.17	56.884	61.364	7.457	7.317
Fe I	5036.9214	54.700	1.31	59.524	64.281	7.516	7.347
Fe I	5058.4966	29.300	1.04	32.716	36.230	7.535	7.419
Fe I	5088.1533	59.900	1.21	64.012	68.170	7.529	7.390
Fe I	5104.4375	60.300	0.89	61.109	65.568	7.594	7.453
Fe I	5115.7769	48.500	0.55	46.682	50.907	7.645	7.540
Fe I	5180.0557	70.200	0.90	72.276	77.716	7.568	7.351
Fe I	5197.9360	53.800	2.04	63.213	67.825	7.430	7.305
Fe I	5236.2021	63.700	3.39	71.531	76.097	7.455	7.314
Fe I	5253.0210	52.300	1.27	55.212	60.806	7.556	7.357
Fe I	5267.2695	55.600	2.65	56.177	60.601	7.599	7.463
Fe I	5285.1274	49.400	0.83	49.141	53.414	7.615	7.494

ξ Hya

		EW_{obs} (mÅ)		EW_{calc} (mÅ)		ε_{Fe} (dex)	
el	λ (air)	EW	σEW	nLTE	LTE	nLTE	LTE
Fe I	5293.9590	54.800	1.08	60.080	64.672	7.507	7.351
Fe I	5294.5474	34.200	0.81	37.163	41.110	7.550	7.426
Fe I	5295.3120	47.900	0.96	53.970	58.472	7.492	7.343
Fe I	5320.0356	48.300	0.71	48.745	53.215	7.602	7.472
Fe I	5326.1426	74.000	1.49	76.709	81.519	7.554	7.369
Fe I	5401.2666	48.800	0.78	47.575	51.768	7.634	7.524
Fe I	5406.7749	58.300	1.07	55.598	59.912	7.661	7.563
Fe I	5412.7837	39.100	0.31	46.551	50.820	7.463	7.334
Fe I	5417.0332	53.400	1.64	55.070	59.535	7.578	7.441
Fe I	5432.9478	80.100	1.22	86.459	91.491	7.487	7.326
Fe I	5436.2949	60.400	3.62	64.464	68.945	7.533	7.387
Fe I	5441.3389	51.500	0.62	58.594	63.004	7.475	7.338
Fe I	5452.0884	36.800	1.09	35.229	39.143	7.642	7.541
Fe I	5460.8726	25.400	0.56	35.378	39.661	7.393	7.302
Fe I	5461.5493	47.500	0.65	41.580	45.492	7.724	7.670
Fe I	5466.9873	66.100	0.42	69.265	74.160	7.547	7.367
Fe I	5470.0928	43.200	1.26	46.316	50.619	7.549	7.413
Fe I	5487.1450	60.900	1.10	63.375	67.926	7.563	7.419
Fe I	5491.8315	27.600	1.09	26.733	29.803	7.630	7.541
Fe I	5494.4624	51.800	1.03	47.421	51.713	7.694	7.613
Fe I	5528.8979	29.900	2.29	34.135	37.677	7.518	7.402
Fe I	5539.2798	39.700	0.30	48.147	52.735	7.447	7.316
Fe I	5543.9355	85.300	0.72	94.372	98.407	7.434	7.322
Fe I	5546.5059	79.700	1.28	77.335	81.836	7.656	7.542
Fe I	5549.9487	28.900	0.40	27.349	30.695	7.645	7.553
Fe I	5552.6919	15.800	0.42	14.400	16.842	7.660	7.555
Fe I	5560.2114	71.300	0.62	80.651	85.255	7.434	7.312
Fe I	5573.1021	71.400	2.91	83.091	87.556	7.392	7.301
Fe I	5636.6958	40.300	0.17	51.248	56.009	7.402	7.298
Fe I	5651.4688	33.700	1.15	35.241	38.854	7.578	7.466
Fe I	5652.3174	46.400	0.91	50.057	54.233	7.540	7.411
Fe I	5653.8652	59.700	0.98	54.317	58.785	7.710	7.638
Fe I	5655.1763	71.600	0.92	65.841	76.559	7.728	8.158
Fe I	5661.3447	44.500	0.73	53.694	57.985	7.436	7.319
Fe I	5680.2402	19.900	0.43	23.162	25.996	7.521	7.413
Fe I	5691.4971	65.800	1.81	68.780	73.483	7.553	7.396
Fe I	5741.8477	50.600	1.61	60.081	64.465	7.432	7.314
Fe I	5742.9600	27.700	2.10	26.541	29.622	7.637	7.549
Fe I	5754.4023	50.100	1.78	46.566	51.228	7.676	7.576
Fe I	5838.3716	50.500	0.54	48.613	53.013	7.645	7.539
Fe I	5848.1265	76.300	1.08	72.167	77.516	7.687	7.568
Fe I	5849.6831	26.200	0.46	24.433	27.608	7.653	7.563
Fe I	5853.1484	41.900	1.26	38.339	44.632	7.675	7.510
Fe I	5855.0757	46.500	0.66	49.901	54.596	7.545	7.392
Fe I	5858.7778	36.400	0.49	36.289	40.098	7.612	7.505
Fe I	5861.1084	24.300	0.35	26.382	29.411	7.559	7.454
Fe I	5873.2124	46.800	0.69	40.976	44.930	7.719	7.663
Fe I	5879.4868	24.800	1.30	19.114	21.476	7.760	7.735
Fe I	5881.2798	39.700	0.66	36.314	40.126	7.678	7.597
Fe I	5898.2153	37.800	1.59	29.967	33.558	7.773	7.752
Fe I	5902.4731	30.300	0.65	38.199	42.396	7.442	7.319
Fe I	5905.6714	81.600	1.25	89.293	95.094	7.471	7.305
Fe I	5909.9722	74.100	0.81	74.450	80.313	7.603	7.389
Fe I	5927.7886	64.400	1.35	73.639	79.352	7.441	7.294
Fe I	5929.6763	68.600	0.83	63.073	67.820	7.712	7.634
Fe I	5940.9912	49.300	0.77	44.615	48.920	7.699	7.621
Fe I	6007.9595	88.600	2.50	95.245	100.469	7.491	7.341
Fe I	6015.2437	25.300	0.30	34.623	39.842	7.410	7.295
Fe I	6034.0352	24.700	0.37	25.117	28.064	7.600	7.504
Fe I	6054.0732	26.600	0.33	21.657	24.252	7.732	7.692
Fe I	6079.0078	72.000	1.01	73.220	78.227	7.588	7.441
Fe I	6082.7100	82.800	1.17	81.921	88.948	7.627	7.283
Fe I	6093.6431	55.700	0.70	54.546	59.548	7.631	7.494
Fe I	6096.6641	68.700	0.82	70.128	74.525	7.584	7.458
Fe I	6098.2441	39.700	0.70	33.346	37.010	7.738	7.693
Fe I	6120.2466	35.100	0.60	32.012	38.662	7.670	7.457
Fe I	6127.9063	79.700	1.07	82.925	88.406	7.550	7.361
Fe I	6151.6172	93.200	1.66	100.239	108.249	7.472	7.191
Fe I	6165.3599	74.400	0.78	79.010	84.503	7.524	7.335
Fe I	6187.3979	20.500	0.90	17.474	20.319	7.697	7.618
Fe I	6187.9893	79.400	1.04	84.706	89.070	7.513	7.382
Fe I	6226.7344	57.200	0.81	60.156	65.034	7.556	7.405
Fe I	6229.2261	82.100	0.69	85.948	92.417	7.536	7.264

ξ Hya

		EW_{obs} (mÅ)		EW_{calc} (mÅ)		ε_{Fe} (dex)	
el	λ (air)	EW	σEW	nLTE	LTE	nLTE	LTE
Fe I	6240.6460	92.800	1.85	100.220	107.996	7.460	7.225
Fe I	6271.2778	57.200	0.96	61.872	67.694	7.525	7.321
Fe I	6293.9243	30.900	0.39	26.197	29.468	7.718	7.659
Fe I	6311.4995	66.600	0.62	69.174	75.435	7.563	7.324
Fe I	6315.8110	72.200	1.13	74.955	80.338	7.559	7.376
Fe I	6338.8760	65.700	0.61	67.389	73.090	7.579	7.391
Fe I	6380.7432	84.600	0.93	82.269	87.988	7.653	7.494
Fe I	6495.7412	65.800	1.73	72.279	78.564	7.495	7.296
Fe I	6496.4658	99.500	1.29	91.982	97.957	7.739	7.663
Fe I	6533.9282	60.600	0.73	60.972	66.130	7.603	7.456
Fe I	6591.3130	22.700	0.46	23.158	26.227	7.598	7.487
Fe I	6597.5591	64.300	0.68	68.525	73.921	7.535	7.368
Fe I	6608.0249	55.800	0.39	61.522	68.663	7.510	7.244
Fe I	6627.5439	54.700	0.29	49.219	53.615	7.709	7.641
Fe I	6633.7485	91.200	0.83	93.773	98.917	7.567	7.427
Fe I	6667.4180	30.400	1.42	32.053	37.055	7.576	7.406
Fe I	6667.7104	24.100	0.34	21.796	24.712	7.670	7.588
Fe I	6699.1411	21.200	0.35	21.874	24.800	7.592	7.482
Fe I	6703.5659	77.600	0.89	79.876	87.011	7.568	7.247
Fe I	6713.7427	41.800	0.28	34.099	38.185	7.761	7.728
Fe I	6746.9536	19.800	0.17	21.906	25.621	7.553	7.401
Fe I	6752.7065	62.500	1.28	65.145	69.898	7.563	7.424
Fe I	6786.8584	51.200	0.37	51.179	55.751	7.610	7.492
Fe II	5000.7305	25.300	1.43	24.716	24.351	7.626	7.635
Fe II	5100.6548	38.900	0.94	46.757	46.066	7.434	7.452
Fe II	5256.9321	38.200	0.79	43.259	42.620	7.495	7.512
Fe II	5264.8022	63.900	1.19	75.271	74.232	7.361	7.386
Fe II	5325.5522	64.300	0.68	74.399	73.372	7.389	7.416
Fe II	5534.8379	78.200	3.00	87.297	85.922	7.413	7.448
Fe II	6084.1016	41.300	0.31	41.591	40.856	7.603	7.620
Fe II	6113.3193	27.300	0.74	25.931	25.498	7.647	7.657
Fe II	6149.2461	52.200	0.63	55.354	54.536	7.541	7.561
Fe II	6238.3857	62.500	0.51	66.821	65.769	7.518	7.544
Fe II	6247.5571	68.900	1.00	74.682	73.506	7.488	7.518
Fe II	6369.4590	34.000	0.51	46.511	45.554	7.337	7.357
Fe II	6416.9189	56.000	0.26	59.474	64.928	7.546	7.365
Fe II	6416.9189	56.000	0.26	53.471	52.629	7.546	7.365
Fe II	6416.9189	56.000	0.26	59.474	64.928	7.546	7.678
Fe II	6416.9189	56.000	0.26	53.471	52.629	7.546	7.678
Fe II	6416.9189	56.000	0.26	59.474	64.928	7.665	7.365
Fe II	6416.9189	56.000	0.26	53.471	52.629	7.665	7.365
Fe II	6416.9189	56.000	0.26	59.474	64.928	7.665	7.678
Fe II	6416.9189	56.000	0.26	53.471	52.629	7.665	7.678
Fe II	6456.3794	79.800	0.91	86.701	85.252	7.469	7.504
Fe II	6516.0767	85.400	1.94	87.282	85.403	7.572	7.610

61 Cyg B

		EW_{obs} (mÅ)		EW_{calc} (mÅ)		ε_{Fe} (dex)	
el	λ (air)	EW	σEW	nLTE	LTE	nLTE	LTE
Fe I	4787.8267	59.100	3.94	51.399	51.399	7.189	7.189
Fe I	4802.8745	37.500	5.25	33.817	33.851	7.141	7.140
Fe I	4875.8770	69.500	3.87	77.490	77.490	6.973	6.973
Fe I	4905.1328	36.900	2.19	33.694	33.728	7.133	7.132
Fe I	4917.2300	57.600	2.70	57.852	57.968	7.067	7.065
Fe I	4918.0127	35.500	3.32	41.730	41.814	6.962	6.961
Fe I	5002.7920	101.800	6.30	116.493	116.493	6.935	6.934
Fe I	5159.0576	54.200	10.08	69.183	69.322	6.879	6.877
Fe I	5196.0591	102.800	11.34	96.200	96.393	7.137	7.135
Fe I	5223.1826	37.400	3.57	51.101	51.152	6.836	6.835
Fe I	5235.3867	57.900	5.46	77.682	77.838	6.805	6.803
Fe I	5243.7764	46.600	1.78	51.724	51.776	6.992	6.992
Fe I	5253.4619	87.900	6.11	112.808	112.808	6.822	6.822
Fe I	5288.5249	53.700	4.07	67.150	67.217	6.879	6.878
Fe I	5295.3120	16.900	2.25	14.922	14.937	7.136	7.136
Fe I	5398.2793	58.900	4.89	68.540	68.677	6.951	6.949
Fe I	5400.5010	100.500	2.00	131.611	131.875	6.815	6.811
Fe I	5436.2949	21.100	2.86	20.860	20.881	7.077	7.076
Fe I	5436.5879	88.100	4.01	81.849	81.849	7.160	7.160
Fe I	5466.3960	85.200	5.46	74.958	75.108	7.183	7.182
Fe I	5473.9004	70.100	3.12	80.633	80.795	6.936	6.933
Fe I	5483.0986	27.000	4.32	34.447	34.481	6.907	6.906
Fe I	5543.1470	54.700	3.16	51.421	51.472	7.130	7.129
Fe I	5560.2114	23.800	3.67	34.387	34.456	6.848	6.846
Fe I	5584.7646	25.900	3.81	38.063	38.101	6.813	6.812
Fe I	5618.6323	38.700	1.84	37.504	37.542	7.093	7.092
Fe I	5636.6958	17.000	1.30	15.380	15.395	7.126	7.125
Fe I	5638.2622	64.100	1.07	73.305	73.452	6.946	6.944

61 Cyg B

		EW_{obs} (mÅ)		EW_{calc} (mÅ)		ε_{Fe} (dex)	
el	λ (air)	EW	σEW	nLTE	LTE	nLTE	LTE
Fe I	5641.4341	48.900	3.34	44.763	44.853	7.140	7.139
Fe I	5679.0229	39.500	1.11	35.314	35.420	7.142	7.140
Fe I	5691.4971	27.200	2.45	23.123	23.169	7.172	7.171
Fe I	5701.5444	107.500	5.08	120.396	120.396	6.931	6.931
Fe I	5705.4644	20.900	1.33	27.089	27.143	6.910	6.909
Fe I	5717.8325	48.900	2.45	48.137	48.233	7.083	7.081
Fe I	5720.8862	9.300	0.56	9.443	9.462	7.062	7.061
Fe I	5754.4023	15.000	1.66	12.836	12.849	7.154	7.154
Fe I	5760.3438	16.400	1.63	19.019	19.038	6.985	6.985
Fe I	5848.1265	27.500	0.96	23.800	23.872	7.159	7.158
Fe I	5853.1484	24.400	2.60	19.934	19.954	7.195	7.194
Fe I	5855.0757	12.400	1.17	11.031	11.042	7.129	7.129
Fe I	5905.6714	30.900	0.88	42.315	42.442	6.870	6.868
Fe I	5909.9722	40.900	1.94	35.351	35.351	7.173	7.173
Fe I	5916.2471	66.800	1.83	65.258	65.258	7.095	7.095
Fe I	5927.7886	31.000	0.95	25.441	25.518	7.188	7.187
Fe I	5930.1797	70.200	1.39	81.413	81.658	6.948	6.945
Fe I	5934.6543	70.700	3.60	86.684	86.684	6.897	6.896
Fe I	5940.9912	9.500	1.39	9.903	9.913	7.049	7.048
Fe I	5952.7178	46.600	1.42	56.030	56.030	6.937	6.937
Fe I	5956.6938	95.700	3.58	94.140	94.140	7.094	7.094
Fe I	5976.7769	61.000	2.05	67.966	67.966	6.984	6.983
Fe I	5984.8149	57.500	2.36	76.110	76.339	6.858	6.855
Fe I	5987.0649	44.600	0.90	49.544	49.743	6.999	6.996
Fe I	6003.0112	83.100	1.93	89.141	89.141	7.007	7.007
Fe I	6005.5415	27.500	1.66	23.981	23.981	7.160	7.160
Fe I	6007.9595	40.800	2.05	44.872	45.007	7.001	6.998
Fe I	6008.5557	86.300	2.69	102.443	102.443	6.914	6.913
Fe I	6012.2100	24.600	1.90	25.926	25.952	7.035	7.035
Fe I	6020.1685	78.600	5.66	80.997	81.241	7.044	7.042
Fe I	6024.0576	89.200	2.52	104.496	104.705	6.926	6.924
Fe I	6027.0508	49.700	0.91	63.701	63.765	6.877	6.876
Fe I	6056.0044	49.500	2.33	63.502	63.693	6.890	6.887
Fe I	6078.4912	53.000	1.04	57.554	57.727	7.011	7.008
Fe I	6079.0078	22.400	0.47	23.729	23.777	7.037	7.036
Fe I	6082.7100	53.200	0.97	48.458	48.507	7.159	7.158
Fe I	6093.6431	12.000	0.58	12.662	12.687	7.042	7.041
Fe I	6096.6641	27.100	0.73	25.159	25.159	7.114	7.114
Fe I	6127.9063	34.000	1.72	36.191	36.227	7.029	7.028
Fe I	6136.9937	102.600	4.84	92.938	92.938	7.195	7.195
Fe I	6151.6172	59.900	3.67	69.647	69.647	6.909	6.908
Fe I	6157.7280	52.700	1.46	57.410	57.467	7.003	7.002
Fe I	6165.3599	36.800	1.65	32.033	32.065	7.161	7.160
Fe I	6173.3345	82.500	2.22	95.448	95.448	6.893	6.892
Fe I	6180.2026	55.400	3.83	69.810	69.810	6.841	6.841
Fe I	6187.9893	38.200	1.69	39.031	39.031	7.056	7.056
Fe I	6200.3125	91.400	2.57	93.198	93.198	7.047	7.047
Fe I	6220.7798	18.800	2.09	20.852	20.852	7.012	7.012
Fe I	6229.2261	45.000	5.05	46.651	46.651	7.039	7.039
Fe I	6232.6401	80.500	3.27	100.902	100.902	6.860	6.860
Fe I	6240.6460	75.500	3.98	69.813	69.813	7.161	7.161
Fe I	6254.2578	120.000	5.93	131.369	131.369	6.955	6.955
Fe I	6265.1323	113.500	3.27	134.454	134.454	6.858	6.858
Fe I	6270.2236	57.500	2.58	66.851	66.851	6.921	6.921
Fe I	6297.7925	98.400	2.04	109.330	109.330	6.939	6.938
Fe I	6315.8110	31.300	1.91	27.959	27.987	7.142	7.141
Fe I	6322.6851	84.500	3.17	96.147	96.147	6.919	6.919
Fe I	6355.0283	77.700	1.63	77.785	77.785	7.069	7.069
Fe I	6358.6968	111.600	2.31	109.001	109.001	7.104	7.104
Fe I	6364.3638	9.600	1.08	8.969	8.996	7.103	7.102
Fe I	6380.7432	32.100	2.00	34.163	34.197	7.029	7.029
Fe I	6400.3169	123.800	4.96	116.224	116.224	7.159	7.159
Fe I	6408.0176	102.400	3.45	124.217	124.217	6.879	6.878
Fe I	6475.6240	61.300	2.85	61.185	61.185	7.072	7.072
Fe I	6481.8696	82.300	4.24	83.879	83.879	7.047	7.047
Fe I	6496.4658	40.400	1.66	39.830	39.950	7.080	7.077
Fe I	6518.3657	71.200	4.11	72.513	72.513	7.051	7.051
Fe I	6569.2139	61.600	2.09	55.331	55.497	7.152	7.151
Fe I	6574.2266	67.200	2.41	62.702	62.765	7.153	7.152
Fe I	6581.2090	43.400	0.94	43.521	43.565	7.068	7.067
Fe I	6593.8696	107.500	3.95	116.300	116.300	6.973	6.973
Fe I	6608.0249	29.300	2.81	28.184	28.212	7.097	7.096
Fe I	6609.1099	79.900	1.93	78.973	78.973	7.083	7.083
Fe I	6627.5439	10.200	0.47	9.574	9.584	7.102	7.102
Fe I	6633.7485	40.500	0.57	39.392	39.471	7.089	7.088
Fe I	6710.3179	37.000	2.87	39.508	39.548	7.017	7.017
Fe I	6733.1504	21.500	1.16	17.976	18.012	7.174	7.173
Fe I	6739.5205	29.400	1.10	33.278	33.311	6.981	6.981
Fe I	6750.1514	84.100	2.17	99.061	99.061	6.876	6.876

ϵ Eri

		EW_{obs} (mÅ)		EW_{calc} (mÅ)		ε_{Fe} (dex)	
el	λ (air)	EW	σEW	nLTE	LTE	nLTE	LTE
Fe I	4787.8267	62.100	1.16	60.670	61.594	7.388	7.387
Fe I	4793.9614	17.100	0.83	17.945	18.405	7.333	7.332
Fe I	4799.4058	48.400	1.01	49.217	50.068	7.344	7.344
Fe I	4808.1479	40.200	1.52	40.079	40.855	7.363	7.363
Fe I	4875.8770	81.900	1.29	88.390	89.464	7.261	7.255
Fe I	4892.8589	67.300	1.47	68.316	69.568	7.344	7.344
Fe I	4896.4385	46.900	1.53	46.904	47.715	7.360	7.360
Fe I	4917.2300	76.900	1.42	85.709	87.103	7.234	7.219
Fe I	4918.0127	69.500	2.49	69.638	70.914	7.358	7.358
Fe I	4979.5859	26.400	1.12	22.747	23.282	7.453	7.447
Fe I	5023.1860	48.000	1.92	49.568	50.580	7.333	7.333
Fe I	5023.4976	41.600	1.26	37.873	38.685	7.430	7.426
Fe I	5031.9141	36.400	0.50	40.438	41.348	7.285	7.282
Fe I	5054.6426	50.100	1.63	54.637	55.525	7.256	7.247
Fe I	5067.1494	85.100	1.44	92.260	93.665	7.261	7.254
Fe I	5088.1533	47.300	1.75	45.902	46.791	7.386	7.385
Fe I	5109.6519	87.900	1.09	85.879	87.364	7.388	7.387
Fe I	5129.6309	59.000	2.22	64.240	65.285	7.279	7.276
Fe I	5228.3760	72.100	0.98	67.018	68.177	7.443	7.437
Fe I	5247.0503	97.900	2.42	93.933	96.838	7.452	7.453
Fe I	5253.0210	34.400	1.26	31.542	32.417	7.427	7.422
Fe I	5285.1274	33.100	1.04	31.930	32.682	7.384	7.383
Fe I	5293.9590	34.200	1.29	39.915	40.771	7.241	7.231
Fe I	5315.0698	40.600	1.32	41.068	41.949	7.351	7.351
Fe I	5320.0356	31.300	0.55	28.359	29.027	7.429	7.425
Fe I	5322.0405	81.700	1.51	87.262	88.862	7.250	7.229
Fe I	5326.1426	54.400	1.07	54.847	55.796	7.351	7.351
Fe I	5361.6250	56.200	2.29	52.155	53.274	7.429	7.424
Fe I	5401.2666	31.700	0.54	29.618	30.315	7.406	7.403
Fe I	5409.1333	66.200	1.13	63.695	64.863	7.400	7.398
Fe I	5412.7837	23.300	0.62	29.159	29.876	7.225	7.213
Fe I	5417.0332	37.300	1.66	37.142	38.016	7.363	7.363
Fe I	5432.9478	80.500	1.33	78.216	79.812	7.393	7.392
Fe I	5436.2949	47.100	0.71	46.926	47.933	7.363	7.363
Fe I	5441.3389	35.300	0.98	39.922	40.778	7.270	7.265
Fe I	5452.0884	20.300	0.31	18.724	19.224	7.407	7.405
Fe I	5460.8726	14.300	0.20	18.229	18.754	7.227	7.214
Fe I	5466.9873	44.200	1.01	46.632	47.535	7.309	7.308
Fe I	5470.0928	33.600	0.52	28.896	29.637	7.460	7.452
Fe I	5472.7085	55.100	0.82	51.497	52.494	7.429	7.424
Fe I	5473.1626	25.000	0.92	25.579	26.208	7.346	7.346
Fe I	5483.0986	55.500	1.15	61.068	62.124	7.258	7.250
Fe I	5487.1450	45.200	0.62	45.801	46.783	7.349	7.349
Fe I	5522.4463	53.000	0.63	54.136	55.185	7.338	7.338
Fe I	5524.2495	6.000	0.24	5.783	5.950	7.377	7.377
Fe I	5539.2798	23.600	0.41	28.103	28.794	7.249	7.241
Fe I	5543.9355	74.800	0.86	79.838	81.136	7.278	7.271
Fe I	5546.5059	62.200	0.90	62.448	63.657	7.356	7.356
Fe I	5549.9487	13.700	0.68	13.528	13.903	7.367	7.367
Fe I	5560.2114	59.000	0.94	67.221	68.523	7.232	7.217
Fe I	5567.3911	87.700	1.65	83.118	84.555	7.450	7.441
Fe I	5600.2241	47.600	0.40	52.941	54.021	7.259	7.251
Fe I	5618.6323	61.700	0.44	65.544	66.678	7.290	7.286
Fe I	5619.5952	44.600	0.36	37.551	38.396	7.494	7.481
Fe I	5622.9453	11.300	0.30	10.714	11.023	7.387	7.387
Fe I	5636.6958	28.100	0.74	30.553	31.272	7.303	7.301
Fe I	5641.4341	78.100	0.88	74.557	75.846	7.420	7.416
Fe I	5650.7056	41.600	0.25	39.069	40.655	7.406	7.402
Fe I	5651.4688	22.900	0.42	19.775	20.282	7.445	7.440
Fe I	5652.3174	33.600	0.51	30.411	31.127	7.432	7.427
Fe I	5655.1763	60.300	1.08	57.515	59.849	7.403	7.400
Fe I	5661.3447	30.200	0.30	33.681	34.474	7.283	7.279
Fe I	5679.0229	71.200	0.86	73.763	75.499	7.324	7.323
Fe I	5680.2402	14.000	0.35	11.608	11.930	7.456	7.450
Fe I	5691.4971	49.400	0.53	48.868	49.916	7.370	7.370
Fe I	5698.0200	22.100	0.38	27.532	28.209	7.223	7.210
Fe I	5701.5444	108.900	1.89	115.451	117.567	7.267	7.253
Fe I	5705.4644	49.600	0.44	54.390	55.500	7.270	7.264
Fe I	5717.8325	73.200	1.40	79.041	80.408	7.265	7.255
Fe I	5731.7617	71.200	0.97	66.680	67.833	7.440	7.434
Fe I	5741.8477	43.000	0.44	39.403	40.248	7.434	7.429
Fe I	5754.4023	22.300	0.94	26.654	27.337	7.249	7.241
Fe I	5759.2622	9.000	0.38	7.248	7.464	7.464	7.457
Fe I	5760.3438	30.900	0.71	36.347	37.165	7.242	7.232
Fe I	5838.3716	29.700	0.34	29.669	30.367	7.361	7.361
Fe I	5849.6831	11.200	0.48	11.828	12.169	7.332	7.331
Fe I	5853.1484	20.100	0.29	18.880	19.687	7.397	7.396
Fe I	5855.0757	28.400	0.53	32.408	33.239	7.275	7.271
Fe I	5858.7778	19.700	0.43	19.812	20.341	7.357	7.357

ϵ Eri

		EW_{obs} (mÅ)		EW_{calc} (mÅ)		ε_{Fe} (dex)	
el	λ (air)	EW	σEW	nLTE	LTE	nLTE	LTE
Fe I	5861.1084	13.200	0.29	13.412	13.784	7.352	7.352
Fe I	5873.2124	25.700	0.45	24.076	24.693	7.398	7.397
Fe I	5881.2798	17.000	0.65	20.700	21.274	7.252	7.245
Fe I	5909.9722	46.200	0.48	52.049	53.111	7.249	7.240
Fe I	5927.7886	52.300	0.65	59.863	61.398	7.241	7.227
Fe I	5940.9912	26.400	0.31	25.763	26.397	7.376	7.376
Fe I	5952.7178	78.900	1.81	87.072	88.398	7.247	7.237
Fe I	6003.0112	107.700	2.06	119.237	120.685	7.231	7.218
Fe I	6012.2100	37.600	0.81	31.660	32.639	7.495	7.478
Fe I	6034.0352	9.900	0.26	12.836	13.192	7.232	7.223
Fe I	6079.0078	56.500	0.86	57.526	58.880	7.343	7.343
Fe I	6082.7100	57.000	0.81	53.693	55.013	7.434	7.427
Fe I	6093.6431	36.700	0.48	36.471	37.406	7.365	7.364
Fe I	6096.6641	51.500	0.36	50.781	51.765	7.372	7.372
Fe I	6098.2441	21.800	0.28	18.299	18.807	7.460	7.453
Fe I	6120.2466	17.500	0.35	14.934	15.753	7.448	7.440
Fe I	6127.9063	58.200	0.92	66.746	68.039	7.222	7.204
Fe I	6151.6172	69.900	1.51	70.949	72.694	7.338	7.336
Fe I	6165.3599	54.300	0.74	61.638	62.896	7.238	7.225
Fe I	6170.5059	93.000	1.97	95.332	97.676	7.331	7.330
Fe I	6173.3345	93.000	1.26	91.127	93.272	7.395	7.395
Fe I	6180.2026	76.000	1.28	77.749	79.336	7.326	7.324
Fe I	6187.3979	8.800	0.13	7.883	8.160	7.414	7.412
Fe I	6187.9893	63.900	0.80	68.032	69.209	7.295	7.293
Fe I	6199.5063	8.400	0.17	8.221	8.528	7.371	7.370
Fe I	6200.3125	96.200	1.32	95.065	97.005	7.380	7.380
Fe I	6226.7344	39.400	0.26	39.677	40.570	7.355	7.355
Fe I	6229.2261	55.500	0.77	59.213	60.483	7.283	7.277
Fe I	6240.6460	71.400	1.13	71.395	73.076	7.360	7.360
Fe I	6265.1323	114.200	1.62	121.176	124.283	7.264	7.238
Fe I	6271.2778	36.600	0.71	39.277	40.202	7.306	7.304
Fe I	6293.9243	15.200	0.24	13.927	14.358	7.406	7.404
Fe I	6297.7925	101.200	1.15	102.549	105.071	7.338	7.336
Fe I	6311.4995	45.300	0.46	43.097	44.157	7.407	7.404
Fe I	6315.8110	52.300	0.64	55.433	56.564	7.305	7.303
Fe I	6322.6851	98.200	1.13	97.518	99.610	7.372	7.372
Fe I	6338.8760	49.600	0.26	52.195	53.643	7.317	7.316
Fe I	6355.0283	90.200	1.63	86.302	88.063	7.431	7.425
Fe I	6364.3638	35.300	0.56	30.436	31.345	7.459	7.450
Fe I	6380.7432	60.200	0.62	65.528	66.865	7.273	7.267
Fe I	6469.1919	67.700	0.84	66.058	67.891	7.384	7.384
Fe I	6481.8696	85.800	0.83	83.845	85.907	7.398	7.397
Fe I	6495.7412	51.100	2.55	58.102	59.714	7.251	7.238
Fe I	6496.4658	77.000	2.18	85.143	87.237	7.252	7.235
Fe I	6518.3657	76.800	0.96	82.389	84.156	7.258	7.240
Fe I	6533.9282	45.500	0.41	41.286	42.345	7.440	7.433
Fe I	6574.2266	58.200	0.73	53.009	55.046	7.478	7.458
Fe I	6581.2090	39.300	0.32	41.726	43.284	7.307	7.303
Fe I	6591.3130	13.500	0.15	11.562	11.920	7.441	7.436
Fe I	6593.8696	110.100	2.08	111.865	114.616	7.334	7.331
Fe I	6597.5591	51.100	0.51	51.551	52.873	7.352	7.353
Fe I	6608.0249	33.900	0.21	35.258	36.386	7.330	7.329
Fe I	6609.1099	87.000	1.45	83.457	85.422	7.428	7.423
Fe I	6625.0215	41.000	1.78	36.261	37.890	7.464	7.450
Fe I	6627.5439	34.500	0.27	29.424	30.178	7.473	7.463
Fe I	6633.7485	76.600	1.31	78.703	80.391	7.329	7.328
Fe I	6667.4180	12.900	0.11	15.406	15.981	7.265	7.257
Fe I	6667.7104	14.000	0.15	10.735	11.067	7.497	7.485
Fe I	6699.1411	10.300	0.22	10.786	11.120	7.337	7.336
Fe I	6703.5659	54.300	0.51	52.242	53.527	7.403	7.400
Fe I	6710.3179	35.100	0.18	38.042	39.545	7.295	7.289
Fe I	6732.0649	9.700	0.24	12.902	13.301	7.216	7.201
Fe I	6746.9536	8.700	0.22	9.979	10.362	7.292	7.288
Fe I	6750.1514	94.000	1.05	97.706	100.109	7.296	7.285
Fe I	6752.7065	42.300	0.72	44.394	45.532	7.319	7.318
Fe I	6786.8584	32.800	0.46	31.453	32.226	7.388	7.387
Fe I	6804.2710	18.400	0.23	19.084	19.654	7.339	7.339
Fe I	6810.2622	57.200	1.07	61.805	63.195	7.284	7.279
Fe II	5325.5522	29.200	1.12	25.064	24.742	7.483	7.494
Fe II	5425.2485	20.900	0.74	23.659	23.355	7.270	7.271
Fe II	5534.8379	34.100	0.60	34.660	34.181	7.345	7.344
Fe II	6084.1016	8.600	0.20	7.516	7.405	7.431	7.434
Fe II	6149.2461	14.300	0.54	14.102	13.949	7.369	7.369
Fe II	6238.3857	20.800	0.32	20.268	20.028	7.379	7.380
Fe II	6247.5571	27.400	0.18	25.281	24.957	7.425	7.430
Fe II	6369.4590	6.400	0.15	8.691	8.529	7.203	7.211
Fe II	6456.3794	35.000	0.19	33.637	33.173	7.397	7.399
Fe II	6516.0767	30.400	0.32	30.798	30.135	7.349	7.348

E | List of publications

Refereed

1- Non-LTE iron abundances in cool stars: The role of hydrogen collisions (submitted to Astronomische Nachrichten)

2- The role of Hydrogen collisions in non-LTE iron abundances: Introducing the quantum fitting method (in prep.)

Non-refereed conference proceedings

1- Non-LTE iron abundance determination of a sample of *Kepler* red giants (EAS Publications Series, Vol. 63, 2013, pp.407-409).

2- NLTE iron abundance determination in red giants (SF2A-2013: Proceedings of the Annual meeting of the French Society of Astronomy and Astrophysics. Eds.: L. Cambresy, F. Martins, E. Nuss, A. Palacios, pp.119-121)

Non-LTE iron abundances in cool stars: The role of hydrogen collisions

Rana Ezzeddine[1,⋆], **Thibault Merle**[2], and **Bertrand Plez**[1]

[1] Laboratoire Univers et Particules de Montpellier, Université de Montpellier, CNRS UMR-5299, Montpellier, France
[2] Institut d'Astronomie et d'Astrophysique, Université Libre de Bruxelles, CP 226, Boulevard du Triomphe, 1050 Brussels, Belgium

Received XXXX, accepted XXXX
Published online XXXX

Key words non-LTE – line: formation – stars: abundances – hydrogen collisions

In the aim of determining accurate iron abundances in stars, this work is meant to empirically calibrate H-collisions cross-sections with iron, where no quantum mechanical calculations have been published yet. Thus, a new iron model atom has been developed, which includes hydrogen collisions for excitation, ionization and charge transfer processes. We show that collisions with hydrogen leading to charge transfer are important for an accurate non-LTE modeling. We apply our calculations on several benchmark stars including the Sun, the metal-rich star α Cen A and the metal-poor star HD140283.

1 Introduction

Iron plays an important role in studying the atmospheres of cool stars. It is often used as a proxy to the total metal content and metallicities in stars.

Neutral iron lines, Fe I, have been shown to be subject to non-LTE effects (Lind et al. 2012; Mashonkina et al. 2011; Thévenin & Idiart 1999). This deviation from LTE grows towards lower metallicities, due to a decreasing number of electrons donated by metals which decreases the collisional rates. Thus, a non-LTE modeling of the spectra of these stars becomes important, which in turn requires a good knowledge of a bulk of atomic data for each atom under consideration. A common problem in non-LTE calculations comes from uncertainties in the underlying atomic data, of which, in cool stars, the inelastic neutral hydrogen collisional rates are the most significant source.

Quantum calculations for hydrogen collisional rates have recently been calculated for a small number of elements including Li (Belyaev & Barklem 2003), Na (Barklem et al. 2010), Mg (Belyaev et al. 2012), Al (Belyaev 2013) and Si (Belyaev et al. 2014). For iron, however, no quantum calculations have been published yet.
In the lack of quantum data, a common practice is to estimate the hydrogen collisional rates using the classical Drawin approximation (Drawin 1968, 1969) which is a modified version of Thomson (1912) classical e^- + atom ionization rate equation, extended by Drawin to that of same atoms ($A + A$) excitation and ionization collisions, where A corresponds to an element species.
Drawin's approximation was then rewritten by Steenbock & Holweger (1984) for inelastic H + atom collisions, which was then reviewed and re-derived by Lambert (1993). Both their approaches apply only to allowed excitation collisional transitions due to the dependence of the collisional rates on the transition's oscillator strength f-value in Drawin's equation.

Upon comparison with quantum calculations, the Drawin approximation has been shown to overestimate the collisional rates by several orders of magnitude (Barklem et al. 2011), which is commonly treated by applying a multiplicative scaling fudge factor S_H to the Drawin rate equation by using different calibration methods on reference stars.

Recent non-LTE abundance studies using quantum calculations revealed that charge transfer (CT) process, i.e. $A + H \rightleftharpoons A^+ + H^-$, can play a more important role than excitation (Lind et al. 2011; Osorio et al. 2015). To our knowledge, no study has yet tested the inclusion of H+Fe charge transfer collision in their non-LTE calculations, which was an important reason that motivated this work.

In this article, we aim at testing the role of the different H+Fe collisional processes including excitation, ionization and charge transfer in non-LTE calculations, using a newly developed iron model atom, and starting from well defined non-spectroscopic atmospheric parameters for a set of benchmark stars.

2 Method

We performed non-LTE, 1D modeling of Fe I and Fe II spectral lines using the radiative transfer code `MULTI2.3` (Carlsson 1986, 1992), which solves the statistical equilibrium and radiative transfer equations simultaneously for the

⋆ Corresponding author: rana.ezzeddine@umontpellier.fr

element in question, through the Accelerated Lambda Iteration (ALI) approximation (Scharmer 1981). In the sections below, we present the observational data including the spectra and measured equivalent widths in Sect. 2.1, the model atmospheres and atmospheric parameters adopted for the stars under study in Sect. 2.2, and the newly developed Fe I/Fe II model atom used in the non-LTE calculations in Sect. 2.3.

2.1 Observational data

The spectra of the stars in this work were obtained from the *Gaia*-ESO survey collaboration. They were observed by the UVES spectrograph of the VLT, and reduced by the standard UVES pipeline version 3.2 (Ballester et al. 2000). All the spectra have high signal to noise ratios (S/N > 110), and a high resolution of $R = 70\,000$.

The equivalent widths (EW) for each star were measure automatically using a Gaussian fitting method with the Automated Equivalent Width Measurement code `Robospect` (Waters & Hollek 2013). The Fe I and Fe II linelist chosen in the analysis is a subset of the Gaia-ESO survey "golden" linelist (v4 Heiter et al. (2015)), which was tested on the Sun. All lines that are blended and whose relative errors $\left(\frac{\sigma EW}{EW}\right) > 0.3$, were removed from the linelist. In addition, only lines with EW between 10 Å and 100 Å in the Solar spectrum were included. The final number of lines used for each star is ∼ 100 Fe I lines and 10 Fe II lines.

2.2 Model atmospheres

Three benchmark stars of different metallicities and stellar parameters were considered in this study, namely the Sun, the metal-rich dwarf α Centauri A and the metal-poor halo subgiant HD140283. Their atmospheric parameters were adopted from the study of the *Gaia* benchmark stars by Jofré et al. (2014), where the effective temperatures $T_{\rm eff}$ and surface gravities log g were determined homogeneously and independently from spectroscopic models, while the stellar metallicities were determined spectroscopically from Fe I lines by fixing $T_{\rm eff}$ and log g to the previous values and applying a line-by-line non-LTE correction to each line. The parameters are listed in Table 1.

1D MARCS (Gustafsson et al. 2008) atmospheric models were interpolated to the atmospheric parameters of each star using the code `interpol_marcs.f` written by Thomas Masseron[1], except for the Solar case where the reference Solar MARCS model was used. Background line opacities except iron, calculated for each star as a function of its atmospheric parameters and sampled to ∼ 153 000 wavelength points using the MARCS opacity package, were also employed in the `MULTI2.3` calculations.

[1] http://marcs.astro.uu.se/software.php

Table 1 Atmospheric parameters of the stars used in this study, adopted from Jofré et al. (2014).

Star	$T_{\rm eff}$	log g	[Fe/H]
Sun	5777	4.43	+0.00
α Cen A	5840	4.31	+0.26
HD140283	5720	3.67	-2.36

2.3 Model atom

A new iron model atom including Fe I and Fe II energy levels, as well as the Fe III ground level has been developed with the most up-to-date atomic data available, including radiative and collisional transitions for all the levels.

2.3.1 Energy levels

The Fe I and Fe II energy levels were adopted from the NIST database[2] from the calculations of Nave et al. (1994) and Nave & Johansson (2013) respectively and supplemented by the predicted high-lying Fe I levels from Peterson & Kurucz (2015) up to an excitation energy of 8.392 eV. The model was completed with the ground Fe III energy level. In order to reduce the large number of energy levels (initially 1939 fine structure levels), all the levels in our iron model atom, except the ground and first ionized states of Fe I and Fe II, were grouped into mean term levels from their respective fine structure levels using the code `FORMATO` (Merle et al., in prep.). In addition, all mean levels above 5 eV and lying within an energy interval of 0.0124 eV (100 cm^{-1}) were combined into superlevels. The excitation potential of each superlevel is a weighted mean by the statistical weights of the excitation potentials of its corresponding mean levels.

The final number of levels in the model atom is 135 Fe I levels (belonging to 911 fine structure levels and 203 spectroscopic terms) and 127 Fe II levels (belonging to 1027 fine structure levels and 189 terms).

2.3.2 Radiative transitions

For our Fe I/Fe II model, we used the VALD3 (Ryabchikova et al. 2011) interface database[3] to extract all the Fe I and Fe II radiative bound-bound transitions. In addition, the UV and IR lines corresponding to transitions from and to the predicted high lying levels have also been included in the model (Peterson & Kurucz 2015). Individual transitions belonging to levels that have been combined to superlevels have also been combined into superlines using `FORMATO`. The superline total transition probability is a weighted average of gf-values of individual transitions, combined via the relation of Martin et al. (1988). Our final FeI/FeII model includes 9816 FeI (belonging to 81162 lines) and 16745

[2] http://www.nist.gov/pml/data/asd.cfm

[3] http://vald.inasan.ru/~vald3/php/vald.php

FeII (belonging to 113964 transitions) super transitions combined from the individual lines.

In addition to the b-b transitions, Fe I and Fe II energy levels were coupled via photoionization to the Fe II and Fe III ground levels respectively. For Fe I levels, the corresponding photoionization cross-section tables were calculated by Bautista (1997) for 52 LS terms and those for Fe II by Nahar & Pradhan (1994) for 86 LS terms, and were extracted from the NORAD[4] database (Nahar & Collaboration). For the rest of the levels, the hydrogenic approximation was used to calculate threshold cross-sections via Kramer's semi-classical relation (Travis & Matsushima 1968). All the photoionization energies extracted from NORAD were shifted to match the threshold ionization energies in NIST due to existing energy differences between their theoretical values (Verner et al. 1994). Sharp cross-section resonance peaks in the tables were smoothed as a function of photon frequencies and then using an opacity sampling method they were resampled to a maximum of 200 frequency points per transition.

2.3.3 Collisional transitions

All levels in our iron model were coupled via electron and neutral hydrogen atom collisional transitions. e^- b-b effective collisional strengths were included from the calculations of Pelan & Berrington (1997) for the ground and first excited states of Fe I, and from Zhang & Pradhan (1995) and Bautista & Pradhan (1996) for 142 Fe II fine structure levels. For the rest of the levels, the Seaton (1962a) and Seaton (1962b) impact approximations were used to calculate the cross-sections for the allowed and forbidden transitions respectively. In addition, e^- ionization collisional transitions were included using the semi-classical approximation of Bely & van Regemorter (1970).

For the H collisions, Lambert (1993) derivation of the Drawin approximation was used to calculate the rate coefficients $\langle\sigma v\rangle$, with the oscillator strength f set to 1 for all transitions. This was motivated by the approach adopted by Steenbock (1985) who set the Q-factor[5] in their Mg+H rate equations equal to 1 for forbidden transitions. Another attempt to remove the oscillator strength dependence from the rate equations was by Collet et al. (2005), who set a constant $f = 10^{-3}$ in the van Regemorter (1962) equation for the e^- collisions for all transitions. In addition, recent quantum calculations for Mg and other elements found large H-collisional rates for forbidden transitions, which were comparable to the allowed ones (Feautrier et al. 2014).
We also adopt the Drawin approximation for charge transfer H collisions in the absence of any other suitable approximation.

All the levels in the model were coupled with b-b, b-f and charge transfer ($Fe + H \rightleftharpoons Fe^+ + H^-$) H collisions. The rates were scaled with a different global multiplicative scaling factor, as follows:

- S_H: multiplicative factor for b-b and b-f H collision rates.
- S_H(CT): multiplicative factor for charge transfer H collision rates.

Several modified model atoms were created using different scaling factors for each H collisional process. S_H was varied between 0.0001 and 10, in multiplication steps of 10, while S_H(CT) was varied between 0.1 and 10 in multiplication steps of 10, in addition to the S_H(CT)=0 models.

3 non-LTE calculations and results

Non-LTE calculations were performed for each atomic model with a given S_H and S_H(CT). Thus, a total of 24 models were computed for each star. The calculated EW(calc) for each model were compared to the measured EW(obs) using the χ^2 test:

$$\chi^2 = \frac{1}{N_{lines}} \sum_{lines} \left(\frac{EW(calc) - EW(obs)}{\sigma EW(obs)} \right)^2 \quad (1)$$

where N_{lines} is the total number of lines used in the χ^2 test. The variation of χ^2 as a function of S_H and S_H(CT) for each star is shown in Fig. 1. The LTE χ^2 are also shown for comparison.

For the Sun, it can be seen that when charge transfer rates are neglected, the best fit is obtained at S_H=0.01. Upon including charge transfer rates, smaller S_H values are needed. For the metal-rich star α Cen A, larger values of S_H and S_H(CT) are favored. For the metal-poor star HD140283, large variations in χ^2 are obtained with S_H and S_H(CT) showing that charge transfer process plays an important role in producing the best-fit. Similar to the Sun, the best fit is also obtained at S_H=0.01 upon neglecting the charge transfer rates, while smaller values of S_H are needed when including them.

Comparing to recent studies, Mashonkina et al. (2011) and Bergemann et al. (2012) used Fe I/Fe II model atoms in their non-LTE abundance determinations, which are comparable to our model. Their calculations were also tested on benchmark stars including the Sun and HD140283, where they used the Drawin approximation scaled with an S_H-factor for the excitation and ionization H collisional rates. Charge transfer rates were not included in their calculations. They could not find a single S_H-factor that

[4] http://www.astronomy.ohio-state.edu/~csur/NORAD/norad.html

[5] $Q = \left(\frac{\chi_H^\infty}{\Delta E^A} \right)^2 f$, where χ_H^∞ = 13.6 eV is the ionization potential of hydrogen, ΔE^A is the transition energy of atom A and f is the oscillator strength of the transition.

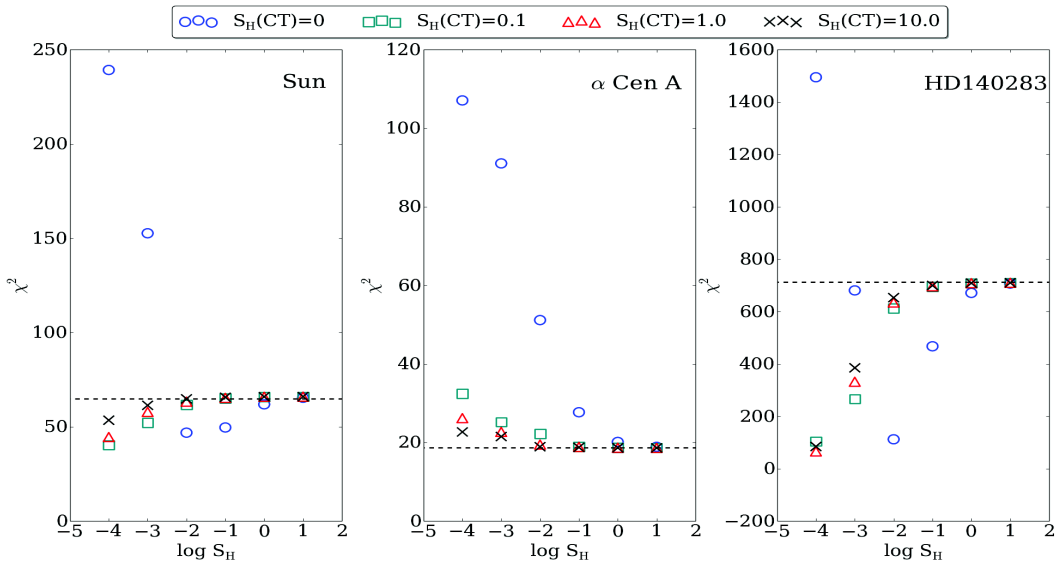

Fig. 1 χ^2 as a function of scaling factors S_H and S_H(CT) for the Sun, HD140283 and α Cen A. The dotted lines represent the χ^2 values obtained in LTE.

would fit all stars. For metal-poor stars, Mashonkina et al. (2011) determined a value of S_H=0.1 while Bergemann et al. (2012) determined an optimum value of S_H=1. For solar-metallicity stars, both studies found that different S_H values had no significant effect on the calculated abundances.

Similarly, we could not find a single set of S_H values that would ensure a best fit for all stars. We could, however, note that including charge transfer H collisional rates is important in iron non-LTE calculations. When neglecting charge transfer rates, however, a large value of S_H is needed for α Cen A ($S_H > 1$), while a smaller value is needed for the Sun and HD140283 ($S_H \leq 0.01$), which is not in accordance with previous studies.

4 Conclusions

We performed iron non-LTE spectral line calculations for three benchmark stars with well determined atmospheric parameters, using hydrogen collisions for excitation and ionization processes, and including charge transfer rates for the first time. We show that the charge transfer rates are important to include in the non-LTE calculations, especially for the metal-poor star. They were found, however, to play a less important role with increasing metallicity for the Sun and the metal-rich star α Cen A, where non-LTE effects are of smaller magnitude. No single set of values for the scaling factors S_H and S_H(CT) was obtained for the different types of stars. This demonstrates the inability of the Drawin approximation to reproduce the correct behavior and magnitudes of hydrogen collision rates (see Barklem et al. (2011)). In the lack of quantum calculations for the hydrogen collision rates, more efficient models than the classical Drawin approximation are required. We are working on such a method based on semi-empirical fitting of the available quantum data for other chemical species.

Acknowledgements. We would like to acknowledge the GES-CoRoT collaboration for providing us with the UVES spectra for the benchmark stars, which have been used in this work. This work has made use of the VALD database, operated at Uppsala University, the Institute of Astronomy RAS in Moscow, and the University of Vienna.

References

Ballester, P., Modigliani, A., Boitquin, O., et al. 2000, The Messenger, 101, 31
Barklem, P. S., Belyaev, A. K., Dickinson, A. S., & Gadéa, F. X. 2010, A&A, 519, A20
Barklem, P. S., Belyaev, A. K., Guitou, M., et al. 2011, A&A, 530, A94
Bautista, M. A. 1997, A&AS, 122, 167
Bautista, M. A. & Pradhan, A. K. 1996, A&AS, 115, 551
Bely, O. & van Regemorter, H. 1970, ARA&A, 8, 329
Belyaev, A. K. 2013, A&A, 560, A60
Belyaev, A. K. & Barklem, P. S. 2003, Phys. Rev. A, 68, 062703
Belyaev, A. K., Barklem, P. S., Spielfiedel, A., et al. 2012, Phys. Rev. A, 85, 032704
Belyaev, A. K., Yakovleva, S. A., & Barklem, P. S. 2014, A&A, 572, A103
Bergemann, M., Lind, K., Collet, R., Magic, Z., & Asplund, M. 2012, MNRAS, 427, 27
Carlsson, M. 1986, Uppsala Astronomical Observatory Reports, 33
Carlsson, M. 1992, in Astronomical Society of the Pacific Conference Series, Vol. 26, Cool Stars, Stellar Systems, and the Sun, ed. M. S. Giampapa & J. A. Bookbinder, 499
Collet, R., Asplund, M., & Thévenin, F. 2005, A&A, 442, 643

Drawin, H.-W. 1968, Zeitschrift fur Physik, 211, 404
Drawin, H. W. 1969, Zeitschrift fur Physik, 225, 470
Feautrier, N., Spielfiedel, A., Guitou, M., & Belyaev, A. K. 2014, in SF2A-2014: Proceedings of the Annual meeting of the French Society of Astronomy and Astrophysics, ed. J. Ballet, F. Martins, F. Bournaud, R. Monier, & C. Reylé, 475–478
Gustafsson, B., Edvardsson, B., Eriksson, K., et al. 2008, A&A, 486, 951
Heiter, U., Lind, K., Asplund, M., et al. 2015, Phys. Scr, 90, 054010
Jofré, P., Heiter, U., Soubiran, C., et al. 2014, A&A, 564, A133
Lambert, D. L. 1993, Physica Scripta Volume T, 47, 186
Lind, K., Asplund, M., Barklem, P. S., & Belyaev, A. K. 2011, A&A, 528, A103
Lind, K., Bergemann, M., & Asplund, M. 2012, MNRAS, 427, 50
Martin, G. A., Fuhr, J. R., & Wiese, W. L. 1988, Atomic transition probabilities. Scandium through Manganese
Mashonkina, L., Gehren, T., Shi, J.-R., Korn, A. J., & Grupp, F. 2011, A&A, 528, A87
Nahar, S. N. & Pradhan, A. K. 1994, Journal of Physics B Atomic Molecular Physics, 27, 429
Nave, G. & Johansson, S. 2013, ApJS, 204, 1
Nave, G., Johansson, S., Learner, R. C. M., Thorne, A. P., & Brault, J. W. 1994, ApJS, 94, 221
Osorio, Y., Barklem, P. S., Lind, K., et al. 2015, A&A, 579, A53
Pelan, J. & Berrington, K. A. 1997, A&AS, 122, 177
Peterson, R. C. & Kurucz, R. L. 2015, ApJS, 216, 1
Ryabchikova, T. A., Pakhomov, Y. V., & Piskunov, N. E. 2011, Kazan Izdatel Kazanskogo Universiteta, 153, 61
Scharmer, G. B. 1981, ApJ, 249, 720
Seaton, M. J. 1962a, Proceedings of the Physical Society, 79, 1105
Seaton, M. J. 1962b, in Atomic and Molecular Processes, ed. D. R. Bates, 375
Steenbock, W. 1985, in Astrophysics and Space Science Library, Vol. 114, Cool Stars with Excesses of Heavy Elements, ed. M. Jaschek & P. C. Keenan, 231–234
Steenbock, W. & Holweger, H. 1984, A&A, 130, 319
Thévenin, F. & Idiart, T. P. 1999, ApJ, 521, 753
Thomson, J. J. 1912, Philosophical Magazine, 23, 499
Travis, L. D. & Matsushima, S. 1968, ApJ, 154, 689
van Regemorter, H. 1962, ApJ, 136, 906
Verner, D. A., Barthel, P. D., & Tytler, D. 1994, A&AS, 108, 287
Waters, C. Z. & Hollek, J. K. 2013, PASP, 125, 1164
Zhang, H. L. & Pradhan, A. K. 1995, A&A, 293, 953

SF2A 2013
L. Cambrésy, F. Martins, E. Nuss and A. Palacios (eds)

NON-LTE IRON ABUNDANCE DETERMINATION OF A SAMPLE OF KEPLER RED GIANTS

Rana Ezzeddine[1], Thibault Merle[2] and Bertrand Plez[1]

Abstract. In the aim of calibrating non-LTE effects in atoms, particularly iron, for which quantum mechanical calculations for collisions with neutral hydrogen do not exist, we re-analyzed a sample of *Kepler* K red giant stars and determined both LTE and non-LTE FeI and FeII abundances, using asteroseismic fundamental atmospheric parameters. 1D, spherical MARCS model atmospheres were used for the abundance determinations. FeI and FeII lines with reliable oscillator strength values were selected. Results show better mutual agreement in abundances between neutral and singly ionized Fe lines as a function of equivalent width and excitation potential in NLTE as compared to that in LTE.

Keywords: Iron abundances, NLTE, Red Giants

1 Introduction

The study of iron abundances in cool stars plays an important role in understanding the Galactic chemical evolution, since there exists a wealth of Fe spectral lines even in metal-poor stars, which makes it a proxy for the total metal content in the star. Iron is also an important opacity contributor in the stellar atmosphere of late-type stars. Moreover, iron lines are used to derive fundamental atmospheric parameters (Effective temperature $T_{\rm eff}$, surface gravity log$g$ and microturbulent velocity ξ) of the star.

In stellar atmospheres, the statistical equilibrium of neutral iron can deviate from thermodynamic equilibrium due to the deviation of the mean intensity of ionizing radiation J_ν from the Planck function B_ν (Mashonkina et al. 2011), and thus it is important to perform non-local thermodynamic equilibrium (NLTE) line formation calculations in order to accurately determine abundances.

In his review, Asplund (2005) described NLTE as the case where "Everything depends on everything, everywhere". And thus in order to correctly synthesize and model stellar spectra to determine NLTE abundances, one has to take into account accurate atomic data including all possible radiative and collisional transitions between the corresponding levels of a model atom of the element under study, especially the collisions with neutral hydrogen which become important in metal poor stars where $\rm n_H/n_e \sim 10^5$. However, collisional rates with hydrogen are usually treated using the semi-classical Drawin approximation (Drawin 1969) which is based on classical rather than quantum mechanics, and has been shown to overestimate the collisional rates up to 5 orders of magnitude (Belyaev & Barklem 2003). And since quantum mechanical data are not yet available for iron, we attempt to calibrate these collisional rates by accurately modelling and determining NLTE FeI/FeII abundances.

2 Method

For this study, we selected a sample of bright *Kepler* red giants which have reliable asteroseismic fundamental atmospheric parameters, $T_{\rm eff}$ and log g. We used high resolution (R=67000) spectra (Thygesen et al. 2012) from the FIES (FIber-fed Echelle Spectrograph) spectrograph of the NOT (Nordic Optical Telescope) at La Palma,

[1] Laboratoire Univers et Particules de Montpellier (LUPM), Université de Montpellier 2-CNRS, France.
[2] Institut d'Astronomie et Astrophysique, Université Libre de Bruxelles, Belgique.

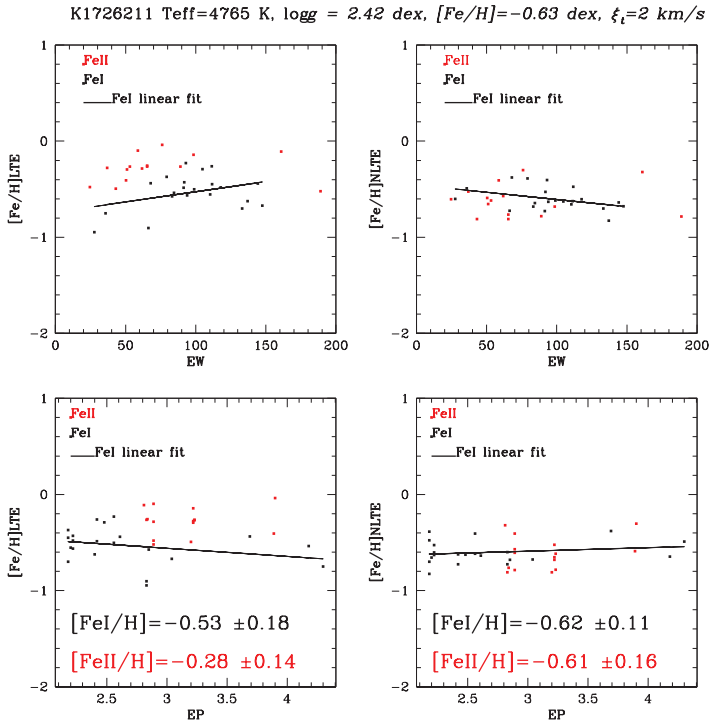

Fig. 1. Diagnostic plots of the results for FeI and FeII in LTE (left column) and NLTE (right column): abundances versus excitation potential and equivalent width for one of the sample stars of KIC ID 1726211.

to measure equivalent widths of a well selected list of non-blended lines from the INSPECT database* (Bergemann et al. 2012). The chosen lines have up-to-date averaged experimental oscillator strengths values from Gehren et al. (2001). Spherical 1D model atmospheres were interpolated† from the MARCS database (Gustafsson et al. 2008) and used with an FeI/FeII model atom (Thévenin & Idiart 1999) to determine NLTE abundances using the spectral synthesis code MULTI2.2 (Carlsson 1986) and a curve-of-growth technique, while LTE abundances were calculated using the TURBOSPECTRUM code (Alvarez & Plez 1998), (Plez 2012).

3 Results and Conclusions

Our LTE results show less deviations with respect to the mean in FeI abundances as a function of excitation potential and equivalent width ($\sim$ 0.25 dex) as compared to that of previous work on these stars. Bruntt et al. (2011) calculated LTE abundances and imposed ionization equilibrium between FeI and FeII lines to derive atmospheric parameters ($T_{\rm eff}$, log g and ξ). The deviations from the mean in their plots are up to 0.5 dex. It is important to note that there is also a difference of up to 400 K in $T_{\rm eff}$, 0.23 dex in log g and 0.2 dex in metallicity, between our asteroseismic and their spectroscopic values of atmospheric parameters. This can have serious consequences on the further abundance determination using these parameters, and thus they have to be carefully chosen.

Our results also show better mutual agreement between FeI and FeII lines in NLTE as compared to LTE (see Fig.1) as a function of equivalent width and excitation potential, without imposing ionization equilibrium between the singly and ionized iron lines.

Future work aims at improving our results by calculating more accurate NLTE abundances, using a better and more complete iron model atom with up-to-date atomic data, and using the updated version of MULTI

*www.inspect-stars.net
†Masseron code: http://marcs.astro.uu.se/software.php

(MULTI2.3). This will allow us to quantify the effects of collision with neutral hydrogen and electrons, leading to more accurate iron abundance determinations in giant stars.

References

Alvarez, R. & Plez, B. 1998, A&A, 330, 1109
Belyaev, A. K. & Barklem, P. S. 2003, Phys. Rev. A, 68, 062703
Bergemann, M., Lind, K., Collet, R., Magic, Z., & Asplund, M. 2012, MNRAS, 427, 27
Bruntt, H., Frandsen, S., & Thygesen, A. O. 2011, A&A, 528, A121
Carlsson, M. 1986, Uppsala Astronomical Observatory Reports, 33
Drawin, H. W. 1969, Zeitschrift fur Physik, 228, 99
Gehren, T., Butler, K., Mashonkina, L., Reetz, J., & Shi, J. 2001, A&A, 366, 981
Gustafsson, B., Edvardsson, B., Eriksson, K., et al. 2008, A&A, 486, 951
Mashonkina, L., Gehren, T., Shi, J.-R., Korn, A. J., & Grupp, F. 2011, A&A, 528, A87
Plez, B. 2012, Turbospectrum: Code for spectral synthesis, astrophysics Source Code Library
Thévenin, F. & Idiart, T. P. 1999, ApJ, 521, 753
Thygesen, A. O., Frandsen, S., Bruntt, H., et al. 2012, A&A, 543, A160

New Advances in Stellar Physics: From Microscopic to Macroscopic Processes
G. Alecian, Y. Lebreton, O. Richard and D. Vauclair (eds)
EAS Publications Series, **63** *(2013) 407-409*

NLTE IRON ABUNDANCE DETERMINATION IN RED GIANTS

R. Ezzeddine[1], T. Merle[2] and B. Plez[1]

Abstract. Our aim is to perform Non-LTE iron abundance calculations on a sample of *Kepler* red giants with reliable fundamental atmospheric parameters from asteroseismology, specifically log g, in order to calibrate for unknown atomic collisional effects with neutral hydrogen for which quantum mechanical data does not yet exist. Preliminary results show better mutual agreement between FeI and FeII lines as compared to LTE, as well as less FeI abundance dispersion than that of previous work.

1 Introduction

Iron is often considered as a proxy for the total metal content in a star, due to the wealth of lines in the optical spectrum. Its contribution to the opacity in the atmospheres of cool stars is large. Iron is also of prime interest for the understanding of the Galactic chemical evolution. Neutral iron line formation is known to deviate from local thermodynamic equilibrium (LTE) (See Asplund 2005) and thus it is vital to perform non-LTE calculations to accurately determine abundances

In order to correctly synthesize and model stellar spectra, one has to take into account accurate atomic data including all possible radiative and collisional transitions between the corresponding levels of a model atom of the element under study. This data is not always available, or of high enough quality. Specifically, the inelastic collisions with neutral hydrogen have been considered as the main source of uncertainty in atomic modelling (Barklem *et al.* 2011). It is usually treated using the semi-classical Drawin approximation (Drawin 1969), which is based on classical rather than quantum mechanics, and has been shown to overestimate the collisional rates up to 5 orders of magnitudes (Belyaev & Barklem 2003). And since

[1] Laboratoire Univers et Particules de Montpellier (LUPM), Université de Montpellier 2, CNRS, France

[2] Institut d'Astronomie et Astrophysique, Université Libre de Bruxelles, Belgique

DOI: 10.1051/eas/1363046

quantum mechanical collisional data are not yet available for iron, we attempt at calibrating these collisional rates by accurately modelling and determining NLTE FeI/FeII abundances.

2 Method

For this study, we selected a sample of bright *Kepler* red giants which have reliable asteroseismic fundamental atmospheric parameters, $T_{\rm eff}$ and log g. We used high resolution (R = 67 000) spectra (Thygesen *et al.* 2012) from the FIES (FIber-fed Echelle Spectrograph) spectrograph of the NOT (Nordic Optical Telescope) at La Palma. We measured equivalent widths of a well selected non-blended lines from the INSPECT database[3] (Bergemann *et al.* 2012). We have chosen the most accurate log gf values based on the experimental averaged values of Gehren *et al.* (2001). Spherical 1D model atmospheres were interpolated[4] from the MARCS database (Gustafsson *et al.* 2008) and used with an FeI/FeII model atom (Thévenin & Idiart 1999) to determine NLTE abundances using the spectral synthesis code MULTI2.2 (Carlsson 1986) and a curve-of-growth technique, while LTE abundances were calculated using the TURBOSPECTRUM code (Alvarez & Plez 1998; Plez 2012). The inelastic collisions with neutral hydrogen have been treated using the semi-classical Drawin approximation (Drawin 1969) with a scaling fudge factor of $S_H = 1$.

3 Results and conclusions

Bruntt *et al.* (2011) used the same spectra to derive LTE abundances imposing ionization equilibrium between FeI and FeII lines to derive atmospheric parameters ($T_{\rm eff}$, log g and the microturbulent velocity ξ). Their method leads to a deviations in FeI abundance as a function of excitation potential and equivalent width of up to 0.5 dex with respect to the mean. It is important to note that there is a difference of up to 400 K in $T_{\rm eff}$, 0.23 dex in log g and 0.2 dex in metallicity, between the asteroseismic and their spectroscopic values of atmospheric parameters. These differences have serious consequences on the abundance determination and thus have to be carefully chosen.

Our results show a better mutual agreement between FeI and FeII lines in NLTE as compared to LTE as a function of equivalent width and excitation potential. They also show less deviations with respect to the mean in LTE as compared to Bruntt *et al.* (2011) and even less deviations in NLTE (of up to $\sim$0.25 dex). This shows that a more careful selection of lines with good log gf values, and starting with asteroseismic parameters leads to different less dispersed abundances.

Future work, aims at improving the obtained results (less dispersion, better ionization equilibrium) by using a more complete iron model atom with up-to-date atomic data and an updated version of the NLTE spectral synthesis code

[3] `www.inspect-stars.net`
[4] Masseron code: `http://marcs.astro.uu.se/software.php`

MULTI2.3 in order to be able to calibrate the uncertain collisional effects of iron with neutral hydrogen and electrons. This should result in more accurate iron abundance determinations in red giants.

References

Alvarez, R., & Plez, B., 1998, A&A, 330, 1109

Asplund, M., 2005, ARA&A, 43, 481

Barklem, P.S., *et al.*, 2011, A&A, 530, A94

Belyaev, A.K., Barklem, P.S., 2003, Phys. Rev. A, 68, 062703

Bergemann, M., *et al.*, 2012, MNRAS, 427, 27

Bruntt, H., *et al.*, 2011, A&A, 528, 121

Carlsson, M., 1986, Uppsala Astronomical Observatory Reports, 33

Drawin, H.W., 1969, Zeitschrift fur Physik, 225, 483

Gehren, T., *et al.*, 2001, A&A, 366, 981

Gustafsson, B., *et al.*, 2008, A&A, 486, 951

Mashonkina, L., *et al.*, 2011, A&A, 528, 87

Plez, B., 2012, Turbospectrum: Code for spectral synthesis, Astrophysics Source Code Library

Thevenin, F., & Idiart, T.P., 1999, ApJ, 521, 753

Thygesen, A.O., *et al.*, 2012, A&A, 543, 160

Bibliography

(2000). Book Review: Allen's astrophysical quantities. - 4th ed. / Springer, 2000. *S&T*, 100(1):72.

Allen, C. W. (1973). *Astrophysical quantities*.

Allende Prieto, C., Majewski, S. R., Schiavon, R., Cunha, K., Frinchaboy, P., Holtzman, J., Johnston, K., Shetrone, M., Skrutskie, M., Smith, V., and Wilson, J. (2008). APOGEE: The Apache Point Observatory Galactic Evolution Experiment. *Astronomische Nachrichten*, 329:1018.

Alonso, A., Arribas, S., and Martínez-Roger, C. (1999). The effective temperature scale of giant stars (F0-K5). I. The effective temperature determination by means of the IRFM. *A&AS*, 139:335–358.

Andersen, J. (1999). Proceedings of the Twenty-third General Assembly. *Transactions of the International Astronomical Union, Series B*, 23.

Anstee, S. D. and O'Mara, B. J. (1995). Width cross-sections for collisional broadening of s-p and p-s transitions by atomic hydrogen. *MNRAS*, 276:859–866.

Asplund, M. (2005). New Light on Stellar Abundance Analyses: Departures from LTE and Homogeneity. *ARA&A*, 43:481–530.

Asplund, M. and García Pérez, A. E. (2001). On OH line formation and oxygen abundances in metal-poor stars. *A&A*, 372:601–615.

Asplund, M., Grevesse, N., Sauval, A. J., and Scott, P. (2009). The Chemical Composition of the Sun. *ARA&A*, 47:481–522.

Asplund, M., Nordlund, Å., and Trampedach, R. (1999a). Confrontation of Stellar Surface Convection Simulations with Stellar Spectroscopy. In Gimenez, A., Guinan, E. F., and Montesinos, B., editors, *Stellar Structure: Theory and Test of Connective Energy Transport*, volume 173 of *Astronomical Society of the Pacific Conference Series*, page 221.

Asplund, M., Nordlund, Å., Trampedach, R., and Stein, R. F. (1999b). 3D hydrodynamical model atmospheres of metal-poor stars. Evidence for a low primordial Li abundance. *A&A*, 346:L17–L20.

Asplund, M., Nordlund, Å., Trampedach, R., and Stein, R. F. (2000). Line formation in solar granulation. II. The photospheric Fe abundance. *A&A*, 359:743–754.

Auer, L. H., Heasley, J. N., and Milkey, R. W. (1972). A computational program for the solution of non-LTE transfer problems by the complete linearization method. *Contributions from the Kitt Peak National Observatory*, 555.

Bagnulo, S., Jehin, E., Ledoux, C., Cabanac, R., Melo, C., Gilmozzi, R., and ESO Paranal Science Operations Team (2003). The UVES Paranal Observatory Project: A Library of High- Resolution Spectra of Stars across the Hertzsprung-Russell Diagram. *The Messenger*, 114:10–14.

Ballester, P., Modigliani, A., Boitquin, O., Cristiani, S., Hanuschik, R., Kaufer, A., and Wolf, S. (2000). The UVES Data Reduction Pipeline. *The Messenger*, 101:31–36.

Barklem, P. S., Anstee, S. D., and O'Mara, B. J. (1998). Line Broadening Cross Sections for the Broadening of Transitions of Neutral Atoms by Collisions with Neutral Hydrogen. *PASA*, 15:336–338.

Barklem, P. S., Anstee, S. D., and O'Mara, B. J. (2015). abo-cross: Hydrogen broadening cross-section calculator. Astrophysics Source Code Library.

Barklem, P. S., Belyaev, A. K., and Asplund, M. (2003). Inelastic H+Li and H^-+Li^+ collisions and non-LTE Li I line formation in stellar atmospheres. *A&A*, 409:L1–L4.

Barklem, P. S., Belyaev, A. K., Dickinson, A. S., and Gadéa, F. X. (2010). Inelastic Na+H collision data for non-LTE applications in stellar atmospheres. *A&A*, 519:A20.

Barklem, P. S., Belyaev, A. K., Guitou, M., Feautrier, N., Gadéa, F. X., and Spielfiedel, A. (2011). On inelastic hydrogen atom collisions in stellar atmospheres. *A&A*, 530:A94.

Barklem, P. S., Belyaev, A. K., Spielfiedel, A., Guitou, M., and Feautrier, N. (2012). Inelastic Mg+H collision data for non-LTE applications in stellar atmospheres. *A&A*, 541:A80.

Barklem, P. S. and O'Mara, B. J. (1997). The broadening of p-d and d-p transitions by collisions with neutral hydrogen atoms. *MNRAS*, 290:102–106.

Barklem, P. S., Stempels, H. C., Allende Prieto, C., Kochukhov, O. P., Piskunov, N., and O'Mara, B. J. (2002). Detailed analysis of Balmer lines in cool dwarf stars. *A&A*, 385:951–967.

Bautista, M. A. (1997). Atomic data from the IRON Project. XX. Photoionization cross sections and oscillator strengths for Fe I. *A&AS*, 122:167–176.

Bautista, M. A. and Pradhan, A. K. (1996). Atomic data from the Iron project. XIII. Electron excitation rates and emissivity ratios for forbidden transitions in NI II and Fe II. *A&AS*, 115:551–559.

Bazot, M., Ireland, M. J., Huber, D., Bedding, T. R., Broomhall, A.-M., Campante, T. L., Carfantan, H., Chaplin, W. J., Elsworth, Y., Meléndez, J., Petit, P., Théado, S., Van Grootel, V., Arentoft, T., Asplund, M., Castro, M., Christensen-Dalsgaard, J., Do Nascimento, J. D., Dintrans, B., Dumusque, X., Kjeldsen, H., McAlister, H. A., Metcalfe, T. S., Monteiro, M. J. P. F. G., Santos, N. C., Sousa, S., Sturmann, J., Sturmann, L., ten Brummelaar, T. A., Turner, N., and Vauclair, S. (2011). The radius and mass of the close solar twin 18 Scorpii derived from asteroseismology and interferometry. *A&A*, 526:L4.

Belkacem, K., Goupil, M. J., Dupret, M. A., Samadi, R., Baudin, F., Noels, A., and Mosser, B. (2011). The underlying physical meaning of the ν_{max} - ν_c relation. *A&A*, 530:A142.

Bely, O. and van Regemorter, H. (1970). Excitation and Ionization by Electron Impact. *ARA&A*, 8:329.

Belyaev, A. K. (2013). Inelastic aluminium-hydrogen collision data for non-LTE applications in stellar atmospheres. *A&A*, 560:A60.

Belyaev, A. K. and Barklem, P. S. (2003). Cross sections for low-energy inelastic H+Li collisions. *Phys. Rev. A*, 68(6):062703.

Belyaev, A. K., Barklem, P. S., Spielfiedel, A., Guitou, M., Feautrier, N., Rodionov, D. S., and Vlasov, D. V. (2012). Cross sections for low-energy inelastic Mg + H and Mg^+ + H^- collisions. *Phys. Rev. A*, 85(3):032704.

Belyaev, A. K., Grosser, J., Hahne, J., and Menzel, T. (1999). Ab initio cross sections for low-energy inelastic H+Na collisions. *Phys. Rev. A*, 60:2151–2158.

Belyaev, A. K., Yakovleva, S. A., and Barklem, P. S. (2014). Inelastic silicon-hydrogen collision data for non-LTE applications in stellar atmospheres. *A&A*, 572:A103.

Bergemann, M., Lind, K., Collet, R., Magic, Z., and Asplund, M. (2012). Non-LTE line formation of Fe in late-type stars - I. Standard stars with 1D and <3D> model atmospheres. *MNRAS*, 427:27–49.

Bergemann, M. and Nordlander, T. (2014). Non-LTE radiative transfer in cool stars. Theory and applications to the abundance analysis for 24 chemical elements. *ArXiv e-prints*.

Blackwell, D. E., Shallis, M. J., and Selby, M. J. (1979). The infrared flux method for determining stellar angular diameters and effective temperatures. *MNRAS*, 188:847–862.

Blanco-Cuaresma, S., Soubiran, C., Jofré, P., and Heiter, U. (2014). The Gaia FGK benchmark stars. High resolution spectral library. *A&A*, 566:A98.

Böhm-Vitense, E. (1958). Über die Wasserstoffkonvektionszone in Sternen verschiedener Effektivtemperaturen und Leuchtkräfte. Mit 5 Textabbildungen. *ZAp*, 46:108.

Born, M. (1926). Zur Quantenmechanik der Stoßvorgänge. *Zeitschrift fur Physik*, 37:863–867.

Bransden, B. H. and Joachain, C. J. (2003). *Physics of Atoms and Molecules*.

Brogaard, K., Sandquist, E., Jessen-Hansen, J., Grundahl, F., and Frandsen, S. (2015). Exploiting the Open Clusters in the Kepler and CoRoT Fields. *Astrophysics and Space Science Proceedings*, 39:51.

Brown, T. M., Gilliland, R. L., Noyes, R. W., and Ramsey, L. W. (1991). Detection of possible p-mode oscillations on Procyon. *ApJ*, 368:599–609.

Bruntt, H., Bedding, T. R., Quirion, P.-O., Lo Curto, G., Carrier, F., Smalley, B., Dall, T. H., Arentoft, T., Bazot, M., and Butler, R. P. (2010). Accurate fundamental parameters for 23 bright solar-type stars. *MNRAS*, 405:1907–1923.

Burbidge, E. M., Burbidge, G. R., Fowler, W. A., and Hoyle, F. (1957). Synthesis of the Elements in Stars. *Reviews of Modern Physics*, 29:547–650.

Carlsson, M. (1986). A computer program for solving multi-level non-LTE radiative transferproblems in moving or static atmospheres. *Uppsala Astronomical Observatory Reports*, 33.

Carlsson, M. (1992). The MULTI Non-LTE Program (Invited Review). In Giampapa, M. S. and Bookbinder, J. A., editors, *Cool Stars, Stellar Systems, and the Sun*, volume 26 of *Astronomical Society of the Pacific Conference Series*, page 499.

Casagrande, L. (2009). The effective temperature scale: resolving different versions. *Mem. Soc. Astron. Italiana*, 80:727.

Casagrande, L., Portinari, L., and Flynn, C. (2006). Accurate fundamental parameters for lower main-sequence stars. *MNRAS*, 373:13–44.

Casagrande, L., Ramírez, I., Meléndez, J., Bessell, M., and Asplund, M. (2010). An absolutely calibrated T_{eff} scale from the infrared flux method. Dwarfs and subgiants. *A&A*, 512:A54.

Castelli, F. and Kurucz, R. L. (2004). New Grids of ATLAS9 Model Atmospheres. *ArXiv Astrophysics e-prints*.

Christensen-Dalsgaard, J. (1991). Some aspects of the theory of solar oscillations. *Geophysical and Astrophysical Fluid Dynamics*, 62:123–152.

Cohen, M., Walker, R. G., Carter, B., Hammersley, P., Kidger, M., and Noguchi, K. (1999). Spectral Irradiance Calibration in the Infrared. X. A Self-Consistent Radiometric All-Sky Network of Absolutely Calibrated Stellar Spectra. *AJ*, 117:1864–1889.

Collet, R., Asplund, M., and Thévenin, F. (2005). Effects of line-blocking on the non-LTE Fe I spectral line formation. *A&A*, 442:643–650.

Collet, R., Asplund, M., and Trampedach, R. (2006). *3D Hydrodynamical Simulations of Convection in Red-Giants Stellar Atmospheres*, page 306.

Collet, R., Nordlund, Å., Asplund, M., Hayek, W., and Trampedach, R. (2009). Abundance analysis of the halo giant HD 122563 with three-dimensional model stellar atmospheres. *Mem. Soc. Astron. Italiana*, 80:719.

Crandall, D. H. (1983). Electron-Impact Excitation of Ions. In Brouillard, F. and McGowan, J. W., editors, *NATO Advanced Science Institutes (ASI) Series B*, volume 83 of *NATO Advanced Science Institutes (ASI) Series B*, page 201.

Cunto, W., Mendoza, C., Ochsenbein, F., and Zeippen, C. J. (1993). TOPBASE: the Opacity Project atomic database. *Bulletin d'Information du Centre de Donnees Stellaires*, 42:39.

De Silva, G. M., Freeman, K. C., Bland-Hawthorn, J., Martell, S., de Boer, E. W., Asplund, M., Keller, S., Sharma, S., Zucker, D. B., Zwitter, T., Anguiano, B., Bacigalupo, C., Bayliss, D., Beavis, M. A., Bergemann, M., Campbell, S., Cannon, R., Carollo, D., Casagrande, L., Casey, A. R., Da Costa, G., D'Orazi, V., Dotter, A., Duong, L., Heger, A., Ireland, M. J., Kafle, P. R., Kos, J., Lattanzio, J., Lewis, G. F., Lin, J., Lind, K., Munari, U., Nataf, D. M., O'Toole, S., Parker, Q., Reid, W., Schlesinger, K. J., Sheinis, A., Simpson, J. D., Stello, D., Ting, Y.-S., Traven, G., Watson, F., Wittenmyer, R., Yong, D., and Žerjal, M. (2015). The GALAH survey: scientific motivation. *MNRAS*, 449:2604–2617.

Drawin, H.-W. (1968). Zur formelmäßigen Darstellung des Ionisierungsquerschnitts für den Atom-Atomstoß und über die Ionen-Elektronen-Rekombination im dichten Neutralgas. *Zeitschrift fur Physik*, 211:404–417.

Drawin, H. W. (1969). Collisional-radiative ionization and recombination coefficients for quasi-stationary homogeneous hydrogen and hydrogenic ion plasmas. *Zeitschrift fur Physik*, 225:470–482.

Drummond, J. D., Christou, J. C., and Fugate, R. Q. (1995). Full Adaptive Optics Images of ADS 9731 and MU Cassiopeiae: Orbits and Masses. *ApJ*, 450:380.

Feautrier, N., Spielfiedel, A., Guitou, M., and Belyaev, A. K. (2014). Non-LTE modeling of cold stellar atmospheres. In Ballet, J., Martins, F., Bournaud, F., Monier, R., and Reylé, C., editors, *SF2A-2014: Proceedings of the Annual meeting of the French Society of Astronomy and Astrophysics*, pages 475–478.

Fisher, V., Bernshtam, V., Golten, H., and Maron, Y. (1996). Electron-impact excitation cross sections for allowed transitions in atoms. *Phys. Rev. A*, 53:2425–2432.

Fite, W. L. and Brackmann, R. T. (1958). Collisions of Electrons with Hydrogen Atoms. I. Ionization. *Physical Review*, 112:1141–1151.

Fleck, I., Grosser, J., Schnecke, A., Steen, W., and Voigt, H. (1991). Na atom excitation in low energy H+Na collisions. *Journal of Physics B Atomic Molecular Physics*, 24:4017–4023.

Fleischmann, H. H. and Dehmel, R. C. (1972). On Drawin's formula for ionization in atom-atom collisions. *Zeitschrift fur Physik*, 252:435–442.

Freytag, B., Steffen, M., Ludwig, H.-G., Wedemeyer-Böhm, S., Schaffenberger, W., and Steiner, O. (2012). Simulations of stellar convection with CO5BOLD. *Journal of Computational Physics*, 231:919–959.

Fuhrmann, K., Axer, M., and Gehren, T. (1993). Balmer lines in cool dwarf stars. 1. Basic influence of atmospheric models. *A&A*, 271:451.

Gai, N., Basu, S., Chaplin, W. J., and Elsworth, Y. (2011). An In-depth Study of Grid-based Asteroseismic Analysis. *ApJ*, 730:63.

Garstang, R. H. (1961). Atomic Transition Probability Calculations. *AJ*, 66:284.

Gehren, T. (1975). Kinetic equilibrium and line formation of NA I in the solar atmosphere. *A&A*, 38:289–302.

Gehren, T., Korn, A. J., and Shi, J. (2001). Kinetic equilibrium of iron in the atmospheres of cool dwarf stars. II. Weak Fe I lines in the solar spectrum. *A&A*, 380:645–664.

Gilmore, G., Randich, S., Asplund, M., Binney, J., Bonifacio, P., Drew, J., Feltzing, S., Ferguson, A., Jeffries, R., Micela, G., and et al. (2012a). The Gaia-ESO Public Spectroscopic Survey. *The Messenger*, 147:25–31.

Gilmore, G., Randich, S., Asplund, M., Binney, J., Bonifacio, P., Drew, J., Feltzing, S., Ferguson, A., Jeffries, R., Micela, G., and et al. (2012b). The Gaia-ESO Public Spectroscopic Survey. *The Messenger*, 147:25–31.

Girard, T. M., Wu, H., Lee, J. T., Dyson, S. E., van Altena, W. F., Horch, E. P., Gilliland, R. L., Schaefer, K. G., Bond, H. E., Ftaclas, C., Brown, R. H., Toomey, D. W., Shipman, H. L., Provencal, J. L., and Pourbaix, D. (2000). A Redetermination of the Mass of Procyon. *AJ*, 119:2428–2436.

Gorshanov, D. L., Shakht, N. A., and Kisselev, A. A. (2006). Observations of the binary star 61 Cyg on the 26 inch refractor at the Pulkovo observatory. *Astrophysics*, 49:386–396.

Gratton, R. G., Carretta, E., Eriksson, K., and Gustafsson, B. (1999). Abundances of light elements in metal-poor stars. II. Non-LTE abundance corrections. *A&A*, 350:955–969.

Gray, D. F. (2008). *The Observation and Analysis of Stellar Photospheres*.

Grevesse, N., Asplund, M., and Sauval, A. J. (2007). The Solar Chemical Composition. *Space Sci. Rev.*, 130:105–114.

Griem, H. R. (1974). *Spectral line broadening by plasmas*.

Grupp, F. (2004). MAFAGS-OS: New opacity sampling model atmospheres for A, F and G stars. II. Temperature determination and three "standard" stars. *A&A*, 426:309–322.

Gustafsson, B., Bell, R. A., Eriksson, K., and Nordlund, A. (1975). A grid of model atmospheres for metal-deficient giant stars. I. *A&A*, 42:407–432.

Gustafsson, B., Edvardsson, B., Eriksson, K., Jørgensen, U. G., Nordlund, Å., and Plez, B. (2008). A grid of MARCS model atmospheres for late-type stars. I. Methods and general properties. *A&A*, 486:951–970.

Hauschildt, P. H., Baron, E., and Allard, F. (1997). Parallel Implementation of the PHOENIX Generalized Stellar Atmosphere Program. *ApJ*, 483:390–398.

Hebb, M. H. and Menzel, D. H. (1940). Physical Processes in Gaseous Nebulae. X. Collisional Excitation of Nebulium. *ApJ*, 92:408.

Heiter, U., Jofré, P., Gustafsson, B., Korn, A. J., Soubiran, C., and Thévenin, F. (2015a). Gaia FGK Benchmark Stars: Effective temperatures and surface gravities. *ArXiv e-prints*.

Heiter, U., Lind, K., Asplund, M., Barklem, P. S., Bergemann, M., Magrini, L., Masseron, T., Mikolaitis, Š., Pickering, J. C., and Ruffoni, M. P. (2015b). Atomic and molecular data for optical stellar spectroscopy. *Phys. Scr*, 90(5):054010.

Hekker, S., Elsworth, Y., De Ridder, J., Mosser, B., García, R. A., Kallinger, T., Mathur, S., Huber, D., Buzasi, D. L., Preston, H. L., Hale, S. J., Ballot, J., Chaplin, W. J., Régulo, C., Bedding, T. R., Stello, D., Borucki, W. J., Koch, D. G., Jenkins, J., Allen, C., Gilliland, R. L., Kjeldsen, H., and Christensen-Dalsgaard, J. (2011). Solar-like oscillations in red giants observed with Kepler: comparison of global oscillation parameters from different methods. *A&A*, 525:A131.

Hekker, S. and Meléndez, J. (2007). Precise radial velocities of giant stars. III. Spectroscopic stellar parameters. *A&A*, 475:1003–1009.

Henyey, L., Vardya, M. S., and Bodenheimer, P. (1965). Studies in Stellar Evolution. III. The Calculation of Model Envelopes. *ApJ*, 142:841.

Hjerting, F. (1938). Tables Facilitating the Calculation of Line Absorption Coefficients. *ApJ*, 88:508.

Hummer, D. G., Berrington, K. A., Eissner, W., Pradhan, A. K., Saraph, H. E., and Tully, J. A. (1993). Atomic data from the IRON Project. 1: Goals and methods. *A&A*, 279:298–309.

Jofré, P., Heiter, U., Soubiran, C., Blanco-Cuaresma, S., Masseron, T., Nordlander, T., Chemin, L., Worley, C. C., Van Eck, S., Hourihane, A., Gilmore, G., Adibekyan, V., Bergemann, M., Cantat-Gaudin, T., Delgado-Mena, E., González Hernández, J. I., Guiglion, G., Lardo, C., de Laverny, P., Lind, K., Magrini, L., Mikolaitis, S., Montes, D., Pancino, E., Recio-Blanco, A., Sordo, R., Sousa, S., Tabernero, H. M., and Vallenari, A. (2015). Gaia FGK benchmark stars: abundances of alpha and iron-peak elements. *ArXiv e-prints*.

Jofré, P., Heiter, U., Soubiran, C., Blanco-Cuaresma, S., Worley, C. C., Pancino, E., Cantat-Gaudin, T., Magrini, L., Bergemann, M., González Hernández, J. I., Hill, V., Lardo, C., de Laverny, P., Lind, K., Masseron, T., Montes, D., Mucciarelli, A., Nordlander, T., Recio Blanco, A., Sobeck, J., Sordo, R., Sousa, S. G., Tabernero, H., Vallenari, A., and Van Eck, S. (2014). Gaia FGK benchmark stars: Metallicity. *A&A*, 564:A133.

Johansson, S., Lundberg, H., Li, Z., Nilsson, H., Sikström, C. M., Zethson, T., Hartman, H., Karlsson, H., Dolk, L., Mannervik, S., Raassen, T., and Leckrone, D. (2000). The FERRUM Project. In *IAU Joint Discussion*, volume 1 of *IAU Joint Discussion*, page 20.

Johnson, H. R. and Krupp, B. M. (1976). Treatment of atomic and molecular line blanketing by opacity sampling. *ApJ*, 206:201–207.

Kallinger, T., Weiss, W. W., Barban, C., Baudin, F., Cameron, C., Carrier, F., De Ridder, J., Goupil, M.-J., Gruberbauer, M., Hatzes, A., Hekker, S., Samadi, R., and Deleuil, M. (2010). Oscillating red giants in the CoRoT exofield: asteroseismic mass and radius determination. *A&A*, 509:A77.

Kervella, P. and Fouqué, P. (2008). The angular sizes of dwarf stars and subgiants. Non-linear surface brightness relations in BVR_cI$_c$ from interferometry. *A&A*, 491:855–858.

Kervella, P., Thévenin, F., Di Folco, E., and Ségransan, D. (2004). The angular sizes of dwarf stars and subgiants. Surface brightness relations calibrated by interferometry. *A&A*, 426:297–307.

Kjeldsen, H. and Bedding, T. R. (1995). Amplitudes of stellar oscillations: the implications for asteroseismology. *A&A*, 293:87–106.

Kupka, F. G., Ryabchikova, T. A., Piskunov, N. E., Stempels, H. C., and Weiss, W. W. (2000). VALD-2 – The New Vienna Atomic Line Database. *Baltic Astronomy*, 9:590–594.

Kurucz, R. and Bell, B. (1995). Atomic Line Data. *Atomic Line Data (R.L. Kurucz and B. Bell) Kurucz CD-ROM No. 23. Cambridge, Mass.: Smithsonian Astrophysical Observatory, 1995.*, 23.

Kurucz, R. L. (1979). Model atmospheres for G, F, A, B, and O stars. *ApJS*, 40:1–340.

Kurucz, R. L. (1993). Atomic data for interpreting stellar spectra: isotopic and hyperfine data. *Physica Scripta Volume T*, 47:110–117.

Kurucz, R. L. (2009). Including All the Lines. In Hubeny, I., Stone, J. M., MacGregor, K., and Werner, K., editors, *American Institute of Physics Conference Series*, volume 1171 of *American Institute of Physics Conference Series*, pages 43–51.

Lallement, R., Vergely, J.-L., Valette, B., Puspitarini, L., Eyer, L., and Casagrande, L. (2014). 3D maps of the local ISM from inversion of individual color excess measurements. *A&A*, 561:A91.

Lambert, D. L. (1993). Quantitative stellar spectroscopy with large optical telescopes. *Physica Scripta Volume T*, 47:186–198.

Landau, L. D. and Lifshitz, E. M. (1965). *Quantum mechanics*.

Lind, K., Asplund, M., Barklem, P. S., and Belyaev, A. K. (2011). Non-LTE calculations for neutral Na in late-type stars using improved atomic data. *A&A*, 528:A103.

Magic, Z., Collet, R., Asplund, M., Trampedach, R., Hayek, W., Chiavassa, A., Stein, R. F., and Nordlund, Å. (2013a). The Stagger-grid: A grid of 3D stellar atmosphere models. I. Methods and general properties. *A&A*, 557:A26.

Magic, Z., Collet, R., Hayek, W., and Asplund, M. (2013b). The Stagger-grid: A grid of 3D stellar atmosphere models. II. Horizontal and temporal averaging and spectral line formation. *A&A*, 560:A8.

Majewski, S. R. (2010). The Future of Stellar Populations Studies in the Milky Way and the Local Group. In Bruzual, G. R. and Charlot, S., editors, *IAU Symposium*, volume 262 of *IAU Symposium*, pages 99–110.

Martin, G. A., Fuhr, J. R., and Wiese, W. L. (1988). *Atomic transition probabilities. Scandium through Manganese*.

Martin, W. C. and Zalubas, R. (1983). Energy levels of silicon, si i through si xiv. *J. Phys. Chem. Ref. Data*, 12:323–380.

Mashonkina, L. (2009). Atomic data necessary for the non-LTE analysis of stellar spectra. *Physica Scripta Volume T*, 134(1):014004.

Mashonkina, L., Gehren, T., Shi, J.-R., Korn, A. J., and Grupp, F. (2011). A non-LTE study of neutral and singly-ionized iron line spectra in 1D models of the Sun and selected late-type stars. *A&A*, 528:A87.

Massey, H. S. W. (1949). Collisions between atoms and molecules at ordinary temperatures. *Reports on Progress in Physics*, 12:248–269.

McAlister, H. A., ten Brummelaar, T. A., Gies, D. R., Huang, W., Bagnuolo, Jr., W. G., Shure, M. A., Sturmann, J., Sturmann, L., Turner, N. H., Taylor, S. F., Berger, D. H., Baines, E. K., Grundstrom, E., Ogden, C., Ridgway, S. T., and van Belle, G. (2005). First Results from the CHARA Array. I. An Interferometric and Spectroscopic Study of the Fast Rotator α Leonis (Regulus). *ApJ*, 628:439–452.

McCallion, P., Shah, M. B., and Gilbody, H. B. (1992). Multiple ionization of magnesium by electron impact. *Journal of Physics B Atomic Molecular Physics*, 25:1051–1060.

Merle, T. (2012). *NLTE radiative transfer in stellar photospheres and chromospheres: application to atoms of magnesium, calcium and iron in late-type stars*. PhD thesis, Université de Nice Sophia-Antipolis, Observatoire de la Côte d'Azur.

Mermilliod, J.-C., Mermilliod, M., and Hauck, B. (1997). The General Catalogue of Photometric Data (GCPD). II. *A&AS*, 124:349–352.

Mihalas, D. (1978). *Stellar atmospheres /2nd edition/*.

Morel, T. and Miglio, A. (2012). Assessing the accuracy of the surface gravity determination in late-type stars with solar-like pulsators. *MNRAS*, 419:L34–L38.

Mosser, B., Michel, E., Belkacem, K., Goupil, M. J., Baglin, A., Barban, C., Provost, J., Samadi, R., Auvergne, M., and Catala, C. (2013). Asymptotic and measured large frequency separations. *A&A*, 550:A126.

Nahar, S. N. (1993). Transition probabilities for dipole allowed fine structure transitions in Si-like ions: Si I, S III, Ar V and Ca VII. *Phys. Scr*, 48:297–325.

Nahar, S. N. and Pradhan, A. K. (1994). Atomic data for opacity calculations: XX. Photoionization cross sections and oscillator strengths for Fe II. *Journal of Physics B Atomic Molecular Physics*, 27:429–446.

Nave, G. and Johansson, S. (2013). The Spectrum of Fe II. *ApJS*, 204:1.

Nave, G., Johansson, S., Learner, R. C. M., Thorne, A. P., and Brault, J. W. (1994). A new multiplet table for Fe I. *ApJS*, 94:221–459.

Nordlund, A. (1982). Numerical simulations of the solar granulation. I - Basic equations and methods. *A&A*, 107:1–10.

Nordlund, A. ø. and Stein, R. F. (2009). Accurate Radiation Hydrodynamics and MHD Modeling of 3-D Stellar Atmospheres. In Hubeny, I., Stone, J. M., MacGregor, K., and Werner, K., editors, *American Institute of Physics Conference Series*, volume 1171 of *American Institute of Physics Conference Series*, pages 242–259.

Osorio, Y., Barklem, P. S., Lind, K., Belyaev, A. K., Spielfiedel, A., Guitou, M., and Feautrier, N. (2015). Mg line formation in late-type stellar atmospheres. I. The model atom. *A&A*, 579:A53.

Pelan, J. and Berrington, K. A. (1997). Atomic data from the IRON Project. XXI. Electron excitation of fine-structure transitions involving the 3dˆ64sˆ2 ˆ5D ground state and the 3dˆ74s ^{5}F metastable state of Fe i. *A&AS*, 122:177–180.

Percival, I. C. and Seaton, M. J. (1957). The partial wave theory of electron-hydrogen atom collisions. *Proceedings of the Cambridge Philosophical Society*, 53:654–662.

Perryman, M. A. C., de Boer, K. S., Gilmore, G., Høg, E., Lattanzi, M. G., Lindegren, L., Luri, X., Mignard, F., Pace, O., and de Zeeuw, P. T. (2001). GAIA: Composition, formation and evolution of the Galaxy. *A&A*, 369:339–363.

Peterson, R. C. (2011). The Extreme Overabundance of Molybdenum in Two Metal-poor Stars. *ApJ*, 742:21.

Peterson, R. C. (2013). Molybdenum, Ruthenium, and the Heavy r-process Elements in Moderately Metal-poor Main-sequence Turnoff Stars. *ApJ*, 768:L13.

Peterson, R. C. and Kurucz, R. L. (2015). New Fe I Level Energies and Line Identifications from Stellar Spectra. *ApJS*, 216:1.

Piskunov, N. E., Kupka, F., Ryabchikova, T. A., Weiss, W. W., and Jeffery, C. S. (1995). VALD: The Vienna Atomic Line Data Base. *A&AS*, 112:525.

Plaskett, H. H. (1955). Interpretation of Fraunhofer-line profiles. *MNRAS*, 115:256.

Plez, B. (1992). Spherical opacity sampling model atmospheres for M-giants and supergiants. II - A grid. *A&AS*, 94:527–552.

Pourbaix, D., Nidever, D., McCarthy, C., Butler, R. P., Tinney, C. G., Marcy, G. W., Jones, H. R. A., Penny, A. J., Carter, B. D., Bouchy, F., Pepe, F., Hearnshaw, J. B., Skuljan, J., Ramm, D., and Kent, D. (2002). Constraining the difference in convective blueshift between the components of alpha Centauri with precise radial velocities. *A&A*, 386:280–285.

Pradhan, A. K. and Nahar, S. N. (2011). *Atomic Astrophysics and Spectroscopy*.

Pradhan, A. K. and Zhang, H. L. (1993). New excitation rates and line ratios for (Fe II). *ApJ*, 409:L77–L79.

Ralchenko, Y., Reader, J., and Kramida, A. (2006). New and Updated Atomic Databases at NIST. In *APS Division of Atomic, Molecular and Optical Physics Meeting Abstracts*, page G1002.

Ramírez, I., Meléndez, J., and Asplund, M. (2009). Accurate abundance patterns of solar twins and analogs. Does the anomalous solar chemical composition come from planet formation? *A&A*, 508:L17–L20.

Reader, J., Wiese, W. L., Martin, W. C., Musgrove, A., and Fuhr, J. R. (2002). NIST Databases on Atomic Spectra. In Salama, F. and et al., editors, *NASA Laboratory Astrophysics Workshop*, page 80.

Retter, A., Bedding, T. R., Buzasi, D. L., Kjeldsen, H., and Kiss, L. L. (2003). Oscillations in Arcturus from WIRE Photometry. *ApJ*, 591:L151–L154.

Rudge, M. R. (1968). Theory of the Ionization of Atoms by Electron Impact. *Reviews of Modern Physics*, 40:564–590.

Rutten, R. J. (2003). *Radiative Transfer in Stellar Atmospheres*.

Ryabchikova, T. A., Pakhomov, Y. V., and Piskunov, N. E. (2011). New release of Vienna Atomic Line Database (VALD) and its integration in Virtual Atomic and Molecular Data Centre (VAMDC). *Kazan Izdatel Kazanskogo Universiteta*, 153:61–66.

Rybicki, G. B. and Hummer, D. G. (1991). An accelerated lambda iteration method for multilevel radiative transfer. I - Non-overlapping lines with background continuum. *A&A*, 245:171–181.

Scharmer, G. B. (1981). Solutions to radiative transfer problems using approximate lambda operators. *ApJ*, 249:720–730.

Seaton, M. J. (1953). The Hartree-Fock Equations for Continuous States with Applications to Electron Excitation of the Ground Configuration Terms of O $_I$. *Royal Society of London Philosophical Transactions Series A*, 245:469–499.

Seaton, M. J. (1955). Cross Sections for 2s-2p Transitions in H and 3s-3p Transitions in Na Produced by Electron and by Proton Impact. *Proceedings of the Physical Society A*, 68:457–473.

Seaton, M. J. (1962a). The Impact Parameter Method for Electron Excitation of Optically Allowed Atomic Transitions. *Proceedings of the Physical Society*, 79:1105–1117.

Seaton, M. J. (1962b). The Theory of Excitation and Ionization by Electron Impact. In Bates, D. R., editor, *Atomic and Molecular Processes*, page 375.

Shah, M. B., Elliott, D. S., and Gilbody, H. B. (1987). Pulsed crossed-beam study of the ionisation of atomic hydrogen by electron impact. *Journal of Physics B Atomic Molecular Physics*, 20:3501–3514.

Shah, M. B., McCallion, P., Okuno, K., and Gilbody, H. B. (1993). Multiple ionization of iron by electron impact. *Journal of Physics B Atomic Molecular Physics*, 26:2393–2401.

Shchukina, N., Sukhorukov, A., and Trujillo Bueno, J. (2012). Non-LTE Determination of the Silicon Abundance Using a Three-dimensional Hydrodynamical Model of the Solar Photosphere. *ApJ*, 755:176.

Sobelman, I. I., Vainshtein, L. A., and Yukov, E. A. (1981). *Excitation of atoms and broadening of spectral lines*.

Söderhjelm, S. (1999). Visual binary orbits and masses POST HIPPARCOS. *A&A*, 341:121–140.

Steenbock, W. (1985). Statistical equilibrium of Fe I/Fe II in cool stars. In Jaschek, M. and Keenan, P. C., editors, *Cool Stars with Excesses of Heavy Elements*, volume 114 of *Astrophysics and Space Science Library*, pages 231–234.

Steenbock, W. and Holweger, H. (1984). Statistical equilibrium of lithium in cool stars of different metallicity. *A&A*, 130:319–323.

Stein, R. F. and Nordlund, Å. (1998). Simulations of Solar Granulation. I. General Properties. *ApJ*, 499:914–933.

Steinmetz, M., Zwitter, T., Siebert, A., Watson, F. G., Freeman, K. C., Munari, U., Campbell, R., Williams, M., Seabroke, G. M., Wyse, R. F. G., Parker, Q. A., Bienaymé, O., Roeser, S., Gibson, B. K., Gilmore, G., Grebel, E. K., Helmi, A., Navarro, J. F., Burton, D., Cass, C. J. P., Dawe, J. A., Fiegert, K., Hartley, M., Russell, K. S., Saunders, W., Enke, H., Bailin, J., Binney, J., Bland-Hawthorn, J., Boeche, C., Dehnen, W., Eisenstein, D. J., Evans, N. W., Fiorucci, M., Fulbright, J. P., Gerhard, O., Jauregi, U., Kelz, A., Mijović, L., Minchev, I., Parmentier, G., Peñarrubia, J., Quillen, A. C., Read, M. A., Ruchti, G., Scholz, R.-D., Siviero, A., Smith, M. C., Sordo, R., Veltz, L., Vidrih, S., von Berlepsch, R., Boyle, B. J., and Schilbach, E. (2006). The Radial Velocity Experiment (RAVE): First Data Release. *AJ*, 132:1645–1668.

Strom, S. E. and Kurucz, R. (1966). Statistical Procedure for Computing Line-Blanketed Model Stellar Atmospheres. *AJ*, 71:181.

Takeda, Y. (1994). Non-LTE effect on CNO abundance determinations for solar-type stars: The Sun, Procyon, and the oxygen problem in metal-poor dwarfs. *PASJ*, 46:53–72.

Thévenin, F. and Idiart, T. P. (1999). Stellar Iron Abundances: Non-LTE Effects. *ApJ*, 521:753–763.

Thompson, W. R., Shah, M. B., and Gilbody, H. B. (1995). Single and double ionization of atomic oxygen by electron impact. *Journal of Physics B Atomic Molecular Physics*, 28:1321–1330.

Thomson, J. J. (1912). Ionization by moving electrified particles. *Philosophical Magazine*, 23:499.

Travis, L. D. and Matsushima, S. (1968). Radiative Opacity in Stellar Atmospheres. I. Metal Absorption Coefficients. *ApJ*, 154:689.

Turon, C., O'Flaherty, K. S., and Perryman, M. A. C., editors (2005). *The Three-Dimensional Universe with Gaia*, volume 576 of *ESA Special Publication*.

Unsold, A. (1955). *Physik der Sternatmospharen, MIT besonderer Berucksichtigung der Sonne.*

van Leeuwen, F., editor (2007). *Hipparcos, the New Reduction of the Raw Data*, volume 350 of *Astrophysics and Space Science Library*.

van Regemorter, H. (1962). Rate of Collisional Excitation in Stellar Atmospheres. *ApJ*, 136:906.

VandenBerg, D. A., Bond, H. E., Nelan, E. P., Nissen, P. E., Schaefer, G. H., and Harmer, D. (2014). Three Ancient Halo Subgiants: Precise Parallaxes, Compositions, Ages, and Implications for Globular Clusters. *ApJ*, 792:110.

Vernazza, J. E., Avrett, E. H., and Loeser, R. (1973). Structure of the Solar Chromosphere. Basic Computations and Summary of the Results. *ApJ*, 184:605–632.

Verner, D. A., Barthel, P. D., and Tytler, D. (1994). Atomic data for absorption lines from the ground level at wavelengths greater than 228A. *A&AS*, 108:287–340.

Waters, C. Z. and Hollek, J. K. (2013). ROBOSPECT: Automated Equivalent Width Measurement. *PASP*, 125:1164–1178.

Yi, S. K., Kim, Y.-C., and Demarque, P. (2003). The Y^2 Stellar Evolutionary Tracks. *ApJS*, 144:259–261.

Zhang, H. L. and Pradhan, A. K. (1995). Atomic data from the Iron Project. VI. Collision strengths and rate coefficients for Fe II. *A&A*, 293:953–966.

Zhao, G. and Gehren, T. (2000). Non-LTE analysis of neutral magnesium in cool stars. *A&A*, 362:1077–1082.